Advances in Clinical and Experimental Medicine

MONTHLY ISSN 1899-5276 (PRINT) ISSN 2451-2680 (ONLINE) advances.umw.edu.pl

2025, Vol. 34, No. 11 (November)

Impact Factor (IF) – 1.9
Ministry of Science and Higher Education – 70 pts
Index Copernicus (ICV) – 161.00 pts

Wroclaw Medical University

Advances
in Clinical and Experimental
Medicine

Advances
in Clinical and Experimental Medicine

ISSN 1899-5276 (PRINT) ISSN 2451-2680 (ONLINE) advances.umw.edu.pl

MONTHLY 2025
Vol. 34, No. 11
(November)

Advances in Clinical and Experimental Medicine (*Adv Clin Exp Med*) publishes high-quality original articles, research-in-progress, research letters and systematic reviews and meta-analyses of recognized scientists that deal with all clinical and experimental medicine.

Editorial Office
ul. Marcinkowskiego 2–6
50-368 Wrocław, Poland
Tel.: +48 71 784 12 05
E-mail: redakcja@umw.edu.pl

Publisher
Wroclaw Medical University
Wybrzeże L. Pasteura 1
50-367 Wrocław, Poland

Online edition is the original version of the journal

Editorial Policy

Advances in Clinical and Experimental Medicine (Adv Clin Exp Med) is an independent multidisciplinary forum for exchange of scientific and clinical information, publishing original research and news encompassing all aspects of medicine, including molecular biology, biochemistry, genetics, biotechnology and other areas. During the review process, the Editorial Board conforms to the "Uniform Requirements for Manuscripts Submitted to Biomedical Journals: Writing and Editing for Biomedical Publication" approved by the International Committee of Medical Journal Editors (www.ICMJE.org). The journal publishes (in English only) original papers and reviews. Short works considered original, novel and significant are given priority. Experimental studies must include a statement that the experimental protocol and informed consent procedure were in compliance with the Helsinki Convention and were approved by an ethics committee.

For all subscription-related queries please contact our Editorial Office: redakcja@umw.edu.pl
For more information visit the journal's website: advances.umw.edu.pl

Pursuant to the ordinance of the Rector of Wroclaw Medical University No. 37/XVI R/2024, from March 1, 2024, authors are required to pay a fee for each manuscript accepted for publication in the journal Advances in Clinical and Experimental Medicine. The fee amounts to 1600 EUR for all types of papers.

Indexed in: MEDLINE, Science Citation Index Expanded, Journal Citation Reports/Science Edition, Scopus, EMBASE/Excerpta Medica, Ulrich's™ International Periodicals Directory, Index Copernicus

Typographic design: Piotr Gil, Monika Kolęda
DTP: Wydawnictwo UMW
Cover: Monika Kolęda
Printing and binding: Drukarnia I-BiS Bierońscy Sp.k.

Advances
in Clinical and Experimental Medicine

MONTHLY 2025, Vol. 34, No. 11 (November)

ISSN 1899-5276 (PRINT)
ISSN 2451-2680 (ONLINE)
advances.umw.edu.pl

Contents

Editorials

1797 Krzysztof Simon, Monika Pazgan-Simon
HCV infection: Extrahepatic manifestations of infection and treatment options

1803 Yuko Hakamata, Hiroaki Hori
Neurobiological effects of childhood maltreatment: Health consequences, recovery pathways and clinical implications for holistic care

1807 Timothy Daly
Blood biomarkers of Alzheimer's disease: Balancing clinical relevance with improved accessibility and sustainability

1813 Yuchen Sun, Shengtao Hu, Ming Yi, Zhijun Dai
Immune reprogramming of cold tumors using TGF-β/PD-L1 bispecific antibody and armed oncolytic virus therapy

Meta-analysis

1819 Xiaoxia Zhang, Ruoling Mo, Yue Liu, Xiuying Guo
A meta-analysis examining the impact of the continuous intervention for intraoperative pressure wound ulcers associated problems in women with breast cancer

1827 Xiaoping Ren, Shuyan Liu, Ju Gao, Rupshikha Choudhury, Sanjay Rastogi
Clearing the path: Hypertonic saline's impact on intracranial pressure in traumatic brain injury. A systematic review and meta-analysis

Original papers

1841 Shasha Liu, Yue Wang, Yuling Guo, Xinran Xu, Yiping Gao, Lan Cheng
***MiR-204-5p* promoted maternally expressed gene 3 (*MEG3*) through *SP1*-mediated *DNMT1* pathway in trophoblast cells in recurrent miscarriage**

1851 Jie Ruan, Ying Xie, Huifang Zhou, Libo Su, Chao Liu, Chaoqun Zhang, Sun Dianxing
Mesoderm/mesenchyme homeobox l as a potential target that orchestrates hepatic stellate cell activation

1863 Xupeng Wu, Hong Liu, Liangliang Cui, Mengyan Mo, Changxin Li
Genetically determined thyroid function and cerebral cortex structure: A Mendelian randomization study

1881 Yanqiong Liu, Lian Li, Shasha Wang, Shuangyan Zhou, Jianhui Zou
Epidemiological characteristics of thyroid cancer worldwide and construction of a machine learning diagnostic model

1897 Xiaoyan Wang, Zhufeng Chen, Shanshan Wu, Xuemei Fan
Effects of echinacoside on the regulation of mitochondrial fission induced by TBK1/Drp1 in rheumatoid arthritis

1907 Li Wang, Xue Wang, Ying Zheng, Jiao Kong, Lin-Mei Zheng, Ai-Hua He, Xiao-Ju Chen
Parkin aggravates symptoms of preeclampsia through promoting mitophagy and apoptosis

1921 Jun Miao, Lu Wang, Min Feng
Association between proinflammatory cytokines and pain intensity in patients with postherpetic neuralgia

1929 ZongHui Feng, Yan Chen, FengMei Yi, Min Li, ShuMin Jiang, ChunYue He, YangLi Chen, MaoSheng Chen, WenCheng Li
Importance of single nucleotide polymorphism microarray in prenatal diagnosis

1937 Bo Li, Si-Ying Li, Yi-Chao Yan
IGF2BP2-mediated m^{6}A modifies SLC7A11 to regulate proliferation and ferroptosis in non-small cell lung cancer cells

1947 Michał Zawistowski, Piotr Niecikowski, Magdalena Durlik, Joanna Nowaczyk, Jan Broda, Bartosz Foroncewicz, Krzysztof Mucha, Monika Widera, Robert Król, Honorata Stadnik, Marek Karczewski, Tomasz Kruszyna, Bogdan Niekowal, Justyna Korus, Dorota Kamińska, Magdalena Krajewska, Maciej Kosieradzki, Piotr Domagała
Peritoneal dialysis catheter removal at the time or after kidney transplantation: A multicenter cardinality-matched cohort study

1959 Paulina Szabelska, Joanna Brydak-Godowska, Przemysław Krajewski, Radosław Różycki, Joanna Gołębiewska
Correlations between OCT, OCT angiography and fundus autofluorescence in adults with superficial optic disc drusen: The importance of multimodal imaging

1969 Maria Jędrzejczyk, Christopher S. Lee, Ercole Vellone, Anna Gozdzik, Remigiusz Szczepanowski, Michał Czapla, Izabella Uchmanowicz
Analysis of changes in mental health, cognitive function and self-care behaviors in patients with heart failure: A prospective cohort study

Reviews

1981 Aleksandra A. Nasiadka, Alicja Rydzewska-Rosołowska, Katarzyna Kakareko, Irena Głowińska, Tomasz Hryszko
The role of urinary biomarkers in the diagnosis, prognosis and pathophysiology of heart failure with preserved ejection fraction

Editorial

HCV infection: Extrahepatic manifestations of infection and treatment options

Krzysztof Simon[1,2,A–F], Monika Pazgan-Simon[2,A–F]

[1] Department of Infectious Diseases and Hepatology, Faculty of Medicine, Wroclaw Medical University, Poland
[2] First Department of Infectious Diseases, Regional Specialistic Hospital, Wrocław, Poland

A – research concept and design; B – collection and/or assembly of data; C – data analysis and interpretation; D – writing the article; E – critical revision of the article; F – final approval of the article

Advances in Clinical and Experimental Medicine, ISSN 1899–5276 (print), ISSN 2451–2680 (online) *Adv Clin Exp Med*. 2025;34(11):1797–1802

Address for correspondence
Krzysztof Simon
E-mail: krzysztof.simon@umw.edu.pl

Funding sources
None declared

Conflict of interest
None declared

Received on August 22, 2025
Accepted on September 3, 2025

Published online on September 26, 2025

Abstract

Currently, there is no doubt that hepatitis C virus (HCV) infection is a systemic disease affecting not only the liver but also a range of other organs – extrahepatic manifestations (EHMs). Extrahepatic manifestations usually occur concurrently with liver disease, primarily have an immunological basis, and/or are a consequence of the direct impact of HCV on virtually all organs. The scope of the problem is significant; it has been shown that 30–40% of HCV-infected individuals are affected, which aligns with our own observations. Viral elimination (either spontaneous HCV clearance or as a result of pharmacotherapy) is crucial for the patient's prognosis, both in terms of liver disease and EHM. Achieving a sustained virological response (SVR) only in many cases of EHMs is associated with remission of clinical symptoms of EHMs.

Key words: HCV, liver, mixed cryoglobulinemia

Cite as
Simon K, Pazgan-Simon M. HCV infection: Extrahepatic manifestations of infection and treatment options. *Adv Clin Exp Med*. 2025;34(11):1797–1802. doi:10.17219/acem/210248

DOI
10.17219/acem/210248

Highlights

- Hepatitis C virus (HCV) is a systemic disease, with 30–40% of patients developing extrahepatic manifestations (EHMs) alongside liver involvement.
- EHMs in HCV are driven by immune-mediated mechanisms or direct viral effects, impacting multiple organ systems.
- Sustained virological response (SVR) after HCV clearance improves outcomes, often leading to remission or significant improvement of extrahepatic manifestations.

Introduction

The term "viral hepatitis C" is a significant oversimplification of the problem, as it does not encompass a range of highly diverse liver diseases associated with HCV, nor the numerous extrahepatic manifestations of this infection. Currently, there is no doubt that HCV infection is a systemic disease affecting not only the liver but also a variety of other organs – extrahepatic manifestations (EHMs). Extrahepatic manifestations typically occur alongside liver disease, are largely immunologically mediated, and/or result from the direct effects of HCV on multiple organs. Most experts believe that at least 1 form of EHM appears in 30–40% of those infected with HCV. Viral elimination (either spontaneous clearance of HCV or as a result of pharmacotherapy) is crucial for the patient's prognosis, both in terms of liver disease – regardless of its stage – and extrahepatic manifestations. In many cases, achieving a sustained virological response (SVR) is associated with remission of clinical symptoms of EHMs. However, causal treatment initiated at a late stage of HCV-related disease often does not bring significant clinical benefits; hence, early diagnosis and therapy of HCV infection are of vital importance.[1]

Epidemiology

Infections caused by primary hepatotropic viruses – HBV, HCV, HAV, HEV, and HDV – are among the most serious infectious disease challenges in the modern world. According to the WHO, an estimated 50 million people are currently infected with HCV, compared with approx. 71 million a decade ago. In 2022, 242,000 deaths were attributed to chronic HCV infection, primarily from liver cirrhosis or hepatocellular carcinoma. Spontaneous elimination of HCV occurs in about 15–45% of infected individuals, usually within a few months, while the remaining 55–85% develop chronic infection. For untreated patients with chronic HCV, the risk of cirrhosis ranges from 15% to 30% within 20 years. The highest prevalence of HCV infection is observed in the Mediterranean region, China, India, Russia, as well as in Alaska and the USA. On the other hand, many countries – primarily wealthy, but not only European – are on a fast track to eliminate HCV by 2030, such as Canada, Australia, and Japan. The global decline in infections is due to advances in knowledge, improved sanitary and epidemiological standards, the use of disposable medical equipment, easier access to diagnostics – especially molecular techniques – and better availability of safe, well-tolerated antiviral therapies based on direct-acting antivirals (DAAs). In Poland, approx. 700,000 individuals have anti-HCV antibodies, but active viral replication (HCV RNA positive) is detected in only about 150,000. In 2024, according to NIZ-PZH data, just 3,526 cases of chronic HCV-related liver disease and 44 cases of acute hepatitis were diagnosed – figures that are highly concerning given the estimated number of individuals with active replication. Notably, the registry does not capture cases presenting with extrahepatic manifestations of HCV infection. At the current rate of diagnosis, elimination of HCV in Poland may not be achieved until around 2060, a timeline similar to that projected for the United States.[1–5]

Extrahepatic manifestations of HCV infection

The hepatic manifestations of HCV infection are well characterized. In contrast, EHMs are often not linked to HCV in the absence of active biochemical liver disease. This frequently delays initiation of antiviral therapy, thereby reducing the likelihood of cure and adversely affecting mortality and treatment costs (Fig. 1,2).[6–9] Moreover, numerous diseases involving different organs show a statistically significant association with HCV infection, although the nature of this relationship remains unclear. Does HCV infection increase the risk of these conditions? What immunological mechanisms are involved? (Fig. 3).[10–17]

HCV extrahepatic manifestations in details

Mixed cryoglobulinemia

Mixed cryoglobulinemia (MC), most commonly type II, is the most frequent EHM of HCV infection. It is defined

Typical HCV extrahepatic manifestations
Mixed cryoglobulinemia syndrome
Non-Hodgkin lymphoma
Porphyria cutanea tarda
Lichen planus
Necrolytic acral erythema
Autoimmune thyreoiditis
Diabetes mellitus t. 2
Kidney diseases
Arthritis, myalgias, sicca symptoms
Cardiovascular diesases
Depression

Fig. 1. Typical HCV extrahepatic manifestations

by the presence of cryoglobulins–immune complexes that precipitate at temperatures below 37°C – and is associated with vasculitis and multiorgan involvement. Mixed cryoglobulinemia occurs approx. 11 times more often in HCV-infected individuals than in uninfected ones, affecting about 4.9% of patients with HCV. Notably, around 90% of patients with cryoglobulins have detectable anti-HCV antibodies and HCV RNA, confirming active infection. Mixed cryoglobulinemia is both an autoimmune and lymphoproliferative disorder, resulting from persistent activation of B lymphocytes by HCV to produce

Less known and discussed extrahepatic manifestations of HCV infection
Chronic fatigue
Slowed cognitive processes
Encephalopathy not associated with liver cirrhosis
Inflammation of the spinal cord
Cerebral circulation disorders and their consequences
Polyneuropathies, including restless legs syndrome

Fig. 2. Less known and discussed extrahepatic manifestations of HCV infection

antibodies. Clinically, MC is usually mild, but in 5–10% of cases it progresses to non-Hodgkin lymphoma, with a risk 35 times higher than in the general population. Cryoglobulins precipitate and deposit in the walls of small- and medium-sized blood vessels, leading to vasculitis. The organs most commonly affected are the skin, joints, kidneys, central and peripheral nervous systems, gastrointestinal tract, and heart. Typical symptoms include weakness, purpura (skin hemorrhages), and joint pain, usually without true arthritis. The joints most frequently affected are the proximal interphalangeal and metacarpophalangeal joints of the hands, as well as the knees and hips. Renal involvement is manifested by proteinuria and hematuria, which may progress to membranoproliferative glomerulonephritis and renal failure. Neurological symptoms include paresthesias, tingling, and burning sensations in the feet and hands, reflecting peripheral polyneuropathy, while isolated mononeuropathies are uncommon. In severe cases,

Other diseases statistically significantly associated with HCV infection (lack of data on the effectiveness of DAA)
Gastrointestinal diseases: Celiac disease, inflammatory bowel diseases, irritable bowel syndrome, gastroesophageal reflux disease
Cancers: Prostate cancer, esophageal cancer, pancreatic cancer, anal cancer; other head and neck cancers
Others: Parkinson's disease, pulmonary fibrosis, immune thrombocytopenic purpura, antiphospholipid syndrome, systemic lupus erythematosus, keratitis (Mooren's ulcer)
Dermatoses with presumed association with HCV Infection: Nodular arteritis, sicca syndrome – incomplete Sjögren's syndrome, psoriasis
Dermatoses with incidental association with HCV Infection: Prurigo
Dermatoses with casuistic association with HCV Infection: Erythema nodosum, erythema multiforme, vascular urticaria (usually in the acute phase; also occurring in the course of infections with other viruses), annular granuloma, vitiligo, Behçet's disease

Fig. 3. Other diseases statistically significantly associated with HCV infection (lack of data on the effectiveness of direct-acting antivirals (DAAs)

MC can progress rapidly, leading to renal failure, intestinal ischemia, and pulmonary hemorrhage.

Treatment involves DAAs. Achieving SVR leads to remission of symptoms in about 70% of treated patients. In patients with clinically severe MC, unfortunately, the pharmacological elimination of HCV does not affect the course of this condition. This group of patients requires immunosuppressive treatment.[6,8,9]

Non-Hodgkin lymphomas

The risk of developing B-cell non-Hodgkin's lymphoma (B-NHL) is increased by 28% among individuals infected with HCV compared to uninfected persons. A meta-analysis based on 48 clinical studies demonstrated that HCV infection is present in approx. 15% of patients with B-NHL. Furthermore, 90% of patients with NHL and circulating cryoglobulins have detectable HCV viremia. The most common subtypes of NHL associated with HCV infection include: diffuse large B-cell lymphoma (DLBCL), lymphoplasmacytic lymphoma (Waldenström's macroglobulinemia), marginal zone lymphoma (MZL) – particularly splenic marginal zone lymphoma (SMZL) and nodal marginal zone lymphoma (NMZL) – and MALT lymphoma. It has been shown that 2/3 of HCV-associated lymphomas tend to have a less aggressive clinical course. Approximately 10% of HCV-infected patients develop monoclonal gammopathy, characterized by the production of IgM kappa antibodies, which may indicate an increased risk of multiple myeloma. HCV infection can also be associated with polyclonal or oligoclonal hypergammaglobulinemia, most often involving IgG, which correlates with the severity of hepatitis. Coexisting chronic hepatitis further increases the risk of hepatotoxicity during lymphoma therapy, particularly with rituximab..

Treatment: DAAs should be considered as first-line treatment in cases of indolent lymphomas. For more aggressive lymphomas (intermediate and high-grade), initial treatment with immunochemotherapy followed by antiviral therapy is recommended. It has also been demonstrated that effective HCV treatment (achieving sustained virologic response, SVR) statistically reduces the risk of developing NHL in previously infected patients.[6,8–13]

Dermatological diseases

Compared with uninfected individuals, HCV infection increases the risk of porphyria cutanea tarda (PCT) more than 8.5-fold and of lichen planus (LP) approx. twofold, particularly in patients with HCV genotypes 1 and 4. Both PCT and LP occur in 1–2% of HCV-infected individuals, independent of the cutaneous manifestations seen in MC.

Treatment: Effective antiviral therapy reduces the severity of PCT symptoms. However, its impact on the incidence and clinical course of lichen planus has not been demonstrated. Necrolytic acral erythema, a rare skin condition associated with HCV and clinically resembling psoriasis, may recur even after successful antiviral treatment. The association between other dermatological diseases and chronic HCV infection remains unclear.[6,8–12,17]

Endocrine diseases

Type 2 diabetes and insulin resistance occur in up to 15% of HCV-infected individuals and are more than 1.5 times more common than in uninfected populations. HCV is an independent risk factor, conferring a 70% higher likelihood of developing insulin resistance and type 2 diabetes. Impaired glucose metabolism, in turn, accelerates the progression of liver cirrhosis, increases the risk of hepatocellular carcinoma, and contributes to cardiovascular complications. Antiviral therapy with DAAs reduces the incidence of insulin resistance and type 2 diabetes, while in patients with pre-existing diabetes, it improves glycemic control. Achieving sustained virological response (SVR) lowers the risk of vascular complications, including end-stage renal disease (by 84%), ischemic stroke (by 47%), and acute coronary syndromes (by 36%).

Thyroid disorders, most commonly autoimmune conditions such as Hashimoto's thyroiditis and Graves' disease, constitute the 2nd major group of endocrine diseases associated with HCV infection. They occur in 2–13% of HCV-infected individuals, most frequently presenting as hypothyroidism. An increased risk of papillary thyroid carcinoma has also been reported in this population.

Treatment: Antiviral therapy with DAAs is considered the standard approach for all forms of HCV-associated thyroid disease.[6,10,12]

Kidney diseases

Compared with uninfected individuals, those with HCV infection have an approx. 26% higher risk of developing and progressing kidney disease. The clinical spectrum is diverse – about 10% of HCV-infected individuals eventually develop renal manifestations, most commonly membranoproliferative glomerulonephritis (MPGN) and, less frequently, nephrotic syndrome. Membranoproliferative glomerulonephritis is typically associated with mixed cryoglobulinemia.

Treatment: The first-line therapy is antiviral treatment with DAAs. Effective antiviral therapy reduces proteinuria, although it usually does not result in complete resolution of kidney disease. In cases with rapidly progressive renal deterioration, immunosuppressive therapy remains the primary treatment approach.[6,9,12]

Arthritis, myalgias, sicca symptoms

The prevalence of musculoskeletal symptoms (myalgia and arthralgia) and sicca syndrome among individuals infected with HCV is more than twice as high as in uninfected individuals. Joint pain occurs in 6–20% of patients, while arthritis is observed in a significantly smaller percentage of HCV-infected individuals (about 4–5%). In patients with circulating cryoglobulins, joint pain is more frequently observed, affecting even 40–80% of those infected with HCV. Arthritis is usually polyarticular, symmetrical, and involves the joints of the hands, knees, ankles, and spine. Clinically, it often resembles rheumatoid arthritis, but without accompanying joint surface erosion and deformities. The detection of rheumatoid factor may lead to misdiagnosis of rheumatoid arthritis, as it is also present in 40% of HCV-infected individuals. Approximately 10–30% of individuals infected with HCV experience symptoms related to dryness of the mouth, eyes, and genital organs. Significantly fewer, about 5%, have Sjögren's syndrome defined by the presence of specific antibodies (anti-SSA and anti-SSB) and histological changes.

Treatment involves the use of DAAs, regardless of immunosuppressive and biological therapy.[6,8,10]

Cardiovascular diseases

The risk of cardiovascular complications (ischemic heart disease, chronic heart failure, ischemic stroke, carotid artery atherosclerosis) in patients infected with HCV is approx. 20% higher than in the uninfected population, particularly in those with active HCV replication (HCV RNA positive). This also applies to patients with HIV/HCV co-infection, which presents a more complex issue. There are reports from Japan linking HCV infection with myocarditis and cardiomyopathy. The presence of HCV has also been demonstrated within atherosclerotic plaques. Undoubtedly, these relationships result from the influence of many not fully understood factors associated with chronic HCV infection, including endothelial dysfunction and low-grade systemic inflammation.

Treatment with DAAs significantly reduces the risk of developing cardiovascular diseases.[8,10–12]

Neuropsychiatric disorders

The HCV infection has been shown to be associated with more than a twofold increased risk of a range of neuropsychiatric disorders, including mood disorders, depression, cognitive dysfunction, sleep disturbances, and chronic fatigue syndrome. There is also evidence of HCV's involvement in demyelinating processes, functional and organic brain disorders, and even a connection with certain forms of encephalitis. Various forms of depression occur in 24.5% of individuals infected with HCV, while sleep disturbances and chronic fatigue affect as many as 60%. In our observations, these issues are seen in nearly all patients infected with HCV.

Treatment: DAAs should be considered as first-line treatment in milder cases and in the course of neurological diseases of vascular and demyelinating origin, particularly those associated with cryoglobulinemia. Achieving SVR is associated with the resolution of neuropsychiatric symptoms, mainly chronic fatigue symptoms, and allows for the discontinuation of antidepressant medications in some patients.[10,14–16]

Treatment summary: Extrahepatic manifestations of HCV infection

Elimination of the virus through pharmacotherapy with DAAs is crucial for patient outcomes in both liver disease and EHMs. In most, though not all, cases, achieving a sustained virological response (SVR) is associated with remission of EHM symptoms. When treatment is initiated at an advanced stage of HCV-related disease, however, clinical benefits are often limited, underscoring the importance of early diagnosis and therapy. In a large cohort of more than 25,000 individuals with HCV in British Columbia, Canada, DAA treatment significantly reduced EHM-related mortality risk by 78–84%.[18–23]

Conclusions

Chronic HCV infection is associated with a wide spectrum of clinical conditions beyond liver disease. Antiviral therapy with DAAs, irrespective of its effect on liver disease regression or progression, has a significant impact on the remission of selected EHMs. In addition, successful DAA therapy improves quality of life and positively affects overall wellbeing.[18–23]

Use of AI and AI-assisted technologies

Not applicable.

ORCID iDs

Krzysztof Simon https://orcid.org/0000-0002-8040-0412
Monika Pazgan-Simon https://orcid.org/0000-0002-0226-6836

References

1. World Health Organization (WHO). Fact Sheets: Hepatitis C. Geneva, Switzerland: World Health Organization (WHO); 2025. https://www.who.int/news-room/fact-sheets/detail/hepatitis-c. Accessed July 25, 2025.
2. Hwang SY, Danpanichkul P, Agopian V, et al. Hepatocellular carcinoma: Updates on epidemiology, surveillance, diagnosis and treatment. *Clin Mol Hepatol*. 2025;31(Suppl):S228–S254. doi:10.3350/cmh.2024.0824

3. Zakład Epidemiologii Chorób Zakaźnych i Nadzoru Narodowy Instytut Zdrowia Publicznego Państwowego Zakładu Higieny – Państwowy Instytut Badawczy (NIZP PZH-PIB), Departament Zapobiegania i Kontroli Chorób Zakaźnych Głównego Inspektoratu Sanitarnego (GIS). Zachorowania na wybrane choroby zakaźne w Polsce od 1 stycznia do 31 grudnia 2024 r. oraz w porównywalnym okresie 2023 r. Warsaw, Poland: National Institute of Public Health – National Institute of Hygiene; 2025. https://wwwold.pzh.gov.pl/oldpage/epimeld/2024/INF_24_12B.pdf. Accessed July 25, 2025.
4. Cui F, Blach S, Manzengo Mingiedi C, et al. Global reporting of progress towards elimination of hepatitis B and hepatitis C. *Lancet Gastroenterol Hepatol*. 2023;8(4):332–342. doi:10.1016/S2468-1253(22)00386-7
5. Kim NH. Extrahepatic Conditions Related to HCV Infection. Hepatitis C Online; 2024. https://www.hepatitisc.uw.edu/go/evaluation-staging-monitoring/extrahepatic-conditions/core-concept/all?%20Hepatitis%20C. Accessed July 25, 2025.
6. Chopra S, Flamm S. Extrahepatic manifestations of hepatitis C virus infection. Waltham, USA: UpToDate, Inc.; 2025. https://ff.uptodate.com/contents/extrahepatic-manifestations-of-hepatitis-c-virus-infection. Accessed August 7, 2025.
7. World Health Organization (WHO). *Global Hepatitis Report 2024: Action for Access in Low- and Middle-Income Countries*. Geneva, Switzerland: World Health Organization (WHO); 2024. ISBN:978-92-4-009167-2.
8. World Health Organization (WHO). Hepatitis B & C Burden, Gaps and Priorities Towards 2030 Elimination Targets. Geneva, Switzerland: World Health Organization (WHO); 2025. https://cdn.who.int/media/docs/default-source/hq-hiv-hepatitis-and-stis-library/2025-world-hepatitis-day-presentation-hep-b-and-c-burden--gaps-and-priorities.pdf. Accessed August 15, 2025.
9. Garg B, Arbabi A, Kirkland PA. Extrahepatic manifestations of chronic hepatitis C virus (HCV) infection. *Cureus*. 2024;16(3):e57343. doi:10.7759/cureus.57343
10. Songtanin B, Nugent K. Burden, outcome, and comorbidities of extrahepatic manifestations in hepatitis C virus infection. *Biology (Basel)*. 2022;12(1):23. doi:10.3390/biology12010023
11. Kuna L, Jakab J, Smolic R, Wu GY, Smolic M. HCV extrahepatic manifestations. *J Clin Transl Hepatol*. 2019;7(2):172–182. doi:10.14218/JCTH.2018.00049
12. Rincón-Choles H. Extrahepatic manifestations of chronic HCV infection. N Engl J Med. 2021;385(1):94–95. doi:10.1056/NEJMc2106143
13. Zińczuk A, Janocha-Litwin J, Rostkowska K, Simon K. Pozawątrobowe manifestacje zakażenia wirusem zapalenia wątroby typu C: epidemiologia, patofizjologia i leczenie. *Hepatologia*. 2018;18:28–36. doi:10.5114/hepatologia.2018.75977
14. Moretti R, Giuffrè M, Merli N, et al. Hepatitis C virus-related central and peripheral nervous system disorders. *Brain Sci*. 2021;11(12):1569. doi:10.3390/brainsci11121569
15. Mathew S, Faheem M, Ibrahim SM, et al. Hepatitis C virus and neurological damage. *World J Hepatol*. 2016;8(12):545. doi:10.4254/wjh.v8.i12.545
16. Alsop D, Younossi Z, Stepanova M, Afdhal NH. Cerebral MR spectroscopy and patient-reported mental health outcomes in hepatitis C genotype 1 naive patients treated with ledipasvir and sofosbuvir (abstr 48). *Hepatology*. 2014;60:221A. https://journals.lww.com/hep/citation/2014/10001/cerebral_mr_spectroscopy_and_patient_reported.48.aspx.
17. Walczak-Koszela I, Sysa-Jędrzejowska A, Woźniacka A. Dermatozy współistniejące z wirusowymi chorobami wątroby. *Postepy Hig Med Dosw (Online)*. 2015;69:1325–1330. https://ws.studylibpl.com/doc/835535/dermatozy-wsp%C3%B3%C5%82istniej%C4%85ce-z-wirusowymi-chorobami-w%C4%85troby-...
18. Zignego AL, Ramos-Casals M, Ferri C, et al. International therapeutic guidelines for patients with HCV-related extrahepatic disorders: A multidisciplinary expert statement. *Autoimmun Rev*. 2017;16(5):523–541. doi:10.1016/j.autrev.2017.03.004
19. Mazzaro C, Quartuccio L, Adinolfi LE, et al. A review on extrahepatic manifestations of chronic hepatitis C virus infection and the impact of direct-acting antiviral therapy. *Viruses*. 2021;13(11):2249. doi:10.3390/v13112249
20. Pawlotsky JM, Negro F, Aghemo A, et al. EASL recommendations on treatment of hepatitis C: Final update of the series. *J Hepatol*. 2020;73(5):1170–1218. doi:10.1016/j.jhep.2020.08.018
21. Tomasiewicz K, Flisiak R, Jaroszewicz J, et al. Recommendations of the Polish Group of Experts for HCV for the treatment of hepatitis C in 2023. *Clin Exp Hepatol*. 2023;9(1):1–8. doi:10.5114/ceh.2023.125957
22. Reau N, Vekeman F, Wu E, Bao Y, Gonzalez YS. Prevalence and economic burden of extrahepatic manifestations of hepatitis C virus are underestimated but can be improved with therapy. *Hepatol Commun*. 2017;1(5):439–452. doi:10.1002/hep4.1049
23. Jeong D, Luster D. Extrahepatic manifestations: Impacts of hepatitis C beyond the liver. CatieBlog. 2024. https://blog.catie.ca/2024/04/22/extrahepatic-manifestations-impacts-of-hepatitis-c-beyond-the-liver. Accessed July 25, 2025.

Neurobiological effects of childhood maltreatment: Health consequences, recovery pathways and clinical implications for holistic care

Yuko Hakamata[1,2,D–F], Hiroaki Hori[2,E,F]

[1] Department of Clinical and Cognitive Neuroscience, Toyama University School of Medicine, Japan
[2] Department of Behavioral Medicine, National Institute of Mental Health, National Center of Neurology and Psychiatry (NCNP), Tokyo, Japan

A – research concept and design; B – collection and/or assembly of data; C – data analysis and interpretation;
D – writing the article; E – critical revision of the article; F – final approval of the article

Advances in Clinical and Experimental Medicine, ISSN 1899–5276 (print), ISSN 2451–2680 (online) *Adv Clin Exp Med*. 2025;34(11):1803–1806

Address for correspondence
Yuko Hakamata
E-mail: hakamata@med.u-toyama.ac.jp

Funding sources
None declared

Conflict of interest
None declared

Received on July 22, 2025
Reviewed on September 1, 2025
Accepted on October 15, 2025

Published online on October 29, 2025

Abstract

Adverse childhood experiences (ACEs), such as childhood abuse and neglect, have a profound impact on our bodies, affecting the brain, autonomic nervous system, endocrine system, immune and inflammatory systems, as well as genetic expressions. Childhood maltreatment can leave long-lasting neurobiological scars, significantly increasing the risk of developing both physical and mental disorders, including depression and posttraumatic stress disorder (PTSD). The ICD-11, an international disease classification system, has recently introduced new diagnostic criteria for what is known as complex PTSD. In this context, we will briefly overview the neurobiological effects of ACEs, the associated health conditions they can lead to, and potential pathways to recovery. These pathways include promoting the reinstatement of emotional and interpersonal skills that may have been impaired during early development. Approaching ACEs from a holistic perspective may open new avenues for more effective clinical practices for individuals suffering both physically and mentally.

Key words: childhood trauma, childhood adverse experiences (ACEs), posttraumatic stress disorder (PTSD), complex PTSD, evidence-based psychotherapy

Cite as
Hakamata Y, Hori H. Neurobiological effects of childhood maltreatment: Health consequences, recovery pathways and clinical implications for holistic care. *Adv Clin Exp Med*. 2025;34(11):1803–1806. doi:10.17219/acem/212649

DOI
10.17219/acem/212649

Highlights

- Childhood maltreatment has profound and wide-ranging effects on long-term physical and mental health.
- Early-life trauma can cause persistent alterations in the brain, autonomic nervous system, endocrine, and immune pathways.
- Exposure to childhood abuse increases the risk of developing chronic physical illnesses and psychiatric disorders.
- Complex PTSD (CPTSD) is strongly linked to childhood maltreatment and involves disturbances in emotional regulation, self-concept, and relationships.
- Treatment for CPTSD emphasizes rebuilding emotional regulation and interpersonal skills as well as restoring functional self-organization.

Introduction

Medicine is the science and practice of diagnosing, treating, managing, and preventing diseases, injuries, and related health conditions in humans. Clinicians recognize the importance of viewing diseases and health problems from a holistic, biopsychosocial framework. For example, the cause of a liver disease can be attributed to habitual excessive alcohol intake. In that case, we need to consider and address the maladaptive alcohol intake in treating the disease itself. External stressors (e.g., pathogens, allergens and harmful substance exposure) have, of course, detrimental effects on the body, but scientists have revealed that psychological stressors, such as trauma, also significantly affect our physical conditions – the brain, autonomic nervous system, endocrine system, immune/inflammatory system, and gene expressions.

Unfortunately, in psychiatry, there is no established objective marker to determine the presence of mental illnesses. Stressful life events and dysfunctional family environments often precede the development of psychiatric diseases; however, it is challenging to clarify the causal relationship between them. Thus, psychiatric diagnoses are primarily based on the information collected during a medical interview, including the types and duration of symptoms that the patient experiences. Among these conditions, posttraumatic stress disorder (PTSD) is unique in that its diagnostic criteria explicitly require exposure to a life-threatening event – a clearly defined environmental factor. Such traumatic events include combat experience, natural disaster, motor vehicle accident, and sexual assault.

Recently, the International Classification of Diseases, 11th Revision (ICD-11), introduced new diagnostic criteria for complex posttraumatic stress disorder (CPTSD). It is a disease strongly associated with long-term, repeated traumas, rather than a single trauma, which include adverse childhood experiences (ACEs), such as abuse and neglect from a principal caregiver. Notably, ACEs are one of the most serious social problems, affecting over 1/3 of the population in developed countries, as indicated by extensive epidemiological studies.[1] In addition, physically and sexually abused individuals are reported to have a 40% prevalence rate of CPTSD.[2] Its diagnostic criteria consist of the disturbance of self-organization (DSO), in addition to 3 PTSD criteria of trauma re-experience, avoidance and sense of threat. Disturbance of self-organization further has 3 types of symptoms: 1) affect dysregulation (e.g., sudden outbursts of anger and intense mood swings), 2) negative self-concept (e.g., feeling of self-worthlessness) and 3) disturbances in relationships (e.g., overdependence on or overavoidance from others). It can overlap with the symptoms of attachment disorders and borderline personality disorder.[3]

Here, we provide a brief overview of the neurobiological impacts of ACEs, the associated health conditions, and possible pathways to recovery, with a focus on CPTSD.

ACEs and neurobiological scars

Substantial evidence indicates that, irrespective of the presence or absence of psychiatric diagnosis, individuals with ACEs exhibit blunted cortisol responses to psychosocial stressors, and increased levels of inflammatory markers such as C-reactive protein (CRP). In addition, they show exaggerated amygdala responses to emotionally negative stimuli and possess decreased hippocampal grey matter volume (see Hakamata et al.[4] for a comprehensive review).

Although the mechanisms underlying these neurobiological alterations remain unclear, animal studies have reported elevated glucocorticoid and glutamate levels, as well as overactivation of N-methyl-D-aspartate (NMDA) receptors, in mice exposed to repetitive stressors during early development. Among them, NMDA receptor overstimulation is known to cause neuronal death, inhibit neurogenesis, and reduce dendritic branching in the hippocampus.[5] In contrast, decreased cortisol secretion is observed in adults who have experienced ACEs,[6] which initially seems to contradict the findings on excessive glucocorticoid secretion in animal studies. However, cortisol levels may have similarly increased in humans who

experienced ACEs at certain points in early life, potentially leading to disruptions in neuronal growth and generation in the hippocampus, as well as dysfunction of the hypothalamic–pituitary–adrenal (HPA) axis. Supporting this notion, a few longitudinal studies demonstrated the decline of cortisol levels over time in adolescents with ACEs,[7,8] while their CRP levels increased as time passed,[9] suggesting low-grade inflammation caused by blunted cortisol secretion. Furthermore, peripheral inflammatory markers can penetrate the blood–brain barrier when systemic inflammation persists,[10] exerting detrimental effects on the central nervous system through multiple pathways.[11]

Importantly, ACEs increase the risk of developing stress-related mental disorders such as PTSD and depression by approx. 4–5 times.[12,13] In addition, childhood maltreatment confers a 1.5-fold increased risk of lung disease, gastric ulcers, and arthritis. Sexual abuse increases the risk of heart diseases by about 4 times, and neglect increases the risk of autoimmune diseases by 4 times.[14]

The neurobiological alterations associated with ACEs can exist transdiagnostically and lead to the development or the increased risk of mental (and/or physical) diseases through complex interactions between various environmental and genetic factors. Future research should elucidate the neurobiological alterations and the pathways leading to each medical disease.

Recovery from ACEs

The diagnostic notion of CPTSD is relatively new, and systematic research on its effective treatment is still underway. However, according to a meta-analysis on previous randomized controlled trials for PTSD patients with at least 1 symptom among the DSO (i.e., CPTSD syndrome), cognitive behavioral therapy (CBT), exposure component alone (EA) and eye movement and desensitization reprocessing (EMDR), which are evidence-based psychological treatments for PTSD, improve interpersonal difficulties with moderate-to-large effect sizes.[15] Despite the lack of EMDR findings, CBT and EA also alleviate negative self-concept with moderate-to-large effect sizes. Nonetheless, the effectiveness of treatments for affect dysregulation remains unclear.

Recently, the Skills Training in Affective and Interpersonal Regulation (STAIR) Narrative Therapy,[16] developed for childhood trauma survivors, has attracted significant attention as a new, promising treatment for DSO in CPTSD. STAIR Narrative Therapy consists of 16 sessions, including skills training in affect regulation and interpersonal difficulties (i.e., STAIR), and repeated imaginal exposure to trauma with cognitive restructuring (i.e., Narrative Therapy). Narrative Therapy is similar to CBT and exposure therapy, which encourage patients to recall trauma memories vividly and repeatedly and thereby help them integrate fragmented memories into a part of their autobiographical memory in a less threatening manner through cognitive restructuring.[17] The key feature of this psychotherapy is that it includes the component of STAIR to develop and strengthen patients' skills to be aware of, accept and manage their feelings and emotions, and express them more adaptively. The STAIR is also similar to the emotion regulation group therapy,[18] whose effectiveness has been shown in patients with borderline personality disorder with significant problems in regulating their intense emotions.[19] STAIR focuses on the recovery and redevelopment of emotional and interpersonal skills impaired due to chronic childhood abuse, and has been demonstrated to effectively improve CPTSD symptoms, including DSO.[20,21]

A meta-analysis, although a preliminary quantitative synthesis, has found that evidence-based PTSD psychological treatments reduced the exaggerated amygdala activity towards negative stimuli, accompanying decreased activity in the insula and anterior cingulate cortex, in PTSD patients.[22] These findings suggest that individuals with ACEs can recover from the neurobiological scars they have sustained. Future research should elucidate the neurobiological mechanisms by which STAIR Narrative Therapy or other potential treatments can ameliorate DSO, addressing the difficulties stemming from ACEs.

Conclusions

Clinicians and scientists find essential to consider the effects of psychosocial stressors that significantly affect our mind and body – from the brain, autonomic nervous system, endocrine system, immune/inflammatory system, up to gene expressions – especially for individuals with ACEs associated with various mental and physical health problems towards better medical practice, holistic treatment, and support for them.

Use of AI and AI-assisted technologies

Not applicable.

ORCID iDs

Yuko Hakamata https://orcid.org/0000-0002-5717-8091
Hiroaki Hori https://orcid.org/0000-0002-4548-7110

References

1. Gilbert R, Widom CS, Browne K, Fergusson D, Webb E, Janson S. Burden and consequences of child maltreatment in high-income countries. *Lancet*. 2009;373(9657):68–81. doi:10.1016/S0140-6736(08)61706-7
2. Huynh PA, Kindred R, Perrins K, et al. Prevalence of complex post-traumatic stress disorder (CPTSD): A systematic review and meta-analysis. *Psychiatry Res*. 2025;351:116586. doi:10.1016/j.psychres.2025.116586
3. Ford JD, Courtois CA. Complex PTSD, affect dysregulation, and borderline personality disorder. *Bord Personal Disord Emot Dysregul*. 2014;1(1):9. doi:10.1186/2051-6673-1-9

4. Hakamata Y, Suzuki Y, Kobashikawa H, Hori H. Neurobiology of early life adversity: A systematic review of meta-analyses towards an integrative account of its neurobiological trajectories to mental disorders. *Front Neuroendocrinol*. 2022;65:100994. doi:10.1016/j.yfrne.2022.100994
5. Sandi C. Stress, cognitive impairment and cell adhesion molecules. *Nat Rev Neurosci*. 2004;5(12):917–930. doi:10.1038/nrn1555
6. Meewisse ML, Reitsma JB, De Vries GJ, Gersons BPR, Olff M. Cortisol and post-traumatic stress disorder in adults: Systematic review and meta-analysis. *Br J Psychiatry*. 2007;191(5):387–392. doi:10.1192/bjp.bp.106.024877
7. Hagan M, Coccia M, Rivera L, et al. Longitudinal hair cortisol in low-income young children: A useful biomarker of behavioral symptom change? *Psychoneuroendocrinology*. 2021;133:105389. doi:10.1016/j.psyneuen.2021.105389
8. Simsek S, Uysal C, Kaplan I, Yuksel T, Aktas H. BDNF and cortisol levels in children with or without post-traumatic stress disorder after sustaining sexual abuse. *Psychoneuroendocrinology*. 2015;56:45–51. doi:10.1016/j.psyneuen.2015.02.017
9. Slopen N, Kubzansky LD, McLaughlin KA, Koenen KC. Childhood adversity and inflammatory processes in youth: A prospective study. *Psychoneuroendocrinology*. 2013;38(2):188–200. doi:10.1016/j.psyneuen.2012.05.013
10. Galea I. The blood–brain barrier in systemic infection and inflammation. *Cell Mol Immunol*. 2021;18(11):2489–2501. doi:10.1038/s41423-021-00757-x
11. Dantzer R, O'Connor JC, Freund GG, Johnson RW, Kelley KW. From inflammation to sickness and depression: When the immune system subjugates the brain. *Nat Rev Neurosci*. 2008;9(1):46–56. doi:10.1038/nrn2297
12. Scott KM, Smith DR, Ellis PM. Prospectively ascertained child maltreatment and its association with DSM-IV mental disorders in young adults. *Arch Gen Psychiatry*. 2010;67(7):712. doi:10.1001/archgenpsychiatry.2010.71
13. Hughes K, Bellis MA, Hardcastle KA, et al. The effect of multiple adverse childhood experiences on health: A systematic review and meta-analysis. *Lancet Public Health*. 2017;2(8):e356–e366. doi:10.1016/S2468-2667(17)30118-4
14. Goodwin RD, Stein MB. Association between childhood trauma and physical disorders among adults in the United States. *Psychol Med*. 2004;34(3):509–520. doi:10.1017/S003329170300134X
15. Karatzias T, Murphy P, Cloitre M, et al. Psychological interventions for ICD-11 complex PTSD symptoms: Systematic review and meta-analysis. *Psychol Med*. 2019;49(11):1761–1775. doi:10.1017/S0033291719000436
16. Cloitre M, Koenen KC, Cohen LR, Han H. Skills training in affective and interpersonal regulation followed by exposure: A phase-based treatment for PTSD related to childhood abuse. *J Consult Clin Psychol*. 2002;70(5):1067–1074. doi:10.1037/0022-006X.70.5.1067
17. Lanius RA, Williamson PC, Densmore M, et al. The nature of traumatic memories: A 4-T fMRI functional connectivity analysis. *Am J Psychiatry*. 2004;161(1):36–44. doi:10.1176/appi.ajp.161.1.36
18. Gratz KL, Tull MT, Levy R. Randomized controlled trial and uncontrolled 9-month follow-up of an adjunctive emotion regulation group therapy for deliberate self-harm among women with borderline personality disorder. *Psychol Med*. 2014;44(10):2099–2112. doi:10.1017/S0033291713002134
19. Stoffers-Winterling JM, Storebø OJ, Kongerslev MT, et al. Psychotherapies for borderline personality disorder: A focused systematic review and meta-analysis. *Br J Psychiatry*. 2022;221(3):538–552. doi:10.1192/bjp.2021.204
20. Cloitre M, Stovall-McClough KC, Nooner K, et al. Treatment for PTSD related to childhood abuse: A randomized controlled trial. *Am J Psychiatry*. 2010;167(8):915–924. doi:10.1176/appi.ajp.2010.09081247
21. Niwa M, Kato T, Narita-Ohtaki R, et al. Skills training in affective and interpersonal regulation narrative therapy for women with ICD-11 complex PTSD related to childhood abuse in Japan: A pilot study. *Eur J Psychotraumatol*. 2022;13(1):2080933. doi:10.1080/20008198.2022.2080933
22. Aarts I, Thorsen AL, Vriend C, Planting C, Van Den Heuvel OA, Thomaes K. Effects of psychotherapy on brain activation during negative emotional processing in patients with posttraumatic stress disorder: A systematic review and meta-analysis. *Brain Imaging Behav*. 2023;18(2):444–455. doi:10.1007/s11682-023-00831-0

Blood biomarkers of Alzheimer's disease: Balancing clinical relevance with improved accessibility and sustainability

Timothy Daly[A,C–F]

Bioethics Program, Latin American University of Social Sciences (FLACSO) Argentina, Buenos Aires, Argentina

A – research concept and design; B – collection and/or assembly of data; C – data analysis and interpretation;
D – writing the article; E – critical revision of the article; F – final approval of the article

Advances in Clinical and Experimental Medicine, ISSN 1899–5276 (print), ISSN 2451–2680 (online) *Adv Clin Exp Med*. 2025;34(11):1807–1812

Address for correspondence
Timothy Daly
E-mail: tdaly@flacso.org.ar

Funding sources
None declared

Conflict of interest
None declared

Received on July 27, 2025
Accepted on August 2, 2025

Published online on November 5, 2025

Abstract

The U.S. Food and Drug Administration (FDA) recently approved a blood-based biomarker to confirm diagnosis of Alzheimer's disease (AD-BBMs). When used in conjunction with human expertise in the diagnosis of neurocognitive disorder due to Alzheimer's disease (AD), blood-based biomarkers could increase both the accessibility and sustainability of medical practice and research. Indeed, AD-BBMs are likely to be more cost-effective in the long term and conservative calculations performed here suggest that they would have an approx. 10-fold and 36-fold lower carbon footprint compared to cerebrospinal fluid (CSF) lumbar punctures and amyloid positron emission tomography (PET) scans, respectively. Their use will require a careful balance of trade-offs to maximize benefits and minimize harms for current patients, while ensuring the sustainable integration of these tools into healthcare systems so that diagnostic precision remains accessible to present and future generations in an aging global population amid anthropogenic climate change.

Key words: biomarkers, Alzheimer's disease, access, sustainability, climate change

Cite as
Daly T. Blood biomarkers of Alzheimer's disease: Balancing clinical relevance with improved accessibility and sustainability. *Adv Clin Exp Med*. 2025;34(11):1807–1812. doi:10.17219/acem/208917

DOI
10.17219/acem/208917

Highlights

- Alzheimer's disease blood-based biomarkers (AD-BBMs), when combined with clinical expertise, can improve accessibility of Alzheimer's disease diagnosis.
- Sustainability analysis indicates that AD-BBMs have a significantly lower carbon footprint – approx. 10 times less than CSF lumbar punctures and ~36 times less than amyloid PET scans.
- AD-BBMs may reduce healthcare costs and promote environmentally sustainable Alzheimer's research and clinical practice by lowering medical emissions and resource use.

Introduction: A newly-approved blood test to help in the diagnosis of Alzheimer's disease

According to the World Health Organization (WHO), in 2021, over 55 million people were living with dementia, a clinical syndrome of neurocognitive disorder defined by the coexistence of acquired cognitive impairment, associated with behavioral and psychological symptoms leading to functional impairment.[1]

Alzheimer's disease (AD), first described as a rare condition in the early 1900s, became widely recognized in the 1970s as the predominant cause of late-life dementia based on converging clinical and pathological evidence.[2] It is now estimated to account for approx. 40 million cases of dementia worldwide. Alzheimer's disease is a progressive neurodegenerative disorder characterized by the accumulation of amyloid-β and tau proteins in the brain, leading to progressive memory loss, cognitive and functional decline, and neuropsychiatric symptoms.

Historically, AD was defined and confirmed by post-mortem neuropathological examination in people who died with neurocognitive dementia. This neuropathological examination typically revealed the presence of senile plaques containing amyloid-beta outside neurons, and neurofibrillary degeneration containing tau protein inside neurons. For as long as in vivo biomarkers of amyloid and tau protein were not available, in vivo diagnosis of AD was probabilistic. However, since the late 2000s, in vivo biomarkers – positron emission tomography (PET) imaging and cerebrospinal fluid (CSF) lumbar punctures – have been used to confirm diagnosis of AD, mostly in high-income countries.[3] These biomarkers are also increasingly used to define, explain, and treat AD.[2] Some anti-amyloid antibodies with modest effects on the slowing of cognitive decline in AD have recently been approved in different health systems.[4]

Against this backdrop, on May 16th 2025, the U.S. Food and Drug Administration (FDA) approved the first blood test for in vitro diagnosis of AD via the FDA Breakthrough Device Designation mechanism:

The Lumipulse G pTau217/β-Amyloid 1-42 Plasma Ratio is for the early detection of amyloid plaques associated with Alzheimer's disease in adult patients, aged 55 years and older, exhibiting signs and symptoms of the disease … [in] a multi-center clinical study of 499 individual plasma samples from adults who were cognitively impaired … 91.7% of individuals with … Plasma Ratio positive results had the presence of amyloid plaques by PET scan or CSF test result, and 97.3 % of individuals with negative results had a negative amyloid PET scan or CSF test result. Less than 20% of the 499 patients tested received an indeterminate … Plasma Ratio result … the new blood test can reliably predict the presence or absence of amyloid pathology associated with Alzheimer's disease at the time of the test in patients who are cognitively impaired. The test is intended for patients presenting at a specialized care setting with signs and symptoms of cognitive decline. The results must be interpreted in conjunction with other patient clinical information.[5]

I will analyze this regulatory decision and argue that for the global community to capitalize on this significant moment in the history of AD, there will be an important trade-off to be made between clinical relevance in medical practice, increased accessibility to a diagnosis of AD and improved environmental sustainability of healthcare practices.

In clinical practice, blood tests in AD should only be used after evaluation by a physician

The regulatory approval of a drug, diagnostic test or medical device should be understood in the context of a whole health system.[6] The health system in the USA has a decades-long tradition of governance and oversight of medical decision-making. One of the founding distinctions of regulatory oversight in the USA is the analytic separation between medical research – contributing to generalizable knowledge, and clinical practice – using existing medical knowledge with the intention of improving lives.[7] As the FDA approval states, this AD blood test is "intended for patients presenting at a specialized care setting with signs and symptoms of cognitive decline … in diagnosing Alzheimer's disease".[5] In other words, this blood test has been approved for clinical use. While the primary focus here is on its application in diagnostic practice, its potential role in medical research

– particularly in efforts to make academic medicine more sustainable – will also be considered.

How, then, is AD diagnosed? Here, there is another important distinction to draw, this time with regards to the meaning of AD. The Alzheimer's Association in the USA, the largest patient association with significant global influence in research, policy and advocacy, has a specialist workgroup which defends a "continuum" concept based on the famous amyloid cascade hypothesis of AD.[2] According to this definition, AD starts with Aβ accumulation, which triggers downstream biomarkers of tau and neurodegeneration, and ultimately ending in dementia.[8] Importantly, these authors believe that AD should be understood in deterministic terms, with the arrival of dementia a matter of time in Aβ-positive individuals, even though the timescale between Aβ accumulation and cognitive decline remains unspecified and would happen after death due to other causes in many or even most people. However, the authors argue that "mortality from unrelated causes should not be a criterion used to define what is and what is not a disease".[8]

Global estimates suggest that over 400 million people are on the AD continuum,[9] that is, they are amyloid-positive and have AA-2024-defined biological AD (bAD), even though most of them will never develop dementia during their lifetime.[10] Hypothetically, these new blood tests could be used to diagnose bAD in more than 400 million people, with the aim of offering a significant proportion of them anti-Aβ antibody therapy to reduce the risk of future cognitive decline. We will argue in the following paragraphs that this would be a mistake because bAD does not meet the criterion of clinical relevance to current and future patients.

The authors of the AA-2024 diagnostic criteria themselves argue that "AD can be diagnosed in asymptomatic individuals, but we do not believe this should be done for clinical purposes at this time" (though the authors also state that this recommendation "would change in the future if disease-targeted therapies, currently being evaluated in trials, demonstrate benefit in preventing cognitive decline and are approved for clinical use in individuals with preclinical AD").[8] Therefore, to maximize the clinical relevance of blood tests in AD, a different definition of AD will have to be used. The International Working Group 2024 Clinical-Biological Construct of Alzheimer Disease (IWG-2024) is grounded in a probabilistic, rather than deterministic, relationship between amyloid accumulation and the clinical state of cognitive decline.[11] The IWG-2024 argues that symptoms of a neurocognitive disorder and AD biomarkers are both required to establish a diagnosis of AD.[11] The neurocognitive disorder is typically characterized by progressive amnesia, language impairment (aphasia), and behavioral dysregulation, although atypical forms also exist. For most people, accumulation of AD biomarkers alone is a state of risk for AD: Aβ+ individuals are at risk of AD, and according to IWG-2024, the term "preclinical AD" is reserved for people with genetic risk profiles that make dementia "in the near future" the exception rather than the rule for those people.[11]

Only the IWG definition of AD can ensure the clinical relevance of blood tests in clinical practice, i.e., their use only after expert evaluation.[12] A blood test on its own without knowing someone's cognitive status will not provide clinically meaningful information to those who need it,[13] and asymptomatic bAD could lead to psychosocial harms, including legal and financial consequences, and unnecessary treatment.[11] Primary care physicians should also be wary of direct-to-consumer promotion of these blood tests which may brush over the issue of clinical relevance in the name of access.[12] Commercial entities thus have an obligation to avoid overstating the clinical relevance of blood tests for asymptomatic people.[14]

Finally, it is vital that the diagnostic performance of blood tests is confirmed in diverse, global populations.[15] Inconclusive test results (up to 1 in 5) should motivate more sophisticated imaging technologies to enhance diagnostic accuracy. Now that we have established clinical relevance as a necessary safeguarding criterion for the use of blood tests in confirming diagnosis of AD, we can now explore the 2 potential benefits they offer to global health: improved accessibility to diagnostic confirmation and more sustainable healthcare actions.

Confirmation of AD diagnosis is currently high-tech, high-cost, and low-accessibility: Blood biomarkers could improve access to diagnostic confirmation

The FDA's language to describe their approval and the IWG definition of AD lead us to the following claims. Blood tests do not answer the question: Does this asymptomatic person have AD? They instead provide a (high-probability) answer to the question: Is this person's neurocognitive disorder due to AD? Thus, all that blood biomarkers can currently do is confirm or rule out a diagnosis of AD as part of a (simplified) 2-step clinical-biological process (Fig. 1) that is required to establish diagnosis of AD according to best practices.[16]

Both Step 1 and Step 2 suffer from low access both within countries (e.g., rural vs urban settings), including high-income countries,[17] and between countries. The majority of over 55 million cases of dementia worldwide are undiagnosed, though in richer countries, this trend is reducing.[18] Thus, investing in human expertise to establish cases of neurocognitive disorder is arguably the most important step that global medicine can take to improve access to diagnosis of AD and dementia worldwide, rather than overly focusing on technological development.[19] Blood-based biomarkers of AD cannot directly bolster this process due

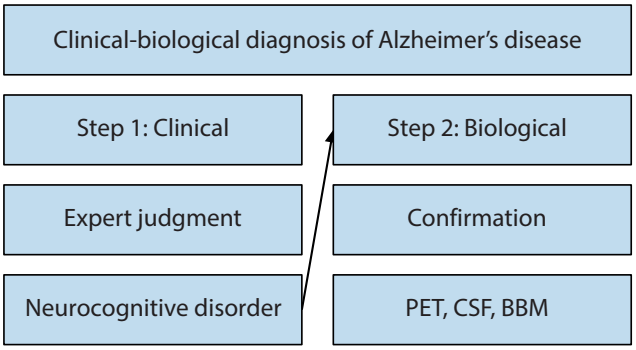

Fig. 1. Simplified 2-step process for diagnosing clinical-biological Alzheimer's disease (AD) following the approval of blood-based biomarkers. Step 1 involves establishing an AD phenotype, a complex process in itself, while Step 2 uses biomarkers to confirm the clinical-biological diagnosis of AD

to the need for robust health systems to perform the expert clinical work of Step 1 that requires years of trying in neuropsychological assessment.[15]

As for Step 2, prior to the approval of AD-BBMs, AD diagnosis has required detecting the presence of pathophysiologic biomarkers with high specificity for post-mortem neuropathology, including amyloid PET scans and CSF concentrations of amyloid and tau proteins via lumbar puncture or "spinal tap". Topographic biomarkers are also used to study the regional consequences of AD pathology, such as regional hypometabolism on fluorodeoxyglucose (FDG)-PET, tau PET, and atrophy on structural magnetic resonance imaging (MRI), which can be used to measure disease progression.[16]

Globally, Step 2 of the AD diagnostic process also suffers from low accessibility, because neither PET scanners nor CSF lumbar punctures are available in many countries. Even in high-income countries where specialist infrastructure exists, the average time from symptom onset to an established diagnosis is approx. 3.5 years.[20] Moreover, CSF punctures involve some degree of invasiveness and significant rates of patient refusal in global contexts, and there are important contraindications for use in AD.[21]

Furthermore, cost is an important factor. In the USA, PET scans cost at least 5,000 USD and are not reimbursed by medical insurance except when performed in research contexts.[22] Lumbar punctures cost approx. 1,000 USD and are more likely to be reimbursed; therefore, they are used more frequently in routine clinical practice. But for memory clinics, performing lumbar punctures is expensive due to the staff required for the long procedure.[23] While blood tests are thought to be marketed at 500–1,000 USD[24] competing tests are deliberately being designed to lower costs.[25] In the long term, it is likely that blood tests will remain the most cost-effective option, but more universal, equitable access will only be attained with insurance coverage.[26]

Thus, diagnostic confirmation of AD is currently high-tech, high-cost, low-accessibility. The overall low accessibility of AD diagnosis worldwide is a barrier to the right to healthcare, the founding mission of the WHO.[27] If – and only if – used in conjunction with human expertise to establish clinical-biological AD, access to BBM-ADs worldwide could be a boon for accessibility to timely diagnosis by reducing technological, financial and time barriers to achieve the goal of timely diagnosis of AD.[28]

In research and practice, blood tests for use in Alzheimer's disease could be a step towards more sustainable healthcare

Current healthcare practices take place within a period of human-exacerbated climate change. Climate change is arguably the greatest health threat facing humanity across the global population, and health impacts will follow and further exacerbate existing gradients of health inequalities facing people with neurological disorders, which are the most burdensome diseases worldwide, affecting around 3.4 billion people.[29,30] The effects of climate change exacerbate ill health across the spectrum of neurodevelopmental, neurological and neurodegenerative diseases.[31,32] There is an emerging brain-climate research program to study the vulnerability of the human brain to the effects of climate change.[33]

But health research and clinical practice themselves are a significant source of carbon emissions, due to wet laboratory and clinical research, diagnostics, therapeutics and anesthetics, and computational research.[34,35] It is now recognized that there is a major need for sustainable healthcare practices in neurology.[32] However, as mentioned in Section 1, healthcare systems involve both clinical practice (e.g., diagnostics) and research, the latter meaning the creation of generalizable knowledge about health and disease.[7] Thus, awareness of climate change should lead us to think of both research and clinical practice in the light of a "healthcare-harm" trade-off: Energy-intensive actions in both practice and research actually contribute to worsened emissions and climate change, and thus worsened (brain) health worldwide. Thus, AD-BBMs could be used to make this healthcare-harm trade-off more favorable by making diagnostic practices and research projects more environmentally sustainable.

Let us take the example of imaging and AD diagnosis and calculate approximate carbon footprints per patient. PET scanners used to confirm AD diagnosis have an annual energy consumption of approx. 10–11 4-person households, leading to the annual emission of approx. 15 tons of carbon dioxide (CO_2), and they cannot usefully be switched off due to the hours-long process of recalibration for routine use.[36] Excluding all of the costs of making a PET scanner as well as the indirect energy costs during the 2–3 h period of a patient being in the hospital (e.g., heating and lighting) for a PET scan, let us focus just on the amyloid PET scan itself,

which takes around 30 min. Assuming scanner availability for a 40-h working week in non-hospitalized (i.e., new) patients, approx. 80 patients could be scanned per week. Assuming some operational time costs due to preparing the scanner for different patients, let us say that a single PET scanner can be used to scan 70 patients per week, for 50 weeks of the year to allow for holidays, meaning 70 × 50 = 3,500 patients per year. Dividing the 15,000 kg of annual emissions by 3,500 patients leaves us with approx. 4.25 kg of CO_2 emissions per new patient scanned in a PET scanner. Conversely, a full blood test, leads to the emission of approx. 116 g of CO_2, accounting for all consumables, associated waste for blood draw, and electricity and water use for laboratory analyses.[37] A rough estimate indicates that a BBM-AD blood test produces approx. ×36 fewer CO_2 emissions than a PET scan (4,250/116).

How about the carbon footprint of lumbar punctures? Once more, we will not calculate indirect emissions due to a longer procedure. However, no specific calculations exist for the carbon footprint of lumbar punctures. Related data from anesthesia and surgical interventions provide a rough benchmark, as lumbar punctures require both anesthetic agents and consumables. The anesthetics themselves have a low median converted carbon footprint, e.g., of approx. 75 g,[38] whereas the footprint of the surgical consumables (i.e., a spinal anesthesia administration set) and the preparatory consumables (e.g., gowns) are closer to a kilogram.[39] Given the 116 g CO_2 footprint of a full blood draw, it can be reasonably stated that AD-BBMs generate approx. 10-fold lower CO_2 emissions compared with lumbar punctures.

These rough estimates suggest that AD-BBMs have an approx. 10-fold and 36-fold lower carbon footprint compared with CSF lumbar puncture and amyloid PET scanning, respectively. This means that they can increase resource stewardship[40] and make for more sustainable healthcare actions when used in line with best practice recommendations.

This could also include healthcare research, for instance, to replace PET in low-precision studies including exploratory longitudinal studies, pilot intervention studies, feasibility studies, and proof-of-concept studies. However, the scope of AD-BBMs is likely to be more limited to research and diagnostic practice, as they cannot achieve other goals of medical imaging, e.g., the use of precision MRI in monitoring the side effects of current and future treatments for AD. It is vital that the sustainability gains from the lower carbon footprint of blood tests do not lead to their misuse in diagnostic practice, which could lead to a loss of those gains in reduced emissions if they are used excessively.[37] There are many instances when blood-tests are overused,[40] and given the unmet needs of people with AD, there is the risk that these diagnostic aids contribute to overtesting, particularly if the warnings of the defenders of the clinical-biological definition of AD are not heeded.

Conclusions

A recent analysis found significant evidence gaps for AD-BBMs: Most research focuses on their technical capacity; many other papers tend to promote them in commentaries and reviews; a handful of papers have addressed their diagnostic accuracy, whereas hardly any have studied their impact on patients and society.[41] These gaps, alongside the revised biological criteria for AD proposed by the Alzheimer's Association in 2024, suggest the possibility of widespread, clinically irrelevant use of AD-BBMs. This bias should be corrected by refocusing research on findings that meet the criterion of relevance to current and future patients.

Nevertheless, if their relevance to global populations is confirmed, and if they are used wisely in conjunction with clinical expertise, AD-BBMs could be an accessible, sustainable front-line tool to increase the coverage of confirmation of timely AD diagnosis. Their use will require a logic of trade-offs to maximize gains and limit harms for current and future patients.

Use of AI and AI-assisted technologies

Not applicable.

ORCID iDs

Timothy Daly https://orcid.org/0000-0003-1650-242X

References

1. World Health Organization (WHO). Dementia. Geneva, Switzerland: World Health Organization (WHO); 2024. https://www.who.int/news-room/fact-sheets/detail/dementia. Accessed July 27, 2025.
2. Daly T. The meanings of Alzheimer's disease. *Phil Med*. 2025;6(1):251. doi:10.5195/pom.2025.251
3. Van Der Molen LH, Boenink M, Van Lente H, Richard E. Changing definitions of disease: Transformations in the diagnostic criteria for Alzheimer's disease. *Alzheimers Dement*. 2025;21(4):e70133. doi:10.1002/alz.70133
4. Daly T, Olluri A, Kurkinen M. Anti-amyloid treatments in Alzheimer's disease: Elegance, evidence and ethics. *Adv Clin Exp Med*. 2024;33(12):1303–1309. doi:10.17219/acem/198674
5. U.S. Food and Drug Administration (FDA). FDA Clears First Blood Test Used in Diagnosing Alzheimer's Disease. Silver Spring, USA: U.S. Food and Drug Administration (FDA); 2024. https://www.fda.gov/news-events/press-announcements/fda-clears-first-blood-test-used-diagnosing-alzheimers-disease. Accessed July 27, 2025.
6. World Health Organization (WHO). Health Systems Governance. Geneva, Switzerland: World Health Organization (WHO); 2024. https://www.who.int/health-topics/health-systems-governance. Accessed July 27, 2025.
7. Miracle VA. The Belmont Report: The triple crown of research ethics. *Dimens Crit Care Nurs*. 2016;35(4):223–228. doi:10.1097/DCC.0000000000000186
8. Jack CR, Andrews JS, Beach TG, et al. Revised criteria for diagnosis and staging of Alzheimer's disease: Alzheimer's Association Workgroup. *Alzheimers Dement*. 2024;20(8):5143–5169. doi:10.1002/alz.13859
9. Gustavsson A, Norton N, Fast T, et al. Global estimates on the number of persons across the Alzheimer's disease continuum. *Alzheimers Dement*. 2023;19(2):658–670. doi:10.1002/alz.12694
10. Brookmeyer R, Abdalla N. Estimation of lifetime risks of Alzheimer's disease dementia using biomarkers for preclinical disease. *Alzheimers Dement*. 2018;14(8):981–988. doi:10.1016/j.jalz.2018.03.005

11. Dubois B, Villain N, Schneider L, et al. Alzheimer disease as a clinical-biological construct: An International Working Group Recommendation. *JAMA Neurol*. 2024;81(12):1304. doi:10.1001/jamaneurol.2024.3770
12. Widera E, Covinsky K. The limited role of Alzheimer disease blood-based biomarkers in primary care. *JAMA Intern Med*. 2025;185(7):755. doi:10.1001/jamainternmed.2025.0976
13. Bouteloup V, Villain N, Vidal JS, et al. Cognitive phenotyping and interpretation of Alzheimer blood biomarkers. *JAMA Neurol*. 2025;82(5):506. doi:10.1001/jamaneurol.2025.0142
14. Ventola CL. Direct-to-consumer pharmaceutical advertising: Therapeutic or toxic? *P T*. 2011;36(10):669–684. PMID:22346300. PMCID: PMC3278148.
15. Mielke MM, Anderson M, Ashford JW, et al. Considerations for widespread implementation of blood-based biomarkers of Alzheimer's disease. *Alzheimers Dement*. 2024;20(11):8209–8215. doi:10.1002/alz.14150
16. Dubois B, von Arnim CAF, Burnie N, Bozeat S, Cummings J. Biomarkers in Alzheimer's disease: Role in early and differential diagnosis and recognition of atypical variants. *Alz Res Therapy*. 2023;15(1):175. doi:10.1186/s13195-023-01314-6
17. Giebel C, Cannon J, Komuravelli A, Whittington R. Challenges of dementia care in the UK. *BMJ*. 2025;389:r1135. doi:10.1136/bmj.r1135
18. Yu J, Wang P, Xie S, et al. Prevalence and progress of underdiagnosis of probable dementia: A repeated cross-sectional study in 19 European countries. *BMC Med*. 2025;23(1):395. doi:10.1186/s12916-025-04196-7
19. Sarfati M, Senequier A, Bihouix P, Marrauld L, Manet R. Preventing a global health care systems collapse through low-tech medicine. *J Glob Health*. 2024;14:03035. doi: 10.7189/jogh.14.03035.
20. Kusoro O, Roche M, Del-Pino-Casado R, Leung P, Orgeta V. Time to diagnosis in dementia: A systematic review with meta-analysis. *Int J Geriatr Psychiatry*. 2025;40(7):e70129. doi: 10.1002/gps.70129.
21. Wan Sulaiman WA, Muhamad Saliluddin S, Ong YJ, et al. A cross sectional study assessing the knowledge and attitudes towards lumbar puncture among the staff of a public university in Malaysia. *Clin Epidemiol Global Health*. 2018;6(1):29–33. doi:10.1016/j.cegh.2017.05.002
22. Schindler SE, Atri A. The role of cerebrospinal fluid and other biomarker modalities in the Alzheimer's disease diagnostic revolution. *Nat Aging*. 2023;3(5):460–462. doi:10.1038/s43587-023-00400-6
23. Bonomi S, Gupta MR, Schindler SE. Inadequate reimbursement for lumbar puncture is a potential barrier to accessing new Alzheimer's disease treatments. *Alzheimers Dement*. 2023;19(12):5849–5851. doi:10.1002/alz.13473
24. The Fisher Center for Alzheimer's Research Foundation. What to know about the new blood test for Alzheimer's. New York, USA: The Fisher Center for Alzheimer's Research Foundation; 2025. https://www.alzinfo.org/articles/diagnosis/what-to-know-about-the-new-blood-test-for-alzheimers. Accessed July 27, 2025.
25. Keck School of Medicine of USC. USC researchers develop low-cost blood test for early Alzheimer's detection. Los Angeles, USA: Keck School of Medicine of USC; 2025. https://keck.usc.edu/news/usc-researchers-develop-low-cost-blood-test-for-early-alzheimers-detection/. Accessed July 27, 2025.
26. Deverka PA, Lin GA, Phillips KA. Payer coverage considerations for Alzheimer disease blood-based biomarker tests. *JAMA*. 2024;332(22):1877. doi:10.1001/jama.2024.19084
27. Meier BM. Human rights in the World Health Organization: Views of the director-general candidates. *Health Hum Rights*. 2017;19(1):293–298.
28. Dhedhi SA, Swinglehurst D, Russell J. 'Timely' diagnosis of dementia: what does it mean? A narrative analysis of GPs' accounts. *BMJ Open*. 2014;4(3):e004439. doi:10.1136/bmjopen-2013-004439
29. Sheather J, Littler K, Singh JA, Wright K. Ethics, climate change and health: A landscape review. *Wellcome Open Res*. 2023;8:343. doi:10.12688/wellcomeopenres.19490.1
30. Steinmetz JD, Seeher KM, Schiess N, et al. Global, regional, and national burden of disorders affecting the nervous system, 1990–2021: A systematic analysis for the Global Burden of Disease Study 2021. *Lancet Neurol*. 2024;23(4):344–381. doi:10.1016/S1474-4422(24)00038-3
31. Nomura Y, Newcorn JH, Ginalis C, et al. Prenatal exposure to a natural disaster and early development of psychiatric disorders during the preschool years: Stress in pregnancy study. *Child Psychol Psychiatry*. 2023;64(7):1080–1091. doi:10.1111/jcpp.13698
32. Sisodiya SM, Gulcebi MI, Fortunato F, et al. Climate change and disorders of the nervous system. *Lancet Neurol*. 2024;23(6):636–648. doi:10.1016/S1474-4422(24)00087-5
33. Doell KC, Berman MG, Bratman GN, et al. Leveraging neuroscience for climate change research. *Nature Climate Change*. 2023;13(12):1288–1297. doi:10.1038/s41558-023-01857-4
34. Quann N, Burns S, Hull KL, et al. Reducing the carbon footprint of research: experience from the NightLife study. *BMJ Open*. 2023;13(4):e070200. doi:10.1136/bmjopen-2022-070200
35. Fiske A, Radhuber IM, Willem T, Buyx A, Celi LA, McLennan S. Climate change and health: The next challenge of ethical AI. *Lancet Global Health*. 2025;13(7):e1314–e1320. doi:10.1016/S2214-109X(25)00124-X
36. Merkle EM, Bamberg F, Vosshenrich J. The impact of modern imaging techniques on carbon footprints: Relevance and outlook. *Eur Urol Focus*. 2023;9(6):891–893. doi:10.1016/j.euf.2023.09.009
37. McAlister S, Barratt AL, Bell KJ, McGain F. The carbon footprint of pathology testing. *Med J Aust*. 2020;212(8):377–382. doi:10.5694/mja2.50583
38. Wang AY, Ahsan T, Kosarchuk JJ, Liu P, Riesenburger RI, Kryzanski J. Assessing the environmental carbon footprint of spinal versus general anesthesia in single-level transforaminal lumbar interbody fusions. *World Neurosurg*. 2022;163:e199–e206. doi:10.1016/j.wneu.2022.03.095
39. Kodumuri P, Joshi P, Malek I. Assessment of the carbon footprint of total hip arthroplasty and opportunities for emission reduction in a UK hospital setting. *Bone Joint Open*. 2024;5(9):742–748. doi:10.1302/2633-1462.59.BJO-2024-0027.R1
40. Spoyalo K, Lalande A, Rizan C, et al. Patient, hospital and environmental costs of unnecessary bloodwork: Capturing the triple bottom line of inappropriate care in general surgery patients. *BMJ Open Qual*. 2023;12(3):e002316. doi:10.1136/bmjoq-2023-002316
41. Van Gool WA, Siebrand JAF, Brayne C, Larson EB, Richard E. Evidence gap in blood biomarkers for Alzheimer's disease. *BMJ*. 2025;390:e084781. doi: 10.1136/bmj-2025-084781.

Immune reprogramming of cold tumors using TGF-β/PD-L1 bispecific antibody and armed oncolytic virus therapy

Yuchen Sun[B–D,F], Shengtao Hu[B–D,F], Ming Yi[A,D–F], Zhijun Dai[A,D–F]

Department of Breast Surgery, The First Affiliated Hospital, College of Medicine, Zhejiang University, Hangzhou, China

A – research concept and design; B – collection and/or assembly of data; C – data analysis and interpretation;
D – writing the article; E – critical revision of the article; F – final approval of the article

Advances in Clinical and Experimental Medicine, ISSN 1899–5276 (print), ISSN 2451–2680 (online) *Adv Clin Exp Med*. 2025;34(11):1813–1817

Address for correspondence
Ming Yi
E-mail: mingyi2022@zju.edu.cn

Funding sources
This work was supported by the National Natural Science Foundation of China (grant No. 82373281) and the Natural Science Foundation of Zhejiang Province (grant No. LQ24H160007).

Conflict of interest
None declared

Received on August 3, 2025
Reviewed on September 13, 2025
Accepted on September 17, 2025

Published online on November 13, 2025

Abstract

Immunotherapy has revolutionized oncology; however, its efficacy remains limited by the immunosuppressive tumor microenvironment (TME). This editorial synthesizes recent advances demonstrating how rationally designed combination strategies – particularly those incorporating the transforming growth factor beta/programmed death-ligand 1 (TGF-β/PD-L1) bispecific antibody platform (YM101/BiTP) and the multi-cytokine-armed oncolytic virus VG161 – can overcome resistance mechanisms. By concurrently dismantling immunosuppressive networks, activating innate immunity and remodeling the TME, these approaches show superior preclinical activity across challenging tumor phenotypes. The integration of mechanistic insights with evolving biomarker-driven strategies heralds a new era of personalized combination immunotherapy.

Key words: immunotherapy, tumor microenvironment, antibodies, bispecific, oncolytic virotherapy

Cite as
Sun Y, Hu S, Yi M, Dai Z. Immune reprogramming of cold tumors using TGF-β/PD-L1 bispecific antibody and armed oncolytic virus therapy. *Adv Clin Exp Med*. 2025;34(11):1813–1817. doi:10.17219/acem/210993

DOI
10.17219/acem/210993

Highlights

- TGF-β/PD-L1 bispecific antibody (YM101/BiTP) effectively reprograms the tumor microenvironment, overcomes immune exclusion and enhances antitumor immune activation, highlighting its potential for clinical translation in cancer immunotherapy.
- VG161, a multi-cytokine-armed oncolytic virus, exhibits synergistic effects by activating innate immunity and enhancing antitumor immune responses, providing a promising therapeutic strategy for immunologically "cold" tumors.

Introduction

The advent of immune checkpoint blockade (ICB) targeting the programmed cell death protein 1 (PD-1)/programmed death-ligand 1 (PD-L1) axis has marked a paradigm shift in cancer therapy.[1,2] While a subset of patients experience durable responses, the overall response rate remains limited.[3] This limitation is primarily due to the complex immunosuppressive mechanisms within the tumor microenvironment (TME).[4,5] The TME comprises a heterogeneous network of cellular and molecular components – including immunosuppressive factors such as tumor growth factor beta (TGF-β) and PD-L1, impaired antigen presentation, and physical or structural barriers that limit immune cell infiltration – that collectively hinder effective antitumor immune responses.

As a result, non-inflamed tumors – often classified as immune-excluded (T cells restricted to the stromal margin) or immune-desert (minimal T cell infiltration) – exhibit resistance to ICB monotherapy.[6,7] Overcoming this resistance requires combination strategies that not only relieve immunosuppression but also enhance immune activation.[8] Recent preclinical studies have highlighted 2 promising modalities: bispecific antibodies targeting complementary immunosuppressive pathways, and oncolytic viruses engineered to deliver immunostimulatory payloads.[9–11] This editorial focuses on how these approaches, particularly when combined, may reshape current strategies to overcome ICB resistance.

The immunosuppressive TME as the primary barrier

The TME functions as an immunosuppressive niche that actively inhibits antitumor immunity.[12–14] Among the key mediators, TGF-β and PD-L1 signaling pathways play central roles. Transforming growth factor beta suppresses the effector function of cytotoxic T lymphocytes (CTLs) and natural killer (NK) cells, promotes the differentiation of regulatory T cells (Tregs), induces cancer-associated fibroblast (CAF) activation, thereby generating desmoplastic stroma that limits T cell infiltration, and promotes the expansion of immunosuppressive myeloid populations.[15–18] Concurrently, PD-1/PD-L1 signaling impairs the function of activated T cells by inducing exhaustion, characterized by reduced cytokine production and proliferative capacity.[19,20] Therefore, the co-expression and spatial proximity of TGF-β and PD-L1 signaling contribute to a synergistic suppression of antitumor immunity.

In addition, defective innate immune activation – particularly the failure of immature dendritic cells (DCs) to present tumor antigens and prime T cells – underlies the immune-desert phenotype.[6] Myeloid-derived suppressor cells (MDSCs) and M2-like tumor-associated macrophages (TAMs) further exacerbate immunosuppression by producing arginase, indoleamine 2,3-dioxygenase (IDO) and interleukin 10 (IL-10).[21–25] This complex interplay between stromal, immune and tumor components results in T cell exclusion or dysfunction, thereby limiting the efficacy of ICB in the majority of patients.[26] A comprehensive understanding of these mechanisms is critical for designing rational and effective combination therapies.

Combination therapy: A mechanistic approach to overcome resistance

Given the redundancy and compensatory nature of immunosuppressive pathways within the TME, monotherapies targeting individual molecules are insufficient to restore antitumor immunity. Combination approaches that simultaneously modulate multiple aspects of the cancer-immunity cycle offer a more effective strategy.[8] Several therapeutic modalities have demonstrated potential in combination with ICB. Chemotherapy and radiotherapy promote immunogenic cell death, leading to antigen release and activation of DCs.[27–29] Anti-angiogenic agents normalize tumor vasculature, reduce hypoxia and facilitate immune cell infiltration.[30,31] Co-stimulatory receptor agonists (e.g., CD40, OX40, GITR) enhance T cell activation and expansion.[32] Agonists of the stimulator of interferon genes (STING) pathway

activate type I interferon responses in DCs, promoting cross-priming of CD8+ T cells.[33–36] Epigenetic modulators reverse exhaustion-associated transcriptional programs in T cells,[37] while metabolic regulators improve nutrient availability and reduce acidity in the TME, thus enhancing T cell viability and function.[38,39] In this context, bispecific antibodies that co-target non-redundant immunosuppressive pathways provide a spatially coordinated mechanism to inhibit immune evasion. These molecules offer dual blockade within the tumor site and may enhance efficacy while limiting systemic toxicity. [40] Ultimately, the effectiveness of combination regimens relies on mechanistic synergy – defined as the capacity to overcome multiple rate-limiting steps across antigen release, presentation, T cell priming, infiltration, and effector function.

VG161 oncolytic virus: Multi-mechanistic immune activation

Oncolytic viruses are a class of immunotherapeutic agents capable of inducing direct tumor cell lysis while stimulating innate and adaptive immunity.[41] VG161 is a genetically modified oncolytic herpes simplex virus type 1 (oHSV-1) that encodes 3 immunostimulatory transgenes: *IL-12*, a single-chain *IL-15/IL-15RA* fusion protein and a *PD-L1*-targeting peptide.[42] These payloads are designed to enhance local immune activation and counteract tumor-associated immunosuppression.

Upon intertumoral injection, VG161 selectively replicates in tumor cells, leading to immunogenic cell death and release of tumor-associated antigens (TAAs). This promotes the recruitment and activation of antigen-presenting cells, particularly DCs.[11] The locally expressed IL-12 facilitates DC maturation and promotes Th1-type immune responses. The IL-15/IL-15RA fusion protein supports the survival and expansion of NK cells and CD8+ T cells, while the PD-L1-targeting fusion protein blocks inhibitory signaling in the TME.[43–45]

Preclinical studies in breast cancer models have demonstrated that VG161 increases the infiltration of CD4+ and CD8+ T cells, as well as NK cells, while enhancing the production of pro-inflammatory cytokines such as tumor necrosis factor alpha (TNF-α) and interferon gamma (IFN-γ).[11] Notably, VG161 exhibits strong synergy with paclitaxel (PTX). In addition to its cytotoxic effects, PTX facilitates antigen release and alters the TME to support viral replication and immune cell infiltration.[46,47] Sequential administration of VG161 followed by PTX results in enhanced tumor growth suppression, reduced pulmonary metastasis and increased CD3+ and CD8+ T cell infiltration in metastatic sites. These effects are more pronounced with VG161 than with its parental virus VG160, underscoring the importance of its immunomodulatory transgenes.

Bispecific targeting of TGF-β and PD-L1: From YM101 to BiTP

To overcome the limited efficacy of PD-1/PD-L1 blockade in immunosuppressive microenvironment, especially in immune-excluded tumors, a bispecific antibody strategy targeting both TGF-β and PD-L1 has been developed. YM101, constructed using the Check-BODY™ platform, combines binding domains for TGF-β and PD-L1 in a single molecule.[10] Preclinical studies showed that YM101 effectively inhibited TGF-β–Smad and PD-L1–PD-1 signaling pathways, reversed epithelial–mesenchymal transition (EMT) and enhanced T cell activation in vitro. In murine tumor models, YM101 exhibited superior antitumor activity compared to monotherapy. This was accompanied by increased infiltration of CD8+ T cells and dendritic cells, a higher M1/M2 macrophage ratio, and enhanced cytokine production, collectively promoting a 'hot' tumor phenotype.

Building on these results, a humanized version of YM101 – termed BiTP – was developed to enable translational application.[9] BiTP retained high binding affinity and functional activity against both TGF-β and human PD-L1. In humanized TNBC models, BiTP exhibited enhanced antitumor efficacy over anti-PD-L1 or anti-TGF-β monotherapy. Mechanistically, BiTP reduced stromal collagen deposition, improved CD8+ T cell infiltration and increased tumor-infiltrating lymphocyte density. These changes contributed to immune reprogramming within the TME and reinforced antitumor immunity. Together, YM101 and BiTP exemplify a promising bispecific antibody approach that simultaneously alleviates immune exclusion and checkpoint-mediated suppression, offering a novel therapeutic strategy for immune-excluded tumors.

Future perspectives

Current limitations of immune checkpoint blockade highlight the essential role of the immunosuppressive TME in mediating therapeutic resistance. Accumulating preclinical evidence supports the need for combination strategies that concurrently target multiple immunosuppressive mechanisms within the TME. In our recent studies, we employed the TGF-β/PD-L1 bispecific antibody platform and the cytokine-armed oncolytic virus VG161 as complementary strategies to address TME-associated immune exclusion and desert-like features.

The therapeutic efficacy of these platforms is further enhanced when used in combination with agents targeting innate immune activation or adaptive resistance. For example, YM101 demonstrates improved antitumor activity when combined with STING agonists, which enhance antigen presentation and type I interferon responses within the TME.[36,48] In addition, resistance-associated features

such as *CCR5*$^{+}$ T cell enrichment – identified through single-cell RNA sequencing – may be targeted by agents such as Maraviroc to further optimize therapeutic response.[49] VG161 also exhibits synergy with chemotherapeutic agents such as paclitaxel, which not only induces direct cytotoxicity but also modulates suppressive myeloid cells, thereby amplifying systemic antitumor immunity and inhibiting metastatic dissemination.

To facilitate successful clinical translation, several key factors must be addressed. First, the development and validation of predictive biomarkers are critical for stratifying patients according to TME immunophenotypes (inflamed, excluded, desert) and dominant resistance mechanisms. This will enable rational selection of personalized combination regimens. Second, optimization of treatment sequencing and dosing is required to balance efficacy with toxicity. Third, ongoing exploration of novel combination strategies – including integration of bispecific antibodies or oncolytic viruses with metabolic modulators, epigenetic therapies, co-stimulatory receptor agonists, or adoptive cell therapies – holds considerable therapeutic potential.[50] Finally, advances in spatial and single-cell multi-omics technologies are expected to provide high-resolution insights into TME dynamics during treatment, facilitating the identification of emergent resistance pathways and novel therapeutic targets.[51]

Conclusions

The integration of multi-targeted agents such as YM101/BiTP and VG161, informed by mechanistic insights and supported by biomarker-driven patient selection, represents a rational and promising approach to overcoming the immunosuppressive TME. These strategies may substantially broaden the clinical benefit of immunotherapy across a wider range of tumor types and patient populations.

Use of AI and AI-assisted technologies

Not applicable.

ORCID iDs

Yuchen Sun https://orcid.org/0009-0004-8017-7507
Shengtao Hu https://orcid.org/0009-0006-5264-6315
Ming Yi https://orcid.org/0000-0001-5243-6613
Zhijun Dai https://orcid.org/0000-0001-5209-8626

References

1. Verma V, Sharma G, Singh A. Immunotherapy in extensive small cell lung cancer. *Exp Hematol Oncol*. 2019;8(1):5. doi:10.1186/s40164-019-0129-x
2. Reck M, Rodríguez-Abreu D, Robinson AG, et al. Pembrolizumab versus chemotherapy for PD-L1-positive non-small-cell lung cancer. *N Engl J Med*. 2016;375(19):1823–1833. doi:10.1056/NEJMoa1606774
3. Akinleye A, Rasool Z. Immune checkpoint inhibitors of PD-L1 as cancer therapeutics. *J Hematol Oncol*. 2019;12(1):92. doi:10.1186/s13045-019-0779-5
4. Liu F, Qin L, Liao Z, et al. Microenvironment characterization and multi-omics signatures related to prognosis and immunotherapy response of hepatocellular carcinoma. *Exp Hematol Oncol*. 2020;9(1):10. doi:10.1186/s40164-020-00165-3
5. Mariathasan S, Turley SJ, Nickles D, et al. TGFβ attenuates tumour response to PD-L1 blockade by contributing to exclusion of T cells. *Nature*. 2018;554(7693):544–548. doi:10.1038/nature25501
6. Hegde PS, Karanikas V, Evers S. The where, the when, and the how of immune monitoring for cancer immunotherapies in the era of checkpoint inhibition. *Clin Cancer Res*. 2016;22(8):1865–1874. doi:10.1158/1078-0432.CCR-15-1507
7. Hegde PS, Chen DS. Top 10 challenges in cancer immunotherapy. *Immunity*. 2020;52(1):17–35. doi:10.1016/j.immuni.2019.12.011
8. Smyth MJ, Ngiow SF, Ribas A, Teng MWL. Combination cancer immunotherapies tailored to the tumour microenvironment. *Nat Rev Clin Oncol*. 2016;13(3):143–158. doi:10.1038/nrclinonc.2015.209
9. Yi M, Wu Y, Niu M, et al. Anti-TGF-β/PD-L1 bispecific antibody promotes T cell infiltration and exhibits enhanced antitumor activity in triple-negative breast cancer. *J Immunother Cancer*. 2022;10(12):e005543. doi:10.1136/jitc-2022-005543
10. Yi M, Zhang J, Li A, et al. The construction, expression, and enhanced anti-tumor activity of YM101: A bispecific antibody simultaneously targeting TGF-β and PD-L1. *J Hematol Oncol*. 2021;14(1):27. doi:10.1186/s13045-021-01045-x
11. Deng X, Shen Y, Yi M, et al. Combination of novel oncolytic herpesvirus with paclitaxel as an efficient strategy for breast cancer therapy. *J Med Virol*. 2023;95(5):e28768. doi:10.1002/jmv.28768
12. Jia Q, Wang A, Yuan Y, Zhu B, Long H. Heterogeneity of the tumor immune microenvironment and its clinical relevance. *Exp Hematol Oncol*. 2022;11(1):24. doi:10.1186/s40164-022-00277-y
13. Muenst S, Läubli H, Soysal SD, Zippelius A, Tzankov A, Hoeller S. The immune system and cancer evasion strategies: Therapeutic concepts. *J Intern Med*. 2016;279(6):541–562. doi:10.1111/joim.12470
14. Yan Y, Huang L, Liu Y, et al. Metabolic profiles of regulatory T cells and their adaptations to the tumor microenvironment: Implications for antitumor immunity. *J Hematol Oncol*. 2022;15(1):104. doi:10.1186/s13045-022-01322-3
15. Park BV, Freeman ZT, Ghasemzadeh A, et al. TGFβ1-mediated SMAD3 enhances PD-1 expression on antigen-specific T cells in cancer. *Cancer Discov*. 2016;6(12):1366–1381. doi:10.1158/2159-8290.CD-15-1347
16. Thomas DA, Massagué J. TGF-β directly targets cytotoxic T cell functions during tumor evasion of immune surveillance. *Cancer Cell*. 2005;8(5):369–380. doi:10.1016/j.ccr.2005.10.012
17. Kanamori M, Nakatsukasa H, Okada M, Lu Q, Yoshimura A. Induced regulatory T cells: Their development, stability, and applications. *Trends Immunol*. 2016;37(11):803–811. doi:10.1016/j.it.2016.08.012
18. Peng D, Fu M, Wang M, Wei Y, Wei X. Targeting TGF-β signal transduction for fibrosis and cancer therapy. *Mol Cancer*. 2022;21(1):104. doi:10.1186/s12943-022-01569-x
19. Okazaki T, Honjo T. The PD-1–PD-L pathway in immunological tolerance. *Trends Immunol*. 2006;27(4):195–201. doi:10.1016/j.it.2006.02.001
20. Xu-Monette ZY, Zhang M, Li J, Young KH. PD-1/PD-L1 blockade: Have we found the key to unleash the antitumor immune response? *Front Immunol*. 2017;8:1597. doi:10.3389/fimmu.2017.01597
21. Xu Y, Zeng H, Jin K, et al. Immunosuppressive tumor-associated macrophages expressing interlukin-10 conferred poor prognosis and therapeutic vulnerability in patients with muscle-invasive bladder cancer. *J Immunother Cancer*. 2022;10(3):e003416. doi:10.1136/jitc-2021-003416
22. Wu Y, Yi M, Niu M, Mei Q, Wu K. Myeloid-derived suppressor cells: An emerging target for anticancer immunotherapy. *Mol Cancer*. 2022;21(1):184. doi:10.1186/s12943-022-01657-y
23. Dancsok AR, Gao D, Lee AF, et al. Tumor-associated macrophages and macrophage-related immune checkpoint expression in sarcomas. *Oncoimmunology*. 2020;9(1):1747340. doi:10.1080/2162402X.2020.1747340
24. Arlauckas SP, Garren SB, Garris CS, et al. Arg1 expression defines immunosuppressive subsets of tumor-associated macrophages. *Theranostics*. 2018;8(21):5842–5854. doi:10.7150/thno.26888

25. Holmgaard RB, Zamarin D, Li Y, et al. Tumor-expressed IDO recruits and activates MDSCs in a Treg-dependent manner. *Cell Rep*. 2015; 13(2):412–424. doi:10.1016/j.celrep.2015.08.077
26. Sun JY, Zhang D, Wu S, et al. Resistance to PD-1/PD-L1 blockade cancer immunotherapy: Mechanisms, predictive factors, and future perspectives. *Biomark Res*. 2020;8(1):35. doi:10.1186/s40364-020-00212-5
27. Hwang WL, Pike LRG, Royce TJ, Mahal BA, Loeffler JS. Safety of combining radiotherapy with immune-checkpoint inhibition. *Nat Rev Clin Oncol*. 2018;15(8):477–494. doi:10.1038/s41571-018-0046-7
28. Obeid M, Tesniere A, Ghiringhelli F, et al. Calreticulin exposure dictates the immunogenicity of cancer cell death. *Nat Med*. 2007;13(1):54–61. doi:10.1038/nm1523
29. Zhu H, Shan Y, Ge K, Lu J, Kong W, Jia C. Oxaliplatin induces immunogenic cell death in hepatocellular carcinoma cells and synergizes with immune checkpoint blockade therapy. *Cell Oncol*. 2020;43(6): 1203–1214. doi:10.1007/s13402-020-00552-2
30. Pan C, Liu H, Robins E, et al. Next-generation immuno-oncology agents: Current momentum shifts in cancer immunotherapy. *J Hematol Oncol*. 2020;13(1):29. doi:10.1186/s13045-020-00862-w
31. Viallard C, Larrivée B. Tumor angiogenesis and vascular normalization: Alternative therapeutic targets. *Angiogenesis*. 2017;20(4):409–426. doi:10.1007/s10456-017-9562-9
32. Pourakbari R, Hajizadeh F, Parhizkar F, Aghebati-Maleki A, Mansouri S, Aghebati-Maleki L. Co-stimulatory agonists: An insight into the immunotherapy of cancer. *EXCLI J*. 2021;20:1055–1085. doi:10.17179/EXCLI 2021-3522
33. Abe T, Barber GN. Cytosolic-DNA-mediated, STING-dependent proinflammatory gene induction necessitates canonical NF-κB activation through TBK1. *J Virol*. 2014;88(10):5328–5341. doi:10.1128/JVI.00037-14
34. Ablasser A, Goldeck M, Cavlar T, et al. cGAS produces a 2′-5′-linked cyclic dinucleotide second messenger that activates STING. *Nature*. 2013;498(7454):380–384. doi:10.1038/nature12306
35. Jiang M, Chen P, Wang L, et al. cGAS-STING, an important pathway in cancer immunotherapy. *J Hematol Oncol*. 2020;13(1):81. doi:10.1186/ s13045-020-00916-z
36. Yi M, Niu M, Wu Y, et al. Combination of oral STING agonist MSA-2 and anti-TGF-β/PD-L1 bispecific antibody YM101: A novel immune cocktail therapy for non-inflamed tumors. *J Hematol Oncol*. 2022;15(1):142. doi:10.1186/s13045-022-01363-8
37. Khan ANH, Magner WJ, Tomasi TB. An epigenetically altered tumor cell vaccine. *Cancer Immunol Immunother*. 2004;53(8):748–754. doi:10.1007/ s00262-004-0513-0
38. Leone RD, Emens LA. Targeting adenosine for cancer immunotherapy. *J Immunother Cancer*. 2018;6(1):57. doi:10.1186/s40425-018-0360-8
39. Borodovsky A, Barbon CM, Wang Y, et al. Small molecule AZD4635 inhibitor of A_{2A} R signaling rescues immune cell function including $CD103^{+}$ dendritic cells enhancing anti-tumor immunity. *J Immunother Cancer*. 2020;8(2):e000417. doi:10.1136/jitc-2019-000417
40. Yi M, Zheng X, Niu M, Zhu S, Ge H, Wu K. Combination strategies with PD-1/PD-L1 blockade: Current advances and future directions. *Mol Cancer*. 2022;21(1):28. doi:10.1186/s12943-021-01489-2
41. Kohlhapp FJ, Kaufman HL. Molecular pathways: Mechanism of action for talimogene laherparepvec, a new oncolytic virus immunotherapy. *Clin Cancer Res*. 2016;22(5):1048–1054. doi:10.1158/1078-0432.CCR-15-2667
42. Chouljenko DV, Ding J, Lee IF, et al. Induction of durable antitumor response by a novel oncolytic herpesvirus expressing multiple immunomodulatory transgenes. *Biomedicines*. 2020;8(11):484. doi:10.3390/ biomedicines8110484
43. Quetglas JI, Labiano S, Aznar MÁ, et al. Virotherapy with a Semliki forest virus-based vector encoding IL12 synergizes with PD-1/PD-L1 blockade. *Cancer Immun Res*. 2015;3(5):449–454. doi:10.1158/2326-6066.CIR-14-0216
44. Ge Y, Wang H, Ren J, et al. Oncolytic vaccinia virus delivering tethered IL-12 enhances antitumor effects with improved safety. *J Immunother Cancer*. 2020;8(1):e000710. doi:10.1136/jitc-2020-000710
45. Robinson TO, Schluns KS. The potential and promise of IL-15 in immuno-oncogenic therapies. *Immunol Lett*. 2017;190:159–168. doi:10.1016 /j.imlet.2017.08.010
46. Zhang B, Cheng P. Improving antitumor efficacy via combinatorial regimens of oncolytic virotherapy. *Mol Cancer*. 2020;19(1):158. doi:10.1186/s12943-020-01275-6
47. Jung KH, Choi IK, Lee HS, et al. Oncolytic adenovirus expressing relaxin (YDC002) enhances therapeutic efficacy of gemcitabine against pancreatic cancer. *Cancer Lett*. 2017;396:155–166. doi:10.1016/j.canlet.2017.03.009
48. Yi M, Niu M, Zhang J, et al. Combine and conquer: Manganese synergizing anti-TGF-β/PD-L1 bispecific antibody YM101 to overcome immunotherapy resistance in non-inflamed cancers. *J Hematol Oncol*. 2021;14(1):146. doi:10.1186/s13045-021-01155-6
49. Jiao X, Nawab O, Patel T, et al. Recent advances targeting CCR5 for cancer and its role in immuno-oncology. *Cancer Res*. 2019;79(19): 4801–4807. doi:10.1158/0008-5472.CAN-19-1167
50. Bahreyni A, Mohamud Y, Luo H. Oncolytic virus-based combination therapy in breast cancer. *Cancer Lett*. 2024;585:216634. doi:10.1016/j.canlet.2024.216634
51. Vandereyken K, Sifrim A, Thienpont B, Voet T. Methods and applications for single-cell and spatial multi-omics. *Nat Rev Genet*. 2023; 24(8):494–515. doi:10.1038/s41576-023-00580-2

A meta-analysis examining the impact of the continuous intervention for intraoperative pressure wound ulcers associated problems in women with breast cancer

Xiaoxia Zhang[B], Ruoling Mo[C], Yue Liu[D], Xiuying Guo[A]

Internal School of Nursing, Hainan Vocational University of Science and Technology, Haikou, China

A – research concept and design; B – collection and/or assembly of data; C – data analysis and interpretation;
D – writing the article; E – critical revision of the article; F – final approval of the article

Advances in Clinical and Experimental Medicine, ISSN 1899–5276 (print), ISSN 2451–2680 (online) *Adv Clin Exp Med*. 2025;34(11):1819–1826

Address for correspondence
Xiuying Guo
E-mail: Xiuying.Guo11@outlook.com

Funding sources
None declared

Conflict of interest
None declared

Received on September 5, 2024
Reviewed on November 10, 2024
Accepted on December 12, 2024

Published online on April 29, 2025

Abstract

Background. Even though ongoing intervention is essential, several uncertainties remain about the management of intraoperative pressure wound ulcers in breast cancer patients.

Objectives. To evaluate the impact of the ongoing intervention for intraoperative pressure wound ulcer problems related with female breast cancer patients, a meta-analysis study was conducted.

Materials and methods. Up until June 2024, comprehensive literature study was completed and 2,720 related studies were found. At the beginning point, 9 studies that were chosen included 1,467 women with breast cancer. Using dichotomous or continuous techniques and a random model, the odds ratio (OR) and mean difference (MD) and 95% confidence intervals (95% CIs) were used to evaluate the impact of continuous intervention for intraoperative pressure wound ulcers-associated difficulties in women with breast cancer.

Results. In comparison to the control group of female breast cancer patients, continuous intervention resulted in significantly better quality of life (QoL) (MD = 8.07; 95% CI: 4.84–11.29, $p < 0.001$), fewer intraoperative pressure wound ulcers (OR = 0.18; 95% CI: 0.13–0.24, $p < 0.001$) and higher Braden risk score (OR = 2.11; 95% CI: 1.91–2.31, $p < 0.001$).

Conclusions. In comparison to the control group, women with breast cancer undergoing continuous intervention experienced a significantly better QoL fewer intraoperative pressure wound ulcers, and had a higher Braden risk score. However, because there were not many studies chosen for comparison in the meta-analysis, reader's discretion is advised regarding its results.

Key words: breast cancer, continuous intervention, Braden risk score, intraoperative pressure wound ulcer

Cite as
Zhang X, Mo R, Liu Y, Guo X. A meta-analysis examining the impact of the continuous intervention for intraoperative pressure wound ulcers associated problems in women with breast cancer. *Adv Clin Exp Med*. 2025;34(11):1819–1826. doi:10.17219/acem/197323

DOI
10.17219/acem/197323

Highlights

- A meta-analysis study was done to find out how the current intervention is affecting problems with pressure wound ulcers during surgery in women with breast cancer.
- Compared to the control group, women with breast cancer receiving ongoing intervention had a much higher Braden risk score, a much better quality of life and fewer pressure wound ulcers during surgery.
- However, because there weren't many studies chosen for comparison in the meta-analysis, its results should be used with care.

Background

In China, approx. 500,000 new tumor cases and 300,000 cancer-related deaths were recorded in 2024, accounting for around 30% of global tumor incidence and mortality rates, respectively.[1] Malignant tumors are extremely common and have a high death rate, making them a serious threat to human health and life. In 2018, about 2 million new cases and 1.5 million deaths globally made breast cancer the most prevalent malignant tumor.[2] The symptoms experienced by patients with breast cancer are intricate and varied.[3] In therapeutic practice, pressure ulcers are commonly shown as a shared clinical outcome.[4] Pressure wound ulcers affect millions people in the USA, the Netherlands, Germany, and Australia.[5] In China, the prevalence of pressure ulcers among the population ranges between 1.14% and 1.78%.[6] In addition to experiencing increased pain, patients with pressure ulcers may also suffer from feelings of depression, anxiety and loneliness. Longer hospital stays result in increased financial hardship on society and families as a result of rising hospitalization costs and social resource waste. As a result, this impacts the diagnosis and progression of the primary illness, potentially complicating treatment outcomes. Pressure wound ulcers are among the most costly medical conditions due to the high expenses associated with their management and treatment. Continuous intervention, based on a specialized technical framework, encompasses a range of activities guided by diagnosis and targeted intervention strategies. These interventions are chosen based on diagnostic characteristics, research findings, the potential for functional recovery in women, and the capabilities of both patients and healthcare providers. Young in a single-center randomized controlled trial (RCT) demonstrated that the experimental group had a significantly lower incidence of PRESSURE wound ulcer complications compared to the control group as a result of continuous care.[7] Nevertheless, this study showed that pressure ulcer complications in breast cancer patients after surgery were inevitable, depending on the length of bed rest and whether continuous care was provided.[8]

Caregivers must take appropriate preventive measures to reduce the risk of pressure wound ulcers and enhance the quality of life (QoL) for immobile patients. There is a positive correlation between the behavior of primary caregivers and the severity of pressure ulcers.[9] Pressure wound ulcers increase the strain on patients and caregivers. It is critical to consider and investigate strategies that improve patients' QoL while reducing the incidence of pressure wound ulcers in those with advanced breast cancer. The usefulness of continuous care for breast cancer patients who are having issues related to intraoperative pressure wound ulcers is a hotly debated topic. Therefore, to evaluate and resolve this issue, a comprehensive meta-analysis is necessary. Even though ongoing intervention is essential, several uncertainties remain about the management of intraoperative pressure wound ulcers in breast cancer patients.

Objectives

We investigated the efficacy of continuous management in preventing intraoperative pressure wound ulcers in women with breast cancer using the meta-analysis approach.

Methods

Eligibility criteria

To provide an overview, studies demonstrating how continuous intervention can mitigate issues related to intraoperative pressure wound ulcers in women with breast cancer were selected.[10]

Information sources

Figure 1 provides a comprehensive overview of the investigation. The literature was included in the study when the following inclusion criteria were met[11]:

1. The study was an RCT, observational, prospective, or retrospective study.
2. The individuals under investigation were women who had breast cancer.
3. The intervention was carried out continuously.

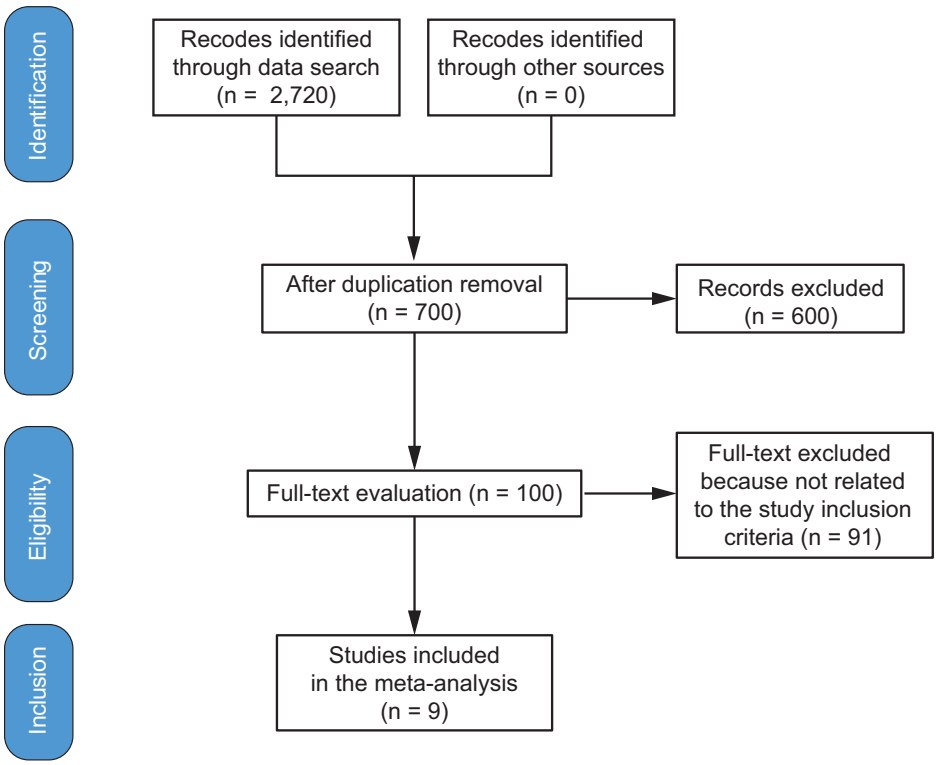

Fig. 1. A procedure flowchart for the research

4. The study evaluated the impact of ongoing intervention for issues related to intraoperative pressure wound ulcers in women with breast cancer.

Research on intraoperative pressure wound ulcers in women without continuous intervention, research on the characteristics of the effect of continuous intervention for problems associated with intraoperative pressure ulcers in breast cancer patients, and research that did not emphasize the significance of the comparison were all excluded.[12]

Search strategy

Based on the PICOS approach, a search protocol operation was identified. We classified it as follows: QoL, intraoperative pressure wound ulcers and Braden risk score were the "outcomes", continuous intervention was the "intervention" or "exposure," while the "comparison" was between continuous intervention and control. Finally, "research design" meant that the planned research had no boundaries.[13]

Until June 2024, we conducted a comprehensive search across the following databases: Google Scholar, Embase, Chinese Biomedical Literature Database, Cochrane Library, PubMed, and OVID. We did this by organizing keywords and adding more keywords related to breast cancer, intraoperative pressure wound ulcers, Braden risk score, and continuous intervention (Table 1).[14–16] To ensure that the investigation accurately established a link between the impact of continuous intervention on intraoperative pressure wound ulcers in female breast cancer patients, duplicate papers were removed and compiled into an EndNote file, and their titles and abstracts were reassessed.[17,18]

Table 1. Methods of searching for selected databases

Database	Search strategy
PubMed	#1 "breast cancer"[MeSH terms] OR "intraoperative pressure wound ulcers"[MeSH Terms] [All fields] #2 "Braden risk score"[MeSH terms] OR "continuous intervention"[MeSH terms] [All fields] #3 #1AND #2
Embase	#1 'breast cancer'/exp OR 'intraoperative pressure wound ulcers' #2 'Braden risk score'/exp OR ' continuous intervention' #3 #1AND #2
Cochrane Library	#1 (breast cancer) :ti,ab,kw (intraoperative pressure wound ulcers):ti,ab,kw (word variations have been searched) #2 (Braden risk score):ti,ab,kw OR (continuous intervention):ti,ab,kw (word variations have been searched) #3 #1AND #2

Selection process

The meta-analysis method was used to organize and assess the procedure that followed the epidemiological proclamation.

Data collection process

Some of the criteria used to collect data included the first author's name, research data, year of study, country or region, population type, medical and treatment characteristics, classification categories, quantitative and qualitative evaluation methods, data sources, outcome assessments, and statistical analysis.[19]

Data items

Main consequences of the inclusion parameter were analyzed. All studies were conducted on females; language of publication was neither an inclusion nor an exclusion criterion. There were no restrictions on the number of volunteers who could be found for the research. As letters, reviews and editorials are not appropriate for meta-analysis, these were not included in our study.[20,21]

Study risk of bias assessment

Two authors evaluated the selected papers' methods independently to assess the possibility of bias in each study. Procedural quality was assessed using the "risk of bias instrument" from the Cochrane Handbook for Systematic Reviews of Interventions, v. 5.1.0.22.[22] After each study was classified using the assessment criteria, they were categorized as having a medium bias risk if 1 or more quality requirements were not met, and as having a low bias risk if all requirements were met. The research was deemed to have a significant bias risk if multiple quality standards were either fully or partially satisfied.

Effect estimates

Sensitivity analysis was limited to studies that assessed and detailed the impact of continuous management for intraoperative pressure wound ulcer issues related with female breast cancer patients. The limited availability of demographic data, such as age and ethnicity, for comparison outcomes hindered the application of stratified models to examine the effects of specific factors.[23–25]

Statistical analyses

Using either dichotomous or continuous methods within a random-effects model, the odds ratio (OR) and mean difference (MD), along with their 95% confidence intervals (95% CIs), were calculated. The I^2 index was calculated using a range from 0% to 100%, where values of 0%, 25%, 50%, and 75% indicated no, low, moderate, and high heterogeneity, respectively.[26] The analysis used a p-value of less than 0.05 to define the statistical significance of differences among subgroups.[27]

Reporting bias assessment

We used the Egger's regression test and funnel plots, displaying the logarithm of the ORs against their standard errors (SEs), to quantitatively and qualitatively assess publication bias. A p-value of less than 0.05 indicated the presence of significant bias.[28]

Certainty assessment

Two-tailed testing was utilized to examine every p-value. Graphs and statistical analyses were produced using Reviewer Manager v. 5.3 (The Nordic Cochrane Centre, the Cochrane Collaboration, Copenhagen, Denmark).[29,30]

Results

Out of 2,720 relevant studies meeting the inclusion criteria, 9 articles published between 2015 and 2024 were selected for inclusion in this analysis.[31–39] Table 2 summarizes the findings of these studies. At the outset, the research included 1,467 women with breast cancer, of whom 702 received continuous intervention and 765 were assigned to the control group. The sample sizes across studies ranged from 68 to 260 women. Figures 2–4 illustrate that, compared to the control group, continuous intervention in women with breast cancer resulted in significantly improved QoL (MD = 8.07; 95% CI: 4.84–11.29, $p < 0.001$) with high heterogeneity ($I^2 = 97\%$), a significantly lower incidence of intraoperative pressure wound ulcers (OR = 0.18; 95% CI: 0.13–0.24, $p < 0.001$) with no heterogeneity ($I^2 = 0\%$), and a higher Braden risk score (OR = 2.11; 95% CI: 1.91–2.31, $p < 0.001$) with no heterogeneity ($I^2 = 0\%$). Using the quantitative Egger's regression test and visual interpretation of the funnel plots presented in Fig. 5–7, no evidence of publication bias was detected ($p = 0.90$). However, as illustrated in Fig. 8, while there was no bias in selective reporting, the majority of the included RCTs exhibited poor procedural quality.

Discussion

A total of 1,467 female breast cancer patients were included at the outset of the studies selected for the meta-analysis. Among them, 702 patients received continuous intervention, while 765 were in the control group.[31–39]

Table 2. Features of the chosen studies for the meta-analysis

Study	Country	Total	Continuous intervention	Control
Zeng and Yang, 2015[31]	China	68	35	33
Guan et al, 2015[32]	China	218	110	108
Hu et al, 2016[33]	China	260	130	130
Wang, 2017[34]	China	165	83	82
Cao et al., 2017[35]	China	130	65	65
Lilly et al., 2017[36]	China	200	100	100
Chen et al, 2017[37]	China	120	60	60
Liu et al. 2019[38]	China	106	53	53
Kong et al, 2024[39]	China	200	66	134
Total		1,467	702	765

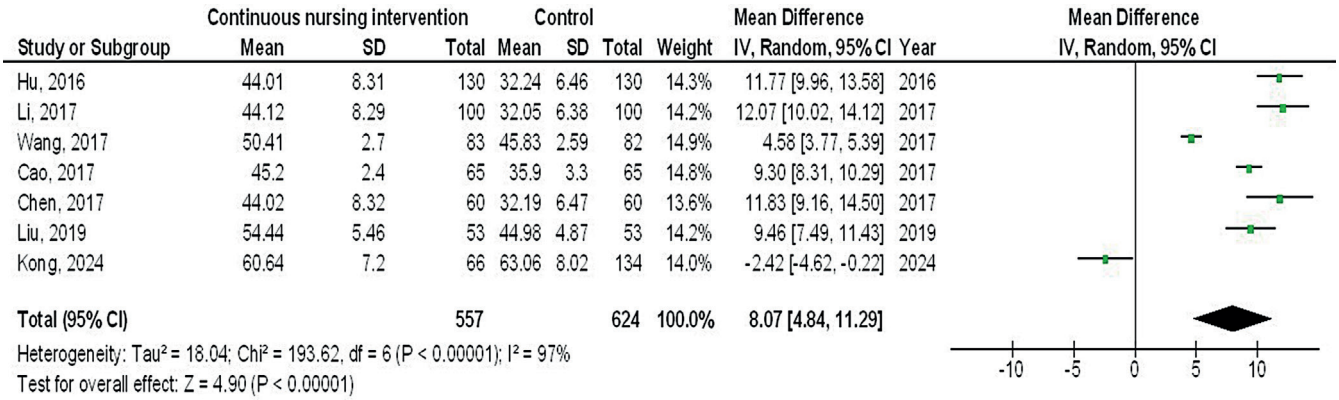

Fig. 2. The forest plot of the continuous intervention's impact on breast cancer patients' quality of life in comparison to the control group

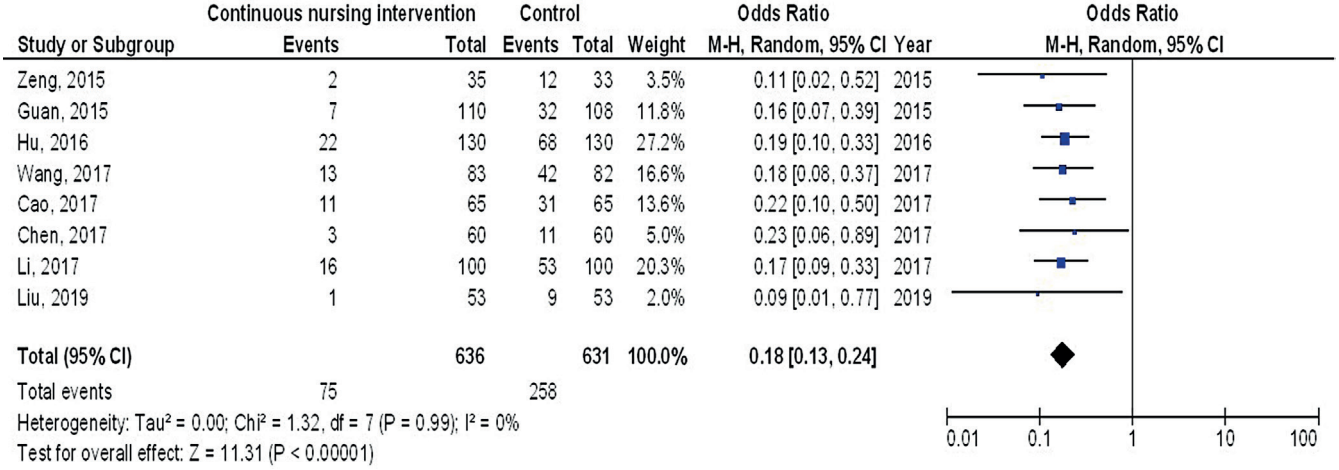

Fig. 3. The forest plot of the continuous intervention's impact on intraoperative pressure wound ulcers in breast cancer patients in comparison to the control group

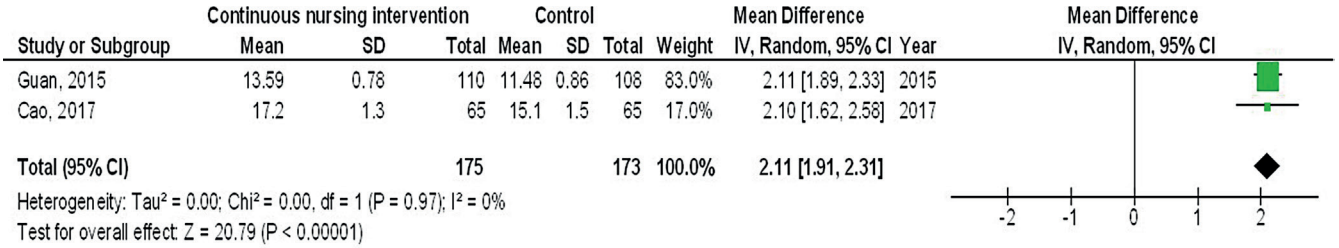

Fig. 4. The forest plot of the continuous intervention's impact on the Braden risk score for breast cancer in comparison to the control group

In comparison to the control group, female breast cancer patients undergoing continuous intervention experienced a significantly better QoL and fewer intraoperative pressure wound ulcers, and had a higher Braden risk score. However, due to the limited number of studies included in the meta-analysis for comparison, such as those utilizing the Braden risk score, caution must be exercised when interpreting the results, as this may affect the significance of the evaluated assessments.[40–50]

The overall death rate for breast cancer is the highest among all malignant tumors in women.[51] Because of the complex and varied symptoms that affect this population, pressure wound ulcers are significantly more common in women with breast cancer. Many anti-tumor medications can lead to hypoalbuminemia, acute malnutrition, increased cancer-related pain, and other adverse effects in patients.[40,41,44,45] These treatments also impact patients' nutritional metabolism, food intake, nutrient absorption barriers, tumor cell catabolism, and the biological activity of tumors. Inadequate prompt intervention might lead to the rapid formation of pressure wound ulcers.[52] The community healthcare system in China is still developing and has yet to reach an optimal level. Patients with advanced breast cancer are primarily cared for at home by their relatives, and the patient's QoL is directly affected by their understanding

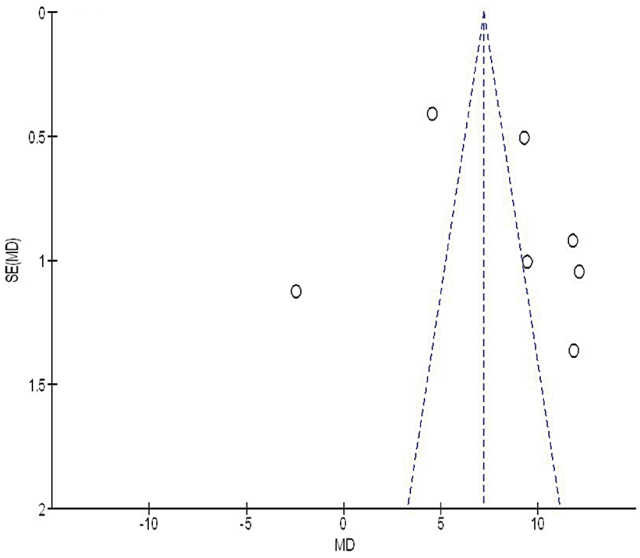

Fig. 5. The continuous intervention's funnel plot on breast cancer patients' quality of life in comparison to the control group

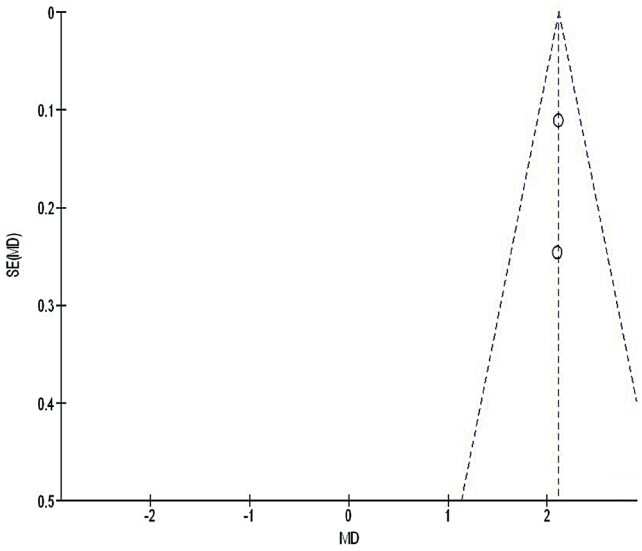

Fig. 7. The continuous intervention's funnel plot on the Braden risk score for breast cancer in comparison to the control group

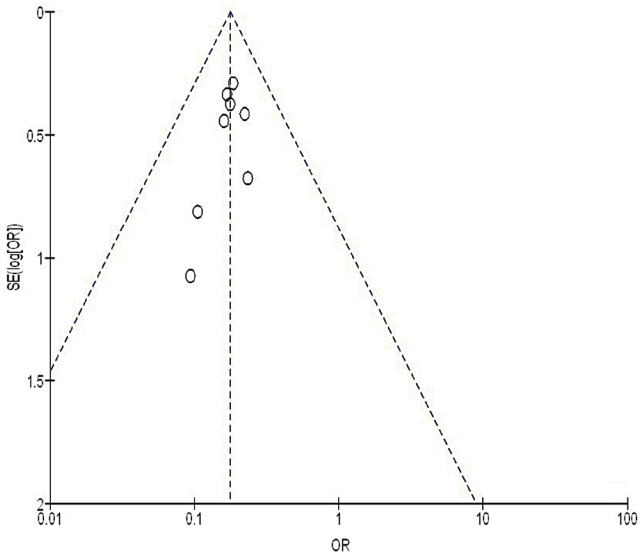

Fig. 6. The intraoperative pressure wound ulcer control vs ongoing intervention funnel plot for breast cancer

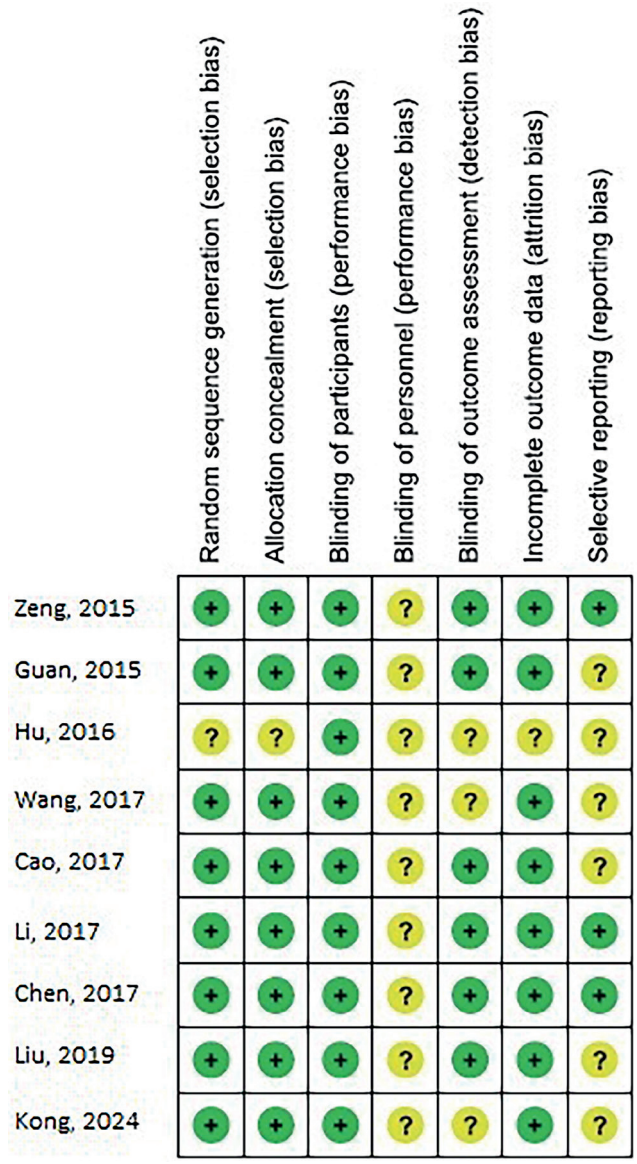

Fig. 8. Risk-of-bias plot

of pressure wound ulcers. The incidence of pressure ulcers is also strongly linked to life satisfaction.[53] As patients transition from the hospital back to their families or communities, aftercare includes hospital discharge planning, referrals, ongoing follow-up, and counseling. The integration of the telemedicine-specific model and telemedicine platform, which includes the use of web-based education programs, encouraging self-management patient applications, and the peer-based patient-driven platform of pressure wound ulcer continuity care model, are the main components of the care model continuity, as reported in various experiments.[54,55] Researchers from many places are progressively employing a multidisciplinary approach to pressure wound ulcer therapy.[42,46–50] The guidelines for treating pressure wound ulcers include

laser therapy as the lowest recommended grade of treatment. However, they also contribute to a broader understanding of the management of the disease.[56] Patients' firsthand experience with the coordination and continuation of medical treatments is what continuity of care is all about. They will be naturally encouraged by this, and it will help to promote their health.

Limitations

Assortment bias may have occurred. We also lacked the information needed to conclude whether certain characteristics, such as race and age, had an impact on outcomes. Bias may have been amplified due to the inclusion of incomplete or inaccurate data from previous studies. Factors such as age, race and nutritional status of the women were likely sources of bias. Additionally, incomplete data and unpublished research could have unintentionally led to skewed values.

Conclusions

In comparison to the control group, women with breast cancer undergoing continuous intervention experienced a significantly better QoL and fewer intraoperative pressure wound ulcers, and had a higher Braden risk score. However, due to the limited number of studies included in the meta-analysis for comparison, such as those utilizing the Braden risk score, caution must be exercised when interpreting the results. This limitation may affect the significance and reliability of the evaluated assessments.

Data availability

The datasets generated and/or analyzed during the current study are available from the corresponding author on reasonable request.

Consent for publication

Not applicable.

Use of AI and AI-assisted technologies

Not applicable.

ORCID iDs

Xiuying Guo https://orcid.org/0009-0002-7240-260X

References

1. Ebrahimbaygi P, Khazaei MR, Valadbeigi P, et al. Recent advances in scaffold based electrospun for breast cancer research. *Polym Adv Technol*. 2024;35(7):e6499. doi:10.1002/pat.6499
2. Xu X, Zhang M, Xu F, Jiang S. Wnt signaling in breast cancer: Biological mechanisms, challenges and opportunities. *Mol Cancer*. 2020; 19(1):165. doi:10.1186/s12943-020-01276-5
3. Liang Y, Zhang H, Song X, Yang Q. Metastatic heterogeneity of breast cancer: Molecular mechanism and potential therapeutic targets. *Semin Cancer Biol*. 2020;60:14–27. doi:10.1016/j.semcancer.2019.08.012
4. Li H, Liu ZY, Chen YC, Zhang XY, Wu N, Wang J. Identification and validation of an immune-related lncRNAs signature to predict the overall survival of ovarian cancer. *Front Oncol*. 2022;12:999654. doi:10.3389/fonc.2022.999654
5. Hahnel E, El Genedy M, Tomova-Simitchieva T, et al. The effectiveness of two silicone dressings for sacral and heel pressure ulcer prevention compared with no dressings in high-risk intensive care unit patients: A randomized controlled parallel-group trial. *Br J Dermatol*. 2020;183(2):256–264. doi:10.1111/bjd.18621
6. Du Y, Wu F, Lu S, et al. Efficacy of pressure ulcer prevention interventions in adult intensive care units: A protocol for a systematic review and network meta-analysis. *BMJ Open*. 2019;9(4):e026727. doi:10.1136/bmjopen-2018-026727
7. Young C. Using the 'aSSKINg' model in pressure ulcer prevention and care planning. *Nurs Stand*. 2021;36(2):61–66. doi:10.7748/ns.2021.e11674
8. Díaz-Valenzuela A, García-Fernández FP, Carmona Fernández PJ, Valle Cañete MJ, Pancorbo-Hidalgo PL. Effectiveness and safety of olive oil preparation for topical use in pressure ulcer prevention: Multicentre, controlled, randomised, and double-blinded clinical trial. *Int Wound J*. 2019;16(6):1314–1322. doi:10.1111/iwj.13191
9. Taylor C, Mulligan K, McGraw C. Barriers and enablers to the implementation of evidence-based practice in pressure ulcer prevention and management in an integrated community care setting: A qualitative study informed by the theoretical domains framework. *Health Soc Care Community*. 2021;29(3):766–779. doi:10.1111/hsc.13322
10. Stroup DF, Berlin JA, Morton SC, et al. Meta-analysis of observational studies in epidemiology: A proposal for reporting. *JAMA*. 2000; 283(15):2008–2012. doi:10.1001/jama.283.15.2008
11. Emad M, Osama H, Rabea H, Saeed H. Dual compared with triple antithrombotics treatment effect on ischemia and bleeding in atrial fibrillation following percutaneous coronary intervention: A meta-analysis. *Int J Clin Med Res*. 2023;1(2):77–87. doi:10.61466/ijcmr1020010
12. Zangeneh MM, Zangeneh A. Prevalence of wound infection following right anterolateral thoracotomy and median sternotomy for resection of benign atrial masses that induce heart failure, arrhythmia, or thromboembolic events: A meta-analysis. *Int J Clin Med Res*. 2023; 2(1):27–33. doi:10.61466/ijcmr2010004
13. Liberati A, Altman DG, Tetzlaff J, et al. The PRISMA Statement for Reporting Systematic Reviews and Meta-Analyses of studies that evaluate health care interventions: Explanation and elaboration. *PLoS Med*. 2009;6(7):e1000100. doi:10.1371/journal.pmed.1000100
14. Saeed H, Aldhalmi AK, AbdElrahman M, O. Elgendy M. A meta-analysis evaluating the effect of N95 respirators in healthcare and non-healthcare providers on laboratory-confirmed respiratory virus infection. *Al-Mustaqbal J Pharm Med Sci*. 2024;1(1):Article 1. doi:10.62846/3006-5909.1000
15. Saeed H, Al-Athari AJH, O. Elgendy M. Effect of Chinese herbal medicine as an adjunctive technique to standard treatment for people with diabetic foot ulcers: A meta-analysis. *Al-Mustaqbal J Pharm Med Sci*. 2024;1(1):Article 3. doi:10.62846/3006-5909.1002
16. Aldhalmi AK, AbdElrahman M, Adbelrahim EAM. Effect of external application of traditional herbal medicine on burn wound ulcers: A meta-analysis. *Al-Mustaqbal J Pharm Med Sci*. 2024;1(1):Article 2. doi:10.62846/3006-5909.1001
17. Osama H, Saeed H, Nicola M, Emad M. Neuraxial anesthesia compared to general anesthesia in subjects with hip fracture surgery: A meta-analysis. *Int J Clin Med Res*. 2023;1(2):66–76. doi:10.61466/ijcmr1020009
18. Sundaresan A. Wound complications frequency in minor technique gastrectomy compared to open gastrectomy for gastric cancer: A meta-analysis. *Int J Clin Med Res*. 2023;1(3):100–107. doi:10.61466/ijcmr1030012
19. Perazzo H, Castro R, Luz PM, et al. Effectiveness of generic direct-acting agents for the treatment of hepatitis C: Systematic review and meta-analysis. *Bull World Health Organ*. 2020;98(3):188–197K. doi:10.2471/BLT.19.231522
20. Singh RK. A meta-analysis of the impact on gastrectomy versus endoscopic submucosal dissection for early stomach cancer. *Int J Clin Med Res*. 2023;1(3):88–99. doi:10.61466/ijcmr1030011

21. Amin MA. A meta-analysis of the eosinophil counts in the small intestine and colon of children without obvious gastrointestinal disease. *Int J Clin Med Res*. 2023;1(1):1–8. doi:10.61466/ijcmr1010001
22. Higgins JPT, Thomas J, Chandler J, Cumpston M, Li T, Page MJ, Welch VA, eds. *Cochrane Handbook for Systematic Reviews of Interventions*. 2nd ed. Chichester, UK: Wiley & Sons; 2019. doi:10.1002/9781119536604
23. Giong Z, Lie N. A meta-analysis of the impact of a phosphate-specific diet on serum phosphate levels in people receiving hemodialysis. *Int J Clin Med Res*. 2024;2(4):135–142. doi:10.61466/ijcmr2040005
24. Jiany L, Xiu W. A meta-analysis evaluated the effectiveness of Chinese herbal medicine as a supplement to conventional care for patients with diabetic foot ulcers. *Int J Clin Med Res*. 2024;2(4):116–123. doi:10.61466/ijcmr2040003
25. Weang Z. A meta-analysis examining the impact of antibiotic prophylaxis on surgical site wound infection during third molar surgery. *Int J Clin Med Res*. 2024;2(4):127–134. doi:10.61466/ijcmr2040004
26. Sheikhbahaei S, Trahan TJ, Xiao J, et al. FDG-PET/CT and MRI for evaluation of pathologic response to neoadjuvant chemotherapy in patients with breast cancer: A meta-analysis of diagnostic accuracy studies. *Oncologist*. 2016;21(8):931–939. doi:10.1634/theoncologist.2015-0353
27. Shaaban MAE, Mohamed AIM. Determining the efficacy of N-acetyl cysteine in treatment of pneumonia in COVID-19 hospitalized patients: A meta-analysis. *Int J Clin Med Res*. 2023;1(2):36–42. doi:10.61466/ijcmr1020006
28. Higgins JPT, Thompson SG, Deeks JJ, Altman DG. Measuring inconsistency in meta-analyses. *BMJ*. 2003;327(7414):557–560. doi:10.1136/bmj.327.7414.557
29. Gu R, Xu G. A meta-analysis looking at the effects of continuous management for complications related to intraoperative pressure wound ulcers in women with breast cancer. *Int J Clin Med Res*. 2024;2(4):100–106. doi:10.61466/ijcmr2040001
30. Koang Y. A meta-analysis on the use of photobiomodulation to regulate gingival wound healing in addition to periodontal therapies. *Int J Clin Med Res*. 2024;2(4):107–115. doi:10.61466/ijcmr2040002
31. Ding L, Ding S, He C, Zhang Q, An J. The efficacy of continuing nursing interventions on intraoperative pressure ulcer-related complications in breast cancer patients: Systematic review and meta-analysis. *Gland Surg*. 2022;11(6):1078–1085. doi:10.21037/gs-22-258
32. Zhu YT, Jiang YX, Pei L, Zhu WC, Jin XG. Application of quality control circle in the management of early ambulation after cesarean section: An observational study. *Medicine (Baltimore)*. 2024;103(14):e37633. doi:10.1097/MD.0000000000037633
33. Hu B, Wang Q, Wang YA, et al. Epigenetic activation of WNT5A drives glioblastoma stem cell differentiation and invasive growth. *Cell*. 2016;167(5):1281–1295.e18. doi:10.1016/j.cell.2016.10.039
34. Wang L. Early diagnosis of breast cancer. *Sensors*. 2017;17(7):1572. doi:10.3390/s17071572
35. Cao MD, Lamichhane S, Lundgren S, et al. Metabolic characterization of triple negative breast cancer. *BMC Cancer*. 2014;14(1):941. doi:10.1186/1471-2407-14-941
36. Lilly AJ, Johnson M, Kuzmiak CM, et al. MRI-guided core needle biopsy of the breast: Radiology-pathology correlation and impact on clinical management. *Ann Diagn Patol*. 2020;48:151563. doi:10.1016/j.anndiagpath.2020.151563
37. Chen Q, Xu M, Zheng W, Xu T, Deng H, Liu J. Se/Ru-decorated porous metal–organic framework nanoparticles for the delivery of pooled siRNAs to reversing multidrug resistance in taxol-resistant breast cancer cells. *ACS Appl Mater Interfaces*. 2017;9(8):6712–6724. doi: 10.1021/acsami.6b12792
38. Liu N, Qi ES, Xu M, Gao B, Liu GQ. A novel intelligent classification model for breast cancer diagnosis. *Information Processing & Management*. 2019;56(3):609–623. doi:10.1016/j.ipm.2018.10.014
39. Kong LX, Zhao YH, Feng ZL, Liu TT. Personalized and continuous care intervention affects rehabilitation, living quality, and negative emotions of patients with breast cancer. *World J Psychiatry*. 2024;14(6):876–883. doi:10.5498/wjp.v14.i6.876
40. Saeed H, Salem HF, Rabea H, Abdelrahim MEA. Effect of human error, inhalation flow, and inhalation volume on dose delivery from Ellipta® dry-powder inhaler. *J Pharm Innov*. 2019;14(3):239–244. doi:10.1007/s12247-018-9352-y
41. Nicola M, Elberry A, Sayed O, Hussein R, Saeed H, Abdelrahim M. The impact of adding a training device to familiar counselling on inhalation technique and pulmonary function of asthmatics. *Adv Ther*. 2018;35(7):1049–1058. doi:10.1007/s12325-018-0737-6
42. Elgendy MO, Abdelrahim ME, Salah Eldin R. Potential benefit of repeated MDI inhalation technique counselling for patients with asthma. *Eur J Hosp Pharm*. 2015;22(6):318–322. doi:10.1136/ejhpharm-2015-000648
43. Saeed H, Mohsen M, Fink JB, et al. Fill volume, humidification and heat effects on aerosol delivery and fugitive emissions during noninvasive ventilation. *J Drug Deliv Sci Technol*. 2017;39:372–378. doi:10.1016/j.jddst.2017.04.026
44. Hassan A, Rabea H, Hussein RRS, et al. In-vitro characterization of the aerosolized dose during non-invasive automatic continuous positive airway pressure ventilation. *Pulm Ther*. 2016;2(1):115–126. doi:10.1007/s41030-015-0010-y
45. Elgendy MO, Hassan AH, Saeed H, Abdelrahim ME, Eldin RS. Asthmatic children and MDI verbal inhalation technique counseling. *Pulm Pharmacol Ther*. 2020;61:101900. doi:10.1016/j.pupt.2020.101900
46. Harb HS, Elberry AA, Rabea H, Fathy M, Abdelrahim ME. Performance of large spacer versus nebulizer T-piece in single-limb noninvasive ventilation. *Respir Care*. 2018;63(11):1360–1369. doi:10.4187/respcare.05976
47. Madney YM, Fathy M, Elberry AA, Rabea H, Abdelrahim MEA. Nebulizers and spacers for aerosol delivery through adult nasal cannula at low oxygen flow rate: An in-vitro study. *J Drug Deliv Sci Technol*. 2017;39:260–265. doi:10.1016/j.jddst.2017.04.014
48. Vecellio L, Abdelrahim ME, Montharu J, Galle J, Diot P, Dubus JC. Disposable versus reusable jet nebulizers for cystic fibrosis treatment with tobramycin. *J Cyst Fibros*. 2011;10(2):86–92. doi:10.1016/j.jcf.2010.10.004
49. Zawbaa HM, Osama H, El-Gendy A, et al. Effect of mutation and vaccination on spread, severity, and mortality of COVID-19 disease. *J Med Virol*. 2022;94(1):197–204. doi:10.1002/jmv.27293
50. Mäkinen M, Haavisto E, Lindström V, Brolin K, Castrén M. Finnish and Swedish prehospital emergency care providers' knowledge and attitudes towards pressure ulcer prevention. *Int Emerg Nurs*. 2021;55:100873. doi:10.1016/j.ienj.2020.100873
51. Parisod H, Holopainen A, Kielo-Viljamaa E, Puukka P, Beeckman D, Haavisto E. Attitudes of nursing staff towards pressure ulcer prevention in primary and specialised health care: A correlational cross-sectional study. *Int Wound J*. 2022;19(2):399–410. doi:10.1111/iwj.13641
52. Nadukkandiyil N, Syamala S, Saleh HA, et al. Implementation of pressure ulcer prevention and management in elderly patients: A retrospective study in tertiary care hospital in Qatar. *Aging Male*. 2020;23(5):1066–1072. doi:10.1080/13685538.2019.1670156
53. Delawder JM, Leontie SL, Maduro RS, Morgan MK, Zimbro KS. Predictive validity of the Cubbin–Jackson and Braden Skin Risk Tools in critical care patients: A multisite project. *Am J Crit Care*. 2021;30(2):140–144. doi:10.4037/ajcc2021669
54. Wei M, Wu L, Chen Y, Fu Q, Chen W, Yang D. Predictive validity of the Braden Scale for pressure ulcer risk in critical care : A meta-analysis. *Nurs Crit Care*. 2020;25(3):165–170. doi:10.1111/nicc.12500
55. Anrys C, Van Tiggelen H, Verhaeghe S, Van Hecke A, Beeckman D. Independent risk factors for pressure ulcer development in a high-risk nursing home population receiving evidence-based pressure ulcer prevention: Results from a study in 26 nursing homes in Belgium. *Int Wound J*. 2019;16(2):325–333. doi:10.1111/iwj.13032
56. Reddy TP, Rosato RR, Li X, Moulder S, Piwnica-Worms H, Chang JC. A comprehensive overview of metaplastic breast cancer: Clinical features and molecular aberrations. *Breast Cancer Res*. 2020;22(1):121. doi:10.1186/s13058-020-01353-z

Clearing the path: Hypertonic saline's impact on intracranial pressure in traumatic brain injury. A systematic review and meta-analysis

*Xiaoping Ren[1,A], *Shuyan Liu[2,B], Ju Gao[3,C,D], Rupshikha Choudhury[4,D,E], Sanjay Rastogi[4,E,F]

[1] Department of Rehabilitation, Affiliated Hangzhou First People's Hospital, School of Medicine, Westlake University, China
[2] Department of Neurology, The People's Hospital of Danyang – Affiliated Danyang Hospital of Nantong University, China
[3] Department of Neurology, Huanggang Central Hospital, China
[4] Department of Oral and Maxillofacial Surgery, Regional Dental College, Guwahati, India

A – research concept and design; B – collection and/or assembly of data; C – data analysis and interpretation;
D – writing the article; E – critical revision of the article; F – final approval of the article

Advances in Clinical and Experimental Medicine, ISSN 1899–5276 (print), ISSN 2451–2680 (online) *Adv Clin Exp Med*. 2025;34(11):1827–1840

Address for correspondence
Ju Gao
E-mail: gaoju202311@sina.com

Funding sources
Project name: Correlation study between subclinical hypothyroidism and carotid atherosclerosis in patients with acute ischemic stroke and vascular dementia (grant No. FZ2023006)

Conflict of interest
None declared

*Xiaoping Ren and Shuyan Liu contributed equally to this work.

Received on June 17, 2024
Reviewed on September 27, 2024
Accepted on December 16, 2024

Published online on March 24, 2025

Abstract

Background. Elevated intracranial pressure (ICP) significantly worsens neurological outcomes and mortality rates in patients with traumatic brain injury (TBI). Hypertonic saline (HTS), a hyperosmolar treatment, controls elevated ICP in TBI patients. However, there is still debate regarding the efficacy of HTS in managing TBI.

Objectives. To assess the effectiveness of HTS in lowering elevated ICP in TBI patients with TBI.

Materials and methods. A systematic search was conducted using 4 electronic databases (PubMed, Embase, Scopus, and Cochrane Library) to select relevant articles published in peer-reviewed journals. The risk ratio (RR) and mean difference (MD) were calculated, along with their 95% confidence intervals (95% CIs). Heterogeneity was assessed using Cochrane Q, I^2 statistics and p-value. RevMan 5.4 was used.

Results. The current meta-analysis included 965 TBI patients from 15 randomized controlled trials (RCTs). We found that HTS was significantly more effective than other ICP-lowering agents with RR of 0.74 (95% CI: 0.58–0.94) for reduction of elevated ICP; RR = 0.57 (95% CI: 0.40–0.81) for all-cause mortality; RR = 0.68 (95% CI: 0.49–0.95) for rate of adverse hypernatremia; RR = 0.73 (95% CI: 0.60–0.88) for substantial change in the Glasgow Outcome Scale (GOS) score and shorter period of hospital stay with MD of –1.26 (95% CI: –2.30 to –0.21).

Conclusions. We found that HTS is considerably effective in reducing elevated ICP with improvement in long-term neurological functions, all-cause mortality, rate of hypernatremia, and length of hospital stay in TBI patients.

Key words: hypertonic saline, intracranial pressure, traumatic brain injury, neurological outcomes, mortality rates

Cite as
Ren X, Liu S, Gao J, Choudhury R, Rastogi S. Clearing the path: Hypertonic saline's impact on intracranial pressure in traumatic brain injury. A systematic review and meta-analysis. *Adv Clin Exp Med*. 2025;34(11):1827–1840. doi:10.17219/acem/197437

DOI
10.17219/acem/197437

Highlights

1. Traumatic brain injury (TBI) occurs when the brain is harmed by a quick, external and violent impact, such as in sports or car accidents. Worldwide, it is a leading cause of mortality and lasting disability in people.
2. Increased intracranial pressure (ICP) has a major negative impact on neurological outcomes and mortality rates in individuals with TBI.
3. Hypertonic saline (HTS), a hyperosmolar therapy, manages increased ICP in TBI patients. However, there is still some dispute over the efficacy of HTS in TBI treatment.
4. The present analysis shows that HTS outperforms other hyperosmolar agents like mannitol in reducing ICP, improving neurological outcomes, reducing mortality and shortening hospital or ICU stays in acute TBI patients.

Introduction

Traumatic brain injury (TBI) occurs when the brain is damaged due to a sudden, external and forceful impact[1] often caused by serious sports-related accidents or vehicular collisions.[2] This condition is a leading cause of fatalities and permanent disabilities in adults worldwide.[3] Possible symptoms of TBI include cognitive disorientation, impaired visual acuity and difficulty concentrating, which may manifest either promptly or with a delay.[4] Following a TBI, blood leakage from blood vessels between the meninges leads to the development of subdural hematomas[5] and an increase in intracranial pressure (ICP),[6] which in turn increases the risk of brain herniation and is associated with worse clinical outcomes. Most TBI fatalities result from an uncontrolled increase in ICP, which often occurs within the first 48 h following the event.[7]

Emergency care for moderate-to-severe TBI emphasizes ensuring that the patient has enough oxygen and blood flow, keeping blood pressure stable and preventing further head or neck injury.[8] Therefore, reducing ICP using potential hyperosmolar treatments, including mannitol and hypertonic saline (HTS), is a critical part of treating patients with mild-to-severe TBI.[9] The initial rapid infusion of large volumes of mannitol and a hypertonic crystalloid solution helps restore blood pressure and blood volume.[10] A hyperosmolar solution changes the viscosity and microcirculation of blood, causes the pial arteriolar constriction, creates an osmotic gradient that pulls cerebral edema fluid from brain tissue into the bloodstream, and lets the cerebrospinal fluid leave the brain and lowers the ICP.[11,12]

Since TBI severely impairs the quality of life. Researchers are investigating numerous therapeutic approaches to address this issue. Hypertonic saline is an osmotic agent that can be beneficial to patients during the acute phase of severe TBI as it reduces the detrimental consequences of secondary brain injury and regulates ICP by extracting fluid from enlarged cerebral tissue.[13,14] Nevertheless, the most recent guidelines from the Brain Trauma Foundation 2016[15] state that there is "insufficient evidence available from comparative studies to support a formal recommendation" for the use of HTS, even though it is becoming more popular in this setting and earlier studies have shown its clinical benefits. One possible side effect linked to HTS use is severe hypernatremia.[16]

Therefore, researchers have conducted numerous randomized clinical trials (RCTs), comparing infusions of different hyperosmolar treatments with HTS to investigate their efficacy in terms of reducing ICP in patients suffering from acute TBI. However, the impact of a continuous HTS infusion on neurological function, long-term functional results, all-cause mortality, long-term ICP management, and adverse effects as compared to standard treatments is still not clear. Therefore, in the present study, 15 RCTs[17–31] comparing the effect of HTS with other ICP-lowering hyperosmolar treatments were selected according to predefined inclusion-exclusion criteria and meta-analyzed.

Objectives

The aim of this systematic review and meta-analysis was to assess the effectiveness of HTS on the reduction of elevated ICP in patients with TBI.

Materials and methods

Search strategy and selection criteria

This meta-analysis and systematic review comply with the reporting standards established in the Preferred Reporting Items for Systematic Reviews and Meta-analysis (PRISMA) statement.[32] We conducted a systematic review of RCTs that compared the efficacy of HTS with other ICP-reducing agents in the reduction of elevated ICP in patients with TBI. The investigation concentrated on individuals of all ages who were experiencing elevated ICP as a result of TBI.

The primary outcome of interest was the change in Glasgow Outcome Scale (GOS) scores after 6 months, all-cause mortality, rate of hypernatremia, rate of uncontrolled ICP, and length of hospital stay. The investigation did not include trials that involved animal studies, studies that were not randomized, or studies that did not provide

Table 1. Database search strategy

Database	Search strategy
Scopus	#1 "Hypertonic Saline" OR "HTS" OR "Intracranial Pressure Lowering Agents" OR "Traumatic Brain Injury" OR "TBI" OR "Intracranial Pressure" OR "ICP" OR "Glasgow Outcome Scale (GOS) score" #2 "All-cause mortality" OR "total length of stay" OR "Osmotherapy" OR "reduction in uncontrolled ICP" OR "Hypernatremia" OR "Mannitol," OR "Mechanical ventilation" OR "Intravenous bolus infusion" OR "Cerebral perfusion pressure" OR "Randomized controlled trial" OR "RCT" OR "Systematic review" OR "meta-analysis" #3 #1 AND #2
PubMed	#1 "Hypertonic Saline" OR "HTS" [MeSH Terms]# OR "Intracranial Pressure Lowering Agents" [All Fields] OR "Traumatic Brain Injury" [MeSH terms] OR "TBI" [All fields] OR "Intracranial Pressure" [All Fields] OR "ICP" [All Fields] OR "Glasgow Outcome Scale (GOS) score" [All fields]. #2 "All-cause mortality" [MeSH Terms] OR "total length of stay" [All Fields] OR "Osmotherapy" [All Fields] OR "reduction in uncontrolled ICP" [All Fields] OR "Hypernatremia" OR "mannitol" [All Fields] OR "Mechanical ventilation" [All Fields] OR "Intravenous bolus infusion" [All Fields] OR "Cerebral perfusion pressure" [All Fields] OR "Randomized controlled trial" [All Fields] OR "RCT" [All Fields] OR "systematic review" [All Fields] OR "meta-analysis" [All Fields] #3 #1 AND #2
Embase	#1 "Hypertonic Saline"/exp$ OR "HTS"/exp OR "Intracranial Pressure Lowering Agents"/exp OR "Traumatic Brain Injury"/exp OR "TBI"/exp OR "Intracranial Pressure"/exp OR "ICP"/exp OR "Glasgow Outcome Scale (GOS) score". #2 "All-cause mortality"/exp OR "total length of stay"/exp OR "Osmotherapy"/exp OR "reduction in uncontrolled ICP"/exp OR "Hypernatremia"/exp OR "Mannitol"/exp OR "Mechanical ventilation"/exp OR "Intravenous bolus infusion"/exp OR "Cerebral perfusion pressure"/exp OR "Randomized controlled trial"/exp OR "RCT"/exp OR "Systematic review"/exp OR "meta-analysis"/exp #3 #1 AND #2
Cochrane Library	#1 (Hypertonic Saline): ti, ab, kw@ OR (HTS): ti, ab, kw OR (Intracranial Pressure Lowering Agents): ti, ab, kw OR (Traumatic Brain Injury) ti, ab, kw OR (TBI): ti, ab, kw OR (Intracranial Pressure): ti, ab, kw OR (ICP): ti, ab, kw OR (Glasgow Outcome Scale (GOS) score): ti, ab, kw (Word variations have been searched) #2 (All-cause mortality): ti, ab, kw OR (total length of stay): ti, ab, kw OR (Osmotherapy): ti, ab, kw OR (reduction in uncontrolled ICP): ti, ab, kw OR (Hypernatremia): ti, ab, kw OR (Mannitol): ti, ab, kw OR (Mechanical ventilation): ti, ab, kw OR (Intravenous bolus infusion): ti, ab, kw OR (Cerebral perfusion pressure): ti, ab, kw OR (Randomized controlled trial): ti, ab, kw OR (RCT): ti, ab, kw OR (Systematic review): ti, ab, kw OR (meta-analysis): ti, ab, kw OR (Word variations have been searched) #3 #1 AND #2

MeSH terms – Medical Subject Headings; $ exp – explosion in Emtree-searching of selected subject terms and related subjects; @ ti, ab, kw: either title or abstract or keyword fields.

hyperosmolar prophylaxis. There were no restrictions regarding language or year of publication. We conducted an exhaustive search of the scientific literature databases Embase, PubMed, Scopus, and Cochrane Library for publications released prior to April 30, 2024.

The following search terms were employed: "Hypertonic Saline" OR "HTS" OR "Intracranial Pressure Lowering Agents" OR "Traumatic Brain Injury" OR "TBI" OR "Intracranial Pressure" OR "ICP" OR "Glasgow Outcome Scale (GOS) score", "All-cause mortality" OR "total length of stay" OR "Osmotherapy" OR "reduction in uncontrolled ICP" OR "Hypernatremia" OR "Mannitol," OR "Mechanical ventilation" OR "Intravenous bolus infusion" OR "Cerebral perfusion pressure" OR "Randomized controlled trial" OR "RCT" OR "Systematic review" OR "meta-analysis". Keywords were identified and evaluated for agreement in both the MEDLINE and Embase databases in accordance with the PICOS criteria.[33]

The keywords that were specified were inserted into the Title (ti)-Abstract (abs)-Keyword (keyword) field during the Scopus search. The Cochrane Library database employed the search keywords "traumatic brain injury," "elevated intracranial pressure" and "hypertonic saline." The PICO framework was employed to establish precise selection criteria. The letter "P" was employed to identify patients who had experienced TBI. Hypertonic saline was implemented by the intervention group to mitigate elevated ICP. Mannitol and other ICP-lowering agents were represented by the letter "C." The change in GOS scores at 6 months, all-cause mortality, rate of hypernatremia, rate of uncontrolled ICP, and duration of hospital stay associated with the use of HTS compared to control agents were the primary clinical outcomes, denoted by "O."

The design of the study was confined to the application of RCTs. The methodology utilized in our investigation was based on the approach used in the formulation of the World Health Organization (WHO) guideline.[34] Further articles were discovered by employing backward and forward citation tracking on previously published meta-analyses and the studies included therein.

Table 1,[17–31] delineates the comprehensive search strategy. The titles, abstracts and full texts of potentially qualifying publications were independently evaluated by 2 reviewers, X.R. and S.L. Any discrepancies between the 2 reviewers were resolved through discussion, and the 3rd author (J.G.) was consulted as needed.

Data analysis

The current investigation encompassed studies that provided comparative data on the efficacy of HTS compared to other ICP lowering agents in the reduction of elevated ICP in TBI patients. The studies were selected on the basis of their ability to provide full texts and an adequate amount of data for a 2×2 table. Bibliographic references that were outdated, anecdotal or wholly expert-based were

excluded from the examination process. The demographic profiles of the patients and event data, including relevant components, were independently collected from the studies included in the analysis by 2 researchers (X.R. and S.L.). The data were collected using a predetermined form and comprised the following: the authors, publication year, country, total number of patients, age of patients, condition of patients at admission, intervention and control doses, and primary and secondary outcomes. In the event that the publishers' data was insufficient or ambiguous, they were contacted to obtain supplementary information. For instance, clarification was sought when the dosage of ICP lowering agents was unclear. All-cause mortality, rate of hypernatremia, rate of uncontrolled ICP, length of hospital stay, and change in GOS scores at 6 months were the primary outcomes evaluated.

Risk of bias assessment of included studies

The researchers employed a standardized questionnaire to evaluate the studies under investigation for any potential biases. The Cochrane Risk-of-Bias tool v. 2 was employed by 2 authors to independently assess the risk of bias in individual investigations.[35] Five components comprised the tool: bias induced by randomization, bias resulting from deviations from intended interventions, bias due to lacking outcome information, bias during outcome evaluation, and bias in selecting out the reported outcomes. In order to evaluate potential bias, 2 researchers (X.R. and S.L.) conducted an impartial evaluation. An additional reviewer (J.G.), assumed the role of an arbitrator to resolve any remaining disputes. Ultimately, the potential bias was evaluated and classified as either "uncertain risk", "high risk" or "low risk".

Statistical analyses

A comparison-adjusted funnel plot was employed to evaluate publication bias and small-study effects.[36] Begg's test[37] was implemented by MedCalc software v. 23.1.7 (MedCalc, Ostend, Belgium).[38] to verify the statistically significant impact of this bias. The software program Review Manager (RevMan) v. 5.4 (The Cochrane Collaboration, The Nordic Cochrane Centre, Copenhagen, Denmark)[39] was implemented to assess and analyze the impact of various continuous and dichotomous outcomes. In order to evaluate binary outcomes, relative risks (RRs) were calculated for each study, along with 95% confidence intervals (95% CIs)[40] and the mean difference (MD).[41] The risk ratio (RR) was computed using the DerSimonian-Lair method[42] and a 2×2 table[43] that contained event data. The quantitative evaluation excluded studies that did not report any selected primary or secondary outcome. The objective of forest plots[44] were created to assess the impact of various outcome determinants. The heterogeneity was evaluated using statistical methods, including the I^2 test[45] and the χ^2 test,[46] which were used in conjunction with a p-value. A random effect model[47] was implemented due to the fact that the investigations were conducted in different settings. Statistical significance is defined as a p-value that is less than 0.05.[48] In order to evaluate the efficacy of HTS in reducing elevated ICP in acute TBI patients in comparison to control agents, a subgroup analysis was conducted.

Results

Study selection outcomes

An extensive electronic survey was done by searching across multiple databases. A total of 318 papers were identified that satisfied the inclusion criteria specified in the PICOS criteria. Out of the 265 articles that were considered, 53 papers were excluded because they had duplicate content or titles and abstracts that were not relevant. After conducting additional screening, a total of 135 papers were then evaluated to determine their eligibility. However, after applying the inclusion-exclusion criteria, it was determined that 130 research did not meet the requirements and were consequently excluded. Subsequently, the remaining 65 articles were assessed to determine their suitability. Among the whole pool of studies examined, 50 were eliminated, mostly because they did not match the inclusion criteria, did not provide enough data to create 2×2 tables or did not have significant outcome measures. Ultimately, this meta-analysis included a total of 15 RCTs that met the predefined inclusion-exclusion criteria, as depicted in Fig. 1. The researches included in the analysis involve a combined total of 965 participants, spanning various age groups. The salient features of the publications considered in this meta-analysis are outlined in Table 2. The text provides information on the authors' identification and the year of publication, the study design, the condition of the patients, the total number of patients, the age of the participants, the dosage of the intervention and comparator, as well as the primary and secondary outcomes. In addition, data regarding the events in the 2×2 table were obtained from the aforementioned research for the purpose of conducting a meta-analysis.

Quality assessment of the included studies

An assessment of potential risk of bias was executed out to calculate the overall rating for the study's quality. Table 3 displays the results of the risk of bias assessment for each of the 15 RCTs that were included, using the predetermined questionnaire. The current meta-analysis exhibits a low risk of bias, as indicated by the traffic light plot in Fig. 2 and the summary plot for bias assessment displayed in Fig. 3. Among the 15 RCTs, 11 studies were determined to have a low risk of bias.

Two RCTs, of Du et al.[18] and Jagannatha et al.,[23] demonstrate a moderate level of bias. This is attributed to issues

Table 2. Characteristics of the included studies

Study ID and year	Type of study	Country of study	Age of participants [years]	Number of participants	Condition of participants	Intervention	Control	Primary outcomes	Secondary outcomes
Cottenceau et al.[17]	two-center parallel RCT	France and Israel	>16	47	GCS ≤ 8 at time of admission, severe TBI require ICP monitoring and mechanical ventilation.	7.5% hypertonic saline bolus infused intravenously over 20 min (2 mL/kg dose).	20% mannitol bolus infused intravenously over 20 min (4 mL/kg dose).	Maximal ICP reduction and alteration in cerebral perfusion pressure from baseline after hyperosmolar therapy over a duration of 120 min.	Neurological outcome at 6 months (GOS). All-cause mortality by 6 months, hypernatremia, uncontrolled ICP, defined as average time ICP > 20 mm Hg, length of hospital stay.
Du et al.[18]	single-center parallel RCT	China	>18	67	Severe TBI, ICP > 20 mm Hg.	3% hypertonic saline bolus infused intravenously.	20% mannitol bolus infused intravenously.	Maximal ICP reduction and alteration in cerebral perfusion pressure from baseline after hyperosmolar therapy over a duration of 120 min.	Hypernatremia, neurological outcome at 6 months (GOS). All-cause mortality by 6 months. Uncontrolled ICP, defined as average time ICP > 20 mm Hg, duration of hospital stay.
Francony et al.[19]	single-center parallel RCT	France	>18	20	Sustained elevation of ICP > 20 mm Hg for more than 10 min. Patients with TBI, stroke, and spontaneous hemorrhage, mechanically ventilated.	100 mL of 7.45% hypertonic saline bolus infused via CVC over 20 min.	231 mL of 20% mannitol bolus infused via CVC over 20 min.	ICP magnitude and change in cerebral perfusion pressure after hyperosmolar therapy during the 120-min monitoring period.	Rebound phenomenon, hypernatremia, neurological outcome at 6 months (GOS), all-cause mortality by 6 months, uncontrolled ICP defined as average time ICP > 20 mm Hg, duration of hospital stay.
Harutjunyan et al.[20]	single-center parallel RCT	Germany	>18	32	Patients with severe neuronal damage and at risk of increased ICP with cerebral trauma, spontaneous intracerebral hemorrhage or subarachnoid hemorrhage.	7.2% hypertonic saline and hydroxyethyl starch 200/0.5 via CVC at variable rate until ICP < 15 mm Hg.	Variable dose 15% mannitol via CVC at variable rate until ICP < 15 mm Hg.	ICP reduction below 15 mm Hg (% maximal decrease in ICP from baseline).	All-cause mortality by 6 months, refractory ICP (>15 mm Hg) requiring thiopentone administration, duration of hospital stay.
Hendoui et al.[21]	three-center parallel RCTs	Iran	18–65	33	Patients with GCS ≤ 12 and evidence of brain edema on CT scan and with TBI.	Intervention 1: 125 Ml, 5% hypertonic saline bolus dose infused over 1 h every 6 h for 3 days intervention 2: 500 mL, 5% hypertonic saline continuous infusion over 3 days.	1 g/kg 20% mannitol bolus dose infused over 20 min, 0.25–0.5 g/kg repeat dose every 6 h for 3 days.	GCS reduction, S100B biomarker measurement, lowest ICP achieved for each bolus and time required to achieve ICP < 20 mm Hg.	Hypernatremia, mortality and 60-day survival length of ICU and hospital stay.
Huang and Yang[22]	single-center parallel RCT	China	>18	83	Severe TBI with intracranial hypertension.	10% hypertonic saline bolus infused via CVC over 20 min.	20% mannitol bolus infused intravenously.	ICP reduction below 15 mm Hg (% maximal decrease in ICP from baseline).	All-cause mortality by 6 months, refractory ICP (>15 mm Hg) requiring thiopentone administration.

Table 2. Characteristics of the included studies – cont.

Study ID and year	Type of study	Country of study	Age of participants [years]	Number of participants	Condition of participants	Intervention	Control	Primary outcomes	Secondary outcomes
Jagannatha et al.[23]	single-center parallel RCT	India	15–70	38	Patients with severe TBI within 24 h of injury.	2.5 mL/kg bolus dose, 3% hypertonic saline infused via CVC over 5 min; maximum of 3 doses given.	2.5 mL/kg bolus dose 20% mannitol infused via CV, cover 5 min; max of 3 doses given.	Lowest ICP achieved for each bolus and time required to achieve ICP < 20 mm Hg.	Duration of ICU and hospital stay, in-hospital mortality, GOS at 6 months, uncontrolled ICP after maximum of 3 doses hyperosmolar therapy, hypernatremia.
Kumar et al.[24]	single-center parallel RCT	India	1–16	30	Children with severe TBI and pediatric GCS ≤ 8 presenting within 24 h of trauma.	2.5-mL/kg bolus dose, 3% hypertonic saline infused via CVC over 5 min, 2nd dose given if 1st bolus failed.	2.5 mL/kg bolus dose 20% mannitol infused via CV, cover 5 min, 2nd dose given if 1st bolus failed.	Mean reduction in ICP, defined as the difference between baseline ICP and lowest ICP after completion of bolus foreach dose.	GOS score at 6 months, mortality, length of hospital stay, number of raised ICP episodes, uncontrolled ICP, as case of refractory-ICP despite 3 consecutive doses of hyperosmolar therapy.
Patil and Gupta[25]	single-center parallel RCT	India	>18	120	Severe TBI but no immediate need for surgery, GCS ≤ 8, with sustained elevated ICP > 20 mm Hg for >5 min.	Variable bolus dose, 3% hypertonic saline infused via CVC at infusion rate of 6 mL per minute until ICP < 15 mm Hg.	1. Variable bolus dose 20% mannitol infused via CVC at infusion rate of 6 mL per minute. 2. Variable bolus dose 10% mannitol and 10% glycerol infused via CVC at infusion rate of 6 mL per min, both until ICP < 15 mm Hg.	Reduction in ICP below 15 mm Hg (maximal ICP reduction).	Hypernatremia, mortality and 60-day survival length of ICU and hospital stay.
Qin et al.[26]	single-center parallel RCT	China	>18	24	Severe TBI after decompressive craniectomy, ICP > 20 mm Hg > 5 min.	3% hypertonic saline bolus infused via CVC over 20 min.	20% mannitol bolus infused intravenously.	Lowest ICP achieved for each bolus and time required to achieve ICP < 20 mm Hg.	Duration of ICU and hospital stay, in-hospital mortality. GOS at 6 months, uncontrolled ICP after maximum of 3 doses hyperosmolar therapy, hypernatremia.
Roquilly et al.[27]	multicenter parallel RCT	France	18–80	370	Moderate-to-severe TBI defined as GCS 12 or lower and traumatic abnormal brain CT findings of extradural, subdural hematoma within 24 h of injury.	Continuous intravenous infusion of 20% hypertonic saline at variable infusion rate for 48 h longer if patients remained at high risk of raised ICP.	Standard care to include hypertonic saline boluses, mannitol boluses, hypothermia, and other ICP-lowering methods.	Extended GOS score at 6 months, lowest ICP achieved for each bolus and time required to achieve ICP < 20 mm Hg.	Mortality rate in ICU, length of ICU stay, uncontrolled ICP, defined as ICP > 22 mm Hg for >20 min, change in ICP during study period hypernatremia.
Tsaousi et al.[28]	single-center parallelRCT	Greece	>18	51	Undergoing elective supratentorial craniotomy.	7.5% hypertonic saline bolus infused via CVC over 20 min.	20% mannitol bolus infused intravenously.	Lowest ICP achieved for each bolus and time required to achieve ICP < 20 mm Hg.	Duration of ICU and hospital stay, in-hospital mortality, GOS at 6 months, uncontrolled ICP after maximum of 3 doses hyperosmolar therapy, hypernatremia.

Table 2. Characteristics of the included studies – cont.

Study ID and year	Type of study	Country of study	Age of participants [years]	Number of participants	Condition of participants	Intervention	Control	Primary outcomes	Secondary outcomes
Vialet et al.[29]	single-center parallel RCT	France	>18	20	Head trauma and persistent coma and GCS < 8 requiring ICP monitoring and infusion of an osmotic agent.	2 mL/kg bolus dose 7.5% hypertonic saline infused over 20 min, 2nd dose given within 10 min if 1st dose failed.	2 mL/kg bolus dose, 20% mannitol infused over 20 min, 2nd dose given within 10 min if 1st dose failed.	ICP control, defined as the number of episodes and duration of intracranial hypertension per day.	Duration of hospital stay, uncontrolled ICP, defined as rate of failure of each treatment, 90-day GOS score, all-cause mortality by 6 months.
Wahdan et al.[30]	single-center parallel RCT	Egypt	18–60	50	Severe TBI, GCS 4–12.	0.5 mL/kg/h continuous hypertonic saline infusion over 48 h.	3 mL/kg boluses (infused over 30 min) every 6 h for 48 h.	Reduction in ICP below 15 mm Hg (maximal ICP reduction).	Length of ICU stay, mortality in ICU.
Yan et al.[31]	single-center parallel RCT	China	>18	60	Severe TBI after decompressive craniectomy, ICP > 25 mm Hg >5 min.	3% hypertonic saline bolus infused via CVC over 20 min.	20% mannitol bolus infused intravenously.	Lowest ICP achieved for each bolus and time required to achieve ICP < 20 mm Hg.	Duration of ICU and hospital stay, in-hospital mortality, GOS at 6 months, uncontrolled ICP after max of 3 doses hyperosmolar therapy, hypernatremia.

RCT – randomized controlled trial; ICP – intracranial pressure; TBI – traumatic brain injury; ICU – intensive care unit; GCS – Glasgow Coma Scale; CVC – central venous catheter.

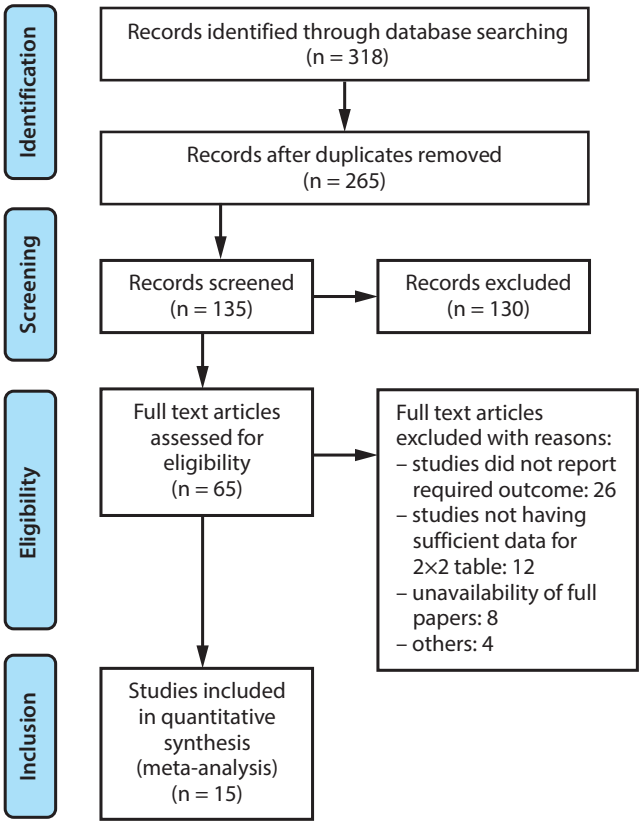

Fig. 1. Preferred Reporting Items for Systematic reviews and Meta-Analyses (PRISMA) study flow diagram

with the randomization method and the deviation from the intended intervention, respectively. The other 2 RCTs conducted by Hendoui et al.[21] and Vialet et al.[29] demonstrate a high risk of bias pertaining to the randomization method and the selection of reported outcomes, respectively.

Findings derived from the statistical investigation

In all, 965 TBI patients from 15 selected RCTs were included in the current meta-analysis to evaluate the efficacy of HTS compared to other ICP-lowering agents on the reduction of elevated ICP in patients with TBI. The following conclusions were obtained from the statistical analysis of the primary study outcome:

Comparison of the efficacy of HTS and other ICP lowering agents in controlling the elevated ICP in TBI patients

The included studies defined the elevated ICP as a requirement of "stage 3 therapies" in accordance with the Brain Trauma Foundation guidelines, which include barbiturates to reduce ICP.[11] Elevated ICP is defined as the "persistently elevated ICP greater than 20 mm Hg despite a maximum of 3 doses of hyperosmolar therapy,"

Table 3. Risk assessment of included studies

Study ID and year	Cottenceau et al.[17]	Du et al.[18]	Francony et al.[19]	Harutjunyan et al.[20]	Hendoui et al.[21]	Huang and Yang[22]	Jagannatha et al.[23]	Kumar et al.[24]	Patil and Gupta[25]	Qin et al.[26]	Roquilly et al.[27]	Tsaousi et al.[28]	Vialet et al.[29]	Wahdan et al.[30]	Yan et al.[31]
Was a consecutive or random sample of patients enrolled?	Y	Y	Y	Y	Y	Y	Y	Y	Y	Y	Y	Y	Y	Y	Y
Did the study avoid inappropriate exclusions?	Y	Y	Y	Y	Y	Y	Y	Y	Y	Y	Y	Y	Y	Y	Y
Did all patients receive the same reference standard?	Y	Y	Y	Y	Y	Y	Y	Y	Y	Y	Y	Y	Y	Y	Y
Were all patients included in the analysis?	N	N	N	N	N	N	N	N	N	N	N	N	N	N	N
Was the sample frame appropriate to address the target population?	Y	Y	Y	Y	Y	Y	Y	Y	Y	Y	Y	Y	Y	Y	Y
Were study participants sampled in an appropriate way?	Y	Y	Y	Y	Y	Y	Y	Y	Y	Y	Y	Y	Y	Y	Y
Were the study subjects and the setting described in detail?	Y	Y	Y	Y	Y	Y	Y	Y	Y	Y	Y	Y	Y	Y	Y
Were valid methods used for the identification of the condition?	Y	Y	Y	Y	Y	Y	Y	Y	Y	Y	Y	Y	Y	Y	Y
Was the condition measured in a standard, reliable way for all participants?	Y	Y	Y	Y	Y	Y	Y	Y	Y	Y	Y	Y	Y	Y	Y

[#] Y – yes; N – no.

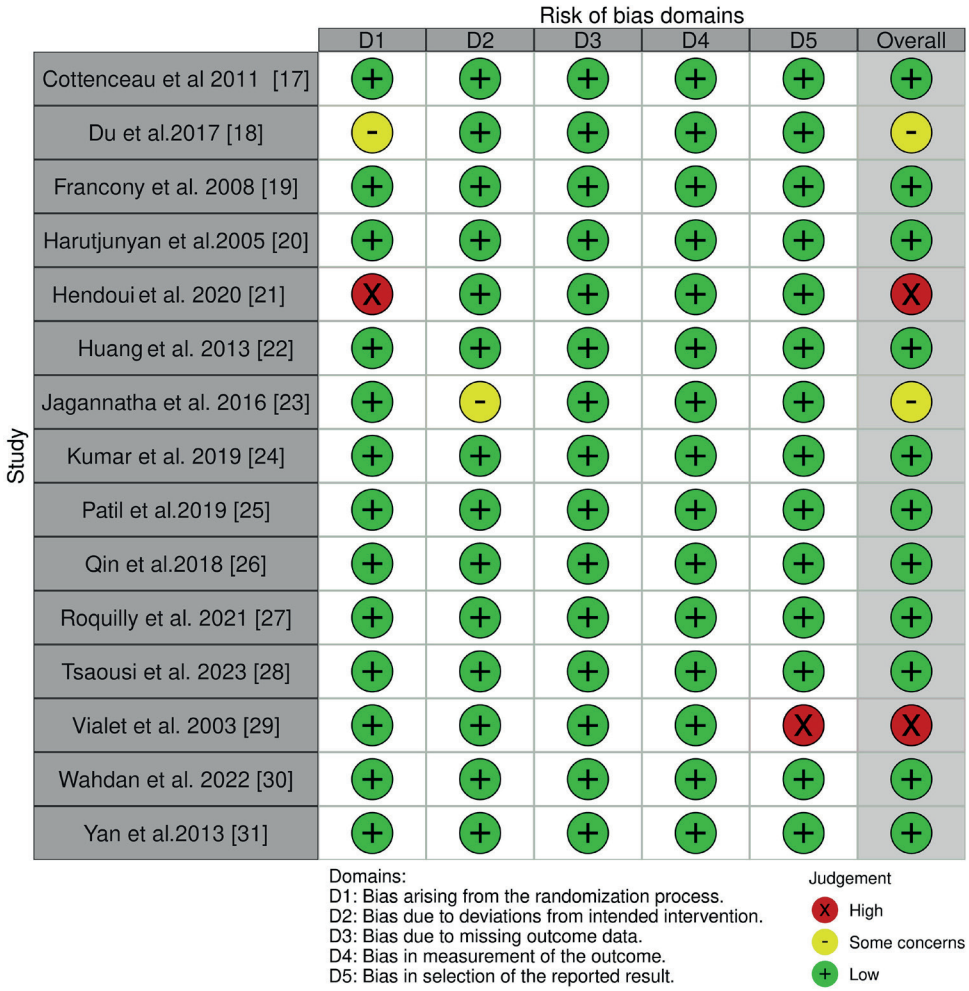

Fig. 2. Traffic light plot for assessment of risk of bias

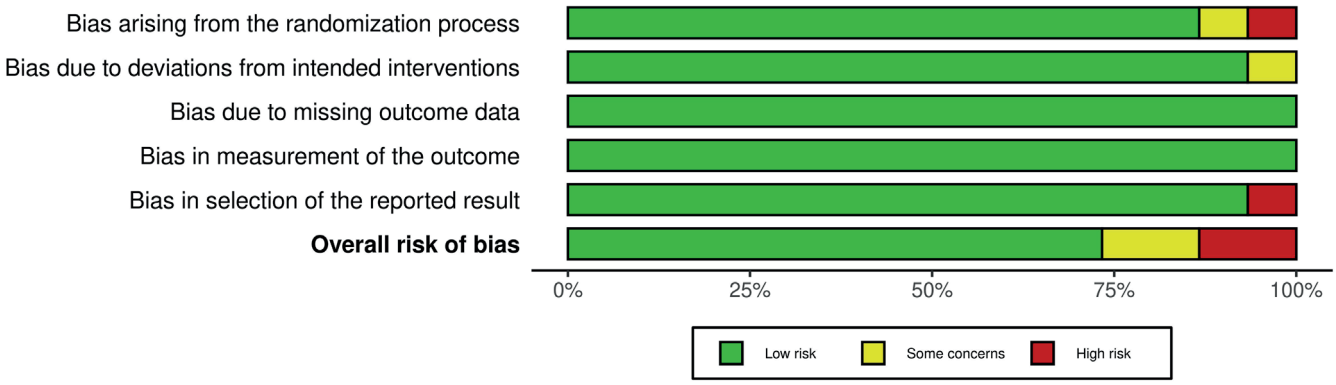

Fig. 3. Risk of bias summary plot

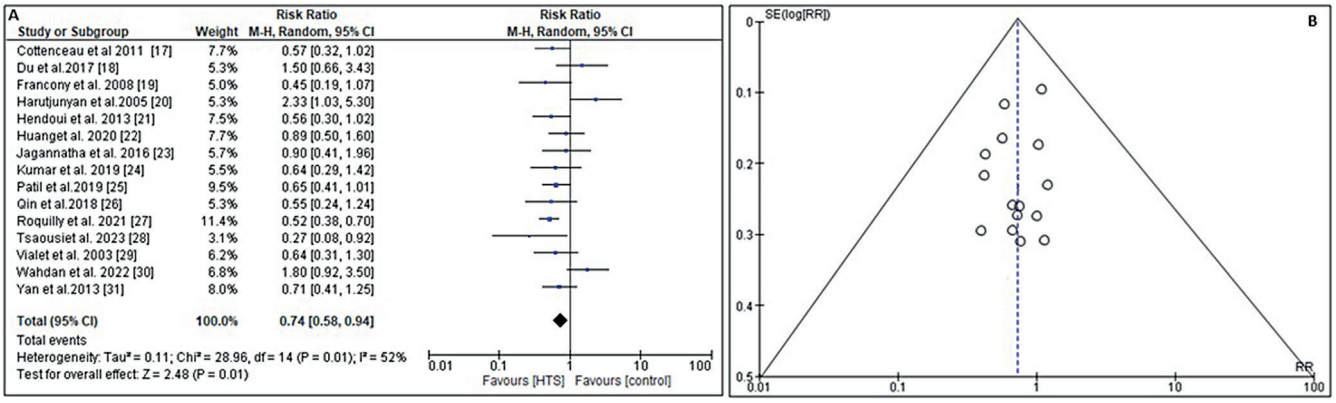

Fig. 4. A. Forest plot comparing the effect of HTS vs control on rate of uncontrolled intracranial pressure; B. Funnel plot

HTS – hypertonic saline: RR – risk ratio; 95% CI – 95% confidence interval; M-H random – Mantel–Haenszel random-effects model.

necessitating the use of further ICP-lowering measures, such as hyperventilation, propofol, cerebrospinal fluid drainage, or decompressive craniectomy.[49]

Treatment failure is defined as a sustained raised ICP greater than 35 mm Hg despite 2 consecutive infusions of hyperosmolar or an average time ICP exceeding 20 mm Hg, barbiturate requirement, and/or episodes of refractory ICP after 3 consecutive doses of hyperosmolar therapy.[50] In order to evaluate the overall efficacy of HTS in managing the rate of elevated ICP in TBI patients in comparison to other ICP lowering agents, the RR and 95% CI were calculated using event data from the included studies (Fig. 4). This meta-analysis demonstrated that HTS was significantly more effective than other agents in reducing ICP (RR = 0.74, 95% CI: 0.58–0.94, $Tau^2 = 0.11$, $\chi^2 = 28.96$, degrees of freedom (df) = 14, $I^2 = 52\%$, Z = 2.48, and p = 0.01) as shown in Fig. 4A. Additionally, the symmetrical funnel diagram in Fig. 4B and a statistically insignificant p-statistic of Begg's test (p = 0.312), which exceeds the predefined significance threshold of 0.05, suggested a minimal likelihood of publication bias.

Subgroup analysis

A subgroup analysis was conducted to investigate the effectiveness of HTS and other ICP lowering agents in controlling elevated ICP in TBI patients. The analysis focused on evaluating changes in GOS scores at 6 months, all-cause mortality, the rate of hypernatremia, and the length of hospital stay.

All-cause mortality

To determine the impact of infusing HTS vs other ICP lowering comparator on all-cause mortality, the RR and 95% CI were calculated using the event data extracted from the included trials (Fig. 5A). In comparison to the comparator, the administration of HTS results in a lower mortality rate with an RR of 0.57 (95% CI: 0.40–0.81) and Tau^2 value of 0.24, χ^2 value of 29.47, df = 14, Z = 3.10, $I^2 = 52\%$, and p = 0.002. In addition, the symmetrical funnel plots (Fig. 5B) and the statistically insignificant p value (p = 0.104) from Begg's test, (>0.05) indicate a low probability of publication bias.

Rate of adverse hypernatremia

To find out the impact of infusing HTS vs other ICP lowering comparator on the rate of adverse hypernatremia or defined as a rise in serum sodium concentration to a value exceeding 145 mmol/L,[51] the RR and 95% CI were calculated using the event data extracted from

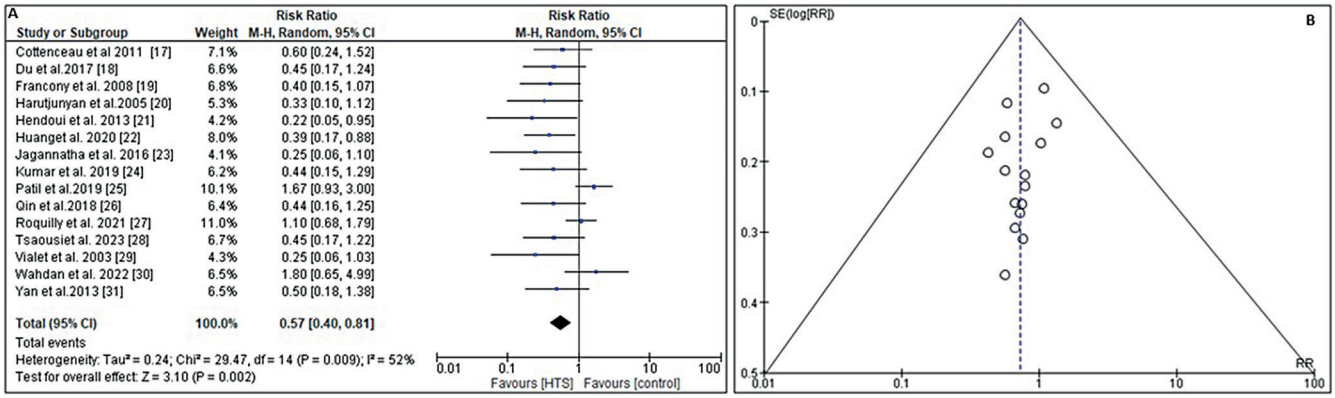

Fig. 5. A. Forest plot comparing the effect of HTS vs control on all-cause mortality; B. Funnel plot

HTS – hypertonic saline: RR – risk ratio; 95% CI – 95% confidence interval; M-H random – Mantel–Haenszel random-effects model.

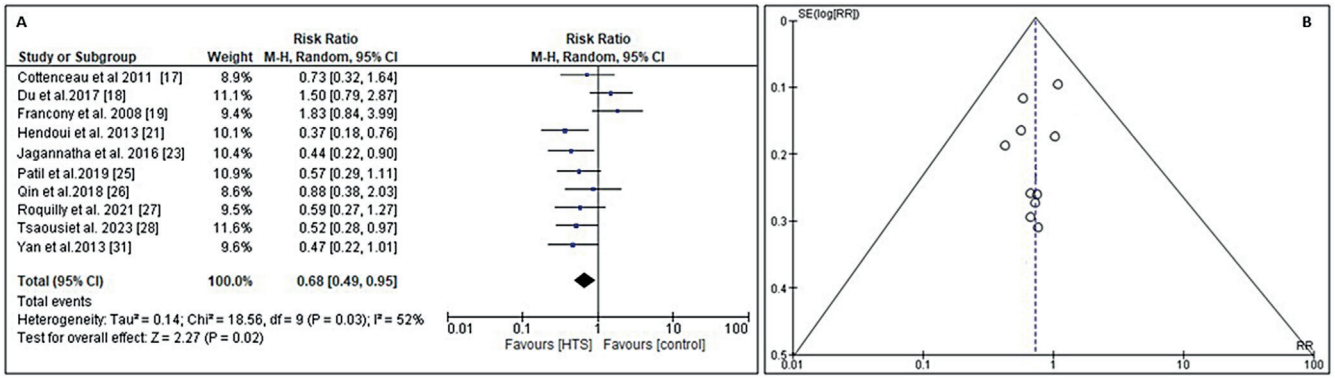

Fig. 6. A. Forest plot comparing the effect of HTS vs control on rate of adverse hypernatremia; B. Funnel plot

HTS – hypertonic saline: RR – risk ratio; 95% CI – 95% confidence interval; M-H random – Mantel–Haenszel random-effects model.

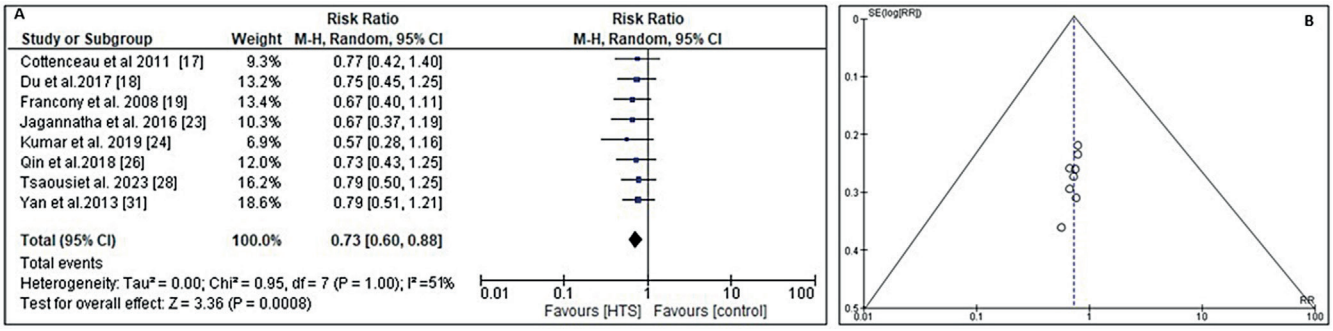

Fig. 7. A. Forest plot comparing the effect of HTS vs control on GOS score at 6 months; B. Funnel plot

HTS – hypertonic saline: RR – risk ratio; 95% CI – 95% confidence interval; M-H random – Mantel–Haenszel random-effects model.

the included RCTs (Fig. 6A). In comparison to the comparator, the administration of HTS results in lower rate of adverse hypernatremia with an RR of 0.68 (95% CI: 0.49–0.95) and Tau^2 value of 0.14, χ^2 value of 18.56, df = 9, Z = 2.27, I^2 = 52%, and p = 0.02. Moreover, the symmetrical funnel plots depicted in Fig. 6B, along with the statistically negligible p-value (p = 0.284) obtained from Begg's test (p > 0.05), suggest a little likelihood of publication bias.

Change in GOS scale score

The GOS score[52] is an ordinal scale used to assess patients' functional outcomes following brain injury, taking into account the patients' level of consciousness and ability to perform activities of daily living (ADLs). The RR and 95% CI were calculated using the event data extracted from the included RCTs to determine the impact of infusing HTS vs other ICP lowering comparator on the change

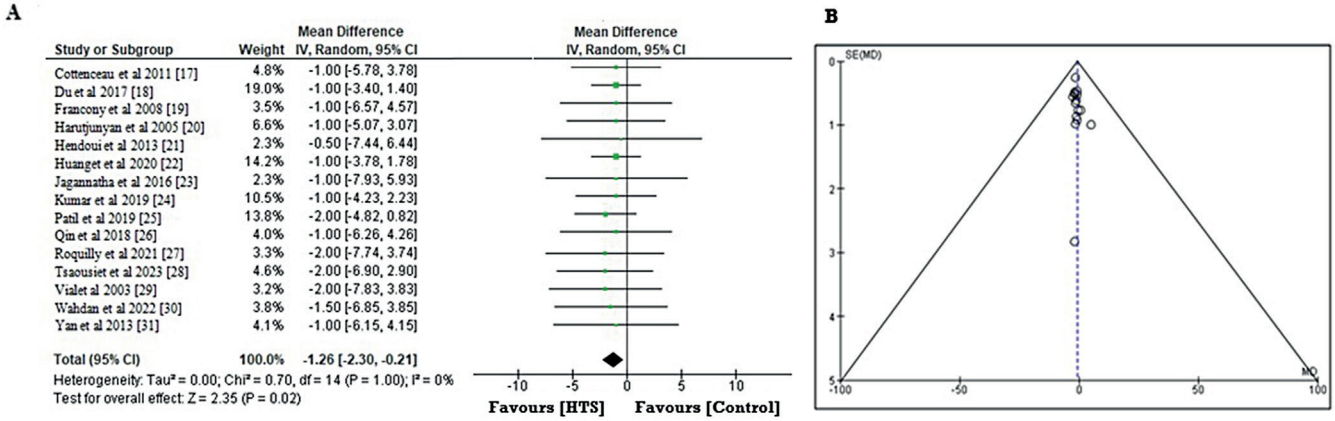

Fig. 8. A. Forest plot comparing the effect of HTS vs control on length of hospital stay; B. Funnel plot

HTS – hypertonic saline: RR – risk ratio; 95% CI – 95% confidence interval.

in the GOS score (Fig. 7A). Compared to the comparator, the administration of HTS leads to a substantial change in GOS scale score. The relative risk (RR) is 0.73 (95% CI: 0.60–0.88), with a Tau^2 value of 0.00, χ^2 value of 0.95, df = 7, Z-score of 3.36, I^2 value of 51%, and a $p < 0.001$. In addition, the symmetrical funnel plots shown in Fig. 7B, coupled with the statistically insignificant p-value of 0.144 obtained from Begg's test ($p > 0.05$), indicate a low probability of publication bias.

Length of hospital stay

To investigate the beneficial impact of infusing HTS compared to other ICP lowering comparator on the total length of hospital stay, the MD and the 95% CI were calculated using the event data extracted from the included RCTs (Fig. 8A). Compared to the comparator, the administration of HTS leads to a shorter period of hospital stay. The estimated MD is –1.26 (95% CI: –2.30 to –0.21), with a Tau^2 value of 0.00, χ^2 value of 0.70, df = 14, Z = 2.35, $I^2 = 70\%$, and $p = 0.02$. In addition, the symmetrical funnel plots shown in Fig. 8B, combined with the statistically insignificant p-value of 0.246 calculated from the Begg's test ($p > 0.05$), stipulate a low probability of publication bias.

From the abovementioned statistical analysis of the included RCTs,[17–31] we found that HTS was significantly more effective than other hyperosmolar agents in reducing ICP (RR = 0.74 (95% CI: 0.58–0.94)), mortality rate (RR = 0.57 (95% CI: 0.40–0.81)) and rate of adverse hypernatremia (RR = 0.68 (95% CI: 0.49–0.95)), providing substantial change in GOS scale score (RR = 0.73 (95% CI: 0.60–0.88)), with shorter period of hospital stay (MD = –1.26 (95% CI: –2.30 to –0.21)). These values of RR 1 indicate that HTS is substantially more effective than other ICP-lowering agents for improving long-term neurological function, all-cause mortality and length of hospital stay in patients with acute TBI.

Discussion

According to our systematic review and meta-analysis including 15 RCTs[17–31] that incorporated 965 TBI patients of all age groups, HTS was found to be considerably more effective than other ICP-lowering agents. The following are the primary findings that were determined: 1) HTS was substantially more effective than primarily mannitol in improving the long-term neurological outcome in patients with elevated ICP; 2) HTS was more effective in lowering the all-cause mortality and length of hospital stay and reducing risk of adverse hypernatremia. The wide 95% CIs for all the evaluated outcomes indicate the therapeutically significant differences between HTS and other hyperosmolar treatments for decreasing ICP, such as mannitol. Our findings are in accordance with the findings of a systematic review and meta-analysis conducted by Bernhardt et al.,[53] who concluded that there is no evidence of an effect of HTS on clinically significant outcomes and that HTS is associated with adverse hypernatremia. In spite of the fact that HTS was found to be not related to deleterious hypernatremia when compared with other agents, this result must be viewed with care due to the fact that the majority of the weighting for this point estimate is based on a single large multicenter trial.[27] This research was significant since it explored the continuous infusion of a larger dosage of HTS (20%) than is often used in clinical settings (range: 1.8–5%). The infusion was administered for a minimum of 48 h. Therefore, it is conceivable that the apparent increased risk of hypernatremia in the patients who were investigated is mostly because of the lengthy continuous infusion of concentrated HTS. Similarly, our findings are align with recent practice surveys, which revealed that most centers use HTS as first-line hyperosmolar therapy rather than mannitol.[54,55]

However, our findings contradict the findings of prior research that suggested that HTS is not more successful than

its comparators (e.g., mannitol), such as Chen et al.,[56] who conducted a Cochrane review in which they analyzed trials that compared HTS to a potential range of other ICP-lowering agents, including mannitol or mannitol in combination with glycerol. They contended that HTS is not superior to mannitol in terms of efficacy and safety in the long-term management of acute TBI, based on the limited data and weak evidence. The majority of their included RCTs were at a high or ambiguous risk of bias due to selective reporting, incomplete outcome data and a lack of blinding. Additionally, certain studies have indicated that there is no difference in plasma sodium concentration between patients who are getting HTS and those who are receiving mannitol boluses. This difference may indicate that certain delivery procedures are not successful in achieving a hyperosmolar state.[57,58] The effect of bolus compared to continuous infusion of HTS on plasma sodium levels should be investigated further to discover whether or not there is an optimal administration route that can generate a therapeutic hyperosmolar state without causing deleterious hypernatremia. Continued research is required to answer this question. It is likely that using near-patient salt monitoring, such as blood gas analysis, will make it easier for clinicians to give and alter the dosage of HTS.

Within the setting of TBI, there is a dearth of large-scale RCTs that compare ICP-lowering treatments due to the relatively low occurrence of severe TBI in critical care settings, which necessitates the use of ICP-lowering medicines. Similarly, RCT data from nations with lower middle incomes and RCT involving pediatric populations are scarce. In this particular review, for example, there is only 1 pediatric trial that reports a GOS score of ≤12 and primarily included trials involving adult patients from higher-income countries.[21] In order to address the existing lack of high-quality evidence and to ascertain whether or not HTS is a preferred ICP-lowering agent in particular patient population, there is a pressing need for larger international and multicenter trials to be conducted in a range of contexts.

Finally, the inconsistent reporting of outcomes following TBI among clinical trials, such as long-term functional outcome ratings using the GOS score, undermines the validity of comparisons between studies and impedes advancement in this area of research. For instance, 3 studies reported GOS scores in formats that were not suitable for inclusion in a pooled analysis. Vialet et al.[29] only provided statistics on the number of patients who had died or had severe disability at the 90-day point. In the RCT by Jagannatha et al.,[23] the term "favorable" outcome was defined as "good recovery," "moderate disability" or "severe disability." This definition is likely to be in conflict with what the majority of patients would view as a favorable outcome. Similarly, Kumar et al.[21] recorded the number of patients who survived with or without disability, as well as the number of patients who were in a vegetative state or had passed away during the first 6 months of their illness. It is not certain whether these methods of GOS reporting will be beneficial to clinicians or patients, which highlights the importance of having a core outcome set that is standardized for TBI.

Therefore, there is an obvious need for the execution of more trials in substantial TBI (COSTS-TBI) projects[59,60] in the future for establishing a standard set for analyzing patients with moderate to severe TBI and to provide more accurate evaluations of blood pressure-lowering medicines in a variety of critical care settings, the thresholds for hazardous hypernatremia, the optimal range of plasma sodium concentration, and other clinical characteristics of patients.

Limitations

The limitations of this analysis can be attributed to the clinical and methodological disparities among trials, which also encompassed predominantly small sample sizes. In addition, variations in the methodologies used to report outcomes restricted the available data that could be included in meta-analyses. Furthermore, the subgroup analyses were based on different age groups, degrees of TBI and methods of administration. Additionally, it remains uncertain whether there is an optimal hyperosmolar therapy that varies according to the age group of the patient or the severity of TBI. Along with this, the classification between "favorable" and "unfavorable" outcomes was based on what most patients and physicians would agree upon. Therefore, it is conceivable that significant data regarding the long-term neurological prognosis, which could potentially impact and direct decisions made by patients and clinicians, may not be reflected in these findings.

Conclusions

This systematic review and meta-analysis provide substantial evidence that HTS is more effective to other hyperosmolar agents, such as mannitol, in decreasing ICP, enhancing neurological outcomes (measured using GOS score), reducing overall mortality, and shortening the duration of hospital or ICU stay in patients with acute TBI. However, this conclusion is derived from a limited number of trials with a small sample size, necessitating a comprehensive investigation into the potential benefits of HTS and the risks associated with hypernatremia. Hence, it is imperative to carry out future research that includes a substantial number of trials and a sufficient sample size in order to ensure the accuracy and reliability of the findings regarding the effectiveness of HTS for acute TBI.

Data availability

The datasets generated and/or analyzed during the current study are available from the corresponding author on reasonable request.

Consent for publication

Not applicable.

Use of AI and AI-assisted technologies

Not applicable.

ORCID iDs

Xiaoping Ren https://orcid.org/0009-0009-1661-6057
Shuyan Liu https://orcid.org/0009-0005-4313-9250
Ju Gao https://orcid.org/0009-0005-3088-4817
Rupshikha Choudhury https://orcid.org/0000-0002-9956-0133
Sanjay Rastogi https://orcid.org/0000-0001-8573-3075

References

1. Capizzi A, Woo J, Verduzco-Gutierrez M. Traumatic brain injury: An overview of epidemiology, pathophysiology, and medical management. *Med Clin North Am*. 2020;104(2):213–238. doi:10.1016/j.mcna.2019.11.001
2. Thapa K, Khan H, Singh TG, Kaur A. Traumatic brain injury: Mechanistic insight on pathophysiology and potential therapeutic targets. *J Mol Neurosci*. 2021;71(9):1725–1742. doi:10.1007/s12031-021-01841-7
3. Faul M, Coronado V. Epidemiology of traumatic brain injury. *Handb Clin Neurol*. 2015;127:3–13. doi:10.1016/B978-0-444-52892-6.00001-5
4. Bergman K, Given B, Fabiano R, Schutte D, Von Eye A, Davidson S. Symptoms associated with mild traumatic brain injury/concussion: The role of bother. *J Neurosci Nurs*. 2013;45(3):124–132. doi:10.1097/JNN.0b013e31828a418b
5. Zhang S, Chen Q, Xian L, Chen Y, Wei L, Wang S. Acute subdural haematoma exacerbates cerebral blood flow disorder and promotes the development of intraoperative brain bulge in patients with severe traumatic brain injury. *Eur J Med Res*. 2023;28(1):138. doi:10.1186/s40001-023-01100-y
6. O'Phelan KH, Park D, Efird JT, et al. Patterns of increased intracranial pressure after severe traumatic brain injury. *Neurocrit Care*. 2009;10(3):280–286. doi:10.1007/s12028-008-9183-7
7. Gedeno K, Neme D, Jemal B, et al. Evidence-based management of adult traumatic brain injury with raised intracranial pressure in intensive critical care unit at resource-limited settings: A literature review. *Ann Med Surg (Lond)*. 2023;85(12):5983–6000. doi:10.1097/MS9.0000000000001291
8. Lynch DG, Narayan RK, Li C. Multi-mechanistic approaches to the treatment of traumatic brain injury: A review. *J Clin Med*. 2023;12(6):2179. doi:10.3390/jcm12062179
9. Gu J, Huang H, Huang Y, Sun H, Xu H. Hypertonic saline or mannitol for treating elevated intracranial pressure in traumatic brain injury: A meta-analysis of randomized controlled trials. *Neurosurg Rev*. 2019;42(2):499–509. doi:10.1007/s10143-018-0991-8
10. Wiórek A, Jaworski T, Krzych ŁJ. Hyperosmolar treatment for patients at risk for increased intracranial pressure: A single-center cohort study. *Int J Environ Res Public Health*. 2020;17(12):4573. doi:10.3390/ijerph17124573
11. Fenn NE, Sierra CM. Hyperosmolar therapy for severe traumatic brain injury in pediatrics: A review of the literature. *J Pediatr Pharmacol Ther*. 2019;24(6):465–472. doi:10.5863/1551-6776-24.6.465
12. Mangat HS, Härtl R. Hypertonic saline for the management of raised intracranial pressure after severe traumatic brain injury. *Ann N Y Acad Sci*. 2015;1345(1):83–88. doi:10.1111/nyas.12704
13. Froese L, Dian J, Batson C, Gomez A, Unger B, Zeiler FA. The impact of hypertonic saline on cerebrovascular reactivity and compensatory reserve in traumatic brain injury: An exploratory analysis. *Acta Neurochir*. 2020;162(11):2683–2693. doi:10.1007/s00701-020-04579-0
14. Berger-Pelletier E, Émond M, Lauzier F, Shields JF, Turgeon AF. Erratum: Hypertonic saline in severe traumatic brain injury: A systematic review and meta-analysis of randomized controlled trials. *CJEM*. 2016;18(3):243–243. doi:10.1017/cem.2016.323
15. Maas AIR, Menon DK, Adelson PD, et al. Traumatic brain injury: Integrated approaches to improve prevention, clinical care, and research. *Lancet Neurol*. 2017;16(12):987–1048. doi:10.1016/S1474-4422(17)30371-X
16. Kolmodin L, Sekhon MS, Henderson WR, Turgeon AF, Griesdale DE. Hypernatremia in patients with severe traumatic brain injury: A systematic review. *Ann Intensive Care*. 2013;3(1):35. doi:10.1186/2110-5820-3-35
17. Cottenceau V, Masson F, Mahamid E, et al. Comparison of effects of equiosmolar doses of mannitol and hypertonic saline on cerebral blood flow and metabolism in traumatic brain injury. *J Neurotrauma*. 2011;28(10):2003–2012. doi:10.1089/neu.2011.1929
18. Du DY, Sun LT, Zhang WS, Li K, Xu C, Li ZF. The clinical efficacy of hypertonic saline in reducing intracranial pressure in patients with severe traumatic brain injury [in Chinese]. *Neural Inj Funct Reconstr*. 2017;12:215–217.
19. Francony G, Fauvage B, Falcon D, et al. Equimolar doses of mannitol and hypertonic saline in the treatment of increased intracranial pressure. *Crit Care Med*. 2008;36(3):795–800. doi:10.1097/CCM.0B013E3181643B41
20. Harutjunyan L, Holz C, Rieger A, Menzel M, Grond S, Soukup J. Efficiency of 7.2% hypertonic saline hydroxyethyl starch 200/0.5 versus mannitol 15% in the treatment of increased intracranial pressure in neurosurgical patients: A randomized clinical trial [ISRCTN62699180]. *Crit Care*. 2005;9(5):R530. doi:10.1186/cc3767
21. Hendoui N, Beigmohammadi MT, Mahmoodpoor A, et al. Reliability of calcium-binding protein S100B measurement toward optimization of hyperosmolal therapy in traumatic brain injury. *Eur Rev Med Pharmacol Sci*. 2013;17(4):477–485. PMID:23467946.
22. Huang X, Yang L. Comparison of 20% mannitol and 15% hypertonic saline in doses of similar osmotic burden for treatment of severe traumatic brain injury with intracranial hypertension [in Chinese]. *Nan Fang Yi Ke Da Xue Xue Bao*. 2014;34(5):723–726. PMID:24849445.
23. Jagannatha AT, Sriganesh K, Devi BI, Rao GSU. An equiosmolar study on early intracranial physiology and long term outcome in severe traumatic brain injury comparing mannitol and hypertonic saline. *J Clin Neurosci*. 2016;27:68–73. doi:10.1016/j.jocn.2015.08.035
24. Kumar SA, Devi BI, Reddy M, Shukla D. Comparison of equiosmolar dose of hyperosmolar agents in reducing intracranial pressure: A randomized control study in pediatric traumatic brain injury. *Childs Nerv Syst*. 2019;35(6):999–1005. doi:10.1007/s00381-019-04121-3
25. Patil H, Gupta R. A comparative study of bolus dose of hypertonic saline, mannitol, and mannitol plus glycerol combination in patients with severe traumatic brain injury. *World Neurosurg*. 2019;125:e221–e228. doi:10.1016/j.wneu.2019.01.051
26. Qin D, Huang W, Yang L, et al. Hypertonic saline in treatment of intracranial hypertension caused by severe cerebral trauma after decompressive craniectomy. *Chin J Neuromed*. 2018;15:1267–1273.
27. Roquilly A, Moyer JD, Huet O, et al. Effect of continuous infusion of hypertonic saline vs standard care on 6-month neurological outcomes in patients with traumatic brain injury: The COBI randomized clinical trial. *JAMA*. 2021;325(20):2056. doi:10.1001/jama.2021.5561
28. Tsaousi GG, Pezikoglou I, Nikopoulou A, et al. Comparison of equiosmolar doses of 7.5% hypertonic saline and 20% mannitol on cerebral oxygenation status and release of brain injury markers during supratentorial craniotomy: A randomized controlled trial. *J Neurosurg Anesthesiol*. 2023;35(1):56–64. doi:10.1097/ANA.0000000000000791
29. Vialet R, Albanèse J, Thomachot L, et al. Isovolume hypertonic solutes (sodium chloride or mannitol) in the treatment of refractory posttraumatic intracranial hypertension: 2 mL/kg 7.5% saline is more effective than 2 mL/kg 20% mannitol. *Crit Care Med*. 2003;31(6):1683–1687. doi:10.1097/01.CCM.0000063268.91710.DF
30. Wahdan AS, Al-Madawi AA, El-Shafey KA, Othman SH. Comparison of intermittent versus continuous infusion of 3% hypertonic saline on intracranial pressure in traumatic brain injury using ultrasound assessment of optic nerve sheath. *Egypt J Anaesth*. 2022;38(1):291–299. doi:10.1080/11101849.2022.2077052
31. Yan YF, Yao HB, Shen X, Yao-Dong. Hypertonic saline for the treatment of intracranial hypertension due to traumatic brain edema. *J Trauma Surg*. 2013;15:296–300.
32. Liberati A, Altman DG, Tetzlaff J, et al. The PRISMA statement for reporting systematic reviews and meta-analyses of studies that evaluate healthcare interventions: Explanation and elaboration. *BMJ*. 2009;339:b2700. doi:10.1136/bmj.b2700

33. Brown D. A review of the PubMed PICO tool: Using evidence-based practice in health education. *Health Promot Pract*. 2020;21(4):496–498. doi:10.1177/1524839919893361
34. Kuo CY, Liou TH, Chang KH, et al. Functioning and disability analysis of patients with traumatic brain injury and spinal cord injury by using the World Health Organization Disability Assessment Schedule 2.0. *Int J Environ Res Public Health*. 2015;12(4):4116–4127. doi:10.3390/ijerph120404116
35. Higgins JPT, Altman DG, Gotzsche PC, et al. The Cochrane Collaboration's tool for assessing risk of bias in randomised trials. *BMJ*. 2011;343:d5928. doi:10.1136/bmj.d5928
36. Sterne JAC, Egger M. Funnel plots for detecting bias in meta-analysis. *J Clin Epidemiol*. 2001;54(10):1046–1055. doi:10.1016/S0895-4356(01)00377-8
37. Begg CB, Mazumdar M. Operating characteristics of a rank correlation test for publication bias. *Biometrics*. 1994;50(4):1088–1101. PMID:7786990.
38. Elovic A, Pourmand A. MDCalc Medical Calculator App review. *J Digit Imaging*. 2019;32(5):682–684. doi:10.1007/s10278-019-00218-y
39. Schmidt L, Shokraneh F, Steinhausen K, Adams CE. Introducing RAPTOR: RevMan Parsing Tool for Reviewers. *Syst Rev*. 2019;8(1):151. doi:10.1186/s13643-019-1070-0
40. Noma H, Misumi M, Tanaka S. Risk ratio and risk difference estimation in case-cohort studies. *J Epidemiol*. 2023;33(10):508–513. doi:10.2188/jea.JE20210509
41. Andrade C. Mean difference, dtandardized mean difference (SMD), and their use in meta-analysis: As simple as it gets. *J Clin Psychiatry*. 2020;81(5):20f13681. doi:10.4088/JCP.20f13681
42. George BJ, Aban IB. An application of meta-analysis based on DerSimonian and Laird method. *J Nucl Cardiol*. 2016;23(4):690–692. doi:10.1007/s12350-015-0249-6
43. Freidlin B, Korn EL. Two-by-two factorial cancer treatment trials: Is sufficient attention being paid to possible interactions? *J Nat Cancer Inst*. 2017;109(9):djx146. doi:10.1093/jnci/djx146
44. Dettori JR, Norvell DC, Chapman JR. Seeing the forest by looking at the trees: How to interpret a meta-analysis forest plot. *Global Spine J*. 2021;11(4):614–616. doi:10.1177/21925682211003889
45. Huedo-Medina TB, Sánchez-Meca J, Marín-Martínez F, Botella J. Assessing heterogeneity in meta-analysis: Q statistic or I^2 index? *Psychol Methods*. 2006;11(2):193–206. doi:10.1037/1082-989X.11.2.193
46. McHugh ML. The Chi-square test of independence. *Biochem Med (Zagreb)*. 2013;23(2):143–149. doi:10.11613/BM.2013.018
47. Barili F, Parolari A, Kappetein PA, Freemantle N. Statistical Primer: Heterogeneity, random- or fixed-effects model analyses? *Interact Cardiovasc Thorac Surg*. 2018;27(3):317–321. doi:10.1093/icvts/ivy163
48. Andrade C. The p-value and statistical significance: Misunderstandings, explanations, challenges, and alternatives. *Indian J Psychol Med*. 2019;41(3):210–215. doi:10.4103/IJPSYM.IJPSYM_193_19
49. Leinonen V, Vanninen R, Rauramaa T. Raised intracranial pressure and brain edema. *Handb Clin Neurol*. 2018;145:25–37. doi:10.1016/B978-0-12-802395-2.00004-3
50. Mataczyński C, Kazimierska A, Uryga A, Kasprowicz M. Intracranial pressure pulse morphology-based definition of life-threatening intracranial hypertension episodes. In: *2022 44th Annual International Conference of the IEEE Engineering in Medicine & Biology Society (EMBC)*. Glasgow, UK: IEEE; 2022:1742–1746. doi:10.1109/EMBC48229.2022.9871403
51. Yun G, Baek SH, Kim S. Evaluation and management of hypernatremia in adults: Clinical perspectives. *Korean J Intern Med*. 2023;38(3):290–302. doi:10.3904/kjim.2022.346
52. Yamal JM, Hannay HJ, Gopinath S, Aisiku IP, Benoit JS, Robertson CS. Glasgow Outcome Scale measures and impact on analysis and results of a randomized clinical trial of severe traumatic brain injury. *J Neurotrauma*. 2019;36(17):2484–2492. doi:10.1089/neu.2018.5939
53. Bernhardt K, McClune W, Rowland MJ, Shah A. Hypertonic saline versus other intracranial-pressure-lowering agents for patients with acute traumatic brain injury: A systematic review and meta-analysis. *Neurocrit Care*. 2024;40(2):769–784. doi:10.1007/s12028-023-01771-9
54. Cook AM, Morgan Jones G, Hawryluk GWJ, et al. Guidelines for the acute treatment of cerebral edema in neurocritical care patients. *Neurocrit Care*. 2020;32(3):647–666. doi:10.1007/s12028-020-00959-7
55. Rowland M, Veenith T, Scomparin C, et al. Sugar or salt ("SOS"): A protocol for a UK multicentre randomised trial of mannitol and hypertonic saline in severe traumatic brain injury and intracranial hypertension [update in: *Cochrane Database Syst Rev*. 2020;1:CD010904. doi:10.1002/14651858.CD010904.pub3]. *J Intensive Care Soc*. 2022;23(2):222–232. doi:10.1177/1751143720901690
56. Chen H, Song Z, Dennis JA. Hypertonic saline versus other intracranial pressure-lowering agents for people with acute traumatic brain injury. *Cochrane Database Syst Rev*. 2019;1(1):CD010904. doi:10.1002/14651858.CD010904.pub2
57. Boone M, Oren-Grinberg A, Robinson T, Chen C, Kasper E. Mannitol or hypertonic saline in the setting of traumatic brain injury: What have we learned? *Surg Neurol Int*. 2015;6(1):177. doi:10.4103/2152-7806.170248
58. Dabrowski W, Siwicka-Gieroba D, Robba C, et al. Potentially detrimental effects of hyperosmolality in patients treated for traumatic brain injury. *J Clin Med*. 2021;10(18):4141. doi:10.3390/jcm10184141
59. Vella MA, Crandall ML, Patel MB. Acute management of traumatic brain injury. *Surg Clin North Am*. 2017;97(5):1015–1030. doi:10.1016/j.suc.2017.06.003
60. Freeman N, Welbourne J. Osmotherapy: Science and evidence-based practice [erratum in: *BJA Educ*. 2019;19(1):34. doi:10.1016/j.bjae.2018.10.002]. *BJA Educ*. 2018;18(9):284–290. doi:10.1016/j.bjae.2018.05.005

MiR-204-5p promoted maternally expressed gene 3 (*MEG3*) through *SP1*-mediated *DNMT1* pathway in trophoblast cells in recurrent miscarriage

Shasha Liu[A,B], Yue Wang[B,C], Yuling Guo[C], Xinran Xu[D], Yiping Gao[E], Lan Cheng[F]

Department of Obstetrics, Tianjin Central Hospital of Obstetrics and Gynecology, China

A – research concept and design; B – collection and/or assembly of data; C – data analysis and interpretation;
D – writing the article; E – critical revision of the article; F – final approval of the article

Advances in Clinical and Experimental Medicine, ISSN 1899–5276 (print), ISSN 2451–2680 (online) *Adv Clin Exp Med*. 2025;34(11):1841–1849

Address for correspondence
Lan Cheng
E-mail:chenlancl0b@126.com

Funding sources
The study was financially supported by the Tianjin Key Medical Discipline (Specialty) Construction Project (grant No. TJYXZDXK-043A).

Conflict of interest
None declared

Received on July 27, 2024
Reviewed on August 21, 2024
Accepted on November 13, 2024

Published online on April 8, 2025

Abstract

Background. Recurrent miscarriage (RM) affects 1–2% of couples. Maternally expressed gene 3 (*MEG3*) is aberrantly expressed in RM patients.

Objectives. To investigate a novel regulatory mechanism, we examined the *miR-204-5p*/Specificity protein 1 (*SP1*)/DNA methyltransferase 1 (*DNMT1*)/*MEG3* axis in the trophoblast cell line HTR-8/SVneo.

Materials and methods. Human trophoblast cell line HTR-8/SVneo was used and cells were transfected with siRNA targeting *SP1*, *miR-204-5p* mimics, pcDNA3.1-*DNMT1*, or their negative controls (NCs). The methylation inhibitor, 5-azadC, was used to treat the cells transfected with pcDNA3.1-*SP1*. The reverse transcription quantitative polymerase chain reaction (RT-qPCR) method was used to examine the relative RNA levels of *SP1*, *DNMT1* and *MEG3*. Western blot assay was performed to measure the protein levels of *SP1* and *DNMT1*. The dual-luciferase reporter gene assay was used to validate the *miR-204-5p* bindings to *SP1*. Functional assays were utilized to assess cell apoptosis, colony formation, migration, and invasion.

Results. *SP1* knockdown inhibited *DNMT1* and increased *MEG3* expression. The expression of *MEG3* was enhanced by methylation inhibition through 5-azadC, but *SP1* upregulation reversed this effect. *SP1* knockdown increased apoptosis and decreased migration and invasion, which was reversed by *DNMT1* overexpression. *SP1* was targeted and inhibited by *miR-204-5p*. *miR-204-5p* also inhibited *DNMT1*, and enhanced the expression of *MEG3*. *miR-204-5p* inhibited cell proliferation, migration and invasion, and promoted apoptosis. Overexpression of *SP1* partially reversed these effects by activating *DNMT1* and inhibiting *MEG3*.

Conclusions. *miR-204-5p* promoted *MEG3* expression in trophoblast cells via *SP1*-mediated *DNMT1* inhibition, leading to reduced cell migration, proliferation and invasion, as well as increased apoptosis. This study reveals a novel regulatory axis in trophoblast cells, providing insights into potential regulatory mechanisms in RM.

Key words: *MEG3*, *SP1*, *DNMT1*, recurrent miscarriage, trophoblast cells

Cite as
Liu S, Wang Y, Guo Y, Xu X, Gao Y, Cheng L. *MiR-204-5p* promoted maternally expressed gene 3 (*MEG3*) through *SP1*-mediated *DNMT1* pathway in trophoblast cells in recurrent miscarriage. *Adv Clin Exp Med*. 2025;34(11):1841–1849. doi:10.17219/acem/195925

DOI
10.17219/acem/195925

Background

Recurrent miscarriage (RM) affects 1–2% of women attempting to conceive, imposing both emotional and clinical burden.[1] Despite extensive research, the underlying causes of RM remain incompletely understood, often involving a complex interplay of genetic, epigenetic and environmental factors, including endocrine disruptors such as mancozeb.[2–7]

Recent advances in molecular biology have revealed the crucial role of extravillous trophoblast cells in maintaining a successful pregnancy by mediating implantation and placental development.[8] Previous research has also shown that severe acute respiratory syndrome coronavirus-2 (SARS-CoV-2) affects female reproductive health by targeting trophoblasts.[9] Dysfunction of trophoblasts is a well-established contributor to pregnancy loss.

Previously, specificity protein 1 (*SP1*), also known as a transcriptional factor *SP1*, was found to be reduced in the chorionic villus tissues in the placentas from RM patients, and the downregulation of *SP1* by upregulation of *miR-4497* could induce the apoptosis of trophoblast cells, which is associated with RM occurrences.[10,11] *SP1* regulates genes essential for cellular growth and differentiation, while *DNMT1* is correlated with DNA methylation patterns, and is of significance in maintaining genomic stability and gene expression.[12,13] Similar to *miR-4497*, *miR-204-5p* was also involved in studies focusing on unexplained recurrent spontaneous abortion.[14] *miR-204-5p* plays a role in placental development and function. For instance, *miR-204-5p* has been revealed to modulate the trophoblast cell proliferation and invasion, which are essential for proper placental development.[15] Dysregulation of *miR-204-5p* was revealed to be associated with pregnancy-related disorders, including preeclampsia (PE).[16,17] *miR-204-5p* expression was downregulated in PE and the upregulation of *miR-204-5p* was related to the decreased migration of trophoblast cells.[17]

Long non-coding RNA (lncRNA), such as maternally expressed gene 3 (*MEG3*), is a known regulator in tumor suppression and regulation of cell growth and death.[18] Studies have unveiled that *MEG3* expression is downregulated in blood samples, embryonic villus and chorionic villus tissues from RM patients, indicating its potential role in the pathogenesis of RM.[19–21] Further, *MEG3* was validated to stimulate the invasion and proliferation of trophoblast cells.[20,21] Similarly, in PE, downregulation of *MEG3* was discovered to increase apoptosis of trophoblast cells and inhibit cell invasion.[22] Previously, *DNMT1* was discovered to enhance methylation of *MEG3* promoter and decrease *MEG3* expression, thereby mediating the disease progression in breast cancer,[23] anemia,[24] diabetic retinopathy,[25] etc. However, such interaction between *DNMT1* and *MEG3* has not been validated in trophoblast cells.

In this study, we hypothesized that *miR-204-5p*/*SP1*/*DNMT1* axis plays a pivotal role in modulating trophoblast cell invasion, proliferation and apoptosis, processes essential for placental development and successful pregnancy, through *MEG3* modulation via epigenetic modifications.

Objectives

Our research aims to elucidate a novel modulatory mechanism of *miR-204-5p* in trophoblast cells via *SP1*/*DNMT1*/*MEG3* pathway and its impact on cell invasion, proliferation and apoptosis.

Materials and methods

Culture of cells

HTR-8/SVneo cells, derived from human first-trimester chorionic villi, were obtained from Procell (Wuhan, China). The cells were cultured in Roswell Park Memorial Institute Medium (RPMI) 1640 medium supplemented with 10% fetal bovine serum (FBS; Gibco, Waltham, USA) at 37°C in a humidified atmosphere containing 5% CO_2.

Cell transfection and treatment

Cells were reseeded in 6-well plates at a density of 5×10^5 cells per well and incubated overnight. On the 2nd day, cells were transfected with specific siRNAs, overexpressed plasmids, miRNA mimics, or their negative controls (NC) (GenePharma, Tianjin, China), using Lipofectamine 2000 kit (Invitrogen, Waltham, USA). Following the protocols, cells were transfected with 50 nM siRNA targeting *SP1* (si-*SP1*) or negative control siRNA (si-NC) (GenePharma). For miRNA overexpression, cells were transfected with 50 nM *miR-204-5p* mimics (*miR-204-5p*), mimics negative control (NC mimics). For overexpression of *SP1* or *DNMT1*, cells were collected for transfection, with 2 μg of pcDNA3.1 empty vector (Ctrl), pcDNA3.1-*SP1* (*SP1*) or pcDNA3.1-*DNMT1* (*DNMT1*) (GenePharma). In addition, the methylation inhibitor, 5-azadC (1 μM; Aladdin, Tianjin, China) was used to treat the cells for methylation inhibition.

RNA isolation and reverse transcription quantitative polymerase chain reaction method

RNA was extracted from all cell groups using TRIzol Kit (Beyotime, Beijing, China). Complementary DNA (cDNA) was synthesized using a PrimeScript RT reagent Kit (TaKaRa, Tokyo, Japan). The reverse transcription quantitative polymerase chain reaction (RT-qPCR) assay was performed using the SYBR Taq II Kit (TaKaRa) on Step OnePlus RT-PCR (Applied Biosystems, Waltham, USA). The specific primers used for RT-qPCR are listed below:

miR-204-5p:
Forward(F) 5'-TGCGGTTCCCTTTGTCATCCTATG-3';
Reverse (R) 5'-GTCGTATCCAGTGCAGGGTCCGAG-GTGCACTGGATACGACAGGCATAG-3'.

U6:
F 5'-CTCGCTTCGGCAGCACA-3',
R 5'-AACGCTTCACGAATTTGCGT-3'.
SP1:
F 5′-CTGGTCCCATCATCATCCGG-3′,
R 5′-TGTTTGGGCTTGTGGGTTCT-3′.
DNMT1:
F 5′-TGGTGAAGACGCCAGTGGA-3′,
R 5′-CGTGGCTGTGGAGGGATTTCG-3′.
MEG3:
F 5′-CGGCTGAAGAACTGCGGATGG-3′,
R 5′-CGTGGCTGTGGAGGGATTTCG-3′.
GAPDH:
F 5'-GCACCGTCAAGGCTGAGAAC-3',
R 5'- TGGTGAAGACGCCAGTGGA -3'.

The expression levels were analyzed in Microsoft Excel 2013 software (Microsoft Corp., Redmond, USA) using the $2^{-\Delta\Delta Ct}$ method, with U6 (for *miR-204-5p*) or GAPDH (for the rest) as the house keeping reference.

Western blot analysis

Cells were lysed in radioimmunoprecipitation assay (RIPA) buffer with phenylmethylsulfonyl fluoride (PMSF) (Beyotime). Proteins were separated by using the sodium dodecyl sulfate–polyacrylamide gel electrophoresis (SDS-PAGE) methods, and transferred to polyvinylidene difluoride (PVDF) (Millipore, St. Louis, USA). The membranes were then blocked in 5% skim milk for 1 h at room temperature and then incubated overnight at 4°C with the following primary antibodies: SP1 (1:1000, #5931; Cell Signaling Technology (CST), Danvers, USA), DNMT1 (1:1000, #5032; CST) and glyceraldehyde 3-phosphate dehydrogenase (GAPDH) (1:10,000, AB2000; Abways, Tianjin, China). Membranes were incubated with horseradish peroxidase (HRP)-conjugated secondary antibodies (1:20,000, AB0101; Abways) for 1 h at room temperature. Immunoblots were then visualized using an enhanced chemiluminescence (ECL) kit, and images were captured using the SCG-W3000 imaging system (ServiceBio, Wuhan, China).

Dual-luciferase reporter assays

The binding sites were predicted using StarBase database (https://rnasysu.com/encori). The pmirGLO-*SP1*-3′UTR-wild type (*SP1*-UTR-wt) and mutant type (*SP1*-UTR-mt) were constructed using the pmirGLO vector (Promega, Madison, USA). Cells were co-transfected with 50 ng of *SP1*-UTR-wt or *SP1*-UTR-mt and 50 nM *miR-204-5p* mimics/inhibitors, or respective controls (GenePharma). After 48 h, luciferase activity was measured on a multifunctional microplate after using the Dual-Luciferase Reporter Assay kit (Beyotime).

Flow cytometry for apoptosis analysis

Apoptosis was assessed using Cell Apoptosis Kit (Bioss, Beijing, China). Transfected cells were collected, washed with precooled phosphate-buffered saline (PBS) and suspended using binding buffer. As per the manufacturer's protocol, cells were stained in Annexin V-FITC and propidium iodide (PI) for 15 min at room temperature in dark. Cell apoptosis was analyzed with flow cytometry (BD FACSCanto II; BD Biosciences, Franklin Lakes, USA).

Colony formation assay

Cells after transfection were collected and reseeded in 6-well plates with a density of 600 cells per well. Cells were observed every day till the formation of colonies. Cells were fixed using 4% paraformaldehyde for 20 min and then stained with 0.1% crystal violet for 30 min in dark. Colonies with more than 50 cells were counted in each group.

Transwell assays

The transwell chambers with 8-μm pores were obtained from Jet Biotech (Guangzhou, China). For migration assays, cells were washed in PBS twice and seeded in the upper chamber with serum-free medium at a density of 5×10^4 per well, while culture medium with 15% FBS was added in the lower chamber. For invasion assays, the upper chambers were pre-coated with Matrigel (Corning Company, Corning, USA). Cells were observed under an optical microscope (model Ts2; Nikon Corp., Tokyo, Japan) every 6 h. After 36 h, cells that had migrated or invaded to the lower surface were washed using PBS twice gently and fixed using 4% paraformaldehyde for 20 min, and then stained in crystal violet for 30 min. Cells were then observed and counted under an optical microscope (model Ts2; Nikon Corp.) from 5 different fields.

Statistical analyses

Due to the small sample size, non-normal distribution was assumed. The statistical significance of difference was determined with the nonparametric Kruskal–Wallis test with Dunn's post hoc test, and Mann–Whitney U test for comparison within 2 groups using GraphPad v. 9.0 (GraphPad Software, San Diego, USA). Bonferroni correction was performed for multiple testing. The results from statistical analysis in this study were included in Supplementary Tables 1 and 2. The figures were generated based on statistical data and cell images from experiments mentioned above using GraphPad. Data in replicates are presented in figures as scatter dots with the median and range lines. The p-values less than 0.05 were considered statistically significant.

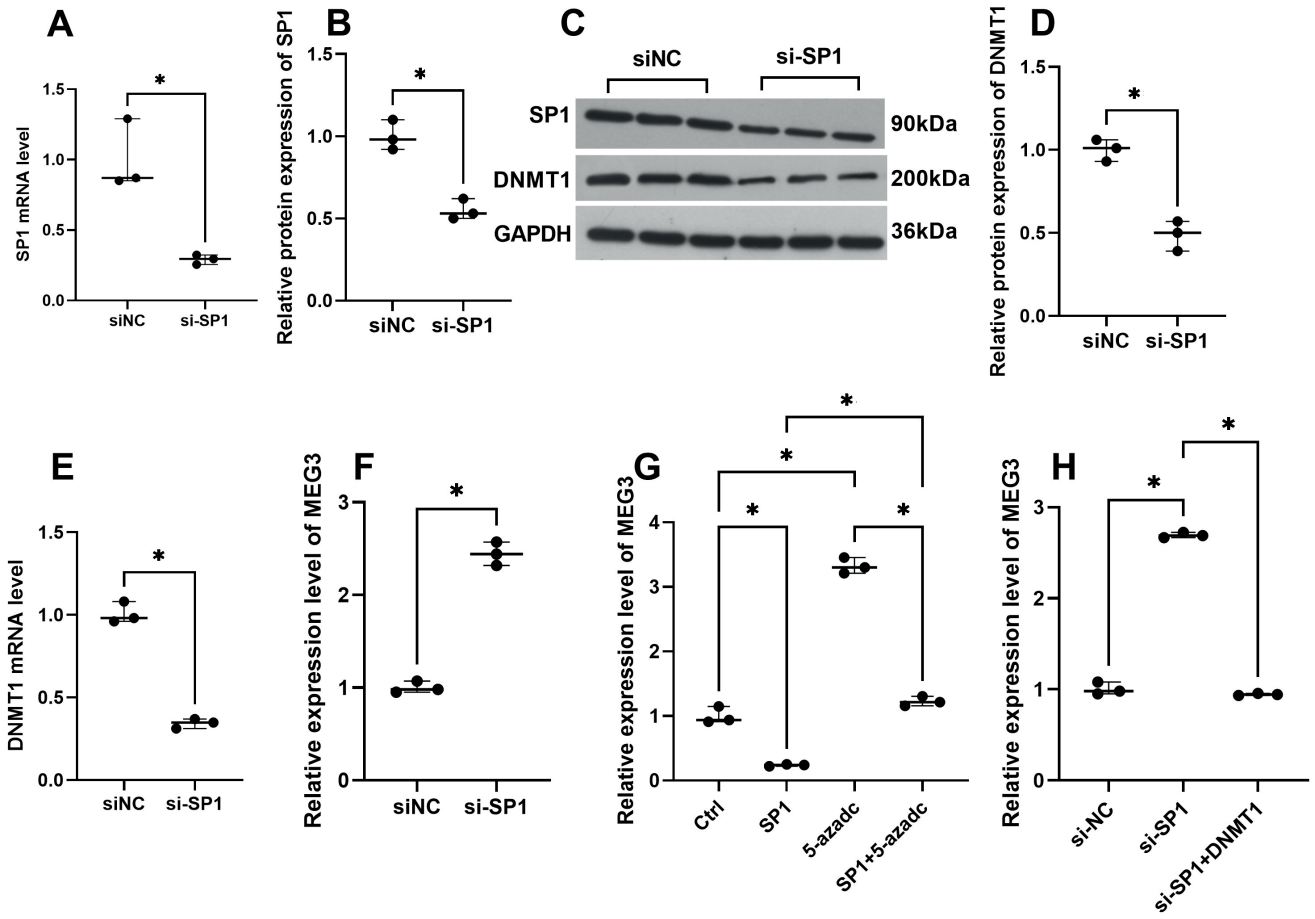

Fig. 1. Downregulation of *SP1* promoted *MEG3* through methylation inhibition in trophoblast cells. A. HTR-8/SVneo cells were transfected with siRNA that targeted *SP1* (si-*SP1*) and its control (si-NC). The reverse transcription quantitative polymerase chain reaction (RT-qPCR) method was used to determine the mRNA levels of *SP1* with reference to GAPDH; B–D. Western blot method was used to analyze the protein expression levels of *SP1* and *DNMT1*; E,F. The RNA levels of *DNMT1* and *MEG3* were analyzed by applying the RT-qPCR method; G. Cells were transfected with pcDNA3.1 empty vector (Ctrl) and plasmid overexpressing *SP1*(*SP1*), and then the transfected cells were further divided by treatment of methylation inhibitor, 5-azadC. *MEG3* expression was measured; H. Cells were transfected with si-*SP1* alone, or co-transfected with pcDNA3.1 plasmid overexpressing *DNMT1*(*DNMT1*) and si-*SP1*. *MEG3* expression was measured. Data in replicates are presented in figures as scatter dots with the median and range lines. Kruskal–Wallis test with Dunn's post hoc and Bonferroni correction was performed for multiple comparisons, and Mann–Whitney U test for comparison within 2 groups

*p < 0.050. *SP1* – specificity protein 1; DNMT1 – DNA methyltransferase 1; si-*SP1* – siRNA targeting SP1; si-NC – siRNA negative control; *MEG3* – maternally expressed gene 3.

Results

Downregulation of *SP1* promoted *MEG3* through methylation inhibition in trophoblast cells

SP1 mRNA and protein levels were inhibited in HTR-SV/neo cells transfected with si-*SP1* (Fig. 1A–C). Furthermore, *SP1* knockdown in cells inhibited both *DNMT1* mRNA and protein levels (Fig. 1C–E). Additionally, SP1 knockdown upregulated *MEG3* expression, an effect that was reversed by *DNMT1* overexpression (Fig. 1F,H). A methylation inhibitor, 5-azadC, promoted the *MEG3* expression and overexpression of *SP1* could partly reverse the effect of 5-azadC (Fig. 1G). The findings suggest that *SP1* knockdown enhanced *MEG3* by *DNMT1*-mediated methylation in trophoblast cells.

SP1 knockdown decreased trophoblast cell invasion, proliferation and migration and increased apoptosis through *DNMT1* modulation

Downregulation of *SP1* induced cell apoptosis in HTR-SV/neo cells but the overexpression of *DNMT1* could counteract this (Fig. 2A). Colony formation results showed that the number of colonies was decreased by *SP1* knockdown but was restored by the overexpression of *DNMT1* (Fig. 2B). Cell migration and invasion were also inhibited by *SP1* knockdown and restored by *DNMT1* overexpression (Fig. 2C,D).

miR-204-5p inhibited *SP1/DNMT1* by targeting *SP1* in HTR-8/SVneo cells

Based on predictions from the Starbase database, miR-204-5p is predicted to bind to SP1, and the putative binding

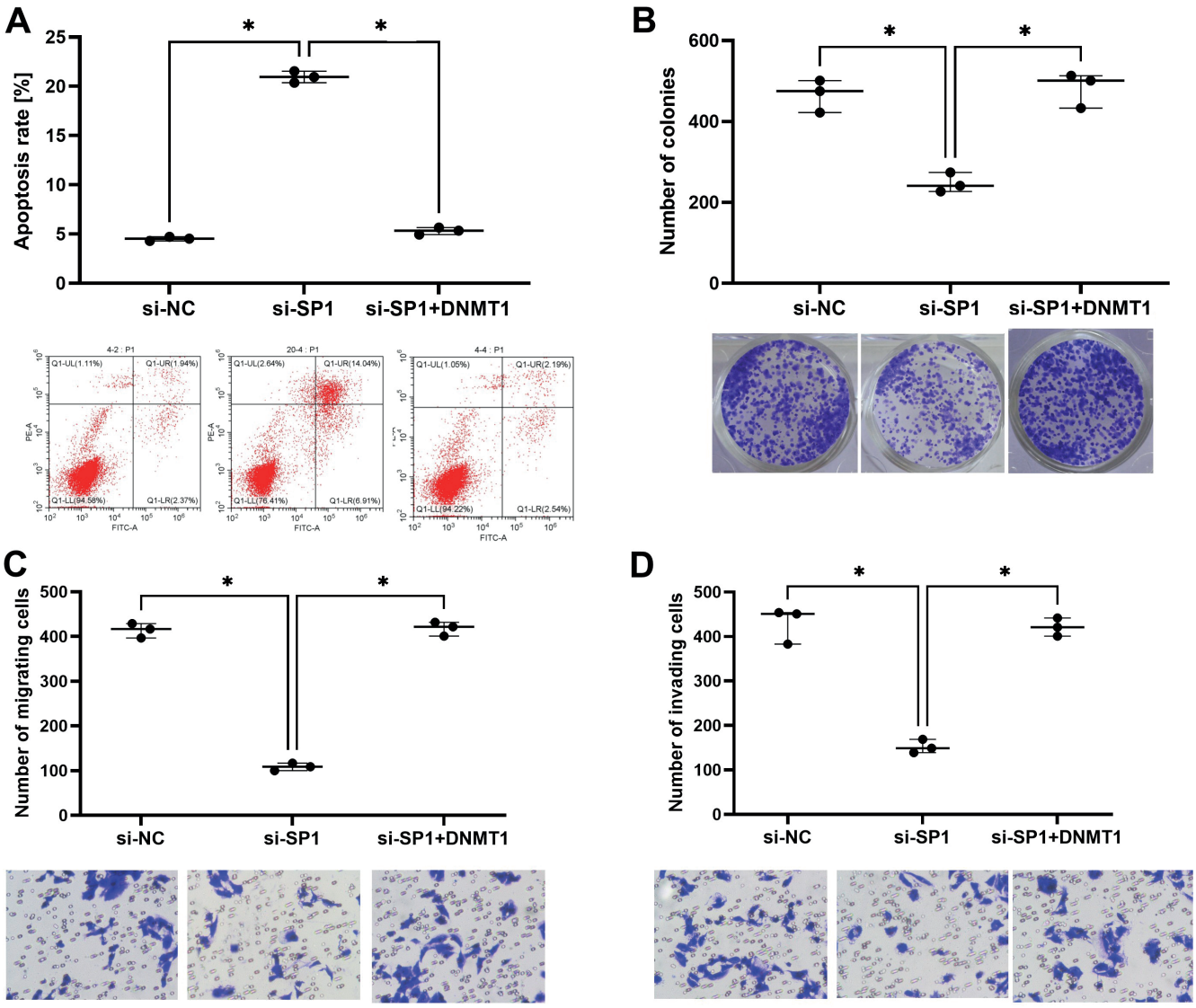

Fig. 2. *SP1* knockdown decreased cell invasion and migration and increased apoptosis through *DNMT1* modulation in trophoblast cells. HTR-8/SVneo cells were transfected with si-*SP1* alone, or together with pcDNA3.1-*DNMT1*. A. Flow cytometry method was used to analyze cellular apoptosis; B. Colony formation assays were performed to analyze cell proliferation; C,D. Transwell assays were performed to analyze the cell capability of invasion and migration in each group. Data in replicates are presented in figures as scatter dots with the median line and range lines. Kruskal–Wallis test with Dunn's post hoc and Bonferroni correction was performed for multiple comparisons, and Mann–Whitney U test for comparison within 2 groups

*p < 0.050. *SP1* – specificity protein 1; *DNMT1* – DNA methyltransferase 1; si-*SP1* – siRNA targeting SP1; si-NC – siRNA negative control; *MEG3* – maternally expressed gene 3.

sites are illustrated in Fig. 3A. The cells were transfected with *miR-204-5p* mimics (*miR-204-5p*) or its negative control (NC mimics), *miR-204-5p* inhibitor or its negative control (inhibitor NC), and the pmirGLO plasmids containing the *SP1*-UTR-wt/mt. Dual luciferase reporter gene assays were performed to analyze the relative luciferase activity, and results showed that the relative luciferase activity was significantly reduced in cells co-transfected with *miR-204-5p* and *SP1*-UTR-wt and increased in cells transfected with *miR-204-5p* inhibitor and *SP1*-UTR-wt (Fig. 3B). In addition, *miR-204-5p* upregulation inhibited *SP1* and *DNMT1* in mRNA and protein levels (Fig. 3C–G). Conversely, overexpression of *miR-204-5p* upregulated *MEG3* expression, an effect that was reversed by overexpression of *SP1* (Fig. 3H). The inhibitory effect of *miR-204-5p* on *SP1*/*DNMT1* could be reversed by overexpression of *SP1* (Fig. 3I–K).

miR-204-5p regulated the invasion and migration of trophoblast cells by targeting *SP1*

Overexpression of *miR-204-5p* inhibited cell proliferation, invasion and migration but the inhibitory effect was recovered by *SP1* overexpression in HTR-8/SVneo cells (Fig. 4A,C,D). On the contrary, *miR-204-5p* overexpression enhanced apoptosis rates and *SP1* overexpression reversed this (Fig. 4B).

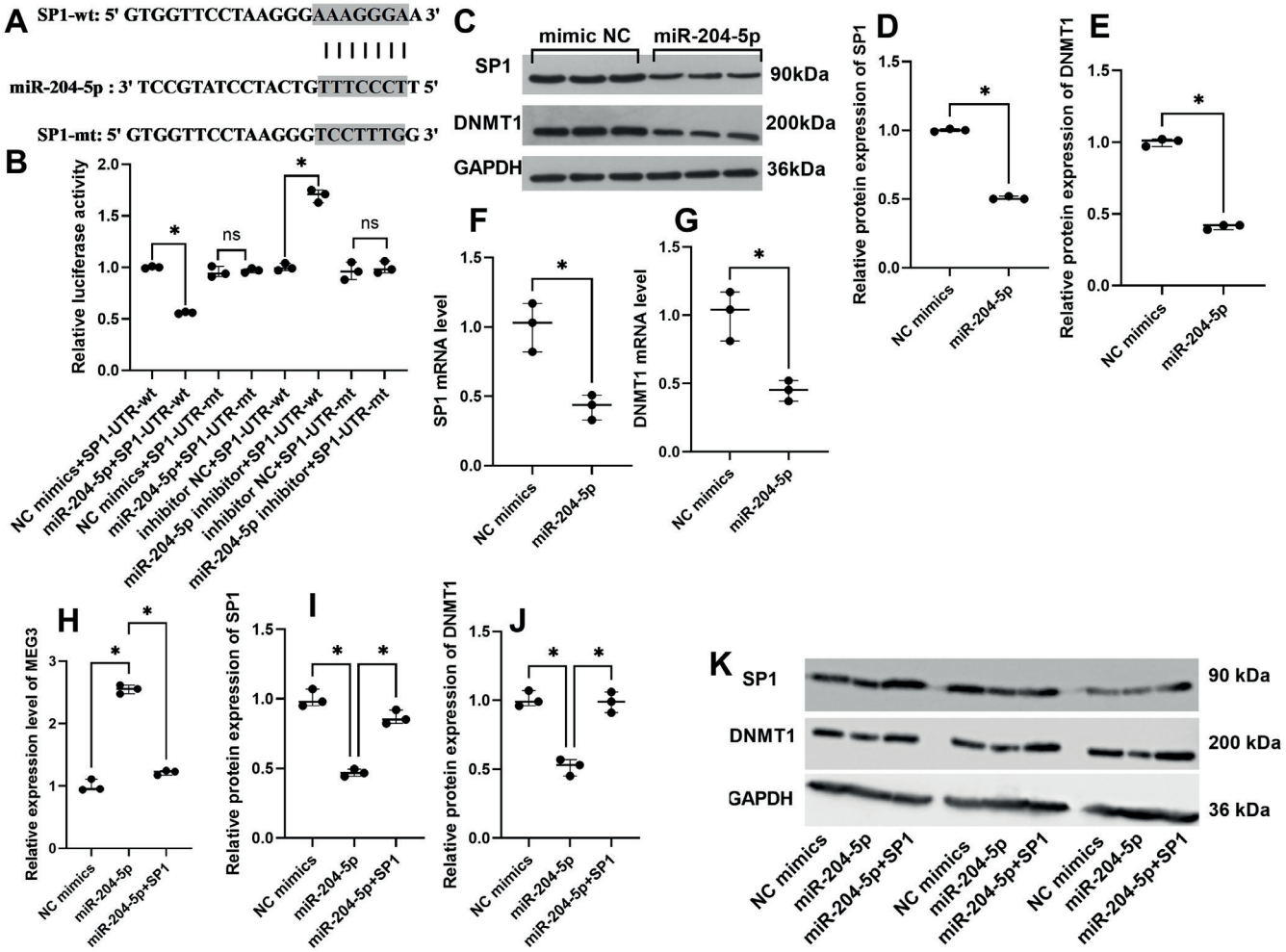

Fig. 3. *miR-204-5p* inhibited *SP1/DNMT1* by targeting *SP1* in HTR-8/SVneo cells. A. The binding sites between *SP1* and *miR-204-5p* were predicted using StarBase database; B. pmirGLO-*SP1*-3'UTR-wild type (*SP1*-UTR-wt) and mutant type (*SP1*-UTR-mt) were constructed using pmirGLO vector. Then, cells were transfected with *miR-204-5p* mimics (*miR-204-5p*) or its negative control (NC mimics), or *miR-204-5p* inhibitor or its negative control (inhibitor NC). Dual luciferase reporter gene assays were performed to analyze the relative luciferase activity; C–E. The protein expression levels of *SP1* and *DNMT1* were measured in cells with *miR-204-5p* upregulation; F–G. The mRNA levels of *SP1* and *DNMT1*; H. Cells were transfected with *miR-204-5p* mimic, or co-transfected with *miR-204-5p* mimic and pcDNA3.1-*SP1*. *MEG3* expression was measured; I–K. Western blot analysis for protein levels of *SP1* and *DNMT1*. Data in replicates are presented in figures as scatter dots with the median and range lines. Kruskal–Wallis test with Dunn's post hoc and Bonferroni correction was performed for multiple comparisons, and Mann–Whitney U test for comparison within 2 groups

*p < 0.050, ns – not significant. *SP1* – specificity protein 1; *DNMT1* – DNA methyltransferase 1; si-*SP1* – siRNA targeting SP1; si-NC – siRNA negative control; *MEG3* – maternally expressed gene 3.

Discussion

This study advances the understanding of epigenetic regulation in RM. By elucidating the *miR-204-5p*/*SP1*/*DNMT1*/*MEG3* axis, it provides insights into the molecular pathways contributing to trophoblast cell function and pregnancy maintenance. Specifically, it identifies *miR-204-5p* as a critical regulator of *SP1* and *DNMT1*, influencing *MEG3* expression and thereby affecting trophoblast cell behavior. These findings suggest potential therapeutic targets for managing RM, focusing on the modulation of *miR-204-5p* and its downstream effectors. In this study, we demonstrated that *SP1* knockdown leads to a significant reduction in *DNMT1* levels, which in turn upregulates *MEG3* expression. This finding is consistent with existing literature that indicates *SP1* enhances *DNMT1* transcription.[26] It was unveiled previously that protein expression levels of *SP1* and *DNMT1* were significantly low in human villous specimen from RM patients, in comparison with those from the patients with induced abortion or sporadic abortion; in vitro, knockdown of *SP1* or *DNMT1* could decrease the invasion and migration in trophoblast cells.[27] In our study, the increase in apoptosis and decrease in migration and invasion following *SP1* knockdown in trophoblast cells also reveal critical roles of *SP1* in maintaining cell function. Further, these effects were reversed by *DNMT1* overexpression, highlighting *DNMT1*'s role in cell proliferation and motility, and indicating that *SP1* modulated the cell phenotypes via *DNMT1*. Such interactions have been well documented in cancer cells, where *SP1* increases the activity of *DNMT1*,

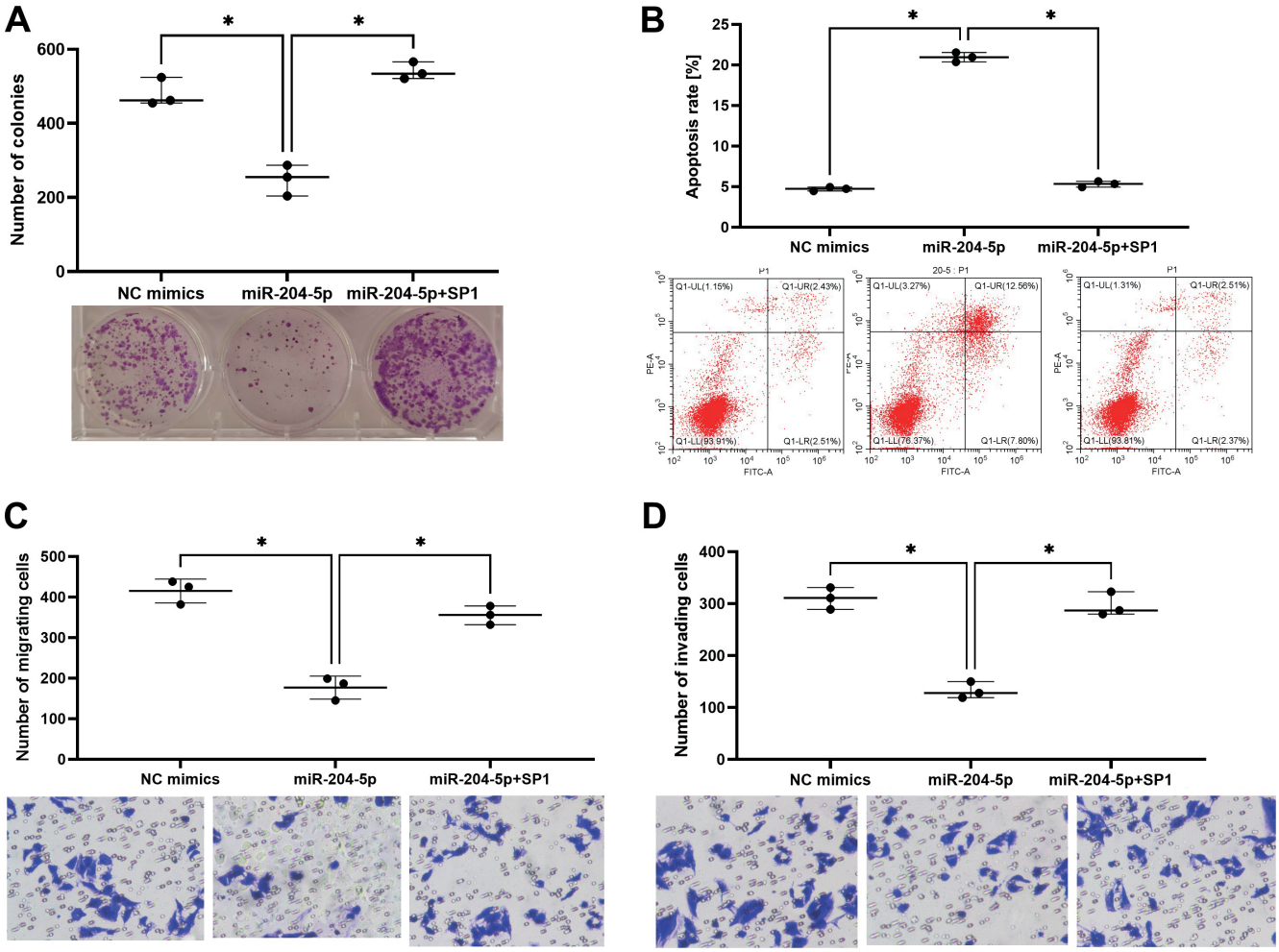

Fig. 4. *miR-204-5p* decreased HTR-8/SVneo cell invasion and migration and increased apoptosis through targeting *SP1*. Cells were transfected with *miR-204-5p* mimic, or co-transfected with *miR-204-5p* mimic and pcDNA3.1-*SP1*. A. Colony formation; B. Apoptosis rates; C,D. Migration and invasion. Data in replicates are presented in figures as scatter dots with the median and range lines. Kruskal–Wallis test with Dunn's post hoc and Bonferroni correction was performed for multiple comparisons, and Mann–Whitney U test for comparison within 2 groups

*p < 0.050. *SP1* – specificity protein 1; *DNMT1* – DNA methyltransferase 1; si-*SP1* – siRNA targeting SP1; si-NC – siRNA negative control; *MEG3* – maternally expressed gene 3.

DNMT3A and *DNMT3B*, leading to hypermethylation of tumor suppressor gene.[28–30] In our study, the decreased *DNMT1* levels following *SP1* knockdown suggest a similar regulatory mechanism in trophoblast cells, underscoring the broader implications of *SP1-DNMT1* interactions beyond oncogenesis. In addition, the methylation inhibitor, 5-azadC, was used to induce the cells and we found that *MEG3* expression was increased by 5-azadC, suggesting that *MEG3* was regulated in trophoblast cells likely due to methylation. Furthermore, upregulation of *SP1*/*DNMT1* in cells was found to partly reverse the change in *MEG3* expression induced by 5-azadC. These results suggest that *SP1*/*DNMT1* inhibited *MEG3* expression via methylation regulation.

Previously, *DNMT1* was identified to be essential for maintaining DNA methylation patterns during DNA replication, crucial for gene silencing and genomic stability.[31,32] For instance, in breast cancer, *MEG3* expression was enhanced by knockdown of *DNMT1* through demethylation of *MEG3* promoter.[23,33] Our findings extend the interaction of *DNMT1*/*MEG3* to trophoblast cells, suggesting that *DNMT1*-mediated methylation is vital for placental development and function.

A significant finding of this study is that *miR-204-5p* directly targets *SP1*, leading to decreased levels of both *SP1* and *DNMT1*, which in turn upregulates *MEG3* expression in trophoblast cells. This regulatory pathway was confirmed through dual-luciferase activity, RT-qPCR and western blot methods; *miR-204-5p* has been previously identified as a tumor suppressor in various cancers, regulating genes involved in proliferation and apoptosis.[34,35] Our study shows that *miR-204-5p* similarly impacts the apoptosis, invasion and migration of trophoblast cells, highlighting its role in reproductive health. *MEG3* expression was increased by *miR-204-5p* overexpression, which was reversed by *SP1* overexpression, indicates a complex regulatory mechanism involving *miR-204-5p*, *SP1* and *DNMT1* in trophoblast cells.

Limitations

Despite the significant findings, this study has limitations. First, the research was conducted in vitro using HTR-8/SVneo trophoblast cells, which may not fully replicate in vivo environment of placental tissue. Second, although the study identifies *miR-204-5p* as a regulator of *SP1* and *DNMT1*, the broader regulatory network involving other miRNAs and transcription factors was not explored. Additionally, the clinical relevance of these findings needs further validation through studies involving human study participants and clinical samples.

Conclusions

The elucidation of the *miR-204-5p*/*SP1*/*DNMT1*/*MEG3* pathway offers new perspectives on the molecular mechanisms in regulating trophoblast cells. Future research should explore therapeutic interventions targeting this pathway to improve pregnancy outcomes in preclinical animal studies. Additionally, investigating other miRNAs and lncRNAs involved in trophoblast function could further enhance the understanding of the complex regulatory networks in placental development.

Supplementary data

The supplementary materials are available at https://doi.org/10.5281/zenodo.14043134. The package includes the following files:

Supplementary Table 1. The results of homogeneity of variance test.

Supplementary Table 2. Statistical methods (Mann–Whitney U test) and test results used.

Supplementary Table 3. Kruskal–Wallis test with Dunn's post hoc and Bonferroni correction and test results used.

Data availability

The datasets generated and/or analyzed during the current study are available from the corresponding author on reasonable request.

Consent for publication

Not applicable.

Use of AI and AI-assisted technologies

Not applicable.

ORCID iDs

Shasha Liu https://orcid.org/0000-0001-6516-7168
Yue Wang https://orcid.org/0009-0001-3433-4960
Yuling Guo https://orcid.org/0009-0009-9825-9398
Xinran Xu https://orcid.org/0009-0008-0916-0488
Yiping Gao https://orcid.org/0009-0009-4411-7204
Lan Cheng https://orcid.org/0009-0004-9164-2646

References

1. Dunne J, Foo D, Dachew BA, et al. Diabetic and hypertensive disorders following early pregnancy loss: A systematic review and meta-analysis. *eClinicalMedicine*. 2024;71:102560. doi:10.1016/j.eclinm.2024.102560
2. Lin YJ, Chang WH, Kuo PL, Chen HC, Chang WT, Huang PC. Oxidative/nitrosative stress increased the risk of recurrent pregnancy loss: Taiwan Recurrent Pregnancy Loss and Environmental Study (TREPLES). *Redox Biol*. 2023;68:102940. doi:10.1016/j.redox.2023.102940
3. Sun JX, Yao Y, Li WX, et al. Upregulation of *GPR133* expression impaired the phagocytosis of macrophages in recurrent spontaneous miscarriage. *Epigenetics*. 2024;19(1):2337087. doi:10.1080/15592294.2024.2337087
4. Mu F, Wang M, Zeng X, Wang F. Predicting risk of subsequent pregnancy loss among women with recurrent pregnancy loss: An immunological factor-based multivariable model. *Am J Reprod Immunol*. 2024;91(3):e13837. doi:10.1111/aji.13837
5. Kuroda K. A review of the optimization of thyroid function, thrombophilia, immunity and uterine milieu: OPTIMUM treatment strategy for recurrent implantation failure and recurrent pregnancy loss. *Reprod Med Biol*. 2024;23(1):e12561. doi:10.1002/rmb2.12561
6. Bamba C, Rohilla M, Kumari A, Kaur A, Srivastava P. Influence of forkhead box protein 3 gene polymorphisms in recurrent pregnancy loss: A meta-analysis. *Placenta*. 2024;146:79–88. doi:10.1016/j.placenta.2024.01.003
7. Bianchi S, Nottola SA, Torge D, Palmerini MG, Necozione S, Macchiarelli G. Association between female reproductive health and mancozeb: Systematic review of experimental models. *Int J Environ Res Public Health*. 2020;17(7):2580. doi:10.3390/ijerph17072580
8. Liu Z, Wang C, Tang Y, et al. ENO1 promotes trophoblast invasion regulated by E2F8 in recurrent miscarriage. *FASEB J*. 2024;38(8):e23631. doi:10.1096/fj.202302032RR
9. Torge D, Bernardi S, Arcangeli M, Bianchi S. Histopathological features of SARS-CoV-2 in extrapulmonary organ infection: A systematic review of literature. *Pathogens*. 2022;11(8):867. doi:10.3390/pathogens11080867
10. Safe S, Imanirad P, Sreevalsan S, Nair V, Jutooru I. Transcription factor SP1, also known as specificity protein 1 as a therapeutic target. *Exp Opin Ther Targets*. 2014;18(7):759–769. doi:10.1517/14728222.2014.914173
11. Tang H, Pan L, Xiong Y, et al. Down-regulation of the SP1 transcription factor by an increase of microRNA-4497 in human placenta is associated with early recurrent miscarriage. *Reprod Biol Endocrinol*. 2021;19(1):21. doi:10.1186/s12958-021-00701-8
12. Deng K, Wu M. Leucine-rich repeats containing 4 protein (LRRC4) in memory, psychoneurosis, and glioblastoma. *Chin Med J (Engl)*. 2023;136(1):4–12. doi:10.1097/CM9.0000000000002441
13. Qiu W, Guo Q, Guo X, et al. Mesenchymal stem cells, as glioma exosomal immunosuppressive signal multipliers, enhance MDSCs immunosuppressive activity through the miR-21/SP1/DNMT1 positive feedback loop. *J Nanobiotechnol*. 2023;21(1):233. doi:10.1186/s12951-023-01997-x
14. Liu X, Wu J, Nie H, et al. Comprehensive analysis of circRNAs, miRNAs, and mRNAs expression profiles and ceRNA networks in decidua of unexplained recurrent spontaneous abortion. *Front Genet*. 2022;13:858641. doi:10.3389/fgene.2022.858641
15. Yu Y, Wang L, Gao M, Guan H. Long non-coding RNA TUG1 regulates the migration and invasion of trophoblast-like cells through sponging miR-204-5p. *Clin Exp Pharmacol Physiol*. 2019;46(4):380–388. doi:10.1111/1440-1681.13058
16. Yu Y, Wang L, Liu T, Guan H. MicroRNA-204 suppresses trophoblast-like cell invasion by targeting matrix metalloproteinase-9. *Biochem Biophys Res Commun*. 2015;463(3):285–291. doi:10.1016/j.bbrc.2015.05.052

17. Ding Y, Yuan X, Gu W, Lu L. Treatment with metformin prevents preeclampsia by suppressing migration of trophoblast cells via modulating the signaling pathway of UCA1/miR-204/MMP-9. *Biochem Biophys Res Commun*. 2019;520(1):115–121. doi:10.1016/j.bbrc.2019.09.099
18. Hayashi-Okada M, Sato S, Nakashima K, et al. Identification of long noncoding RNAs downregulated specifically in ovarian high-grade serous carcinoma. *Reprod Med Biol*. 2024;23(1):e12572. doi:10.1002/rmb2.12572
19. Al-Rubaye S, Ghaderian SMH, Salehpour S, et al. Aberrant expression of BAX, MEG3, and miR-214-3P genes in recurrent pregnancy loss. *Gynecol Endocrinol*. 2021;37(7):660–664. doi:10.1080/09513590.2021.1897098
20. Zhang J, Liu X, Gao Y. The long noncoding RNA MEG3 regulates Ras-MAPK pathway through RASA1 in trophoblast and is associated with unexplained recurrent spontaneous abortion. *Mol Med*. 2021;27(1):70. doi:10.1186/s10020-021-00337-9
21. Zhang J, Liu X, Gao Y. FTO protein regulates the TGF-β signalling pathway through RNA N6-methyladenosine modification to induce unexplained recurrent spontaneous abortion. *FEBS J*. 2024;291(7):1545–1559. doi:10.1111/febs.17053
22. Wang R, Zou L. Downregulation of LncRNA-MEG3 promotes HTR8/SVneo cells apoptosis and attenuates its migration by repressing Notch1 signal in preeclampsia. *Reproduction*. 2020;160(1):21–29. doi:10.1530/REP-19-0614
23. Pan T, Ding H, Jin L, et al. DNMT1-mediated demethylation of lncRNA MEG3 promoter suppressed breast cancer progression by repressing Notch1 signaling pathway. *Cell Cycle*. 2022;21(21):2323–2337. doi:10.1080/15384101.2022.2094662
24. Li H, Xu X, Wang D, et al. Hypermethylation-mediated downregulation of long non-coding RNA MEG3 inhibits osteogenic differentiation of bone marrow mesenchymal stem cells and promotes pediatric aplastic anemia. *Int Immunopharmacol*. 2021;93:107292. doi:10.1016/j.intimp.2020.107292
25. He Y, Dan Y, Gao X, Huang L, Lv H, Chen J. DNMT1-mediated lncRNA MEG3 methylation accelerates endothelial-mesenchymal transition in diabetic retinopathy through the PI3K/Akt/mTOR signaling pathway. *Am J Physiol Endocrinol Metab*. 2021;320(3):E598–E608. doi:10.1152/ajpendo.00089.2020
26. Duan P, Huang X, Ha M, Li L, Liu C. miR-142-5p/DAX1-dependent regulation of P450c17 contributes to triclosan-mediated testosterone suppression. *Sci Total Environ*. 2020;717:137280. doi:10.1016/j.scitotenv.2020.137280
27. Li S, Zhai J, Liu J, et al. BMAL1 facilitates trophoblast migration and invasion via SP1-DNMT1/DAB2IP pathway in recurrent spontaneous abortion. *Oncotarget*. 2017;8(52):89451–89464. doi:10.18632/oncotarget.20702
28. Wang XX, Guo GC, Qian XK, et al. miR-506 attenuates methylation of lncRNA MEG3 to inhibit migration and invasion of breast cancer cell lines via targeting SP1 and SP3. *Cancer Cell Int*. 2018;18(1):171. doi:10.1186/s12935-018-0642-8
29. Ren G, Li H, Hong D, et al. LINC00955 suppresses colorectal cancer growth by acting as a molecular scaffold of TRIM25 and SP1 to inhibit DNMT3B-mediated methylation of the PHIP promoter. *BMC Cancer*. 2023;23(1):898. doi:10.1186/s12885-023-11403-2
30. Chuang TD, Khorram O. Glucocorticoids regulate MiR-29c levels in vascular smooth muscle cells through transcriptional and epigenetic mechanisms. *Life Sci*. 2017;186:87–91. doi:10.1016/j.lfs.2017.08.007
31. Yuan L, Liang X, He L. Unveiling dissociation mechanisms and binding patterns in the UHRF1-DPPA3 complex via multi-replica molecular dynamics simulations. *J Mol Model*. 2024;30(6):173. doi:10.1007/s00894-024-05946-9
32. Işık A, Fırat D. Letter to the editor concerning "Most cited 100 articles from Turkey on abdominal wall hernias: A bibliometric study." *Turk J Surg*. 2021;37(2):193–194. doi:10.47717/turkjsurg.2021.4973
33. Zhu X, Lv L, Wang M, et al. DNMT1 facilitates growth of breast cancer by inducing MEG3 hyper-methylation. *Cancer Cell Int*. 2022;22(1):56. doi:10.1186/s12935-022-02463-8
34. Ma X, Chen Z, Chen W, et al. LncRNA AL139294.1 can be transported by extracellular vesicles to promote the oncogenic behaviour of recipient cells through activation of the Wnt and NF-κB2 pathways in non-small-cell lung cancer. *J Exp Clin Cancer Res*. 2024;43(1):20. doi:10.1186/s13046-023-02939-z
35. Jiang W, Yu Y, Ou J, Li Y, Zhu N. Exosomal circRNA RHOT1 promotes breast cancer progression by targeting miR-204-5p/PRMT5 axis. *Cancer Cell Int*. 2023;23(1):260. doi:10.1186/s12935-023-03111-5

Mesoderm/mesenchyme homeobox I as a potential target that orchestrates hepatic stellate cell activation

Jie Ruan[1,A,D], Ying Xie[2,B,D], Huifang Zhou[3,C,D], Libo Su[2,C,D], Chao Liu[2,B,D,E], Chaoqun Zhang[1,D,E], Sun Dianxing[1,3,D–F]

[1] Department of Internal Medicine, Hebei Medical University, Shijiazhuang, China
[2] Hebei Key Laboratory of Laboratory Animal Science, Hebei Medical University, Shijiazhuang, China
[3] The Liver Disease Center of PLA, The 980th Hospital of PLA Joint Logistics Support Force, Shijiazhuang, China

A – research concept and design; B – collection and/or assembly of data; C – data analysis and interpretation; D – writing the article; E – critical revision of the article; F – final approval of the article

Advances in Clinical and Experimental Medicine, ISSN 1899–5276 (print), ISSN 2451–2680 (online) *Adv Clin Exp Med*. 2025;34(11):1851–1862

Address for correspondence
Sun Dianxing
E-mail: sundx9@163.com

Funding sources
This study was supported by a grant from the National Natural Science Foundation of China (No. 81672041, http://isisn.nsfc.gov.cn/egrantweb).

Conflict of interest
None declared

Acknowledgements
The authors would like to express their gratitude to Hebei Key Laboratory of Laboratory Animal Science, which contributed to the efficacy of the experimental technique.

Received on July 23, 2024
Reviewed on November 16, 2024
Accepted on December 12, 2024

Published online on March 12, 2025

Cite as
Ruan J, Xie Y, Zhou H, et al. Mesoderm/mesenchyme homeobox I as a potential target that orchestrates hepatic stellate cell activation. *Adv Clin Exp Med*. 2025;34(11):1851–1862. doi:10.17219/acem/197320

DOI
10.17219/acem/197320

Abstract

Background. Hepatic stellate cell (HSC) activation is a critical factor in the development of liver fibrosis. Recent research indicates that mesoderm/mesenchyme homeobox 1 (*Meox1*) contributes to fibrosis in organs like the skin and heart.

Objectives. To investigate the potential impact of *Meox1* on HSC activation and provide an available target for hepatic fibrosis research.

Materials and methods. The human HSC cell line LX-2 was utilized to investigate the role of *Meox1* in HSC activation. Fibrotic gene expression was analyzed, and assays were conducted to assess cell proliferation, migration and the cell cycle.

Results. *Meox1* was identified as a positive regulator of HSC activation. We found that transforming growth factor-β1 (TGF-β1) treatment significantly upregulated *Meox1* expression in a dose-dependent manner in LX-2 cells, and the expression levels of α-smooth muscle actin (α-SMA), collagen type I (collagen-I) and matrix metalloproteinase-2 (MMP-2) also increased progressively with higher concentrations of TGF-β1. Knockdown of *Meox1* via small interfering RNA (siRNA) inhibited TGF-β1-induced expression of HSC activation markers and fibrotic genes, including α-SMA, collagen-I and MMP-2. Conversely, *Meox1* overexpression promoted HSC activation, evidenced by increased levels of α-SMA, collagen-I and MMP-2. Meanwhile, *Meox1* overexpression accelerated cell proliferation and enhanced cell migration. Additionally, forced expression of *Meox1* in LX-2 cells elevated Smad3 phosphorylation level, although TGF-β1 and total Smad3 protein levels remained unchanged. Furthermore, we observed that *Meox1* could induce a redistribution of the cell population, extending the G1 phase, and that *Meox1*-upregulated p21CIP1/WAF1 expression in LX-2 cells was independent of p53.

Conclusions. Our findings suggest that *Meox1* plays a pivotal role in HSC activation and may be involved in the canonical TGF-β1/Smad pathway.

Key words: transforming growth factor-β1, fibrosis, Smad3, hepatic stellate cell, mesoderm/mesenchyme homeobox I

Highlights

- Meox1 was identified as a key regulator of hepatic stellate cell activation in liver fibrosis.
- TGF-β1 upregulates *Meox1* expression in Lx-2 cells, promoting fibrotic gene expression and HSC activation.
- Meox1 overexpression enhances HSC proliferation, migration, and Smad3 phosphorylation, linking it to the TGF-β1/Smad pathway.
- Knockdown of *Meox1* suppresses HSC activation, reducing α-SMA, collagen-I and MMP-2 expression.
- *Meox1* induces cell cycle redistribution and upregulates p21CIP1/WAF1 independently of *p53*, suggesting a novel regulatory mechanism.

Background

Liver fibrosis is a common pathological change seen in various chronic hepatic diseases, including alcoholic liver disease, nonalcoholic steatohepatitis (NASH), chronic hepatitis C virus (HCV), and hepatitis B virus (HBV) infections, as well as autoimmune diseases. These conditions can ultimately progress to cirrhosis and hepatocellular carcinoma (HCC).[1–4] A defining feature of liver fibrosis is the extensive accumulation of extracellular matrix (ECM), which is continuously synthesized by myofibroblasts, leading to abnormal connective tissue proliferation. Recent studies have identified activated hepatic stellate cells (HSCs) as the primary source of myofibroblasts, highlighting their crucial role in liver fibrosis.[5–7]

Hepatic stellate cells (HSCs) constitute about 1/3 of the liver's nonparenchymal cells.[6–9] When the liver is subjected to pathological stimuli, quiescent HSCs become activated and differentiate into myofibroblasts, producing ECM to aid tissue regeneration during wound healing. However, prolonged HSC activation disrupts the balance between ECM synthesis and degradation, leading to excessive accumulation of ECM components such as collagen type I (collagen-I), tissue inhibitors of metalloproteinases (TIMPs) and matrix metalloproteinases (MMPs). This imbalance contributes to liver fibrosis and organ dysfunction. Inhibiting HSC activation may help alleviate liver fibrosis.[10–14] Therefore, investigating the molecular mechanisms of HSC activation is crucial for understanding liver fibrosis and identifying potential therapeutic targets to reverse this process.

Mesoderm/mesenchyme homeobox 1 (*Meox1*) is a member of the homeobox transcription factor subfamily.[15–17] Previous research has demonstrated that *Meox1* is essential for organ and cell differentiation during embryonic development, including somite differentiation,[18] axial skeleton formation,[19,20] and the development of muscles[21,22] and blood vessels.[23,24] In pathological conditions, *Meox1* plays a role in tissue repair, such as neointima formation following vascular injury[25] and osteoblastic differentiation in skeletal diseases.[26]

Recent studies have increasingly focused on the role of *Meox1* in the pathogenesis of organ fibrosis. In the skin, *Meox1* significantly enhances the proliferation and migration of human dermal fibroblasts and contributes to hypertrophic scar formation in burn patients.[27,28] In vascular diseases, *Meox1* induces endothelial cell senescence, promoting atherosclerosis progression,[29] and is upregulated in arterial smooth muscle cells following balloon injury, driving their phenotypic transformation and pathological vascular remodeling.[30] In the heart, *Meox1* expression is markedly increased in hypertrophic cardiomyopathy patients and accelerates hypertrophy decompensation through interaction with the transcriptional target gene *GATA4*.[31] Furthermore, a recent study identified *Meox1* as a central regulator in the transition from fibroblasts to profibrotic myofibroblasts in myocardial fibrosis, essential for TGF-β-induced fibroblast activation.[32] Additionally, *Meox1* is upregulated in lung tissue of idiopathic pulmonary fibrosis patients.[33] However, the role of *Meox1* in hepatic stellate cell (HSC) activation and its relationship with liver fibrosis remain largely unexplored.

LX-2 cells, an immortalized human hepatic stellate cell line, exhibit typical characteristics of primary HSCs, including expression of glial acidic fibrillary protein and desmin, and responsiveness to platelet-derived growth factor BB and transforming growth factor-β (TGF-β), making them ideal for studying liver fibrosis.[34] In this study, we not only evaluated the expression level of *Meox1* in TGF-β1-induced LX-2 cells and observed the role of *Meox1* in regulating HSC activation, but also tentatively explored the potential mechanism of *Meox1*-orchestrated HSC activation.

Objectives

The aim of this study was to investigate the potential impact of *Meox1* on HSC activation and provide an available target for hepatic fibrosis research.

Materials and methods

Data sources/measurement

Cell culture and reagent

The LX-2 cell lines (Procell CL-0560; Procell Life Science & Technology Co., Ltd., Wuhan, China) were authenticated

via short tandem repeat (STR) profiling. Cells were cultured in Dulbecco's modified Eagle's medium (DMEM; Thermo Fisher Scientific, Waltham, USA) supplemented with 10% fetal bovine serum (FBS; Lanzhou Minhai Bio-Engineering Co., Ltd., Gansu, China) at 37°C in a humidified atmosphere with 5% CO_2. TGF-β1 (ab50036; Abcam, Cambridge, UK) was stored at –20°C. For TGF-β1 stimulation experiments, cells were starved overnight and then treated with increasing concentrations of TGF-β1 (0, 0.5, 1, 5, 10, and 20 ng/mL) for 72 h to collect protein.[12,27,35]

The full-length peptide coding sequence of *homo sapiens Meox1* was synthesized by Sangon Biological Engineering Technology & Services Co., Ltd. (Shanghai, China) and inserted into the multiple cloning sites of pCDNA3.1(+) to generate the expression plasmid pcDNA3.1-*Meox1*. LX2-*Meox1* cell lines were established by stable transfection of pcDNA3.1-*Meox1* into LX-2 cells using hygromycin B selection. Plasmid transfection was performed using Lipofectamine™ 3000 reagent according to the manufacturer's instructions (Invitrogen, Thermo Fisher Scientific, Waltham, USA).

Study design and setting

RNA interference

For *Meox1* inhibition experiments, LX-2 cells were transfected with either Meox1-specific small interfering RNA (siRNA) or a negative control using Lipofectamine RNAiMAX reagent, following the manufacturer's instructions (Invitrogen, Thermo Fisher Scientific). The siRNAs were synthesized by Genepharma Co., Ltd. (Shanghai, China). The sequence for the negative control siRNA was:
5'-TTC TCC GAA CGT GTC ACG TTT-3' (sense) and
5'-ACG TGA CAC GTT CGG AGA ATT-3' (antisense).

The sequence for Meox1-specific siRNA was:
5'-CTG CCA ATG AGA CAG AGA ATT-3' (sense) and
5'-TTC TCT GTC TCA TTG GCA GTT-3' (antisense).[27]

RT-qPCR

Total RNA was extracted from the cells using TRIzol Reagent following the manufacturer's instructions (TaKaRa, Otsu, Japan). Reverse transcription was then performed using the PrimeScript™ RT reagent kit according to the manufacturer's protocol (TaKaRa). Quantitative reverse transcription polymerase chain reaction (RT-qPCR) was performed using the TB Green® Premix Ex Taq™ II kit (TaKaRa) on a QuantStudio 5 Real-Time PCR System (Applied Biosystems, Thermo Fisher Scientific, Waltham, USA). All primers were synthesized by Sangon. The primer sequences used were as follows:

α-SMA forward
5'-CTTCGTTACTACTGCTGAGCGTGAG-3',
α-SMA reverse
5'-CCCATCAGGCAACTCGTAACTCTTC-3',
collagen-1(1A1) forward
5'-TGATCGTGGTGAGACTGGTCCTG-3',
collagen-1(1A1) reverse
5'-CTTTATGCCTCTGTCGCCCTGTTC-3',
MMP-2 forward
5'-CACCTACACCAAGAACTTCCGTCTG-3',
MMP-2 reverse
5'-GTGCCAAGGTCAATGTCAGGAGAG-3',
TGF-β1 forward
5'-TACAGCAACAATTCCTGGCGATACC-3',
TGF-β1 reverse
5'-CTCAACCACTGCCGCACAACTC-3',
Meox-1 forward
5'-AAGGATGAAGTGGAAGCGTGTGAAG-3',
Meox-1 reverse
5'-TCTGAACTTGGAGAGGCTGTGGAG-3',

The *GAPDH* internal reference primer was purchased from Sangon (B661104-0001).

Western blotting

Cellular total protein extraction utilized radioimmunoprecipitation assay (RIPA) lysis buffer (Solarbio, Beijing, China) supplemented with freshly added phenylmethylsulfonyl fluoride (PMSF) and a protein phosphatase inhibitor (Solarbio). Protein concentrations were determined using a bicinchoninic acid (BCA) protein assay kit (Solarbio). Equal amounts of protein were separated by sodium dodecyl sulfate–polyacrylamide gel electrophoresis (SDS-PAGE) and transferred onto nitrocellulose or polyvinylidene difluoride (PVDF) membranes (Millipore, Bedford, USA), each blocked with 5% bovine serum album (BSA) or 5% nonfat dry milk.

Primary antibodies included: anti-Meox1 (1:1,000, ab105349; Abcam), anti-α-SMA (1:500, ab5694; Abcam), anti-collagen-I (1:2,000, 66761-1-Ig; Proteintech, Chicago, USA), anti-MMP-2 (1:1,000, 66366-1-Ig; Proteintech), anti-TGF-β1 (1:1,000, 21898-1-AP; Proteintech), anti-Smad3 (1:1,000, 66516-1-Ig; Proteintech), anti-phospho-Smad3 (1:1,000, 9520T; Cell Signaling Technology (CST), Danvers, USA), anti-p53 (1:5,000, 60283-2-Ig; Proteintech), anti-p21 (1:1,000, 10355-1-AP; Proteintech), anti-p16 (1:2,000, 10883-1-AP; Proteintech), and anti-GAPDH (1:10,000, ab181602; Abcam).

Due to the host of primary antibodies, including anti-Meox1 (1:1,000, ab105349; Abcam), anti-α-SMA (1:500, ab5694; Abcam), anti-TGF-β1 (1:1,000, 21898-1-AP; Proteintech), anti-phospho-Smad3 (1:1,000, 9520T; CST), anti-p21 (1:1,000, 10355-1-AP; Proteintech), anti-p16 (1:2,000, 10883-1-AP; Proteintech), and anti-GAPDH (1:10,000, ab181602; Abcam), was rabbit, we performed western blotting utilized horseradish peroxidase (HRP)-conjugated AffiniPure goat anti-rabbit IgG (H+L) (1:5,000, SA00001-2; Proteintech) as secondary antibodies.

Due to the host of primary antibodies, including anti-collagen-I (1:2,000, 66761-1-Ig; Proteintech), anti-MMP-2 (1:1,000, 66366-1-Ig; Proteintech), anti-Smad3 (1:1,000,

66516-1-Ig; Proteintech), and anti-p53 (1:5,000, 60283-2-Ig; Proteintech), was mouse, we performed western blotting utilizing HRP-conjugated AffiniPure goat anti-mouse IgG (H + L) (1:5,000; SA00001-1; Proteintech) as secondary antibodies.

Protein expression levels were visualized using an enhanced chemiluminescence (ECL) kit (New Cell & Molecular Biotech Co., Ltd., Suzhou, China) and imaged with the ChemiDoc™ Touch imaging system (Thermo Fisher Scientific).

Cell proliferation assay

Cell Counting Kit-8 (CCK-8; Dojindo Lab, Kumamoto, Japan) was used to assess cell proliferation. Cell lines in the logarithmic growth phase were resuspended and seeded into 96-well plates at a density of 1×10^3 cells/well. At designated time points (0, 24, 48, 72, and 96 h), 10 mL of CCK-8 solution was added to each well, followed by a 2-h incubation at 37°C in a 5% CO_2 humidified atmosphere. Optical density (OD) at 450 nm was measured every 24 h using a microplate reader (Bio-Tek Instruments, Winooski, USA).

Cell migration assay

Transwell chambers with 8-micrometer polycarbonate filters (Corning Company, Corning, USA) were used for the cell migration assay. Cell lines in the logarithmic growth phase were resuspended in serum-free DMEM and seeded into the Transwell upper chamber at a density of 1×10^4 cells/well. Then, 600 µL of DMEM containing 10% FBS was added to the Transwell lower chamber. After a 24-h incubation period, the filters were fixed with methyl alcohol for 1 h and stained with 0.5% crystal violet for 20 min. Stained cells were observed and photographed under an inverted microscope (model DMI6000 B; Leica Camera AG, Wetzlar, Germany) in 5 randomly selected fields (including 1 each from the upper, lower, central, left, and right positions) at ×100 magnification. Subsequently, ImageJ v. 1.8.0 (National Institutes of Health (NIH), Bethesda, USA) was used for cell counting.

Flow cytometry assay

Flow cytometry was used to analyze the cell cycle using the Cell Cycle Assay Kit Plus (C6078; Shanghai Bioscience Technology Co. Ltd., Shanghai, China), following the manufacturer's instructions. Cells were collected during the logarithmic growth phase, washed twice with pre-cooled PBS, and then resuspended in approx. 1 mL of pre-cooled staining buffer to prepare a single-cell suspension.

The single-cell suspension was mixed with 1 mL of pre-cooled 75% ethanol and stored at –20°C overnight for fixation. After incubation, cells were collected and resuspended in 1 mL of PBS. Then, 4 µL of RedNucleus I staining solution was added to each tube, mixed gently and thoroughly and incubated at room temperature in the dark for 20 min. Following staining, the cell suspension was filtered through a nylon mesh into a flow cytometry tube.

Flow cytometry assays were conducted using a fluorescence-activated cell sorting (FACS) Aria II flow cytometer (BD Biosciences, Pharmingen, San Diego, USA).

Statistical analyses

Statistical analysis was conducted using IBM SPSS software v. 26.0 (IBM Corp., Armonk, USA) and R v. 4.4.2 (R Foundation for Statistical Computing, Vienna, Austria). Each experiment (RT-qPCR, western blotting, cell proliferation, cell migration, and flow cytometry assay) was performed in triplicate. Medians (1st and 3rd quartile; Q1–Q3) was used to represent the values. For small samples, testing for normality was not feasible with sufficient reliability; therefore, a nonparametric test was used. The nonparametric Mann–Whitney U test and Kruskal–Wallis H test with Dunn's post hoc tests were utilised for examining the data as appropriate. For comparisons between the 2 groups, we utilized the nonparametric Mann–Whitney U test. For comparisons involving more than 2 groups, we utilized the Kruskal–Wallis H test with Dunn's post hoc tests, with significance values adjusted using the Bonferroni correction for multiple testing. In the case of repetition measurements, differences in characteristics between groups were analyzed using the ARTool package in R.[36,37] All comparisons were 2-tailed, with statistical significance set at $p < 0.05$.

Results

Meox1 was upregulated in TGFβ1-induced HSC activation

To determine if *Meox1* was upregulated in activated HSCs, we used LX-2 cells, a commonly employed model for studying fibrogenesis and HSC activation.[34] Transforming growth factor-β1 is well known for inducing HSC activation.[9,38–40] Therefore, we examined the effect of TGF-β1 on *Meox1* expression in LX-2 cells. Treating the cells with increasing concentrations of TGF-β1 resulted in a dose-dependent upregulation of *Meox1*, with significant increases observed at concentrations up to 10 ng/mL (Fig. 1A,B). We also evaluated the expression levels of HSC activation markers and fibrosis-related factors in TGF-β1-treated LX-2 cells. Consistent with previous reports,[12,35,41,42] the expression levels of α-smooth muscle actin (α-SMA) (Fig. 1A,C), collagen-I (Fig. 1A,D) and MMP-2 (Fig. 1A,E) increased progressively with higher concentrations of TGF-β1. These results indicate that *Meox1* is induced during HSC activation.

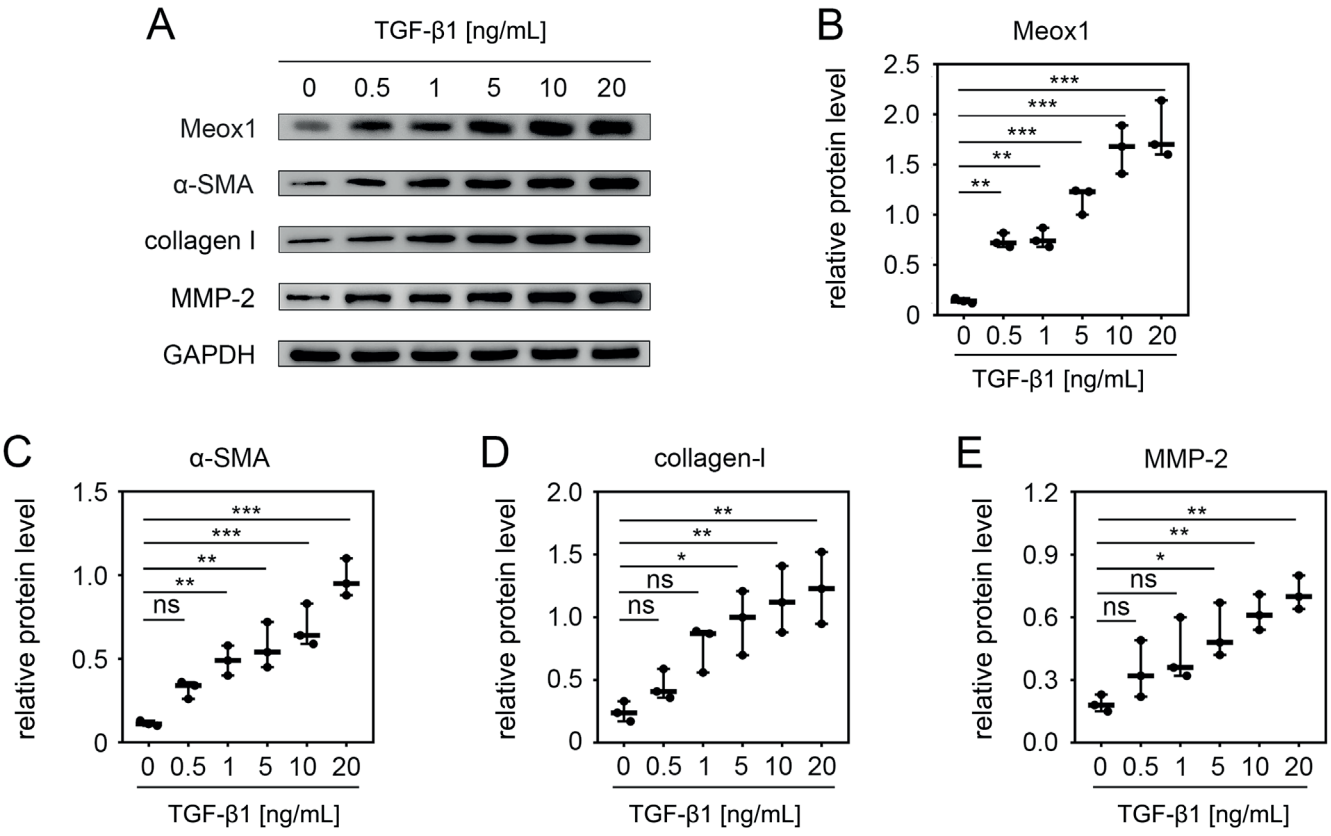

Fig. 1. TGF-β1 dose-dependently upregulated *Meox1* and HSC activation markers expression in LX-2 cells. A. Western blotting analysis the *Meox1*, α-SMA, collagen-I, and MMP-2 expression. The LX-2 cells were starved overnight and subsequently treated with increasing concentration of TGF-β1 (0, 0.5, 1, 5 10, and 20 ng/mL) for 72 h to collect protein; B–E. Quantification of *Meox1* and HSC activation markers level shown in A by normalized to GAPDH level. Western blot scanning densitometry for 3 independent experiments was analyzed with ImageJ software (Kruskal–Wallis H-test; *Meox1*, p = 0.008; α-SMA, p = 0.008; collagen-I, p = 0.016; MMP-2, p = 0.032). The line in the middle of the box represents the median, the upper whisker represents the extension from the median to the maximum value, and the lower whisker represents the extension from the median to the minimum value

TGF-β1 – transforming growth factor-β1; *Meox1* – mesoderm/mesenchyme homeobox gene l; HSC – hepatic stellate cell; α-SMA – α smooth muscle actin; collagen-I – collagen type I; MMP-2 – matrix metalloproteinase-2; GAPDH – glyceraldehyde phosphate dehydrogenase; ns – no significant difference; *p < 0.05; **p < 0.01; ***p < 0.001.

Meox1 was essential for TGFβ1-induced HSC activation

To further investigate the role of *Meox1* in TGF-β1-stimulated HSC activation, we knocked down *Meox1* in LX-2 cells using specific siRNA (si-*Meox1*). As shown in Fig. 2A,B, TGF-β1 stimulation increased the expression of *Meox1* and HSC activation markers. However, *Meox1* expression was significantly reduced by its specific siRNA. Upon *Meox1* knockdown, the expression of TGF-β1-induced HSC activation markers, including α-SMA (Fig. 2A,C), collagen-I (Fig. 2A,D) and MMP-2 (Fig. 2A,E), was significantly reduced.

Notably, *Meox1* knockdown also reduced the expression of these markers at the basal level, without TGF-β1 stimulation. These findings confirm that TGF-β1 enhances the expression of HSC activation markers and that this activation can be inhibited by *Meox1* knockdown, suggesting that *Meox1* is essential for TGF-β1-induced HSC activation.

Overexpression of *Meox1* promoted HSC activation

Given that *Meox1* was upregulated during HSC activation, suggesting its involvement in transdifferentiation, we examined the effect of *Meox1* alone on HSC activation. We stably transfected the *Meox1* gene into LX-2 cells and analyzed the expression levels of HSC activation markers. The results showed that *Meox1* mRNA (Fig. 3A) and protein (Fig. 3E) levels were significantly increased compared to the control, confirming the successful establishment of LX-2-*Meox1* cell lines with stable *Meox1* expression. In these cell lines, the mRNA levels of α-SMA (Fig. 3B), collagen-I (Fig. 3C) and MMP-2 (Fig. 3D) were significantly upregulated. Western blot analysis also indicated that *Meox1* overexpression significantly increased the protein levels of α-SMA, collagen-I and MMP-2 (Fig. 3E), suggesting that *Meox1* promotes the expression of these HSC activation markers at the transcriptional level.

Cell proliferation and migration are key functional characteristics of HSC activation.[9] Therefore, we further

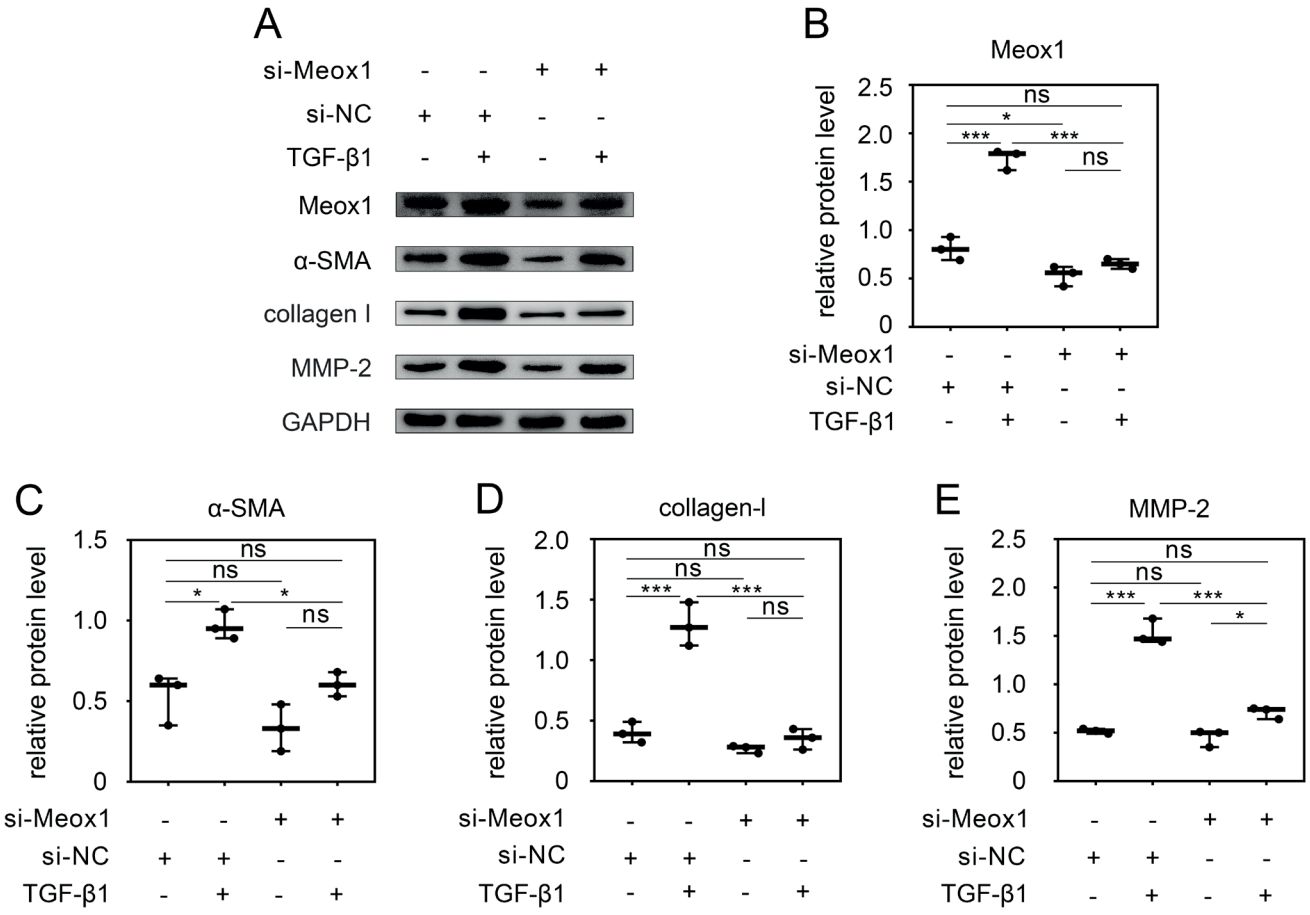

Fig. 2. *Meox1* was essential for TGF-β1-induced HSC activation. A. The *Meox1* knockdown inhibited TGF-β1-induced HSC activation markers protein expression in LX-2 cells. LX-2 cells were transfected with control (si-*NC*) or *Meox1* siRNA (si-*Meox1*). Following incubation for 48 h, LX-2 cells were treated with 10 ng/mL TGF-β1 for 72 h to collect protein. The protein expression level of *Meox1* and HSC activation markers were detected with western blotting; B–E. Quantification of protein levels shown in A by normalized to GAPDH for each individual protein. Western blot scanning densitometry for 3 independent experiments was analyzed with ImageJ software (Kruskal–Wallis H-test; *Meox1*, p = 0.023; α-SMA, p = 0.032; collagen-I, p = 0.038; MMP-2, p = 0.022). The line in the middle of the box represents the median, the upper whisker represents the extension from the median to the maximum value, and the lower whisker represents the extension from the median to the minimum value

TGF-β1 – transforming growth factor-β1; *Meox1* – mesoderm/mesenchyme homeobox gene l; HSC – hepatic stellate cell; GAPDH – glyceraldehyde phosphate dehydrogenase; ns – no significant difference; *p < 0.05; **p < 0.01; ***p < 0.001.

evaluated the effect of *Meox1* on HSC proliferation using the CCK-8 assay (Fig. 3F). The data indicated that the growth rate of LX-2-*Meox1* cells was faster than that of the control group at 48, 72 and 96 h, demonstrating that *Meox1* accelerates cell proliferation. Additionally, we assessed the role of *Meox1* in HSC migration using a Transwell assay. The results showed that the number of migrating cells increased compared to the control group when *Meox1* was upregulated (Fig. 3G). Overall, these findings suggest that *Meox1* promotes HSC phenotypic transformation as well as subsequent proliferation and migration.

The Smad3 phosphorylation level increased in LX-2 *Meox1* cells

We first investigated whether there was a regulatory loop between *Meox1* and TGF-β1 during HSC activation. As shown in Fig. 4A, the mRNA level of TGF-β1 did not significantly change after the stable transfection of the *Meox1* gene into LX-2 cells. Additionally, *Meox1* overexpression did not upregulate the protein level of TGF-β1 in LX-2 cells (Fig. 4B). Previous studies have highlighted the critical role of the canonical receptor-activated Smad pathway in mediating TGF-β1 signaling.[9,43] We therefore examined whether *Meox1* was involved in the Smad-dependent TGF-β1 pathway. Smad3 is essential for mediating TGF-β1 signaling in HSC activation and the expression of profibrogenic genes, including collagen-I and α-SMA.[9,44] Consequently, we focused on the impact of *Meox1* on Smad3. Western blot analysis revealed that while the total protein level of Smad3 remained unchanged in LX-2 cells following *Meox1* overexpression, the phosphorylation of Smad3 was elevated (Fig. 4B). These findings suggest that *Meox1* operates downstream of TGF-β1 without forming a feedback loop and potentially participates in the TGF-β1/Smad3 pathway.

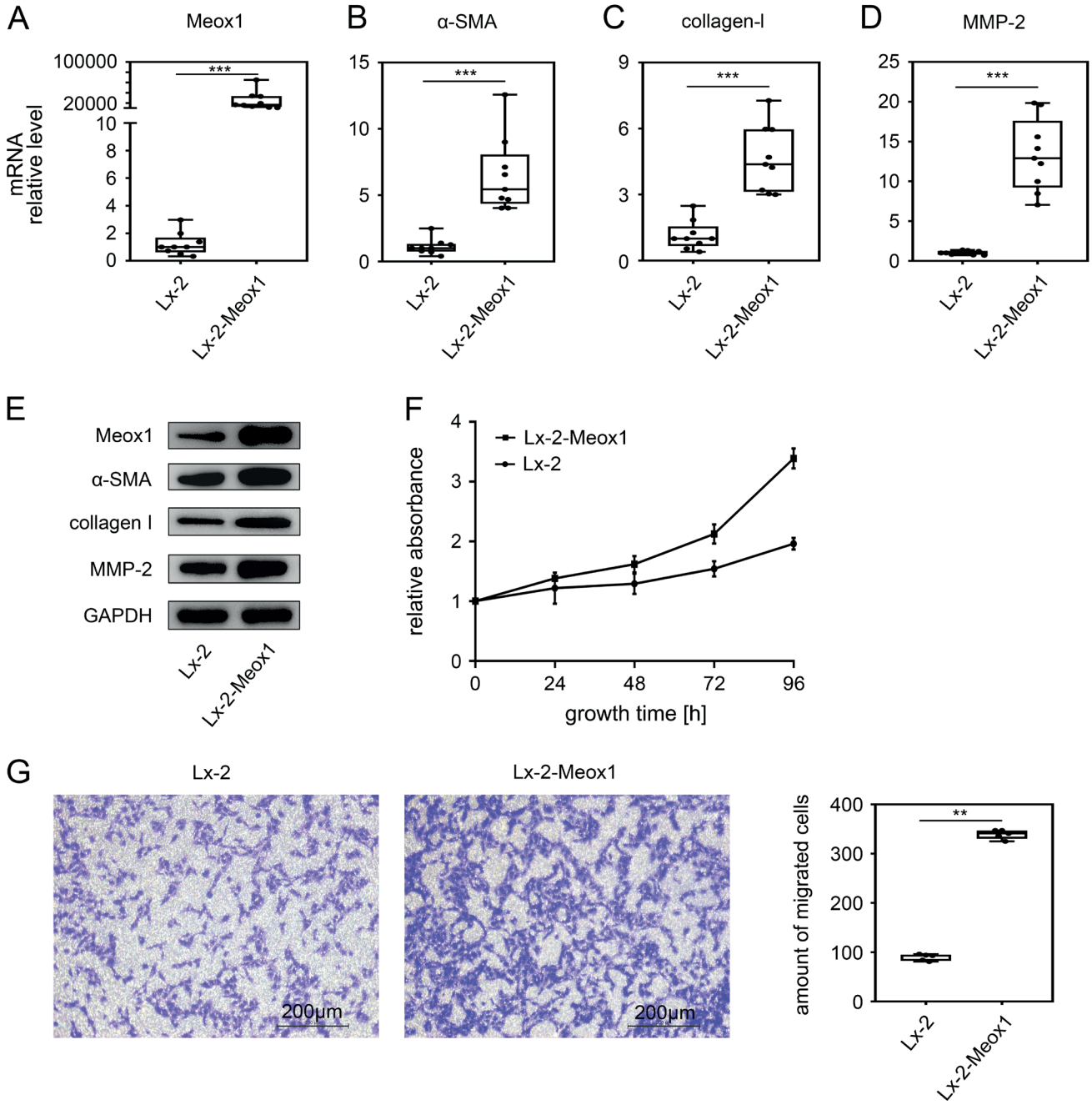

Fig. 3. *Meox1* induced HSC activation markers expression and accelerated HSC proliferation/migration. The LX2-*Meox1* cell lines were established by stably transfecting *pcDNA3.1-Meox1* into LX-2 cells with hygromycin B selection. A–D. Quantitative reverse transcription polymerase chain reaction (RT-qPCR) analysis of *Meox1*, α-SMA, collagen-I, and MMP-2 mRNA expression level in LX2-*Meox1* cell lines. The mRNA expression level of α-SMA increased by 5.44 (4.3584, 8.0645) fold ($p < 0.001$, Mann–Whitney U test), collagen-I increased by 4.379 (3.1230, 5.9695) fold ($p < 0.001$, Mann–Whitney U test) and MMP-2 increased by 12.899 (9.2280, 17.6105) fold ($p < 0.001$, Mann–Whitney U test) when *Meox1* was overexpressed in LX-2 cells; E. Western blotting analysis of *Meox1*, α-SMA, collagen-I, and MMP-2 protein expression level in LX2-*Meox1* cell lines (n = 3); F. Proliferation effect of *Meox1* in LX-2 cells. The growth rate of LX-2-*Meox1* cells was significantly increased compared to LX-2 cells at 48 h ($p < 0.001$, ARTool package in R); the same phenomenon was also found at 72 h ($p < 0.001$, ARTool package in R) and 96 h ($p < 0.001$, ARTool package in R); G. Representative phase contrast image and quantitative analysis of transwell migration assay in LX-2 and LX-2-*Meox1* cells. The migration number of LX-2 cells was 93 (82.5, 95), LX-2-*Meox1* cells was 314 (330.5, 347) and the migration of LX-2-*Meox1* cells was significantly increased compared to the LX-2 cells ($p = 0.009$, Mann–Whitney U test). The line in the middle of the box represents the median, while the upper and lower boundaries of the box correspond to the 3rd quartile (Q3) and the 1st quartile (Q1), respectively. The upper whisker represents the extension from the Q3 to the maximum value, and the lower whisker represents the extension from the Q1 to the minimum value

TGF-β1 – transforming growth factor-β1; *Meox1* – mesoderm/mesenchyme homeobox gene l; HSC – hepatic stellate cell; α-SMA – α smooth muscle actin; collagen-I – collagen type I; MMP-2 – matrix metalloproteinase-2.

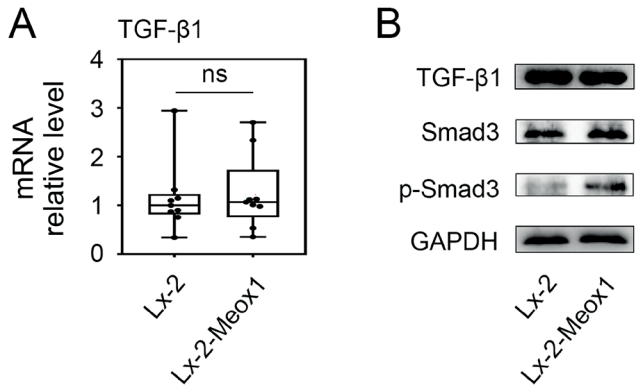

Fig. 4. The Smad3 phosphorylation level increased in LX-2-*Meox1* cells. A. Quantitative reverse transcription polymerase chain reaction (RT-qPCR) analysis of TGF-β1 mRNA expression level in LX2-*Meox1* cell lines. The mRNA expression level of TGF-β1 increased by 1.067 (0.7580, 1.7325) fold (p = 0.690, Mann–Whitney U test) when *Meox1* was overexpressed in LX-2 cells. The line in the middle of the box represents the median, while the upper and lower boundaries of the box correspond to the 3rd quartile (Q3) and the 1st quartile (Q1), respectively. The upper whisker represents the extension from the Q3 to the maximum value, and the lower whisker represents the extension from the Q1 to the minimum value. B. Western blotting analysis of TGF-β1, total Smad3 and phosphorylated Smad3 expression level in LX2-*Meox1* cell lines (n = 3)

TGF-β1 – transforming growth factor-β1; *Meox1* – mesoderm/mesenchyme homeobox gene l.

Meox1 induced LX-2 cells population redistribution

To determine if *Meox1* affects cell cycle progression, we used flow cytometry to analyze cell population distribution. The results showed a significant increase in the proportion of cells in the G1 phase and no significant difference in the G2 phase in LX-2-*Meox1* cells compared to the LX-2 control group (Fig. 5A). This indicates that *Meox1* can induce a redistribution of the cell population, extending the G1 phase.

Meox1 activated p21$^{CIP1/WAF1}$ expression in HSCs

Meox1 acts as a transcriptional inducer of *p16*^{INK4a} and *p21*$^{CIP1/WAF1}$ in vascular endothelial cells (VECs).[29] Therefore, we also examined its impact on stimulating the expression of *p16*^{INK4a} and *p21*$^{CIP1/WAF1}$ in HSCs. Western blot analysis revealed a significant increase in *p21*$^{CIP1/WAF1}$ protein expression in LX-2-*Meox1* cells compared to the control, whereas no notable change was observed in *p16*^{INK4a} protein levels (Fig. 5B). Despite *p53* being a well-established transcriptional activator of the *p21*$^{CIP1/WAF1}$ gene,[45] its protein expression did not differ between LX-2-*Meox1* cells and control cells (Fig. 5B). These findings suggest that the upregulation of *p21*$^{CIP1/WAF1}$ during *Meox1*-induced HSC activation is independent of *p53*.

Discussion

Mounting evidence supports that HSC activation and their transformation into myofibroblasts are critical stages in hepatic fibrosis. Inhibiting HSC activation represents a promising treatment approach to alleviate fibrosis progression.[8,9] Nevertheless, the safety and efficacy of this therapeutic strategy remain uncertain. Therefore, further research is essential to identify new therapeutic targets.

Several gene expression profiles undergo changes during fibrosis and play crucial roles in the transdifferentiation of myofibroblasts and fibrogenesis.[4,8,46] *Meox1* has recently emerged as a significant regulator of fibroblast activation across various types of organ fibrosis, including skin,[27] vessel,[30] heart,[31,32] and lung fibrosis.[33] Importantly, *Meox1* is specifically expressed in activated fibroblasts, orchestrating a comprehensive fibrotic gene expression program and is essential for TGF-β-induced fibroblast activation.[32]

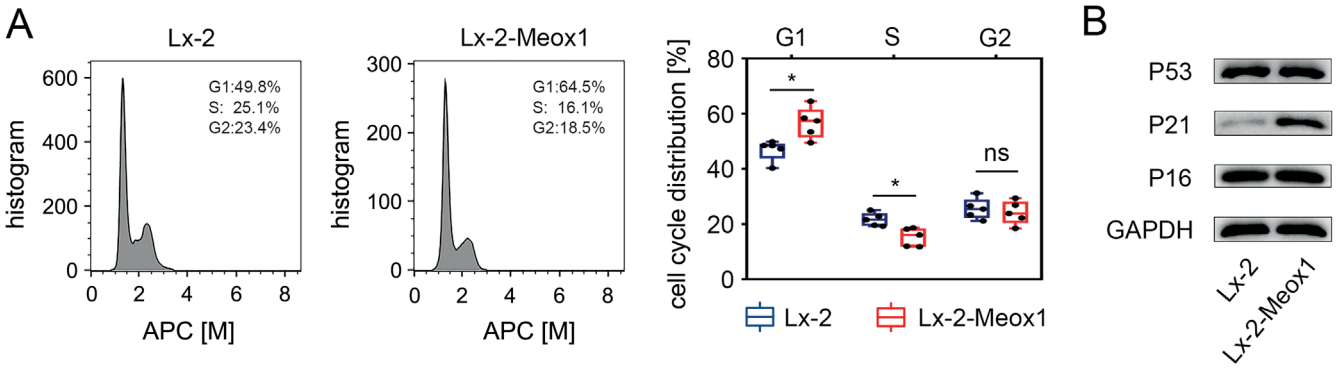

Fig. 5. *Meox1* induced cell population redistribution and *p21*$^{CIP1/WAF1}$ expression in LX-2 cells. A. Effect of *Meox1* on cell cycle distribution in LX-2 cells was assessed with flow cytometry. Compared to the LX-2 control group, the proportion of cells in the G1 phase in LX-2-*Meox1* cells was increased (p = 0.016, Mann–Whitney U test), while the proportion of cells in the G2 phase exhibited no significant difference (p = 0.754, Mann–Whitney U test). The line in the middle of the box represents the median, while the upper and lower boundaries of the box correspond to the 3rd quartile (Q3) and the 1st quartile (Q1), respectively. The upper whisker represents the extension from the Q3 to the maximum value, and the lower whisker represents the extension from the Q1 to the minimum value. B. Western blotting analysis of *p53*, *p21*$^{CIP1/WAF1}$ and *p16*^{INK4a} protein expression level in LX2-*Meox1* cell lines (n = 3)

Meox1 – mesoderm/mesenchyme homeobox gene l.

Therefore, we investigated the impact of *Meox1* on human HSC activation.

TGF-β1, a key inflammatory mediator, is recognized as the principal profibrogenic cytokine that triggers HSC activation and ECM production.[9,44] The α-SMA, a hallmark of HSC activation, serves as an indicator of activation severity.[8,9] Additionally, collagen-I and MMP-2 are integral components of the ECM and are widely used to assess fibrosis severity.[8,9] Our study revealed that *Meox1* expression increased concurrently with α-SMA and the accumulation of collagen-I and MMP-2 in TGF-β1-treated LX-2 cells. Interestingly, inhibiting *Meox1* expression blocked TGF-β1-induced synthesis of α-SMA, collagen-I and MMP-2, thereby reducing ECM accumulation. These findings suggest that *Meox1* may contribute to TGF-β1-induced HSC activation and subsequent ECM deposition.

Hepatic stellate cell activation is a multifaceted process involving changes in phenotype and function crucial for ECM production, proliferation and migration.[8] Our study demonstrated that overexpression of *Meox1* significantly elevated α-SMA levels in LX-2 cells. Similarly, expression levels of collagen-I and MMP-2 were robustly enhanced, indicating that *Meox1* can drive the transformation of quiescent HSCs into a myofibroblastic phenotype. Previous studies have indicated that approx. 80% of fibrillary collagen-I is synthesized by activated HSCs, with MMP-2 playing a regulatory role in this process.[8] Matrix metalloproteinase-2, a profibrotic mediator secreted by activated HSCs, contributes to ECM degradation and enhances HSC activation and migration.[12] Conversely, inhibition of *Meox1* reduced basal levels of both collagen-I and MMP-2 expression. These findings suggest that *Meox1* functions as an inducer of collagen-I and MMP-2, thereby regulating ECM production in HSCs.

Furthermore, our observations indicated that *Meox1* significantly promoted the proliferation and migration of LX-2 cells. These data underscore the crucial role of *Meox1* in HSC activation, aligning with previous research demonstrating *Meox1*'s ability to modulate phenotypes and functions of human dermal fibroblasts[27] and smooth muscle cells (SMCs).[24,30]

The TGF-β1/Smad signaling pathway is crucial in liver fibrosis by activating HSCs.[9,40] Transforming growth factor-β1 induces *Meox1* expression, and blocking *Meox1* inhibits TGF-β1-induced ECM synthesis. Interestingly, TGF-β1 expression did not significantly vary with *Meox1* overexpression in LX-2 cells, suggesting that *Meox1* likely acts downstream of TGF-β1 without forming a feedback loop with it. Upon active TGF-β binding to the TGF-β type II receptor, transforming growth factor-β type I receptor (TβRI) is phosphorylated, activating its catalytic activity and initiating signaling through phosphorylation of Smad family members.[9,40] Studies indicate *Smad3* as a critical mediator of HSC profibrogenic responses,[9,44] crucial for liver fibrosis progression through ECM expression.[40,47] Smad3 activity, modulated by expression, phosphorylation and nuclear translocation, induces transcription of target genes.[24] Our study observed increased Smad3 phosphorylation but no significant change in total Smad3 levels upon forced *Meox1* expression in LX-2 cells, suggesting *Meox1* may regulate Smad3 phosphorylation. However, *Meox1*'s localization in the nucleus makes direct promotion of TGF-β-induced Smad3 phosphorylation in the cytoplasm unlikely. Research on SMCs suggests *Meox1* maintains nuclear Smad3 phosphorylation by inhibiting protein phosphatase, Mg^{2+}/Mn^{2+} dependent 1A (PPM1A), a Smad3 phosphatase blocking TGF-β signaling.[24] Thus, we propose TGF-β1-induced *Meox1* preserves Smad3 phosphorylation to promote HSC activation, yet the detailed mechanisms of *Meox1* in HSC activation require further exploration.

Furthermore, our findings indicate that increased *Meox1* expression lengthens the G1 phase. Previous studies have shown that $p21^{CIP1/WAF1}$ and $p16^{INK4a}$ are downstream transcriptional targets of *Meox1* and can be directly activated by *Meox1* in VECs.[29] These genes act as cyclin-dependent kinase inhibitors essential for G1 phase arrest.[48] In LX-2 cells, *Meox1* overexpression significantly induced $p21^{CIP1/WAF1}$ expression, whereas $p16^{INK4a}$ levels remained unchanged compared to the negative control. We speculate that this discrepancy may result from different intracellular responses in different cell types.

Increased $p21^{CIP1/WAF1}$ expression was observed at both protein and mRNA levels, while *p53* expression, a known transcriptional activator of $p21^{CIP1/WAF1}$,[48] was unaffected by *Meox1* expression in LX-2 cells. This suggests that *Meox1*-induced $p21^{CIP1/WAF1}$ expression at the transcriptional level is independent of *p53*. This independence may explain *Meox1*'s role in lengthening the G1 phase. Studies have shown that $p21^{CIP1/WAF1}$ plays a crucial role in hepatocyte development, differentiation and cell cycle regulation, with Smad family members mediating the activation of the $p21^{CIP1/WAF1}$ promoter. Truncated Smad3 blocks this transactivation.[49]

Previous research has confirmed that *Meox1* can regulate muscle tissue growth and differentiation by controlling the cell cycle.[21] Extensive research has demonstrated the close connection between cell fate decisions and cell cycle machinery,[50–52] revealing how cells use distinct cell cycle states to regulate biochemical and physical changes, such as metabolism, gene expression profiles and differentiation. Extending the G1 phase allows cells to respond more efficiently to signals, activate developmental gene transcription and initiate differentiation programs while maintaining the differentiation state.[53–55]

A study demonstrated that *Mteox1* is necessary for TGF-β1-induced SMC differentiation from mesenchymal progenitors[24] and acts as a central transcriptional switch governing TGF-β1-induced fibroblast activation in myocardial fibrosis.[32] Our results suggest that *Meox1* mediates TGF-β1-stimulated transdifferentiation of quiescent HSCs into a myofibroblastic phenotype that accumulates fibrillary collagens. Interestingly, previous research suggested that $p21^{CIP1/WAF1}$ enhances the sensitivity of cell response to TGF-β.[56] Therefore, we speculate that *Meox1*-induced G1

phase extension may create a temporal window that enhances HSC response to various profibrogenic cytokines, allowing for more efficient activation and maintenance of the transdifferentiation state, thereby promoting fibrosis. These findings indicate a more complex relationship between *Meox1* and HSC activation that warrants further investigation.

Limitations

Our study has several limitations. Primarily, the use of the LX-2 cell line may not fully represent primary hepatic stellate cells or the in vivo environment, potentially leading to over- or underestimation of *Meox1* effects. The reliance on a single cell line and in vitro conditions further limits the generalizability and physiological relevance of the findings. Transient knockdown and overexpression techniques introduce variability and may not capture long-term regulatory mechanisms. The absence of in vivo validation means systemic factors are not considered, affecting translational potential. Additionally, RT-qPCR and western blot analyses could introduce technical biases, impacting result precision. Future studies should incorporate primary HSCs, validate findings in animal models, use stable genetic manipulation techniques, and replicate results across multiple cell lines to mitigate these biases and enhance study precision.

Conclusions

Our research identifies *Meox1* as a key factor in TGF-β1-induced HSC activation, significantly influencing HSC phenotypic modulation. While the precise mechanisms remain unclear, changes in Smad3 phosphorylation suggest that *Meox1* may regulate HSC activation through the TGF-β/Smad signaling pathway. Given its role in promoting HSC activation, *Meox1* warrants further investigation and may represent a promising antifibrotic drug target for treating hepatic fibrosis.

Supplementary data

The supplementary materials are available at https://doi.org/10.5281/zenodo.14232390. The package includes the following files:

Supplementary Fig. 1A. Kruskal–Wallis H test was utilized for examining the data from western blotting assay of *Meox1*.

Supplementary Fig. 1B. Kruskal–Wallis H test was utilized for examining the data from western blotting assay of α-SMA.

Supplementary Fig. 1C. Kruskal–Wallis H test was utilized for examining the data from western blotting assay of collagen-I.

Supplementary Fig. 1D. Kruskal–Wallis H test was utilized for examining the data from western blotting assay of MMP-2.

Supplementary Fig. 2A. Kruskal–Wallis H test was utilized for examining the data from western blotting assay of *Meox1*.

Supplementary Fig. 2B. Kruskal–Wallis H test was utilized for examining the data from western blotting assay of α-SMA.

Supplementary Fig. 2C. Kruskal–Wallis H test was utilized for examining the data from western blotting assay of collagen-I.

Supplementary Fig. 2D. Kruskal–Wallis H test was utilized for examining the data from western blotting assay of MMP-2.

Supplementary Fig. 3A. The nonparametric Mann–Whitney U test was utilized for examining the data from qPCR assay of Meox1.

Supplementary Fig. 3B. The nonparametric Mann–Whitney U test was utilized for examining the data from qPCR assay of α-SMA.

Supplementary Fig. 3C. The nonparametric Mann–Whitney U test was utilized for examining the data from qPCR assay of collagen I.

Supplementary Fig. 3D. The nonparametric Mann–Whitney U test was utilized for examining the data from RT-qPCR assay of MMP-2.

Supplementary Fig. 3E. The ARTool package in R was utilized for examining the data from CCK-8 cell proliferation assay.

Supplementary Fig. 3F. The nonparametric Mann–Whitney U test was utilized for examining the data from cell migration assay.

Supplementary Fig. 4. The nonparametric Mann–Whitney U test was utilized for examining the data from RT-qPCR assay of TGF.

Supplementary Fig. 5A. The nonparametric Mann–Whitney U test was utilized for examining the data from cell cycle assay in G1.

Supplementary Fig. 5B. The nonparametric Mann–Whitney U test was utilized for examining the data from cell cycle assay in S.

Supplementary Fig. 5C. The nonparametric Mann–Whitney U test was utilized for examining the data from cell cycle assay in G2.

Data availability

The datasets generated and/or analyzed during the current study are available from the corresponding author on reasonable request.

Consent for publication

Not applicable.

Use of AI and AI-assisted technologies

Not applicable.

ORCID iDs

Jie Ruan https://orcid.org/0000-0002-5250-6287
Ying Xie https://orcid.org/0000-0001-5147-874X
Huifang Zhou https://orcid.org/0000-0002-9177-8672
Libo Su https://orcid.org/0000-0003-0525-9890
Chao Liu https://orcid.org/0009-0006-8051-5830
Chaoqun Zhang https://orcid.org/0009-0003-4760-8515
Sun Dianxing https://orcid.org/0000-0002-6015-7435

References

1. Schuppan D, Ashfaq-Khan M, Yang AT, Kim YO. Liver fibrosis: Direct antifibrotic agents and targeted therapies. *Matrix Biol*. 2018;68–69:435–451. doi:10.1016/j.matbio.2018.04.006
2. Ebrahimi H, Naderian M, Sohrabpour AA. New concepts on pathogenesis and diagnosis of liver fibrosis: A review article. *Middle East J Dig Dis*. 2016;8(3):166–178. doi:10.15171/mejdd.2016.29
3. Weiskirchen R, Tacke F. Liver fibrosis: From pathogenesis to novel therapies. *Dig Dis*. 2016;34(4):410–422. doi:10.1159/000444556
4. Parola M, Pinzani M. Liver fibrosis: Pathophysiology, pathogenetic targets and clinical issues. *Mol Aspects Med*. 2019;65:37–55. doi:10.1016/j.mam.2018.09.002
5. Elpek GÖ. Cellular and molecular mechanisms in the pathogenesis of liver fibrosis: An update. *World J Gastroenterol*. 2014;20(23):7260. doi:10.3748/wjg.v20.i23.7260
6. Puche JE, Saiman Y, Friedman SL. Hepatic stellate cells and liver fibrosis. *Compr Physiol*. 2013;3(4):1473–1492. doi:10.1002/cphy.c120035
7. Moreira RK. Hepatic stellate cells and liver fibrosis. *Arch Pathol Lab Med*. 2007;131(11):1728–1734. doi:10.5858/2007-131-1728-HSCALF
8. Yan Y, Zeng J, Xing L, Li C. Extra- and intra-cellular mechanisms of hepatic stellate cell activation. *Biomedicines*. 2021;9(8):1014. doi:10.3390/biomedicines9081014
9. Dewidar B, Meyer C, Dooley S, Meindl-Beinker AN. TGF-β in hepatic stellate cell activation and liver fibrogenesis: Updated 2019. *Cells*. 2019;8(11):1419. doi:10.3390/cells8111419
10. Lu DH, Guo XY, Qin SY, et al. Interleukin-22 ameliorates liver fibrogenesis by attenuating hepatic stellate cell activation and downregulating the levels of inflammatory cytokines. *World J Gastroenterol*. 2015;21(5):1531–1545. doi:10.3748/wjg.v21.i5.1531
11. Zhang G, Liu Y, Liu P. Active components from sea buckthorn (*Hippophae rhamnoides* L.) regulate hepatic stellate cell activation and liver fibrogenesis. *J Agric Food Chem*. 2018;66(46):12257–12264. doi:10.1021/acs.jafc.8b05306
12. Coppola N, Perna A, Lucariello A, et al. Effects of treatment with Maraviroc a CCR5 inhibitor on a human hepatic stellate cell line. *J Cell Physiol*. 2018;233(8):6224–6231. doi:10.1002/jcp.26485
13. Luo J, Li L, Chang B, et al. Mannan-binding lectin via interaction with cell surface calreticulin promotes senescence of activated hepatic stellate cells to limit liver fibrosis progression. *Cell Mol Gastroenterol Hepatol*. 2022;14(1):75–99. doi:10.1016/j.jcmgh.2022.03.011
14. Roehlen N, Crouchet E, Baumert TF. Liver fibrosis: Mechanistic concepts and therapeutic perspectives. *Cells*. 2020;9(4):875. doi:10.3390/cells9040875
15. Candia AF, Hu J, Crosby J, et al. *Mox-1* and *Mox-2* define a novel homeobox gene subfamily and are differentially expressed during early mesodermal patterning in mouse embryos. *Development*. 1992;116(4):1123–1136. doi:10.1242/dev.116.4.1123
16. Samuel S, Naora H. Homeobox gene expression in cancer: Insights from developmental regulation and deregulation. *Eur J Cancer*. 2005;41(16):2428–2437. doi:10.1016/j.ejca.2005.08.014
17. Candia AF, Wright CV. Differential localization of Mox-1 and Mox-2 proteins indicates distinct roles during development. *Int J Dev Biol*. 1996;40(6):1179–1184. PMID:9032023.
18. Mankoo BS, Skuntz S, Harrigan I, et al. The concerted action of Meox homeobox genes is required upstream of genetic pathways essential for the formation, patterning and differentiation of somites. *Development*. 2003;130(19):4655–4664. doi:10.1242/dev.00687
19. Bayrakli F, Guclu B, Yakicier C, et al. Mutation in *MEOX1* gene causes a recessive Klippel–Feil syndrome subtype. *BMC Genet*. 2013;14(1):95. doi:10.1186/1471-2156-14-95
20. Stamataki D, Kastrinaki MC, Mankoo BS, Pachnis V, Karagogeos D. Homeodomain proteins Mox1 and Mox2 associate with Pax1 and Pax3 transcription factors. *FEBS Lett*. 2001;499(3):274–278. doi:10.1016/S0014-5793(01)02556-X
21. Nguyen PD, Gurevich DB, Sonntag C, et al. Muscle stem cells undergo extensive clonal drift during tissue growth via *Meox1*-mediated induction of G2 cell-cycle arrest. *Cell Stem Cell*. 2017;21(1):107–119.e6. doi:10.1016/j.stem.2017.06.003
22. Sutcu HH, Ricchetti M. Loss of heterogeneity, quiescence, and differentiation in muscle stem cells. *Stem Cell Investig*. 2018;5:9. doi:10.21037/sci.2018.03.02
23. Nguyen PD, Hollway GE, Sonntag C, et al. Haematopoietic stem cell induction by somite-derived endothelial cells controlled by *Meox1*. *Nature*. 2014;512(7514):314–318. doi:10.1038/nature13678
24. Dong K, Guo X, Chen W, et al. Mesenchyme homeobox 1 mediates transforming growth factor-β (TGF-β)-induced smooth muscle cell differentiation from mouse mesenchymal progenitors. *J Biol Chem*. 2018;293(22):8712–8719. doi:10.1074/jbc.RA118.002350
25. Wu Y, Li YJ, Shi LL, et al. Spatio-temporal model of *Meox1* expression control involvement of Sca-1-positive stem cells in neointima formation through the synergistic effect of Rho/CDC42 and SDF-1α/CXCR4. *Stem Cell Res Ther*. 2021;12(1):387. doi:10.1186/s13287-021-02466-8
26. Huang M, Li X, Li G. Mesenchyme homeobox 1 mediated-promotion of osteoblastic differentiation is negatively regulated by mir-3064-5p. *Differentiation*. 2021;120:19–27. doi:10.1016/j.diff.2021.05.002
27. Wei Z, Han C, Li H, et al. Molecular mechanism of mesenchyme homeobox 1 in transforming growth factor β1-induced *P311* gene transcription in fibrosis. *Front Mol Biosci*. 2020;7:59. doi:10.3389/fmolb.2020.00059
28. Stelnicki EJ, Harrison MR, Holmes D, et al. The human homeobox genes *MSX-1*, *MSX-2*, and *MOX-1* are differentially expressed in the dermis and epidermis in fetal and adult skin. *Differentiation*. 1997;62(1):33–41. doi:10.1046/j.1432-0436.1997.6210033.x
29. Douville JM, Cheung DYC, Herbert KL, Moffatt T, Wigle JT. Mechanisms of MEOX1 and MEOX2 regulation of the cyclin dependent kinase inhibitors p21CIP1/WAF1 and p16INK4a in vascular endothelial cells. *PLoS One*. 2011;6(12):e29099. doi:10.1371/journal.pone.0029099
30. Wu B, Zhang L, Zhu YH, et al. Mesoderm/mesenchyme homeobox gene l promotes vascular smooth muscle cell phenotypic modulation and vascular remodeling. *Int J Cardiol*. 2018;251:82–89. doi:10.1016/j.ijcard.2017.10.098
31. Lu D, Wang J, Li J, et al. *Meox1* accelerates myocardial hypertrophic decompensation through Gata4. *Cardiovasc Res*. 2018;114(2):300–311. doi:10.1093/cvr/cvx222
32. Alexanian M, Przytycki PF, Micheletti R, et al. A transcriptional switch governs fibroblast activation in heart disease. *Nature*. 2021;595(7867):438–443. doi:10.1038/s41586-021-03674-1
33. Sivakumar P, Thompson JR, Ammar R, et al. RNA sequencing of transplant-stage idiopathic pulmonary fibrosis lung reveals unique pathway regulation. *ERJ Open Res*. 2019;5(3):00117–02019. doi:10.1183/23120541.00117-2019
34. Xu L, Hui AY, Albanis E, et al. Human hepatic stellate cell lines, LX-1 and LX-2: New tools for analysis of hepatic fibrosis. *Gut*. 2005;54(1):142–151. doi:10.1136/gut.2004.042127
35. Guimarães EL, Stradiot L, Mannaerts I, Schroyen B, Van Grunsven LA. P311 modulates hepatic stellate cells migration. *Liver Int*. 2015;35(4):1253–1264. doi:10.1111/liv.12691
36. Wobbrock JO, Findlater L, Gergle D, Higgins JJ. The aligned rank transform for nonparametric factorial analyses using only anova procedures. In: *Proceedings of the SIGCHI Conference on Human Factors in Computing Systems*. Vancouver, Canada: Association for Computing Machinery (ACM); 2011:143–146. doi:10.1145/1978942.1978963
37. Elkin LA, Kay M, Higgins JJ, Wobbrock JO. An aligned rank transform procedure for multifactor contrast tests. In: *The 34th Annual ACM Symposium on User Interface Software and Technology*. Virtual Event USA: Association for Computing Machinery (ACM); 2021:754–768. doi:10.1145/3472749.3474784
38. Fabregat I, Moreno-Càceres J, Sánchez A, et al. TGF -β signalling and liver disease. *FEBS J*. 2016;283(12):2219–2232. doi:10.1111/febs.13665
39. Dooley S, Ten Dijke P. TGF-β in progression of liver disease. *Cell Tissue Res*. 2012;347(1):245–256. doi:10.1007/s00441-011-1246-y

40. Caja L, Dituri F, Mancarella S, et al. TGF-β and the tissue microenvironment: Relevance in fibrosis and cancer. *Int J Mol Sci*. 2018;19(5):1294. doi:10.3390/ijms19051294
41. Zhang DW, Zhao YX, Wei D, et al. HAb18G/CD147 promotes activation of hepatic stellate cells and is a target for antibody therapy of liver fibrosis. *J Hepatol*. 2012;57(6):1283–1291. doi:10.1016/j.jhep.2012.07.042
42. Li HY, Ju D, Zhang DW, et al. Activation of TGF-β1-CD147 positive feedback loop in hepatic stellate cells promotes liver fibrosis. *Sci Rep*. 2015;5(1):16552. doi:10.1038/srep16552
43. Matsuzaki K. Smad phosphoisoform signals in acute and chronic liver injury: Similarities and differences between epithelial and mesenchymal cells. *Cell Tissue Res*. 2012;347(1):225–243. doi:10.1007/s00441-011-1178-6
44. Xu F, Liu C, Zhou D, Zhang L. TGF-β/SMAD pathway and its regulation in hepatic fibrosis. *J Histochem Cytochem*. 2016;64(3):157–167. doi:10.1369/0022155415627681
45. el-Deiry WS, Harper JW, O'Connor PM, et al. WAF1/CIP1 is induced in p53-mediated G1 arrest and apoptosis. *Cancer Res*. 1994;54(5):1169–1174. PMID:8118801.
46. Tu S, Huang W, Huang C, Luo Z, Yan X. Contextual regulation of TGF-β signaling in liver cancer. *Cells*. 2019;8(10):1235. doi:10.3390/cells8101235
47. Dufton NP, Peghaire CR, Osuna-Almagro L, et al. Author Correction: Dynamic regulation of canonical TGFβ signalling by endothelial transcription factor ERG protects from liver fibrogenesis. *Nat Commun*. 2020;11(1):1301. doi:10.1038/s41467-020-15151-w
48. Ekholm SV, Reed SI. Regulation of G1 cyclin-dependent kinases in the mammalian cell cycle. *Curr Opin Cell Biol*. 2000;12(6):676–684. doi:10.1016/S0955-0674(00)00151-4
49. Moustakas A, Kardassis D. Regulation of the human p21/WAF1/Cip1 promoter in hepatic cells by functional interactions between Sp1 and Smad family members. *Proc Natl Acad Sci U S A*. 1998;95(12):6733–6738. doi:10.1073/pnas.95.12.6733
50. Blomen VA, Boonstra J. Cell fate determination during G1 phase progression. *Cell Mol Life Sci*. 2007;64(23):3084–3104. doi:10.1007/s00018-007-7271-z
51. Alenzi FQB. Links between apoptosis, proliferation and the cell cycle. *Br J Biomed Sci*. 2004;61(2):99–102. doi:10.1080/09674845.2004.11732652
52. Pauklin S, Vallier L. The cell-cycle state of stem cells determines cell fate propensity [published correction appears in: *Cell*. 2014;156(6):1338. doi:10.1016/j.cell.2014.02.044]. *Cell*. 2013;155(1):135–147. doi:10.1016/j.cell.2013.08.031
53. Calder A, Roth-Albin I, Bhatia S, et al. Lengthened G1 phase indicates differentiation status in human embryonic stem cells. *Stem Cells Dev*. 2013;22(2):279–295. doi:10.1089/scd.2012.0168
54. Sela Y, Molotski N, Golan S, Itskovitz-Eldor J, Soen Y. Human embryonic stem cells exhibit increased propensity to differentiate during the G1 phase prior to phosphorylation of retinoblastoma protein. *Stem Cells*. 2012;30(6):1097–1108. doi:10.1002/stem.1078
55. Clegg CH, Linkhart TA, Olwin BB, Hauschka SD. Growth factor control of skeletal muscle differentiation: Commitment to terminal differentiation occurs in G1 phase and is repressed by fibroblast growth factor. *J Cell Biol*. 1987;105(2):949–956. doi:10.1083/jcb.105.2.949
56. Li CY, Suardet L, Little JB. Potential role of WAF1/Cip1/p21 as a mediator of TGF-β cytoinhibitory effect . *J Biol Chem*. 1995;270(10):4971–4974. doi:10.1074/jbc.270.10.4971

Genetically determined thyroid function and cerebral cortex structure: A Mendelian randomization study

Xupeng Wu[1,2,A], Hong Liu[2,A], Liangliang Cui[2,B], Mengyan Mo[2,C], Changxin Li[1,D–F]

[1] Department of Neurology, First Hospital of Shanxi Medical University, Taiyuan, China
[2] Department of Neurology, Peace Hospital affiliated to Changzhi Medical College, China

A – research concept and design; B – collection and/or assembly of data; C – data analysis and interpretation; D – writing the article; E – critical revision of the article; F – final approval of the article

Advances in Clinical and Experimental Medicine, ISSN 1899–5276 (print), ISSN 2451–2680 (online) *Adv Clin Exp Med*. 2025;34(11):1863–1879

Address for correspondence
Changxin Li
E-mail: Leeverygreat@outlook.com

Funding sources
None declared

Conflict of interest
None declared

Acknowledgements
We would like to thank the THYROIDOMICS and ENIGMA consortia for providing GWAS data.

Received on August 30, 2024
Reviewed on December 1, 2024
Accepted on December 18, 2024

Published online on July 23, 2025

Abstract

Background. A correlation between thyroid function and cognitive impairment has been well established; however, the impact of thyroid dysfunction on structural changes in the brain cortex remains largely unexplored.

Objectives. The study describes a 2-sample Mendelian randomization (MR) analysis to elucidate the relationship between thyroid malfunction and brain structure and function.

Materials and methods. Eight phenotypes of thyroid function were extracted from THYROIDOMICS consortium by determining free thyroxine (FT4) and thyroid-stimulating hormone (TSH) levels in both men and women separately and together, as well as in individuals with increased or decreased TSH levels. The results were assessed in terms of overall brain cortical thickness and the surface area (SA) of grey matter, along with 34 specific measurements for various regions. The primary method employed for the analysis was the inverse-variance weighted (IVW) approach.

Results. The data were subjected to MR Egger regression, Cochrane's Q statistic and leave-one-out analysis to determine the correlation between the variables. The FT4 in men, women and overall was statistically associated with cortical thickness of entorhinal cortex (EC). Overall TSH and TSH in men were associated with cortical thickness of caudal anterior cingulate. Additionally, in men, TSH levels showed an association with cortical thickness in the cuneus gyrus. Increased TSH was associated with decreased SA of lateral occipital (LO) and increased SA of lateral orbitofrontal, medial orbitofrontal and superior frontal cortex. Decreased TSH was negatively associated with the SA of pars opercularis (PO) and the cortical thickness of posterior cingulate cortex. No pleiotropy was detected.

Conclusions. Our findings indicate a possible causal link between thyroid function and the cortical architecture of particular functional areas associated with neurodegenerative and psychiatric conditions.

Key words: cognitive function, thyroid function, Mendelian randomization, cerebral cortex structure, psychological diseases

Cite as
Wu X, Liu H, Cui L, Mo M, Li C. Genetically determined thyroid function and cerebral cortex structure: A Mendelian randomization study. *Adv Clin Exp Med*. 2025;34(11):1863–1879. doi:10.17219/acem/199321

DOI
10.17219/acem/199321

Highlights

- Thyroid hormones (THs) play an essential role in regulating the development and differentiation of neurons and neuroglia, alongside the overall development and functionality of the central nervous system (CNS).
- A relationship between thyroid function and cognitive impairment has been noted; however, the effects of thyroid dysfunction on alterations in brain cortex structure remain to be explored.
- Researchers can visualize psychiatric diseases and cognitive decline by modifying cerebral cortex anatomy. Thus, various research have examined how thyroid function affects cerebral cortex structure.
- Mendelian randomization (MR) techniques were developed to determine the potential relationship between genetically influenced exposures and clinical outcomes.
- Our findings indicate a possible causal link between thyroid function and the cortical architecture of particular functional areas associated with neurodegenerative and psychiatric conditions.

Background

The central nervous system (CNS) and the endocrine system are inextricably connected. Thyroid hormones (THs) are critical for the regulation of the development and differentiation of neurons and neuroglia, as well as the development and function of the CNS. Tri-iodothyronine (T_3) stimulates the nervous system, enabling vigilance, wakefulness and responsiveness to external stimuli. Moreover, TH stimulates the peripheral nervous system, enhancing gastrointestinal tone, motility and peripheral reflexes. Neurological impairments and psychiatric abnormalities can result from aberrant TH levels, which are essential for the maintenance of normal brain functions.[1,2] Emerging evidence suggests a potential causal relationship between TH regulation and specific cortical structures, providing novel insights into the neurobiological mechanisms underlying the cognitive and psychiatric manifestations of thyroid dysfunction. This association has significant implications for understanding the pathophysiology of conditions like hypothyroidism-induced depression and cognitive impairment, informing novel therapeutic strategies.[3] The relationships between thyroid function and specific cortical structures may be mediated by neural substrates involving the hypothalamic–pituitary–thyroid axis, influencing neuroplasticity and synaptic pruning. Key regions include the hippocampus, amygdala and prefrontal cortex, where THs regulate gene expression, neurotrophic factors and neurotransmitter modulation, impacting cognitive and emotional processing.[4] Patients with hypothyroidism frequently experience neurological and psychiatric symptoms, such as mood disorders, impaired memory and lack of concentration.[5] Untreated long-term hypothyroidism can cause peripheral neuropathy. Hyperthyroidism can induce various neuropsychiatric symptoms, including anxiety, restlessness, mood instability, insomnia, memory loss, and psychosis.[6–9] Moreover, cognitive decline can occur due to variations in serum TH levels, even within the reference range.[10–12]

By altering the structure of the cerebral cortex, it is possible to visualize psychiatric disorders and cognitive decline.[13,14] Consequently, numerous studies have documented the impact of thyroid function on the structural characteristics of the cerebral cortex. For instance, investigations have indicated that subclinical hypothyroidism notably decreases the gray matter volume (GMV) in several brain areas, including the orbitofrontal gyrus and right inferior occipital gyrus, which are involved in sensory functions, impulses and learning.[15] Su et al. found that the GMV of specific functional regions, such as the right superior frontal gyrus, superior temporal gyrus, medial frontal gyrus, and supplementary motor area, showed notable decreases in patients with untreated hypothyroidism.[16]

Similarly, Göbel et al. observed changes in GMV in specific brain regions among individuals with hyperthyroidism.[17] The condition results in a reduction of GMV in the bilateral hippocampus and para-hippocampal gyrus, left temporal pole and bilateral primary visual cortex.[18] Nevertheless, these studies failed to elucidate the directionality of these relationships. Moreover, the studies conducted with a limited sample size present several significant limitations, such as the challenge of determining reverse causality, the presence of potential confounding variables and discrepancies in interpretations. In light of this, it is crucial to investigate the possible causal impacts of thyroid function on the structure of the cerebral cortex. Examining causal effects can aid in pinpointing risk factors and mitigating the occurrence of thyroid disorders linked to neurological or psychological conditions.

Randomized controlled trials have proven to be valuable in exploring causal relationships; nonetheless, they face challenges such as inadequate long-term compliance from participants and several other complications. The examination of various genetic factors for their correlation with particular studies was facilitated by the accessibility of data from extensive genome-wide association studies (GWAS). As a result, methodologies based on Mendelian randomization (MR) were developed to determine the possible interaction between genetically influenced exposures and clinical outcomes. Genetic variations are considered crucial components in these methodologies.[19] Marouli et al.[20] previously

conducted a study utilizing MR to clarify the risk linked to a reduced likelihood of developing Alzheimer's disease (AD). The findings indicated that individuals with AD showed an elevation in genetically anticipated thyroid-stimulating hormone (TSH) levels, all while remaining within the normal range. A separate MR study indicated that hypothyroidism may lower the risk of developing schizophrenia. Consequently, it was hypothesized that THs could impact cognitive function and mental state by modifying the structure of particular cerebral functional regions.[21]

Consequently, we utilized the MR method to explore the causal relationships between thyroid function, both within normal and aberrant ranges, and the structure of the cerebral cortex, which includes the global cerebral cortex along with its 34 functional subdivisions.[22] The MR method is utilized for its ability to leverage genetic diversity in examining the causal relationship between exposures and outcomes. This approach utilizes genetic variants as natural experiments, randomly distributed during meiosis, which helps to reduce confounding and misinterpretation of results from epidemiological studies. It effectively avoids reverse causation, ensuring that the genetic variations used in these studies are not influenced by the onset or progression of outcomes. This method provides unbiased estimates of the effects of a causal variable without requiring a traditional randomized controlled trial. As a result, MR is primarily utilized in conjunction with various forms of information for the purpose of causal inference. We investigated single nucleotide polymorphisms (SNPs) to assess whether there is a relationship between an SNP and thyroid function, and how it may influence specific cortical thickness (CT) or surface area (SA) outcomes. After performing a comprehensive literature review, no MR-based study was identified that explored the relationship between cortical thickness, SA of the cerebral cortex and thyroid function phenotypes.

Objectives

This paper presents a 2-sample MR analysis to elucidate the relationship between thyroid dysfunction and brain structure and function.

Materials and methods

Study design and data sources

The guidelines outlined in Strengthening the Reporting of Observational Studies in Epidemiology using MR (STROBE-MR) were followed.[23] We accessed the online database (Datasets – The ThyroidOmics Consortium, uni-greifswald.de), which includes GWAS summary data from a meta-analysis conducted by the THYROIDOMICS consortium, to obtain TH measurements. The database includes participants of European ancestry. We analyzed data from 54,288 individuals across 22 independent cohorts for TSH and 49,269 study participants across 19 independent cohorts for free thyroxine (FT4), providing sufficient power (≥80%) to detect small-to-moderate effects (0.1–0.3 standard deviations (SDs)) with a type I error rate of 0.05. The analysis employed MR methods (inverse-variance weighted (IVW), weighted median and MR-Egger regression) and addressed pleiotropy and heterogeneity, ensuring robust estimates of causal relationships. We excluded the data from participants taking thyroid medications or undergoing thyroid surgery. We considered the eligible participants with hormone levels within the cohort-specific reference range to have continuous phenotypes. To gain a comprehensive perspective, we also identified participants with TSH levels exceeding the upper and lower cohort-specific reference ranges, both elevated and decreased, using the summary data.

Assumptions

Three basic assumptions provided the basis of the MR analysis. First, the relevance assumption established a robust correlation between the exposure and the genetic variants. Second, we analyzed the genetic variants to ensure they were not associated with any confounding factors that could influence the exposure–outcome relationship. Finally, we examined the SNPs as genetic variants that influenced the outcome, such as changes in TH levels and/or brain structure, without being affected by alternative pathways. We primarily collected data on normal range thyroid function, as indicated by TSH and FT4 levels, and correlated them with functional regions of the brain. We assessed changes in brain regions by considering variations in cortical thickness and SA. Consequently, we analyzed the causal effects of thyroid dysfunction, specifically hyperthyroidism or hypothyroidism, as indicated by TSH levels, on the cortical structure of 34 distinct brain regions. Figure 1 depicts the overview of this study.

Statistical analyses

Thirty-four specific brain regions were considered as phenotypes. Bonferroni-corrected p-values (i.e., $0.05/544 = 9.192 \times 10^{-5}$) were used to analyze brain region-level data in 544 MR estimates, accounting for multiple testing. The correlation data were considered significant if the p-value exceeded the Bonferroni-corrected threshold but remained below 0.05. A stronger association between the parameters was declared if the p-value was below 0.01. The study employed Bonferroni correction to adjust for multiple testing, reducing the risk of type I errors. However, the stringent p-value threshold ($p < 0.001$) may have increased the risk of type II errors in this study, potentially obscuring true associations. For the analysis of changes in cortical regions at the global cortical level, statistical significance was considered if the p-value was < 0.05.

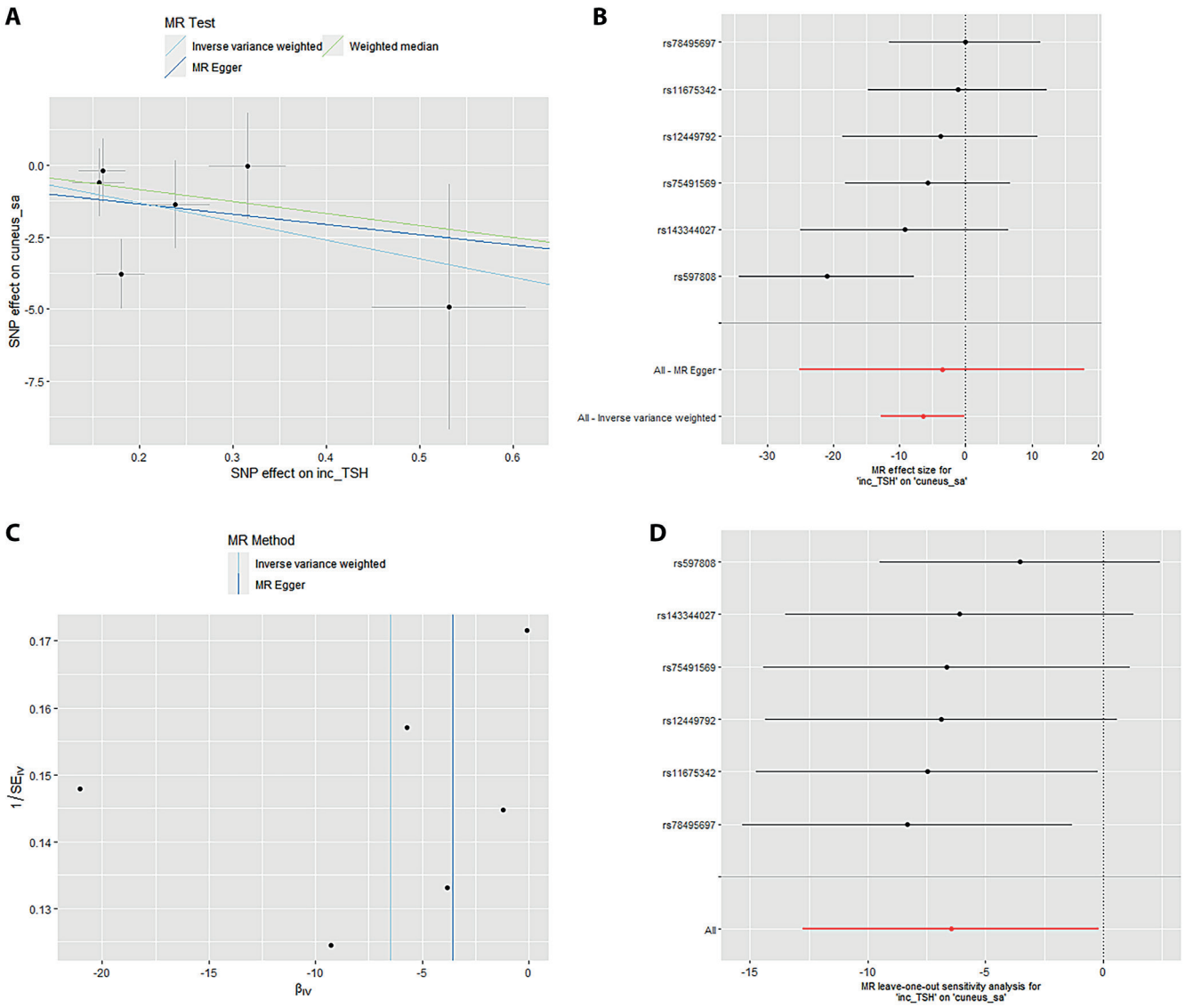

Fig. 1. Analysis of incTSH_cuneus_SA. A. Scatter plot; B. Forest plot; C. Funnel plot; D. Leave-one-out sensitivity analysis

MR – Mendelian randomization; TSH – thyroid-stimulating hormone; SNP – single nucleotide polymorphism.

Mendelian randomization analysis

To address pleiotropy, SNPs were selected using thyroid-related GWAS data and proxy SNPs ($R^2 > 0.8$) for index SNPs that had not been explicitly genotyped in this study. The MR methods used were the IVW method for estimating causal effects using SNPs as instruments to account for multiplicative random effects,[24] the weighted median method and the MR-Egger regression. In order to mitigate the potential influence of horizontal pleiotropy on IVW estimations, MR-Egger regression was used for analyzing pleiotropy and estimated causal effects, and weighted median, weighted mode and simple mode methods were employed for addressing the potential heterogeneity. The MR-Egger method is commonly employed to detect instances of directional pleiotropy caused by genetic variants. Additionally, it can identify pleiotropic effects that are not associated with genetic variant exposure in general.[25] The presence of horizontal pleiotropy was assessed using the weighted median approach. The instrument variables were considered valid if they accounted for more than 50% of the variation.[26] The utilization of the weighted mode approach can effectively yield reliable estimates for both valid and invalid cases in general.[27]

Sensitivity analyses and outlier analyses

Several sensitivity studies were conducted to account for pleiotropy and obtain dependable MR outcomes. The presence of putative directional horizontal pleiotropy was assessed using Merger regression, with a p-value of less than 0.05 for the intercept term.[28] The occurrence of pleiotropy was assessed for heterogeneity using Cochran's

Q statistic,[25] with a significance level of $p < 0.001$. In addition, the existence of horizontal pleiotropy ($p < 0.001$) was assessed using the MR Pleiotropy Residual Sum and Outlier (MR-PRESSO) global tests.[29] To assess an outlier, a leave-one out study was conducted. In this analysis, a p-value of less than 0.05 was used to determine if the MR results were significantly influenced by the exclusion of a single SNP.

Assessment of assumptions

For the MR analysis, this study considered the SNP as a genetic instrument. The associations between SNPs and the disorder were included if they exhibited genome-wide significance with $p < 0.001$ and the same was ascertained by excluding SNPs in linkage disequilibrium ($R^2 > 0.001$ and clump window <10,000 kb). The strength of genetic instruments was determined through F-statistics and SNPs with an F-value <10 were excluded. The data were harmonized, and SNPs with either palindromic or intermediate allele frequencies were excluded, as were outcome-related SNPs that did not meet the genome-wide significance threshold ($p \geq 0.001$). To exclude potential bias by risk factors and fulfill the requirements of the 2nd MR hypothesis, the reminding SNPs were searched in the PhenoScanner database.[30] The study included 9 possible confounders[31–38]: habits of smoking, coffee, and alcohol, diagnosed psychiatric disorders, years of educational attainment, migraine, diagnosed coronary artery diseases, body mass index (BMI), and sleep disorders. The PhenoScanner database revealed that no SNP was associated with migraine, educational attainment, psychiatric disorders, sleep disorders, or coffee intake. However, we identified 1 SNP (rs597808) associated with smoking and cardiovascular diseases, while 3 SNPs (rs1045476, rs4445669 and rs11039355) were linked to BMI. The remaining SNPs were excluded from further analysis due to their lack of direct association with brain structure and related confounders.

Software and data analysis

An online database (https://enigma.ini.usc.edu/research/download-enigma-gwas-results) was browsed and the summary of statistical data from the ENIGMA consortium was downloaded.[39] The data on cerebral cortical SA [mm^2] and CT [mm] were obtained from a meta-analysis. This GWAS summary data provided access to 51,665 individuals, mainly from the European population (94%). The data were analyzed across 60 cohorts using T1-weighted magnetic resonance imaging (MRI). An additive model was constructed for adjusted routine personal data (including sex, age, their squared values, their interaction, and their squared value), and the genetic associations for each cohort were analyzed. The Desikan–Killiany atlas[40] was referred to as state 34 brain regions with known functional specializations. These functional regions of brains were analyzed through the MR approach by using globally weighted estimates and excluding the measures of regional phenotypes. It was carried out to avoid neuroanatomical variability between different individuals in regional phenotypes.

Results

Thyroid function is linked to specific brain regions, impacting neurobiological mechanisms. Hypothyroidism is associated with reduced hippocampal volume, leading to impairments in memory and learning. It affects amygdala activity, altering emotional regulation. Thyroid hormones modulate neurotransmitter balance, impacting cerebral cortex, basal ganglia and cerebellum, influencing mood, cognition and motor function, respectively.

Causal estimation for all brain regions

Initially, 4 indicator SNPs were screened separately for the data related to FT4 of men (FT4_men) and women (FT4_women) prediction while 10 indicator SNPs were analyzed for FT4 overall (FT4_overall). Likewise, 16 indicator SNPs were separately tested for TSH of men (TSH_men) and women (TSH_women) and 25 indicator SNP for overall TSH (TSH_overall). For increased TSH (inc_TSH) and decreased TSH (dec_TSH), 5 and 6 SNPs were included, respectively. As a criterion, the F-statistics of these genetic tools were considered significant if found greater than the normal selection value of 10. The complete results of causal estimation for all brain regions are shown in Fig. 1–6.

Mendelian randomization Egger

Mendelian randomization Egger (MR-Egger) was performed to analyze a directional pleiotropy test, a causal effect test and an estimation of the causal impact assuming that all genetic variants met the primary assumptions. However, the MR-Egger method can determine if genetic variants have pleiotropic effects on the outcome that deviate from 0 on average (directional pleiotropy). Figure 1 displays an analysis of the incTSH_cuneus_SA. Figure 1A depicts a scatter plot that shows the correlation between the effect of SNP on cuneus_SA and its influence on cuneus_TSH. It demonstrates that SNPs influence not only the composition and functionality of the gene product but also its quantity. Meanwhile, Fig. 1B presents a forest plot illustrating the results of the MR analysis, which assesses the relationship between cuneus SA (cuneus_SA) and TSH levels (cuneus_TSH). Point estimations are quantified as the alteration in the magnitude of the MR effect size. Figure 1C depicts the funnel plot, which exhibits asymmetry caused by certain genetic variations that have exceptionally powerful influence on the result

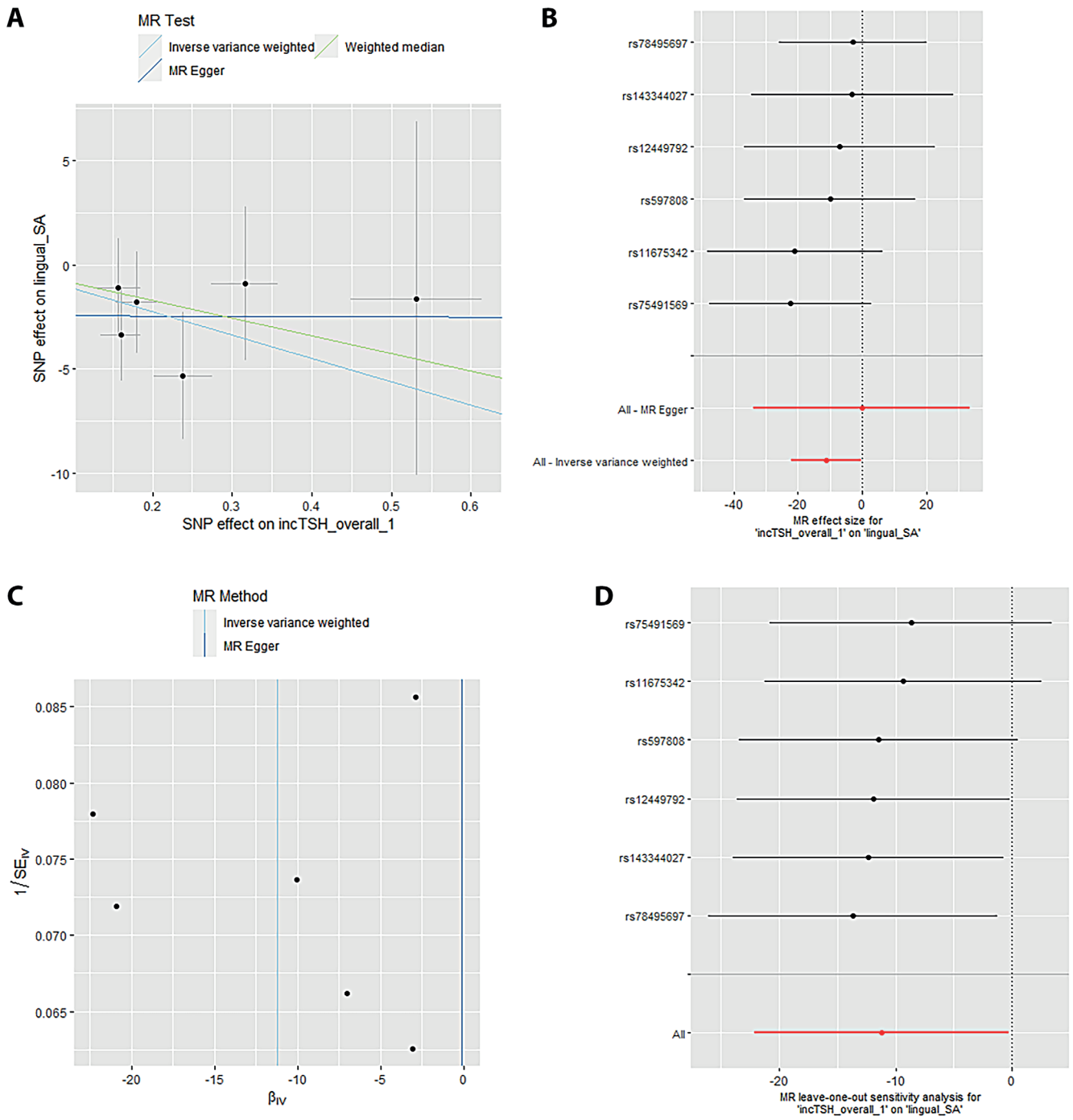

Fig. 2. Analysis of incTSH_overall_1 lingual_SA. A. Scatter plot; B. Forest plot; C. Funnel plot; D. Leave-one-out sensitivity analysis

MR – Mendelian randomization; TSH – thyroid-stimulating hormone; SNP – single nucleotide polymorphism.

despite having poor precision. This asymmetry suggests the presence of directional pleiotropy. Figure 1D presents the leave-one-out sensitivity analysis. This method systematically excludes each genetic variant from the MR analysis one at a time to assess the robustness of the results and identify any influential variants that may disproportionately affect the overall findings. Likewise, Fig. 2 displays the similar analysis of the incTSH_overall_1 lingual_SA, Fig. 3 for incTSH_overall_1 superiorfrontal_thick, Fig. 4 displays a research analysis of the thickness of the lateral occipital (LO) region in men, utilizing FT4 data, Fig. 5 shows analysis of LO thickness in women with FT4, and Fig. 6 presents the study of temporal pole thickness in women with FT4.

The data revealed 7 causal relationships between thyroid function traits and regional cortical thickness, which exhibited nominal statistical significance. Additionally, 5 causal relationships between thyroid function traits and regional cortical SA were observed to be statistically significant. Unfortunately, the study did not find any statistically

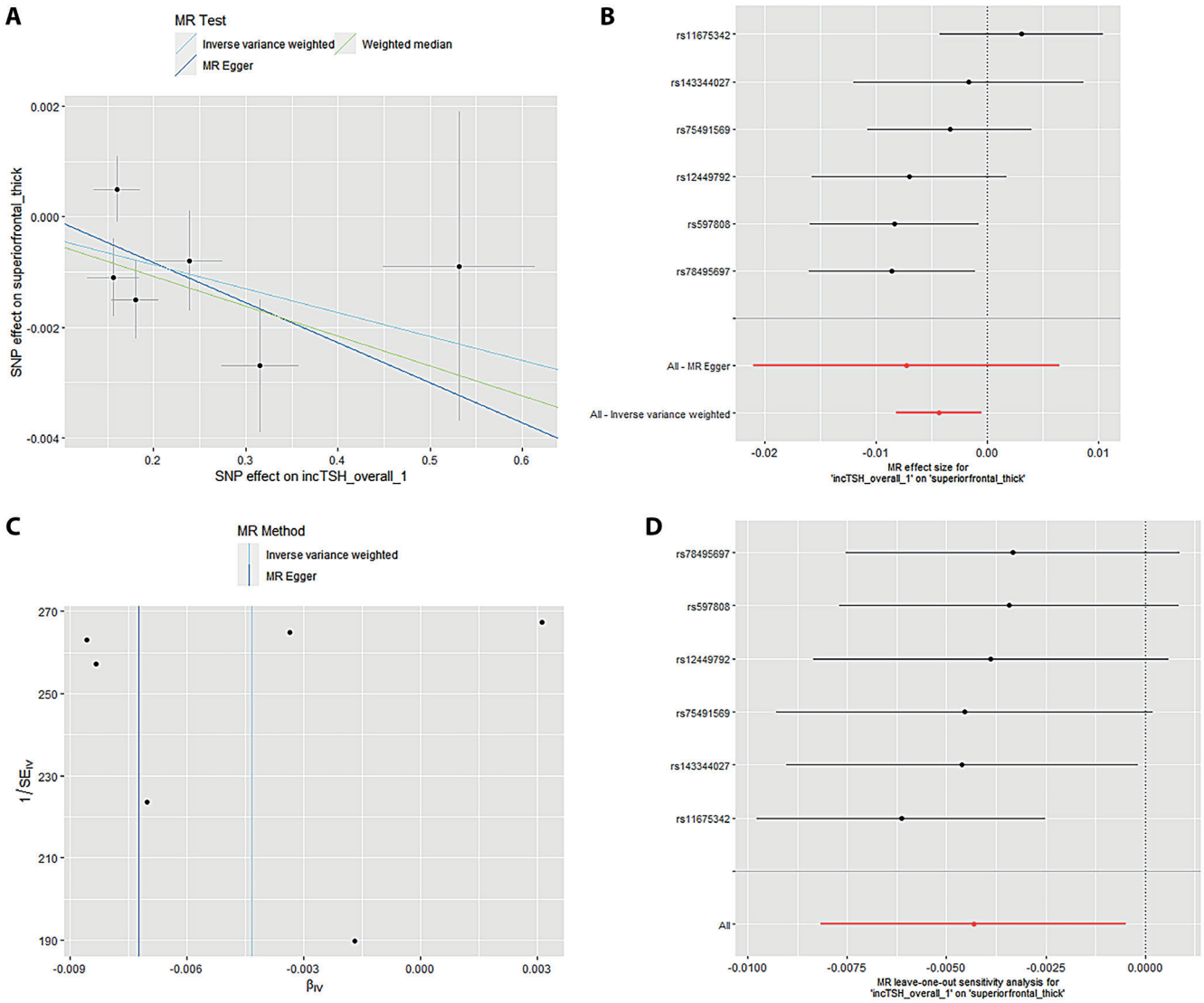

Fig. 3. Analysis of incTSH_overall_1 superiorfrontal_thick. A. Scatter plot; B. Forest plot; C. Funnel plot; D. Leave-one-out sensitivity analysis

MR – Mendelian randomization; TSH – thyroid-stimulating hormone; SNP – single nucleotide polymorphism.

significant results indicating the impact of thyroid function features on cortical structure in 34 brain functional regions (all $p > 0.001$). The data showed 7 causal relationships between thyroid functional trait and regional cortical thickness, which were found to have nominal statistical significance while 5 causal relationships between thyroid function traits and regional cortical SA were observed to be statistically significant. However, the impact of thyroid function traits on cortical structure could not be determined in 34 brain functional regions as the results were not statistically significant (all $p > 0.001$).

The data from the IVW model indicated that, at the functional area level with overall weighted analysis, genetically predicted levels of FT4 in men, women and the overall population were all positively associated with the thickness of the EC. Likewise, for FT4_men and FT4_women, weighted median method was of similar significance. Nonetheless, the consistent direction of association was determined through MR-Egger, simple mode and weighted mode methods. For FT4_overall, the other 4 methods also yielded consistent directions of association with IVW. The data analyzed with overall weighted analysis the IVW model showed that in the functional area level, genetic predicted levels of FT4_men, FT4_women were associated with the thickness of LO sulcus positively with weighted median of similar significance. Moreover, the consistency in the direction of association was strengthened by analysis made through MR-Egger, simple mode and weighted mode methods. Moreover, for another functional area, caudal anterior cingulate cortex (cACC), overall weighted analysis in the IVW model predicted that the level of TSH_overall and TSH_men were separately associated positively with the thickness of this area. For the former, the results were found consistent in the directions of association when analyzed through MR-Egger, weighted median method, simple mode, and

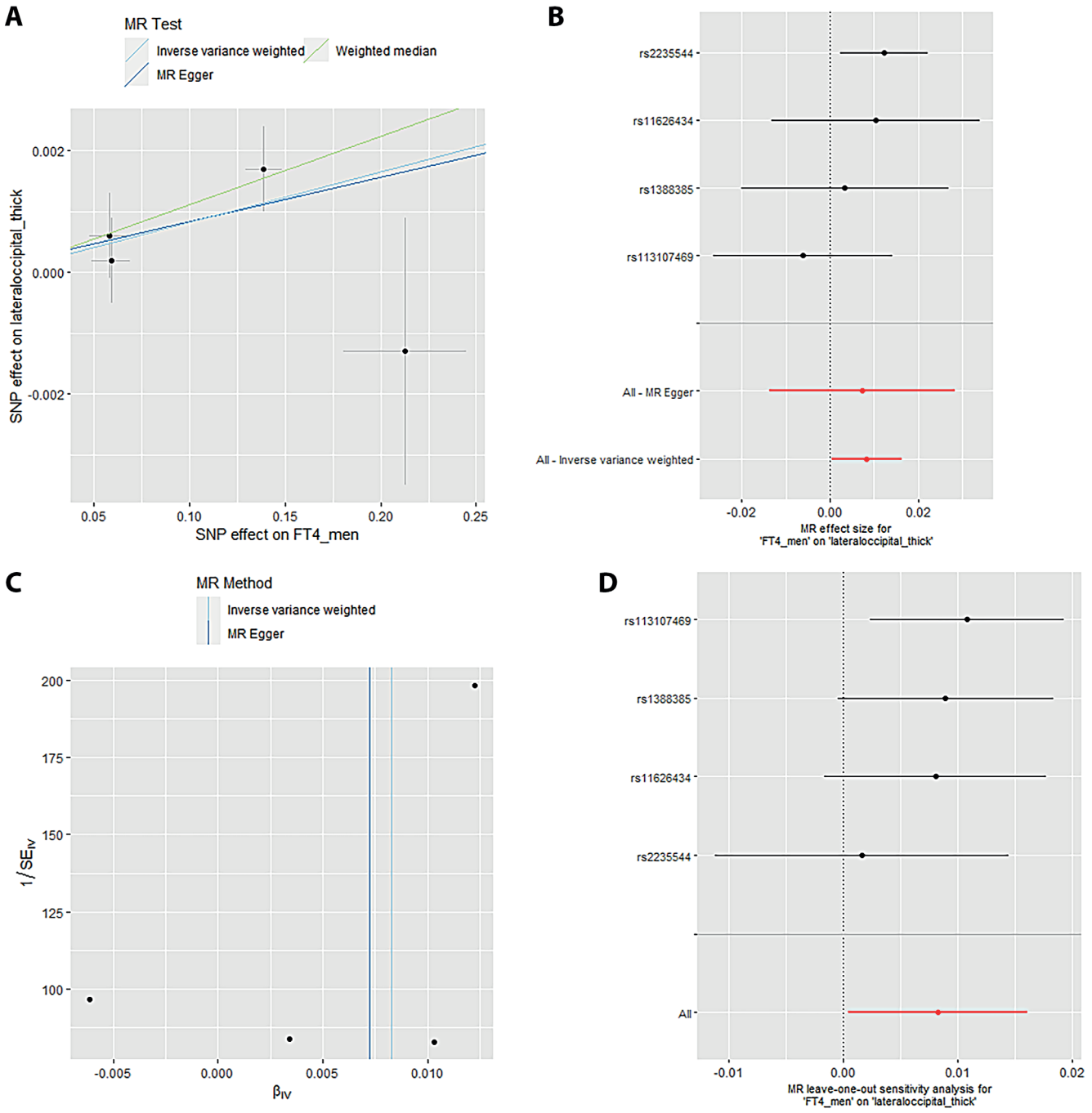

Fig. 4. Analysis of FT4-men lateraloccipital_thick. A. Scatter plot; B. Forest plot; C. Funnel plot; D. Leave-one-out sensitivity analysis

MR – Mendelian randomization; TSH – thyroid-stimulating hormone; SNP – single nucleotide polymorphism.

weighted mode methods. For the latter, except for MR-Egger, the outcome of other methods affirmed the findings obtained with IVW. The genetic predicted level of TSH_men was also found associated with the thickness of cuneus gyri positively (β (SE): 0.007 (0.004, p = 0.040) through overall weighted analysis by the IVW model. Indeed, the weighted median method and simple mode method yielded consistent directions of association. However, MR-Egger and weighted mode methods obtained opposite directions of association. The data from overall weighted analysis and the IVW model showed that genetic predicted level of FT4_women was associated with the thickness of temporal pole positively. Except for simple mode method, MR-Egger, weighted median method and weighted mode methods supported the directions of association with IVW. The IVW model in the functional area level with overall weighted analysis revealed a reduction in the mean SA of LO (β (SE): –20.246 (8.640), p = 0.019) due to genetic predicted hypothyroidism (inc_TSH) and an increase in the mean SA

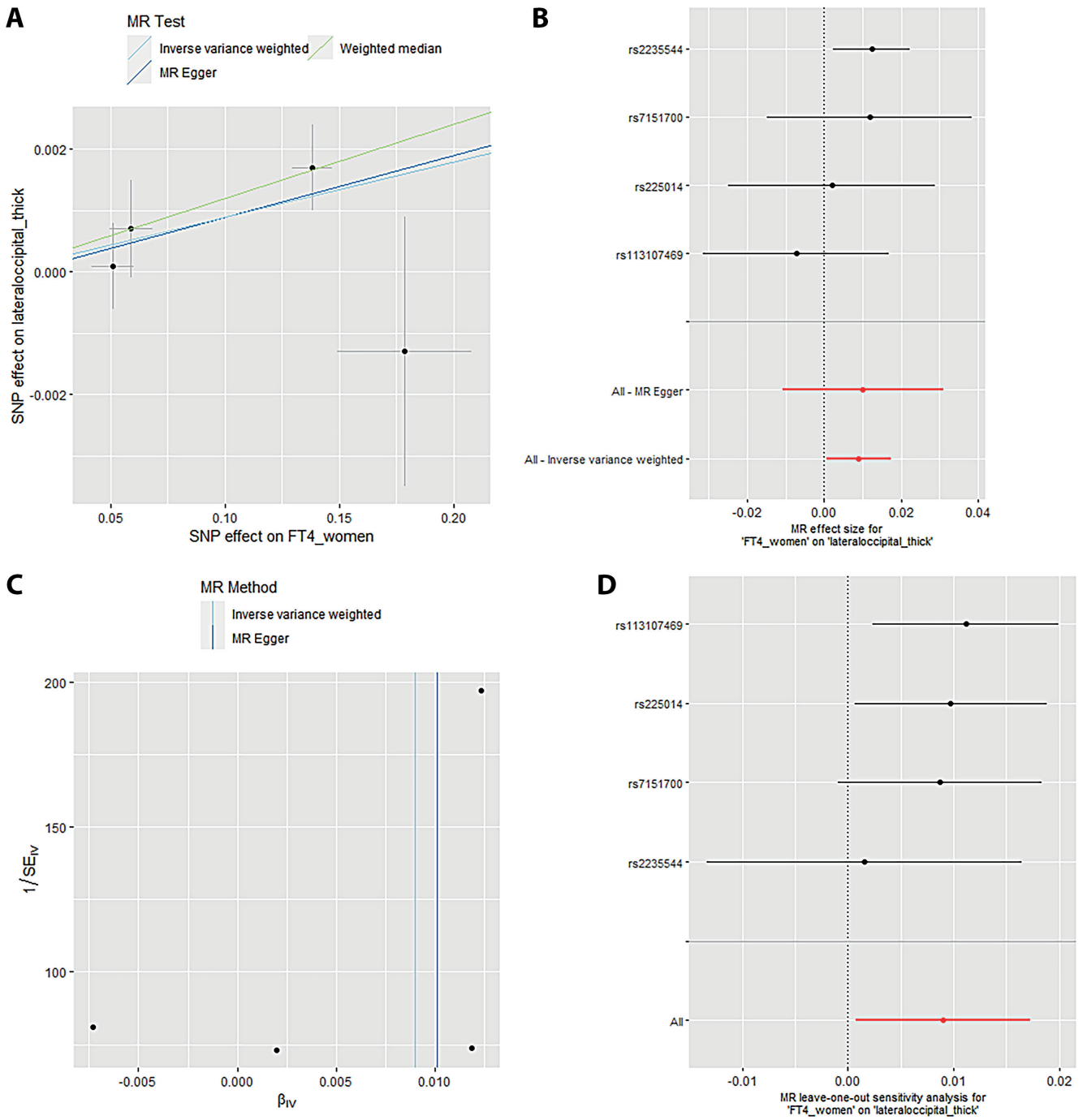

Fig. 5. Analysis of FT4-women lateraloccipital_ thick. A. Scatter plot; B. Forest plot; C. Funnel plot; D. Leave-one-out sensitivity analysis

MR – Mendelian randomization; TSH – thyroid-stimulating hormone; SNP – single nucleotide polymorphism.

of lateral orbitofrontal gyri (LOF), medial orbitofrontal gyri (MOF) and superior frontal gyrus (SFG). The consistency in the direction of this association was affirmed by MR-Egger, weighted median method, simple mode, and weighted mode methods. Moreover, the weighted median method also exhibited similar significance for the association of inc_TSH and the SA of MOF. Regarding genetic predicted hyperthyroidism (dec_TSH), the IVW model presented a reduction in the mean SA of PO and the mean thickness of posterior cingulate cortex (PCC). The weighted median method corroborated this significance. The consistency in the data, particular for the directionality of association was affirmed through MR-Egger, simple mode and weighted mode methods. No significant horizontal pleiotropy (all $p > 0.05$) was detected for the reported significant causalities as was analyzed through MR-Egger intercept test, the MR-PRESSO test and Cochran's Q test. The leave-one-out analyses also confirmed that no SNP could significantly influence the causal estimates.

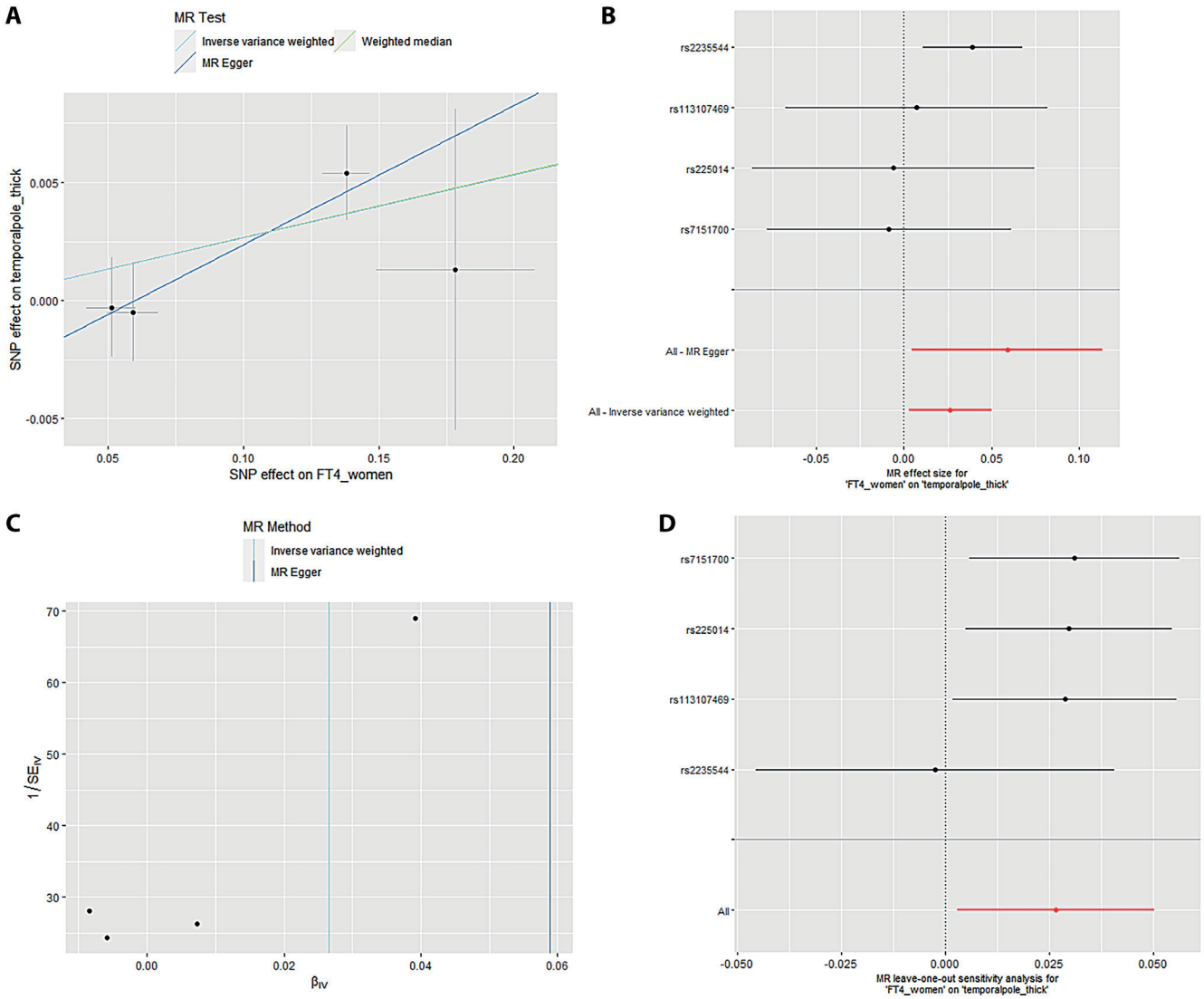

Fig. 6. Analysis of FT4-women temporalpole_thick. A. Scatter plot; B. Forest plot; C. Funnel plot; D. Leave-one-out sensitivity analysis

MR – Mendelian randomization; TSH – thyroid-stimulating hormone; SNP – single nucleotide polymorphism.

Table 1. Horizontal pleiotropy analysis for 6 different outcomes associated with FT4 and TSH levels

Exposure	Outcome	MR-Egger intercept test			MR-PRESSO global test		Cochran's Q
		Egger intercept	SE	p-value	RSS obs	p-value	p-value
inc_TSH cuneus_sa	cuneus_SA	–0.6405	2.294	0.7939	9.865	0.293	0.162
incTSH_overall_1	lingual_SA	–0.1138	17.21	0.9950	3.134	0.836	0.026
incTSH_overall_1	superiorfrontal_thick	–0.0072	0.0070	0.3609	10.510	0.223	0.078
FT4_men	lateraloccipital_thick	0.0001	0.00106	0.9239	2.753	0.4314	0.255
FT4_women	lateraloccipital_thick	–0.00011	0.00104	0.9192	7.1135	0.491	0.292
FT4_women	temporalpole-thick	–0.00349	0.00267	0.3236	10.542	0.413	0.634

TSH – thyroid-stimulating hormone; SA – surface area; FT4 – free thyroxine; SE – standard error; RSS – residual sum of squares.

Examination of horizontal pleiotropy for 6 distinct outcomes

Table 1 displays the examination of horizontal pleiotropy for 6 distinct outcomes linked to FT4 and TSH levels. The Egger intercept for cuneus_SA was –0.6405, with an standard error (SE) of 2.294 and a p-value of 0.794. The observed residual sum of squares (RSS) for the MR-PRESSO global test was 9.86, with a p-value of 0.293. Additionally, the p-value for Cochran's Q test was 0.1619.

The lingual_SA had an Egger intercept value of –0.1138, with SE of 17.21 and a p-value of 0.665. The observed RSS for the MR-PRESSO global test was 3.134, with a p-value of 0.836. Additionally, the p-value for Cochran's Q test was 0.0264. The value of the Egger intercept for superior frontal pole thickness was –0.0072, with SE of 0.007 and a p-value of 0.361. The observed RSS for the MR-PRESSO global test was 10.150, with a p-value of 0.223. Additionally, the p-value for Cochran's Q test was 0.078.

The lateral occipital pole thickness value for men had an Egger intercept of –0.0001 with SE of 0.00106 and a p-value of 0.924. The observed RSS for the MR-PRESSO global test was 2.753 with a p-value of 0.431. Additionally, the p-value for Cochran's Q test was 0.2546. The lateral occipital pole thickness in women had an Egger intercept of –0.00011, with SE of 0.00104 and a p-value of 0.919. The observed RSS for the MR-PRESSO global test was 7.1135, with a p-value of 0.491. Additionally, the p-value for Cochran's Q test was 0.29154. The temporal pole thickness in women had an Egger intercept value of –0.00349, with SE of 0.00267 and a p-value of 0.324. The observed RSS for the MR-PRESSO global test was 10.542, with a p-value of 0.413. Additionally, the p-value for Cochran's Q test was 0.634.

R2_F statistics for single nucleotide polymorphisms

Table 2 presents the R2_F statistics for various SNPs associated with 6 different outcomes related to FT4 and TSH levels. The IVW test computed odds ratios (ORs) for different brain regions (Table 3). The estimated OR for cuneus_SA was 1.147 (with a 95% confidence interval (95% CI) of 1.045–1.457) and a p-value of 0.008. The OR for lingual_SA was calculated to be 1.124 (95% CI: 1.027–1.241), and the p-value associated with this finding was 0.003. The OR for superior frontal thickness was 1.054 (1.004–1.147), and the p-value was 0.002. The OR for lateral occipital _ thickness in men was found to be 1.122 (1.031–1.234), with a p-value of 0.001. The OR for lateral occipital thickness in women was found to be 1.078 (1.005–1.161), accompanied by a p-value of 0.003. Finally, for women, the OR for temporal pole thickness was 1.114 (1.031–1.248) with a p-value of 0.001. Cochran's Q-test was utilized to assess horizontal multiplicity and to obtain more robust association estimates. The analysis revealed no evidence of horizontal multiplicity, as all p-values for the MR-Egger intercept test exceeded 0.05. Indeed, all p-values from Cochran's Q analysis were greater than 0.05.

Leave-one-out analyses

Sensitivity analyses are crucial in MR studies to assess the robustness and reliability of causal estimates, identifying potential biases, outliers or assumption violations. These analyses, including leave-one-out, influence, bootstrap, and robustness checks, increase confidence in findings and provide insight into underlying biological mechanisms. Sensitivity analyses, particularly leave-one-out tests, revealed that SNP (*rs2235544*) substantially influenced the MR estimates for FT4_women on temporal pole and LO thickness, as well as FT4_men on LO thickness in this study. Notably, removing this SNP (*rs2235544*) resolved the causal effects, underscoring the importance of sensitivity analyses in MR studies to identify and address potential outliers and biases. In contrast, other estimates remained robust across all SNPs. Importantly, this study highlights the necessity of rigorous sensitivity testing to ensure reliable causal inference. Moreover, our findings emphasize that normal-range thyroid function does not have a discernible causal effect on global brain cortex thickness or SA, suggesting region-specific effects of THs on brain structure. These results underscore the value of comprehensive sensitivity analyses in MR studies to validate and refine causal relationships.

Our analysis exhibits several notable strengths, ensuring robust and reliable findings. With a substantial sample size, we achieved sufficient statistical power, exceeding 80%, to detect moderate effects. Rigorous multiple testing corrections via Bonferroni adjustment minimized false positives. Leveraging MR, we established causal inference using genetic instruments. Comprehensive sensitivity analyses verified the stability of estimates, and our region-specific examination uncovered novel associations between THs effects and brain structure. These methodological strengths collectively enhance confidence in our findings, providing valuable insights into the complex relationship between thyroid function and brain anatomy. The findings of present MR analysis reveal a causal link between thyroid function and cortical structure, impacting cognitive and emotional processing. Thyroid malfunction, particularly hypothyroidism, alters SA and thickness in brain regions responsible for emotional regulation, cognitive processing and sensory processing, underscoring TH crucial role in maintaining optimal brain health.

Discussion

Although certain observational studies indicate a potential link between thyroid function and the structure of the cerebral cortex, the definitive causal relationship remains to be determined. The advent of GWAS data has enabled the analysis of genetic factors for their potential links to alterations in brain structure, psychological disorders and TH levels. Recent studies indicate that hypothyroidism may lead to a reduction in gray matter; however, there is still no thorough analysis on this subject.[41,42] This report represents a pioneering investigation that employs MR to elucidate the data concerning the causal relationship

Table 2. R2_F statistics of different SNPs of 6 different outcomes associated with FT4 and TSH levels

SNP	effect_allele. exposure	other_allele. exposure	eaf. exposure	beta. exposure	se. exposure	pval. exposure	samplesize. exposure	R^2	F-value
inc_TSH & cuneus_SA									
rs11675342	T	C	0.3988	0.1604	0.025	1.48E–10	53241	0.012337	665.0189
rs12449792	T	C	0.3168	0.1566	0.0281	2.41E–08	46314	0.010616	496.9069
rs143344027	A	G	0.9881	–0.5314	0.0827	1.33E–10	53241	0.006641	355.9136
rs597808	A	G	0.2253	0.1801	0.0259	3.47E–12	53241	0.011323	609.7159
rs75491569	T	C	0.1777	–0.2384	0.0367	8.67E–11	53241	0.01661	899.2163
rs78495697	T	C	0.1424	0.3157	0.0414	2.56E–14	53241	0.024343	1328.332
inc_TSH lingual_SA									
rs11675342	T	C	0.3988	0.1604	0.025	1.48E–10	53241	0.012337	665.0189
rs12449792	T	C	0.3168	0.1566	0.0281	2.41E–08	46314	0.010616	496.9069
rs143344027	A	G	0.9881	–0.5314	0.0827	1.33E–10	53241	0.006641	355.9136
rs597808	A	G	0.2253	0.1801	0.0259	3.47E–12	53241	0.011323	609.7159
rs75491569	T	C	0.1777	–0.2384	0.0367	8.67E–11	53241	0.01661	899.2163
rs78495697	T	C	0.1424	0.3157	0.0414	2.56E–14	53241	0.024343	1328.332
inc_TSH & SFG_TH									
rs11675342	T	C	0.3988	0.1604	0.025	1.48E–10	53241	0.012337	665.0189
rs12449792	T	C	0.3168	0.1566	0.0281	2.41E–08	46314	0.010616	496.9069
rs143344027	A	G	0.9881	–0.5314	0.0827	1.33E–10	53241	0.006641	355.9136
rs597808	A	G	0.2253	0.1801	0.0259	3.47E–12	53241	0.011323	609.7159
rs75491569	T	C	0.1777	–0.2384	0.0367	8.67E–11	53241	0.01661	899.2163
rs78495697	T	C	0.1424	0.3157	0.0414	2.56E–14	53241	0.024343	1328.332
FT4_men&LO_TH									
rs113107469	T	C	0.01465	0.2127	0.0322	4.07E–11	22455	0.001306	29.36535
rs11626434	C	G	0.3741	0.058	0.0102	1.23E–08	22455	0.001575	35.42727
rs1388385	A	G	0.3118	–0.0588	0.0102	7.16E–09	22455	0.001484	33.36527
rs2235544	A	C	0.4432	0.1388	0.0095	5.86E–48	22455	0.009508	215.5418
FT4_women&LO_TH									
rs113107469	T	C	0.01465	0.1784	0.0294	1.35E–09	27380	0.000919	25.1796
rs2235544	A	C	0.4432	0.138	0.0087	8.23E–57	27380	0.009399	259.7707
rs225014	T	C	0.5788	0.0511	0.009	1.30E–08	27380	0.001273	34.90147
rs7151700	A	C	0.4821	0.059	0.0094	4.05E–10	27380	0.001738	47.67321
FT4_women&TP_TH									
rs113107469	T	C	0.01465	0.1784	0.0294	1.35E–09	27380	0.000919	25.1796
rs2235544	A	C	0.4432	0.138	0.0087	8.23E–57	27380	0.009399	259.7707
rs225014	T	C	0.5788	0.0511	0.009	1.30E–08	27380	0.001273	34.90147
rs7151700	A	C	0.4821	0.059	0.0094	4.05E–10	27380	0.001738	47.67321

TSH – thyroid-stimulating hormone; SA – surface area; FT – free thyroxine; SFG-TH – superior frontal gyrus thyroid hormones; LO-TH – lateral occipital thyroid hormones; TP-TH – temporal pole thyroid hormone.

Table 3. Odds ratio (OR) of 6 different outcomes associated with FT4 and TSH levels by inverse variance method

Exposure	Outcome	OR (95% CI)	p-value
inc_TSH cuneus_sa	cuneus_SA	1.147 (1.045–1.457)	0.008
incTSH_overall_1	lingual_SA	1.124 (1.027–1.241)	0.003
incTSH_overall_1	superiorfrontal_thick	1.054 (1.004–1.147)	0.002
FT4_men	lateraloccipital_thick	1.122 (1.031–1.234)	0.001
FT4_women	lateraloccipital_thick	1.078 (1.005–1.161)	0.003
FT4_women	temporalpole_thick	1.114 (1.031–1.248)	0.001

TSH – thyroid-stimulating hormone; SA – surface area; FT– free thyroxine; 95% CI – 95% confidence interval.

between thyroid function and the structure of the cerebral cortex. This includes 34 cortical regions regarding SA and thickness. The findings indicate that the TH or SA of the cortex in particular brain regions linked to cognitive and psychological functions is affected by the characteristics of thyroid function, with no evidence of pleiotropy or heterogeneity.

The entorhinal cortex (EC), situated in the medial temporal lobe, is primarily associated with the regulation of episodic memory; however, its role encompasses functions that go beyond merely facilitating spatial navigation.[43] The stimulation has a beneficial impact on memory and learning processes.[44]

This study investigated a gender-independent positive correlation between FT4 and the thickness of the EC within the normal reference range, suggesting that THs plays a critical role in a variety of brain functions. The influence of AD on EC has been documented in the preclinical stages of the disease.[45–47] Meanwhile; thyroid function has been identified as a critical factor in the pathological progression of AD even within the normal range. Consequently, it is possible to infer that the modulation of EC thickness by THs has an impact on cognitive functions that are involved in the onset and progression of AD.[48]

The cACC serves as a vital neural structure located in the medial prefrontal cortex and plays a significant role in cognitive control, goal-directed cognition and emotional responses.[49] Consequently, the discovery of a positive correlation between the TH of the cACC and the level of TSH_men holds considerable importance.[49] Research has identified a diminished cACC volume in both schizophrenia and autism spectrum disorder (ASD). Consequently, further investigation is essential to clarify the specific role of elevated TSH levels within the normal range in alleviating the symptoms associated with ASD, schizophrenia and depression.[50,51]

The PCC experiences thinning due to a decrease in TSH (dec_TSH), which plays a crucial role in the encoding of episodic memory and self-spatial orientation.[52–54] The PCC has been linked to numerous psychiatric disorders, including schizophrenia, autism, depression, and attention deficit hyperactivity disorder (ADHD), via metabolic abnormalities, functional connectivity challenges and volumetric atrophy.[55–60] Therefore, it is plausible that the structural atrophy of the PCC could be associated with the psychiatric disorders seen in individuals with hyperthyroidism.

The observation in this study that inc_TSH results in an increase in the SA of the cortical region of the SFG without a significant impact on its thickness is incongruous with observational studies that have reported a decrease in the volume of the SFG in such patients. The superior frontal gyrus, which is situated in the upper portion of the frontal lobe cortex, is comprised of Brodmann areas 6, 8, 9, and 32.[61] It is intricately involved in a variety of cognitive functions and motor control tasks, including attention, working memory, cognitive control, and emotional regulation.[62] The SFG also plays a role in psychiatric disorders associated with self-consciousness, introspection and self-awareness.[62] However, this observed correlation suggests that the SA of the SFG region may be influenced by genetically predicted hypothyroidism, underscoring the intricate relationship between brain morphology and thyroid function. This study also observed a decrease in the SA of the PO as a result of hypothyroidism, in addition to SFG. The PO is predominantly involved in language production,[63] lexical selection, phonological processing, and speech encoding.[64–66] Negative changes in PO have been linked to decreased verbal fluency in individuals experiencing normal aging,[67] those with schizophrenia,[68] and patients with AD.[69] Moreover, the volume of this region is reduced in healthy young individuals exhibiting heightened anxiety levels.[70] As a result, this finding suggests that hyperthyroidism could play a role in the deficits observed in advanced language functions and emotional regulation due to a reduction in the TH of the PO.

The medial orbitofrontal cortex (mOFC) and the lateral orbitofrontal cortex (lOFC) are 2 distinct regions of the orbitofrontal cortex (OFC). Our study found that hypothyroidism increased cortical SA in the mOFC and lOFC. Damage to the lOFC can disrupt credit allocation in the value learning process, while damage to the mOFC can impede value-oriented decision-making.[71] A recent MR analysis[72] that links thyroid function and schizophrenia can also be interpreted as a reduction in the mOFC volume in adolescents at familial risk for schizophrenia. This suggests that hypothyroidism may mitigate the risk of developing schizophrenia. Additionally, the GMV in the lOFC has been reduced in patients with depression,[73,74] including school-aged children.[75] Our results indicate a potential inverse relationship between hypothyroidism and depression. In contrast, hypothyroidism has been linked to an elevated incidence of depression in observational studies. As a result, a comprehensive examination is necessary to uncover this correlation. Similarly, patients with obsessive-compulsive disorder, generalized anxiety disorder and ASD have been observed to have expanded OFC SA, reduced mOFC SA and decreased OFC SA, respectively.[76–79] Therefore, comprehending the function of TSH in these conditions would provide a new perspective on the management of these disorders.

In the context of neurodevelopment and neuropsychiatric conditions, the observation made in this study regarding a positive correlation between normal-range TSH levels in men and increased thickness in the cuneus region, while hypothyroidism reduced the SA of the LO cortex, is of particular interest. The cuneus is involved in primary visual processing, which encompasses the interpretation of visual field inputs, face recognition, complex affective expression processing, and visual imagery.[80] The LO cortex is essential for the identification of fundamental features of external objects and extends its capabilities to more complex cognitive tasks.[81–85] The LO and cuneus regions have been observed to exhibit reductions in both functional activity

and SA in children with ASD.[86] Similarly, patients with bipolar disorder show a significant reduction in the bilateral SA of the cuneus.[87] In a bidirectional MR study,[88] the diminished cuneus thickness was also discovered to be associated with an increased risk of AD. Consequently, the results of the present study have exacerbated a complex yet substantial correlation between thyroid function and the emergence of a variety of neuropsychiatric disorders.

It is important to highlight that our study did not find a relationship between the SA of 34 brain regions or the overall cerebral cortex and normal-range thyroid function. This suggests that thyroid function primarily affects the thickness of the cerebral cortex within the normal reference range. Nonetheless, SA of the cerebral cortex is the main focus when considering hypo- or hyperthyroidism. It is crucial to acknowledge that cortical TH and SA serve as 2 relatively independent morphological indicators within the structure of the cerebral cortex.[89] As a result, they are shaped by unique genetic influences and pursue different developmental paths.[90] As a result, the same exposure factor might not produce a simultaneous or symmetrical effect on both indicators. There is evidence to suggest that thyroid function may have an impact on cerebral blood flow and metabolism. Hypothyroidism can lead to reduced cerebral blood flow in various areas, such as the cuneus and the anterior cingulate cortex.[91] Conversely, metabolic irregularities within the limbic lobe may stem from hyperthyroidism.[92] Our MR analysis incorporated stringent quality control protocols, encompassing data cleaning, outlier elimination and validation of genetic instruments. We conducted an evaluation of potential biases via sensitivity analyses, examining for pleiotropy and population stratification. Additionally, we utilized IVW and Egger regression to assess causal estimates, thereby ensuring resilience against horizontal pleiotropy and heterogeneity. The implementation of these measures effectively reduced biases, thereby increasing confidence in our findings and confirming the causal relationships between thyroid function and brain anatomy.

Thyroid hormone influences brain regions by interacting with its receptors in essential areas such as the cingulate gyrus, hippocampus and amygdala.[92] An investigation into the human limbic system carried out through autopsy revealed the existence of TSH receptors in neurons.[93] This finding suggests that variations in FT4 and TSH levels may influence metabolism in this region, resulting in structural alterations. Thyroid hormones play a crucial role in shaping neural development, differentiation and functionality in areas such as the EC, caudal anterior cingulate and cuneus gyri. They regulate neuroplasticity, synaptic function, and neurotrophic factors, such as brain-derived neurotrophic factor (BDNF) and nerve growth factor (NGF), crucial for cognitive processes and emotional regulation. Alterations in TH levels impact neural circuit structure and function, affecting gene expression, axonal growth and synaptic transmission. Thyroid hormones also modulate neurotransmitter systems, including serotonin, dopamine and gamma-aminobutyric acid (GABA), influencing mood and cognition.[94–97]

Existing literature emphasizes the importance of THs in neuronal survival, synaptogenesis and neuronal connectivity, shedding light on the mechanisms that explain the noted relationships between thyroid function and brain structure. The relationship between thyroid function and brain structure carries important clinical implications, indicating that thyroid disorders could play a role in neurodegenerative diseases, cognitive decline and mood disorders. Future studies should explore the neuroprotective effects of THs, optimal treatment strategies and biomarkers for early detection.[94] Possible clinical applications encompass tailored TH therapy, neuroprotective strategies and innovative approaches for AD, depression and anxiety disorders. Recent MR-based studies have uncovered a link between obesity, sleep disorders and cortical structure. The thickness and SA of certain cortical regions can be affected by these conditions.[98–99] Individuals with hypothyroidism often face an increased risk of obesity and sleep disorders.[100] Therefore, it is essential to conduct additional inquiries into the interactive effects of these factors. Future studies on genetically determined thyroid function and cerebral cortex structure should concentrate on exploring the mechanisms that influence the effects of THs on neurogenesis, synaptogenesis and neuronal plasticity. Furthermore, investigating connections with cognitive decline, mood disorders and neurodegenerative diseases will be essential. Longitudinal studies will investigate the impact of thyroid function on brain development and maturation, while genetic and epigenetic analyses will assist in identifying regulatory variants. Investigations will also focus on therapeutic strategies, including hormone supplementation, for addressing thyroid-related brain health issues. Through the integration of knowledge from various fields such as endocrinology, neuroscience, genetics and epidemiology, these studies seek to clarify intricate relationships and enhance clinical practice, with the ultimate goal of advancing brain health outcomes.

Limitations

This investigation is subject to certain limitations. Primarily, the GWAS data used in this research was derived from European populations. Consequently, the applicability of these findings to other ethnic groups should be approached with caution. Second, the absence of age information in the GWAS data is a significant limitation, as age is a crucial factor influencing both thyroid function and brain structure. Furthermore, the objective of this investigation was to investigate the causal relationship between thyroid function and cortical structure by employing specific metrics, including volume, thickness, SA, and gyrification index. A broader array of indicators could be incorporated into comprehensive studies to further investigate the correlation between brain structure and thyroid function. However,

these approaches have certain limitations as well such as MR-Egger assumes instrumental variable independence, potentially leading to biased estimates if pleiotropy exists. Similarly, weighted median methods can be sensitive to outliers and may not perform well with weak instruments or non-causal associations. Additionally, both methods assume linear relationships, potentially masking non-linear effects. Moreover, MR findings should be interpreted cautiously due to limitations, including potential unmeasured confounding variables, pleiotropy and population stratification. Additionally, MR assumes a linear relationship between genetic variants and outcomes, and instrumental variable validity relies on strong assumptions. These limitations may bias or distort causal estimates. It is important to consider the possibility that the exposed and outcome groups may overlap in the 2-sample MR analysis. This overlap could introduce bias into the results, potentially affecting the conclusions.

Conclusions

This innovative MR analysis investigated the causal relationship between thyroid function and cortical structure. The results demonstrate that thyroid dysfunction, especially hypothyroidism, affects the SA of various cortical regions linked to mental and emotional processing. Moreover, optimal thyroid function significantly impacts the thickness of brain regions intricately linked to cognitive function, including the EC. This study provides new evidence that highlights the link between thyroid function and cognitive abilities, along with mental and psychological health. Furthermore, it offers valuable insights into improving the management of related conditions. However, additional studies are needed to validate the relationship between thyroid function and brain structure.

Ethics statement

The dataset mentioned above were all publicly available. The corresponding inform consents from participants were received in the original research. Thus, no ethics was required for our study.

Data availability statement

The thyroid function datasets studied in this study are accessible through the GWAS Public database (Datasets – The ThyroidOmics Consortium (https://www.uni-greifswald.de)). The datasets evaluated in the current study of the human cerebral cortex are available on the ENIGMA Consortium website (https://enigma.ini.usc.edu/research/download-enigma-gwas-results).

Consent for publication

Not applicable.

Use of AI and AI-assisted technologies

Not applicable.

ORCID iDs

Xupeng Wu https://orcid.org/0009-0001-9748-3146
Hong Liu https://orcid.org/0009-0005-8781-7391
Changxin Li https://orcid.org/0009-0009-7640-8663
Liangliang Cui https://orcid.org/0009-0009-8221-7951
Mengyan Mo https://orcid.org/0009-0006-5665-3221

References

1. Liu Y, Brent GA. The role of thyroid hormone in neuronal protection. *Compr Physiol*. 2021;11(3):2075–2095. doi:10.1002/cphy.c200019
2. Bauer M, Goetz T, Glenn T, Whybrow PC. The thyroid-brain interaction in thyroid disorders and mood disorders. *J Neuroendocrinol*. 2008;20(10):1101–1114. doi:10.1111/j.1365-2826.2008.01774.x
3. Chaker L, Bianco AC, Jonklaas J, Peeters RP. Hypothyroidism. *Lancet*. 2017;390(10101):1550–1562. doi:10.1016/S0140-6736(17)30703-1
4. Gold MS, Pottash AL, Extein I. Hypothyroidism and depression: Evidence from complete thyroid function evaluation. *JAMA*. 1981;245(19):1919–1922. doi:10.1001/jama.245.19.1919
5. Samuels MH, Bernstein LJ. Brain fog in hypothyroidism: What is it, how is it measured, and what can be done about it. *Thyroid*. 2022;32(7):752–763. doi:10.1089/thy.2022.0139
6. Demet MM, Özmen B, Deveci A, Boyvada S, Adıgüzel H, Aydemir Ö. Depression and anxiety in hyperthyroidism. *Arch Med Res*. 2002;33(6):552–556. doi:10.1016/S0188-4409(02)00410-1
7. Fardella CE, Gloger S. Neurobehavioral and psychological changes induced by hyperthyroidism: Diagnostic and therapeutic implications. *Exp Rev Neurother*. 2002;2(5):709–716. doi:10.1586/14737175.2.5.709
8. Vogel A, Elberling TinaV, Hørding M, et al. Affective symptoms and cognitive functions in the acute phase of Graves' thyrotoxicosis. *Psychoneuroendocrinology*. 2007;32(1):36–43. doi:10.1016/j.psyneuen.2006.09.012
9. Yuan L, Tian Y, Zhang F, et al. Impairment of attention networks in patients with untreated hyperthyroidism. *Neurosci Lett*. 2014;574:26–30. doi:10.1016/j.neulet.2014.05.016
10. De Jong FJ, Masaki K, Chen H, et al. Thyroid function, the risk of dementia and neuropathologic changes: The Honolulu–Asia Aging Study. *Neurobiol Aging*. 2009;30(4):600–606. doi:10.1016/j.neurobiolaging.2007.07.019
11. Tan ZS, Beiser A, Vasan RS, et al. Thyroid function and the risk of Alzheimer disease: The Framingham Study. *Arch Intern Med*. 2008;168(14):1514–1520. doi:10.1001/archinte.168.14.1514
12. Van Osch LADM, Hogervorst E, Combrinck M, Smith AD. Low thyroid-stimulating hormone as an independent risk factor for Alzheimer disease. *Neurology*. 2004;62(11):1967–1971. doi:10.1212/01.WNL.0000128134.84230.9F
13. Galakhova AA, Hunt S, Wilbers R, et al. Evolution of cortical neurons supporting human cognition. *Trends Cogn Sci*. 2022;26(11):909–922. doi:10.1016/j.tics.2022.08.012
14. Guo J, Yu K, Dong SS, et al. Mendelian randomization analyses support causal relationships between brain imaging-derived phenotypes and risk of psychiatric disorders. *Nat Neurosci*. 2022;25(11):1519–1527. doi:10.1038/s41593-022-01174-7
15. Zhang Y, Yang Y, Tao B, Lv Q, Lui S, He L. Gray matter and regional brain activity abnormalities in subclinical hypothyroidism. *Front Endocrinol (Lausanne)*. 2021;12:582519. doi:10.3389/fendo.2021.582519
16. Su W, Zhao L, Bao S, et al. Alterations in gray matter morphology and functional connectivity in adult patients with newly diagnosed untreated hypothyroidism. *Thyroid*. 2023;33(7):791–803. doi:10.1089/thy.2022.0476
17. Göbel A, Heldmann M, Göttlich M, Dirk AL, Brabant G, Münte TF. Effect of experimental thyrotoxicosis on brain gray matter: A voxel-based morphometry study. *Eur Thyroid J*. 2015;4(Suppl 1):113–118. doi:10.1159/000398793
18. Zhang W, Song L, Yin X, et al. Grey matter abnormalities in untreated hyperthyroidism: A voxel-based morphometry study using the DARTEL approach. *Eur J Radiol*. 2014;83(1):e43–e48. doi:10.1016/j.ejrad.2013.09.019

19. Davey Smith G, Hemani G. Mendelian randomization: Genetic anchors for causal inference in epidemiological studies. *Hum Mol Genet*. 2014; 23(R1):R89–R98. doi:10.1093/hmg/ddu328
20. Marouli E, Yusuf L, Kjaergaard AD, et al. Thyroid function and the risk of Alzheimer's disease: A Mendelian randomization study. *Thyroid*. 2021;31(12):1794–1799. doi:10.1089/thy.2021.0321
21. Freuer D, Meisinger C. Causal link between thyroid function and schizophrenia: A two-sample Mendelian randomization study. *Eur J Epidemiol*. 2023;38(10):1081–1088. doi:10.1007/s10654-023-01034-z
22. Skrivankova VW, Richmond RC, Woolf BAR, et al. Strengthening the Reporting of Observational Studies in Epidemiology Using Mendelian Randomization: The STROBE-MR Statement. *JAMA*. 2021; 326(16):1614. doi:10.1001/jama.2021.18236
23. Teumer A, Chaker L, Groeneweg S, et al. Genome-wide analyses identify a role for SLC17A4 and AADAT in thyroid hormone regulation. *Nat Commun*. 2018;9(1):4455. doi:10.1038/s41467-018-06356-1
24. Burgess S, Butterworth A, Thompson SG. Mendelian randomization analysis with multiple genetic variants using summarized data. *Genet Epidemiol*. 2013;37(7):658–665. doi:10.1002/gepi.21758
25. Bowden J, Del Greco M F, Minelli C, Davey Smith G, Sheehan N, Thompson J. A framework for the investigation of pleiotropy in two-sample summary data Mendelian randomization. *Stat Med*. 2017; 36(11):1783–1802. doi:10.1002/sim.7221
26. Burgess S, Bowden J, Fall T, Ingelsson E, Thompson SG. Sensitivity analyses for robust causal inference from Mendelian randomization analyses with multiple genetic variants. *Epidemiology*. 2017;28(1):30–42. doi:10.1097/EDE.0000000000000559
27. Hartwig FP, Davey Smith G, Bowden J. Robust inference in summary data Mendelian randomization via the zero modal pleiotropy assumption. *Int J Epidemiol*. 2017;46(6):1985–1998. doi:10.1093/ije/dyx102
28. Bowden J, Davey Smith G, Burgess S. Mendelian randomization with invalid instruments: Effect estimation and bias detection through Egger regression. *Int J Epidemiol*. 2015;44(2):512–525. doi:10.1093/ije/dyv080
29. Verbanck M, Chen CY, Neale B, Do R. Detection of widespread horizontal pleiotropy in causal relationships inferred from Mendelian randomization between complex traits and diseases. *Nat Genet*. 2018; 50(5):693–698. doi:10.1038/s41588-018-0099-7
30. Staley JR, Blackshaw J, Kamat MA, et al. PhenoScanner: A database of human genotype–phenotype associations. *Bioinformatics*. 2016; 32(20):3207–3209. doi:10.1093/bioinformatics/btw373
31. Ansari D. Culture and education: New frontiers in brain plasticity. *Trends Cogn Sci*. 2012;16(2):93–95. doi:10.1016/j.tics.2011.11.016
32. Chen W, Feng J, Guo J, et al. Obesity causally influencing brain cortical structure: A Mendelian randomization study. *Cereb Cortex*. 2023; 33(15):9409–9416. doi:10.1093/cercor/bhad214
33. Chen Y, Lyu S, Xiao W, Yi S, Liu P, Liu J. Sleep traits causally affect the brain cortical structure: A Mendelian randomization study. *Biomedicines*. 2023;11(8):2296. doi:10.3390/biomedicines11082296
34. Wang M, Wang Z, Wang Y, Zhou Q, Wang J. Causal relationships involving brain imaging-derived phenotypes based on UKB imaging cohort: A review of Mendelian randomization studies. *Front Neurosci*. 2024 Jul 10;18:1436223. doi:10.3389/fnins.2024.1436223
35. Kang J, Jia T, Jiao Z, et al. Increased brain volume from higher cereal and lower coffee intake: Shared genetic determinants and impacts on cognition and metabolism. *Cereb Cortex*. 2022;32(22):5163–5174. doi:10.1093/cercor/bhac005
36. Logtenberg E, Overbeek MF, Pasman JA, et al. Investigating the causal nature of the relationship of subcortical brain volume with smoking and alcohol use. *Br J Psychiatry*. 2022;221(1):377–385. doi:10.1192/bjp.2021.81
37. Mitchell BL, Diaz-Torres S, Bivol S, et al. Elucidating the relationship between migraine risk and brain structure using genetic data. *Brain*. 2022;145(9):3214–3224. doi:10.1093/brain/awac105
38. Mohanta SK, Yin C, Weber C, et al. Cardiovascular brain circuits. *Circ Res*. 2023;132(11):1546–1565. doi:10.1161/CIRCRESAHA.123.322791
39. Grasby KL, Jahanshad N, Painter JN, et al. The genetic architecture of the human cerebral cortex. *Science*. 2020;367(6484):eaay6690. doi:10.1126/science.aay6690
40. Chen CH, Fiecas M, Gutiérrez ED, et al. Genetic topography of brain morphology. *Proc Natl Acad Sci U S A*. 2013;110(42):17089–17094. doi:10.1073/pnas.1308091110
41. Maass A, Berron D, Libby LA, Ranganath C, Düzel E. Functional subregions of the human entorhinal cortex. *eLife*. 2015;4:e06426. doi:10.7554/eLife.06426
42. Kim IB, Park SC. The entorhinal cortex and adult neurogenesis in major depression. *Int J Mol Sci*. 2021;22(21):11725. doi:10.3390/ijms222111725
43. Nau M, Navarro Schröder T, Bellmund JLS, Doeller CF. Hexadirectional coding of visual space in human entorhinal cortex. *Nat Neurosci*. 2018; 21(2):188–190. doi:10.1038/s41593-017-0050-8
44. Kobayashi K, Yoshinaga H, Ohtsuka Y. Memory enhancement and deep-brain stimulation of the entorhinal area. *N Engl J Med*. 2012;366(20):1945; author reply 1946. doi:10.1056/NEJMc1203204
45. Braak H, Braak E. Neuropathological stageing of Alzheimer-related changes. *Acta Neuropathol*. 1991;82(4):239–259. doi:10.1007/BF00308809
46. Kaufman SK, Del Tredici K, Thomas TL, Braak H, Diamond MI. Tau seeding activity begins in the transentorhinal/entorhinal regions and anticipates phospho-tau pathology in Alzheimer's disease and PART. *Acta Neuropathol*. 2018;136(1):57–67. doi:10.1007/s00401-018-1855-6
47. Yeung LK, Olsen RK, Bild-Enkin HEP, et al. Anterolateral entorhinal cortex volume predicted by altered intra-item configural processing. *J Neurosci*. 2017;37(22):5527–5538. doi:10.1523/JNEUROSCI.3664-16.2017
48. Gray JR, Braver TS. Personality predicts working-memory-related activation in the caudal anterior cingulate cortex. *Cogn Affect Behav Neurosci*. 2002;2(1):64–75. doi:10.3758/CABN.2.1.64
49. Yuan Q, Liang X, Xue C, et al. Altered anterior cingulate cortex subregional connectivity associated with cognitions for distinguishing the spectrum of pre-clinical Alzheimer's disease. *Front Aging Neurosci*. 2022;14:1035746. doi:10.3389/fnagi.2022.1035746
50. Choi JS, Kang DH, Kim JJ, et al. Decreased caudal anterior cingulate gyrus volume and positive symptoms in schizophrenia. *Psychiatry Res Neuroimaging*. 2005;139(3):239–247. doi:10.1016/j.pscychresns.2004.05.008
51. Laidi C, Boisgontier J, De Pierrefeu A, et al. Decreased cortical thickness in the anterior cingulate cortex in adults with autism. *J Autism Dev Disord*. 2019;49(4):1402–1409. doi:10.1007/s10803-018-3807-3
52. Guterstam A, Björnsdotter M, Gentile G, Ehrsson HH. Posterior cingulate cortex integrates the senses of self-location and body ownership. *Curr Biol*. 2015;25(11):1416–1425. doi:10.1016/j.cub.2015.03.059
53. Natu VS, Lin JJ, Burks A, Arora A, Rugg MD, Lega B. Stimulation of the posterior cingulate cortex impairs episodic memory encoding. *J Neurosci*. 2019;39(36):7173–7182. doi:10.1523/JNEUROSCI.0698-19.2019
54. Rolls ET, Cheng W, Feng J. The orbitofrontal cortex: Reward, emotion and depression. *Brain Commun*. 2020;2(2):fcaa196. doi:10.1093/braincomms/fcaa196
55. Byun MS, Kim JS, Jung WH, et al. Regional cortical thinning in subjects with high genetic loading for schizophrenia. *Schizophr Res*. 2012;141(2–3):197–203. doi:10.1016/j.schres.2012.08.028
56. Leech R, Sharp DJ. The role of the posterior cingulate cortex in cognition and disease. *Brain*. 2014;137(1):12–32. doi:10.1093/brain/awt162
57. Narr KL, Toga AW, Szeszko P, et al. Cortical thinning in cingulate and occipital cortices in first episode schizophrenia. *Biol Psychiatry*. 2005; 58(1):32–40. doi:10.1016/j.biopsych.2005.03.043
58. Outen JD, Burhanullah MH, Vandrey R, et al. Cannabinoids for agitation in Alzheimer's disease. *Am J Geriatr Psychiatry*. 2021;29(12):1253–1263. doi:10.1016/j.jagp.2021.01.015
59. Ries ML, Wichmann A, Bendlin BB, Johnson SC. Posterior cingulate and lateral parietal gray matter volume in older adults with depressive symptoms. *Brain Imaging Behav*. 2009;3(3):233–239. doi:10.1007/s11682-009-9065-4
60. Zhou C, Xu J, Ping L, et al. Cortical thickness and white matter integrity abnormalities in obsessive-compulsive disorder: A combined multimodal surface-based morphometry and tract-based spatial statistics study. *Depress Anxiety*. 2018;35(8):742–751. doi:10.1002/da.22758
61. Kraljević N, Schaare HL, Eickhoff SB, et al. Behavioral, anatomical and heritable convergence of affect and cognition in superior frontal cortex. *NeuroImage*. 2021;243:118561. doi:10.1016/j.neuroimage.2021.118561
62. Li W, Qin W, Liu H, et al. Subregions of the human superior frontal gyrus and their connections. *NeuroImage*. 2013;78:46–58. doi:10.1016/j.neuroimage.2013.04.011
63. Tomaiuolo F, MacDonald JD, Caramanos Z, et al. Morphology, morphometry and probability mapping of the pars opercularis of the inferior frontal gyrus: An in vivo MRI analysis. *Eur J Neurosci*. 1999;11(9): 3033–3046. doi:10.1046/j.1460-9568.1999.00718.x

64. Costafreda SG, Fu CHY, Lee L, Everitt B, Brammer MJ, David AS. A systematic review and quantitative appraisal of fMRI studies of verbal fluency: Role of the left inferior frontal gyrus. *Hum Brain Mapp*. 2006; 27(10):799–810. doi:10.1002/hbm.20221
65. Papoutsi M, De Zwart JA, Jansma JM, Pickering MJ, Bednar JA, Horwitz B. From phonemes to articulatory codes: An fMRI study of the role of Broca's area in speech production. *Cereb Cortex*. 2009; 19(9):2156–2165. doi:10.1093/cercor/bhn239
66. Schnur TT, Schwartz MF, Kimberg DY, Hirshorn E, Coslett HB, Thompson-Schill SL. Localizing interference during naming: Convergent neuroimaging and neuropsychological evidence for the function of Broca's area. *Proc Natl Acad Sci U S A*. 2009;106(1):322–327. doi:10.1073/pnas.0805874106
67. Vonk JMJ, Rizvi B, Lao PJ, et al. Letter and category fluency performance correlates with distinct patterns of cortical thickness in older adults. *Cereb Cortex*. 2019;29(6):2694–2700. doi:10.1093/cercor/bhy138
68. North HF, Bruggemann J, Cropley V, et al. Increased peripheral inflammation in schizophrenia is associated with worse cognitive performance and related cortical thickness reductions. *Eur Arch Psychiatry Clin Neurosci*. 2021;271(4):595–607. doi:10.1007/s00406-021-01237-z
69. Yang A, Du L, Gao W, et al. Associations of cortical iron accumulation with cognition and cerebral atrophy in Alzheimer's disease. *Quant Imaging Med Surg*. 2022;12(9):4570–4586. doi:10.21037/qims-22-7
70. Hu Y, Dolcos S. Trait anxiety mediates the link between inferior frontal cortex volume and negative affective bias in healthy adults. *Soc Cogn Affect Neurosci*. 2017;12(5):775–782. doi:10.1093/scan/nsx008
71. Noonan MP, Chau BKH, Rushworth MFS, Fellows LK. Contrasting effects of medial and lateral orbitofrontal cortex lesions on credit assignment and decision-making in humans. *J Neurosci*. 2017;37(29): 7023–7035. doi:10.1523/JNEUROSCI.0692-17.2017
72. Jiang QH, Gong WD. Correlation analyse between thyroid hormone levels and severity of schizophrenia symptoms. *World J Psychiatry*. 2025;15(1):100880. doi:10.5498/wjp.v15.i1.100880
73. Grieve SM, Korgaonkar MS, Koslow SH, Gordon E, Williams LM. Widespread reductions in gray matter volume in depression. *NeuroImage Clin*. 2013;3:332–339. doi:10.1016/j.nicl.2013.08.016
74. Price JL, Drevets WC. Neural circuits underlying the pathophysiology of mood disorders. *Trends Cogn Sci*. 2012;16(1):61–71. doi:10.1016/j.tics. 2011.12.011
75. Fowler CH, Gaffrey MS. Reduced cortical surface area globally and in reward-related cortex is associated with elevated depressive symptoms in preschoolers. *J Affect Disord*. 2022;319:286–293. doi:10.1016 /j.jad.2022.09.075
76. Ecker C, Ginestet C, Feng Y, et al. Brain surface anatomy in adults with autism: The relationship between surface area, cortical thickness, and autistic symptoms. *JAMA Psychiatry*. 2013;70(1):59. doi:10.1001/ jamapsychiatry.2013.265
77. Hirjak D, Kubera KM, Northoff G, et al. Cortical contributions to distinct symptom dimensions of catatonia. *Schizophr Bull*. 2019;45(6): 1184–1194. doi:10.1093/schbul/sby192
78. Rus OG, Reess TJ, Wagner G, Zaudig M, Zimmer C, Koch K. Structural alterations in patients with obsessive–compulsive disorder: A surface-based analysis of cortical volume, surface area and thickness. *J Psychiatry Neurosci*. 2017;42(6):395–403. doi:10.1503/jpn.170030
79. Zhang T, Xie X, Li Q, et al. Hypogyrification in generalized anxiety disorder and associated with insomnia symptoms. *Nat Sci Sleep*. 2022; 14:1009–1019. doi:10.2147/NSS.S358763
80. Palejwala AH, Dadario NB, Young IM, et al. Anatomy and white matter connections of the lingual gyrus and cuneus. *World Neurosurg*. 2021;151:e426–e437. doi:10.1016/j.wneu.2021.04.050
81. Cattaneo Z, Lega C, Ferrari C, et al. The role of the lateral occipital cortex in aesthetic appreciation of representational and abstract paintings: A TMS study. *Brain Cogn*. 2015;95:44–53. doi:10.1016/j.bandc.2015.01.008
82. Grill-Spector K, Kourtzi Z, Kanwisher N. The lateral occipital complex and its role in object recognition. *Vision Res*. 2001;41(10–11): 1409–1422. doi:10.1016/S0042-6989(01)00073-6
83. Gschwind M, Pourtois G, Schwartz S, Van De Ville D, Vuilleumier P. White-matter connectivity between face-responsive regions in the human brain. *Cereb Cortex*. 2012;22(7):1564–1576. doi:10.1093/ cercor/bhr226
84. Guo D, Yang J. Reactivation of schema representation in lateral occipital cortex supports successful memory encoding. *Cereb Cortex*. 2023;33(10):5968–5980. doi:10.1093/cercor/bhac475
85. Libero LE, Maximo JO, Deshpande HD, Klinger LG, Klinger MR, Kana RK. The role of mirroring and mentalizing networks in mediating action intentions in autism. *Mol Autism*. 2014;5(1):50. doi:10. 1186/2040-2392-5-50
86. Jung M, Tu Y, Lang CA, et al. Decreased structural connectivity and resting-state brain activity in the lateral occipital cortex is associated with social communication deficits in boys with autism spectrum disorder. *NeuroImage*. 2019;190:205–212. doi:10.1016/j.neuroimage.2017.09.031
87. Achalia R, Raju VB, Jacob A, et al. Comparison of first-episode and multiple-episode bipolar disorder: A surface-based morphometry study. *Psychiatry Res Neuroimaging*. 2020;302:111110. doi:10.1016/j. pscychresns.2020.111110
88. Seyedsalehi A, Warrier V, Bethlehem RAI, Perry BI, Burgess S, Murray GK. Educational attainment, structural brain reserve and Alzheimer's disease: A Mendelian randomization analysis. *Brain*. 2023;146(5):2059–2074. doi:10.1093/brain/awac392
89. Panizzon MS, Fennema-Notestine C, Eyler LT, et al. Distinct genetic influences on cortical surface area and cortical thickness. *Cereb Cortex*. 2009;19(11):2728–2735. doi:10.1093/cercor/bhp026
90. Wierenga LM, Langen M, Oranje B, Durston S. Unique developmental trajectories of cortical thickness and surface area. *NeuroImage*. 2014; 87:120–126. doi:10.1016/j.neuroimage.2013.11.010
91. Haji M, Kimura N, Hanaoka T, et al. Evaluation of regional cerebral blood flow in Alzheimer's disease patients with subclinical hypothyroidism. *Dement Geriatr Cogn Disord*. 2015;39(5–6):360–367. doi:10.1159 /000375298
92. Schreckenberger MF, Egle UT, Drecker S, et al. Positron emission tomography reveals correlations between brain metabolism and mood changes in hyperthyroidism. *J Clin Endocrinol Metab*. 2006; 91(12):4786–4791. doi:10.1210/jc.2006-0573
93. Naicker M, Naidoo S. Expression of thyroid-stimulating hormone receptors and thyroglobulin in limbic regions in the adult human brain. *Metab Brain Dis*. 2018;33(2):481–489. doi:10.1007/s11011-017-0076-3
94. Battaglia S, Nazzi C, Lonsdorf TB, Thayer JF. Neuropsychobiology of fear-induced bradycardia in humans: Progress and pitfalls. *Mol Psychiatry*. 2024;29(12):3826–3840. doi:10.1038/s41380-024-02600-x
95. Battaglia S, Nazzi C, Fullana MA, Di Pellegrino G, Borgomaneri S. 'Nip it in the bud': Low-frequency rTMS of the prefrontal cortex disrupts threat memory consolidation in humans. *Behav Res Ther*. 2024;178:104548. doi:10.1016/j.brat.2024.104548
96. Tanaka M, Tuka B, Vécsei L. Navigating the neurobiology of migraine: From pathways to potential therapies. *Cells*. 2024;13(13):1098. doi:10.3390/cells13131098
97. Tanaka M, Vécsei L. A decade of dedication: Pioneering perspectives on neurological diseases and mental illnesses. *Biomedicines*. 2024;12(5):1083. doi:10.3390/biomedicines12051083
98. Wei X, Iao WC, Zhang Y, Lin Z, Lin H. Retinal microvasculature causally affects the brain cortical structure: A Mendelian randomization study. *Ophthalmol Sci*. 2024;4(6):100465. doi:10.1016/j. xops. 2024.100465
99. Zhan Y, Zhang Z, Lin S, et al. Causal association of sarcopenia-related traits with brain cortical structure: A bidirectional Mendelian randomization study. *Aging Clin Exp Res*. 2025;37(1):57. doi:10.1007/ s40520-025-02977-x
100. Kalinowska S, Trześniowska-Drukała B, Safranow K, et al. Association between thyroid function and metabolic syndrome in male and female schizophrenia patients. *Psychiatry Res*. 2019;274:167–175. doi:10.1016/j.psychres.2019.02.029

Epidemiological characteristics of thyroid cancer worldwide and construction of a machine learning diagnostic model

Yanqiong Liu[1,A,D], Lian Li[1,B], Shasha Wang[1,B], Shuangyan Zhou[2,C], Jianhui Zou[1,F]

[1] Department of Endocrinology, Zhejiang Provincial People's Hospital Bijie Hospital, China
[2] Department of Thyroid and Breast Surgery, Zhejiang Provincial People's Hospital Bijie Hospital, China

A – research concept and design; B – collection and/or assembly of data; C – data analysis and interpretation;
D – writing the article; E – critical revision of the article; F – final approval of the article

Advances in Clinical and Experimental Medicine, ISSN 1899–5276 (print), ISSN 2451–2680 (online) *Adv Clin Exp Med*. 2025;34(11):1881–1896

Address for correspondence
Jianhui Zou
E-mail: 13985350330@163.com

Funding sources
None declared

Conflict of interest
None declared

Received on September 11, 2024
Reviewed on November 9, 2024
Accepted on December 18, 2024

Published online on April 16, 2025

Abstract

Background. Age and gender have been identified as significant factors contributing to the global rise in thyroid cancer (TC), with this disease predominantly affecting women. It is crucial to thoroughly investigate the trends of the disease over time to better understand its progression and potential risk factors.

Objectives. This study analyzed the global incidence of TC using data from the Global Burden of Disease (GBD) database from 1990 to 2021. Additionally, we aimed to develop a high-performance diagnostic model using machine-learning algorithms and to explore the tumor microenvironment through single-cell sequencing.

Materials and methods. To analyze trends in incidence, age-period cohort models were applied, with a particular focus on birth cohort and period effects. Machine learning algorithms, including least absolute shrinkage and selection operator (LASSO) and Ridge regression, were used for gene feature selection. Subsequently, cross-validation was conducted to validate the diagnostic model. For deeper insights, single-cell RNA sequencing was conducted to analyze myeloid cell subpopulations within the tumor microenvironment.

Results. Age and period effects emerged as the primary drivers in our analysis of TC trends, particularly among women. Machine learning models, specifically LASSO and Ridge regression, demonstrated high predictive accuracy in diagnosing the disease. Additionally, single-cell RNA sequencing unveiled crucial interactions between myeloid cells and the tumor microenvironment.

Conclusions. This study provides a comprehensive analysis of TC trends and introduces a machine-learning-based diagnostic tool. Additionally, single-cell RNA sequencing offers novel insights into the tumor microenvironment, which may help shape future treatment strategies for TC.

Key words: machine learning, epidemiology, gene expression, tumor microenvironment, thyroid neoplasms

Cite as
Liu Y, Li L, Wang S, Zhou S, Zou J. Epidemiological characteristics of thyroid cancer worldwide and construction of a machine learning diagnostic model. *Adv Clin Exp Med*. 2025;34(11):1881–1896. doi:10.17219/acem/199327

DOI
10.17219/acem/199327

Highlights

- Rising thyroid cancer cases worldwide: A comprehensive study from 1990 to 2021 reveals a significant increase in thyroid cancer incidence, especially among women.
- AI-powered thyroid cancer diagnosis: A cutting-edge machine learning model demonstrates high accuracy in predicting thyroid cancer using genetic data.
- Single-cell RNA sequencing insights: Myeloid cells play a crucial role in the thyroid cancer tumor microenvironment, with MIF and *GALECTIN* pathways driving key interactions.
- Genetic markers for early detection: The study identifies critical genetic markers that can enhance early diagnosis and treatment strategies for thyroid cancer.
- Impact of age, gender, and environment: Factors such as aging, gender differences, and environmental influences contribute to the rising global cases of thyroid cancer.
- This research provides valuable insights into thyroid cancer trends, AI-driven diagnostics and potential treatment breakthroughs.

Background

Thyroid cancer (TC) is one of the few proliferative endocrine tumors, and its incidence has significantly increased over the several past decades. Several factors, including advancements in diagnostic techniques, heightened public awareness and changes in environmental exposures, are likely contributing to this rising trend.[1,2] With the global population aging and environmental factors evolving, the epidemiological characteristics of TC are continuously changing. Therefore, updated research and analyses are urgently needed. According to data from the World Health Organization (WHO), TC ranks as the 9th most common cancer globally. In 2020, approx. 586,000 new cases were reported, with nearly 90,000 deaths worldwide. Over the past decades, the incidence of thyroid cancer has been rising, particularly among women.

According to the American Cancer Society (ACS), women are 3 times more likely to develop TC than men. There are significant differences in TC incidence across different regions. For example, South Korea has the highest incidence, while rates are relatively low in Africa and South Asia. According to the International Agency for Research on Cancer (IARC), high-income countries generally have higher TC incidence rates compared to low- and middle-income countries.[1,2]

Previous investigations indicate that age, sex and residential zone are the most influential factors correlating with TC prevalence. For instance, women have greater access to diagnosis compared to men. Moreover, the variations in incidence rates by geography are assumed to be indicative of greater exposure to risk factors within different regions. However, a systematic analysis based on long-term trends and the underlying mechanisms contributing to the increase in TC cases is still lacking.

The current study aims to conduct a comprehensive analysis of the differences in age-standardized incidence and prevalence rates of TC across countries from 1990 to 2021, utilizing data from the Global Burden of Disease (GBD) database.[3,4] We designed this study to explore a large dataset and identify novel trends otherwise hidden from prior analyses. Moreover, we aimed to develop a highly accurate TC diagnostic model using advanced machine learning approaches. This method not only enhances diagnostic precision but also provides a more reliable tool for clinical practice, ultimately improving patient outcomes.

Additionally, we used single-cell RNA sequencing to gain a more precise understanding of the cellular challenges within the tumor microenvironment.[5,6] The exciting component of this method is that we can identify intricate cellular communications and gene expression patterns which are critical in tumorigenesis and progression.

Objectives

The GBD database was used to examine global trends in TC incidence from 1990 to 2021. Additionally, this study aimed to develop a machine learning-based diagnostic model by identifying key genes and to investigate tumor–microenvironment interactions using single-cell sequencing, offering potential therapeutic insights.

Materials and methods

Patients

Study population

The study included patients diagnosed with TC, utilizing data obtained from publicly available datasets (e.g., GBD database, GSE27155, GSE111455, GSE196264, TCGA-THCA). The inclusion criteria encompassed confirmed cases of TC, with documented patient characteristics including age, sex, geographic location, and stage at diagnosis. Exclusion criteria included patients with missing clinical or demographic

data. The datasets were thoroughly cleaned to eliminate inconsistencies or errors, ensuring high-quality data for analysis. Gene expression data were normalized to mitigate batch effects and technical variations across different datasets.

Specimen characteristics

Biological material

Gene expression data from TC patients were collected from the Gene Expression Omnibus (GEO) database and The Cancer Genome Atlas (TCGA). Control samples were also obtained from the same datasets and consisted of non-cancerous thyroid tissue from patients diagnosed with thyroid conditions.

Preservation and storage

Datasets used were publicly available and underwent quality control in their respective studies. Data were stored in compliance with open-source data-sharing standards.

Assay methods

Global Burden of Disease analysis

This study utilized the R programming language for data analysis, primarily leveraging packages such as ggplot2, dplyr, reshape2, readxl, and ggpubr. First, epidemiological data were imported using the read.csvfunction, with a focus on data from 2021. The dataset was categorized into 20 age groups, and the subset function was applied to extract data based on specific conditions, including age group, gender (male and female), geographic location (global), metrics ("rate" or "number"), and measurement type ("prevalence" or "incidence").

Data cleaning was conducted using the gsub function, while order and factor were utilized for sorting and categorization to ensure the correct arrangement of variables. The ggplot2 package was employed to generate visualizations, including line charts for prevalence and incidence trends across different age groups and pyramid charts for case distribution. These visualizations were created using functions such as geom_line, geom_point, geom_ribbon, and geom_bar. Additionally, the ggarrange function from the ggpubr package was used to combine multiple graphs, facilitating easy comparison and effective presentation of results.

In this study, Joinpoint regression analysis and decomposition analysis were conducted on incidence and mortality data using R. Age-standardized incidence data from China and global sources were selected for analysis, and their corresponding standard errors (SE) were calculated. The data were then sorted by gender and year and exported as *csv files for regression analysis in Joinpoint software to identify trends in incidence changes. The annual percent change (AAPC) and segment-specific percent change (APC) were extracted from Joinpoint and formatted using R for further analysis and visualization.

In the decomposition analysis, demographic data were integrated to calculate the population proportions for different age groups in 1990 and 2021. Specific formulas were applied to decompose the total change and distinguish the contributions of age structure, total population growth, and epidemiological changes. Data processing and analysis primarily utilized R packages such as dplyr, tidyr, and ggplot2.

Study design

Case selection and time frame

The study was retrospective, utilizing data from 1990–2021 to analyze global trends in TC incidence using the GBD database. To enhance accuracy, the data were stratified by gender, age and geographical location.

Endpoints

The primary endpoints of this study included age-standardized incidence rates, prevalence and mortality rates of TC. The secondary endpoint focused on exploring gene expression differences within the tumor microenvironment using single-cell sequencing data.

Candidate variables

The variables initially considered in this study included age, sex, geographical region, and gene expression levels, as they are key factors influencing TC prognosis.

Sample size and power

A large dataset from the GBD, TCGA and GEO databases was used to ensure adequate statistical power. The study was designed to detect significant epidemiological trends and gene expression patterns, with a target power of 0.8 to detect medium effect sizes.

Statistical analyses

We processed the sample data using the following methods: TCGA for TC, including 100 normal tissue samples and 507 tumor samples, totaling 607 samples. GSE27155: Human thyroid adenomas, carcinomas and normals. Human samples of various thyroid carcinomas, adenomas and normals (99 samples). GSE111455: Array-based genome-wide transcriptome analysis of minimally invasive follicular thyroid carcinomas (3 samples). GSE196264: Gene profile of human medullary TC. Eight sporadic MTC patients were selected for the gene microarray analysis (17 samples). Joinpoint regression models were employed for trend analysis to assess changes in incidence and prevalence

over time. The age-period-cohort (APC) model was also utilized to evaluate the influence of age, period and cohort on incidence trends. Differentially expressed genes (DEGs) identified by DESeq2 and limma were analyzed using differential gene expression analysis.

Differential gene expression analysis

Differential expression analysis was conducted using the limma package in R, designed for differential expression analysis of microarray and RNA-Seq data. We used normalized expression data from the TCGA dataset. To ensure robust statistical analysis, genes with 0 variance across samples were removed. A linear model was fitted using the lmFit function and a design matrix specifying control and treatment groups. Contrasts were defined to compare treatment and control groups, and Empirical Bayes method (eBayes) was used to compute adjusted t-statistics and log-odds for differential expression. Genes were considered significantly differentially expressed if the absolute $\log_2$ fold change ($|\log_2 FC|$) exceeded 0.585 and the adjusted p-value, corrected for false discovery rate (FDR), was less than 0.05.[7]

Significant genes were further analyzed to visualize expression patterns. Heatmaps were generated using pheatmap in R to display the most significantly differentially expressed genes, applying hierarchical clustering to rows while keeping columns unclustered. Volcano plots were created using ggplot2 in R to illustrate the distribution of $\log_2$ fold changes against the negative log of the adjusted p-value.

KEGG analysis

We conducted gene set enrichment analysis using the Kyoto Encyclopedia of Genes and Genomes database (KEGG, https://www.kegg.jp) to identify significant pathways associated with our gene list of interest. The analysis was performed using the clusterProfiler package in R (v. 4.4.1, a programming language and software environment for statistical computing and data visualization; R Foundation for Statistical Computing, Vienna, Austria). First, gene symbols were converted to Entrez Gene Identifier using the org.Hs.eg.db package. Duplicate entries were removed, and genes without corresponding Entrez IDs were excluded. The enrichKEGG function was used for KEGG pathway enrichment analysis, specifying "hsa" (human) as the organism. The significance threshold for pathway inclusion was set at a p-value of 0.05 and an adjusted p-value (q-value) of 1. Pathway descriptions were simplified by removing redundant species information. Results were filtered to include only pathways meeting the specified significance criteria and saved to a file named "KEGG.txt". Visualization of the top 30 pathways was done using barplot and dotplot functions from the enrichplot package. Plots were colored based on adjusted p-values, using raw p-values if the threshold exceeded 0.05. All visualization results were saved in *pdf format for further analysis and presentation.

WGCNA analysis

Weighted gene co-expression network analysis (WGCNA) was performed using R to identify gene modules associated with clinical traits in the TCGA dataset. First, the expression data were normalized, and genes with low variance (standard deviation (SD) <1.5) were filtered out to ensure robustness. The soft-thresholding power was determined by scale-free topology criteria, selecting a power value X to achieve a scale-free topology fit index of at least 0.8. This power was used to construct an adjacency matrix, which was then transformed into a topological overlap matrix (TOM) to measure network interconnectedness. Gene modules were identified by dynamic tree cutting based on the TOM gene dendrogram, with a minimum module size of 60 genes. Module eigengenes were calculated and similar expression pattern modules were merged based on a height cut of 0.25 on the eigengene dendrogram. Pearson's correlation analysis was used to assess the relationship between module eigengenes and clinical traits (e.g., control and treat), and significant modules were analyzed in depth. Gene significance (GS) and module membership (MM) metrics were calculated for each gene, and scatter plots were generated to visualize the relationship between GS and MM in key modules. All analyses were conducted using the WGCNA package in R, with results visualized through a series of dendrograms, heatmaps and scatter plots. Final module assignments and gene significance metrics were exported for further biological interpretation and validation.

Machine learning models

This study employed a comprehensive machine learning approach to develop and evaluate predictive models for classification tasks. Data were sourced from publicly available GEO datasets and preprocessed to ensure consistency between training and test sets. Key libraries used included randomForestSRC, glmnet, xgboost, and ComplexHeatmap for data processing, model training and visualization. Feature selection was performed using various machine learning algorithms to identify important variables. Model training utilized diverse algorithms, including random forest, least absolute shrinkage and selection operator (LASSO) regression and gradient boosting machine, with hyperparameter optimization to enhance performance. Training data were scaled and centered to standardize input features, ensuring robust model development.

Each model's performance was assessed using cross-validation and evaluated based on the area under the curve (AUC) metric. The best-performing model was selected for further analysis and validated on an independent test dataset. Additionally, a logistic regression model was constructed to compare its performance with machine learning models. Results were visualized using heatmaps to display AUC values across different models and datasets,

facilitating comparative analysis. The final model was saved to ensure reproducibility and future application. This rigorous approach ensured the development of robust predictive models with potential applications in bioinformatics and computational biology.

Single-cell sequencing

Single-cell RNA sequencing (scRNA-seq) data were obtained from publicly available datasets. We used the Matrix package (v. 1.7-2) in R to load the raw count matrix and the Seurat package (v.5.2.1) for further processing. Gene and barcode information were annotated onto the count matrix, creating a Seurat object for downstream analysis. The NormalizeData function was used to normalize the Seurat object, and high-variance features were identified using FindVariableFeatures. The data were then scaled using ScaleData and subjected to principal component analysis (PCA) with RunPCA. The first 10 principal components were used to construct a shared nearest neighbor graph (FindNeighbors) and identify cell clusters using the FindClusters function with a resolution of 0.1. For data visualization, t-distributed stochastic neighbor embedding (t-SNE) was applied using RunTSNE. Cluster-specific marker genes were identified using FindAllMarkers, with criteria set to include genes expressed in at least 10% of cells and a log fold change threshold of 0.1. The top 4 marker genes for each cluster were extracted and saved for further analysis. Cell type annotation was based on known marker genes for various cell types. A DotPlot was generated to visualize the expression of these marker genes across clusters. Annotations were manually added to the metadata of the Seurat object, updating cluster identities accordingly.

Cell–cell communication analysis

Cell–cell communication analysis was performed using the CellChat package (v. 1.5.0). A CellChat object was created from the Seurat object, and the CellChatDB.human database (https://github.com/sqjin/CellChat) was used to identify secreted signaling pathways. Overexpressed genes and ligand-receptor pairs were identified, and communication probabilities were computed using computeCommunProb. Interactions between different cell types and signaling pathways were visualized using various methods, including circle plots, chord diagrams and heatmaps.

Results

Epidemiological trends of thyroid cancer

Incidence by age and gender revealed age-specific incidence rates for both men and women, with incidence increasing with age and peaking in middle age. Women exhibited a higher incidence rate than men (Fig. 1A). The population pyramid illustrates the age and gender distribution, showing a balanced distribution in younger age groups and a higher proportion of women in older age groups (Fig. 1B).

The age- and gender-adjusted incidence rates, as illustrated in Fig. 1A, were further refined by incorporating specific factors such as risk factors and demographic variables, allowing for a more precise and contextualized analysis. The analysis confirms a higher incidence rate among women, with distinct peaks observed during middle age (Fig. 1C). Additionally, the adjusted population pyramid illustrates the population distribution after incorporating these adjustments, highlighting demographic shifts and underscoring trends related to an aging population (Fig. 1D).

Joinpoint analysis of the change of thyroid cancer incidence rate in the general population

Figure 2 results show that Joinpoint analysis revealed significant changes in TC incidence rates at multiple time points for the overall population, females and males, with a more pronounced growth trend after the year 2000. Decomposition analysis indicates that the increase in incidence and mortality rates was primarily influenced by population aging, epidemiological changes and population growth. Among these factors, population aging and epidemiological changes have a more significant impact on women. Collectively, these factors contribute to the increasing burden of TC (Fig. 2).

The clustering of gene expression across different samples

Figure 3A presents differential gene expression between the control and test groups, highlighting genes such as *ETV4, LIPH* and *GABRR2*, which exhibit higher expression (red) in the test group, while *CDR2, HSDL1* and *LRIG1* show lower expression (blue). Figure 3B visualizes the significance and magnitude of gene expression changes, where red dots indicate significantly upregulated genes and green dots represent significantly downregulated genes. The x-axis denotes the log fold change (logFC), while the y-axis represents the negative log of the adjusted p-value.

Weighted gene co-expression network analysis results

In Fig. 4, the sample clustering tree and trait heatmap illustrate the distribution of samples under the "Control" and "Treat" traits, displaying distinct clustering patterns. The gene clustering tree, along with module colors, groups genes into multiple modules, each represented by a different color, highlighting gene co-expression patterns. The module-trait relationship heatmap reveals correlations between gene modules and clinical traits, with certain

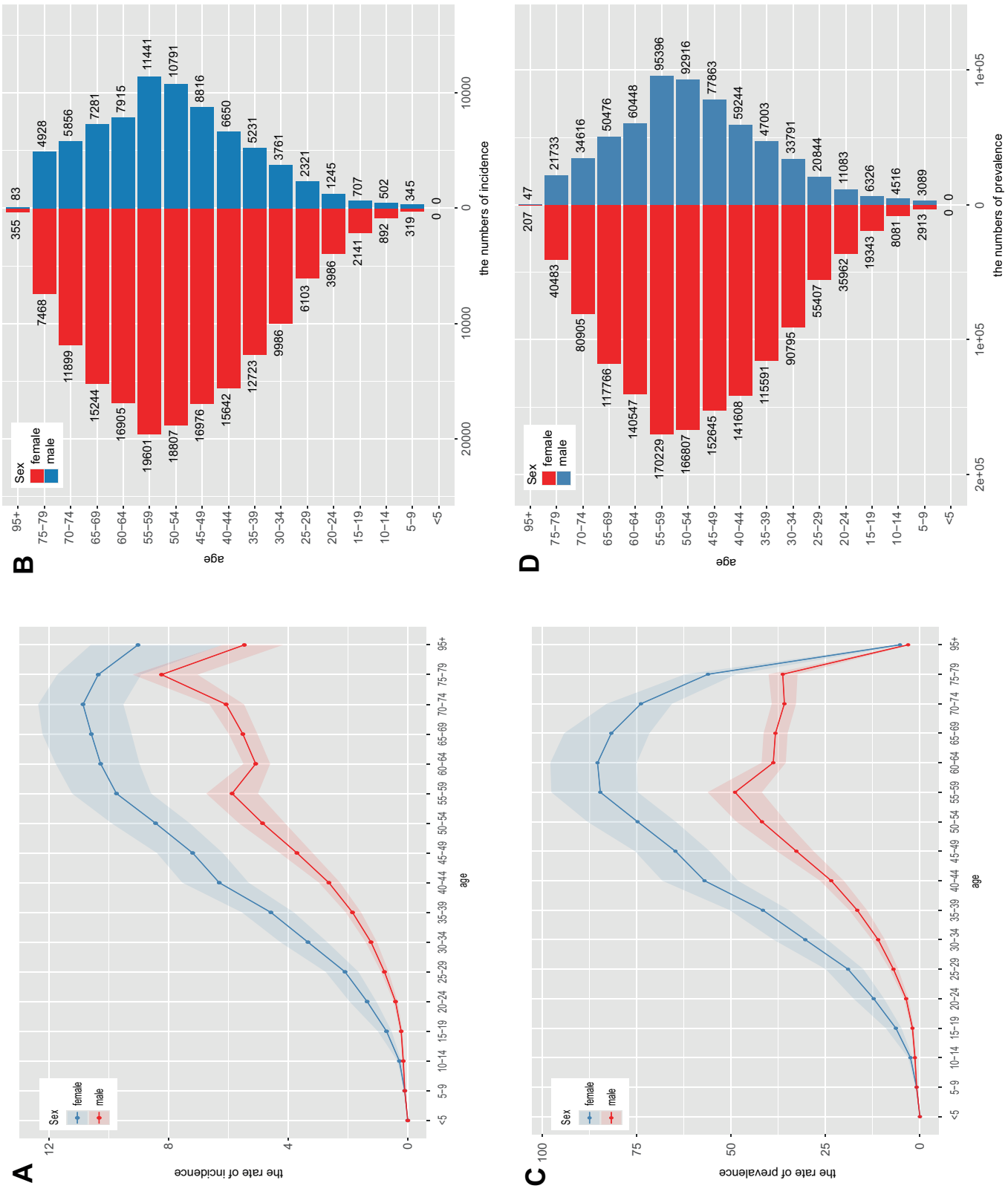

Fig. 1. Epidemiological trends of thyroid cancer (TC). A. Incidence curve graph showing TC incidence rates across different age groups and genders; B. Stacked bar chart displaying the distribution of TC incident cases across different age groups and genders; C. Time trend graph illustrating the number of TC cases and age-standardized incidence rates from 1990 to 2021; D. Prevalence curve graph showing TC prevalence rates across different age groups and genders; E. Stacked bar chart displaying the distribution of TC prevalent cases across different age groups and genders; F. Time trend graph illustrating the number of TC prevalent cases and age-standardized prevalence rates from 1990 to 2021

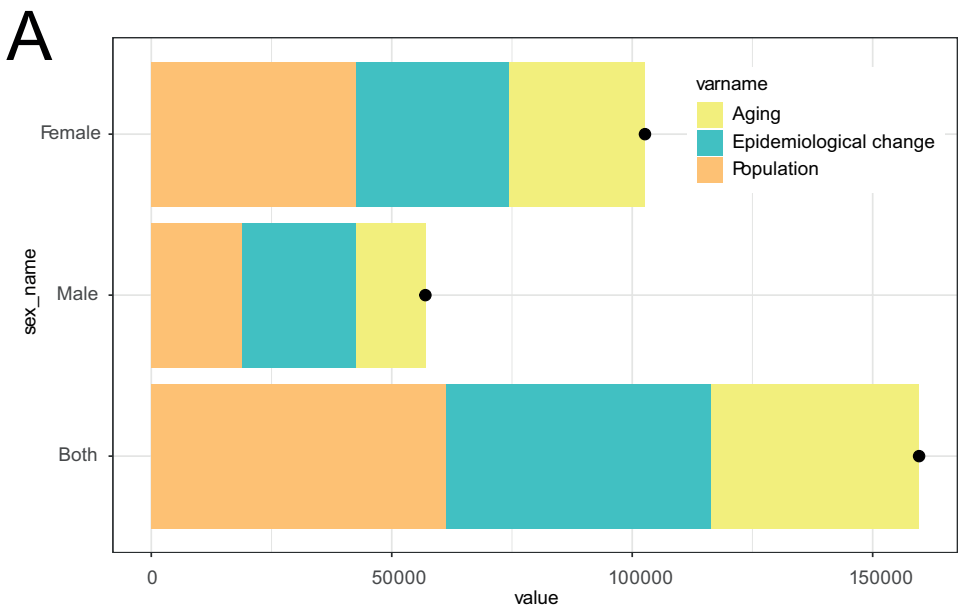

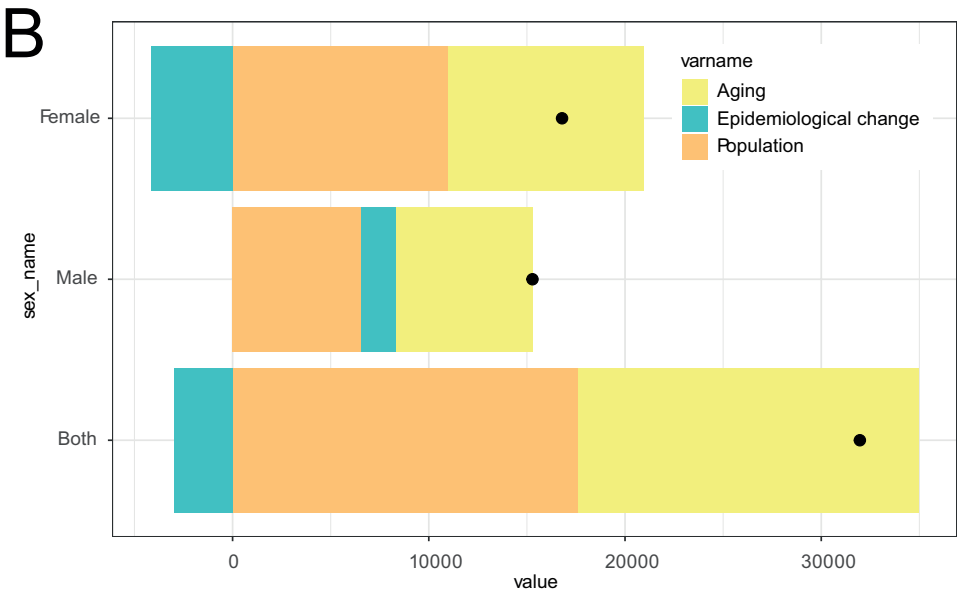

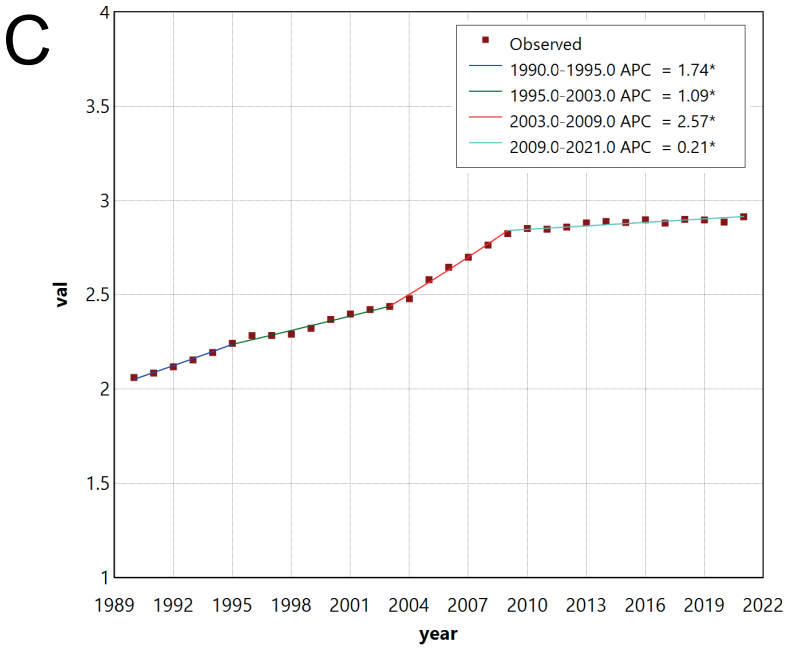

* Indicates that the Annual Percent Change (APC) is significantly different from zero at the alpha = 0.05 level. Final Selected Model: 3 Joinpoints.

Fig. 2. Joinpoint and decomposition analysis. A. Joinpoint analysis for the total population; B. Decomposition analysis of incidence rates; C. Decomposition analysis of mortality rates

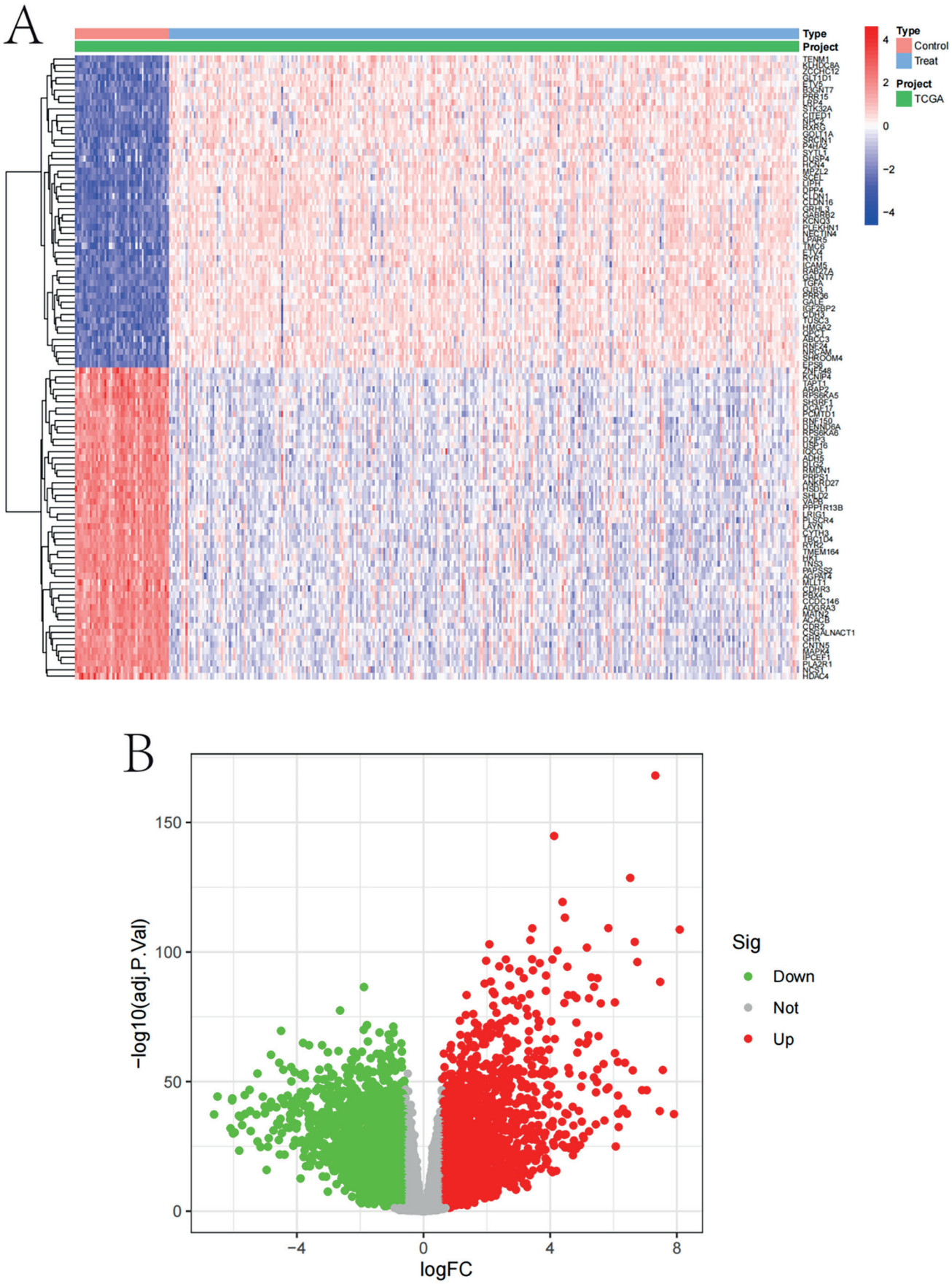

Fig. 3. The clustering of gene expression across different samples. A. Heatmap: Displaying the clustering of gene expression in different samples. Red indicates high expression and blue indicates low expression; B. Volcano plot: Showing the results of gene expression differential analysis. Red points represent significantly upregulated genes, green points represent significantly downregulated genes and grey points indicate genes with no significant change

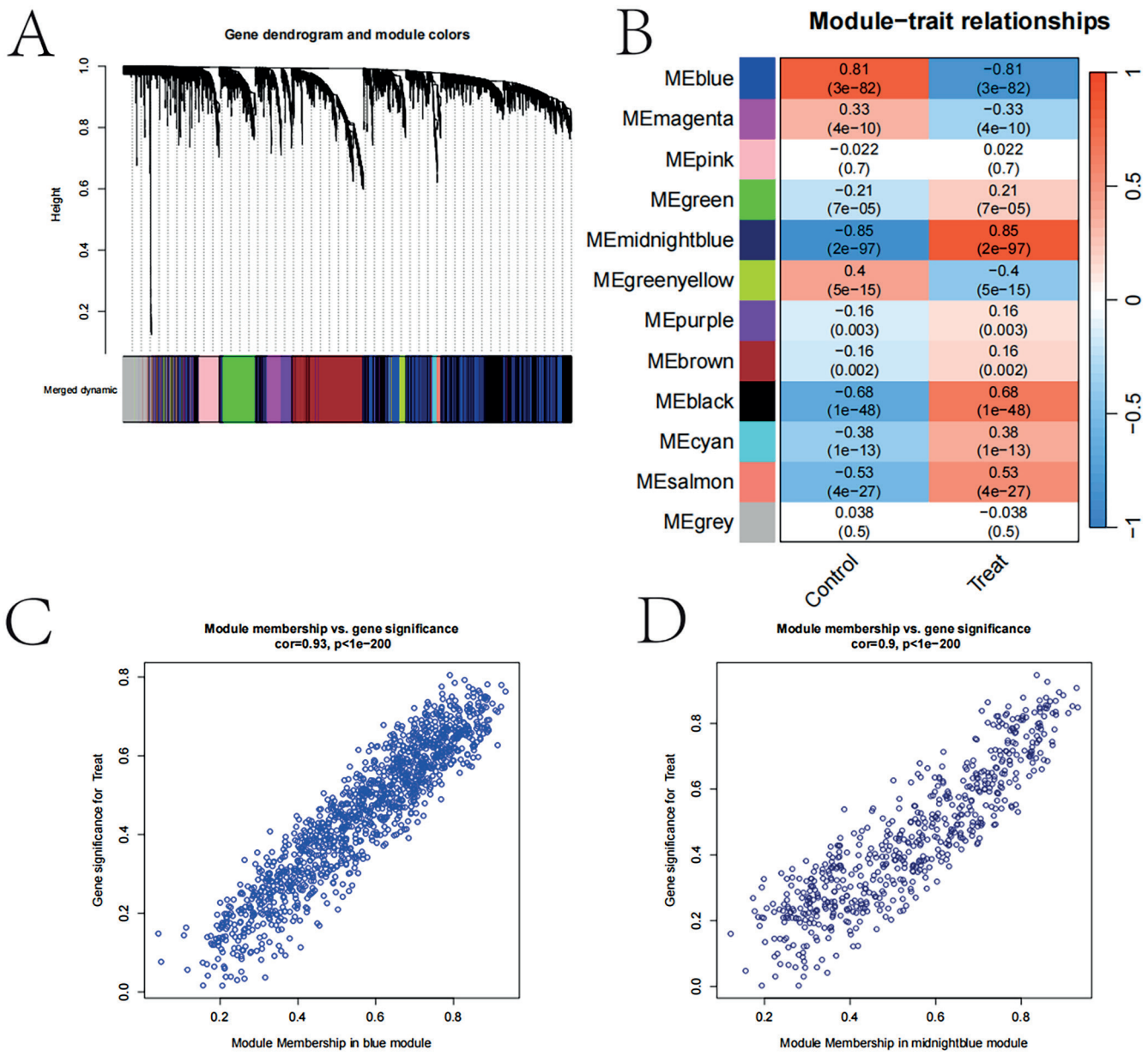

Fig. 4. Weighted gene co-expression network analysis (WGCNA) results. A. Gene clustering tree and module colors; B. Module-trait relationship heatmap; C. Module membership vs gene significance scatter plot (based on module membership (MM)); D. Module membership vs gene significance scatter plot (based on gene significance (GS))

modules, such as MEblue and MEmagenta, showing strong positive correlations with the "Treat" trait. These findings suggest that these modules may play a crucial role in TC.

The gene significance bar plot illustrates the importance and significance of genes within each module, with error bars representing SEs. The scatter plot of module membership compared to gene significance further confirms the strong correlation between module membership and gene significance, particularly in the midnight blue and blue modules. These findings suggest that the gene modules identified through WGCNA may play critical roles in the development and progression of TC, offering valuable insights for further research and potential therapeutic target identification (Fig. 4).

Differential expression gene and WGCNA module overlap and functional enrichment

The analysis results in Fig. 5 indicate that 510 genes overlapped between DEGs and gene modules identified through WGCNA, suggesting that these genes may play critical roles in TC. Gene Ontology (GO) enrichment analysis revealed significant enrichment of these genes in biological processes such as cell proliferation, signal transduction and metabolic regulation. The gene-pathway network diagram illustrated the connections between key genes and multiple pathways, indicating their involvement in various biological processes. The pathway network diagram further highlighted the intricate interactions between pathways.

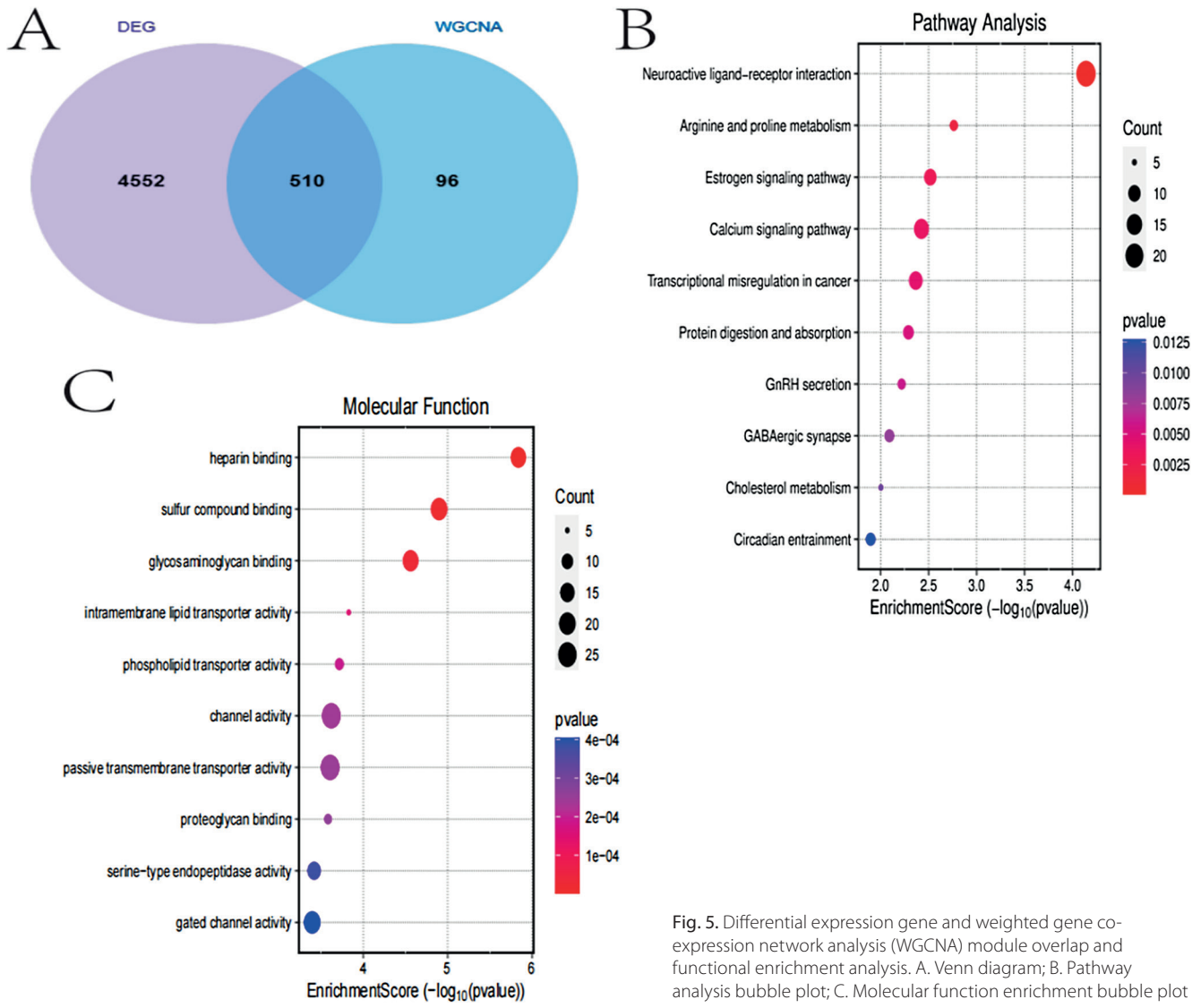

Fig. 5. Differential expression gene and weighted gene co-expression network analysis (WGCNA) module overlap and functional enrichment analysis. A. Venn diagram; B. Pathway analysis bubble plot; C. Molecular function enrichment bubble plot

Molecular function enrichment analysis reveals significant enrichment in functions such as ligand binding and enzyme activity, while pathway analysis underscores the importance of neuroligand-receptor interactions and metabolic pathways. These findings provide valuable insights into the molecular mechanisms of TC and may offer potential directions for developing therapeutic strategies (Fig. 5).

Model performance evaluation, gene expression difference and predictive ability analysis

Figure 6 results demonstrate the performance of various machine learning models across different datasets, using AUC values as evaluation metrics. The Ridge and LASSO models performed best on the GSE27155 dataset, achieving AUC values close to 1. The volcano plot highlights significantly upregulated and downregulated genes, including *ETV4* and *RXRG*. Gene expression box plots showed significant differences in gene expression between control and experimental groups. The gene correlation matrix revealed strong correlations among multiple genes. The receiver operating characteristic (ROC) curve for the GSE27155 dataset indicates excellent model prediction performance, with an AUC of 0.963. Additionally, multiple genes exhibited high predictive potential as biomarkers, with *ETV4* and *KLHDC8A* achieving perfect AUC scores of 1. These analyses suggest that the identified genes hold promise for TC diagnosis and prediction (Fig. 6).

Thyroid cancer single cell RNA sequencing analysis

In Fig. 7, violin plots illustrate the distribution of RNA counts and feature numbers in tumor samples, highlighting variability between samples and indicating diversity in gene expression across different cells. The PCA scatter plot visualizes sample distribution using PCA, with samples clustering along the first 2 principal components (PC1 and PC2), providing insights into the main sources of variation.

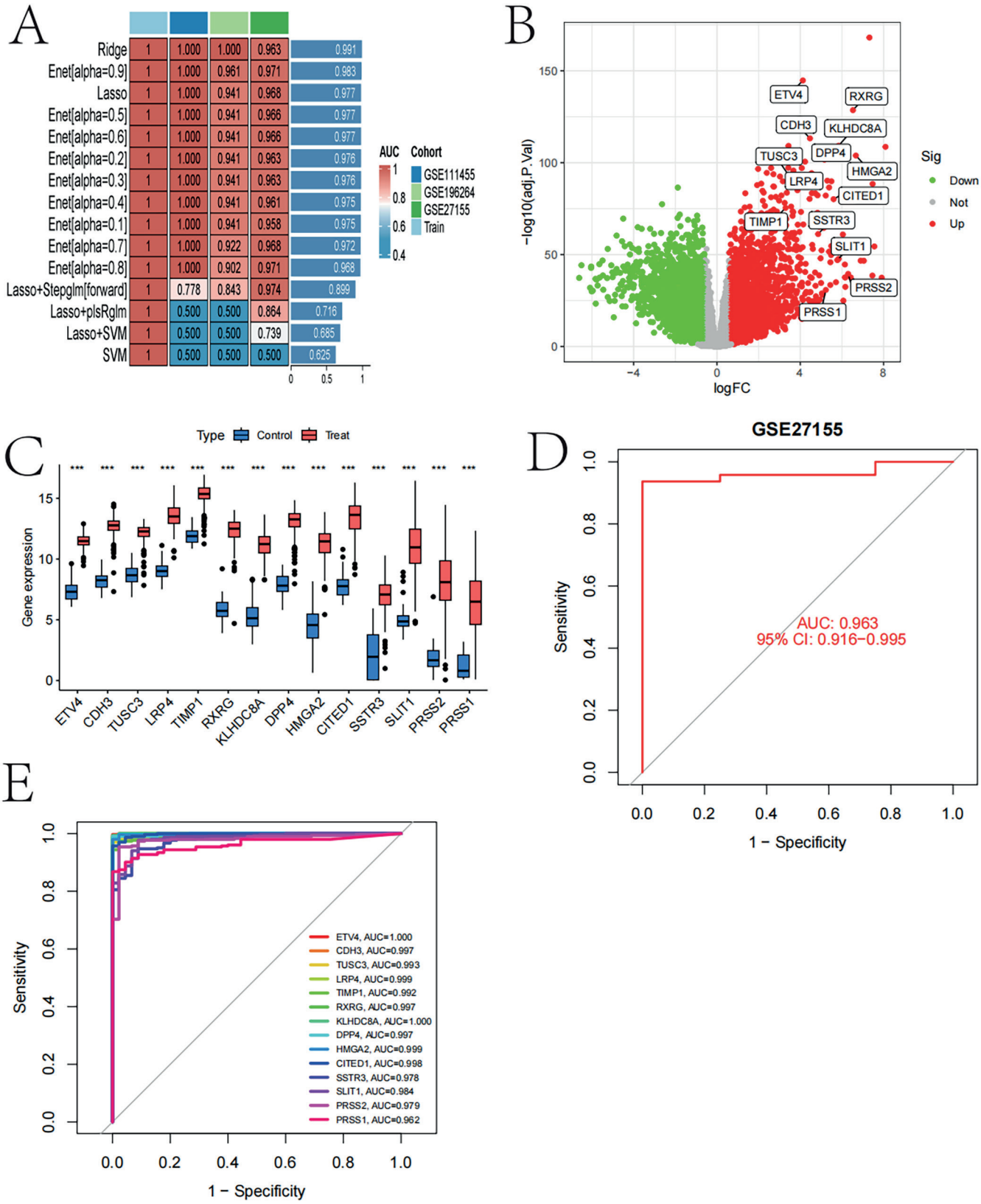

Fig. 6. Model performance evaluation, gene expression difference and predictive ability analysis. A. Model performance heatmap; B. Volcano plot; C. Gene expression box plot; D. Receiver operating characteristic (ROC) curve plot (single dataset); E. ROC curve plot (multiple genes)

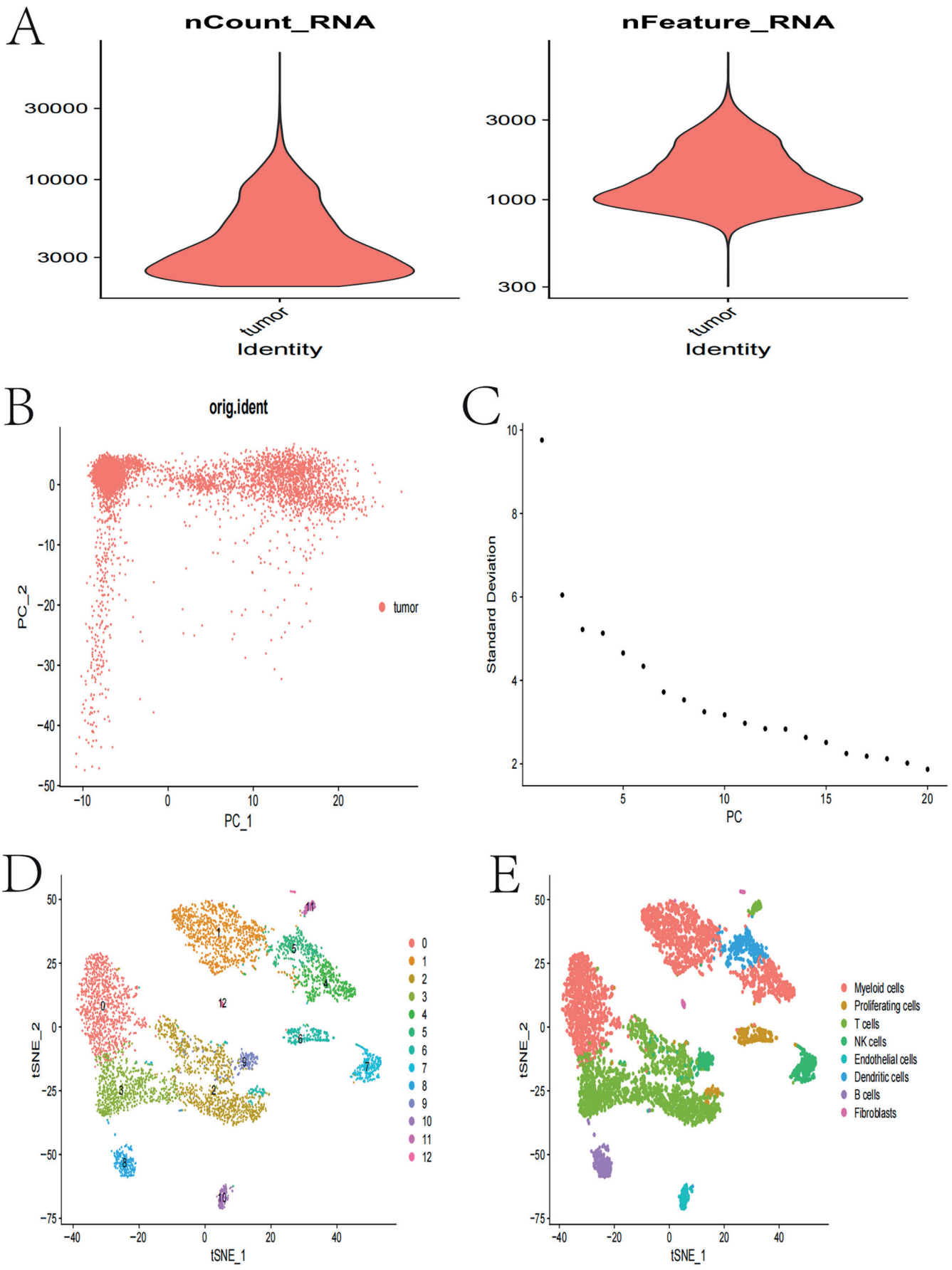

Fig. 7. Thyroid cancer single cell RNA sequencing analysis. A. Violin plot showing the distribution of counts (top) in tumor samples; B. Principal component analysis (PCA) scatter plot; C. The plot of explained variance; D. t-distributed stochastic neighbor embedding (t-SNE) clustering plot; E. t-SNE cell type plot: Cells distinguished and annotated for different types by the result of (tSNE)

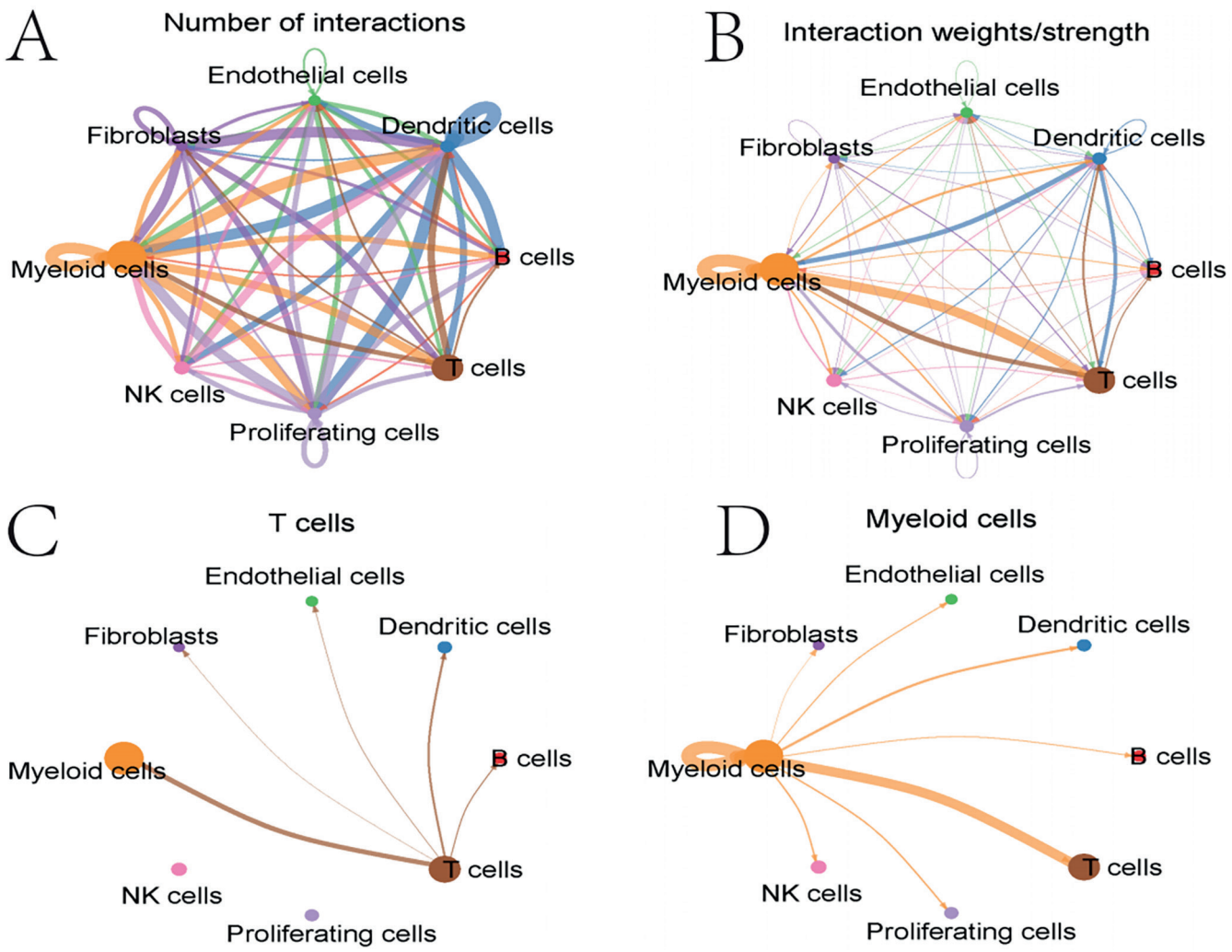

Fig. 8. The network interaction diagram between different TC cells, highlighting their interactions with each other. A. Network diagram of intercellular interaction quantity; B. Network analysis of the intercellular interaction strength; C. T-cell interaction network diagram; D. Myeloid cell interaction network

The variance explained plot displays the SD of each principal component, with the first few components explaining most of the data variance, providing a basis for principal component selection. The t-SNE clustering plot identifies multiple distinct cell populations through t-SNE analysis, revealing cellular diversity and potential subgroups. The t-SNE cell type plot further annotates and distinguishes different cell types based on t-SNE results, including myeloid cells, proliferating cells, T cells, natural killer (NK) cells, endothelial cells, dendritic cells, B cells, and fibroblasts. These analyses provide important information about cellular heterogeneity in TC, contributing to the understanding of its biological characteristics and potential therapeutic targets (Fig. 7).

For network diagram of intercellular interaction quantity

Cell interaction network shows frequent interactions among myeloid cells, T, B, NK cells, endothelial cells, and fibroblasts. Notably, myeloid–NK cell interactions are particularly strong. T-cell network focuses on T cell interactions with myeloid and dendritic cells, crucial for immune responses. Myeloid cell network highlights extensive interactions with T-cells, dividing cells and endothelial cells, emphasizing their role in the tumor microenvironment. Macrophage migration inhibitory factor (MIF) signaling pathway primarily involves myeloid and T cells in the MIF signaling process. *GALECTIN* signaling pathway involves myeloid cells, endothelial cells and fibroblasts, with JAK-STAT as a central signaling pathway (Fig. 8).

Analysis of cell–cell communication and gene expression in the MIF and *GALECTIN* signaling pathways

Among these interactions, the communication between myeloid cells and Treg/NKr is particularly important in the MIF signaling pathway, as it may play a pivotal role in explaining both immunological functions and the relevance to the tumor microenvironment. Among these well-known molecules, genes such as *MIF* and its receptor CD74 (along with CXCR4) are predominantly expressed

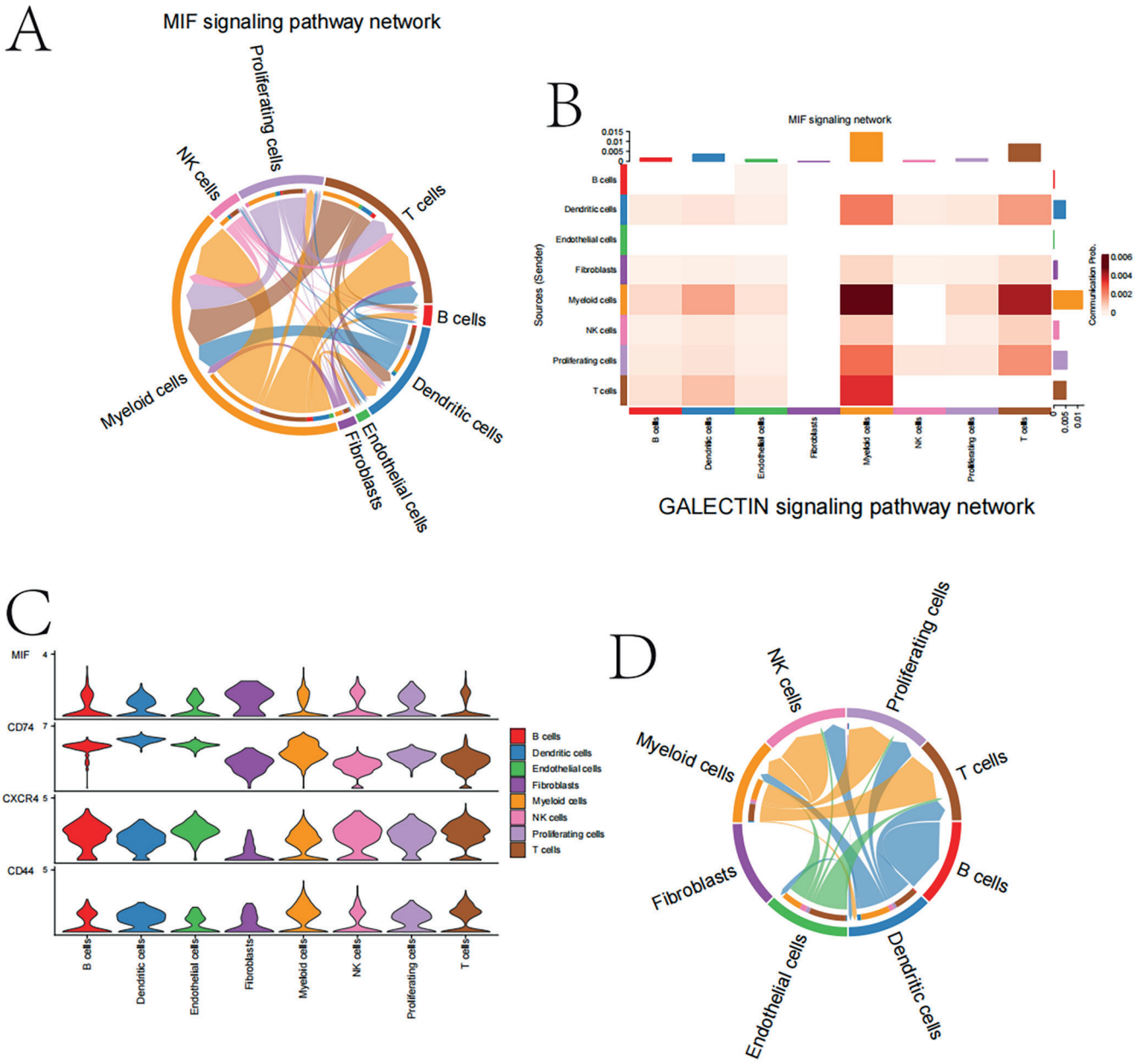

Fig. 9. Cellular interactions and gene expression in migration inhibitory factor (MIF) and *GALECTIN* pathways. A. MIF signaling pathway network diagram; B. Signaling pathway heatmap; C. Violin plot of the expression levels of the 4 target genes in different cell populations; D. *GALECTIN* signaling pathway network map.

by myeloid cells and T cells, suggesting their crucial roles in cell-type signaling and immune regulation.

The interaction between myeloid cells and endothelial cells in the *GALECTIN* signaling pathway emerges as a strong potential mediator of tumor progression, playing an unsuspected yet significant role in angiogenesis. Moreover, the interaction strength was highest between myeloid cells and fibroblasts, with gene expression patterns indicating that many of these cells are actively engaged in central signal transduction processes within this population. Data from the heatmap and violin plot further highlight the differential expression of genes within cell types involved in these pathways, providing insights into intercellular communication.

In summary, our findings reveal a complex interplay between the MIF and *GALECTIN* pathways in papillary TC cells, involving myeloid dendritic cells. This insight may have significant implications for understanding cancer biology and developing future therapeutic targets (Fig. 9).

Discussion

Thyroid cancer is a heterogeneous disease with various subtypes, each exhibiting unique molecular characteristics and biological behaviors. As research progresses, more molecular drivers are being identified, playing key roles in the initiation and progression of TC. These drivers

include gene mutations, gene fusions and changes in expression levels, affecting processes like cell signaling, cell cycle control and apoptosis. Myeloid cells play a crucial role in the tumor microenvironment, where they can be educated or activated by tumor cells to promote tumor development and immune evasion. The expression and function of inflammatory factors or immune-related molecules in myeloid cells may significantly impact the progression of TC. To further elucidate the complex interactions within the tumor microenvironment (TME), advanced technologies, such as single-cell RNA sequencing (scRNA-seq), have emerged as indispensable tools, enabling high-resolution profiling of cellular heterogeneity and intercellular communication. Single-cell RNA sequencing enables the analysis of cellular heterogeneity within the tumor microenvironment at the single-cell level, providing detailed gene expression profiles of various cell subpopulations. This technology facilitates the identification of specific cell types that interact with myeloid cells and their communication patterns through the MIF and *GALECTIN* signaling pathways.[8–10]

Macrophage migration inhibitory factor supports tumor growth and metastasis by enhancing myeloid cell activation and their adaptability to TME.[11–13] The *GALECTIN* signaling pathway, along with other signaling mechanisms, has been identified as a critical contributor to tumorigenesis in various cancers. It primarily functions by disrupting cell–cell interactions and promoting immune evasion.

Our study highlights the crucial role of the *GALECTIN* pathway in mediating interactions between medullary cells, endothelial cells and fibroblasts. This finding is further supported by other studies, emphasizing its significance in tumor cell–stromal cell interactions. Members of the *GALECTIN* family specifically bind to carbohydrates, influencing cell adhesion and migration. This interaction plays a crucial role in tumor cell survival, particularly during migration through the basement membrane or the tumor extracellular matrix (ECM).[15–17]

Therapeutic agents that inhibit *GALECTIN* binding have the potential to reduce tumor cell adhesion and migration, thereby limiting metastasis. This strategy could be particularly effective in preventing tumor cells from interacting with the ECM and stromal cells. Combining *GALECTIN* inhibitors with other treatments, such as immunotherapy or chemotherapy, may enhance overall efficacy by simultaneously targeting multiple aspects of tumor progression and immune evasion.

In this study, leveraging machine learning approaches and demonstrating superior performance compared to several existing studies, we developed a diagnostic model for TC with a high degree of predictive accuracy. The Ridge and LASSO models achieved AUC values close to 1 on the GSE27155 dataset, indicating excellent performance in identifying gene features associated with TC. These results align with findings from other studies utilizing machine learning for cancer prediction, further validating the potential of machine learning in tumor diagnosis.

Limitations

The study has several limitations. First, it relies on publicly available datasets, which may not fully represent all geographic or demographic variations, potentially limiting the generalizability of the results. Second, the machine learning models, though validated, are based on a specific dataset and may require further validation across more diverse populations. Third, while single-cell RNA sequencing provides valuable insights, our analysis focuses primarily on myeloid cells, leaving other cell types underexplored. Lastly, the study does not account for potential changes in diagnostic techniques or environmental factors over the years, which may influence TC trends.

Conclusions

This study conducted a comprehensive analysis of global TC incidence and prevalence from 1990 to 2021, identifying multiple influencing factors and their interactions. Using the age-period-cohort model, we found that TC incidence significantly increases with age, particularly among women. Our findings suggest that population aging, epidemiological shifts and environmental factors collectively contribute to the rising burden of TC.

Data availability statement

The datasets supporting the findings of the current study are openly available in figshare at https://figshare.com/s/5cd186232b9ea779ee41.

Consent for publication

Not applicable.

Use of AI and AI-assisted technologies

Not applicable.

ORCID iDs

Yanqiong Liu https://orcid.org/0009-0000-8468-0821
Lian Li https://orcid.org/0009-0009-5469-072
Shasha Wang https://orcid.org/0009-0003-4222-6702
Shuangyan Zhou https://orcid.org/0009-0001-6920-1324
Jianhui Zou https://orcid.org/0009-0003-9696-0371

References

1. Chen Z, Wang C, Li M, Cai S, Liu X. SPRED3 regulates the NF-κB signaling pathway in thyroid cancer and promotes the proliferation. *Sci Rep*. 2024;14(1):20506. doi:10.1038/s41598-024-61075-6
2. Villanova M, Tolaney SM, Min L. Association between pembrolizumab-related thyroid adverse events and outcomes in early-stage triple-negative breast cancer patients. *Endocr Relat Cancer*. 2024;31(11):e240120. doi:10.1530/ERC-24-0120

3. Li Y, Piao J, Li M. Secular trends in the epidemiologic patterns of thyroid cancer in China over three decades: An updated systematic analysis of Global Burden of Disease Study 2019 data. *Front Endocrinol (Lausanne)*. 2021;12:707233. doi:10.3389/fendo.2021.707233
4. Yang I, Yu JM, Chung HS, et al. Hashimoto thyroiditis and mortality in patients with differentiated thyroid cancer: The national epidemiologic survey of thyroid cancer in Korea and meta-analysis. *Endocrinol Metab*. 2024;39(1):140–151. doi:10.3803/EnM.2023.1748
5. Rojas-Rueda D, Lamsal S, Kak M, El-Saharty S, Herbst CH. Public health impacts of ambient particulate matter pollution in Libya from 1990 to 2019: An analysis of the 2019 Global Burden of Disease (GBD) Study. *Int J Environ Res Public Health*. 2024;21(6):667. doi:10.3390/ijerph21060667
6. Wang Z, Yao W, Wu W, et al. Global incidence trends of early-onset colorectal cancer and related exposures in early-life: An ecological analysis based on the GBD 2019. *Front Public Health*. 2024;12:1367818. doi:10.3389/fpubh.2024.1367818
7. Baltsavia I, Oulas A, Theodosiou T, et al. scRNA-Explorer: An end-user online tool for single cell RNA-seq data analysis featuring gene correlation and data filtering. *J Mol Biol*. 2024;436(17):168654. doi:10.1016/j.jmb.2024.168654
8. Mizukoshi C, Kojima Y, Nomura S, Hayashi S, Abe K, Shimamura T. DeepKINET: A deep generative model for estimating single-cell RNA splicing and degradation rates. *Genome Biol*. 2024;25(1):229. doi:10.1186/s13059-024-03367-8
9. Cheng L, Yang C, Lu J, et al. Oncogenic *SLC2A11–MIF* fusion protein interacts with polypyrimidine tract binding protein 1 to facilitate bladder cancer proliferation and metastasis by regulating mRNA stability. *MedComm*. 2024;5(9):e685. doi:10.1002/mco2.685
10. Suzuki J, Furuta S, Kameoka Y, et al. Dynamics of scFv-targeted VAP2 correlating with IL-16, MIF and IL-1Ra in ANCA-associated vasculitis. *Microvasc Res*. 2024;156:104720. doi:10.1016/j.mvr.2024.104720
11. Zhang F, Meng T, Feng R, et al. MIF aggravates experimental autoimmune prostatitis through activation of the NLRP3 inflammasome via the PI3K/AKT pathway. *Int Immunopharmacol*. 2024;141:112891. doi:10.1016/j.intimp.2024.112891
12. Jia X, Xi J, Tian B, et al. The tautomerase activity of tumor exosomal MIF promotes pancreatic cancer progression by modulating MDSC differentiation. *Cancer Immunol Res*. 2024;12(1):72–90. doi:10.1158/2326-6066.CIR-23-0205
13. Liang J, Lei K, Liang R, et al. Single-cell RNA sequencing reveals the MIF-ACKR3 receptor-ligand interaction between iCAFs and tumor cells in esophageal squamous cell carcinoma. *Cell Signal*. 2024;117:111093. doi:10.1016/j.cellsig.2024.111093
14. Yan L, Wu M, Wang T, et al. Breast cancer stem cells secrete MIF to mediate tumor metabolic reprogramming that drives immune evasion. *Cancer Res*. 2024;84(8):1270–1285. doi:10.1158/0008-5472.CAN-23-2390
15. Wang Y, Sun Y, Li H, Xu J. Galectin-8 alters immune microenvironment and promotes tumor progression. *Am J Cancer Res*. 2023;13(6):2517–2529. PMID:37424827. PMCID:PMC10326578.
16. Xiao Z, Wang S, Chen J, et al. The dual role of the NFATc2/galectin-9 axis in modulating tumor-initiating cell phenotypes and immune suppression in lung adenocarcinoma. *Adv Sci (Weinh)*. 2024;11(20):2306059. doi:10.1002/advs.202306059
17. Yan M, Chen Y, Li M, et al. *Coprinopsis cinerea* galectin CGL1 induces apoptosis and inhibits tumor growth in colorectal cancer cells. *Int J Mol Sci*. 2022;24(1):235. doi:10.3390/ijms24010235

Effects of echinacoside on the regulation of mitochondrial fission induced by TBK1/Drp1 in rheumatoid arthritis

Xiaoyan Wang[1,A–F], Zhufeng Chen[2,B,C,F], Shanshan Wu[3,4,B,C,F], Xuemei Fan[5,A–C,E,F]

[1] Department of Diagnostics, Shaanxi University of Chinese Medicine, Xianyang, China
[2] Department of Orthopedics, Tangdu Hospital, The Second Affiliated Hospital of Air Force Medical University, Xi'an, China
[3] Department of Anatomy, Basic Medical College, Shaanxi University of Chinese Medicine, Xianyang, China
[4] Shaanxi Key Laboratory of Research on Traditional Chinese Medicine Physical Constitution and Treatment, Xianyang, China
[5] Department of Rheumatology, Zibo Central Hospital, China

A – research concept and design; B – collection and/or assembly of data; C – data analysis and interpretation;
D – writing the article; E – critical revision of the article; F – final approval of the article

Advances in Clinical and Experimental Medicine, ISSN 1899–5276 (print), ISSN 2451–2680 (online) *Adv Clin Exp Med*. 2025;34(11):1897–1906

Address for correspondence
Xuemei Fan
E-mail: xuemeifan198@163.com

Funding sources
This work was supported by the Natural Science Basic Research Program of Shaanxi Province (grant No. 2023-JC-QN-0852 and 2024JC-YBQN-0947), the project of Qinchuangyuan Traditional Chinese Medicine industry innovation cluster (grant No. L2024-QYC-ZYYJJQ-X15) and the Shaanxi Key Laboratory of Research on TCM Physical Constitution and Treatment (grant No. KF202308). The funders had no role in the study design, data collection and analysis, decision to publish, or preparation of the manuscript.

Conflict of interest
None declared

Acknowledgements
We thank Medjaden Inc. for providing scientific editing services for this manuscript.

Received on November 6, 2024
Reviewed on December 29, 2024
Accepted on January 8, 2025

Published online on July 2, 2025

Cite as
Wang X, Chen Z, Wu S, Fan X. Effects of echinacoside on the regulation of mitochondrial fission induced by TBK1/Drp1 in rheumatoid arthritis. *Adv Clin Exp Med*. 2025;34(11):1897–1906. doi:10.17219/acem/199920

DOI
10.17219/acem/199920

Abstract

Background. Dysregulated mitochondrial fission in synovial tissue is a key contributor to the progression of rheumatoid arthritis (RA), and echinacoside (ECH) has been shown to modulate this process in a mouse model of RA.

Objectives. This study aimed to investigate the effects of echinacoside (ECH) on the proliferation and inflammatory response of human fibroblast-like synoviocytes (MH7A cells), and to elucidate the potential underlying mechanisms.

Materials and methods. The expression and co-localization of TANK-binding kinase 1 (TBK1) and phosphorylated dynamin-related protein 1 (p-Drp1) in synovial tissues from patients with and without RA were analyzed. MH7A cells were exposed to either ECH or 0.1% dimethyl sulfoxide (DMSO). Cell proliferation was detected using Cell Counting Kit-8 (CCK-8) assay and reactive oxygen species (ROS) expression was detected with dichlorofluorescin (DCFH) staining. The levels of interleukin (IL)-6, IL-8, tumor necrosis factor alpha (TNF-α), cyclooxygenase (COX)-2, IL-1β, TANK-binding kinase 1 (TBK1), and Drp1 and the oxidative stress markers NF-E2-related factor 2 (Nrf2), heme oxygenase-1 (HO-1) and NAD(P)H: quinone oxidoreductase 1 (NQO1) were measured using quantitative real-time polymerase chain reaction (qPCR). The mitochondrial morphology was detected with transmission electron microscopy (TEM), and the expression levels of p-TBK1 (S172), TBK1, p-Drp1 (S616), p-Drp1 (S637), and Drp1 were assessed using western blotting.

Results. Compared to tissue from non-RA patients, RA synovial tissue exhibited higher expression and co-localization of TBK1 and phosphorylated Drp1 (p-Drp1). Following ECH treatment, MH7A cell proliferation and inflammatory cytokine secretion were reduced, while the expression of antioxidant stress markers was significantly increased. Furthermore, ECH treatment led to reduced levels of ROS, mitochondrial fragmentation and dysregulated mitochondrial fission in MH7A cells, along with decreased expression of p-TBK1 (Ser172) and p-Drp1 (Ser616), while p-Drp1 (Ser637) levels were increased.

Conclusions. Echinacoside regulates abnormal mitochondrial fission via the TBK1/Drp1 pathway, reducing the proliferation and inflammatory response of MH7A cells.

Key words: rheumatoid arthritis, mitochondrial fission, echinacoside

Highlight

- TBK1 is highly expressed in rheumatoid arthritis (RA) synovial tissue and may promote inflammation through Drp1-mediated mitochondrial fission.
- Echinacoside reduces inflammation and oxidative stress in RA-derived MH7A synoviocytes, highlighting its potential as a natural anti-inflammatory compound.
- Echinacoside alleviates mitochondrial dysfunction by inhibiting mitochondrial fission in MH7A cells.
- The anti-inflammatory effects of echinacoside in rheumatoid arthritis are linked to its regulation of the TBK1/Drp1 signaling pathway.

Background

Rheumatoid arthritis (RA) is a profoundly disabling disorder that predominantly impacts the joints, with an estimated prevalence of around 0.25–1% within the global population.[1] In China, the prevalence of RA is about 0.42% and the disability rate is as high as 61.3%.[2] At present, drug treatment for this condition achieves primarily symptomatic remission; the progression of RA is difficult to curb, posing a clinical challenge.

Dysregulated mitochondrial fission assumes a crucial role in the progression of numerous diseases.[3,4] Our research group found abnormal mitochondrial fission in synovial tissue and fibroblast-like synoviocytes (FLSs) in patients with RA.[5] Dynamin-related protein 1 (Drp1), a key regulatory molecule, mediates abnormal mitochondrial fission in FLSs, induces synovial proliferation and inflammation, and aggravates the progression of RA.[5] Its effect on the induction of such fission is influenced strongly by post-translational modifications, including phosphorylation, ubiquitination, Simulation of Urban Mobility (SUMO), and acetylation. Phosphorylation of Drp1 at Ser616 promotes mitochondrial fission, whereas phosphorylation at Ser637, Ser412 and Ser684 inhibits the fission process.[4,6]

TANK-binding kinase 1 (TBK1) is a serine/threonine protein kinase that plays a critical role in the initiation and progression of various diseases, particularly cancer and inflammatory disorders, by mediating protein phosphorylation, and has emerged as a key focus of recent research.[7,8] It belongs to the non-classical IκB kinase family and exhibits 64% homology with IκB kinase ε (IKKε, also referred to as IKKi). In recent years, accumulating evidence has indicated that TBK1 is closely associated with the development of various cancers, particularly lung, pancreatic and colorectal cancers. It is significantly upregulated in KRAS-mutant pancreatic ductal adenocarcinoma, and the receptor tyrosine kinase AXL activates it through a RAS-RalB-dependent mechanism, enhancing the epithelial–mesenchymal transition of pancreatic cancer cells, thereby increasing their aggressiveness and metastatic potential.[8] The elimination of TBK1 can reduce the occurrence of immune tolerance, increasing the anti-tumor immunotherapeutic effect of PD1.[7] Inhibitors targeting TBK1 can significantly improve the effect of tumor immunotherapy.[7] On the other hand, overactivation of TBK1 is closely linked to immune dysregulation and is a key contributor to the pathogenesis of autoimmune diseases,[9–11] suggesting that TBK1 may represent a promising therapeutic target for the treatment of RA. However, Hu et al.[12] found that the local expression of TBK1 is low in the joints of patients with osteoarthritis, and that the overexpression of TBK1 ameliorated tumor necrosis factor alpha (TNF-α)-induced apoptosis and mitochondrial dysfunction. In addition, TBK1 mediates Drp1-S637 phosphorylation to inhibit mitochondrial fission, induces mitochondrial autophagy, maintains mitochondrial homeostasis and alleviates local joint inflammation in patients with osteoarthritis.[12]

Echinacoside (ECH) is a phenylethanol glycoside with multiple biological functions. In recent years, the amount of basic research on ECH has increased, with studies focusing on its neuroprotective, anti-tumor, anti-oxidative, anti-inflammatory, and other functions.[13–16] Echinacoside has been shown to provide neuroprotection by suppressing the α-synuclein/TLR2/NF-κB/NLRP3 pathway in microglia within a Parkinson's disease model.[17] Echinacoside has been shown to alleviate osteoarthritis in mice through activation of the Nrf2/HO-1 signaling pathway.[18] Additionally, ECH modulates oxidative stress and reduces alcohol-induced liver injury by targeting Nrf2.[19] We previously found that ECH effectively attenuated the progression of arthritis in CIA mice.[20] However, the effect of ECH on MH7A synovial cells in RA is still not understood.

Objectives

In this study, we investigated the expression of TBK1 in RA synovium and the effect of ECH on RA (MH7A synovial) cells via the TBK1/Drp1 pathway.

Materials and methods

Reagents

A Cell Counting Kit-8 (CCK-8; AC0011S) was purchased from Xi'an AccuRef Scientific (Xi'an, China). The reactive

oxygen species (ROS) probe DCFH-DA (S0033S) was obtained from Beyotime Biotechnology (Shanghai, China). TBK1 antibody (#3504, 51872S), p-TBK1 (S172; #5433), p-Drp1 (S616; #4494, 3455S), and Drp1 antibody (#8570) were purchased from Cell Signaling Technology (CST; Danvers, USA). GAPDH (ab181602) and p-Drp1 (S637; ab193216) were provided by Abcam (Cambridge, UK). Horseradish peroxidase (HRP)-conjugated goat anti-rabbit IgG was purchased from ASPEN (AS1107; Wuhan, China). Dulbecco's modified Eagle's medium (DMEM; G4524), fetal bovine serum (FBS; G8002) and HRP-labeled goat anti-mouse IgG (GB23301) were obtained from Servicebio (Wuhan, China). A sodium dodecyl sulfate-polyacrylamide gel electrophoresis (SDS-PAGE) gel preparation kit (AS1012), a bicinchoninic acid (BCA) protein concentration determination kit (AS1086), radioimmunoprecipitation (RIPA) total protein lysate (AS1004), electrochemiluminescence (ECL) detection kit (AS1059), protease inhibitor cocktail (04693159001), and phosphorylase inhibitor (AS1008) were bought from ASPEN. A rapid RNA extraction kit (RM0051) was purchased from AccuRef Scientific. EntiLink™ 1st-strand cDNA synthesis super mix (EQ031), TRIpure total RNA extraction reagent, and EnTurbo™ SYBR Green PCR SuperMix (EQ001) were acquired from ELK Biotechnology (Wuhan, China). Primers were obtained from Sangong Biotech (Shanghai, China).

Study design

The MH7A cell line (No. CL-474h), an immortalized cell line derived from RA FLS transfected with SV40T antigen gene that has the characteristics of human RA-FLS, was utilized to analyze the impact of ECH on cell proliferation, inflammatory cytokine levels, oxidative stress, mitochondrial morphology, and mitochondrial phosphorylation.

Participants

Patients with RA who underwent knee replacement surgery (n = 6) and those with meniscus injury but not RA who underwent arthroscopic surgery (n = 4) were incorporated into this study. The research recerived approval from the Institutional Review Board of Tangdu Hospital, Air Force Medical University, Xi'an, China (approval No. TDLL-202408-08).

Cell source and culture

MH7A cells (cell line No. CL-474h) were purchased from SAIOS (Wuhan, China). They were removed from storage in liquid nitrogen, immediately placed in a water bath set at 37.5°C, shaken for rapid recovery, and quickly moved to a super-clean table. Each cell sample was moved into a 15-mL centrifuge tube, where 2 mL of DMEM (supplemented with 10% FBS and 1% penicillin–streptomycin solution) was added before centrifuging at 1,000 rpm for 5 min. After discarding the supernatant, 10 mL of medium was added for resuspension, and each sample was then inoculated in a culture bottle and placed in a cell incubator for culture. The medium was changed daily. When the cells reached >80% confluence, as confirmed using optical microscopy (Zeiss Primovert Hdcam; Carl Zeiss AG, Oberkochen, Germany) the trypsin was digested and cultured. Cells in the logarithmic phase of growth were randomly assigned to either the dimethyl sulfoxide (DMSO) group or the ECH group.

Immunofluorescence and co-localization analysis

The synovial tissues were preserved overnight in 10% formalin and subsequently embedded in paraffin. Paraffin sections were dewaxed and hydrated, and antigen repair and hydrogen peroxide and serum sealing were performed. Primary antibodies (TBK1 and p-DRP1 S616, 1:1,000) were added and the samples were left to rest overnight at 4°C. Then, the secondary antibody (1:500) was applied, and the samples were left to incubate for 50 min. The Tyramide Signal Amplification (TSA) was then added, and the samples were kept at room temperature for an additional 10 min. Following microwave treatment, the primary and secondary antibodies were removed, and the samples were incubated with 10% rabbit serum (cat. No. G1209) or 3% BSA at room temperature for 30 min to block nonspecific binding. Subsequently, DAPI (4′,6-diamidino-2-phenylindole) was added to re-stain the nuclei, and the samples were incubated at room temperature for 10 min in the dark. The samples were then washed 3 times with PBS for 5 min each, after which a fluorescence quencher was applied. The tissue slices were loaded into a PANNORAMIC digital slide scanner (3DHISTECH, Budapest, Hungary) for imaging. All tissue imaging information was uploaded into a folder and viewed (at ×1–400 magnification) using CaseViewer v. 2.4 software (3DHISTECH). The Area Quantification FL module v. 2.1.2 (Indica Labs, Albuquerque, USA) was used with the Halo analytical software v. 3.0.311.314 (Indica Labs) to quantify the numbers of gene-positive cells and positive and tissue areas in each section, the positive cell density (number of positive cells/tissue area), and the percentage of positive area (positive area/tissue area × 100%).

Transmission electron microscopy

Six-well plates were inoculated with 1×10^6 cells each. The DMSO group was treated with 0.1% DMSO solution and the ECH group was treated with ECH (100 μmol/L) for 24 h, with or without interleukin (IL)-1β (10 ng/mL) for 30 min. About 1 mL of electron microscopy fixative was added to the cells for 2 h before being stored at 4°C. They were washed 3 times with 0.1 M phosphate buffer (PB; pH 7.4) for 15 min. After fixation, dehydration, permeabilization, embedding, and sectioning, the cells were double-stained with 2% uranyl acetate and lead citrate for 15 min each, then left to dry overnight at room temperature. Samples were examined using transmission electron

microscopy (TEM; HT7700; Hitachi High Technologies, Tokyo, Japan) and super-resolution microscopy, and images were collected for further analysis.

CCK-8 assay

Ninety-six-well plates were inoculated with 1×10^5 cells each, and each group was set with 6 compound pores. The samples were treated with DMSO (0.1%) or ECH (40, 80 and 100 μM). Twenty-four hours later, 10 μL of CCK-8 reagent was added for 2 h. Absorbance (OD450) was detected using a microplate reader (Infinite F50; Tecan, Männedorf, Switzerland)

qPCR

Six-well plates were inoculated with 1×10^6 cells each. The samples were treated with 0.1% DMSO solution or 100 μmol/L ECH for 24 h. Total RNA was isolated using a rapid RNA extraction kit, and its purity and concentration were detected with ultraviolet spectrophotometry. The RNA underwent reverse transcription to cDNA utilizing the EntiLink™ 1st-strand cDNA synthesis super mix kit and was subsequently stored at –20°C. Following this, quantitative real-time polymerase chain reaction (qPCR) was conducted with the EnTurbo™ SYBR Green PCR SuperMix kit, employing a 10-μL reaction system. The CT values were determined based on the $2^{-\Delta\Delta CT}$ method. The primers used are detailed in Table 1.

Table 1. Primer sequences

Gene	Type	Sequence
H-GAPDH	sense	CATCATCCCTGCCTCTACTGG
	antisense	GTGGGTGTCGCTGTTGAAGTC
H-IL-6	sense	TCAGCCCTGAGAAAGGAGACAT
	antisense	GCTCTGGCTTGTTCCTCACTACT
H-IL-8	sense	ACTGAGAGTGATTGAGAGTGGAC
	antisense	AACCCTCTGCACCCAGTTTTC
H-TNF-α	sense	CTCTTCTCCTTCCTGATCGTGG
	antisense	CTTGTCACTCGGGGTTCGAG
H-COX-2	sense	AGATTATGTGCAACACTTGAGTGG
	antisense	ATTCCTACCACCAGCAACCCT
H-IL-1β	sense	ACGATGCACCTGTACGATCACT
	antisense	GAGAACACCACTTGTTGCTCCA
H-TBK1	sense	TATTTGCTATTGAAGAGGAGACAAC
	antisense	TAGTCCATAGGCATTAGAAGGTTCT
H-Drp1	sense	ATTCCATTATCCTCGCTGTCACT
	antisense	TGGCTCCTGTTAACTACTCCAAT
H-NQO1	sense	TGGTGGAGTCGGACCTCTATG
	antisense	CATGGCAGCGTAAGTGTAAGC
H-HO-1	sense	GCCAGCAACAAAGTGCAAGA
	antisense	TAAGGACCCATCGGAGAAGC
H-Nrf2	sense	GACAGCCCTGGTATTGATGTC
	antisense	TCACCTTGTGGAAGAAGTGCTT

Western blotting

Six-well plates were inoculated with 1×10^6 cells each. The samples were exposed to 0.1% DMSO solution or 100 μmol/L ECH for 24 h, with or without IL-1β (10 ng/mL) for 30 min. The protein extraction process was carried out using a RIPA lysate that contained a protease and phosphatase inhibitor. The BCA quantification was performed according to the kit (P0010S; Beyotime) instructions. Briefly, a standard curve was made and sample protein concentrations were determined. Protein denaturation, SDS-PAGE electrophoresis, membrane transfer and closure, primary antibody incubation (p-Drp1 (S616), 1:500; p-Drp1 (S637), 1:500; Drp1, 1:2,000; p-TBK1 (S172), 1:1,000; TBK1, 1:3,000; GAPDH, 1:10,000), secondary antibody incubation (1:10,000), and development were performed. A chemiluminescence imaging analysis system was used for image collection and an AlphaEaseFC software processing system (Alpha lnnotech, San Leandro, USA) was employed to assess the optical densities (ODs) of the specific bands.

ROS DCFH-DA staining

The levels of ROS in the cells were evaluated using dichlorofluorescin (DCFH) staining. Following a 24-h treatment with either DMSO or ECH, the medium was discarded and DCFH (10 μM) was introduced. The samples were incubated at 37°C for 30 min in the dark, then rinsed 3 times with fresh cell medium for 5 min each time. Hoechst nucleic acid stain was applied, and the samples were kept at room temperature away from light for an additional 5 min. Subsequently, the samples were washed 3 additional times with fresh medium for 5 min each, then examined under a fluorescence microscope, and images were captured for analysis.

Statistical analyses

Statistical analysis was conducted using IBM SPSS v. 19.0 (IBM Corp., Armonk, USA). The Shapiro–Wilk test assessed the normality of the data, while the Levene's statistic evaluated homogeneity of variance. For normally distributed data with equal variances, an independent-samples t-test was used for comparisons between 2 groups, while one-way analysis of variance (ANOVA) was applied for comparisons among three groups. Post hoc comparisons were conducted using the Student–Newman–Keuls (SNK) test. Non-normally distributed data were analyzed with the Wilcoxon rank sum test. P-values less than 0.05 were considered statistically significant.

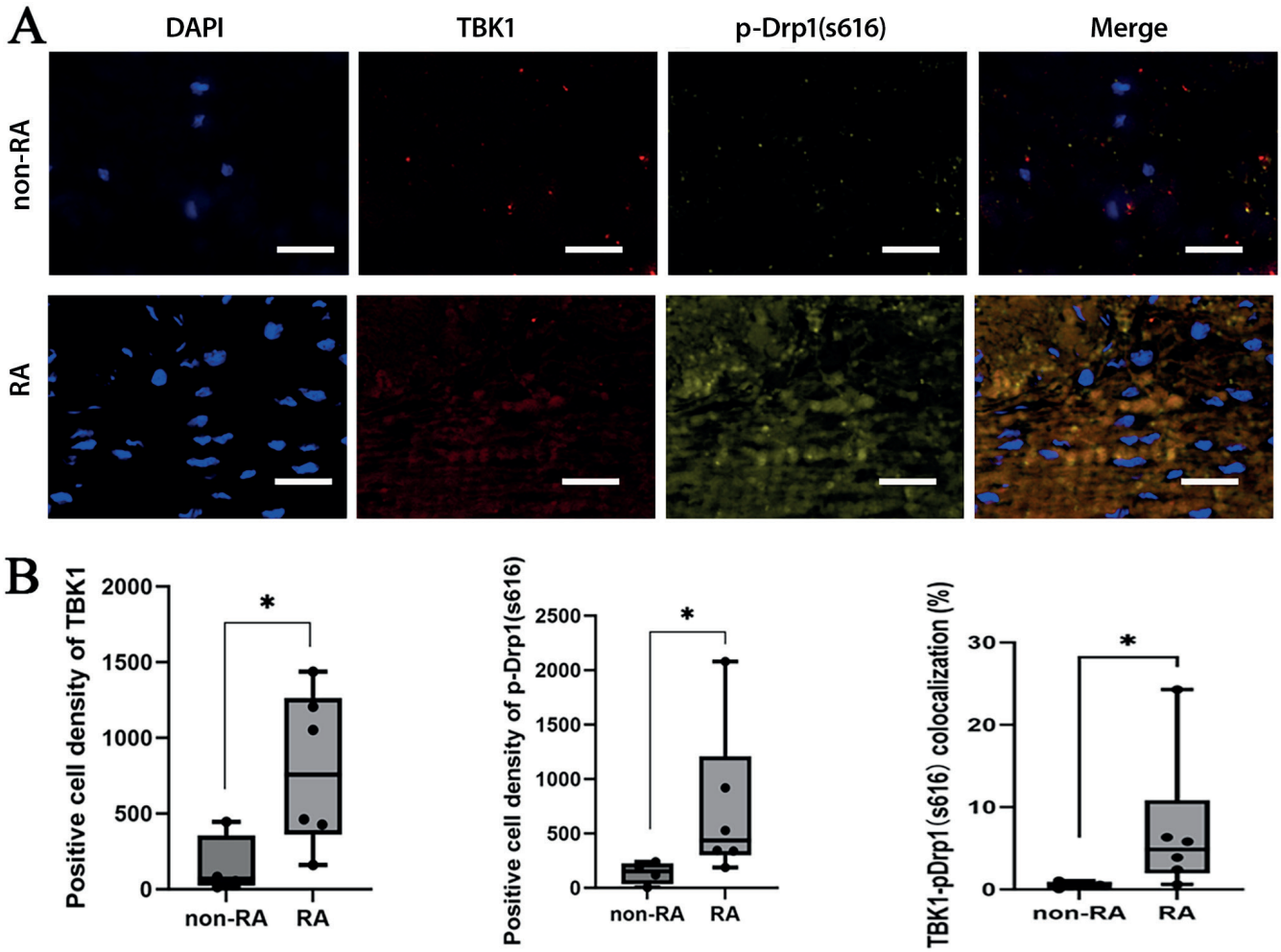

Fig. 1. Expression and co-localization of TANK-binding kinase 1 (TBK1) and phosphorylation dynamin-related protein 1 (p-Drp1) (S616) in rheumatoid arthritis (RA) synovial tissue. A. Expression and co-localization of TBK1 and p-Drp1 (S616) in the synovial tissue of patients with (n = 6) and without (n = 4) RA, detected using immunofluorescence staining (scale: 20 μm); B. Densities and co-localization of TBK1- and p-Drp1 (S616)-positive cells in the synovial tissue of patients with and without RA

*p < 0.05, Wilcoxon rank sum test.

Results

Expression and co-localization of TBK1 and p-Drp1 (S616) in RA synovial tissue

Overactivation of TBK1 is closely associated with dysregulation of the immune response and plays a key role in the pathogenesis of autoimmune diseases. To investigate whether TBK1 is upregulated and involved in Drp1-mediated mitochondrial fission in rheumatoid arthritis (RA), we analyzed the expression and co-localization of TBK1 and phosphorylated Drp1 (p-Drp1) in RA synovial tissues. The expression of TBK1, p-Drp1 (S616) and their co-localization in synovial tissue were higher in the RA group compared to the non-RA group (Fig. 1). This high expression of TBK1 in RA synovium may be related to Drp1-mediated mitochondrial fission.

Effects of ECH on MH7A cell proliferation and inflammation

Previous studies demonstrated that ECH effectively attenuates arthritis progression in collagen-induced arthritis (CIA) mice. Here, we investigate the effects of ECH on MH7A cell proliferation and inflammation. The proliferation of MH7A cells declined after ECH treatment (Fig. 2A). The qPCR analysis revealed that treatment with 100 μmol/L ECH significantly increased the mRNA expression of antioxidant stress markers HO-1, NQO1 and Nrf2 (Fig. 2B), while reducing the expression of inflammatory cytokines IL-6, IL-8, TNF-α, COX-2, and IL-1β (Fig. 2C). These results suggest that ECH alleviated MH7A cell inflammation and oxidative stress.

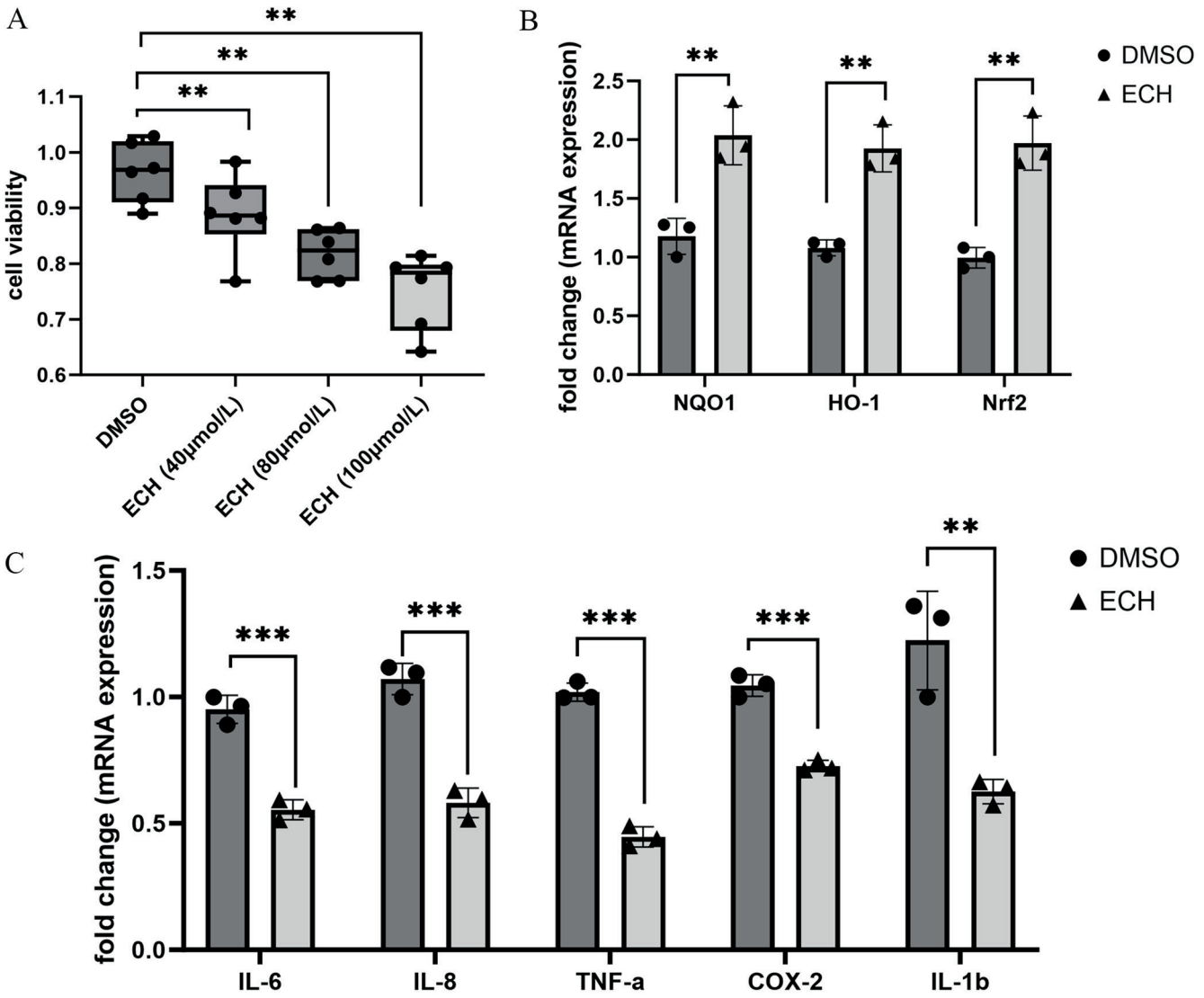

Fig. 2. Effects of echinacoside (ECH) treatment on MH7A cell proliferation and inflammation. A. Cell proliferation activity detected using Cell Counting Kit-8 (CCK-8) assay and assessed with analysis of variance (ANOVA); B. Expression of heme oxygenase-1 (HO-1), NAD(P)H: quinone oxidoreductase 1 (NQO1) and NF-E2-related factor 2 (Nrf2), , detected with quantitative real-time polymerase chain reaction (qPCR). Data are presented as mean ± standard deviation (SD); C. Expression of the inflammatory cytokines interleukin (IL)-6, IL-8, tumor necrosis factor alpha (TNF-α), cyclooxygenase-2 (COX-2), and IL-1β, detected with qRT-PCR

**p < 0.01, ***p < 0.001.

Effects of ECH on oxidative stress and mitochondrial fission of MH7A cells

Mitochondrial fission is involved in synovium inflammation, as it induces oxidative stress. To clarify the effect of ECH on mitochondrial fission, ROS expression and mitochondrial morphology were examined. After ECH treatment, ROS expression was significantly decreased in MH7A cells (Fig. 3A). Transmission electron microscopy revealed that IL-1β induced mitochondrial fission in the cells, but that this fission was significantly reduced after ECH treatment (Fig. 3B). No significant differences were observed in the mRNA expression levels of TBK1 and Drp1 between the treatment and control groups (Fig. 3C). These findings suggest that ECH alleviates inflammation and oxidative stress in MH7A cells by inhibiting mitochondrial fission.

Effects of ECH on TBK1 and Drp1 expression in MH7A cells

Next, we investigated the effects of ECH on the expression levels of TBK1, phosphorylated TBK1 (p-TBK1), Drp1, and phosphorylated Drp1 (p-Drp1). Western blot analysis showed that IL-1β stimulation increased the level of phosphorylated TBK1 at Ser172 (p-TBK1^S172), which was subsequently reduced following ECH treatment (Fig. 4A,B). In addition, IL-1β induced upregulation of phosphorylated Drp1 at Ser616 (p-Drp1^S616) and downregulation at Ser637 (p-Drp1^S637), effects that were reversed by ECH treatment (Fig. 4C,D). These findings suggest that ECH inhibits mitochondrial fission in MH7A cells by regulating the TBK1/Drp1 pathway.

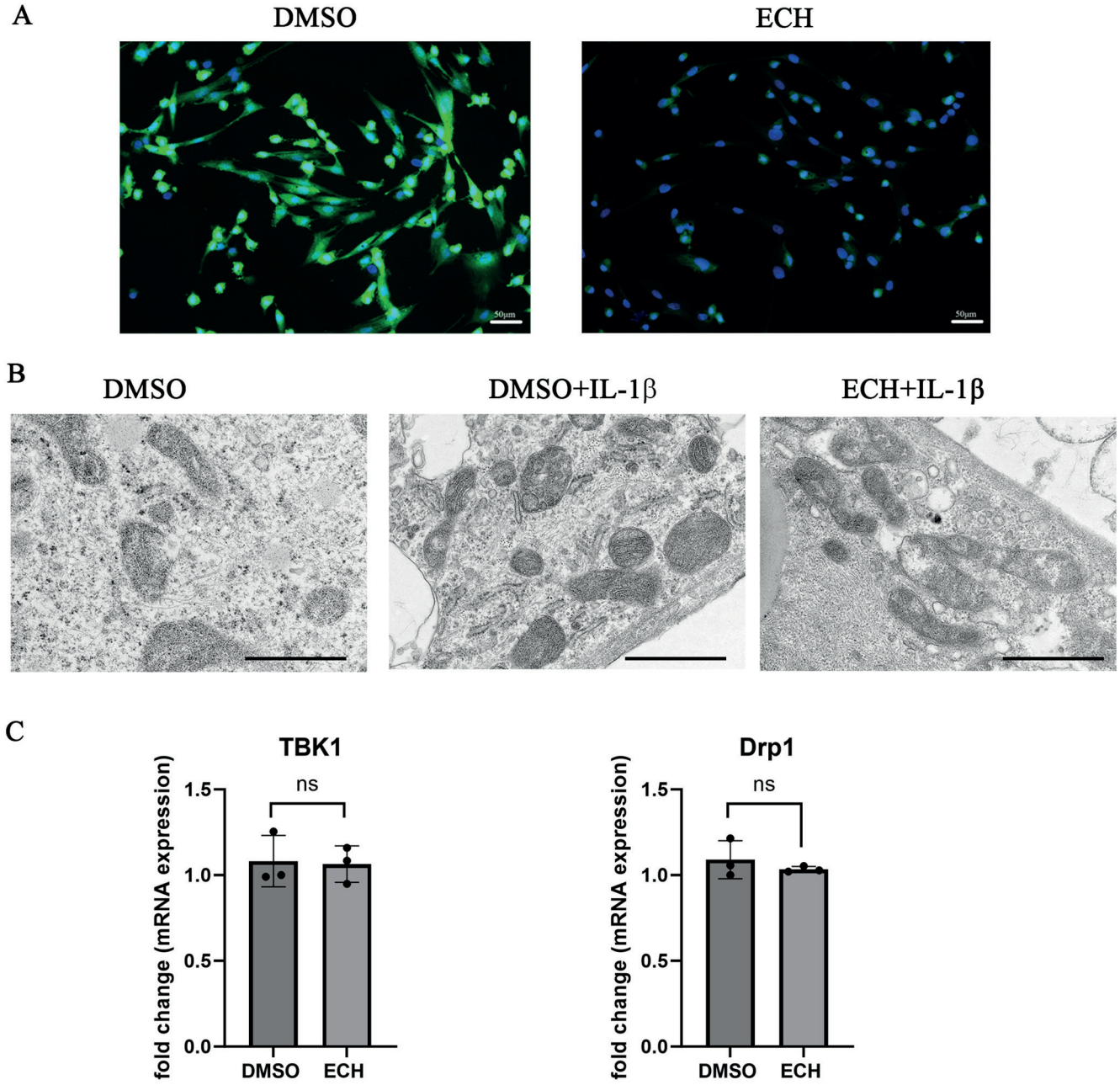

Fig. 3. Effects of echinacoside (ECH) on oxidative stress and mitochondrial fission of MH7A cells. A. Reactive oxygen species (ROS) expression detected using dichlorofluorescein (DCFH) staining (scale: 50 μm); B. Mitochondrial morphology detected with transmission electron microscopy (TEM; scale: 1 μm); C. dynamin-related protein 1 (Drp1) and TANK-binding kinase 1 (TBK1) expression detected with quantitative real-time polymerase chain reaction (qPCR). The data are presented as mean ± standard deviation (SD)

ns – nonsignificant; $p > 0.05$.

Discussion

This study demonstrated that TBK1 expression was markedly elevated in the synovial tissue of RA patients, consistent with findings from animal models of RA, but in contrast to the lower expression levels observed in the synovial tissue of patients with OA.[12] Our results provide further support for TBK1 as a potential therapeutic target for RA.

A 2023 report indicated that local TBK1 expression is low in the joints of patients with OA.[12] In contrast, a 2022 study using a rat model of RA reported elevated levels of phosphorylated TBK1 (p-TBK1). In that study, treatment with CS12192, a novel small-molecule inhibitor selectively targeting JAK3, JAK1, and TBK1, and WEHI112 – a relatively selective TBK1 inhibitor, produced notable immunosuppressive and anti-inflammatory effects.[10] Similar to this report, our findings showed that the expression of TBK1 was upregulated in RA synovial tissues. According to a 2021 report,[21] TBK1 also plays a critical role in the activation of innate immunity by regulating RIPK1-dependent cell death

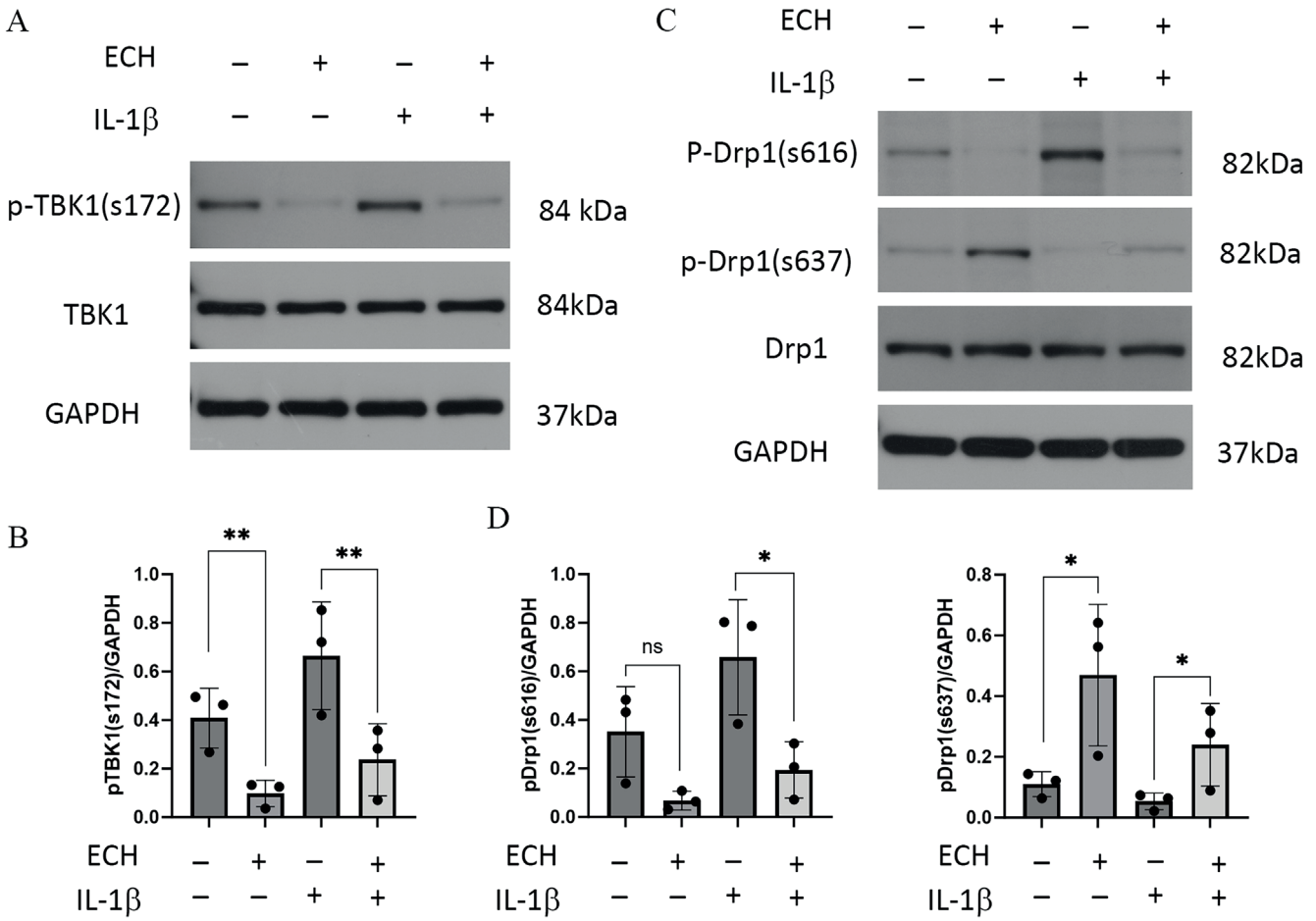

Fig. 4. Effects of echinacoside (ECH) treatment on TANK-binding kinase 1 (TBK1) and dynamin-related protein 1 (Drp1) expression in MH7A cells. A,B. p-TBK1 (s172) and TBK1 expression levels detected with western blotting; C,D. p-Drp1 (S616), p-Drp1 (S637) and Drp1 expression levels detected with western blotting. The concentration of ECH was 100 μmol/L and the concentration of interleukin (IL)-1β was 10 ng/mL. The data are presented as mean ± standard deviation (SD)

ns – nonsignificant; $p > 0.05$; *$p < 0.05$; **$p < 0.01$.

pathways triggered by type I interferons (IFN-I), NF-κB (nuclear factor kappa-light-chain-enhancer of activated B cells) and TNF. In 4 patients with congenital immunodeficiency, a biallelic loss-of-function (LoF) mutation in the *TBK1* gene was identified, which resulted in excessive TNF-induced cell death and subsequent autoimmune inflammation. Notably, treatment with anti-TNF therapy effectively mitigated these pathological effects.[21] These findings further demonstrate the different roles of TBK1 in autoimmune diseases, which may be related to the post-translational modification of TBK1. According to a 2020 report, TBK1 and Drp1 are vital for congenital RNA sensing and antiviral immunity, and TBK1-mediated Drp1 phosphorylation at S412 and S684 affects mitochondrial fission, enhancing the host antiviral defense.[22] In this study, we observed increased colocalization of TBK1 and p-Drp1 (Ser616) in the synovial tissue of patients with RA, suggesting that TBK1 may mediate the activation of p-Drp1 (Ser616), thereby contributing to Drp1-dependent mitochondrial fission in this tissue.

Excessive ROS accumulation is a key factor in the oxidative stress response of FLSs. According to a 2020 report, ROS overexpression in FLSs triggers the secretion of inflammatory mediators, including IL-6 and IL-8, via the NF-κB signaling pathway.[23] In this study, we evaluated the effects of various concentrations of ECH on ROS expression in MH7A cells and found that only 100 μmol/L ECH significantly reduced ROS levels, whereas other concentrations showed no notable effect (data not shown). Therefore, 100 μmol/L ECH was selected as the working concentration for subsequent experiments. Echinacoside effectively reduced the mRNA expression of inflammatory cytokines in MH7A cells, while simultaneously upregulating the expression of antioxidant stress markers, including Nrf2, HO-1 and NQO1. These findings suggest that ECH may alleviated MH7A cell inflammation and oxidative stress. Several studies have reported that ECH effectively modulates the oxidative stress response. A 2019 study reported that ECH significantly reduces ROS and NF-κB levels by inhibiting the NLRP3 inflammasome signaling pathway in spinal cord injury models.[24] Similarly, a 2022 study demonstrated that ECH prevents pyroptosis in cardiomyocytes and improves cardiac function by modulating

the NADPH/ROS/endoplasmic reticulum (ER) stress pathways.[25] Consistent with previous findings,[18,26] these results support the notion that ECH exerts therapeutic effects through its antioxidant properties.

In addition, as reported in 2020, ECH significantly inhibits Drp1, reverses abnormal mitochondrial fission at lesion sites, protects mitochondrial function and inhibits ROS-mediated oxidative stress, thereby reducing neuroinflammation.[27] The anti-oxidative stress effect of ECH may be closely related to the regulation of mitochondrial fission. Consistent with these findings, our team reported in 2024 that ECH reversed abnormal mitochondrial fission in the joints of CIA mice, thereby alleviating arthritic manifestations, by inhibiting Drp1.[20] In this study, we further found that ECH effectively reversed abnormal mitochondrial fission in MH7A cells, strengthening the conclusion that ECH alleviates inflammation and oxidative stress in these cells by inhibiting mitochondrial fission. However, ECH had no effect on Drp1 or TBK1 mRNA expression. The phosphorylated forms of these proteins play important roles in cell signaling, and ECH may regulate their phosphorylation. In this study, ECH notably decreased the levels of p-TBK1 (S172) and p-Drp1 (S616), while simultaneously enhancing the expression of p-Drp1 (S637). We believe that ECH inhibits mitochondrial fission in synovial tissue through the activation of TBK1 to mediate p-Drp1 (S616) phosphorylation and inhibit the proliferation and inflammation and oxidative stress induction of MH7A cells. In contrast to our findings, a 2023 study reported that TBK1 inhibits mitochondrial fission by promoting the phosphorylation of Drp1 at Ser637, thereby inducing mitophagy, maintaining mitochondrial homeostasis and alleviating local joint inflammation.[12] These findings suggest that the mitochondrial functions of TBK1 may differ between the synovial tissue of patients with OA and RA. In RA, TBK1 may contribute to disease progression by promoting mitochondrial fission through the phosphorylation of Drp1 at Ser616. This hypothesis warrants further investigation in future studies.

Limitations

This study has several limitations. First, the safety profile of ECH was not assessed and warrants further investigation. Second, we did not determine whether ECH modulates Drp1 phosphorylation in a TBK1-dependent manner, which remains to be elucidated. Finally, the TBK1-knockout mouse model used in this study requires further refinement to better clarify the mechanistic role of TBK1 in vivo.

Conclusions

The results of this study suggest that ECH treatment inhibits TBK1 phosphorylation, thereby modulating mitochondrial fission and p-Drp1 levels, ultimately leading to reduced ROS production and inflammation in MH7A cells. Echinacoside may suppress abnormal mitochondrial fission in MH7A cells by modulating the TBK1/Drp1 signaling pathway, thereby inhibiting cell proliferation and the inflammatory response. These findings suggest that ECH could represent a promising novel therapeutic option for the treatment of RA.

Data availability statement

The datasets supporting the findings of the current study are openly available in Zenodo repository at https://doi.org/10.5281/zenodo.14783921.

Consent for publication

Not applicable.

Use of AI and AI-assisted technologies

Not applicable.

ORCID

Xiaoyan Wang https://orcid.org/0000-0002-2980-047X
Zhufeng Chen https://orcid.org/0000-0003-4378-5349
Shanshan Wu https://orcid.org/0009-0000-0731-7041
Xuemei Fan https://orcid.org/0009-0006-6281-6023

References

1. Di Matteo A, Bathon JM, Emery P. Rheumatoid arthritis. *Lancet*. 2023; 402(10416):2019–2033. doi:10.1016/S0140-6736(23)01525-8
2. Geng Y, Xie X, Wang Y, et al. The standardized diagnosis and treatment of rheumatoid arthritis [in Chinese]. *Zhonghua Nei Ke Za Zhi*. 2022;61(1):51–59. doi:10.3760/cma.j.cn112138-20210616-00426
3. Kleele T, Rey T, Winter J, et al. Distinct fission signatures predict mitochondrial degradation or biogenesis. *Nature*. 2021;593(7859):435–439. doi:10.1038/s41586-021-03510-6
4. Chen W, Zhao H, Li Y. Mitochondrial dynamics in health and disease: mechanisms and potential targets. *Sig Transduct Target Ther*. 2023;8(1):333. doi:10.1038/s41392-023-01547-9
5. Wang X, Chen Z, Fan X, et al. Inhibition of DNM1L and mitochondrial fission attenuates inflammatory response in fibroblast-like synoviocytes of rheumatoid arthritis. *J Cell Mol Med*. 2020;24(2):1516–1528. doi:10.1111/jcmm.14837
6. Weyand CM, Wu B, Huang T, Hu Z, Goronzy JJ. Mitochondria as disease-relevant organelles in rheumatoid arthritis. *Clin Exp Immunol*. 2023;211(3):208–223. doi:10.1093/cei/uxac107
7. Sun Y, Revach OY, Anderson S, et al. Targeting TBK1 to overcome resistance to cancer immunotherapy. *Nature*. 2023;615(7950):158–167. doi:10.1038/s41586-023-05704-6
8. Xiang S, Song S, Tang H, et al. TANK-binding kinase 1 (TBK1): An emerging therapeutic target for drug discovery. *Drug Discovery Today*. 2021;26(10):2445–2455. doi:10.1016/j.drudis.2021.05.016
9. Louis C, Ngo D, D'Silva DB, et al. Therapeutic effects of a TANK-binding kinase 1 inhibitor in germinal xenter-driven collagen-induced arthritis. *Arthritis Rheum*. 2019;71(1):50–62. doi:10.1002/art.40670
10. Fang Z, Hu Y, Dai J, et al. CS12192, a novel JAK3/JAK1/TBK1 inhibitor, synergistically enhances the anti-inflammation effect of methotrexate in a rat model of rheumatoid arthritis. *Int J Mol Sci*. 2022; 23(21):13394. doi:10.3390/ijms232113394
11. Zeng Y, Ng JPL, Wang L, et al. Mutant p53R211* ameliorates inflammatory arthritis in AIA rats via inhibition of TBK1-IRF3 innate immune response. *Inflamm Res*. 2023;72(12):2199–2219. doi:10.1007/s00011-023-01809-w

12. Hu SL, Mamun AA, Shaw J, et al. TBK1-medicated DRP1 phosphorylation orchestrates mitochondrial dynamics and autophagy activation in osteoarthritis. *Acta Pharmacol Sin*. 2023;44(3):610–621. doi:10.1038/s41401-022-00967-7
13. Song Y, Zeng K, Jiang Y, Tu P. Cistanches Herba, from an endangered species to a big brand of Chinese medicine. *Med Res Rev*. 2021;41(3):1539–1577. doi:10.1002/med.21768
14. Chuang HW, Wang TY, Huang CC, Wei IH. Echinacoside exhibits antidepressant-like effects through AMPAR–Akt/ERK–mTOR pathway stimulation and BDNF expression in mice. *Chin Med*. 2022;17(1):9. doi:10.1186/s13020-021-00549-5
15. Li W, Zhou J, Zhang Y, et al. Echinacoside exerts anti-tumor activity via the miR-503-3p/TGF-β1/Smad aixs in liver cancer. *Cancer Cell Int*. 2021;21(1):304. doi:10.1186/s12935-021-01890-3
16. Ma Y, Yang X, Jiang N, Lu C, Zhang J, Zhuang S. Echinacoside ameliorates doxorubicin-induced cardiac injury by regulating GPX4 inhibition-induced ferroptosis. *Exp Ther Med*. 2023;27(1):29. doi:10.3892/etm.2023.12317
17. Yang XP, Huang JH, Ye FL, et al. Echinacoside exerts neuroprotection via suppressing microglial α-synuclein/TLR2/NF-κB/NLRP3 axis in parkinsonian models. *Phytomedicine*. 2024;123:155230. doi:10.1016/j.phymed.2023.155230
18. Tan Z, Zhang B. Echinacoside alleviates osteoarthritis in rats by activating the Nrf2-HO-1 signaling pathway. *Immunopharmacol Immunotoxicol*. 2022;44(6):850–859. doi:10.1080/08923973.2022.2088384
19. Ding Y, Zhang Y, Wang Z, et al. Echinacoside from *Cistanche tubulosa* ameliorates alcohol-induced liver injury and oxidative stress by targeting Nrf2. *FASEB J*. 2023;37(3):e22792. doi:10.1096/fj.202201430R
20. Wang X, Li L, Zhang M, et al. Anti-inflammatory effect of echinacoside in collagen-induced arthritis via Nrf2/Drp1 pathway [published online as ahead of print on March 20, 2024]. *Adv Clin Exp Med*. 2024. doi:10.17219/acem/184640
21. Taft J, Markson M, Legarda D, et al. Human TBK1 deficiency leads to autoinflammation driven by TNF-induced cell death. *Cell*. 2021;184(17):4447–4463.e20. doi:10.1016/j.cell.2021.07.026
22. Chen S, Liu S, Wang J, et al. TBK1-mediated DRP1 targeting confers nucleic acid sensing to reprogram mitochondrial dynamics and physiology. *Mol Cell*. 2020;80(5):810–827.e7. doi:10.1016/j.molcel.2020.10.018
23. Nygaard G, Firestein GS. Restoring synovial homeostasis in rheumatoid arthritis by targeting fibroblast-like synoviocytes. *Nat Rev Rheumatol*. 2020;16(6):316–333. doi:10.1038/s41584-020-0413-5
24. Gao S, Xu T, Guo H, et al. Ameliorative effects of echinacoside against spinal cord injury via inhibiting NLRP3 inflammasome signaling pathway. *Life Sci*. 2019;237:116978. doi:10.1016/j.lfs.2019.116978
25. Ni Y, Zhang J, Zhu W, Duan Y, Bai H, Luan C. Echinacoside inhibited cardiomyocyte pyroptosis and improved heart function of HF rats induced by isoproterenol via suppressing NADPH/ROS/ER. *J Cell Mol Med*. 2022;26(21):5414–5425. doi:10.1111/jcmm.17564
26. Tao Z, Zhang L, Wu T, Fang X, Zhao L. Echinacoside ameliorates alcohol-induced oxidative stress and hepatic steatosis by affecting SREBP1c/FASN pathway via PPARα. *Food Chem Toxicol*. 2021;148:111956. doi:10.1016/j.fct.2020.111956
27. Zhou L, Yao M, Tian Z, et al. Echinacoside attenuates inflammatory response in a rat model of cervical spondylotic myelopathy via inhibition of excessive mitochondrial fission. *Free Radic Biol Med*. 2020;152:697–714. doi:10.1016/j.freeradbiomed.2020.01.014

Parkin aggravates symptoms of preeclampsia through promoting mitophagy and apoptosis

Li Wang[1,A–F], Xue Wang[2,A–F], Ying Zheng[1,A–C,E,F], Jiao Kong[1,B,C,E,F], Lin-Mei Zheng[1,B,C,E,F], Ai-Hua He[3,B,C,E,F], Xiao-Ju Chen[1,B,C,E,F]

[1] Department of Obstetrics, Hainan General Hospital, Hainan Affiliated Hospital of Hainan Medical University, Haikou, China
[2] Phase 1 Clinical Trial Ward, Hainan General Hospital, Hainan Affiliated Hospital of Hainan Medical University, Haikou, China
[3] Department of Pathology, Hainan General Hospital, Hainan Affiliated Hospital of Hainan Medical University, Haikou, China

A – research concept and design; B – collection and/or assembly of data; C – data analysis and interpretation;
D – writing the article; E – critical revision of the article; F – final approval of the article

Advances in Clinical and Experimental Medicine, ISSN 1899–5276 (print), ISSN 2451–2680 (online) *Adv Clin Exp Med*. 2025;34(11):1907–1919

Address for correspondence
Xiao-Ju Chen
Email: xuexue72108@163.com

Funding sources
This study was supported by the Hainan Provincial Natural Science Foundation High-level Talent Project (grant No. 822RC810).

Conflict of interest
None declared

Received on July 25, 2024
Reviewed on October 19, 2024
Accepted on January 13, 2025

Published online on July 23, 2025

Abstract

Background. Preeclampsia is a serious pregnancy complication with significant maternal and fetal morbidity. Mitophagy plays a crucial role in its pathogenesis. The importance of this study lies in evaluating the role of parkin in preeclampsia, which may offer new insights into the management of this disease.

Objectives. This study was designed to evaluate the role of parkin in preeclampsia.

Materials and methods. To induce a preeclampsia model, pregnant female rats were administered N-nitro-L-arginine methyl ester (L-NAME) subcutaneously at a dose of 50 mg/(kg·day) starting on gestational day 14 for 7 consecutive days. Uteroplacental tissues were then collected, and chorionic trophoblast cells were isolated. Systolic blood pressure (SBP) and urine protein content were measured on days 12 and 20 of pregnancy. Hematoxylin-eosin (H&E) staining and TUNEL staining were employed to assess pathological changes and apoptosis in uteroplacental tissues, respectively. Reverse transcription polymerase chain reaction (RT-qPCR) and western blot analysis were performed to evaluate mRNA and protein expression levels associated with cellular function, mitophagy and the PINK1/parkin signaling pathway.

Results. Compared to the negavtive control (NC) group, rats in the model group showed elevated SBP and urine protein levels ($p < 0.01$). Chorionic trophoblast cells exhibited substantial damage, with significantly increased levels of apoptosis and autophagy. Moreover, parkin mRNA and protein expression levels were markedly upregulated in the model group. Overexpression of parkin in chorionic trophoblast cells enhanced apoptosis and mitophagy, while the autophagy inhibitor 3-methyladenine (3-MA) significantly alleviated the damage caused by overexpression of parkin.

Conclusions. Parkin aggravates the symptoms of preeclampsia by increasing mitophagy and apoptosis.

Key words: apoptosis, preeclampsia, mitophagy, parkin, 3-methyladenine (3-MA)

Cite as
Wang L, Wang X, Zheng Y. Parkin aggravates symptoms of preeclampsia through promoting mitophagy and apoptosis [published online as ahead of print on July 23, 2025]. *Adv Clin Exp Med*. 2025;34(11):1907–1919. doi:10.17219/acem/200059

DOI
10.17219/acem/200059

Highlights

- Parkin overexpression significantly promotes mitophagy and apoptosis in trophoblast cells of preeclampsia rats.
- Elevated parkin levels aggravate preeclampsia symptoms by increasing placental mitochondrial degradation and cell death.
- The mitophagy inhibitor 3-MA partially reverses parkin-induced cell damage in trophoblasts.
- Parkin may serve as a novel therapeutic target for improving placental function in preeclampsia.
- Findings highlight a potential clinical strategy for managing preeclampsia via mitophagy regulation.

Background

Preeclampsia, an obstetric disease, affects 1.5–16.7% of pregnant women and results in 60,000 deaths and 500,000 premature births worldwide every year.[1] Statistics indicate that preeclampsia is the 2nd leading cause of maternal mortality, with maternal mortality rates due to preeclampsia being at least 16% in low-and middle-income countries and as high as 25% in some Latin American countries.[2] Preeclampsia typically develops after the 20th week of pregnancy and is characterized by hypertension, proteinuria, end-organ damage, acute kidney injury(AKI), liver dysfunction, and other systemic complications.[3] Moreover, the impact of preeclampsia is long-lasting. Studies have shown that preeclampsia is associated with an increased risk of future cardiovascular, metabolic and cerebrovascular diseases in mothers. It also raises the risk of fetal growth restriction and placental abruption.[4] The pathogenesis of preeclampsia is believed to be linked to the failure of extravillous trophoblast (EVT) cells to properly migrate and invade the uterine spiral arteries, leading to neovascularization disorders and increased uteroplacental vascular resistance.[5] Currently, aspirin is the only medication recommended for the prevention and treatment of preeclampsia; however, its therapeutic effects are mixed and it is associated with side effects.[6] Previous research has shown that aspirin can reduce the risk of early-onset preeclampsia but is ineffective in alleviating symptoms of late-onset preeclampsia.[7] Therefore, new therapeutic agents are needed to address these challenges.

Mitochondria are the energy powerhouses of cells, essential for placental formation and development throughout pregnancy.[8] They are double-membrane organelles, consisting of an ion-permeable inner membrane and an outer mitochondrial membrane. Mitochondria are crucial for generating the proton gradient and transmembrane potential, with the energy stored in this proton gradient used to synthesize large amounts of adenosine triphosphate (ATP) for energy supply.[9] Although mitochondria cannot be synthesized de novo within cells, they possess their own self-replicating genomes. The coordination between mitophagy and energy production is vital for managing irreparably damaged mitochondria, maintaining mitochondrial volume and ensuring mitochondrial turnover.[10] Mitophagy is the selective process by which autophagosomes and lysosomes remove damaged mitochondrial proteins and dysfunctional mitochondria.[11] When mitochondrial dysfunction occurs, impaired mitophagy can lead to cellular damage and even cell death.[12] Therefore, normal mitophagy is crucial for cell survival. Previous studies have shown that mitophagy primarily relies on parkin mediation.[13] Parkin substrates can generate various ubiquitin chains, including K6, K11, K48, and K63 bonds.[14] Additionally, parkin can facilitate the specific phagocytosis of damaged mitochondria by autophagosomes through ubiquitination-labeled receptor proteins.[15] While the role of parkin in mitophagy is well-established, its impact on preeclampsia remains unclear.

Objectives

The objective of this study was to investigate the specific functions and mechanisms of parkin in preeclampsia by modulating its expression levels in a cell model of the disease. We aimed to provide new insights into the pathogenesis of preeclampsia by uncovering how parkin regulates mitophagy and apoptosis in chorionic trophoblast cells, and to explore its potential as a therapeutic target.

Materials and methods

Study design

All animal-related experiments were approved and supervised by the Animal Ethics Committee of Hainan Affiliated Hospital of Hainan Medical University, Haikou, China (approval No. Med-Eth-Re(2024)254). The Specific Pathogen-Free Sprague Dawley (SPF SD) female rats weighing about 200 g each were purchased from Beijing Vital River Laboratory Animal Technology Co., Ltd. (Beijing, China). All purchased rats were housed in an environment at room temperature of 22–24°C and relative humidity of 50–70%, with free access to food and water.

Participants

Consistent with the previous report, the phase of the estrus cycle was determined by observing cell morphology through vaginal smear.[16] Briefly, female rats in estrus were paired with SPF SD male rats at a ratio of 1:2. Sperm presence was monitored daily through vaginal smears to determine fertilization. Day 0 of pregnancy was defined as the day sperm was first detected. Pregnant rats were then randomly divided into 2 groups: the negative control (NC) group (n = 40) and the model group (n = 40). From the 14th day to 20th day of pregnancy, rats in the model group received subcutaneous injections of 50 mg/(kg·d) N-nitro-L-arginine methyl ester (L-NAME) to induce a preeclampsia model,[17] while rats in the NC group received an equivalent volume of normal saline. On the 20th day, the rats were anesthetized with CO_2 and euthanized. Uteroplacental tissues were collected from the mother rats, with some used for subsequent experiments and others for trophoblast cell isolation. Tissues designated for further experiments were quickly frozen in liquid nitrogen and stored at –80°C.

Variables

The primary variables include blood pressure, urine protein levels, gene expression levels (Beclin-1, p62, mt-parkin (mitochondrial parkin), total-parkin (total cellular parkin) PINK1, NDP52, OPTN), apoptosis rates, and protein expression levels (LC3, Beclin-1, p62, PINK1, parkin, GAPDH).

Data sources and measurements

Isolation and treatment of trophoblast cells

As described in a previous study,[18] uteroplacental tissues from mother rats were meticulously dissected using ophthalmic scissors under aseptic conditions. The tissues were then treated with 2.5 g/L trypsin and digested in a water bath at 37°C for 10 min. This process was repeated 3 times to obtain a cell suspension. The cell suspension was washed twice, re-suspended in Dulbecco's modified Eagle's medium (DMEM)/F12 culture medium containing 10% fetal bovine serum (FBS), and seeded in a culture plate. The cells were then cultured in an incubator with 5% CO_2 at 37°C. Under an optical microscope (model CX43; Olympus Corp., Tokyo, Japan) the isolated cells exhibited typical epithelial-like morphology of trophoblast cells and demonstrated a tendency to spread and grow in sheets. Subsequently, the isolated trophoblast cells were transfected using X-tremeGENE™ (6366244001, MilliporeSigma, St. Louis, USA) with either an overexpression vector for parkin (OE-parkin group) or a corresponding control vector (OE-NC group). Additionally, trophoblast cells transfected with overexpressed parkin and treated with the mitophagy inhibitor 3-methyladenine (3-MA) were designated as the OE-parkin+3-MA group.

Test for blood pressure and urine protein in rats

To measure the systolic blood pressure (SBP) of rats in each group, female rats were fixed in the BP-2000 blood pressure analysis system (Visitech Systems, Apex, USA) on the 12th and 20th days of pregnancy. Once the rats were stabilized, SBP readings were recorded for both the NC group and model group. Additionally, urine samples from the 12th and 20th days of pregnancy were collected. Briefly, rats were placed in a metabolic cage, and urine was collected over a 12-h period. The collected urine was then centrifuged at 4°C and 12,000 rpm for 5 min, and the supernatant was obtained. Total urine protein levels were subsequently measured using a urine protein quantitative test kit (C035-2-1; Jiancheng, Nanjing, China).

Hematoxylin and eosin staining

The obtained uteroplacental tissues were soaked in 4% paraformaldehyde overnight for complete fixation, and then sectioned into 5-μm thick slices. The sections were placed on slides, with resin applied around the edges to prevent slipping. Following the instructions of the hematoxylin and eosin (H&E) staining kit (Beyotime Biotechnology, Shanghai, China), the sections were stained as follows: the nuclei were stained with hematoxylin staining solution for 5 min, then washed with running water and differentiated using 1% hydrochloric acid alcohol for a few seconds. The sections were washed again with running water, blued with 0.6% ammonia, and rinsed with running water. The cytoplasm was then stained with eosin for 3 min, followed by dehydration and mounting. Finally, the sections were observed under an optical microscope (Olympus BX51; Olympus Corp., Tokyo, Japan) and photographed.

RT-qPCR

To extract RNA from mitochondria, mitochondrial isolation kit (C3606; Beyotime Biotechnology) was first used to purify the mitochondria. Subsequently, total RNA from uteroplacental tissues, mitochondria or trophoblast cells was extracted using Trizol reagent (R0016; Beyotime Biotechnology). The RNA concentration from different sources was determined with a NanoDrop spectrophotometer (840-317400; Thermo Fisher Scientific, Waltham, USA). According to the instruction of FastKing cDNA synthesis kit (KR116; Tiangen, Beijing, China), 2 μg of RNA was reverse transcribed into complementary deoxyribonucleic acid (cDNA). The expression levels of Beclin-1, p62, mt-parkin, total-parkin, PINK1, NDP52, and OPTN in tissue or cell samples, along with the internal control GAPDH were detected using RealUniversal Color PreMix (FP201; Tiangen). Relative gene expression was calculated using the $2^{-\Delta\Delta Ct}$ method. All primer sequences are listed in Table 1 and were synthesized by Sangon Biotech Co., Ltd. (Shanghai, China).

Table 1. Primer sequences

Gene name	Primer sequences (5′ to 3′)
Beclin1	F: CAGCCTCTGAAACTGGACACGA
	R: CTCTCCTGAGTTAGCCTCTTCC
p62	F: GCTCTTCGGAAGTCAGCAAACC
	R: GCAGTTTCCCGACTCCATCTGT
Parkin	F: CCAGAGGAAAGTCACCTGCGAA
	R: CTGAGGCTTCAAATACGGCACTG
PINK1	F: CGACAACATCCTTGTGGAGTGG
	R: CATTGCCACCACGCTCTACACT
NDP52	F: ACGCAAGGACTGGATTGGCATC
	R: GGATTTCCTGCTGTGTGGCTGA
OPTN	F: AGGTGGAGAGACTTGAAGTCGC
	R: TCCTCGCTGTCTGCTTCTCAGT
GAPDH	F: GTCTCCTCTGACTTCAACAGCG
	R: ACCACCCTGTTGCTGTAGCCAA

Tunel staining

The collected uteroplacental tissue sections were deparaffinized in xylene, rehydrated through a graded ethanol series, and subsequently treated with Proteinase K working solution for 15–30 min. For the cells, the treated samples were washed twice with phosphate-buffered saline (PBS), fixed with 4% paraformaldehyde for 1 h, and then permeabilized with cell permeabilization solution for 8 min. Following this, tissues and cells were rinsed twice with PBS and stained according to the instructions of TUNEL cell apoptosis detection kit (green fluorescence) (C1086; Beyotime Biotechnology) using the one-step method. Briefly, 50 µL of TUNEL detection solution was added to the cells or sections, which were then incubated in the dark at 37°C for 60 min. Then, the nucleus was stained with DAPI (4′,6-diamidino-2-phenylindole) for 5 min. Finally, cell apoptosis was observed under a fluorescence microscope (Leica DM2500 LED; Leica Camera AG, Wetzlar, Germany) and photographed. The excitation wavelength of TUNEL was 450 nm, and the detection wavelength was 565 nm.

Western blot

Total protein was extracted from tissues, cells and isolated mitochondria using radioimmunoprecipitation assay (RIPA) lysis buffer (P0013B; Beyotime Biotechnology). For cell samples, ultrasonic disruption was performed after collection, while tissues were further homogenized. The cell/mitochondrial lysate and tissue homogenate were then centrifuged at 4°C and 12,000 rpm for 10 min, and the supernatant was collected. Protein concentration was determined using a bicinchoninic acid (BCA) protein assay kit (P0009; Beyotime Biotechnology). Next, 25 µg of total protein was mixed with 5×sodium dodecyl sulfate (SDS) loading buffer and denatured at 99°C for 10 min. Proteins were separated using 10% SDS-polyacrylamide gel electrophoresis (SDS-PAGE), then transferred to a polyvinylidene fluoride (PVDF) membrane via electrotransformation. After transfer, the PVDF membrane was blocked with 5% BCA at ambient temperature for 2 h. The membrane was then incubated overnight at 4°C with primary antibodies (all from Abcam, Cambridge, UK): Anti-LC3 (1:1,000; ab192890), Anti-Beclin1 (1:1000; ab207612), Anti-p62 (1:1,000; ab211324), Anti-PINK1 (1:1,000; ab300623), anti-parkin (1:1,000; ab77924), or Anti-GAPDH (1:1,000; ab8245). On the next day, the membrane was incubated with sheep anti-rabbit or anti-mouse secondary antibodies (1:3,000; ab6721, ab205719) for 1 h of incubation at room temperature. Enhanced chemiluminescence (SuperSignal ECL; Thermo Fisher Scientific) was then used to develop the protein signals on the PVDF membrane. Finally, the expression levels of each protein were visualized using the iBright CL 750 (Thermo Fisher Scientific).

Statistical analyses

All data are presented as mean ± standard deviation (SD), and differences were analyzed using IBM SPSS v. 22.0 software (IBM Corp., Armonk, USA). A t-test was used for analyzing differences between 2 independent samples, while one-way analysis of variance (ANOVA) was employed for comparing multiple independent samples. Post hoc tests were performed using Tukey's test to identify specific group differences. A $p < 0.05$ indicated a significant difference.

Results

Establishment of rat model of preeclampsia

To evaluate the role of parkin in preeclampsia, female rats at 14 days of pregnancy were subcutaneously injected with L-NAME for 7 days to establish a preeclampsia model. Subsequently, the pathological changes in chorionic trophoblast tissues were observed using H&E staining. The H&E staining results showed that, compared to the NC group, the model group exhibited disordered cell arrangement, widened intercellular spaces and thickened basement membrane, indicating severe damage to the chorionic trophoblast tissues in the model group (Fig. 1A). Additionally, SBP and urine protein levels were measured on the 12th and 20th day of pregnancy. The results revealed no significant differences between the 2 groups on the 12th day. However, on the 20th day, the L-NAME-induced preeclampsia rats showed increased blood pressure and urine protein levels, reaching 136.35 mm Hg and 4.4 mg/mL, respectively, compared to the NC group ($p < 0.001$, Fig. 1B and Table 2; Fig. 1C, Table 3). In summary, L-NAME-induced rats displayed clear characteristics of preeclampsia, validating the model for further experiments.

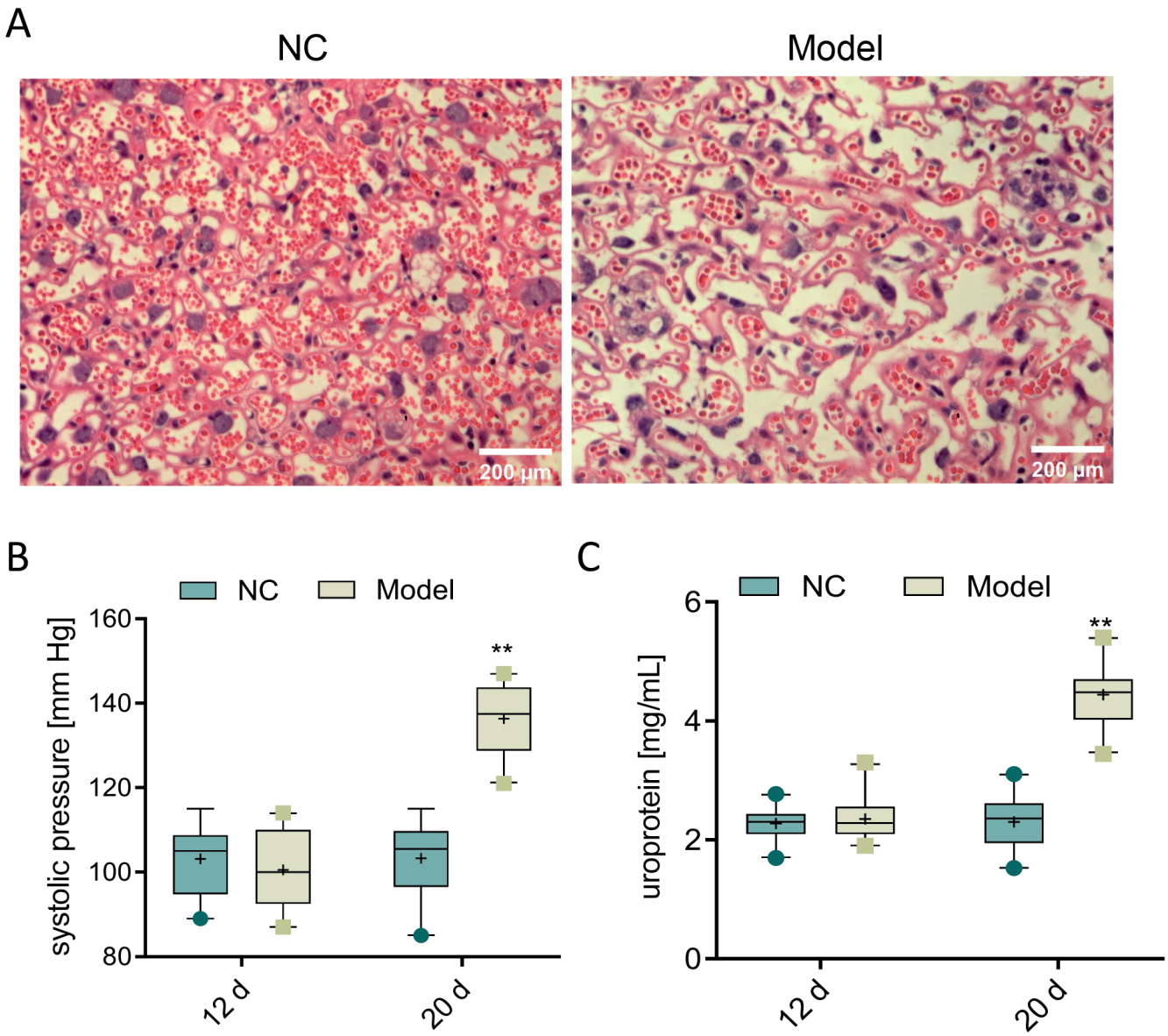

Fig. 1. Construction of rat model of preeclampsia. A. Hematoxylin & eosin (H&E) staining was used to observe the pathological changes of chorionic trophoblast tissues in rats in each group (scale bar = 200 µm); B,C. Measurement of the systolic blood pressure and urine protein content of rats on the 12th and 20th day of pregnancy

**p < 0.01 vs negative control (NC).

Table 2. Independent t-tests were conducted to compare systolic blood pressure between groups on gestational days 12 and 20, as shown in Fig. 1B

Day	Group	Median	t	p-value	df
12	NC	102.15 ±8.34	0.94	0.353	38
	model	100.55 ±9.13			
20	NC	103.30 ±8.77	12.44	<0.001	38
	model	136.35 ±8.01			

df – degrees of freedom; NC – negative control.

L-NAME induction increases the apoptosis level of chorionic trophoblast cells in preeclampsia rats

Additionally, TUNEL staining was used to observe the level of apoptosis in chorionic trophoblast tissues across each group of rats. Compared to the NC group, the TUNEL fluorescence signal in the chorionic trophoblast tissues significantly increased after 7 days of subcutaneous L-NAME injection (Fig. 2). These results indicate a marked upregulation of level of apoptosis in the chorionic trophoblast tissues of the model group.

Table 3. Independent t-tests were used to compare uroprotein levels between groups on gestational days 12 and 20, as shown in Fig. 1C

Day	Group	Median	t	p-value	df
12	NC	2.28 ±0.26	0.84	0.407	38
	model	2.35 ±0.33			
20	NC	2.30 ±0.42	15.03	<0.001	38
	model	4.44 ±0.48			

df – degrees of freedom; NC – negative control.

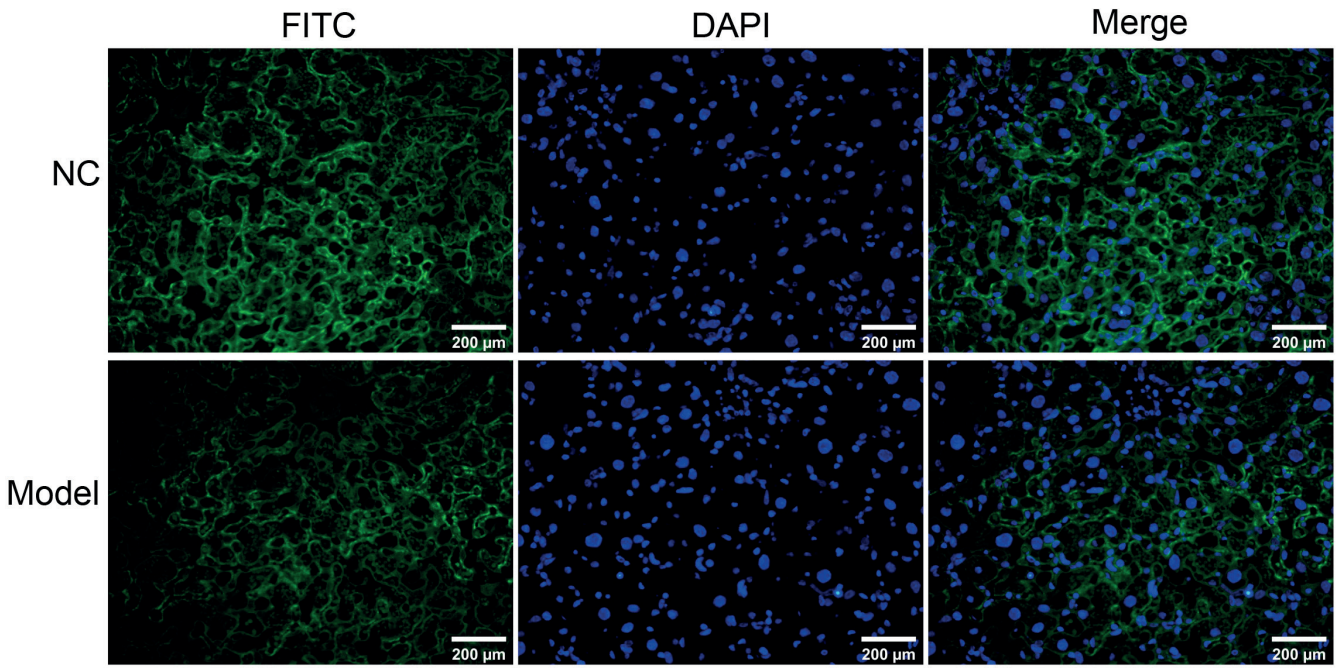

Fig. 2. N-nitro-L-arginine methyl ester (L-NAME) induces the increase of apoptosis level in chorionic trophoblast tissues of preeclampsia rats. TUNEL staining was adopted to observe the level of apoptosis in chorionic trophoblast tissues of rats in each group. TUNEL signal was green, DAPI (4′,6-diamidyno-2-fenyloindol) signal was blue, and the scale bar was 200 μm

L-NAME induces the increase of parkin-dependent mitophagy in chorionic trophoblast tissues of preeclampsia rats

Previous studies have identified the presence of PINK1 and parkin-dependent mitophagy in preeclampsia placenta.[19,20] To further investigate this, we assessed the activities of Beclin-1, PINK1, parkin, p62, NDP52, and OPTN pathways in the chorionic trophoblast tissues of rats at both the mRNA and protein levels. The results showed that, compared to the NC group, the model group exhibited increased mRNA and protein expression levels of Beclin-1 and mt-parkin in chorionic trophoblast tissues, along with decreased mRNA and protein expression levels of p62, NDP52 and OPTN. Additionally, a significant increase in the LC3-II/LC3-I ratio was observed (Fig. 3A–D; Table 4,5). These findings indicate a significant increase in mitophagy in the model group. Taken together, L-NAME induced a notable increase in parkin-dependent mitophagy in the chorionic trophoblast tissues of preeclampsia rats.

3-methyladenine partly reversed the increase of mitophagy and apoptosis of trophoblast cells in preeclampsia rats caused by overexpression of parkin

To clarify the effect of parkin on autophagy and apoptosis in preeclampsia tissues, primary trophoblast cells were isolated from the uteroplacental tissue of preeclampsia rats, and parkin was overexpressed in these cells. Additionally, cells were treated with the autophagy inhibitor 3-MA to determine whether parkin exacerbates preeclampsia symptoms by promoting autophagy and apoptosis. Specifically, compared to the OE-NC group, the OE-parkin group showed increased levels of apoptosis in trophoblast cells. However, when compared to the OE-parkin group, the level of apoptosis in the OE-parkin+3-MA group was reduced (Fig. 4A). Similar results were observed for autophagy. In the OE-parkin group, mRNA and protein expression levels of Beclin-1 and mt-parkin were elevated, while those of p62, NDP52 and OPTN were reduced; the LC3II/LC3I

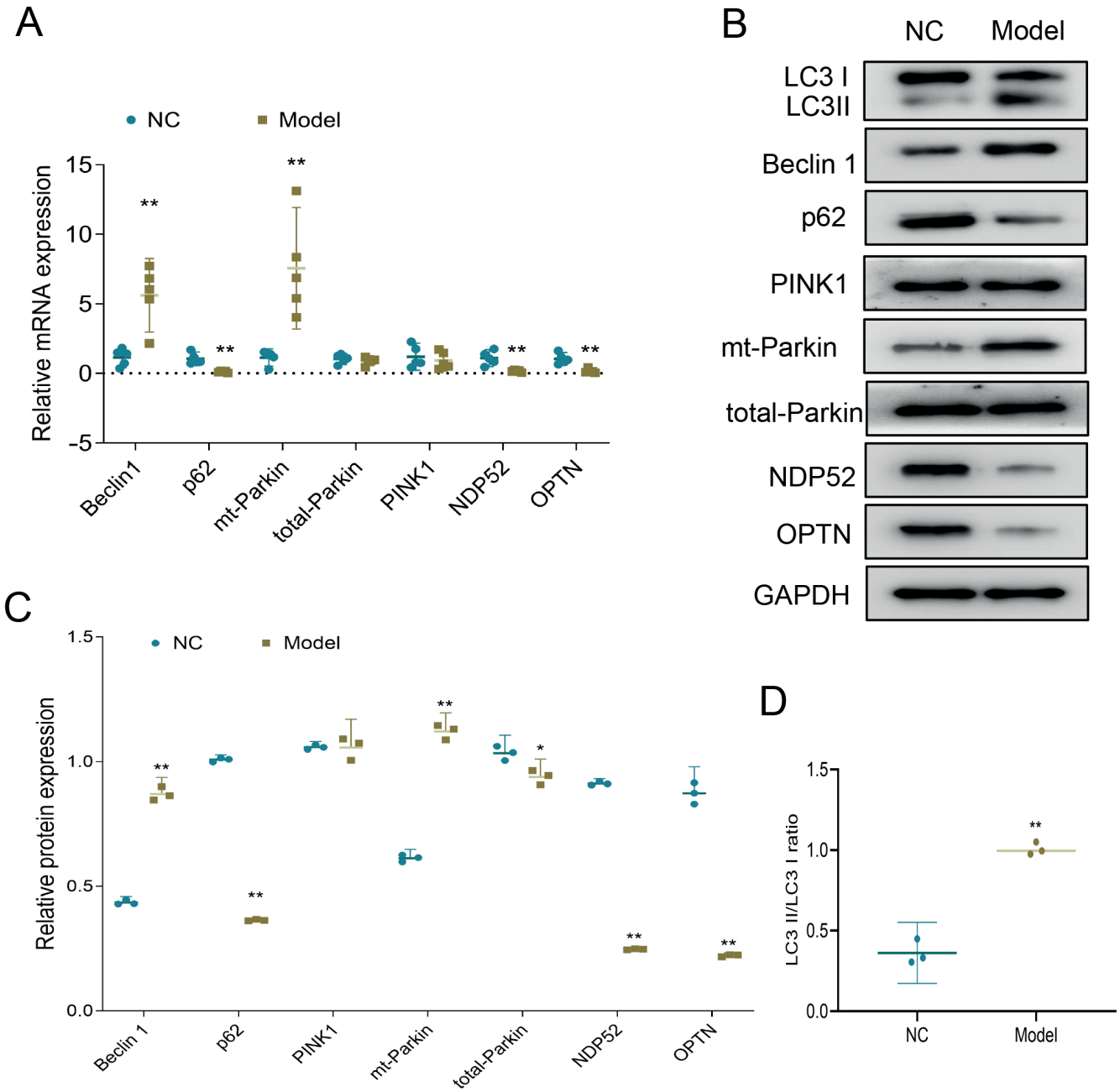

Fig. 3. N-nitro-L-arginine methyl ester (L-NAME) induction increases parkin-dependent mitophagy in chorionic trophoblast tissues of preeclampsia rats. Reverse transcription quantitative polymerase chain reaction (RT-qPCR) and western blot were employed to check the mRNA and protein expression levels of genes related to autophagy dependent on PINK1 and parkin in chorionic trophoblast tissues of rats in each group

**$p < 0.01$ and *$p < 0.05$ vs negative control (NC).

ratio also significantly increased. Notably, in the OE-parkin+3-MA group, mRNA and protein expression levels of LC3I, Beclin-1 and mt-parkin decreased compared to the OE-parkin group, while those of p62, NDP52 and OPTN increased; the LC3II/LC3I ratio also significantly decreased (Fig. 4A–E and Table 6–9). These findings suggest that 3-MA partially reversed the parkin overexpression-induced increase in mitophagy and apoptosis in trophoblast cells of preeclamptic rats.

Discussion

This study explored the role of parkin in preeclampsia by establishing an L-NAME-induced rat model of the condition. The results showed that rats treated with L-NAME exhibited typical symptoms of preeclampsia, including significantly elevated SBP and urine protein levels. Further experiments demonstrated that in the preeclampsia model, the levels of apoptosis and mitophagy in chorionic trophoblast cells were significantly increased, and these changes were closely associated with elevated parkin expression.

Table 4. Independent t-tests were conducted to compare mRNA expression levels of Beclin-1, P62, mt-parkin, total-parkin, PINK1, NDP52, and OPTN between the NC and model groups (Fig. 3A)

Gene	Group	Median	t	p-value	df
Beclin 1	NC	1.16 ±0.60	4.51	0.002	8
	model	5.62 ±2.12			
P62	NC	1.05 ±0.40	5.17	<0.001	8
	model	0.12 ±0.06			
mt-parkin	NC	1.15 ±0.50	4.04	0.004	8
	model	7.56 ±3.51			
total-parkin	NC	1.05 ±0.37	0.75	0.475	8
	model	0.17 ±0.15			
PINK1	NC	1.10 ±0.50	0.57	0.587	8
	model	0.17 ±0.07			
NDP52	NC	1.04 ±0.32	4.16	0.003	8
	model	0.90 ±0.28			
OPTN	NC	2.00 ±0.78	4.90	0.001	8
	model	0.95 ±0.62			

df – degrees of freedom; NC – negative control.

Table 5. Independent t-tests were performed to compare the protein expression levels of Beclin-1, P62, mt-parkin, total-parkin, PINK1, NDP52, OPTN, and the LC3-II/I ratio between the NC and model groups (Fig. 3B–D)

Gene	group	Median	t	p-value	df
Beclin 1	NC	0.44 ±0.01	26.02	<0.001	4
	model	0.87 ±0.03			
P62	NC	1.01 ±0.01	127.70	<0.001	4
	model	0.36 ±0.00			
mt-parkin	NC	1.06 ±0.01	26.60	<0.001	4
	model	1.06 ±0.05			
total-parkin	NC	0.87 ±0.04	4.05	0.016	4
	model	0.22 ±0.00			
PINK1	NC	0.91 ±0.01	0.05	0.962	4
	model	0.25 ±0.00			
NDP52	NC	0.61 ±0.01	145.60	<0.001	4
	model	1.12 ±0.03			
OPTN	NC	1.03 ±0.03	26.25	<0.001	4
	model	0.94 ±0.03			
LC3II/I	NC	0.36 ±0.08	13.07	<0.001	4
	model	1.01 ±0.04			

df – degrees of freedom; NC – negative control.

By overexpressing parkin, it was found that it could promote apoptosis and mitophagy in chorionic trophoblast cells, while the use of the mitophagy inhibitor 3-MA partially reversed these effects. These results indicate that parkin plays a promotive role in the pathological progression of preeclampsia, particularly in terms of mitophagy and apoptosis.

Preeclampsia poses a serious threat to both mother and fetus, yet its pathophysiology remains unclear, and no definitive treatment exists beyond early delivery. Therefore, addressing the current challenges in treating preeclampsia is of critical importance.[21] It is widely believed that insufficient invasion of trophoblast cells into the uterine wall and spiral arteries disrupts uteroplacental circulation, leading to progressive damage as pregnancy progresses.[21,22] Consequently, trophoblast cell damage is considered a key contributing factor in the development of preeclampsia. Many studies have focused on understanding the mechanisms of preeclampsia and exploring new treatment options, often using chorionic trophoblast tissues as a basis for investigation.[23,24] In the present study, a rat model of preeclampsia was established through continuous L-NAME injections.

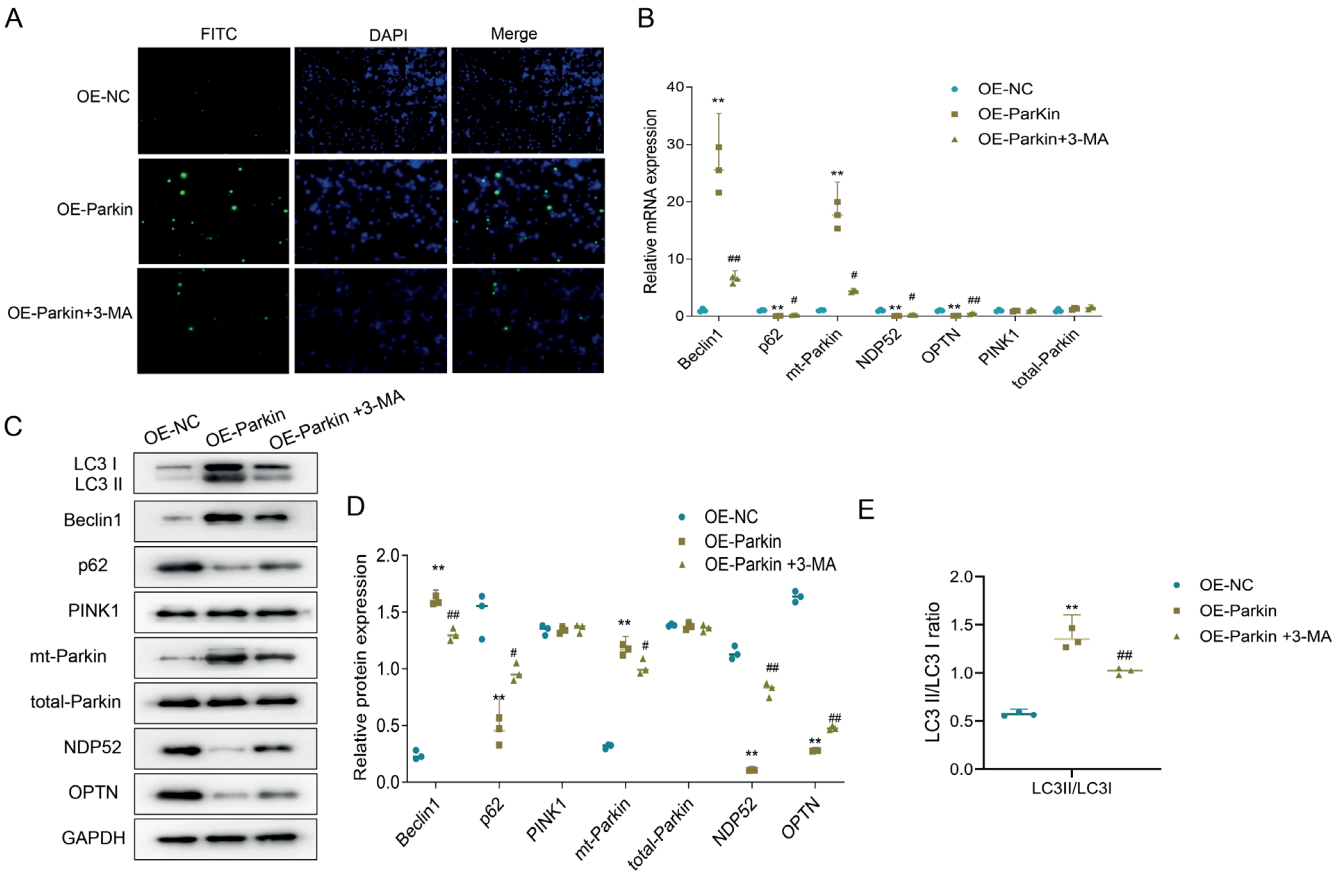

Fig. 4. 3-methyladenine (3-MA) partly reverses the upregulation of mitophagy and apoptosis of trophoblast cells in preeclampsia rats caused by parkin overexpression. A. TUNEL staining was performed to assess the level of apoptosis in trophoblast cells across experimental groups (green: TUNEL-positive signal; blue: DAPI (4′,6-diamidyno-2- fenyloindol) nuclear staining; scale bar = 200 μm); B–E. Reverse transcription quantitative polymerase chain reaction (RT-qPCR) and western blot to detect the mRNA and protein expression levels of mitophagy-related genes in each group of cells

**$p < 0.01$ vs OE-NC; $^{\#}p < 0.05$, $^{\#\#}p < 0.01$ vs OE-parkin; NC – negative control.

Table 6. One-way ANOVA was conducted to compare the immunofluorescence intensity of Beclin-1, P62, mt-parkin, total-parkin, PINK1, NDP52, and OPTN among the OE-NC, OE-parkin, and OE-parkin+3-MA groups (Fig. 4A,B)

Gene	Group	Median	F	p-value	df
Beclin 1	OE-NC	1.05 ±0.28	92.20	<0.001	(2, 6)
	OE-parkin	25.54 ±3.97			
	OE-parkin+3-MA	6.41 ±0.61			
P62	OE-NC	1.02 ±0.08	271.98	<0.001	(2, 6)
	OE-parkin	0.05 ±0.02			
	OE-parkin+3-MA	0.25 ±0.04			
mt-parkin	OE-NC	1.04 ±0.07	126.83	<0.001	(2, 6)
	OE-parkin	17.64 ±2.33			
	OE-parkin+3-MA	4.38 ±0.18			
total-parkin	OE-NC	1.01 ±0.25	3.12	0.118	(2, 6)
	OE-parkin	1.31 ±0.18			
	OE-parkin+3-MA	1.44 ±0.21			
PINK1	OE-NC	1.01 ±0.15	0.400	0.687	(2, 6)
	OE-parkin	0.93 ±0.06			
	OE-parkin+3-MA	1.02 ±0.14			
NDP52	OE-NC	1.03 ±0.14	107.52	<0.001	(2, 6)
	OE-parkin	0.07 ±0.02			
	OE-parkin+3-MA	0.28 ±0.05			
OPTN	OE-NC	1.00 ±0.10	106.87	<0.001	(2, 6)
	OE-parkin	0.09 ±0.01			
	OE-parkin+3-MA	0.44 ±0.09			

df – degrees of freedom; NC – negative control; ANOVA – analysis of variance.

Table 7. Tukey's post hoc test was performed following one-way ANOVA to compare expression levels of Beclin-1, P62, mt-parkin, total-parkin, PINK1, NDP52, and OPTN among the OE-NC, OE-parkin and OE-parkin+3-MA groups (Fig. 4A,B)

Gene	Group	q	p-value
Beclin 1	OE-NC vs OE-parkin	18.26	<0.001
	OE-NC vs OE-parkin+3-MA	4.00	0.068
	OE-parkin vs OE-parkin+3-MA	14.27	<0.001
P62	OE-NC vs OE-parkin	31.28	<0.001
	OE-NC vs OE-parkin+3-MA	24.71	<0.001
	OE-parkin vs OE-parkin+3-MA	6.57	0.008
mt-parkin	OE-NC vs OE-parkin	21.29	<0.001
	OE-NC vs OE-parkin+3-MA	4.28	0.053
	OE-parkin vs OE-parkin+3-MA	17.01	<0.001
total-parkin	OE-NC vs OE-parkin	2.37	0.289
	OE-NC vs OE-parkin+3-MA	3.46	0.110
	OE-parkin vs OE-parkin+3-MA	1.09	0.733
PINK1	OE-NC vs OE-parkin	1.00	0.769
	OE-NC vs OE-parkin+3-MA	0.17	0.992
	OE-parkin vs OE-parkin+3-MA	1.17	0.700
NDP52	OE-NC vs OE-parkin	19.77	<0.001
	OE-NC vs OE-parkin+3-MA	15.30	<0.001
	OE-parkin vs OE-parkin+3-MA	4.47	0.045
OPTN	OE-NC vs OE-parkin	20.48	<0.001
	OE-NC vs OE-parkin+3-MA	12.69	<0.001
	OE-parkin vs OE-parkin+3-MA	8.00	0.004

df – degrees of freedom; NC – negative control; q – Tukey's q statistic; ANOVA – analysis of variance.

Table 8. One-way ANOVA was used to evaluate differences in protein expression levels of Beclin-1, P62, mt-parkin, total-parkin, PINK1, NDP52, and OPTN among the OE-NC, OE-parkin and OE-parkin+3-MA groups (Fig. 4C–E)

Group	Group	Median	F	p-value	df
Beclin 1	OE-NC	0.24 ±0.04	779.40	<0.001	(2, 6)
	OE-parkin	1.60 ±0.04			
	OE-parkin+3-MA	1.30 ±0.05			
P62	OE-NC	1.49 ±0.20	39.59	<0.001	(2, 6)
	OE-parkin	0.46 ±0.12			
	OE-parkin+3-MA	0.97 ±0.08			
mt-parkin	OE-NC	0.32 ±0.02	260.21	<0.001	(2, 6)
	OE-parkin	1.17 ±0.05			
	OE-parkin+3-MA	1.01 ±0.07			
total-parkin	OE-NC	1.38 ±0.01	0.93	0.445	(2, 6)
	OE-parkin	1.37 ±0.03			
	OE-parkin+3-MA	1.36 ±0.03			
PINK1	OE-NC	1.34 ±0.04	0.23	0.802	(2, 6)
	OE-parkin	1.34 ±0.02			
	OE-parkin+3-MA	1.36 ±0.04			
NDP52	OE-NC	1.14 ±0.06	336.17	<0.001	(2, 6)
	OE-parkin	0.11 ±0.00			
	OE-parkin+3-MA	0.82 ±0.06			
OPTN	OE-NC	1.64 ±0.05	1888.33	<0.001	(2, 6)
	OE-parkin	0.28 ±0.00			
	OE-parkin+3-MA	0.48 ±0.02			
LC3II/I	OE-NC	0.57 ±0.02	113.72	<0.001	(2, 6)
	OE-parkin	1.35 ±0.10			
	OE-parkin+3-MA	1.02 ±0.04			

df – degrees of freedom; NC – negative control; ANOVA – analysis of variance.

Table 9. Tukey's post hoc test was performed following one-way ANOVA to compare the expression levels of Beclin-1, P62, mt-parkin, total-parkin, PINK1, NDP52, OPTN, and the LC3-II/I ratio among the OE-NC, OE-parkin and OE-parkin+3-MA groups (Fig. 4C–E)

Gene	Group	q	p-value
Beclin 1	OE-NC vs OE-parkin	53.12	<0.001
	OE-NC vs OE-parkin+3-MA	41.46	<0.001
	OE-parkin vs OE-parkin+3-MA	11.66	<0.001
P62	OE-NC vs OE-parkin	12.58	<0.001
	OE-NC vs OE-parkin+3-MA	6.33	0.010
	OE-parkin vs OE-parkin+3-MA	6.26	0.011
mt-parkin	OE-NC vs OE-parkin	30.29	<0.001
	OE-NC vs OE-parkin+3-MA	24.76	<0.001
	OE-parkin vs OE-parkin+3-MA	5.53	0.018
total-parkin	OE-NC vs OE-parkin	0.94	0.791
	OE-NC vs OE-parkin+3-MA	1.93	0.416
	OE-parkin vs OE-parkin+3-MA	0.99	0.774
PINK1	OE-NC vs OE-parkin	0.29	0.977
	OE-NC vs OE-parkin+3-MA	0.64	0.996
	OE-parkin vs OE-parkin+3-MA	0.94	0.793
NDP52	OE-NC vs OE-parkin	35.83	<0.001
	OE-NC vs OE-parkin+3-MA	11.14	0.001
	OE-parkin vs OE-parkin+3-MA	24.69	<0.001
OPTN	OE-NC vs OE-parkin	80.52	<0.001
	OE-NC vs OE-parkin+3-MA	68.59	<0.001
	OE-parkin vs OE-parkin+3-MA	11.93	<0.001
LC3II/I	OE-NC vs OE-parkin	21.25	<0.001
	OE-NC vs OE-parkin+3-MA	12.17	<0.001
	OE-parkin vs OE-parkin+3-MA	9.09	0.002

df – degrees of freedom; NC – negative control; q – Tukey's q statistic; ANOVA – analysis of variance.

Notably, preeclampsia is characterized by the onset of hypertension and proteinuria in the 2nd half of pregnancy.[7] Consistent with this, our findings showed a significant increase in SBP and urine protein levels in the model group on the 20th day of pregnancy. Furthermore, research indicates that imbalances in apoptosis and proliferation of chorionic trophoblast cells contribute to trophoblast dysfunction and the development of preeclampsia.[25,26] In this study, we observed a marked increase in apoptosis in chorionic trophoblast cells within the model group, confirming the successful construction of an animal model with typical symptoms of preeclampsia. These results further suggest that elevated apoptosis levels in chorionic trophoblast cells may be a key factor in the pathogenesis of preeclampsia.

Mitophagy, an organelle-specific autophagy pathway, plays a crucial role in mitochondrial quality control and in maintaining cellular structure and function.[27] However, excessive mitochondrial damage can also trigger programmed cell death (apoptosis).[28] Previous study have highlighted that mitochondria function in the placental tissue of preeclampsia is severely compromised, including a decrease in ATP production and mitochondrial DNA copy number.[29] Zhou et al. observed an accumulation of mitochondria with impaired mitophagy in preeclamptic placental tissue using a scanning electron microscope.[30] Similarly, Vangrieken et al. discovered a significant increase in the number of mitochondria with impaired mitophagy and notably upregulated mitophagy-related protein expression in preeclamptic placental tissue.[31] These findings collectively suggest that mitophagy plays an important role in the pathogenesis of preeclampsia. In this research, we observed a significant increase in Beclin-1 expression levels, accompanied by a significant decrease in the proteins p62, NDP52 and OPTN in the chorionic trophoblast tissues of rats in the model group. Beclin-1 is widely recognized as a marker protein for measuring autophagy, and the relative binding between Beclin-1 and bcl-2 in cells is indicative of the autophagy level. Generally, a significant increase in Beclin-1 expression reflects an elevated level of cellular autophagy.[32] Additionally, p62 functions as a receptor for autophagic vesicles and ubiquitinated protein aggregates; therefore, reduced p62 expression is indicative of increased autophagic activity.[33] Similarly, NDP52 and OPTN act as receptors that recognize and target vesicles for autophagic degradation.[34,35] These findings suggest that mitophagy levels are significantly

elevated in preeclamptic rats. More importantly, after overexpressing parkin in trophoblast cells from preeclampsia placental tissues, we observed a significant upregulation of both apoptosis and mitophagy levels in this study. This suggests that parkin-dependent autophagy is significantly increased in the chorionic trophoblast of preeclampsia rats. Interestingly, mitophagy does not strictly follow a linear model in which damage sensors and parkin function solely as downstream effectors. The recruitment of autophagy receptor protein mediated by phosphorylated ubiquitin requires PINK1 activity but does not rely solely on parkin.[36] However, previous studies have demonstrated that parkin-mediated ubiquitination of intracellular proteins is also a key signal promoting apoptosis.[37] Consequently, parkin may affect mitophagy and apoptosis in trophoblast cells of preeclamptic rats through multiple pathways.

According to previous studies, 3-MA is a highly effective mitophagy inhibitor.[38] Some studies have also shown that 3-MA can effectively inhibit cell apoptosis.[38] For instance, the study by Seno et al. suggested that 3-MA could effectively inhibit the senescence and autophagy of trophoblast cells.[39] In our study, we similarly found that the levels of apoptosis and autophagy were significantly reduced after parkin overexpression and the incubation of preeclampsia trophoblast cells with 3-MA. However, Dai et al. observed that when trophoblast cells were incubated with 3-MA, the apoptosis level increased significantly when exposed to zearalenone.[40] These differing results may be attributed to the varying states of the cells under different conditions. Additionally, after overexpression of parkin, 3-MA significantly reduced the expression level of mt-parkin, thereby impacting mitophagy and apoptosis in preeclampsia trophoblast cells. Overall, elevated levels of parkin are a key factor in promoting the functional impairment of trophoblast cells in preeclampsia. Thus, inhibiting the parkin pathway may be a promising therapeutic approach for preeclampsia. However, the efficacy of treating preeclampsia by inhibiting parkin requires further validation through in vivo experiments. Although this study primarily focuses on the roles of mitophagy and apoptosis in preeclampsia, it is important to acknowledge that existing research has demonstrated that inflammatory processes play a significant role in the pathophysiology of both preeclampsia and intrauterine growth restriction. Future research could explore the interactions between inflammation, mitophagy and apoptosis to gain a more comprehensive understanding of the mechanisms underlying preeclampsia.[41,42] Furthermore, while this study underscores the critical role of parkin in preeclampsia, these findings require validation in clinical settings. Prioritizing clinical trials to evaluate the potential of parkin inhibitors in the prevention and treatment of preeclampsia is crucial. Additionally, bioinformatics analyses could be employed to further elucidate the specific mechanisms of parkin inhibitors, thereby enhancing our understanding of this therapeutic strategy.

Limitations

This study has several limitations. First, although the rat model of preeclampsia induced by L-NAME closely mimics key clinical features of the disease, it may not fully replicate the complex pathophysiological processes occurring in human pregnancies. Second, the experimental findings were derived primarily from animal tissues and isolated trophoblast cells, without validation in human placental samples or clinical patient cohorts, which limits the translational relevance. Third, the mechanistic exploration was focused mainly on the PINK1/parkin pathway and its influence on mitophagy and apoptosis; other potentially interacting pathways, such as inflammation or oxidative stress, were not evaluated. Fourth, the mitophagy inhibitor 3-MA used in this study may have off-target effects, and more specific tools (e.g., genetic knockdown or clustered regularly interspaced short palindromic repeats (CRISPR)-based editing) are needed to confirm the observed roles of parkin. Finally, the sample size for molecular experiments was relatively small, and the lack of long-term in vivo observations restricts our ability to assess the chronic impact of parkin modulation on pregnancy outcomes.

Conclusion

The overexpression of parkin can aggravate the symptoms of preeclampsia by promoting mitophagy and apoptosis in trophoblast cells in preeclampsia. This study has laid a foundation for clarifying the function of parkin in preeclampsia and suggests that parkin may be an important marker in the treatment of preeclampsia.

Data availability

The datasets generated and/or analyzed during the current study are available from the corresponding author on reasonable request.

Consent for publication

Not applicable.

Use of AI and AI-assisted technologies

Not applicable.

ORCID iDs

Li Wang https://orcid.org/0000-0003-2934-4061
Xue Wang https://orcid.org/0009-0007-1478-0019
Ying Zheng https://orcid.org/0009-0009-1389-2961
Jiao Kong https://orcid.org/0000-0003-1464-7780
Lin-Mei Zheng https://orcid.org/0000-0001-7930-5795
Ai-Hua He https://orcid.org/0009-0004-5060-5937
Xiao-Ju Chen http://orcid.org/0000-0002-7919-0016

References

1. American College of Obstetricians and Gynecologists (ACOG). ACOG Practice Bulletin No. 202: Gestational hypertension and preeclampsia. *Obstet Gynecol*. 2019;133(1):1. doi:10.1097/AOG.0000000000003018
2. Firoz T, Sanghvi H, Merialdi M, Von Dadelszen P. Pre-eclampsia in low and middle income countries. *Best Pract Res Clin Obstet Gynaecol*. 2011;25(4):537–548. doi:10.1016/j.bpobgyn.2011.04.002
3. Ives CW, Sinkey R, Rajapreyar I, Tita ATN, Oparil S. Preeclampsia: Pathophysiology and clinical presentations. *J Am Coll Cardiol*. 2020;76(14):1690–1702. doi:10.1016/j.jacc.2020.08.014
4. Bokslag A, Van Weissenbruch M, Mol BW, De Groot CJM. Preeclampsia: Short and long-term consequences for mother and neonate. *Early Hum Dev*. 2016;102:47–50. doi:10.1016/j.earlhumdev.2016.09.007
5. Zhang H, He Y, Wang JX, et al. miR-30-5p-mediated ferroptosis of trophoblasts is implicated in the pathogenesis of preeclampsia. *Redox Biol*. 2020;29:101402. doi:10.1016/j.redox.2019.101402
6. Man R, Hodgetts Morton V, Devani P, Morris RK. Aspirin for preventing adverse outcomes in low risk nulliparous women with singleton pregnancies: A systematic review and meta-analysis. *Eur J Obstet Gynecol Reprod Biol*. 2021;262:105–112. doi:10.1016/j.ejogrb.2021.05.017
7. Burton GJ, Redman CW, Roberts JM, Moffett A. Pre-eclampsia: Pathophysiology and clinical implications. *BMJ*. 2019;366:l2381. doi:10.1136/bmj.l2381
8. Hu XQ, Zhang L. Hypoxia and mitochondrial dysfunction in pregnancy complications. *Antioxidants (Basel)*. 2021;10(3):405. doi:10.3390/antiox10030405
9. Balaban RS. Regulation of oxidative phosphorylation in the mammalian cell. *Am J Physiol Cell Physiol*. 1990;258(3):C377–C389. doi:10.1152/ajpcell.1990.258.3.C377
10. Peng X, Hou R, Yang Y, Luo Z, Cao Y. Current studies of mitochondrial quality control in the preeclampsia. *Front Cardiovasc Med*. 2022;9:836111. doi:10.3389/fcvm.2022.836111
11. Rodger CE, McWilliams TG, Ganley IG. Mammalian mitophagy: From in vitro molecules to in vivo models. *FEBS J*. 2018;285(7):1185–1202. doi:10.1111/febs.14336
12. Palikaras K, Lionaki E, Tavernarakis N. Mechanisms of mitophagy in cellular homeostasis, physiology and pathology. *Nat Cell Biol*. 2018;20(9):1013–1022. doi:10.1038/s41556-018-0176-2
13. Park J, Lee SB, Lee S, et al. Mitochondrial dysfunction in *Drosophila* PINK1 mutants is complemented by parkin. *Nature*. 2006;441(7097):1157–1161. doi:10.1038/nature04788
14. Ordureau A, Sarraf SA, Duda DM, et al. Quantitative proteomics reveal a feedforward mechanism for mitochondrial PARKIN translocation and ubiquitin chain synthesis. *Mol Cell*. 2014;56(3):360–375. doi:10.1016/j.molcel.2014.09.007
15. Geisler S, Holmström KM, Skujat D, et al. PINK1/parkin-mediated mitophagy is dependent on VDAC1 and p62/SQSTM1. *Nat Cell Biol*. 2010;12(2):119–131. doi:10.1038/ncb2012
16. Willett JA, Cao J, Johnson A, Patel OH, Dorris DM, Meitzen J. The estrous cycle modulates rat caudate–putamen medium spiny neuron physiology. *Eur J Neurosci*. 2020;52(1):2737–2755. doi:10.1111/ejn.14506
17. Zheng L, Tang R, Shi L, Zhong M, Zhou Z. Vagus nerve stimulation ameliorates L-NAME-induced preeclampsia-like symptoms in rats through inhibition of the inflammatory response. *BMC Pregnancy Childbirth*. 2021;21(1):177. doi:10.1186/s12884-021-03650-7
18. Duan L, Liu Z, Wang L, et al. C1q and tumor necrosis factor related protein 4 (CTRP4) suppresses caspase-1/IL-1β inflammatory pathway in trophoblasts of rat models with preeclampsia [in Chinese]. *Xi Bao Yu Fen Zi Mian Yi Xue Za Zhi*. 2016;32(11):1441–1445. PMID:27774931.
19. Kalkat M, Garcia J, Ebrahimi J, et al. Placental autophagy regulation by the BOK-MCL1 rheostat. *Autophagy*. 2013;9(12):2140–2153. doi:10.4161/auto.26452
20. Scarffe LA, Stevens DA, Dawson VL, Dawson TM. Parkin and PINK1: Much more than mitophagy. *Trends Neurosci*. 2014;37(6):315–324. doi:10.1016/j.tins.2014.03.004
21. Ma'ayeh M, Costantine MM. Prevention of preeclampsia. *Semin Fetal Neonatal Med*. 2020;25(5):101123. doi:10.1016/j.siny.2020.101123
22. Robson A, Harris LK, Innes BA, et al. Uterine natural killer cells initiate spiral artery remodeling in human pregnancy. *FASEB J*. 2012;26(12):4876–4885. doi:10.1096/fj.12-210310
23. Knöfler M, Haider S, Saleh L, Pollheimer J, Gamage TKJB, James J. Human placenta and trophoblast development: Key molecular mechanisms and model systems. *Cell Mol Life Sci*. 2019;76(18):3479–3496. doi:10.1007/s00018-019-03104-6
24. Zhang Q, Wang Z, Cheng X, Wu H. lncRNA DANCR promotes the migration an invasion and of trophoblast cells through microRNA-214-5p in preeclampsia. *Bioengineered*. 2021;12(2):9424–9434. doi:10.1080/21655979.2021.1988373
25. Huang Y, Du Y, Zhang X, et al. Down-regulated expression of annexin A7 induces apoptosis in mouse hepatocarcinoma cell line by the intrinsic mitochondrial pathway. *Biomed Pharmacother*. 2015;70:146–150. doi:10.1016/j.biopha.2015.01.009
26. Bailey LJ, Alahari S, Tagliaferro A, Post M, Caniggia I. Augmented trophoblast cell death in preeclampsia can proceed via ceramide-mediated necroptosis. *Cell Death Dis*. 2017;8(2):e2590. doi:10.1038/cddis.2016.483
27. Spinelli JB, Haigis MC. The multifaceted contributions of mitochondria to cellular metabolism. *Nat Cell Biol*. 2018;20(7):745–754. doi:10.1038/s41556-018-0124-1
28. Kerr JFR, Wyllie AH, Currie AR. Apoptosis: A basic biological phenomenon with wide-ranging implications in tissue kinetics. *Br J Cancer*. 1972;26(4):239–257. doi:10.1038/bjc.1972.33
29. Ausman J, Abbade J, Ermini L, et al. Ceramide-induced BOK promotes mitochondrial fission in preeclampsia. *Cell Death Dis*. 2018;9(3):298. doi:10.1038/s41419-018-0360-0
30. Zhou X, Zhao X, Zhou W, et al. Impaired placental mitophagy and oxidative stress are associated with dysregulated BNIP3 in preeclampsia. *Sci Rep*. 2021;11(1):20469. doi:10.1038/s41598-021-99837-1
31. Vangrieken P, Al-Nasiry S, Bast A, et al. Placental mitochondrial abnormalities in preeclampsia. *Reprod Sci*. 2021;28(8):2186–2199. doi:10.1007/s43032-021-00464-y
32. Salminen A, Kaarniranta K, Kauppinen A, et al. Impaired autophagy and APP processing in Alzheimer's disease: The potential role of Beclin 1 interactome. *Prog Neurobiol*. 2013;106–107:33–54. doi:10.1016/j.pneurobio.2013.06.002
33. Gureev AP, Sadovnikova IS, Starkov NN, Starkov AA, Popov VN. p62-Nrf2-p62 mitophagy regulatory loop as a target for preventive therapy of neurodegenerative diseases. *Brain Sci*. 2020;10(11):847. doi:10.3390/brainsci10110847
34. Belousov DM, Mikhaylenko EV, Somasundaram SG, Kirkland CE, Aliev G. The dawn of mitophagy: What do we know by now? *Curr Neuropharmacol*. 2020;19(2):170–192. doi:10.2174/1570159X18666200522202319
35. Yamano K, Youle RJ. Two different axes CALCOCO2-RB1CC1 and OPTN-ATG9A initiate PRKN-mediated mitophagy. *Autophagy*. 2020;16(11):2105–2107. doi:10.1080/15548627.2020.1815457
36. Lazarou M, Sliter DA, Kane LA, et al. The ubiquitin kinase PINK1 recruits autophagy receptors to induce mitophagy. *Nature*. 2015;524(7565):309–314. doi:10.1038/nature14893
37. Ham SJ, Lee D, Yoo H, Jun K, Shin H, Chung J. Decision between mitophagy and apoptosis by parkin via VDAC1 ubiquitination. *Proc Natl Acad Sci U S A*. 2020;117(8):4281–4291. doi:10.1073/pnas.1909814117
38. Kim I, Lemasters JJ. Mitochondrial degradation by autophagy (mitophagy) in GFP-LC3 transgenic hepatocytes during nutrient deprivation. *Am J Physiol Cell Physiol*. 2011;300(2):C308–C317. doi:10.1152/ajpcell.00056.2010
39. Seno K, Tanikawa N, Takahashi H, et al. Oxygen concentration modulates cellular senescence and autophagy in human trophoblast cells. *Am J Reprod Immunol*. 2018;79(6):e12826. doi:10.1111/aji.12826
40. Bai J, Li J, Liu N, et al. Zearalenone induces apoptosis and autophagy by regulating endoplasmic reticulum stress signalling in porcine trophectoderm cells. *Anim Nutr*. 2023;12:186–199. doi:10.1016/j.aninu.2022.08.016
41. Pala Ş, Atılgan R, Ilhan N. High amniotic fluid fractalkine and MIP-1β levels are associated with intrauterine growth restriction: A prospective cohort study. *Turk J Med Sci*. 2024;54(1):280–290. doi:10.55730/1300-0144.5789
42. Açikgözoğlu MK, Pala Ş, Atılgan R, Ilhan N, Ilhan N. High serum angiopoietin-like protein-4 levels are associated with gestational hypertension and preeclampsia: A case-control study. *Turk J Biochem*. 2024;49(3):344–348. doi:10.1515/tjb-2023-0087

Association between proinflammatory cytokines and pain intensity in patients with postherpetic neuralgia

Jun Miao[1,A,D–F], Lu Wang[1,C,D], Min Feng[2,B,C]

[1] Department of Dermatology, Huabei Petroleum Administration Bureau General Hospital, Renqiu, China
[2] Department of Physical Examination Center, Huabei Petroleum Administration Bureau General Hospital, Renqiu, China

A – research concept and design; B – collection and/or assembly of data; C – data analysis and interpretation;
D – writing the article; E – critical revision of the article; F – final approval of the article

Advances in Clinical and Experimental Medicine, ISSN 1899–5276 (print), ISSN 2451–2680 (online) *Adv Clin Exp Med*. 2025;34(11):1921–1928

Address for correspondence
Jun Miao
E-mail: 123950746@qq.com

Funding sources
None declared

Conflict of interest
None declared

Received on September 1, 2024
Reviewed on November 12, 2024
Accepted on January 18, 2025

Published online on July 23, 2025

Abstract

Background. Inflammatory response is involved in the pathogenesis of herpes zoster (HZ) and postherpetic neuralgia (PHN).

Objectives. This study aimed to evaluate levels of proinflammatory factors at different stages of HZ and PHN.

Materials and methods. A total of 154 patients within 72 h of HZ onset and 30 healthy controls were included. Patients were followed up to 90 days. The levels of interleukin 6 (IL-6), tumor necrosis factor alpha (TNF-α) and C-reactive protein (CRP) were measured at baseline and 90 days. The visual analogue scale (VAS) was used to assess the intensity of pain and PHN patients were divided into mild-to-moderate pain and severe pain group.

Results. Interleukin 6, TNF-α and CRP levels in HZ patients at baseline were significantly higher than in healthy controls and decreased as followed up to 90 days. Moreover, PHN patients had a higher level of IL-6, TNF-α or CRP at baseline and 90 days than non-PHN patients. In addition, PHN patients in the severe pain group had a notably higher baseline or 90-day IL-6, TNF-α and CRP level than in the mild-to-moderate pain group. However, the changes of IL-6, TNF-α and CRP levels between 90 days and baseline were significantly less pronounced in the severe pain group than in the mild-to-moderate pain group.

Conclusions. The levels of proinflammatory cytokines were higher in HZ and PHN patients and associated with pain intensity in PNH patients. These findings suggest that repeated measurements of serum proinflammatory cytokines may aid in clinical management and guide anti-inflammatory treatment strategies.

Key words: proinflammatory cytokines, interleukin 6, postherpetic neuralgia, tumor necrosis factor alpha, herpes zoster

Cite as
Miao J, Wang L, Feng M. Association between proinflammatory cytokines and pain intensity in patients with postherpetic neuralgia. *Adv Clin Exp Med*. 2025;34(11):1921–1928. doi:10.17219/acem/200267

DOI
10.17219/acem/200267

Highlights

- Proinflammatory cytokine surge in acute herpes zoster: Cytokine levels peak within 72 h post-rash onset and steadily decline over a 90-day follow-up.
- Higher cytokine burden predicts postherpetic neuralgia (PHN): Patients who develop PHN exhibit significantly elevated proinflammatory cytokines compared to non-PHN cases.
- Cytokine intensity mirrors PHN pain severity: Individuals with severe PHN pain have greater cytokine elevations than those reporting mild-to-moderate pain.
- Blunted cytokine decline in severe PHN: The reduction of proinflammatory cytokines over time is markedly lower in severe-pain patients compared to those with milder symptoms.

Background

Herpes zoster (HZ), caused by varicella-zoster virus, is known as a common skin infectious disease and remains latent in the ganglia after the primary infection. Postherpetic neuralgia (PHN), a significant neuropathic complication of HZ, is clinically defined as persistent neuropathic pain lasting beyond 3 months.[1] Recent studies indicated that the effectiveness of the live zoster vaccine wanes after 10 years in preventing HZ and PHN.[2] Therefore, emerging evidence underscores the necessity of developing multimodal therapeutic interventions targeting both HZ and PHN. Previous studies suggest that combination or interventional therapies may benefit patients with intractable conditions.[3–5] Yet, the incidence of HZ and its sequela, PHN, has continued to rise,[6] with the risk of PHN increasing sharply with age.[7] Therefore, elucidating the underlying pain mechanisms is essential for developing novel treatment options.

Multiple immune cells (mast cells, neutrophils, macrophages, and T lymphocytes) and their secreted mediators contribute to the pathophysiology of neuropathic pain.[8,9] Since proinflammatory cytokines are central to these inflammatory pathways, a broader panel of pertinent biomarkers should be assessed in patients with HZ and PHN.

Proinflammatory cytokines, such as interleukin 6 (IL-6), tumor necrosis factor alpha (TNF-α) and C-reactive protein (CRP), have a trending relationship with pain condition.[10,11] Previous studies also indicated that IL-6 levels were related to the severity of PHN.[12] Compared to non-PHN patients, CRP level increased in PHN patients.[13] Furthermore, recent studies indicated that TNF-α produced by varicella-zoster virus-specific T cells was higher in PHN patients.[14]

Objectives

This study aimed to evaluate the levels of IL-6, TNF-α and CRP at different stages of HZ and PNH.

Materials and methods

Study subjects

The study was approved by the Biomedical Ethics Committee of Huabei Petroleum Administration Bureau General Hospital (approval No. EC-2023-hbyyecky-01) and conducted in accordance with the Declaration of Helsinki. All enrolled patients provided written informed consent. Inclusion criteria for patients with HZ were: 1) fulfilment of the diagnostic criteria for HZ; 2) no speech or cognitive impairment; and 3) capacity to understand and use the visual analogue scale (VAS).

Exclusion criteria were: 1) age <18 or >80 years; 2) concomitant autoimmune disease, including ankylosing spondylitis; 3) active malignancy, bacterial or viral infection other than HZ, or related disorders; 4) recent use of immunosuppressants; 5) severe systemic comorbidities involving the nervous, cardiac, pulmonary, hepatic, or renal systems; and 6) pregnancy or lactation.

Patients with HZ and PHN were administered appropriate comprehensive treatment, including oral valaciclovir, gabapentin and mecobalamin. All patients were followed up for 90 days. Trained clinical professionals conducted face-to-face follow-up visits with the patients. The VAS questionnaire was used to evaluate the pain intensity, ranging from 0 to 10. The VAS pain scale was used as in earlier studies: 0 = no pain; 1–3 = mild, tolerable pain; 4–6 = moderate pain that disrupts sleep; and 7–10 = severe, intolerable pain that interferes with both sleep and appetite.[15,16]

Patients with PHN were stratified by VAS score: a VAS ≤6 defined mild-to-moderate pain (n = 68), whereas a VAS >6 indicated severe pain (n = 25).

Data collection

Baseline demographic and clinical data were recorded within 24 h of admission, including histories of hypertension, diabetes mellitus and dyslipidemia. Serum biomarkers (IL-6, TNF-α and CRP) were also measured.

Hypertension was defined as a systolic blood pressure ≥140 mm Hg, a diastolic blood pressure ≥90 mm Hg

or current use of antihypertensive medication. Diabetes mellitus was diagnosed by a fasting plasma glucose ≥7.0 mmol/L, an HbA1c ≥6.5 %, a 2-h plasma glucose ≥11.1 mmol/L during an oral glucose-tolerance test, or current antidiabetic therapy. Dyslipidemia was defined as a fasting total cholesterol ≥5.2 mmol/L, low-density lipoprotein (LDL) cholesterol ≥3.4 mmol/L, high-density lipoprotein (HDL) cholesterol <1.0 mmol/L, triglycerides ≥1.7 mmol/L, or current use of lipid-lowering agents.

Biochemical measurements

Serum samples from HZ patients and healthy controls were collected at enrollment and again 90 days later, aliquoted into cryotubes, and stored at −80°C without any freeze–thaw cycles. Concentrations of IL-6, TNF-α and CRP were quantified with commercial enzyme-linked immunosorbent assay (ELISA) kits (RapidBio, Arizona, USA) by laboratory staff blinded to the clinical data. Each assay was run in triplicate according to the manufacturer's instructions.

Study size

Between January 2020 and December 2022, 154 patients seen within 72 h of HZ onset and 30 healthy controls were enrolled.

Statistical analyses

Demographic and clinical characteristics of participants were described as frequencies (percentages) and median with interquartile range (IQR; Q1–Q3). The variables included gender, age, a history of hypertension, diabetes mellitus, and dyslipidemia. Significant differences between the 2 groups were tested with the χ^2 or Fisher's exact test for categorical variables and the Mann–Whitney U test for continuous variables. Paired cytokine concentrations in HZ patients (baseline vs day 90) were compared using the Wilcoxon signed-rank test. Baseline HZ patients vs healthy controls, and day-90 HZ patients vs healthy controls, were analyzed with the Mann–Whitney U test, applying a Bonferroni correction (adjusted $\alpha = 0.025$). All analyses were performed with IBM SPSS Statistics v. 26.0 (IBM Corp., Armonk, USA). Two-sided p-values <0.05 were considered statistically significant.

Results

Patient characteristics

From 2020 to 2022, 154 patients and 30 healthy volunteers were enrolled. The HZ and control groups did not differ in age or sex. The patients' median age was 67 years, and 52 (33.8 %) were women. Baseline median serum concentrations of IL-6, TNF-α and CRP were 6.23 pg/mL (IQR: 4.63–9.55), 8.43 pg/mL (IQR: 7.34–9.95) and 12.98 mg/dL (IQR: 11.89–14.69), respectively.

Evaluation of proinflammatory cytokines in HZ patients and healthy controls

To investigate the differences of proinflammatory cytokines between HZ patients and healthy controls, we measured the IL-6, TNF-α and CRP levels. We found that proinflammatory cytokines were significantly higher in HZ patients than in healthy controls (all $p < 0.001$) (Table 1). Subsequently, to further assess the differences in proinflammatory cytokine levels across different stages of HZ, we measured serum IL-6, TNF-α and CRP levels in HZ patients at 90 days. We found that the 90-day levels of these proinflammatory cytokines had significantly decreased compared to baseline (all $p < 0.001$; Table 1). However, IL-6 and CRP levels at 90 days remained significantly higher than those observed in healthy controls (both $p < 0.001$).

Evaluation of proinflammatory cytokines with PHN patients

The demographic and clinical characteristics of PHN and non-PHN patients are presented in Table 2. Among the 154 patients, 93 (60.4%) had PHN, while 61 (39.6%) did not. The PHN patients were generally older, with a higher proportion of males, and showed a higher prevalence

Table 1. Comparison of proinflammatory cytokine levels between HZ patients and healthy controls

Cytokines	Control (n = 30)	HZ at baseline (n = 154)	HZ at 90 days (n = 154)	Z*	p-value*	Z#	p-value#	Z$	p-value$
IL-6 [pg/mL]	4.13 (3.08–4.51)	6.23 (4.62–9.56)	5.24 (4.21–8.39)	−5.86	<0.001	−4.34	<0.001	−9.42	<0.001
TNF-α [pg/mL]	7.30 (5.94–8.02)	8.43 (7.34–9.95)	7.54 (6.04–9.07)	−4.27	<0.001	−1.62	0.106	−8.32	<0.001
CRP [mg/dL]	9.04 (8.53–10.22)	12.98 (11.89–14.69)	11.87 (10.48–13.92)	8.35	<0.001	−6.90	<0.001	−8.29	<0.001

Continuous variables are presented as median and interquartile range (Q1–Q3). *Mann–Whitney test with the Bonferroni correction method was used to compare the levels of cytokines between HZ patients at baseline and healthy controls. #Mann–Whitney test with the Bonferroni correction method was used to compare the levels of cytokines between HZ patients at 90 days and healthy controls. $Wilcoxon signed-rank test for paired data was used to compare the levels of cytokines in HZ patients between at baseline and at 90 days. CRP – C-reactive protein; HZ – herpes zoster; IL-6 – interleukin 6; TNF-α – tumor necrosis factor alpha.

Table 2. Comparison of demographic and clinical characteristics between PHN and non-PHN patients

Characteristics	Non-PHN patients (n = 61)	PHN patients (n = 93)	Z/χ^2	p-value
Age [years]	60 (55–67)	68 (64–69)	–5.116	<0.001
Female, n (%)	22 (36.1)	30 (32.2)	0.239	0.625
History of hypertension, n (%)	19 (31.1)	52 (55.9)	9.903	0.003
History of diabetes mellitus, n (%)	17 (27.9)	46 (49.5)	7.106	0.008
History of dyslipidemia, n (%)	22 (36.1)	29 (32.2)	0.397	0.529
At baseline				
IL-6 [pg/mL]	5.11 (4.42–6.01)	8.13 (4.98–10.94)	–4.89	<0.001
TNF-α [pg/mL]	7.83 (7.34–8.46)	9.43 (7.63–10.32)	–4.28	<0.001
CRP [mg/dL]	11.93 (11.01–12.98)	13.93 (12.77–15.14)	–5.71	<0.001
At 90 days				
IL-6 [pg/mL]	4.36 (4.04–5.24)	7.01 (4.73–9.88)	–4.91	<0.001
TNF-α [pg/mL]	7.04 (5.53–8.04)	8.62 (6.37–9.73)	–4.14	<0.001
CRP [mg/dL]	10.97 (9.92–11.63)	13.22 (11.33–14.79)	–6.36	<0.001

Categorical variables are presented as frequencies (percentage), and continuous variables are presented as median with interquartile range (Q1–Q3); p-value was calculated using χ^2 test or Mann–Whitney test comparing PHN patients to non-PHN patients. CRP – C-reactive protein; IL-6 – interleukin 6; PHN – postherpetic neuralgia; TNF-α – tumor necrosis factor alpha.

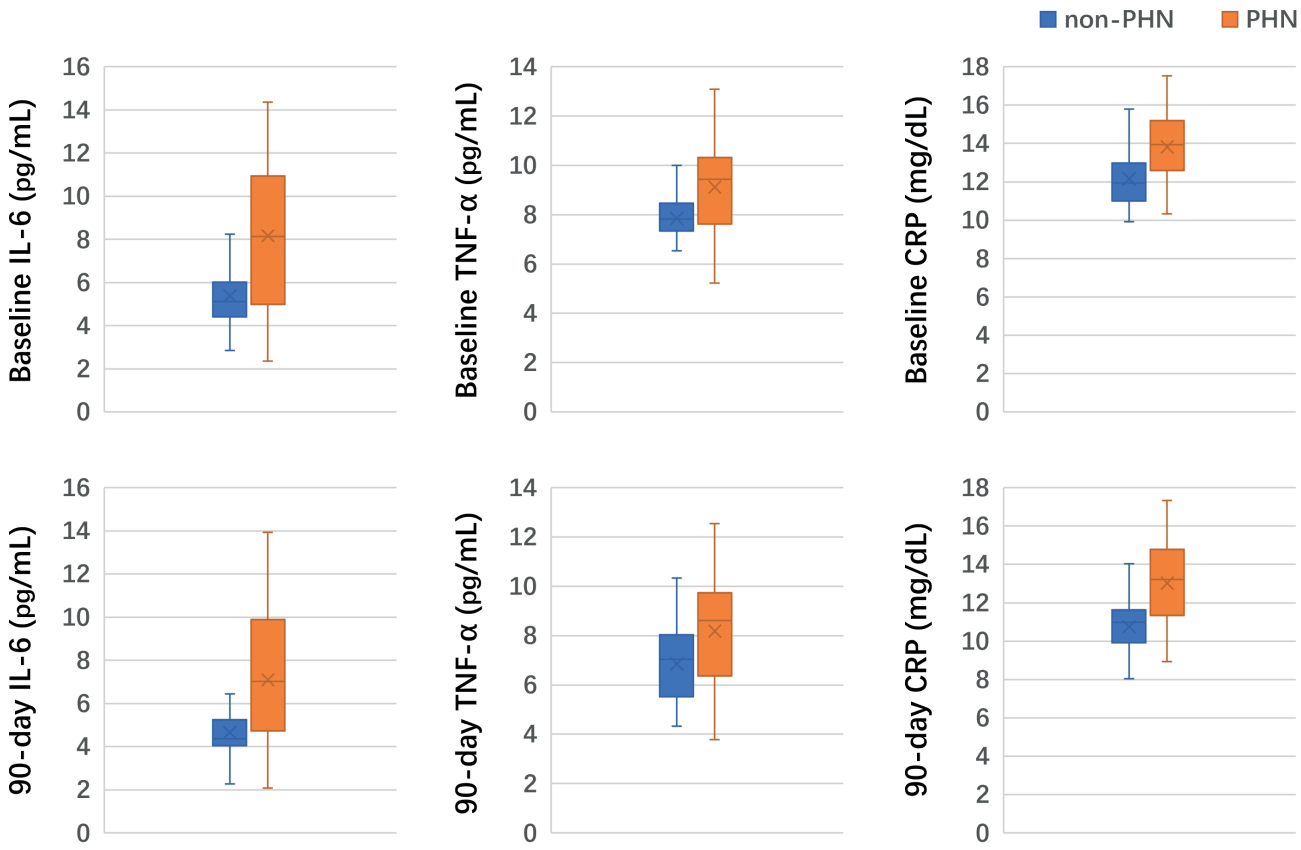

Fig. 1. Comparison of proinflammatory cytokine levels between PHN and non-PHN patients at baseline and after 90 days

CRP – C-reactive protein; IL-6 – interleukin 6; PHN – postherpetic neuralgia; TNF-α – tumor necrosis factor alpha. The chart columns represent the range (whiskers), interquartile range (box), median (line), and mean values (X mark).

of preexisting comorbidities, particularly hypertension and diabetes mellitus. We examined the relationship between baseline proinflammatory cytokine levels and pain intensity in PHN patients (Table 2). As shown in Fig. 1, serum levels of proinflammatory cytokines were markedly higher in PHN patients compared to non-PHN patients. Furthermore, at 90 days, the levels of these cytokines remained significantly elevated in PHN patients (Fig. 1).

Table 3. Comparison of demographic and clinical characteristics based on PHN severity

Characteristics	Mild-to-moderate PHN (n = 68)	Severe PHN (n = 25)	Z/χ^2	p-value
Age [years]	68 (63–69)	81 (75–87)	–6.838	<0.001
Female, n (%)	20 (29.4)	10 (40.0)	0.938	0.333
History of hypertension, n (%)	38 (55.9)	14 (56.0)	0.000	0.992
History of diabetes mellitus, n (%)	32 (34.4)	14 (56.0)	0.585	0.445
History of dyslipidemia, n (%)	22 (32.4)	7 (28.0)	0.161	0.668
At baseline				
IL-6 [pg/mL]	7.20 (4.61–10.23)	10.31 (7.96–12.35)	–3.43	<0.001
TNF-α [pg/mL]	9.05 (7.23–10.08)	9.67 (8.55–11.31)	–2.29	<0.001
CRP [mg/dL]	13.14 (12.05–14.46)	15.22 (14.28–15.89)	–4.47	<0.001
At 90 days				
IL-6 [pg/mL]	6.06 (4.11–8.77)	10.11 (6.41–11.95)	–4.26	<0.001
TNF-α [pg/mL]	7.14 (6.05–9.11)	9.99 (8.62–10.48)	–4.35	<0.001
CRP [mg/dL]	12.38 (10.88–13.90)	14.93 (14.39–15.63)	–5.25	<0.001

Categorical variables are presented as frequencies (percentage), and continuous variables are presented as median with interquartile range (Q1–Q3); p-value was calculated using χ^2 test or Mann–Whitney test comparing mild-to-moderate PHN patients to severe PHN patients. CRP – C-reactive protein; IL-6 – interleukin 6; PHN – postherpetic neuralgia; TNF-α – tumor necrosis factor alpha.

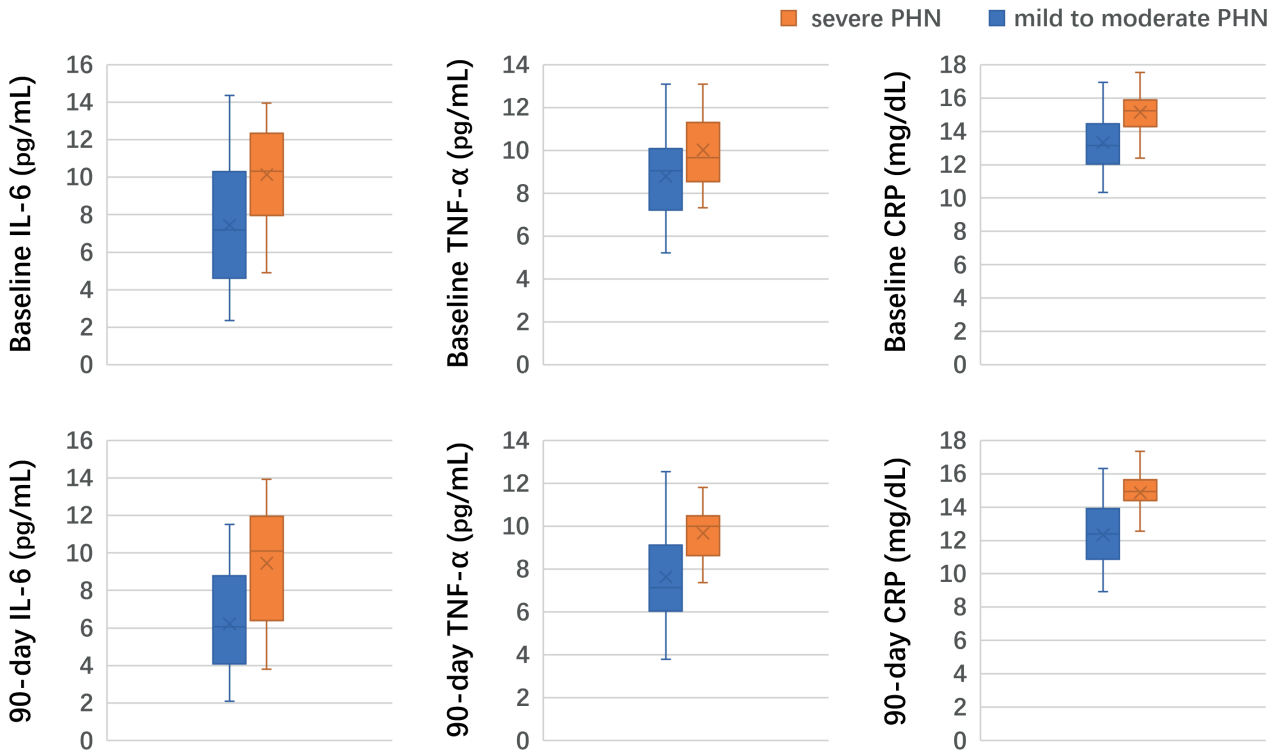

Fig. 2. Comparison of proinflammatory cytokine levels between mild-to-moderate PHN and severe PHN patients at baseline and after 90 days

CRP – C-reactive protein; IL-6 – interleukin 6; PHN – postherpetic neuralgia; TNF-α – tumor necrosis factor alpha. The chart columns represent the range (whiskers), interquartile range (box), median (line), and mean values (X mark).

Association between serum proinflammatory cytokines and VAS score

The demographic and clinical characteristics of PHN patients in relation to VAS scores are presented in Table 3. Among the 93 PHN patients, 68 (73.1%) were classified as having mild-to-moderate pain, while 25 (26.9%) had severe pain. Compared to those with mild-to-moderate PHN, patients with severe PHN were more likely to be older and female and to have a history of diabetes mellitus.

We examined the relationship between proinflammatory cytokine levels and pain intensity in PHN patients (Table 3). As shown in Fig. 2, baseline levels of proinflammatory cytokines were significantly higher in patients with

Table 4. Changes in proinflammatory cytokine levels between mild-to-moderate and severe PHN patients

Changes of cytokines	Mild-to-moderate PHN (n = 68)	Severe PHN (n = 25)	Z	p-value
IL-6 [pg/mL]	−1.09 (−2.00–0.44)	−0.73 (−1.22–0.10)	−2.17	0.030
TNF-α [pg/mL]	−1.31 (−1.84–0.51)	−0.32 (−1.07–0.17)	−3.04	0.002
CRP [mg/dL]	−0.78 (−1.94–0.55)	−0.26 (−0.66–0.00)	−2.29	0.022

Variables are presented as median with interquartile range (Q1–Q3); p-value was calculated using Mann–Whitney test comparing mild-to-moderate PHN patients to severe PHN patients; CRP – C-reactive protein; IL-6 – interleukin 6; PHN – postherpetic neuralgia; TNF-α – tumor necrosis factor alpha.

severe pain compared to those with mild-to-moderate pain. Furthermore, at 90 days, cytokine levels remained notably higher in the severe pain group compared to the mild-to-moderate pain group (Fig. 2).

Changes of proinflammatory cytokines in different pain intensity PHN

To investigate the changes in proinflammatory cytokine levels across different phases in PHN patients, we further analyzed the differences between baseline and 90-day measurements according to pain intensity (Table 4). The results showed that the reduction in proinflammatory cytokine levels over time was smaller in PHN patients with severe pain compared to those with mild-to-moderate pain.

Discussion

In this study, we found that serum proinflammatory cytokine levels in patients with HZ were significantly higher than those in healthy controls. Furthermore, cytokine levels showed a significant decrease at 90 days compared to baseline. Additionally, serum proinflammatory cytokine levels were notably higher in PHN patients compared to non-PHN patients. We also observed that cytokine levels were associated with pain intensity, and the degree of change in serum cytokine levels over time was related to pain intensity as measured using VAS scores.

Interleukin 6 is a key immunomodulatory cytokine that plays a significant role in the pathogenesis of inflammatory conditions.[17] Previous studies have confirmed that blocking the IL-6 pathway is an effective immunotherapeutic strategy.[18,19]Recent research has further demonstrated that targeting the IL-6 pathway, either by interfering with IL-6 itself or its specific receptor, has become a major approach to alleviating inflammatory responses.[20] Additionally, IL-6 levels have been shown to decrease following treatment in PHN patients.[21] Other immune cytokines, such as TNF-α, which regulate both acute and chronic inflammation, also play crucial roles in signal transduction under certain conditions.[22,23]

Monoclonal antibodies have been used to antagonize the TNF-α pathway in inflammatory diseases.[24–26] However, a recent study indicated that TNF-α levels were lower in PHN patients.[27] Additionally, CRP, which is secreted in response to IL-6 stimulation, may serve as a more sensitive biomarker for detecting systemic inflammation following inflammatory events. In turn, CRP interacts with various cell types and stimulates the secretion of IL-6 and TNF-α, thereby promoting proinflammatory effects.[28] Growing evidence has shown that CRP levels are associated with inflammation and disease activity.[29] Furthermore, pharmacological treatments for immune-mediated systemic inflammatory diseases generally reduce systemic inflammation, with CRP levels typically decreasing in accordance with the drug's mechanism of action.[28]

Previous studies have found that CRP levels increase in both HZ and PHN patients and decrease after treatment.[13,30] In summary, although immunological responses are thought to mediate the clinical features of HZ and PHN,[31] the association between serum IL-6, TNF-α or CRP levels and pain intensity in PHN remains not well established. Some studies have shown that IL-6 and CRP levels in HZ patients within seven days of onset are higher than in healthy controls, with these differences potentially linked to pain severity.[32] Additionally, it has been suggested that serum IL-6 levels might serve as a predictor of PHN severity.[12] In contrast, other studies have reported that IL-6 receptor α levels are significantly downregulated in PHN patients compared to healthy controls.[15]

In addition, recent studies with small sample sizes have shown that the concentration of TNF-α secreted by varicella-zoster virus-specific T cells is higher in PHN patients than in non-PHN patients, highlighting the potential role of these specific T cells in the development of PHN.[14] However, further investigation into the interactions among multiple inflammatory factors in HZ and PHN is needed to better understand their combined effects. Moreover, given the large sample size in this study, even minor differences may reach statistical significance. Therefore, additional research is required to clarify the association between proinflammatory cytokines and pain intensity in PHN patients.

In our study, we examined serum proinflammatory cytokine levels in HZ patients within 72 h of onset and in PHN patients at 2 different phases. Additionally, we analyzed whether changes in proinflammatory cytokine levels were associated with pain intensity. We found that serum levels of proinflammatory cytokines in HZ patients were significantly higher at baseline compared to healthy controls and decreased over the 90-day follow-up period. Furthermore,

elevated serum levels of these cytokines were associated with the pain intensity observed in PHN patients. Notably, the reduction in cytokine levels between baseline and 90 days was smaller in PHN patients with severe pain compared to those with mild-to-moderate pain.

Since levels of inflammatory factors change dynamically throughout disease progression, examining these markers at different phases of PHN may help improve our understanding of their relationship with pain intensity. Consistent with previous studies,[12] we found that IL-6 levels significantly decreased at 90 days compared to baseline. However, to date, no studies have assessed serum IL-6, TNF-α and CRP levels both at baseline and at 90 days to explore their association with pain intensity in PHN patients. Our study demonstrated that both baseline and 90-day proinflammatory cytokine levels were elevated in HZ patients and were closely associated with pain intensity in those with PHN.

Several mechanisms might explain this finding. One possible explanation is that pro-nociceptive cytokines, such as IL-6 and TNF-α, promote the activation of nociceptor neurons.[33,34] Previous studies have indicated that macrophages play a key role in both pathological and physiological pain by releasing the nociceptive cytokine IL-6.[35] Additionally, macrophages can regulate the threshold for pain perception by secreting nerve growth factor into the dermis.[36] Another possible explanation is that immune cells and neurons interact to modulate pain sensitivity, contributing to the transition from acute to chronic pain.[37]

Previous studies have suggested that the application of TNF-α can cause axons to produce aberrant electrophysiological activity, and this subsequent ectopic firing by nociceptive axons may generate pain sensations through activation of dorsal horn neurons.[38] Another explanation is that serum CRP levels are higher in HZ patients with severe rash compared to those with mild or moderate rash.[13] Consistent with prior findings, severe rash was significantly associated with severe pain in both univariate and multivariate analyses, indicating that the severity of rash is an important risk factor for pain intensity in PHN patients.[39]

Considering the dynamic changes of inflammatory markers involved in pain sensation,[40] we further evaluated the association between changes in serum proinflammatory cytokine levels (from baseline to 90 days) and pain intensity. To date, these associations with pain intensity in PHN patients have not been clearly defined. We found that smaller reductions in IL-6, TNF-α and CRP levels were associated with an increased risk of severe pain. Therefore, repeated measurements of serum proinflammatory cytokines should be considered in the clinical management of HZ and PHN patients. Our findings suggest that appropriate anti-inflammatory treatments – particularly targeting IL-6, TNF-α and CRP – may help reduce the risk of developing severe pain in HZ patients.

Limitations

This study has several limitations. First, we focused only on IL-6, TNF-α and CRP, while other proinflammatory and anti-inflammatory mediators may also play important roles in pain intensity among PHN patients. Second, we measured serum levels of inflammatory factors without investigating their cellular sources, which could provide deeper insights into the underlying mechanisms. Future studies exploring the origin of these inflammatory mediators may help clarify their specific contributions to pain intensity. Third, we assessed inflammatory factor levels at only 2 time points; more frequent, dynamic measurements over time could offer a better understanding of the temporal relationship between inflammatory responses and pain. Future research should include a broader panel of inflammatory mediators, track their dynamic changes over multiple time points, and explore their cellular origins to provide more precise mechanistic insights and strengthen the biological relevance of the findings.

Conclusions

This study demonstrated that elevated levels of proinflammatory cytokines are associated with pain intensity in patients with PHN. Furthermore, patients with severe pain showed smaller reductions in proinflammatory cytokine levels between baseline and 90 days, suggesting a link between sustained inflammation and pain severity.

Data availability statement

The datasets supporting the findings of the current study are openly available in GitHub at https://github.com/MiaoJun2024/Data.

Consent for publication

Not applicable.

Use of AI and AI-assisted technologies

Not applicable.

ORCID iDs

Jun Miao https://orcid.org/0009-0003-5067-6711
Lu Wang https://orcid.org/0009-0002-9155-824X
Min Feng https://orcid.org/0009-0006-1332-9683

References

1. Scholz J, Finnerup NB, Attal N, et al. The IASP classification of chronic pain for ICD-11: Chronic neuropathic pain. *Pain*. 2019;160(1):53–59. doi:10.1097/j.pain.0000000000001365
2. Klein NP, Bartlett J, Fireman B, et al. Effectiveness of the live zoster vaccine during the 10 years following vaccination: Real-world cohort study using electronic health records. *BMJ*. 2023;383:e076321. doi:10.1136/bmj-2023-076321

3. Tang J, Zhang Y, Liu C, Zeng A, Song L. Therapeutic strategies for postherpetic neuralgia: Mechanisms, treatments, and perspectives. *Curr Pain Headache Rep*. 2023;27(9):307–319. doi:10.1007/s11916-023-01146-x
4. Du Z, Zhang J, Han X, Yu W, Gu X. Potential novel therapeutic strategies for neuropathic pain. *Front Mol Neurosci*. 2023;16:1138798. doi:10.3389/fnmol.2023.1138798
5. Wang R, Zhu T, Han Y. Ultrasound- versus computed tomography-guided cervical dorsal root ganglia pulsed radiofrequencies via intervertebral foramen for the treatment of postherpetic neuralgia: A retrospective cohort study. *Pain Physician*. 2023;26(3):E171–E179. PMID:37192240.
6. Thompson RR, Kong CL, Porco TC, Kim E, Ebert CD, Acharya NR. Herpes zoster and postherpetic neuralgia: Changing incidence rates from 1994 to 2018 in the United States. *Clin Infect Dis*. 2021;73(9):e3210–e3217. doi:10.1093/cid/ciaa1185
7. Muñoz-Quiles C, López-Lacort M, Orrico-Sánchez A, Díez-Domingo J. Impact of postherpetic neuralgia: A six year population-based analysis on people aged 50 years or older. *J Infect*. 2018;77(2):131–136. doi:10.1016/j.jinf.2018.04.004
8. Finnerup NB, Kuner R, Jensen TS. Neuropathic pain: From mechanisms to treatment. *Physiol Rev*. 2021;101(1):259–301. doi:10.1152/physrev.00045.2019
9. Moehring F, Halder P, Seal RP, Stucky CL. Uncovering the cells and circuits of touch in normal and pathological settings. *Neuron*. 2018;100(2):349–360. doi:10.1016/j.neuron.2018.10.019
10. Lutgendorf SK, Zia S, Luo Y, et al. Early and recent exposure to adversity, TLR-4 stimulated inflammation, and diurnal cortisol in women with interstitial cystitis/bladder pain syndrome: A MAPP research network study. *Brain Behav Immun*. 2023;111:116–123. doi:10.1016/j.bbi.2023.03.024
11. Hainsworth KR, Simpson PM, Raff H, Grayson MH, Zhang L, Weisman SJ. Circulating inflammatory biomarkers in adolescents: Evidence of interactions between chronic pain and obesity. *Pain Rep*. 2021;6(1):e916. doi:10.1097/PR9.0000000000000916
12. Lin D, Zhong C, Jiang Q, Huang A, Liu Y. Serum interleukin-6 levels are increased in post-herpetic neuralgia: A single-center retrospective study. *An Bras Dermatol*. 2023;98(2):202–207. doi:10.1016/j.abd.2022.03.007
13. Oskay T, Keskin C, Özen M. Antioxidant and inflammatory biomarkers in herpes zoster. *J Med Virol*. 2022;94(8):3924–3929. doi:10.1002/jmv.27781
14. Peng Q, Guo X, Luo Y, et al. Dynamic immune landscape and VZV-specific T cell responses in patients with herpes zoster and postherpetic neuralgia. *Front Immunol*. 2022;13:887892. doi:10.3389/fimmu.2022.887892
15. Yang X, Yuan C, Wang H, et al. Changes in serum angiogenic factors among patients with acute pain and subacute pain. *Front Mol Neurosci*. 2022;15:960460. doi:10.3389/fnmol.2022.960460
16. Bourdel N, Alves J, Pickering G, Ramilo I, Roman H, Canis M. Systematic review of endometriosis pain assessment: How to choose a scale? *Hum Reprod Update*. 2015;21(1):136–152. doi:10.1093/humupd/dmu046
17. Rose-John S, Jenkins BJ, Garbers C, Moll JM, Scheller J. Targeting IL-6 trans-signalling: Past, present and future prospects. *Nat Rev Immunol*. 2023;23(10):666–681. doi:10.1038/s41577-023-00856-y
18. Tanaka T, Narazaki M, Kishimoto T. Interleukin (IL-6) immunotherapy. *Cold Spring Harb Perspect Biol*. 2018;10(8):a028456. doi:10.1101/cshperspect.a028456
19. Puel A, Picard C, Lorrot M, et al. Recurrent staphylococcal cellulitis and subcutaneous abscesses in a child with autoantibodies against IL-6. *J Immunol*. 2008;180(1):647–654. doi:10.4049/jimmunol.180.1.647
20. Aletaha D, Kerschbaumer A, Kastrati K, et al. Consensus statement on blocking interleukin-6 receptor and interleukin-6 in inflammatoy conditions: An update. *Ann Rheum Dis*. 2023;82(6):773–787. doi:10.1136/ard-2022-222784
21. Zhang W, He C. Clinical efficacy of pulsed radiofrequency combined with intravenous lidocaine infusion in the treatment of subacute herpes zoster neuralgia. *Pain Res Manag*. 2022;2022:5299753. doi:10.1155/2022/5299753
22. Gonzalez Caldito N. Role of tumor necrosis factor-alpha in the central nervous system: A focus on autoimmune disorders. *Front Immunol*. 2023;14:1213448. doi:10.3389/fimmu.2023.1213448
23. van Loo G, Bertrand MJM. Death by TNF: A road to inflammation. *Nat Rev Immunol*. 2023;23(5):289–303. doi:10.1038/s41577-022-00792-3
24. Monaco C, Nanchahal J, Taylor P, Feldmann M. Anti-TNF therapy: Past, present and future. *Int Immunol*. 2015;27(1):55–62. doi:10.1093/intimm/dxu102
25. Medina-Medina R, Iglesias-Flores E, Benítez JM, et al. Development of a prediction model for short-term remission of patients with Crohn's disease treated with anti-TNF drugs. *Int J Mol Sci*. 2023;24(10):8695. doi:10.3390/ijms24108695
26. Meyer A, Drouin J, Weill A, Carbonnel F, Dray-Spira R. Comparative study of pregnancy outcomes in women with inflammatory bowel disease treated with thiopurines and/or anti-TNF: A French nationwide study 2010–2018. *Aliment Pharmacol Ther*. 2021;54(3):302–311. doi:10.1111/apt.16448
27. Gu J, Yuan Y, Wang J, Liu H, Zhang Z, Yan Y. Serum inflammatory cytokine levels in herpes zoster patients and their association with postherpetic neuralgia: A prospective study. *Med Sci Monit*. 2023;29:e941878. doi:10.12659/MSM.941878
28. Sproston NR, Ashworth JJ. Role of C-reactive protein at sites of inflammation and infection. *Front Immunol*. 2018;9:754. doi:10.3389/fimmu.2018.00754
29. Kilcher G, Hummel N, Didden EM, Egger M, Reichenbach S. Rheumatoid arthritis patients treated in trial and real world settings: Comparison of randomized trials with registries. *Rheumatology (Oxford)*. 2018;57(2):354–369. doi:10.1093/rheumatology/kex394
30. Sun H, Yu Z. Effect of extracorporeal shock wave combined with pregabalin on patients with post-herpetic neuralgia. *Medicine (Baltimore)*. 2023;102(30):e34361. doi:10.1097/MD.0000000000034361
31. Yamada K, Mori Y, Cui R, et al. Predictors of herpes zoster severity and immune responses according to pain trajectories: A community-based prospective cohort study. *J Dermatol*. 2023;50(8):1020–1033. doi:10.1111/1346-8138.16829
32. Khazan M, Nasiri S, Riahi SM, Robati RM, Hedayati M. Measurement of melatonin, indole-dioxygenase, IL-6, IL-18, ferritin, CRP, and total homocysteine levels during herpes zoster. *J Med Virol*. 2020;92(8):1253–1259. doi:10.1002/jmv.25484
33. Oggero S, Cecconello C, Silva R, et al. Dorsal root ganglia CX3CR1 expressing monocytes/macrophages contribute to arthritis pain. *Brain Behav Immun*. 2022;106:289–306. doi:10.1016/j.bbi.2022.09.008
34. Gopalsamy B, Farouk AAO, Tengku Mohamad TAS, Sulaiman MR, Perimal EK. Antiallodynic and antihyperalgesic activities of zerumbone via the suppression of IL-1β, IL-6, and TNF-α in a mouse model of neuropathic pain. *J Pain Res*. 2017;10:2605–2619. doi:10.2147/JPR.S143024
35. Zhao J, Huh Y, Bortsov A, Diatchenko L, Ji RR. Immunotherapies in chronic pain through modulation of neuroimmune interactions. *Pharmacol Ther*. 2023;248:108476. doi:10.1016/j.pharmthera.2023.108476
36. Tanaka T, Okuda H, Isonishi A, et al. Dermal macrophages set pain sensitivity by modulating the amount of tissue NGF through an SNX25-Nrf2 pathway. *Nat Immunol*. 2023;24(3):439–451. doi:10.1038/s41590-022-01418-5
37. Ren K, Dubner R. Interactions between the immune and nervous systems in pain. *Nat Med*. 2010;16(11):1267–1276. doi:10.1038/nm.2234
38. Sorkin LS, Xiao WH, Wagner R, Myers RR. Tumour necrosis factor-alpha induces ectopic activity in nociceptive primary afferent fibres. *Neuroscience*. 1997;81(1):255–262. doi:10.1016/s0306-4522(97)00147-4
39. Nagasako EM, Johnson RW, Griffin DRJ, Dworkin RH. Rash severity in herpes zoster: Correlates and relationship to postherpetic neuralgia. *J Am Acad Dermatol*. 2002;46(6):834–839. doi:10.1067/mjd.2002.120924
40. Goldstein RH, Barkai O, Íñigo-Portugués A, Katz B, Lev S, Binshtok AM. Location and plasticity of the sodium spike initiation zone in nociceptive terminals in vivo. *Neuron*. 2019;102(4):801–812.e5. doi:10.1016/j.neuron.2019.03.005

Importance of single nucleotide polymorphism microarray in prenatal diagnosis

ZongHui Feng[A,C–F], Yan Chen[B,C,F], FengMei Yi[B,C,F], Min Li[B,C,F], ShuMin Jiang[B,C,F], ChunYue He[B,C,F], YangLi Chen[B,C,F], MaoSheng Chen[B,C,F], WenCheng Li[B–F]

Prenatal Diagnosis Center, Maternity and Child Care Hospital of Huaihua, China

A – research concept and design; B – collection and/or assembly of data; C – data analysis and interpretation; D – writing the article; E – critical revision of the article; F – final approval of the article

Advances in Clinical and Experimental Medicine, ISSN 1899–5276 (print), ISSN 2451–2680 (online) *Adv Clin Exp Med*. 2025;34(11):1929–1935

Address for correspondence
WenCheng Li
E-mail: liwencheng9743@outlook.com

Funding sources
None declared

Conflict of interest
None declared

Received on February 2, 2023
Reviewed on May 8, 2024
Accepted on July 9, 2024

Published online on May 23, 2025

Abstract

Background. With the increasing number of older pregnant women and environmental pollution, the incidence of congenital malformations increases every year. Prenatal diagnosis is an effective means of identifying congenital malformations.

Objectives. To evaluate the clinical utility of single nucleotide polymorphism (SNP) microarray analysis during prenatal evaluations.

Materials and methods. To assess the similarities and differences between the 2 approaches, 425 pregnant women were selected to undergo prenatal gene SNP microarray analysis and karyotype analysis during prenatal evaluation between January 2020 and August 2021.

Results. The success rate of SNP microarray analysis was 100%, which was statistically different from that of karyotype analysis (92%, Fisher's exact test, $p < 0.001$). The positive rate of SNP detection was 10.4% higher than karyotype analysis, which was 6.6% (Pearson's χ^2 test, $\chi^2 = 3.89$, degrees of freedom (df) = 1, $p = 0.049$). Karyotype analysis detected 28 cases of aneuploidy; SNPs could not only detect these results of karyotype analysis, but 16 cases of copy number variations (CNV) with obvious pathogenicity, including duplications/deletions, chimerism and loss of heterozygosity (LOH).

Conclusions. Single nucleotide polymorphism microarray analysis technology is an important method used in prenatal genetic evaluations, which can find fetal genetic etiologies, correctly evaluate the fetal prognosis during prenatal clinical examination, and provide a more objective basis for whether to continue the pregnancy.

Key words: karyotype analysis, prenatal diagnosis, SNP microarray analysis

Cite as
Feng ZH, Chen Y, Yi FM, et al. Importance of single nucleotide polymorphism microarray in prenatal diagnosis. *Adv Clin Exp Med*. 2025;34(11):1929–1935. doi:10.17219/acem/202728

DOI
10.17219/acem/202728

Highlights

- Single nucleotide polymorphism (SNP) array analysis is an important tool for screening chromosome deletions and replications, especially in fetuses with normal karyotypes.
- The success rate of SNP array analysis was 100%.
- The time for SNP array analysis is much shorter.
- SNP array analysis technology has the advantages of simple operation and fast speed.
- SNP array analysis technology has high throughput and resolution.

Background

With the increasing number of older pregnant women and environmental pollution, the incidence of congenital malformations increases every year. Prenatal diagnosis is an effective means to diagnose congenital malformations.[1] Karyotype analysis is currently the gold standard for the prenatal diagnosis of genetic abnormalities, but it also has drawbacks, including the need for cell culture, long reporting cycles, and an increased risk of sample contamination that can lead to experimental failure.[2] Karyotype analysis can distinguish only fragments larger than 10 megabase (Mb) pairs, and often misses some disease-causing genes smaller than 10 Mb. Microdeletion and microreplication syndrome[3] is caused by the duplication or deletion of chromosomal segments smaller than 5–10 Mb and is associated with a wide range of malformations and dysgnosia. Microreplication and microdeletion of genomic segments (also known as copy number variation (CNV)) are associated with 6–15% of genetic diseases. Detection of CNVs requires high-resolution technology for which traditional karyotype analysis is ineffective.[4] Because of its rapid, high-throughput and high-resolution ability, chromosomal microarray analysis (CMA) has been accepted as a powerful tool for the diagnosis of developmental retardation, intellectual disability, autism, and multiple congenital anomalies.[5–8] Microdeletions and microreplications as small as 50–100 kilobase (kb) pairs can be detected using CMA across the entire genome.[9] Chromosomal microarray analysis is currently classified into 2 categories: array-based comparative genomic hybridization (aCGH) and single nucleotide polymorphism (SNP) array. The aCGH demonstrates the relative amounts of DNA from various areas of the genome by comparing the test DNA sample with a normal reference DNA sample and cannot detect triploidy, while SNP arrays can identify triploidy as well as loss of heterozygosity (LOH) by hybridizing the test sample to the array platform and analyzing the signal intensity of SNP probes.[10,11] The SNP array analysis technology is a new molecular method for karyotype analysis with high resolution, sensitivity, throughput, and accuracy, capable of detecting and analyzing submicroscopic changes in ploidy.[12] The SNP array analysis is effective in the prenatal diagnosis of genetic causes of fetal nasal bone deletion.[13] The SNP array technology has been increasingly applied in prenatal clinical genetic evaluations and has become a recommended genetic testing method for the prenatal diagnosis of fetal growth retardation, mental retardation, autism, and organ malformations, especially when an ultrasound shows fetal abnormalities and a normal karyotype.[14]

Objectives

To evaluate the clinical utility of SNP arrays in prenatal evaluations.

Objects and methods

Research objects

Prenatal SNP array analysis and karyotype analysis were performed on 425 pregnant women aged 19–45 years old between 16 and 31 weeks gestation at our antenatal diagnostic center between January 2020 and August 2021. The main indications of prenatal diagnosis were abnormal prenatal ultrasonography, chromosomal abnormalities of one spouse, advanced maternal age, fetal structural abnormalities, and noninvasive genetic abnormalities. All pregnant women enrolled in the study received technical counseling and signed informed consent forms for the SNP array and conventional karyotypes prior to the study.

Materials and methods

Chromosome karyotype analysis

After samples were centrifuged at 2,000 rpm for 10 min, the supernatant was discarded and the samples were incubated for 8–9 days. Each sample was counted and analyzed for 20–30 mitotic periods, and 5 radionuclide images were observed, analyzed and photographed. If any abnormality was detected, the number of karyotypes increased. Using the International Nomenclature of Human Cytogenetics (ISCN, 2005),[15] the aberrant karyotype was described.

Single nucleotide polymorphism array analysis

Genomic DNA was extracted from fetal umbilical cord blood and amniotic fluid that had never been cultured or previously cultured using a Qiagen kit (Qiagen, Hilden, Germany). The SNP analysis was performed using a genome-wide Affymetrix CytoScan 750 K array (Affymetrix Inc., Santa Clara, USA) containing 500,000 probes for CNV and 200,000 probes for SNPs spread throughout the whole human genome. Data were analyzed using the human genome version of GRCh37 (hg19) and Chromosome Analysis Kit software (Affymetrix). Gains or losses ≥400 kb and LOH ≥ 10 Mb were the most common recommendations. Genome-wide identification of uniparental disomy (UPD) in the offspring-parents triad can be confirmed as having a maternal or paternal origin using the UPDtool.[16] All CNVs found were compared using the following databases: Database of Genomic Variants (DGV, http://projects.tcag.ca/variation), Database of Chromosomal Imbalance and Phenotype in Humans using Ensemble Resources (DECIPHER) database (https://www.deciphergenomics.org), International Standards for Cytogenomic Arrays, and Online Mendelian Inheritance in Man (OMIM) database (http://www.omim.org).[17]

Statistical analyses

For qualitative data, the assumption of expected abundance for the χ^2 test was checked. If the assumption was met, Pearson's χ^2 test of independence was used to analyze the differences between groups. If the assumption was not met, Fisher's exact test for 2×2 tables was used. The analysis was performed using GraphPad Prism v. 9.0 (GraphPad Software, San Diego, USA).

Results

General conditions of study objects

Age composition of objects

There were 425 pregnant women aged 18–45 years old. The distribution of cases by age group is illustrated in Fig. 1. The 18–23 age group had 27 cases, the 24–29 age group had 105 cases, the 30–34 age group had 133 cases, the 35–39 age group had 122 cases, and the 40–45 age group had 38 cases.

Gestational weeks of study participants

The prenatal diagnosis of 425 pregnant women was between 16 and 31 weeks, as shown in Fig. 2. There were 7 cases in the 16+ weeks group, 65 cases in the 17+ weeks group, 89 cases in the 18+ weeks group, 70 cases in the 19+ weeks group, 67 cases in the 20+ weeks group, 28 cases in the 21+ weeks group, 20 cases in the 22+ weeks group, 32 cases in the 23+ weeks group, 11 cases in the 24+ weeks group, 11 cases in the 25+ weeks group, 5 cases in the 26+ weeks group, 2 cases in the 27+ weeks group, 2 cases in the 28+ weeks group, 4 cases in the 29+ weeks group, 10 cases in the 30+ weeks group, and 2 cases in the 31+ weeks group.

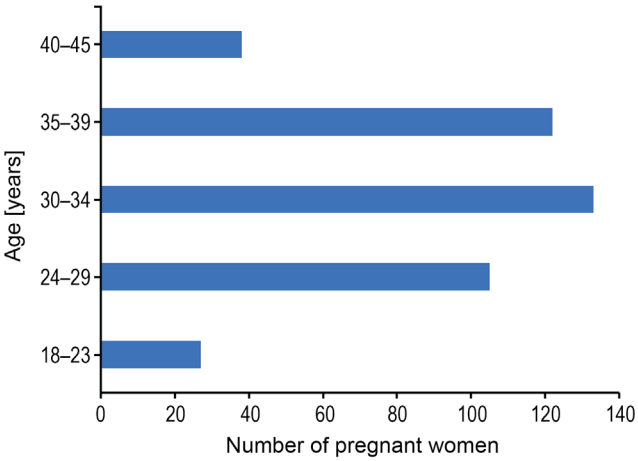

Fig. 1. Age analysis (cases)

Sample type of the study objects

Among the 425 samples, 363 were amniotic fluid, accounting for 85.41% of the total sample size, 30 were miscarriage villi, accounting for 7.06% of the total sample size, and 32 were umbilical cord blood, accounting for 7.53% of the total sample size, as shown in Fig. 3.

Success rate and positive rate of karyotype analysis and SNP array analysis

There were 425 samples, with 391 successful and 34 failed cases (a success rate of 92%). Karyotype analysis identified 28 cases of aberrant karyotypes among the 425 samples, with a positive rate of 6.6%, as shown in Table 1.

In addition, the success rate of SNP array analysis was 100%. Compared with karyotype analysis, the success rate was significantly improved (Table 2, Fisher's exact test, $p < 0.001$). Forty-four cases showed positive results, with a positive rate of 10.4%, which was statistically significant compared to karyotype analysis (Table 3, Pearson's χ^2 test, $\chi^2 = 3.89$, degrees of freedom (df) = 1, $p = 0.049$).

Results of karyotype analysis and SNP array analysis

Among the 28 cases with abnormal karyotypes detected with karyotype analysis, there were 12 cases with trisomy 21, 4 cases with trisomy 18, 2 cases with trisomy 16, 1 case with trisomy 13, 5 cases with 45 X, 1 case with 46 XXX, and 3 cases with 47 XXY. In addition to the abnormal cases, 16 cases with normal karyotypes but abnormal SNP array

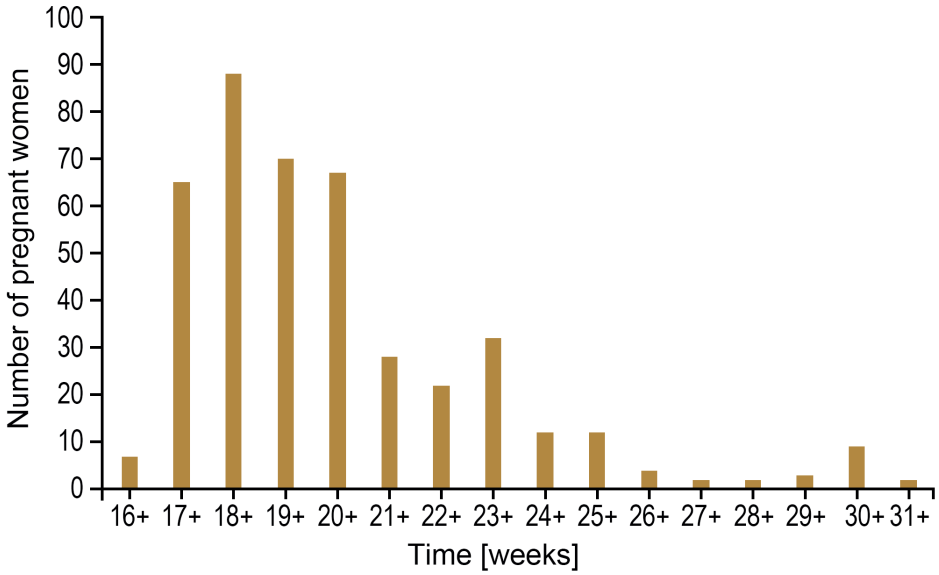

Fig. 2. Gestational weeks (cases)

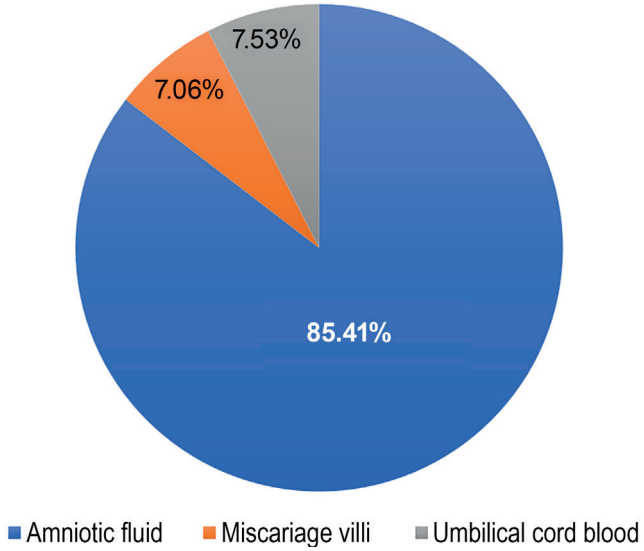

Fig. 3. Sample type of the study object

Table 1. Success rate and positive rate of karyotype analysis and SNP array analysis

Detection items	Total cases	Successful cases	Positive cases
Chromosome karyotype analysis	425	391 (92%)	28 (6.6%)
SNP array analysis	425	425 (100%)	44 (10.4%)

SNP – single nucleotide polymorphism.

Table 2. Fisher's exact test of the success rate of karyotype analysis and SNP array analysis

Detection items	Successful cases	Failed cases	p-value
Chromosome karyotype analysis	391	34	<0.001
SNP array analysis	425	0	–

SNP – single nucleotide polymorphism.

Table 3. Pearson's χ^2 test of independence of the positive rate of karyotype analysis and SNP array analysis

Detection items	Positive cases	Other cases	df	χ^2	p-value
Chromosome karyotype analysis	28	397	1	3.89	0.049
SNP array analysis	44	381	–	–	–

SNP – single nucleotide polymorphism; df – degree of freedom.

analysis were also detected, including 8 cases of duplication/deletion, 3 cases of chimera and 5 cases of LOH. Table 4 summarizes the outcomes.

Results of normal karyotype analysis and abnormal SNP array analysis

Sixteen CNVs with normal karyotype were found to be abnormal in the SNP array analysis results, with a fragment length of 349 kb–14.59 Mb, which was related to microdeletion, microreplication, chimera, and LOH syndrome, as shown in Table 5.

Discussion

Although traditional chromosome karyotyping can identify polyploidy, aneuploidy, translocation, inversion, chimerism, duplication, and deletions larger than 10 Mb, this technique has various limitations, including time-consuming cell cultures, low resolution, high labor demand, and an inability to identify CNVs smaller than 10 Mb.[18–20] Therefore, there is an urgent need for a new testing technique to be used in prenatal evaluations.

Karyotype analysis and CMA are 2 prenatal diagnostic methods that have been widely used over the recent years.[21–23] Chromosomal microarray analysis

Table 4. Comparison of the results of karyotype analysis and SNP array analysis (16 cases with with normal karyotypes but abnormal SNP array analysis, including 8 cases of duplication/deletion, 3 cases of chimera and 5 cases of LOH)

Chromosome karyotype analysis results (cases)	SNP array analysis results (cases)
Trisomy 21 (12)	Trisomy 21 (12)
Trisomy 18 (4)	Trisomy 18 (4)
Trisomy 16 (2)	Trisomy 16 (2)
Trisomy 13 (1)	Trisomy 13 (1)
45, X (5)	45, X (5)
46, XXX (1)	46, XXX (1)
47, XXY (3)	47, XXY (3)

LOH – loss of heterozygosity; SNP – single nucleotide polymorphism.

is a high-resolution technology for whole-genome analysis, detecting micro-deletions and micro-duplications, which are not routinely detected via karyotyping. Chromosomal microarray analysis can be separated into aCGH and SNP array. The SNP array can detect regions of homozygosity, triploidy, and maternal cell contamination, which the aCGH cannot. The SNP array analysis has been widely used in the field of prenatal genetics and has shown tremendous advancement and superiority as a result of scientific and technological developments.[24] Compared to conventional karyotyping, the resolution of SNP array analysis is much greater, allowing the identification of submicroscopic imbalances such as UPDs and LOHs.[25] The value of the additional information provided by SNP array analysis in prenatal diagnosis is evident in reducing the prevalence of fetuses at increased risk of chromosomal imbalances that are undetected or may have genetic disorders.[26] The SNP array analysis can influence pregnancy care and outcomes by offering more precise prognostic information than karyotype analysis.[27]

Compared with traditional karyotypes, the time for SNP array analysis is much shorter, and the time for patients to wait for the genetic results is also significantly shortened.[3] In this study, 425 amniotic fluid, miscarriage villi and umbilical cord blood samples were subjected to traditional cell culture, and karyotype analysis generally takes 12–15 days, with some samples taking up to 20 days due to low cell activity and slow growth.[28] In contrast, the detection period for SNP array analysis is only 3–4 days. Prenatal evaluations are an important means to judge the health state of the fetus. The rapid results of genetics can reduce the waiting time of pregnant women and greatly reduce the psychological burden.[29]

In addition, SNP array analysis technology has the advantages of simple operation and speed, while traditional karyotype analysis technology requires a high level of operation skills, strict aseptic operation of cell cultures, and a tedious and time-consuming chromosome preparation process. The SNP does not require a complex chromosome preparation process or strict aseptic operation, and it only

Table 5. Sixteen cases with normal karyotype results and abnormal SNP results

No.	SNP result	CNV fragment length	CNV type
1	arr[hg19] 10p12.2 (24,110,323-24,477,294)x1	367kb	deletion
2	arr[hg19] 6q26 (162,513,754-163,102,082)x3	588 kb	duplication
3	arr[hg19] 2q13 (110,498,142-111,366,256)x3	868kb	deletion
4	arr[hg19] Xq13.3 (74,524,076-75,360,251)x3	836kb	duplication
5	arr[hg19] 3p26.3p25.3 (61,892-9,122,774)x1	9.06 Mb	deletion
6	arr[hg19] 4q21.3 (87,084,084-87,623,511)x4	539 kb	duplication
7	arr[hg19] 18q22.1 (61,642,539-62,185,405)x1	542kb	deletion
8	arr[hg19] 7p21.3 (10,386,633-10,780,601)x1	349kb	deletion
9	arr[hg19] 5q15q21.3 (93,766,219-107,405,476) x2 hmz	13.60 Mb	LOH
10	arr[hg19] 22q11.1q13.33 (16,888,900-51,197,766)x2-3	trisomy 22	chimera
11	arr[hg19] 18p11.32q23 (136,228-78,013,728)x2-3	trisomy 18	chimera
12	arr[hg19] 21q11.2q22.3 (15,016,487-48,093,361)x3	trisomy 21	chimera
13	2q14.2q21.2 (120,222,604-134,809,504) x2 hmz	14.59 Mb	LOH
14	arr[hg19] 9q21.33q22.33 (89,317,009-102,177,977) x2 hmz	12.80 Mb	LOH
15	arr[hg19] 4q13.2q21.21 (68,443,308-80,883,021) x2 hmz	12.44Mb	LOH
16	arr[hg19] 7p15.2p14.1 (27,122,563-39,324,349) x2 hmz	12.20Mb	LOH

SNP – single nucleotide polymorphism; LOH – loss of heterozygosity; CNV – copy number variation.

utilizes a modest amount of DNA to identify the whole genome's changes in copy number.[30] In this study, 425 samples were cultured under strict aseptic conditions, and 391 samples were successfully cultured with a success rate of 92%. Some samples failed because cells did not adhere to cell walls after culture or cell cloning was stunted, and karyotype isolates were not collected for analysis. This limitation was overcome by the SNP array analysis technology, which obtained results for all 34 samples that failed in culture with a 100% success rate, significantly higher than the karyotyping technique.

The SNP array analysis technology can provide a higher resolution.[31] The number of chromosome bands prepared by traditional karyotype technology is between 300 and 420, and the resolution is low. Theoretically, only 5–10 Mb

chromosome structural abnormalities can be detected.[32] The SNP array analysis technology has high throughput and resolution, enabling the detection of genome-wide CNVs at one time, as well as detecting single gene diploid and small chromosome variants that cannot be identified by karyotype analysis.[33] In addition, SNP probes also provide SNP typing information, which can detect heterozygous loss and can be used for clinical detection of some residual and imprinted genetic diseases. In this study, among the cases with normal karyotypes, 16 CNVs with specific pathogeneses were detected using SNP array analysis, and the length ranged from 349 kb to 14.59 Mb, which involved the microdeletion of a 367 kb fragment in the p12.2 region of chromosome 10, the microreplication of a 588 kb fragment in the q26 region of chromosome 6 and the ROH of about 13.6 Mb in the q15q21.3 region of chromosome 5.

The inability of SNP array analysis to recognize balanced chromosomal structural abnormalities, such as balanced translocations and reversals,[34] prevents them from completely replacing karyotype analysis, despite its many benefits.[35] Although most of these abnormalities are inherited from the parents and do not necessarily affect the phenotype of the fetus, they may still cause spontaneous abortion throughout the reproductive process or cause chromosomal imbalances.[36] A small number of mosaic chromosomal defects may also be undetectable using SNP array analysis. Given that SNP array and karyotype analyses are not substitutable for each other, the combination of the 2 can provide us with more genetic information to avoid a missed diagnosis and provide more basis for genetic counseling.[37]

Limitations

A larger number of participants is suggested to reduce result bias. Moreover, to popularize and generalize SNP array analysis technology, more studies are needed.

Conclusions

The SNP array analysis is an important tool for screening chromosome deletions and replications, especially in fetuses with normal karyotypes. With technical improvements and data accumulation, SNP array analysis will play an important role in prenatal diagnosis.

Ethics statement

The present study was approved by the Ethics Committee of Maternity and Child Care Hospital of Huaihua (approval No. 20200925CZ) and written informed consent was provided by all patients prior to the study. All procedures were performed in accordance with the ethical standards of the Institutional Review Board and The Declaration of Helsinki, and its later amendments and comparable ethical standards.

Data availability

The datasets generated and/or analyzed during the current study are available from the corresponding author on reasonable request.

Consent for publication

Not applicable.

Use of AI and AI-assisted technologies

Not applicable.

ORCID iDs

ZongHui Feng https://orcid.org/0009-0009-3595-0747
Yan Chen https://orcid.org/0009-0008-3490-8275
FengMei Yi https://orcid.org/0009-0008-3490-8275
Min Li https://orcid.org/0009-0009-5832-0537
ShuMin Jiang https://orcid.org/0009-0008-8262-8569
ChunYue He https://orcid.org/0009-0008-2232-3798
YangLi Chen https://orcid.org/0009-0006-1103-3045
MaoSheng Chen https://orcid.org/0009-0005-0768-3179
WenCheng Li https://orcid.org/0000-0002-5211-1074

References

1. Wang Y, Greenfeld E, Watkins N, et al. Diagnostic yield of genome sequencing for prenatal diagnosis of fetal structural anomalies. *Prenat Diagn*. 2022;42(7):822–830. doi:10.1002/pd.6108
2. Wu X, Li Y, Su L, et al. Chromosomal microarray analysis for the fetuses with aortic arch abnormalities and normal karyotype. *Mol Diagn Ther*. 2020;24(5):611–619. doi:10.1007/s40291-020-00474-7
3. Kamath V, Purna Chacko M, Kirubakaran R, Mascarenhas M, Kamath MS. Single nucleotide polymorphism array versus karyotype for prenatal diagnosis in fetuses with abnormal ultrasound: A systematic review and meta-analysis. *Eur J Obstet Gynecol Reprod Biol*. 2022;271:235–244. doi:10.1016/j.ejogrb.2022.02.011
4. Hu L, Yao X, Huang H, et al. Clinical significance of germline copy number variation in susceptibility of human diseases. *J Genet Genomics*. 2018;45(1):3–12. doi:10.1016/j.jgg.2018.01.001
5. Song T, Xu Y, Li Y, et al. Detection of submicroscopic chromosomal aberrations by chromosomal microarray analysis for the prenatal diagnosis of central nervous system abnormalities. *Clin Lab Anal*. 2020;34(10):e23434. doi:10.1002/jcla.23434
6. Werling AM, Grünblatt E, Oneda B, et al. High-resolution chromosomal microarray analysis for copy-number variations in high-functioning autism reveals large aberration typical for intellectual disability. *J Neural Transm*. 2020;127(1):81–94. doi:10.1007/s00702-019-02114-9
7. Hu T, Zhang Z, Wang J, et al. Chromosomal aberrations in pediatric patients with developmental delay/intellectual disability: A single-center clinical investigation. *Biomed Res Int*. 2019;2019:9352581. doi:10.1155/2019/9352581
8. Jang W, Kim Y, Han E, et al. Chromosomal microarray analysis as a first-tier clinical diagnostic test in patients with developmental delay/intellectual disability, autism spectrum disorders, and multiple congenital anomalies: A prospective multicenter study in Korea. *Ann Lab Med*. 2019;39(3):299–310. doi:10.3343/alm.2019.39.3.299
9. Wang H, Dong Z, Zhang R, et al. Low-pass genome sequencing versus chromosomal microarray analysis: Implementation in prenatal diagnosis. *Genet Med*. 2020;22(3):500–510. doi:10.1038/s41436-019-0634-7
10. Wapner RJ, Martin CL, Levy B, et al. Chromosomal microarray versus karyotyping for prenatal diagnosis. *N Engl J Med*. 2012;367(23):2175–2184. doi:10.1056/NEJMoa1203382
11. Levy B, Wapner R. Prenatal diagnosis by chromosomal microarray analysis. *Fertil Steril*. 2018;109(2):201–212. doi:10.1016/j.fertnstert.2018.01.005

12. Xie X, Wu X, Su L, et al. Application of single nucleotide polymorphism microarray in prenatal diagnosis of fetuses with central nervous system abnormalities. *Int J Gen Med*. 2021;14:4239–4246. doi:10.2147/IJGM.S323899
13. Zhang W, Guo Z, Wang W, et al. Application of single nucleotide polymorphism microarray and fluorescence in situ hybridization analysis for the prenatal diagnosis of a case with Pallister–Killian syndrome [in Chinese]. *Zhonghua Yi Xue Yi Chuan Xue Za Zhi*. 2018;35(2): 232–235. doi:10.3760/cma.j.issn.1003-9406.2018.02.019
14. Chen L, Du J, Wang J, et al. Study on the application value of BACs-on-Beads technology combined with chromosome karyotype analysis in prenatal diagnosis. *Transl Pediatr*. 2022;11(2):212–218. doi:10.21037/tp-22-16
15. Call for nomination of members of the International Standing Committee of Human Cytogenomic Nomenclature. *Mol Syndromol*. 2018; 9(2):59–59. doi:10.1159/000487208
16. Monsu M, Comin M. Fast alignment of reads to a variation graph with application to SNP detection. *J Integr Bioinform*. 2021;18(4):20210032. doi:10.1515/jib-2021-0032
17. Huang H, Cai M, Wang Y, Liang B, Lin N, Xu L. SNP array as a tool for prenatal diagnosis of congenital heart disease screened by echocardiography: Implications for precision assessment of fetal prognosis. *Risk Manag Healthc Policy*. 2021;14:345–355. doi:10.2147/RMHP.S286001
18. Pons L, Till M, Alix E, et al. Prenatal microarray comparative genomic hybridization: Experience from the two first years of activity at the Lyon university-hospital. *J Gynecol Obstet Hum Reprod*. 2017;46(3): 275–283. doi:10.1016/j.jogoh.2016.11.004
19. García-Acero M, Suárez-Obando F, Gómez-Gutiérrez A. CGH analysis in Colombian patients: Findings of 1374 arrays in a seven-year study. *Mol Cytogenet*. 2018;11(1):46. doi:10.1186/s13039-018-0398-9
20. Qian YQ, Fu XY, Wang XQ, et al. A feasible diagnostic approach for the translocation carrier from the indication of products of conception. *Mol Cytogenet*. 2018;11(1):12. doi:10.1186/s13039-018-0362-8
21. Hao M, Li L, Zhang H, Li L, Liu R, Yu Y. The difference between karyotype analysis and chromosome microarray for mosaicism of aneuploid chromosomes in prenatal diagnosis. *Clin Lab Anal*. 2020;34(12): e23514. doi:10.1002/jcla.23514
22. Shi Y, Ma J, Xue Y, Wang J, Yu B, Wang T. The assessment of combined karyotype analysis and chromosomal microarray in pregnant women of advanced maternal age: A multicenter study. *Ann Transl Med*. 2019;7(14):318–318. doi:10.21037/atm.2019.06.63
23. Sun W, Su J, Liu T, et al. Comparison of performance of two prenatal diagnostic techniques for the detection of chromosomal mosaicisms in amniocytes [in Chinese]. *Zhonghua Yi Xue Yi Chuan Xue Za Zhi*. 2022;39(8):842–847. doi:10.3760/cma.j.cn511374-20210427-00367
24. Ganapathi M, Nahum O, Levy B. Prenatal diagnosis using chromosomal SNP microarrays. *Methods Mol Biol*. 2019;1885:187–205. doi:10.1007/978-1-4939-8889-1_13
25. Mi X, Shen X, Zhang S. Application value of chromosome microarray analysis for prenatal diagnosis of fetus with ultrasonic abnormalities [in Chinese]. *Zhonghua Yi Xue Yi Chuan Xue Za Zhi*. 2020;37(1):67–70. doi:10.3760/cma.j.issn.1003-9406.2020.01.018
26. Brun S, Pennamen P, Mattuizzi A, et al. Interest of chromosomal microarray analysis in the prenatal diagnosis of fetal intrauterine growth restriction. *Prenat Diagn*. 2018;38(13):1111–1119. doi:10.1002/pd.5372
27. Xiang J, Ding Y, Song X, et al. Clinical utility of SNP array analysis in prenatal diagnosis: A cohort study of 5000 pregnancies. *Front Genet*. 2020;11:571219. doi:10.3389/fgene.2020.571219
28. Fang Y, Wang G, Gu L, et al. Application of karyotype analysis combined with BACs-on-Beads for prenatal diagnosis. *Exp Ther Med*. 2018; 16(4):2895–2900. doi:10.3892/etm.2018.6574
29. Kantor V, Jelsema R, Xu W, et al. Non-invasive prenatal screening for fetal triploidy using single nucleotide polymorphism-based testing: Differential diagnosis and clinical management in cases showing an extra haplotype. *Prenat Diagn*. 2022;42(8):994–999. doi:10.1002/pd.6169
30. Qu S, Wang L, Cai A, et al. Exploring the cause of early miscarriage with SNP-array analysis and karyotyping. *J Matern Fetal Neonatal Med*. 2019;32(1):1–10. doi:10.1080/14767058.2017.1367379
31. Zou Z, Huang L, Lin S, He Z, Luo Y. Unusual twinning: Additional findings during prenatal diagnosis of twin zygosity by single nucleotide polymorphism (SNP) array. *Prenat Diagn*. 2018;38(6):428–434. doi:10.1002/pd.5255
32. Fu F, Deng Q, Lei T ying, et al. Clinical application of SNP array analysis in fetuses with ventricular septal defects and normal karyotypes. *Arch Gynecol Obstet*. 2017;296(5):929–940. doi:10.1007/s00404-017-4518-2
33. Guo YL, Wang L, Xue SW, et al. Application of single nucleotide polymorphism array in prenatal diagnosis for fetuses with abnormal ultrasound findings [in Chinese]. *Zhonghua Fu Chan Ke Za Zhi*. 2018;53(7):464–470. doi:10.3760/cma.j.issn.0529-567x.2018.07.005
34. Xue S, Wang L, Wei J, Liu Y, Ding G, Dai P. Clinical application of single nucleotide polymorphism microarray analysis in pregnancy loss in Northwest China. *Front Genet*. 2023;14:1319624. doi:10.3389/fgene.2023.1319624
35. Cai M, Lin N, Su L, et al. Prenatal diagnosis of 22q11.2 copy number abnormalities in fetuses via single nucleotide polymorphism array. *Mol Biol Rep*. 2020;47(10):7529–7535. doi:10.1007/s11033-020-05815-7
36. Jansen FAR, Hoffer MJV, Van Velzen CL, et al. Chromosomal abnormalities and copy number variations in fetal left-sided congenital heart defects. *Prenat Diagn*. 2016;36(2):177–185. doi:10.1002/pd.4767
37. Chen X, Li H, Chen C, et al. Genome-wide array analysis reveals novel genomic regions and candidate gene for intellectual disability. *Mol Diagn Ther*. 2018;22(6):749–757. doi:10.1007/s40291-018-0358-4

IGF2BP2-mediated m^{6}A modifies SLC7A11 to regulate proliferation and ferroptosis in non-small cell lung cancer cells

*Bo Li[1,A,D-F], *Si-Ying Li[2,A,D–F], Yi-Chao Yan[3,A–F]

[1] Department of Thoracic Surgery, Yingkou Central Hospital, China
[2] Department of Medical Oncology, Yingkou Central Hospital, China
[3] Department of Gastroenterological Surgery, Peking University International Hospital, Beijing, China

A – research concept and design; B – collection and/or assembly of data; C – data analysis and interpretation;
D – writing the article; E – critical revision of the article; F – final approval of the article

Advances in Clinical and Experimental Medicine, ISSN 1899–5276 (print), ISSN 2451–2680 (online) *Adv Clin Exp Med*. 2025;34(11):1937–1946

Address for correspondence
Yi-Chao Yan
E-mail: 18810057399@126.com

Funding sources
None declared

Conflict of interest
None declared

*Si-Ying Li and Bo Li contributed equally to this work.

Received on July 30, 2024
Reviewed on August 28, 2024
Accepted on January 28, 2025

Published online on April 24, 2025

Abstract

Background. Insulin-like growth factor 2 mRNA-binding protein 2 (IGF2BP2) is implicated in various cancers, but its role in modulating ferroptosis and tumor cell behavior in non-small cell lung cancer (NSCLC) remains unclear.

Objectives. This study aimed to investigate how IGF2BP2-mediated N6-methyladenosine (m^{6}A) modification of solute carrier family 7 member 11 (SLC7A11) affects ferroptosis and NSCLC cell viability.

Materials and methods. NSCLC H1299 cells were transfected with either IGF2BP2 or SLC7A11 plasmids and corresponding siRNAs. Expression levels of IGF2BP2, SLC7A11 and ferroptosis markers were analyzed using reverse transcription real-time quantitative polymerase chain reaction (RT-qPCR) and western blot. Cell viability was assessed using the Cell Counting Kit-8 (CCK-8) assay. Reactive oxygen species (ROS) and lipid peroxidation levels were measured with flow cytometry and biochemical kits. The RNA immunoprecipitation (RIP) and mRNA stability assays were utilized to explore the interaction between IGF2BP2 and SLC7A11.

Results. IGF2BP2 expression was significantly upregulated in H1299 cells. Overexpression of IGF2BP2 enhanced cell viability and decreased ferroptosis, whereas its knockdown resulted in reduced cell viability and increased ferroptotic activity. IGF2BP2 enhanced SLC7A11 mRNA stability through m^{6}A modification, and SLC7A11 overexpression reversed the effects of IGF2BP2 knockdown. This interaction increased cell viability and reduced ROS and lipid peroxidation.

Conclusions. IGF2BP2 plays a critical role in NSCLC by stabilizing SLC7A11 mRNA via m^{6}A modification, promoting cell proliferation and suppressing ferroptosis. Targeting the IGF2BP2–SLC7A11 axis may offer a promising therapeutic strategy for NSCLC.

Key words: non-small cell lung cancer, SLC7A11, ferroptosis, IGF2BP2, m^{6}A modification

Cite as
Li B, Li SY, Yan YC. IGF2BP2-mediated m^{6}A modifies SLC7A11 to regulate proliferation and ferroptosis in non-small cell lung cancer cells. *Adv Clin Exp Med*. 2025;34(11):1937–1946. doi:10.17219/acem/200588

DOI
10.17219/acem/200588

Highlights

- IGF2BP2 enhances non-small cell lung cancer (NSCLC) cell proliferation by stabilizing SLC7A11 mRNA through m6A modification, promoting ferroptosis resistance.
- Overexpression of IGF2BP2 boosts SLC7A11 levels, reducing oxidative stress markers and ferroptosis indicators.
- IGF2BP2 stabilizes SLC7A11 mRNA, aiding in the maintenance of redox homeostasis and metabolic reprogramming in cancer cells.
- IGF2BP2 knockdown leads to increased ferroptosis and decreased cell viability, suggesting its potential as a therapeutic target.
- Targeting the IGF2BP2-SLC7A11 axis may provide novel therapeutic strategies for improving clinical outcomes in NSCLC.

Background

Non-small cell lung cancer (NSCLC), the most prevalent form of lung cancer, constitutes nearly 85% of lung cancer diagnoses. Besides, NSCLC is characterized by a complex interplay of genetic and metabolic factors that contribute to lung cancer progression and resistance to treatment.[1] Insulin-like growth factor 2 mRNA-binding protein 2 (IGF2BP2) is pivotal in the context of NSCLC, serving as a regulatory protein related to cancer biology due to its effects on cellular proliferation, metabolism and survival.[2]

IGF2BP2 exerts its biological functions primarily by binding to the mRNAs of various genes, thereby regulating their stability and translation.[3] As a critical target of IGF2BP2, solute carrier family 7 member 11 (SLC7A11) is a crucial transporter in the cellular antioxidant system that maintains intracellular glutathione levels.[4,5] Ferroptosis, a regulated cell death process induced by oxidative stress and characterized by lipid peroxidation, has attracted growing attention in cancer research due to its potential as a therapeutic target.[6] SLC7A11 acts greatly in preventing ferroptosis via promoting the uptake of cystine, which is essential for glutathione synthesis. Glutathione serves as a crucial antioxidant, safeguarding cells against lipid peroxidation and oxidative damage. The capability of cancer cells to evade ferroptosis through metabolic alterations, including the upregulation of glutaminolysis, is considered a hallmark of cancer cell survival and proliferation.[7] The conversion of glutamine into α-ketoglutarate was conducted through this metabolic pathway, thereby fueling the tricarboxylic acid cycle. Additionally, such a pathway is often enhanced in cancer to meet the increased demands of rapidly dividing cells and contribute to the perturbation of redox balance.[8,9] Given the importance of SLC7A11 in maintaining redox homeostasis and preventing ferroptosis, it was specifically chosen for this study.

Objectives

In this context, the present study was designed to elucidate the roles of IGF2BP2 and SLC7A11 in regulating the fate of NSCLC cells, with a particular focus on their contributions to cell viability and resistance to ferroptosis.

We hypothesized that IGF2BP2 was upregulated in NSCLC cells and this upregulation confers a growth advantage through the stabilization of SLC7A11 mRNA, enhanced antioxidant defense and metabolic shifts favoring cell survival.[10–12] The purpose of this study was to explain the regulatory functions of IGF2BP2, examining its impact on the post-transcriptional control of critical genes and its broader effects on the NSCLC cell's metabolic state.

Materials and methods

Cell culture and transfection

Normal human bronchial epithelial (HBE) cells (CRL-2741) and NSCLC H1299 cells (CRL-5803) were provided by the American Type Culture Collection (ATCC; Manassas, USA). The culture of HBE cells and H1299 cells was conducted in Dulbecco's modified Eagle's medium (DMEM)/Nutrient Mixture F-12 medium (cat. No. #11320033; Gibco, Waltham, USA) and Roswell Park Memorial Institute (RPMI) 1640 medium (cat. No. #11875093; Gibco), respectively. Both media contained 1% penicillin/streptomycin (cat. No. #15140122; Gibco) as well as 10% fetal bovine serum (FBS; cat. No. #10082147; Gibco). Cells were incubated at 37°C in a humidified atmosphere containing 5% CO_2.

For transfection, H1299 cells were seeded into 6-well plates to reach 70–80% confluency. Transfections were performed using Lipofectamine 2000 (cat. No. #11668019; Invitrogen, Waltham, USA) according to the manufacturer's instructions. The following experimental groups were established:

SLC7A11 group: transfected with SLC7A11 pcDNA3.1 plasmid; IGF2BP2 group: transfected with IGF2BP2 pcDNA3.1 plasmid; Vector group: transfected with empty vector (control for plasmid transfection); si-IGF2BP2 group: transfected with siRNA targeting IGF2BP2 (sense: 5'-GGGACCAAGAUAACAAUCUTT-3', anti-sense: 5'-AGAUUGUUAUCUUGGUCCCTT-3');

si-NC group: transfected with negative control siRNA (5'-CAACAAGAUGAAGAGCACCAA-3', anti-sense: 5'-UUGGUGCUCUUCAUCUUGUUG-3'; 100 nM final concentration).

For each group, the corresponding controls (empty vector or negative control siRNA) were included to ensure the specificity of the observed effects. Cells were harvested 48 h post-transfection for further analysis. Sangon Biotech Co., Ltd. (Shanghai, China) was responsible for designing and synthesizing the aforementioned plasmids, and the siRNA fragments were provided by GenePharma (Shanghai, China).

RT-qPCR

TRIzol reagent (cat. No. #15596018; Invitrogen) was utilized for extracting total RNA from cells according to the manufacturer's protocol. A NanoDrop spectrophotometer (Thermo Fisher Scientific, Waltham, USA) was adopted to assess the quantity and quality of RNA. Besides, as described by the manufacturer's guidelines, the synthesis of cDNA was conducted using total RNA (1 μg) through the High-Capacity cDNA Reverse Transcription Kit (cat. No. #4368814; Applied Biosystems, Waltham, USA). Reverse transcription real-time quantitative polymerase chain reaction (RT-qPCR) was performed using SYBR Green PCR Master Mix (cat. No. #4309155; Applied Biosystems) on a QuantStudio 5 Real-Time PCR System (Applied Biosystems). Primer sequences applied were as follows:

IGF2BP2:
Reverse 5'-TGGTAGGTGGTCTCGGTGTT-3',
Forward 5'-AGAAGATGTGGAGGAGGCTT-3';

GAPDH (internal control):
Reverse 5'-GAAGATGGTGATGGGATTTC-3',
Forward 5'-GAAGGTGAAGGTCGGAGTC-3';

SLC7A11:
Reverse 5'-AGACTCCCCTCAGTAAAGTGAC-3',
Forward 5'-TCTCCAAAGGAGGTTACCTGC-3'.

Relative gene expression was analyzed using the $2^{-\Delta\Delta Ct}$ method, with GAPDH served as the internal control to normalize the results.

Western blot

Cell were lysed with ice-cold radioimmunoprecipitation assay (RIPA) buffer (cat. No. #R0278; Sigma-Aldrich, St. Louis, USA) supplemented with phosphatase inhibitors (cat. No. #P0044; Sigma-Aldrich) as well as protease (cat. No. #P8340; Sigma-Aldrich). Protein concentrations were measured using the Bicinchoninic Acid (BCA) Protein Assay Kit (cat. No. #23225; Pierce, Rockford, USA). Proteins (30 μg) were separated on 10% sodium dodecyl sulfate-polyacrylamide gel electrophoresis (SDS-PAGE) and transferred to polyvinylidene fluoride (PVDF) membranes (cat. No. #IPVH00010; MilliporeSigma, St. Louis, USA). Membranes were blocked with 5% skimmed milk for 1 h at room temperature and incubated overnight at 4°C with the following primary antibodies: IGF2BP2 (cat. No. #14672S, 1:1,000; Cell Signaling Technology (CST), Danvers, USA), SLC7A11 (cat. No. #ab175186, 1:1,000; Abcam, Cambridge, UK), GPX4 (cat. No. #ab125066, 1:1,000; Abcam), β-actin (cat. No. #A1978, 1:5,000; Sigma-Aldrich), and Acyl-CoA synthetase long-chain family member 4 (ACSL4) (cat. No. #ab155282, 1:1,000; Abcam). Upon rinsing, the membranes were subjected to 1-h incubation with horseradish peroxidase (HRP)-conjugated secondary antibodies (cat. No. #NA931, 1:5,000 for anti-rabbit; cat. No. #NA934, 1:5,000 for anti-mouse; GE Healthcare, Chicago, USA) at ambient temperature. Visualization of the protein bands was achieved using the SuperSignal West Pico PLUS Chemiluminescent Substrate (cat. No. #34580; Thermo Fisher Scientific), followed by imaging on a ChemiDoc XRS+ system (Bio-Rad, Hercules, USA).

Cell viability assay

Cells (5×10^3 cells/well) were seeded into 96-well plates and allowed to adhere overnight. Following treatments, 100 μL of fresh medium containing MTT reagent (0.5 mg/mL, cat. No. #M2128; Sigma-Aldrich) was added and incubated for 4 h. The formazan crystals were dissolved in 100 μL of dimethyl sulfoxide. A microplate reader (Bio-Tek; Winooski, USA) was utilized for measuring the absorbance at 570 nm, with a reference wavelength of 690 nm. Untreated cells served as a control for baseline viability.

ROS detection

The DCFDA Cellular ROS Detection Assay Kit (cat. No. #ab113851; Abcam) was employed for detecting the intracellular ROS levels. Cells (1×10^4 cells/well) were planted in a 96-well plate for cultivation until reaching 70–80% confluency. Upon rinsing with phosphate-buffered saline (PBS), cells was incubated with 25 μM DCFDA in a serum-free medium for 45 min at 37°C in the dark. Fluorescence intensity was measured using a microplate reader (Bio-Tek; excitation: 485 nm, emission: 535 nm). Negative controls (untreated cells) were used to set the baseline fluorescence levels.

Measurement of malondialdehyde and Fe^{2+} levels

Following treatments, the collected cells were rinsed with pre-cooled PBS. Upon centrifugation (3,000 rpm, 4°C, 15 min), the supernatant was collected to assess the levels of Fe^{2+} and malondialdehyde (MDA) using the Iron Assay Kit (cat. No. 3100865; Sigma-Aldrich) and MDA Assay Kit (cat. No. MAK085; Sigma-Aldrich), respectively, as per the manufacturer's protocols. Control samples were prepared from untreated cells to establish baseline levels of Fe^{2+} and MDA.

RNA immunoprecipitation assay

The association between IGF2BP2 and SLC7A11 mRNA was examined using the Magna RIP RNA-Binding Protein Immunoprecipitation Kit (cat. No. #17-700; MilliporeSigma). Cell lysates were incubated with magnetic beads conjugated to anti-IGF2BP2 antibody or normal mouse immunoglobulin G (IgG) (negative control) overnight at 4°C. After incubation, the beads were washed and the RNA was eluted from the beads. Following RNA extraction from the immunoprecipitate, SLC7A11 mRNA levels were measured with RT-qPCR as described previously. An IgG control was included to confirm the specificity of the interaction.

mRNA decay assay

To determine mRNA stability, cells were treated with actinomycin D (5 μg/mL, cat. No. #A9415; Sigma-Aldrich) to suppress RNA synthesis. Samples were collected at 0, 2, 4, 8, and 24 h post-treatment. Total RNA was extracted as previously detailed, and SLC7A11 mRNA levels were quantified with RT-qPCR. The decay rates were calculated by normalizing mRNA levels to the amount at time 0. Non-treated cells served as a control for baseline mRNA stability.

Statistical analyses

Data were analyzed using IBM SPSS v. 23.0 (IBM Corp., Armonk, USA). Results were presented as median with interquartile range (IQR) or mean ± standard deviation (SD). The specific statistical test used was determined based on the data distribution and the number of groups compared.

Due to the small sample size ($n < 10$ per group), nonparametric tests were primarily employed to ensure robust statistical analysis. For comparisons between 2 groups, the Mann–Whitney U test was used. For multiple group comparisons, the Kruskal–Wallis test was applied, followed by Dunn's post hoc test with Bonferroni correction to identify specific differences between groups.

For experiments involving repeated measurements (e.g., measurements taken at multiple time points for the same group), the Friedman's test, a nonparametric alternative to repeated-measures analysis of variance (ANOVA), was performed to evaluate overall differences within each group over time. For post hoc pairwise comparisons between time points, Wilcoxon signed-rank tests were applied with Bonferroni correction for multiple comparisons. For comparisons between groups at the final time point, the Kruskal–Wallis test was performed, followed by Dunn's post hoc test to identify specific between-group differences. A 2-tailed $p < 0.05$ was considered statistically significant for all analyses.

Results

The IGF2BP2 expression is increased in NSCLC H1299 cells

As demonstrated in a previous study, IGF2BP2 expression is elevated in NSCLC, and its overexpression promotes tumor growth and metastasis.[13] Therefore, the differential expression between H1299 cells and HBE cells was first examined. The RT-qPCR findings displayed a remarkable increase in the IGF2BP2 mRNA expression in H1299 cells in comparison with normal HBE cells ($U = 0$, $p = 0.002$). The western blot analysis further verified that the IGF2BP2 protein expression was higher in H1299 cells ($U = 0$, $p = 0.002$) (Fig. 1). These outcomes revealed a marked upregulation of IGF2BP2 expression in H1299 cells, suggesting that IGF2BP2 had a potential function in H1299 cells.

Effects of IGF2BP2 knockdown and overexpression on H1299 cell viability

We further investigated the role of IGF2BP2 in the H1299 cell by knocking down and overexpressing IGF2BP2. According to the analyses of western blot and RT-qPCR, the IGF2BP2 expression levels were evidently raised in the IGF2BP2 group compared to the vector group, while the si-IGF2BP2 group presented a notable reduction in the IGF2BP2 protein expression relative to the si-NC group (mRNA: $H(3, 24) = 19.53$, $p < 0.001$; Protein: $H(3, 24) = 19.55$, $p < 0.001$) (Fig. 2A,B). These findings indicated that we successfully

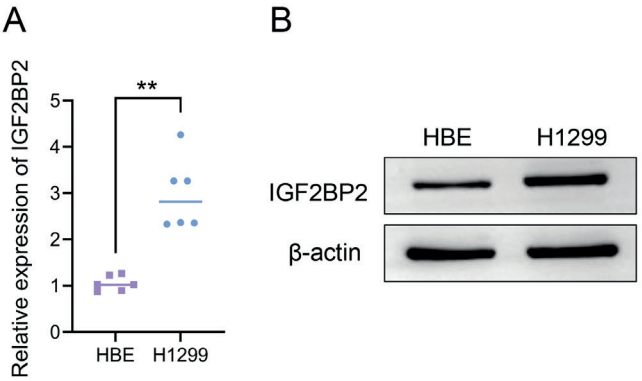

Fig. 1. The IGF2BP2 expression is increased in NSCLC H1299 cells. A. RT-qPCR analysis of IGF2BP2 mRNA levels in HBE and H1299 cells; statistical significance was determined using Mann–Whitney U test; B. Relative protein expression of IGF2BP2 in HBE cells and H1299 cells using western blot; Mann–Whitney U test; **$p < 0.01$

RT-qPCR – reverse transcription real-time quantitative polymerase chain reaction; HBE – human bronchial epithelial; IGF2BP2 – insulin-like growth factor 2 mRNA-binding protein 2.

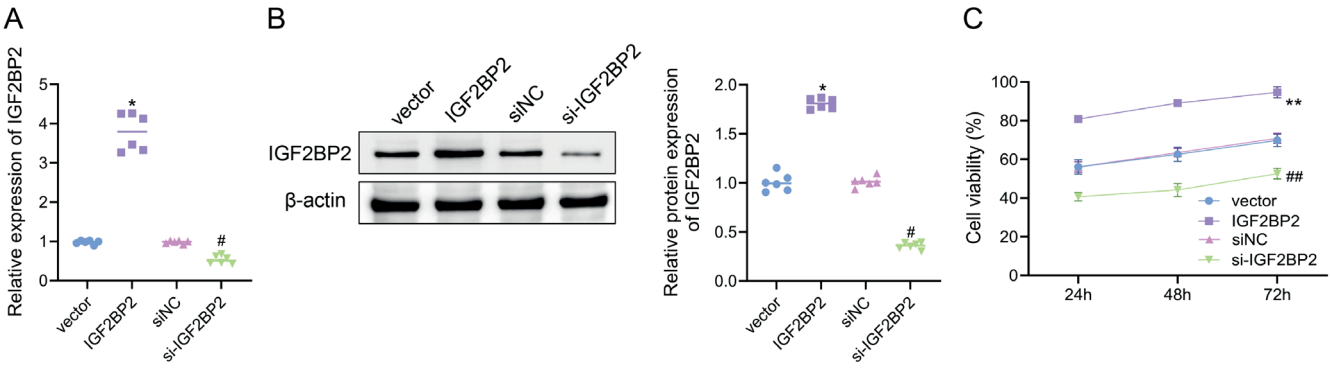

Fig. 2. Effects of IGF2BP2 knockdown and overexpression on H1299 cell viability. A. RT-qPCR analysis of IGF2BP2 mRNA expression; statistical significance was determined using Kruskal–Wallis test; B. Western blot analysis of IGF2BP2 protein levels; One-way analysis of variance (ANOVA) with Dunnett's T3 test; C. Cell viability; Friedman's test assessed within-group differences over time, followed by Wilcoxon signed-rank test for time-point comparisons, while the Kruskal–Wallis test was used for between-group comparisons at 72 h; *p < 0.05; **p < 0.01; IGF2BP2 group vs vector group; #p < 0.05, ##p< 0.01

si-IGF2BP2 group vs siNC group; RT-qPCR – reverse transcription real-time quantitative polymerase chain reaction; IGF2BP2 – insulin-like growth factor 2 mRNA-binding protein 2.

overexpressed and knocked down IGF2BP2 in H1299 cells. The enhancement or suppression of cell viability in H1299 cells was associated with IGF2BP2 overexpression or knockdown, respectively. As disclosed in the findings from cell viability assay, we observed significant changes in cell viability within each group over time (vector group: $\chi^2 = 12$, degrees of freedom (df) = 2, p = 0.002; IGF2BP2 group: $\chi^2 = 10.33$, df = 2, p = 0.006; si-NC group: $\chi^2 = 12$, df = 2, p = 0.002; si-IGF2BP2 group: $\chi^2 = 12$, df = 2, p = 0.002). Post hoc Wilcoxon signed-rank tests revealed that cell viability significantly increased between 24 h and 72 h in each group (p < 0.01). At the final time point (72 h), IGF2BP2 overexpression in H1299 cells significantly increased cell viability, whereas IGF2BP2 knockdown notably reduced it (H (3, 24) = 19.47, p < 0.001) (Fig. 2C). These findings suggested that IGF2BP2 promoted the H1299 cell proliferation.

Different effects of IGF2BP2 knockdown and overexpression on ferroptosis in H1299 cells

The accumulation of lipid peroxidation and reactive oxygen species (ROS) leads to ferroptosis, a form of iron-dependent cell death.[14] Therefore, further exploration was conducted on the impacts of IGF2BP2 knockdown and overexpression on ferroptosis-related markers in H1299 cells. Figure 3A shows that, as opposed to the vector group, ROS levels were considerably declined in the IGF2BP2 overexpression group, while ROS levels were evidently raised in the IGF2BP2 knockdown group (H(3, 24) = 19.46, p < 0.001). No statistical difference were observed between the vector and siNC groups (p > 0.05) (Fig. 3A). Similarly, Fe^{2+} (H(3, 24) = 19.74, p < 0.001) and MDA (H(3, 24) = 19.56, p < 0.001), indicators of iron accumulation and lipid peroxidation, were significantly lower in the IGF2BP2 group and markedly higher in the si-IGF2BP2 group (Fig. 3B,C). ACSL4, a key inducer of ferroptosis,[15] and GPX4, an antioxidant enzyme that scavenges ROS and whose inhibition promotes ferroptosis,[16] were also upregulated.

IGF2BP2 overexpression considerably increased GPX4 protein expression and decreased ACSL4 levels in H1299 cells. Conversely, IGF2BP2 knockdown markedly decreased the GPX4 protein expression (H (3, 24) = 19.50, p < 0.001) and increased ACSL4 expression (H (3, 24) = 19.61, p < 0.001) (Fig. 3D,E). These outcomes indicated that downregulation of IGF2BP2 could evidently enhance ferroptosis in H1299 cells.

IGF2BP2 modulates SLC7A11 expression through m^{6}A modification

SLC7A11 is a key regulator of ferroptosis; its inhibition induces ferroptosis and suppresses tumor growth.[17,18] We first verified the difference in SLC7A11 expression between normal and cancer cells. In contrast to HBE cells, the SLC7A11 protein expression level was remarkably raised in H1299 cells (U = 0, p = 0.002) (Fig. 4A). In H1299 cells, SLC7A11 protein levels were increased in the IGF2BP2 overexpression group and decreased in the si-IGF2BP2 group (H (3, 24) = 19.45, p < 0.001) (Fig. 4B). The RNA immunoprecipitation assays confirmed an interaction between IGF2BP2 and SLC7A11 mRNA in H1299 cells (U = 0 p = 0.002), with the m^{6}A modification levels of SLC7A11 mRNA being higher in the IGF2BP2 group and lower in the si-IGF2BP2 group (H (3, 24) = 19.61, p < 0.001) (Fig. 4C,D). RNA stability assays demonstrated a time-dependent decrease in SLC7A11 mRNA expression across all groups ($\chi^2 = 18$, df = 3, p < 0.001 for all groups). Post hoc Wilcoxon signed-rank tests showed significant differences in SLC7A11 mRNA levels between 0 h and 4 h (p = 0.044), as well as between 0 h and 6 h (p < 0.001), across all groups. At the final time point (6 h), the SLC7A11 mRNA levels were elevated in the IGF2BP2 group and dropped in the si-IGF2BP2 group (H (3, 24) = 18.81, p < 0.001), indicating that IGF2BP2 regulated the stability of SLC7A11 mRNA (Fig. 4E). Overall, IGF2BP2 promoted SLC7A11 expression through m^{6}A modification in H1299 cells.

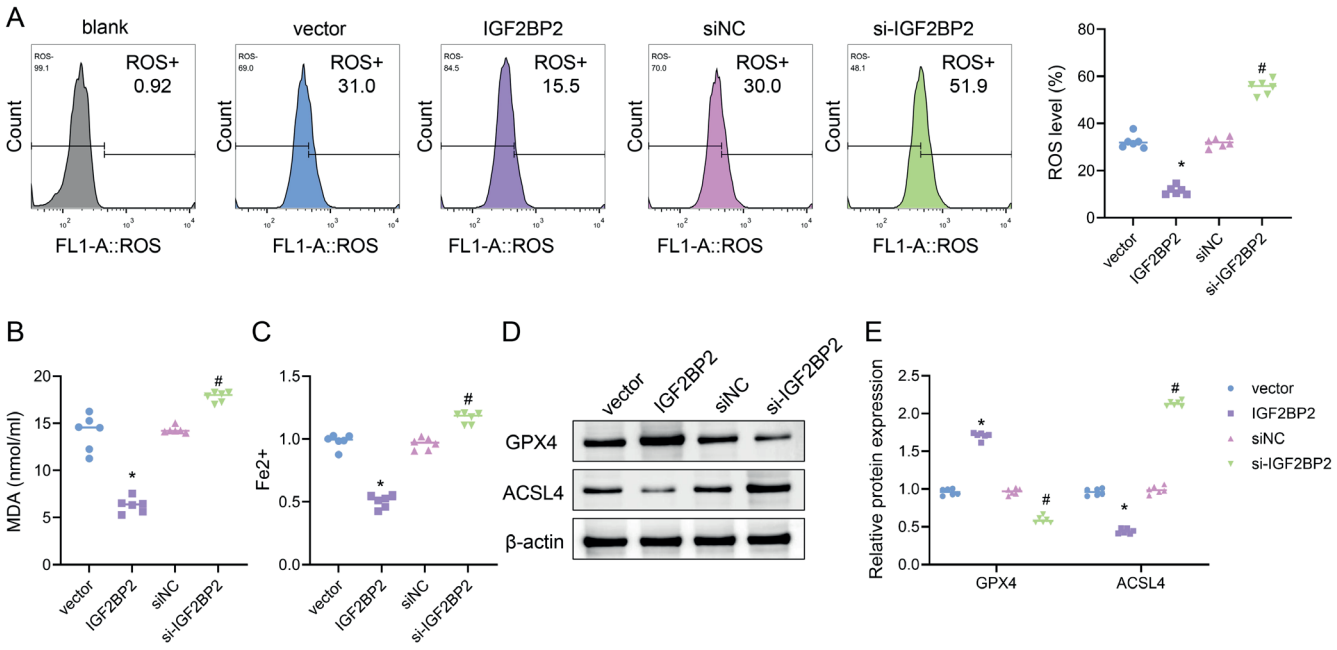

Fig. 3. Different effects of IGF2BP2 knockdown and overexpression on ferroptosis markers in H1299 cells. A. ROS levels; B. MDA level; C. Fe^{2+} level; D. Western blot measurements of the ferroptosis markers GPX4 and ACSL4; E. Relative expression of GPX4 and ACSL4. Statistical significance was determined using Kruskal–Wallis test

*p < 0.05, IGF2BP2 group vs vector group; #p < 0.05, si-IGF2BP2 group vs siNC group. ROS – reactive oxygen species; MDA – malondialdehyde; GPX4 – glutathione peroxidase 4; ACSL4 – Acyl-CoA synthetase long-chain family member 4; IGF2BP2 – insulin-like growth factor 2 mRNA-binding protein 2.

IGF2BP2 regulates cell proliferation and ferroptosis in a SLC7A11-dependent manner

Based on the results presented above, we hypothesized that IGF2BP2 promotes SLC7A11 expression through m^6A modification, thereby moderating ferroptosis and cell proliferation. To test this hypothesis, SLC7A11 was overexpressed in H1299 cells following IGF2BP2 knockdown. Initially, we transfected the SLC7A11 plasmid in H1299 cells. Our results suggested that SLC7A11 protein expression was notably raised in H1299 cells transfected with the SLC7A11 plasmid compared to the vector group, indicating successful overexpression (Supplementary Fig. 1).

As illustrated in Fig. 5A, a remarkable elevation in cell viability was observed over time in all groups (si-NC + vector group: $\chi^2 = 10.33$, df = 2, p = 0.006; si-IGF2BP2 + vector group: $\chi^2 = 12$, df = 2, p = 0.002; si-IGF2BP2 + SLC7A11 group: $\chi^2 = 12$, df = 2, p = 0.002). Post hoc Wilcoxon signed-rank tests indicated significant differences in cell viability between 24 h and 72 h across all groups (p < 0.01). At the final time point (72 h), cell viability was markedly decreased by IGF2BP2 knockdown as opposed to the siNC + vector group, while the SLC7A11 + si-IGF2BP2 group of H1299 cells exhibited an upward trend in cell viability relative to the si-IGF2BP2 + vector group (H (2, 18) = 13.93, p = 0.001). Correspondingly, the ROS levels were markedly raised in the si-IGF2BP2 + vector group, while a notable decline was disclosed in ROS levels in the si-IGF2BP2 + SLC7A11 group (H (2, 18) = 14.36, p < 0.001) (Fig. 5B). Additionally, the si-IGF2BP2 + vector group illustrated a notable elevation in the MDA (H (2, 18) = 14.00, p < 0.001) and Fe^{2+} (H (2, 18) = 14.78, p < 0.001) levels. However, the si-IGF2BP2 + SLC7A11 group presented a marked downward trend in the MDA and Fe^{2+} levels (Fig. 5C,D).

At the protein level, the si-IGF2BP2 + vector group displayed a remarkable downregulation of SLC7A11 and GPX4 and an upregulation of ACSL4 as opposed to the siNC + vector group. However, these changes were remarkably reversed in the si-IGF2BP2 + SLC7A11 group, with upregulation of SLC7A11 (H (2, 18) = 13.35, p < 0.001) and GPX4 (H (2, 18) = 14.75, p < 0.001) and downregulation of ACSL4 (H (2, 18) = 14.36, p < 0.001) (Fig. 5E,F). These outcomes implied that SLC7A11 overexpression reversed the impacts of IGF2BPP2 knockdown on the ferroptosis pathway.

Discussion

A comprehensive study elucidated that IGF2BP2 facilitates a shift in cancer cell metabolism towards glutaminolysis through the post-transcriptional upregulation of SLC7A11, thereby fundamentally contributing to the progression of NSCLC. This metabolic adaptation not only meets the energy and biosynthetic demands of NSCLC cells but also equips them with the ability to counteract oxidative stress, thereby effectively hindering ferroptosis. The elevated levels of IGF2BP2 observed in NSCLC cells are associated with increased cell viability and proliferation, suggesting that IGF2BP2 coordinates the cellular

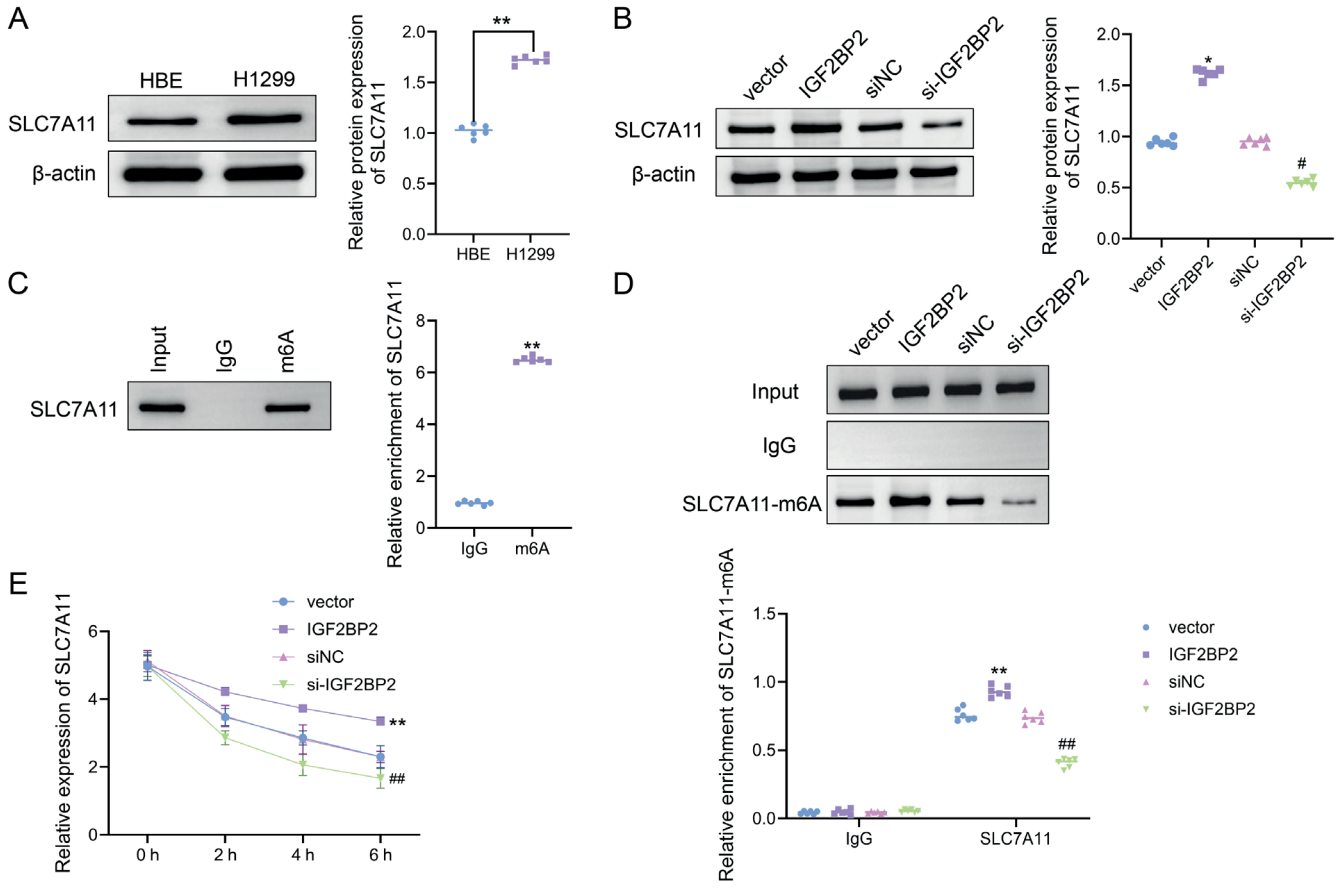

Fig. 4. IGF2BP2 modulates SLC7A11 expression through m^{6}A modification. A. Relative protein expression of SLC7A11 in HBE cells and H1299 cells; statistical significance was determined using Mann–Whitney U test; **p < 0.01, HBE group vs H1299 group; B. Relative protein expression of SLC7A11 in both the overexpression and knockdown of IGF2BP2 in H1299 cells. Statistical significance was determined using Kruskal–Wallis test; *p < 0.05, IGF2BP2 group vs vector group; #p < 0.05, si-IGF2BP2 group vs siNC group; C. The quantification of SLC7A11 mRNA enrichment in H1299 cells subjected to different transfections using RIP assays; statistical significance was determined using Mann–Whitney U test; **p < 0.01; IGF2BP2 group vs IgG group; D. The analysis of changes in m^{6}A modification of SLC7A11 mRNA in H1299 cells subjected to diverse transfection conditions using RIP assays; Kruskal–Wallis test; E. RT-qPCR was used to observe the mRNA decay assay. Friedman's test assessed within-group differences over time, followed by Wilcoxon signed-rank test for time-point comparisons, while the Kruskal–Wallis test was used for between-group comparisons at 6 h; **p < 0.01, IGF2BP2 group vs vector group; ##p < 0.01; si-IGF2BP2 group vs siNC group

SLC7A11 – solute carrier family 7 member 11; HBE – human bronchial epithelial; IGF2BP2 – insulin-like growth factor 2 mRNA-binding protein 2; RIP – RNA immunoprecipitation; RT-qPCR – reverse transcription real-time quantitative polymerase chain reaction ; IgG – immunoglobulin G.

response to the oncogenic stress environments. These outcomes highlight the significance of IGF2BP2 as a therapeutic target and biomarker in NSCLC, which is central to cancer survival, growth and malignant behavior.[19–21]

Further study on the role of IGF2BP2 in NSCLC has positioned it as a potential oncogene, with its upregulation linked to enhanced cell proliferation.[22] Besides, IGF2BP2 is involved in various cancer-promoting pathways, including cell cycle control,[23] evasion of apoptosis[24] and metastasis.[25] In addition, IGF2BP2 has been reported to activate endothelial cells and promote lung adenocarcinoma angiogenesis and metastasis by single-cell sequencing.[26] This aligns with our findings, where we observed that IGF2BP2 promotes NSCLC progression by enhancing cell proliferation and survival, highlighting the role of IGF2BP2 in stabilizing SLC7A11 mRNAs through m^{6}A reading. Furthermore, IGF2BP2 can enhance the colorectal cancer progression by increasing the transferrin receptor expression and promoting iron metabolism.[27] Similarly, our study demonstrated that IGF2BP2 stabilized SLC7A11 mRNA, which was vital for maintaining glutathione levels and protecting against ferroptosis in NSCLC.

To fully understand the oncogenic potential of IGF2BP2, future studies should elucidate its interaction network within cancer cells. This includes identifying its mRNA targets and understanding how IGF2BP2 itself is regulated in the cancer setting. Such endeavors will potentially uncover new therapeutic targets and strategies for NSCLC treatment, offering hope for better treatment of this challenging disease. The regulatory role of IGF2BP2 extends beyond metabolic pathways to include the stabilization of oncogenic mRNAs, such as SLC7A11, which is essential for maintaining redox homeostasis and protecting against ferroptosis.[4] In this study, a significant mechanism in NSCLC pathology was revealed. IGF2BP2 stabilizes SLC7A11 mRNA, which is the core of maintaining cellular

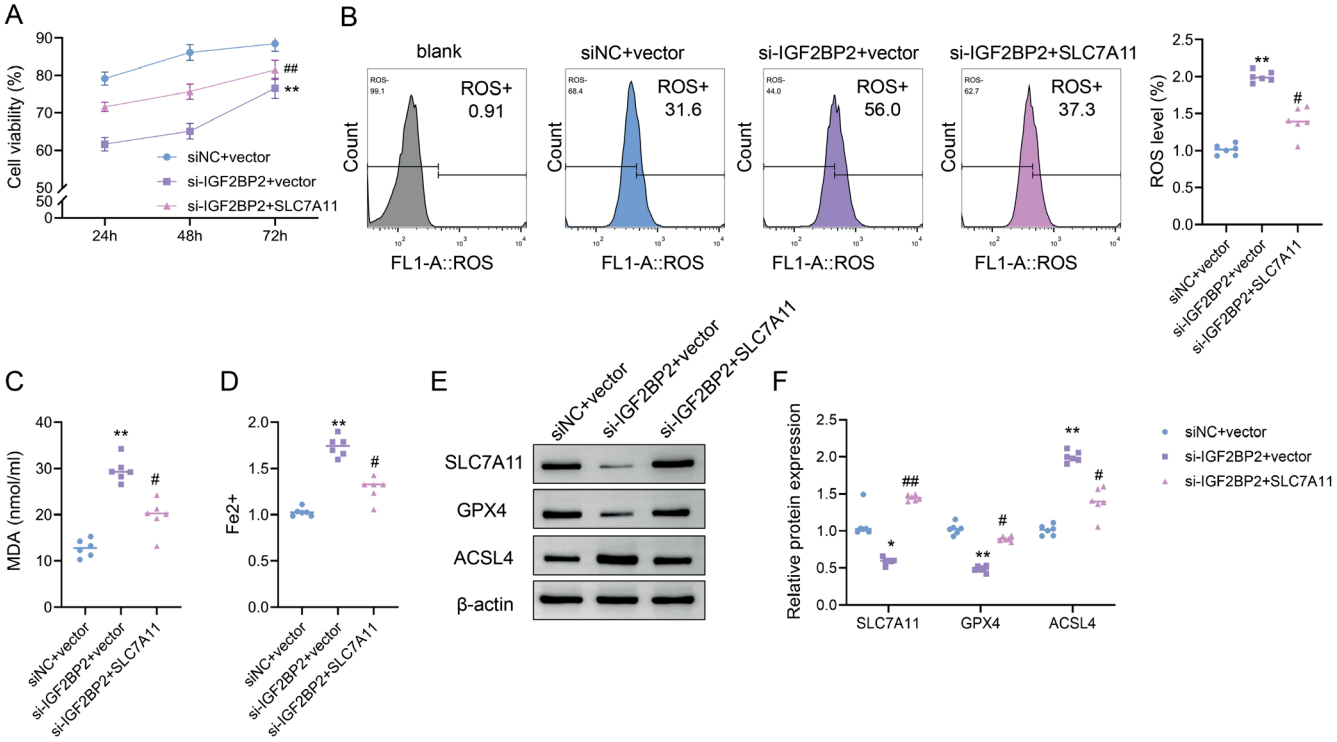

Fig. 5. IGF2BP2 regulates cell proliferation and ferroptosis in a SLC7A11-dependent manner. A. Cell viability; statistical significance was determined using Friedman's test for within-group differences over time, followed by Wilcoxon signed-rank test for time-point comparisons, while the Kruskal–Wallis test was used for between-group comparisons at 72 h; B. ROS levels; C,D. The assay kit results of MDA (C) and Fe^{2+} (D) levels after various transfections; E,F. Relative protein expression of SLC7A11, GPX4 and ACSL4. Statistical significance was determined using Kruskal–Wallis test; *p < 0.05; **p < 0.01; si-IGF2BP2 + vector group vs siNC + vector group; #p < 0.05; ##p < 0.01; si-IGF2BP2 + SLC7A11 group vs si-IGF2BP2 + vector group

ROS – reactive oxygen species; MDA – malondialdehyde; SLC7A11 – solute carrier family 7 member 11; GPX4 – glutathione peroxidase 4; ACSL4 – Acyl-CoA synthetase long-chain family member 4; IGF2BP2 – insulin-like growth factor 2 mRNA-binding protein 2.

redox balance. SLC7A11 ensures the uptake of cystine, which is necessary for glutathione synthesis, enabling cells to withstand oxidative stress and avoid ferroptosis. The effect of IGF2BP2 on SLC7A11 marks a protective mechanism for NSCLC cells, allowing them to thrive in a pro-oxidant tumor microenvironment. The relationship between IGF2BP2 and SLC7A11 suggests that cellular metabolism is closely associated with susceptibility to ferroptosis, potentially reshaping our approach to cancer treatment.

Although this study focused on mRNA stabilization, IGF2BP2 might regulate SLC7A11 through other mechanisms, such as post-translational modifications (like phosphorylation), miRNA interaction and protein-protein interaction.[28–30] In the future, several approaches including phosphoproteomic analysis, miRNA profiling and protein interaction analysis could be employed to further explore these potential mechanisms to comprehensively understand the IGF2BP2's role in regulating SLC7A11.

As is reported, metabolic reprogramming in NSCLC, particularly the shift towards glutaminolysis,[31] is not merely a response to energy demands but a strategic adaptation that confers survival advantages.[32] Through this pathway, NSCLC cells acquire antioxidant capacity by generating nicotinamide adenine dinucleotide phosphate (NADPH), which supports the regeneration of reduced glutathione. The role of IGF2BP2 in this metabolic shift not only supports rapid cell proliferation but also contributes to the cells against ferroptosis.[33] Given this adaptability, targeting metabolic reliance in NSCLC may prove effective, especially when paired with therapies that induce ferroptosis.[34,35] The therapeutic potential of interfering with the IGF2BP2-SLC7A11 interaction and glutaminolysis is substantial. The development of small molecule inhibitors to disrupt this interaction could directly counter the ferroptosis resistance in NSCLC cells. Additionally, targeting glutaminolysis can deplete the metabolic resources of NSCLC cells, making them susceptible to ferroptosis. Such strategies, particularly when combined with existing treatments, can revolutionize NSCLC therapy. The current challenge is to translate these findings into clinical applications, which will involve the development and rigorous testing of targeted pharmacological agents in preclinical and clinical settings. Our findings support a precision medicine approach, suggesting that patient-specific therapies based on the expression of IGF2BP2 and SLC7A11 could enhance treatment outcomes. This study lays a solid foundation for future efforts to conquer NSCLC, highlighting the IGF2BP2–SLC7A11 axis standing as a promising target for novel cancer therapies.

Importantly, this study uncovers a previously unreported regulatory axis where IGF2BP2 stabilizes SLC7A11 mRNA through m^6A reading, providing a novel understanding

of how IGF2BP2 contributes to metabolic adaptation and ferroptosis resistance in NSCLC. This novel mechanism highlights IGF2BP2 as a potential therapeutic target, opening new avenues for developing targeted treatments to improve clinical outcomes in NSCLC.

Limitations

However, certain limitations must be acknowledged. First, we relied on the MTT assay to assess cell viability. However, although this method is efficient and widely accepted, it does not reflect other aspects of cell behavior such as proliferation rate, migration and invasion capabilities. Therefore, further studies incorporating comprehensive assays such as colony formation, migration and invasion are necessary to thoroughly evaluate malignant behavior. Second, this study was conducted primarily in vitro. The use of cell lines may not fully represent the complexity and heterogeneity of tumor behavior in vivo. Moreover, the sample size used in our study was relatively small, which may limit the statistical power and generalizability of the results. Future studies with larger sample sizes will help confirm the robustness of these findings and provide more reliable statistical analysis. Additionally, our study merely offers preliminary data suggesting potential ferroptotic activity and cell proliferation, necessitating additional specific assays to comprehensively confirm ferroptosis. Furthermore, we need to consider the potential compensatory mechanisms that could arise from the inhibition of the IGF2BP2-SLC7A11 axis.[12] Ultimately, although IGF2BP2 has been shown to regulate the stability of SLC7A11 and affect cell viability and ferroptosis, the precise molecular mechanisms and downstream signaling pathways have only been partially elucidated. Comprehensive proteomic and metabolic studies may reveal additional layers of regulation and interaction that contribute to the observed phenotypes. These limitations highlight the importance of future studies with multidimensional approaches, integrating genomic, proteomic and metabolomic data to fully elucidate the role of IGF2BP2 in NSCLC.

Conclusions

IGF2BP2 plays an essential role in NSCLC by modulating m^{6}A modification of SLC7A11 mRNA and enhancing its stability, thereby inhibiting ferroptosis. These findings highlight the therapeutic potential of targeting the IGF2BP2-SLC7A11 axis. Future research should focus on exploring the broader clinical implications, such as the development of small molecule inhibitors or other therapeutic strategies that target this pathway. Additionally, investigating the role of IGF2BP2 in other types of cancers may reveal new insights into its role in cancer progression and ferroptosis regulation, potentially leading to more effective, personalized treatments.

Supplementary data

The supplementary materials are available at https://doi.org/10.5281/zenodo.15074419. The package includes the following files:

Supplementary Fig. 1. Successful overexpression of SLC7A11 in H1299 cells.

Data availability

The datasets generated and/or analyzed during the current study are available from the corresponding author on reasonable request.

Consent for publication

Not applicable.

Use of AI and AI-assisted technologies

Not applicable.

ORCID iDs

Bo Li https://orcid.org/0009-0002-4799-499X
Si-Ying Li https://orcid.org/0009-0001-9653-6410
Yi-Chao Yan https://orcid.org/0000-0002-3816-7610

References

1. Meng X, Xu H, Liang Y, et al. Enhanced CT-based radiomics model to predict natural killer cell infiltration and clinical prognosis in non-small cell lung cancer. *Front Immunol*. 2024;14:1334886. doi:10.3389/fimmu.2023.1334886
2. Zhou Z, Zhang B, Deng Y, et al. FBW7/GSK3β mediated degradation of IGF2BP2 inhibits IGF2BP2-SLC7A5 positive feedback loop and radioresistance in lung cancer. *J Exp Clin Cancer Res*. 2024;43(1):34. doi:10.1186/s13046-024-02959-3
3. Lin CW, Yang WE, Su CW, Lu HJ, Su SC, Yang SF. IGF2BP2 promotes cell invasion and epithelial–mesenchymal transition through Src-mediated upregulation of EREG in oral cancer. *Int J Biol Sci*. 2024;20(3):818–830. doi:10.7150/ijbs.91786
4. Dai Z, Lin B, Qin M, et al. METTL3-mediated m6A modification of SLC7A11 enhances nasopharyngeal carcinoma radioresistance by inhibiting ferroptosis. *Int J Biol Sci*. 2025;21(4):1837–1851. doi:10.7150/ijbs.100518
5. Xu L, Li Q, Wang Y, et al. m6A methyltransferase METTL3 promotes oral squamous cell carcinoma progression through enhancement of IGF2BP2-mediated SLC7A11 mRNA stability. *Am J Cancer Res*. 2021;11(11):5282–5298. PMID:34873461. PMCID:PMC8640804.
6. Zhu F, Ding S, Liu Y, Wang X, Wu Z. Ozone-mediated cerebral protection: Unraveling the mechanism through ferroptosis and the NRF2/SLC7A11/GPX4 signaling pathway. *J Chem Neuroanatom*. 2024;136:102387. doi:10.1016/j.jchemneu.2023.102387
7. Ye J, Jiang X, Dong Z, Hu S, Xiao M. Low-concentration PTX and RSL3 inhibits tumor cell growth synergistically by inducing ferroptosis in mutant p53 hypopharyngeal squamous carcinoma. *Cancer Manag Res*. 2019;11:9783–9792. doi:10.2147/CMAR.S217944
8. Chen C, Wang J, Zhu X, Hu J, Liu C, Liu L. Energy metabolism and redox balance: How phytochemicals influence heart failure treatment. *Biomed Pharmacother*. 2024;171:116136. doi:10.1016/j.biopha.2024.116136
9. Carneiro TJ, Carvalho ALMB, Vojtek M, et al. Disclosing a metabolic signature of cisplatin resistance in MDA-MB-231 triple-negative breast cancer cells by NMR metabolomics. *Cancer Cell Int*. 2023;23(1):310. doi:10.1186/s12935-023-03124-0

10. Wang Z, Wang Y, Shen N, et al. AMPKα1-mediated ZDHHC8 phosphorylation promotes the palmitoylation of SLC7A11 to facilitate ferroptosis resistance in glioblastoma. *Cancer Lett*. 2024;584:216619. doi:10.1016/j.canlet.2024.216619
11. Dang S, Ren Y, Zhao B, et al. Efficacy and safety of warm acupuncture in the treatment of ankylosing spondylitis: A protocol for systematic review and meta-analysis. *Medicine (Baltimore)*. 2021;100(1):e24116. doi:10.1097/MD.0000000000024116
12. Hu N, Hu WH, Zhou SL, et al. SLC7A11 negatively associates with mismatch repair gene expression and endows glioblastoma cells sensitive to radiation under low glucose conditions. *Neoplasma*. 2021; 68(6):1147–1156. doi:10.4149/neo_2021_210327N410
13. Li B, Zhu L, Lu C, et al. circNDUFB2 inhibits non-small cell lung cancer progression via destabilizing IGF2BPs and activating anti-tumor immunity. *Nat Commun*. 2021;12(1):295. doi:10.1038/s41467-020-20527-z
14. Liu P, Wu D, Duan J, et al. NRF2 regulates the sensitivity of human NSCLC cells to cystine deprivation-induced ferroptosis via FOCAD-FAK signaling pathway. *Redox Biol*. 2020;37:101702. doi:10.1016/j.redox.2020.101702
15. Feng S, Rao Z, Zhang J, et al. Inhibition of CARM1-mediated methylation of ACSL4 promotes ferroptosis in colorectal cancer. *Adv Sci (Weinh)*. 2023;10(36):2303484. doi:10.1002/advs.202303484
16. Bersuker K, Hendricks JM, Li Z, et al. The CoQ oxidoreductase FSP1 acts parallel to GPX4 to inhibit ferroptosis. *Nature*. 2019;575(7784): 688–692. doi:10.1038/s41586-019-1705-2
17. Lim JKM, Delaidelli A, Minaker SW, et al. Cystine/glutamate antiporter xCT (SLC7A11) facilitates oncogenic RAS transformation by preserving intracellular redox balance. *Proc Natl Acad Sci U S A*. 2019;116(19): 9433–9442. doi:10.1073/pnas.1821323116
18. Daher B, Parks SK, Durivault J, et al. Genetic ablation of the cystine transporter xCT in PDAC cells inhibits mTORC1, growth, survival, and tumor formation via nutrient and oxidative stresses. *Cancer Res*. 2019;79(15):3877–3890. doi:10.1158/0008-5472.CAN-18-3855
19. Yang J, Qian X, Qiu Q, et al. LCAT1 is an oncogenic LncRNA by stabilizing the IGF2BP2-CDC6 axis. *Cell Death Dis*. 2022;13(10):877. doi:10.1038/s41419-022-05316-4
20. Ma Y, Yang J, Ji T, Wen F. Identification of a novel m5C/m6A-related gene signature for predicting prognosis and immunotherapy efficacy in lung adenocarcinoma. *Front Genet*. 2022;13:990623. doi:10.3389/fgene.2022.990623
21. Han L, Lei G, Chen Z, Zhang Y, Huang C, Chen W. IGF2BP2 regulates MALAT1 by serving as an N6-methyladenosine reader to promote NSCLC proliferation. *Front Mol Biosci*. 2022;8:780089. doi:10.3389/fmolb.2021.780089
22. Xiao Q, Liu L, Qian W, Kang T, Ying R, Nie J. CaMKIIδ, stabilized by RNA N6-methyladenosine reader IGF2BP2, boosts coxsackievirus B3-induced myocardial inflammation via interacting with TIRAP. *J Cardiovasc Transl Res*. 2024;17(3):540–553. doi:10.1007/s12265-023-10478-3
23. Cui Y, Wen Y, Lv C, et al. Decreased RNA-binding protein IGF2BP2 downregulates NT5DC2, which suppresses cell proliferation, and induces cell cycle arrest and apoptosis in diffuse large B-cell lymphoma cells by regulating the p53 signaling pathway. *Mol Med Rep*. 2022;26(3):286. doi:10.3892/mmr.2022.12802
24. Yu HY, Yang L, Liu YC, Yu AJ. Sulforaphene suppressed cell proliferation and promoted apoptosis of COV362 cells in endometrioid ovarian cancer. *PeerJ*. 2023;11:e16308. doi:10.7717/peerj.16308
25. Xu P, Liu K, Huang S, et al. N6-methyladenosine-modified MIB1 promotes stemness properties and peritoneal metastasis of gastric cancer cells by ubiquitinating DDX3X. *Gastric Cancer*. 2024;27(2):275–291. doi:10.1007/s10120-023-01463-5
26. Fang H, Sun Q, Zhou J, et al. m6A methylation reader IGF2BP2 activates endothelial cells to promote angiogenesis and metastasis of lung adenocarcinoma. *Mol Cancer*. 2023;22(1):99. doi:10.1186/s12943-023-01791-1
27. Liu TY, Hu CC, Han CY, et al. IGF2BP2 promotes colorectal cancer progression by upregulating the expression of TFRC and enhancing iron metabolism. *Biol Direct*. 2023;18(1):19. doi:10.1186/s13062-023-00373-x
28. Bell JL, Wächter K, Mühleck B, et al. Insulin-like growth factor 2 mRNA-binding proteins (IGF2BPs): Post-transcriptional drivers of cancer progression? *Cell Mol Life Sci*. 2013;70(15):2657–2675. doi:10.1007/s00018-012-1186-z
29. Hafner M, Landthaler M, Burger L, et al. Transcriptome-wide identification of RNA-binding protein and microRNA target sites by PAR-CLIP. *Cell*. 2010;141(1):129–141. doi:10.1016/j.cell.2010.03.009
30. Hunter T. The age of crosstalk: Phosphorylation, ubiquitination, and beyond. *Mol Cell*. 2007;28(5):730–738. doi:10.1016/j.molcel.2007.11.019
31. Fan TWM, Winnike J, Al-Attar A, et al. Differential inhibition of anaplerotic pyruvate carboxylation and glutaminolysis-fueled anabolism underlies distinct toxicity of selenium agents in human lung cancer. *Metabolites*. 2023;13(7):774. doi:10.3390/metabo13070774
32. Icard P, Simula L, Fournel L, et al. The strategic roles of four enzymes in the interconnection between metabolism and oncogene activation in non-small cell lung cancer: Therapeutic implications. *Drug Resist Updat*. 2022;63:100852. doi:10.1016/j.drup.2022.100852
33. Han S, Yang X, Zhuang J, et al. α-Hederin promotes ferroptosis and reverses cisplatin chemoresistance in non-small cell lung cancer. *Aging*. 2024;16(2):1298–1317. doi:10.18632/aging.205408
34. Deng J, Lin X, Qin J, et al. SPTBN2 suppresses ferroptosis in NSCLC cells by facilitating SLC7A11 membrane trafficking and localization. *Redox Biol*. 2024;70:103039. doi:10.1016/j.redox.2024.103039
35. Mei L, Long J, Wu S, Mei M, Mei D, Qiu H. APOC1 reduced anti-PD-1 immunotherapy of nonsmall cell lung cancer via the transformation of M2 into M1 macrophages by ferroptosis by NRF2/HO-1. *Anticancer Drugs*. 2024;35(4):333–343. doi:10.1097/CAD.0000000000001573

Peritoneal dialysis catheter removal at the time or after kidney transplantation: A multicenter cardinality-matched cohort study

Michał Zawistowski[1,A–D,F], Piotr Niecikowski[1,B,E,F], Magdalena Durlik[2,B,E,F], Joanna Nowaczyk[3,B,E,F], Jan Broda[4,B,E,F], Bartosz Foroncewicz[2,B,E,F], Krzysztof Mucha[2,5,B,E,F], Monika Widera[6,B,E,F], Robert Król[6,B,E,F], Honorata Stadnik[7,B,E,F], Marek Karczewski[7,B,E,F], Tomasz Kruszyna[8,B,E,F], Bogdan Niekowal[8,B,E,F], Justyna Korus[9,B,E,F], Dorota Kamińska[10,B,E,F], Magdalena Krajewska[10,B,E,F], Maciej Kosieradzki[1,B,E,F], Piotr Domagała[1,11,A,E,F]

[1] Department of General and Transplantation Surgery, Medical University of Warsaw, Poland
[2] Department of Transplantology, Immunology, Nephrology and Internal Diseases, Medical University of Warsaw, Poland
[3] Department of Dermatology, German Red Cross (DRK) Hospital Chemnitz-Rabenstein, Germany
[4] student, Faculty of Medicine, Medical University of Warsaw, Poland
[5] Institute of Biochemistry and Biophysics of the Polish Academy of Sciences, Warsaw, Poland
[6] Department of General, Vascular and Transplant Surgery, Medical University of Silesia, Katowice, Poland
[7] Department of General and Transplant Surgery, Clinical Hospital of Poznan, Poznan University of Medical Sciences, Poland
[8] Department of General, Oncological, Gastroenterological and Transplant Surgery, Jagiellonian University Medical College, Cracow, Poland
[9] Department of Nephrology and Transplantation Medicine, Wroclaw Medical University, Poland
[10] Faculty of Medicine, Wroclaw University of Science and Technology, Poland
[11] Department of Surgical Oncology, Transplant and General Surgery, Medical University of Gdansk, Poland

A – research concept and design; B – collection and/or assembly of data; C – data analysis and interpretation;
D – writing the article; E – critical revision of the article; F – final approval of the article

Received on September 23, 2024
Reviewed on December 7, 2024
Accepted on January 14, 2025

Published online on July 31, 2025

Advances in Clinical and Experimental Medicine, ISSN 1899–5276 (print), ISSN 2451–2680 (online) *Adv Clin Exp Med.* 2025;34(11):1947–1957

Address for correspondence
Michał Zawistowski
E-mail: michal.zawistowski@mail.com

Funding sources
None declared

Conflict of interest
None declared

Acknowledgements
We would like to express our gratitude to the medical staff taking care of patients in transplant centers participating in this project. Without their continuous and professional service, we could not have used the data evaluated in this study. We are also thankful to the patients for their anonymous data contribution.

Cite as
Zawistowski M, Niecikowski P, Durlik M, et al. Peritoneal dialysis catheter removal at the time or after kidney transplantation: A multicenter cardinality-matched cohort study. *Adv Clin Exp Med*. 2025;34(11):1947–1957. doi:10.17219/acem/200075

DOI
10.17219/acem/200075

Abstract

Background. Evidence regarding the optimal timing of peritoneal dialysis catheter (PDC) removal in renal graft recipients is limited. While some centers opt for removal during the transplant procedure, others defer catheter removal to various time points post-transplantation.

Objectives. In this multicenter cardinality-matched cohort study, we aimed to determine the optimal timing of PDC removal in patients undergoing kidney transplantation.

Materials and methods. Data from 324 patients were collected across 5 centers. We compared patients who had catheters removed during renal transplant (the PDC-free group) with those who had them removed after the procedure (the PDC group), matched 1:2 by age, sex, body mass index (BMI), living, and extended criteria donor statuses. We evaluated: 1) the need for dialysis within 2 post-transplant months, 2) a composite endpoint of catheter-related infection, peritonitis and/or surgical site infection, and 3) the length of hospitalization.

Results. After cardinality matching, the groups were well-balanced across all matching covariates. Postoperative dialysis was required in 14% of patients, with no statistically significant difference observed between the PDC-free and PDC groups (19% vs 12%; odds ratio (OR) = 1.94; 95% confidence interval (95% CI): 0.78–4.81; p = 0.152). Of the 14 patients in the PDC group who required dialysis postoperatively, only 3 were managed with peritoneal dialysis. No statistically significant difference was noted for the composite endpoint (8.6% vs 6.2%; OR = 0.74; 95% CI: 0.20–2.77; p = 0.656). Hospitalization was significantly longer in patients from the PDC group (median [interquartile range (IQR)]: 11 [9–15] vs 9 [7–12]; BM = –3.036; p = 0.003).

Conclusions. This study did not demonstrate any benefits associated with delaying PDC removal in renal graft recipients. On the contrary, postponing removal was linked to prolonged hospitalization.

Key words: kidney transplantation, peritoneal dialysis, delayed graft function, catheter-related infections

Highlights

- No clear evidence exists on the optimal timing for peritoneal dialysis catheter removal in kidney transplant recipients.
- This is the first multicenter, cardinality-matched cohort study comparing outcomes of peritoneal dialysis catheter removal at the time of transplantation versus delayed removal.
- Study results do not support routine delayed peritoneal dialysis catheter removal after kidney transplantation.
- Peritoneal dialysis catheter management in renal transplant patients should follow an individualized approach, based on comprehensive risk–benefit analysis and patient-centered care.

Background

The perioperative care of peritoneal dialysis patients undergoing renal transplantation involves addressing various challenges across the preoperative, intraoperative and postoperative phases.[1] These include but are not limited to optimizing dialysis, controlling the increased risk of catheter-related infections, including peritonitis, balancing fluid volume and nutritional statuses, monitoring surgical wound healing, ensuring rejection surveillance, and establishing alternative acute or chronic renal replacement therapy in case of graft failure or loss.[2] Another dilemma that transplant surgeons face is related to providing peritoneal dialysis catheter (PDC) management that is most beneficial for the renal recipient. The problem can be summarized by the clinical question of whether PDCs should be left intact or removed during the transplant procedure.[3]

Unfortunately, there is currently no consensus or robust evidence to guide transplant teams on the optimal timing for PDC removal in renal graft recipients.[3,4] Different centers and individual transplant surgeons follow various policies. These include routine removal of the catheters at the time of transplant[3–8] or postponing it until various postoperative time points.[9,10] The European Best Practice Guidelines for peritoneal dialysis suggest they can be left intact for around 3–4 months following transplantation even if good graft function is observed.[11] However, these guidelines, published in 2005, have never been updated (also by other peritoneal dialysis expert groups or societies) and faced criticism due to their methodological constraints.[12]

A recent systematic review and meta-analysis concerning 8 non-randomized studies of interventions did not provide a definitive answer to the question about optimal catheter removal in renal graft recipients due to the high risk of bias of the included studies.[13] It showed that several factors should be taken into account when planning perioperative and post-transplant catheter management, i.e., the risk of early graft dysfunction requiring renal replacement therapy (including acute and chronic dialysis), the risk of infectious or other catheter-related complications, as well as the patient's preferences.

According to Gardezi et al.,[14] patients receiving peritoneal dialysis are more likely to undergo kidney transplantation compared to those on hemodialysis. Similar trends are also observed in Poland where around 4% (4.24% in 2021 and 4.17% in 2022) of dialyzed patients are treated with peritoneal dialysis.[15] Taking that into account, there is an increasing need to provide objective evidence to help clinicians and patients plan optimal dialysis catheter management to ensure the best possible transplant outcome, including quality of life, and potentially reduce the number of subsequent hospitalizations and costs.

Objectives

The objective of this retrospective cohort study was to determine the optimal timing of PDC removal in renal graft recipients by comparing patients with catheters removed at the time of and after kidney transplantation, concerning the incidence of requiring dialysis after the procedure, infectious complications and the length of hospitalization.

Materials and methods

Study design

We conducted a multicenter retrospective cardinality-matched cohort study in peritoneal dialysis patients undergoing kidney transplantation. The reporting of this study conforms to the Strengthening the Reporting of Observational Studies in Epidemiology (STROBE) and Strengthening the Reporting of Cohort Studies in Surgery (STROCSS) 2021 guidelines.[16,17]

Ethical approval

Ethical approval and informed consent collection were waived by the local Ethics Committee of the Medical University of Warsaw, Poland (decision No. AKBE/26/2021) due to the retrospective character of this study. This study was conducted in accordance with the principles of the Declaration of Helsinki.

Setting and participants

Retrospective data concerning adult (≥18 years old) renal graft recipients previously managed with peritoneal dialysis were collected from patient's medical records across 5 kidney transplant centers in Poland. Patients transplanted between 2010 and 2021 were considered eligible for inclusion, ensuring at least 1 year of follow-up. We excluded patients with PDCs removed more than 1 day before the transplant procedure, those who underwent multiorgan transplantation, or individuals with Bricker ileal conduit urinary diversion. Patients with unknown group assignment (no information on whether the PDC was removed at the time or after kidney transplantation) or with missing matching variables were also excluded from the final analyses.

Both deceased donor (all after brain death) and living donor renal transplant procedures were included in the study. The PDC removal timing was at the discretion of the transplant surgeon or other treating physician. Some of them preferred removing the catheters at the time of transplantation, while others postponed it. The achievement of stable graft function most commonly defined the time of delayed removal.

Variables

Medical records from transplant wards and outpatient clinics were searched to collect recipients' and donors' age, sex, body mass index (BMI), subjects' cumulative dialysis vintage (in months), and number of episodes of peritonitis before and after transplantation. Donor characteristics, including extended criteria and living donor status, were identified. Renal graft's cold ischemia, vascular anastomosis and operative times (all in minutes), graft storage modality (including simple cold storage, hypothermic machine perfusion and their combination), and PDC placement site were extracted. Information about the use of central line catheters during surgery, surgical drainage placement, as well as length of hospitalization and surgical drainage use (both in days) were collected. Data concerning intraoperative peritoneum breaches, ascites, urinary leakage, urinary tract infections, catheter-related infections, delayed graft function (defined as the need for dialysis within 7 post-transplant days), types of dialysis used following surgery, and peritoneal dialysis removal time after transplantation (in days), and 1-year graft survival were evaluated.

Study endpoints

The primary endpoint was the incidence of needing dialysis within 2 post-transplant months.[13] Secondary objectives included a composite endpoint defined as the incidence of catheter-related infection, peritonitis and/or surgical site infection, as well as the length of hospitalization.

Cardinality matching

All patients were assigned to the group of recipients whose PDCs were removed at the time of renal transplantation (the PDC-free group) or after the procedure (the PDC group). Cardinality matching[18] was used to match patients 1:2 by 5 covariates, i.e., kidney recipient's age, sex, BMI, living, and extended criteria donor statuses. These factors were selected based on the discussion and consensus among the co-authors, following the evaluation of a web of causation and literature search (to identify factors affecting both the peritoneal dialysis removal and the need for dialysis early after transplantation). Cardinality matching uses advanced programming techniques to find the largest matched sample balanced by prespecified covariates without relying on, and thus overcoming some limitations of, the propensity scores or coarsened covariate values.[19–21] The matching was performed using the MatchIt package[22] in R with the optimization performed by the HiGHs optimization solver.[23] An imbalance between the groups was considered when absolute mean differences were greater than 0.1.

Study size

Assumptions for sample size calculation were based on the study by Kwong et al.[24] and the recent meta-analysis of observational studies.[13] Setting α error at 0.05, β error at 0.2, the allocation ratio 1:2 and assuming the proportion for the primary endpoint at 0.19 in the PDC and 0.05 in the PDC-free group, we calculated the required sample size of 186 (62 subjects in the PDC and 124 in the PDC-free group). The calculations were performed using a priori sample size calculation for Fisher's exact test in G*Power v. 3.1.9.7 (Heinrich Heine University, Düsseldorf, Germany, 2020).[25]

Statistical analyses

Continuous variables were summarized using means with standard deviations (SDs) or medians with interquartile ranges (IQRs), depending on whether the normal distribution was determined using the QQ plot, histogram and the Lilliefors test assessment. The Lilliefors test was given priority over other assessments when evaluating the distribution of continuous data. Categorical covariates were expressed as the number of observations and percentages. No imputation was used to replace missing data (missing data were deleted pairwise). Differences between the groups for categorical variables were evaluated using Fisher's exact (when an expected value was less than 5) or χ^2 tests of independence, as appropriate. For continuous variables, the permuted Brunner–Munzel test was used.

In the matched cohort, the average marginal treatment effect was evaluated with G-computation using robust confidence intervals.[26] For the primary and secondary

composite endpoints, logistic regression models with the matching variables as covariates, and matching weights included, were created. The results were presented using odds ratios (ORs) and robust 95% confidence intervals (95% CIs). Assumptions of the logistic regression models were verified using the Box–Tidwell test, Variance Inflation Factor evaluation and Cook's distance analysis. The Bonferroni correction was applied to account for multiple comparisons. A two-sided p-value less than 0.0167 (to account for the multiple tests performed) was considered statistically significant. All calculations, statistical tests and visualizations were performed using the MatchIt,[22] HiGHS,[23] cobalt,[27] ggplot2,[28] easyalluvial,[29] tableone,[30] and marginaleffects[31] packages in R v. 4.3.2 (R Foundation for Statistical Computing, Vienna, Austria).

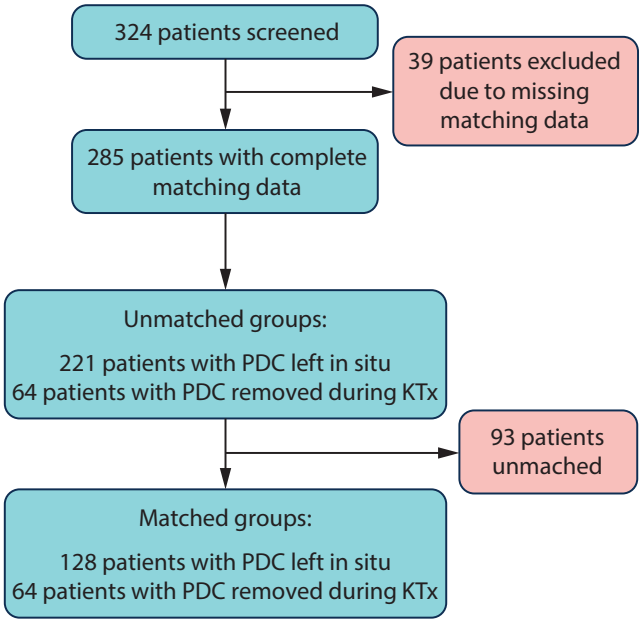

Fig. 1. Study flowchart

PDC – peritoneal dialysis catheter; KTx – kidney transplantation.

Results

Sample characteristics

We collected data from 324 patients from 5 transplant centers. After excluding those with missing data for the matching or grouping variables, 324 were considered eligible for inclusion. In the final analysis, 64 patients from the PDC-free group were matched 1:2 with 128 patients assigned to the PDC group (a total sample size of 192). The flow of patients in the study is summarized in Fig. 1.

After the cardinality matching was conducted, 2 groups balanced (absolute standardized mean difference (SMD) <0.1) in terms of all matching variables were established (Fig. 2,3). The studied population consisted of 47% of females (48% in the subgroup of kidney recipients who had their PDCs removed after and 45% in those with catheters removed at the time of surgery). The operative time was longer in patients with catheters removed at the time of surgery (median [IQR]: 150 [130–181] vs 130 [105–156] min; BM = 3.403, p = 0.002). The peritoneum was left intact following the procedure in 66% (84/128) of subjects from the PDC group and 64% (41/64) of those from the PDC-free group (χ^2_1 = 0.046, p = 0.830). A central venous catheter was inserted more often in the PDC-free group (90% vs 53%; χ^2_1 = 25.991, p < 0.001). Surgical drainage was utilized

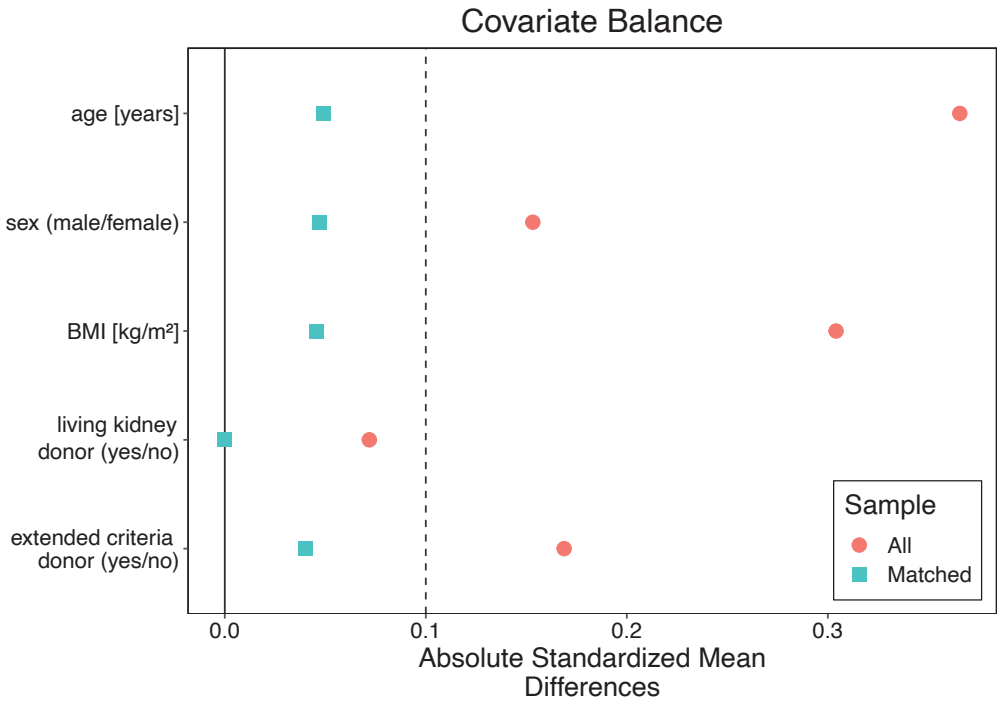

Fig. 2. Absolute standardized mean differences before and after cardinality matching

BMI – body mass index.

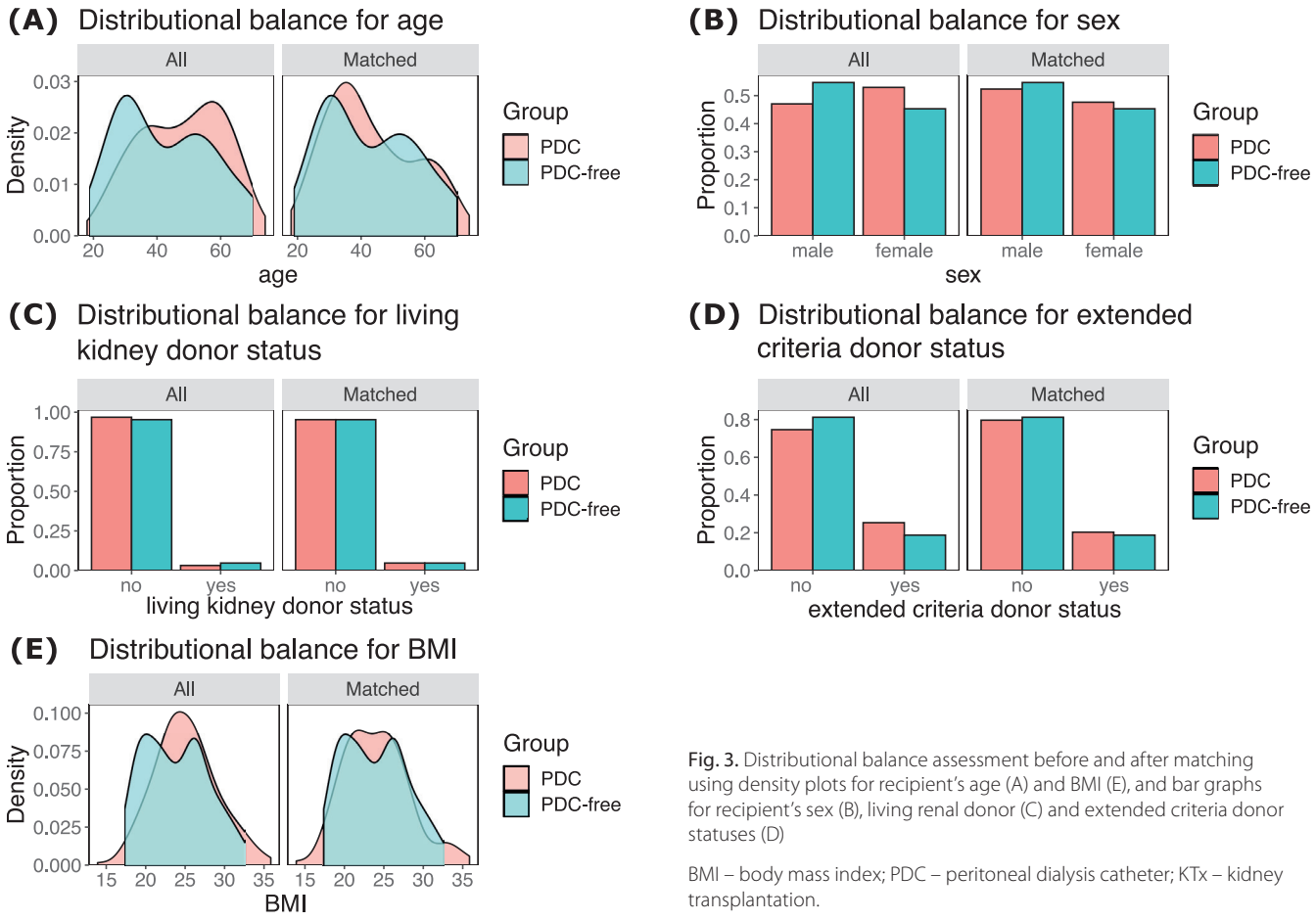

Fig. 3. Distributional balance assessment before and after matching using density plots for recipient's age (A) and BMI (E), and bar graphs for recipient's sex (B), living renal donor (C) and extended criteria donor statuses (D)

BMI – body mass index; PDC – peritoneal dialysis catheter; KTx – kidney transplantation.

in 97% of subjects (98% in the PDC and 95% in the PDC-free group; p = 0.336). The median [IQR] time to PDC removal in the PDC group was 64 [42–97] days (the shortest time was 6 days and the longest one 243). Key baseline characteristics of the studied population are summarized in Table 1, while operative and postoperative characteristics are presented in Table 2.

Primary and secondary endpoints

The primary endpoint, defined as the need for dialysis within 2 post-transplant months was observed in 19% of patients from the PDC-free and 12% of patients from the PDC group, with no statistically significant difference noted between the groups (OR = 1.94; 95% CI: 0.78 – 4.81; p = 0.152, Table 3). Only 3 out of 14 subjects with PDCs available underwent peritoneal dialysis (Table 2). Similarly, no clinically and statistically significant difference was identified for the secondary composite endpoint of the incidence of catheter-related infections, peritonitis and/or surgical site infections. It was detected in 6.2% of patients with PDCs removed at the time of transplant and in 8.6% of recipients with catheters removed after the surgery (OR = 0.74; 95% CI: 0.20 – 2.77; p = 0.656, Table 4). These outcomes are presented graphically in Fig. 4 and Fig. 5. No significant differences were also identified when catheter-related infections other than peritonitis, peritonitis and surgical site infections were evaluated separately (Table 2).

The length of hospitalization was statistically significantly shorter in the PDC-free group (median [IQR], 9 [7–12] vs 11 [9–15] days; BM = –3.036, p = 0.003).

Discussion

In this pragmatic cardinality-matched cohort study, we showed that there was no statistically significant difference in the incidence of needing dialysis within the first 2 post-transplant months between patients whose PDCs were left in situ during kidney transplantation and those whose catheters were removed at the time of the procedure. Accordingly, we could conclude that the current decision-making based solely on the surgeon's discretion is not optimal and fails to predict which patients could potentially benefit from postponing the catheters' removal. Therefore, we seek to determine more objective factors to guide the medical practice on the optimal peritransplant management of peritoneal dialysis patients.

Interestingly, in our study, more patients had their Tenckhoff catheters left in place than removed at the time of transplantation. A similar proportion was

Table 1. Baseline demographic and clinical characteristics of patients before and after matching

Variable		Unmatched comparisons				Matched comparisons			
		overall (n = 285)	PDC group (n = 221)	PDC-free group (n = 64)	ASMD	overall (n = 192)	PDC group (n = 128)	PDC-free group (n = 64)	ASMD
Recipient's age* [years]		48 [35–58]	49 [37–58]	40 [31–54]	0.384	40 [32–54]	40 [33–53]	40 [31–54]	0.051
Recipient's sex: Female*		146/285 (51%)	117/221 (53%)	29/64 (45%)	0.153	90/192 (47%)	61/128 (48%)	29/64 (45%)	0.047
Recipient's BMI* [kg/m^2]		24.8 (3.9)	25.1 (3.9)	23.9 (4.0)	0.306	24.0 (4.0)	24.1 (4.1)	23.9 (4.0)	0.045
Dialysis vintage [months]		19 [12–36]	21 [12–36]	16 [10–25]	0.372	17 [11–33]	18 [12–36]	16 [10–25]	0.256
Donor's age [years]		48 [35–57]	48 [34–57]	48 [37–54]	0.075	48 [35–56]	48 [34–56]	48 [37–54]	0.010
Donor's sex: Female		85/284 (30%)	68/221 (31%)	17/63 (27%)	0.084	55/191 (29%)	38/128 (30%)	17/63 (27%)	0.060
Donor's BMI [kg/m^2]		25.4 [23.1–27.7]	25.6 [23.1–27.7]	25.1 [23.1–27.7]	0.035	25.1 [22.9–27.5]	25.1 [22.9–27.4]	25.1 [23.1–27.7]	0.043
Living renal donor*		10/285 (3.5%)	7/221 (3.2%)	3/64 (4.7%)	0.078	9/192 (4.7%)	6/128 (4.7%)	3/64 (4.7%)	<0.001
Extended criteria donor*		68/285 (24%)	56/221 (25%)	12/64 (19%)	0.159	38/192 (20%)	26/128 (20%)	12/64 (19%)	0.039
Cold ischemia time† [min]		1211 (551)	1286 (533)	1005 (552)	0.520	1159 (559)	1259 (542)	1005 (552)	0.465
Episodes of peritonitis before KTx'	0	229/265 (86%)	173/202 (86%)	56/63 (89%)	0.109	158/183 (86%)	102/120 (85%)	56/63 (89%)	0.121
	1	26/265 (9.8%)	21/202 (10%)	5/63 (7.9%)		17/183 (9.3%)	12/120 (10%)	5/63 (7.9%)	
	2	6/265 (2.3%)	5/202 (2.5%)	1/63 (1.6%)		4/183 (2.2%)	3/120 (2.5%)	1/63 (1.6%)	
	3	4/265 (1.5%)	3/202 (1.5%)	1/63 (1.6%)		4/183 (2.2%)	3/120 (2.5%)	1/63 (1.6%)	
PDC site: Right		68/228 (30%)	48/179 (27%)	20/49 (41%)	0.299	50/149 (34%)	30/100 (30%)	20/49 (41%)	0.228

Continuous variables were summarized using means (standard deviation (SD)) or medians (interquartile range (IQR)), while the categorical ones as n (%). PDC – peritoneal dialysis catheter; KTx – kidney transplantation; ASMD – absolute standardized mean difference (calculated using the tableone package in R); BMI – body mass index. * Matching covariates. † Data were missing for 31 subjects from one of the transplant centers participating in the study.

presented in a study by Warren et al,.[5] who analyzed data from 2 centers in the UK. Unfortunately, it is impossible to retrospectively evaluate why this approach was preferred. What could give some hints is the longer cold ischemia time in the PDC group (Table 2) which, however, was not associated with a higher risk of needing dialysis early after transplantation. Nevertheless, feasible is the evaluation of whether attempts of peritoneal dialysis following transplantation were successful. The results are not very promising. Only 3 out of 14 patients (3 out of 27 in the unmatched cohort, Table 2) requiring dialysis underwent peritoneal dialysis despite having Tenckhoff catheters left intact during their transplant procedures. Reports based on large databases prove that there is potential to use peritoneal dialysis more frequently. In France, according to a report by the Biomedicine Agency from 2013, only 5.1% of patients with failed allografts receive peritoneal dialysis[32] while in the USA this figure was at 16% (data from the United States Renal Data System).[33] Furthermore, the patients' preferences are also important to consider when selecting between various dialysis modalities following graft failure. These are highly individualized and usually depend on various factors, including, i.a., individual circumstances, medical history, lifestyle considerations, experience, expectations, and perceptions.[34] Nevertheless, this is also influenced by the actual availability of both dialysis modalities and whether patients are provided by their healthcare providers or insurers with the option to choose between them.

Assuming that both the clinical team and the patient would consider having a PDC left in place during the transplant procedure, a question remains: How to predict the risk of needing dialysis after the procedure? There are 2 main different scenarios when dialysis might be needed shortly after kidney transplantation, i.e., in case of delayed graft function or primary non-function/early graft loss. Unfortunately, the process of restarting any type of dialysis after kidney transplant failure is not well addressed in clinical guidelines.[35] In the meta-analysis of 8 non-randomized studies of intervention from 2022, the pooled prevalence of needing dialysis early after transplantation for any reason was 15.2% (95% CI: 11.1–20.3%) in patients with PDCs removed at the time of transplantation and 8.6% (95% CI: 2.7–24%) in the group with Tenckhoff catheters removed after surgery.[13] A similar trend was noted in the current study (19% vs 12%), despite cold ischemia time being longer in the PDC group (Table 1). Over a decade ago, a good and practical concept of using web-based calculators to predict delayed graft function was proposed by Irish et al.[36] A similar tool could be developed to help predict primary non-function. Considering the better availability of high-volume real-world data and recent advancements in calculation techniques, we recommend revisiting this idea and creating newer validated predictive models. Bearing in mind the high variability in population characteristics among various continents and countries, it would be appropriate to include as diverse and big a population as possible.

Another dilemma that might appear is whether it is safe to proceed with peritoneal dialysis shortly after kidney

Table 2. Operative and post-transplant characteristics of the patients

Variable		Unmatched comparisons				Matched comparisons			
		overall (n = 285)	PDC group (n = 221)	PDC-free group (n = 64)	ASMD	overall (n = 192)	PDC group (n = 128)	PDC-free group (n = 64)	ASMD
Graft storage modality'	simple cold storage	183/275 (67%)	139/215 (65%)	44/60 (73%)	0.223	122/185 (66%)	78/125 (62%)	44/60 (73%)	0.259
	hypothermic machine perfusion	90/275 (33%)	74/215 (34%)	16/60 (27%)		62/185 (34%)	46/125 (37%)	16/60 (27%)	
	simple cold storage/ hypothermic machine perfusion	2/275 (0.7%)	2/215 (0.9%)	0/60 (0%)		1/185 (0.5%)	1/125 (0.8%)	0/60 (0%)	
Anastomosis time [min]		35 [30–41]	35 [29–41]	33 [30–40]	0.100	33 [30–40]	35 [29–40]	33 [30–40]	0.190
Operative time [min]		135 [105–160]	130 [105–155]	150 [130–181]	0.517	135 [105–160]	130 [105–156]	150 [130–181]	0.565
Intact peritoneum after KTx		189/284 (67%)	148/220 (67%)	41/64 (64%)	0.068	125/192 (65%)	84/128 (66%)	41/64 (64%)	0.033
Central line used during KTx		178/276 (64%)	121/213 (57%)	57/63 (90%)	0.827	121/184 (66%)	64/121 (53%)	57/63 (90%)	0.918
Surgical drainage used after KTx		276/283 (98%)	215/219 (98%)	61/64 (95%)	0.162	186/191 (97%)	125/127 (98%)	61/64 (95%)	0.179
Length of surgical drainage use [days]		3 [2–4]	3 [2–4]	3 [2–5]	0.225	3 [2–4]	3 [2–4]	3 [2–5]	0.361
Length of hospitalization† [days]		11 [8–15]	12 [9–17]	9 [7–12]	0.408	10 [8–14]	11 [9–15]	9 [7–12]	0.274
Infectious complications*		29/285 (10%)	25/221 (11%)	4/64 (6.2%)	0.180	15/192 (7.8%)	11/128 (8.6%)	4/64 (6.2%)	0.090
Urinary tract infection		66/273 (24%)	53/210 (25%)	13/63 (21%)	0.110	38/186 (20%)	25/123 (20%)	13/63 (21%)	0.008
Surgical site infection		17/275 (6.2%)	14/212 (6.6%)	3/63 (4.8%)	0.080	10/187 (5.3%)	7/124 (5.6%)	3/63 (4.8%)	0.040
Episodes of peritonitis after KTx	0	263/272 (97%)	201/210 (96%)	62/62 (100%)	0.299	180/183 (98%)	118/121 (98%)	62/62 (100%)	0.225
	1	9/272 (3.3%)	9/210 (4.3%)	0/62 (0%)		3/183 (1.6%)	3/121 (2.5%)	0/62 (0%)	
PDC-related infection other than peritonitis after KTx		8/274 (2.9%)	7/212 (3.3%)	1/62 (1.6%)	0.109	4/185 (2.2%)	3/123 (2.4%)	1/62 (1.6%)	0.059
Ascites		3/276 (1.1%)	3/213 (1.4%)	0/63 (0%)	0.169	3/187 (1.6%)	3/124 (2.4%)	0/63 (0%)	0.223
Urinary leakage		13/280 (4.6%)	6/218 (2.8%)	7/62 (11%)	0.339	9/190 (4.7%)	2/128 (1.6%)	7/62 (11%)	0.405
Delayed graft function		36/284 (13%)	25/220 (11%)	11/64 (17%)	0.167	23/192 (12%)	12/128 (9.4%)	11/64 (17%)	0.232
Needing dialysis within 2 post-transplant months‡		41/281 (15%)	29/218 (13%)	12/63 (19%)	0.156	27/192 (14%)	15/128 (12%)	12/64 (19%)	0.197
Use of peritoneal dialysis after KTx	hemodialysis	36/39 (92%)	24/27 (89%)	12/12 (100%)	0.500	23/26 (88%)	11/14 (79%)	12/12 (100%)	0.739
	peritoneal dialysis	3/39 (7.7%)	3/27 (11%)	0/12 (0%)		3/26 (12%)	3/14 (21%)	0/12 (0%)	
Graft functioning 1 year after KTx		240/261 (92%)	189/207 (91%)	51/54 (94%)	0.122	163/174 (94%)	112/120 (93%)	51/54 (94%)	0.046
PDC removal time [days]		–	69 [42–100]	–	–	–	64 [42–97]	–	–

Continuous variables were summarized using means (standard deviation (SD)) or median (interquartile range (IQR)) while the categorical ones as n (%). PDC – peritoneal dialysis catheter; KTx – kidney transplantation; ASMD – absolute standardized mean difference (calculated using the tableone package in R); BMI – body mass index. * the composite secondary endpoint defined as the incidence of catheter-related infections, peritonitis, and/or surgical site infection; † the secondary endpoint; ‡ the primary endpoint.

transplantation. Potentially high risk of peritoneal breaches might be concerning to surgeons. In our study, despite grafts being implanted extraperitoneally, the peritoneum was assessed by surgeons to be intact in around 65% of cases, without any notable differences between the evaluated groups. According to Issa and Lakhani,[37] a compromised peritoneum is an indication to remove the PDC during a renal transplant. Nevertheless, in the absence of contraindications, the evidence about peritoneal dialysis initiation shortly after transplantation is compelling and suggests that such treatment is safe.[38] Furthermore, a randomized controlled trial (RCT) proved that it is feasible and safe to use PDCs even immediately after insertion.[39] In that study, no relevant differences were noted when patients with urgent and delayed utilization groups were compared regarding catheter-related complications and catheter survival within 1 year following the insertion. Another doubt might be related to the concern of potential infectious complications, including catheter-related infections and peritonitis.[4,5] The results of our study did not show such trends which is consistent with other reports.[13] We did not identify clinically relevant increased rates of peritonitis shortly after transplantation among patients with catheters left in situ. However, we were not able to evaluate long-term results.

Unfortunately, there is still insufficient evidence available to compare the 2 approaches to peritransplant PDC management in terms of the patient's outcomes, including

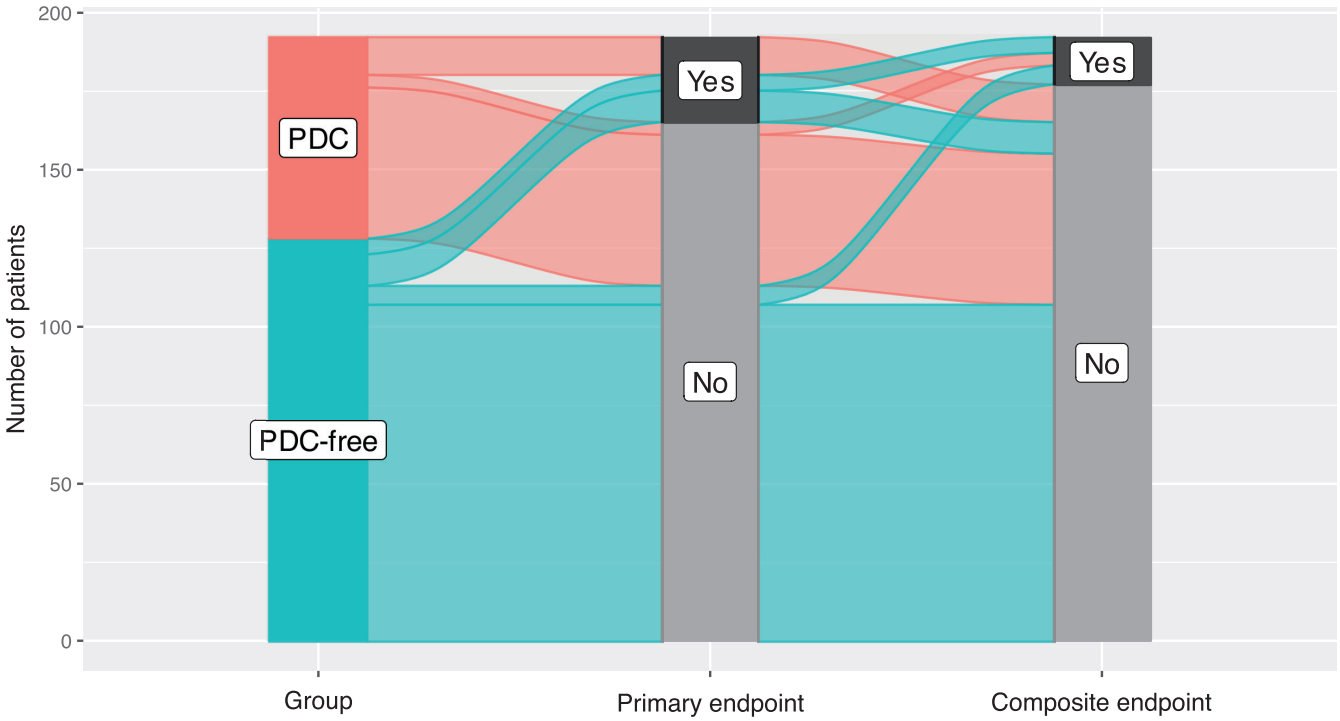

Fig. 4. Alluvial diagram summarizing rates for the primary and secondary composite endpoints. Number of flows: 7. Maximum weight of a single flow: 55.7%

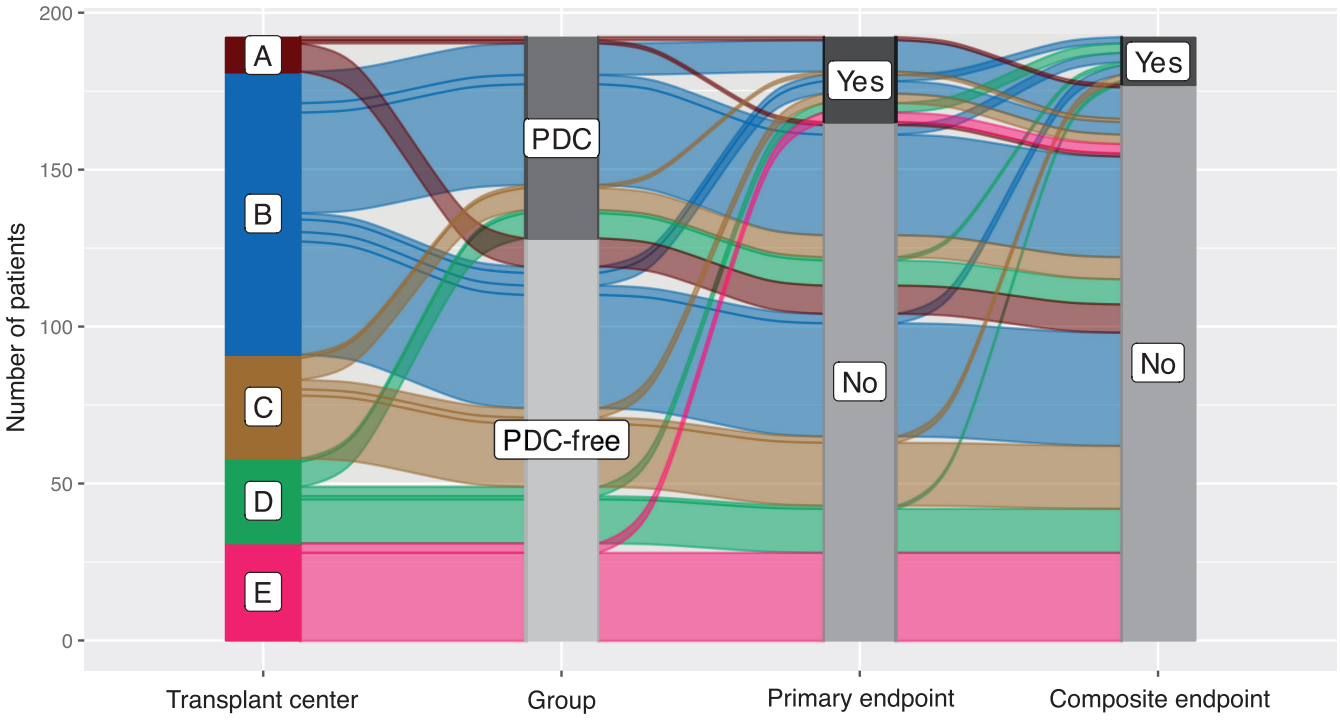

Fig. 5. Alluvial diagram summarizing rates for the primary and secondary composite endpoints, split by the participating transplant center. Number of flows: 22. Maximum weight of a single flow: 18.8%

overall graft survival and quality of life, as well as short and long-term costs. We noticed that the removal of PDCs during surgery prolongs the procedures by around 20 min. The costs to the healthcare system can go up when the catheters are left intact due to the need for subsequent hospitalizations and procedures required to eventually remove them. Costs and additional risks might be also related to potential complications associated with such interventions, including those related to the use of general anesthesia that might be used in some cases. Unfortunately, the retrospective nature of data collection and the variability in local treatment practices limited our ability to evaluate such complications in detail. However, what was identified in our study is that patients with catheters left

Table 3. Logistic regression model for the primary endpoint analysis

Covariate	OR	95% CI	p-value
Peritoneal dialysis catheter removal			
After kidney transplant	–	–	0.152
At the time of kidney transplant	1.94	0.78–4.81	
Recipient's age*	1.00	0.93–1.08	0.963
Recipient's sex*			
Male	–	–	0.768
Female	1.24	0.29–5.26	
Recipient's BMI*	1.09	0.88–1.35	0.442
Living kidney donor*			
No	–	–	0.539
Yes	3.17	0.08–126.31	
Extended criteria donor*			
No	–	–	0.319
Yes	2.64	0.39–17.89	

*Matching variables. OR – odds ratio; 95% CI – 95% confidence interval; BMI – body mass index.

Table 4. Logistic regression model for the composite secondary endpoint analysis

Covariate	OR	95% CI	p-value
Peritoneal dialysis catheter removal			
After kidney transplant	–	–	0.656
At the time of kidney transplant	0.74	0.20–2.77	
Recipient's age*	0.96	0.90–1.10	0.928
Recipient's sex*			
Male	–	–	0.217
Female	0.30	0.04–2.05	
Recipient's BMI*	1.00	0.74–1.35	0.993
Living kidney donor*			
No	–	–	<0.001
Yes	8.2×10^{-7}	1.5×10^{-8} –4.4×10^{-5}	
Extended criteria donor*			
No	–	–	0.192
Yes	6.11	0.40–92.40	

*Matching variables. OR – odds ratio; 95% CI – 95% confidence interval; BMI – body mass index.

in situ stayed statistically significantly longer in the hospital after their transplant procedures. The hospitalization prolongation was about 2 days, which for patients on immunosuppression may be considered clinically significant due to increased risk of hospital-acquired infections. This outcome has an uncertain origin and, to our knowledge, was not described before. We hypothesize that it might be related to the desire to observe such patients more closely for signs of potential catheter-related infections early after transplantation. It could also be related to delayed graft function or the need for dialysis before the initial discharge. However, delayed graft function was more frequent in the PDC-free group (17% vs 9.4%, Table 2). It is also possible that it was due to some other unidentified factors.

With an increasing number of patients using peritoneal dialysis worldwide, the dilemma of Tenckhoff catheter removal in such patients might become more frequent and put a more noticeable burden on healthcare systems in the future. What is worth pointing out is that based on various, often negative experiences, some authors declared to switch to a routine of removing PDCs during kidney transplantation.[3–5]

Limitations

The present study study is limited by its retrospective design. This issue was mitigated by the use of cardinality matching, which yielded satisfactory results in terms of getting balanced groups. Nevertheless, the risk of unmeasured confounding persists.[19] Despite including patients from 5 transplant centers and setting a broad data collection period, the sample size was not very big. This proves that although an RCT would be the best method to answer the studied dilemma, it requires a large number of participating sites and countries and/or a long enrollment period which would significantly increase its potential costs. In contrast, no external funding was needed to complete this matched cohort study which to some extent emulates a true RCT.[19,40] Moreover, cardinality matching is thought to bring some advantages in the setting of a small sample size when compared to other observational data analysis methods.[41] Our data can be used to power a prospective study. What should be considered in future research that could not be evaluated in ours are patient-reported outcomes, including quality of life and satisfaction assessments.

Conclusions

We did not identify any significant benefits from postponing PDC removal in patients undergoing kidney transplantation. Neither clinically nor statistically significant differences were noted for the need for dialysis within 2 post-transplant months when patients with catheters removed at the time and after the procedure were compared. Postponed catheter removal was not associated with an increased rate of infectious complications. However, it was associated with prolonged hospitalization. An individual approach based on a detailed risk-benefit assessment and patient preferences should be taken into account when planning PDC management in renal graft recipients.

Data Availability Statement

The datasetssupporting the findings of the current study are openly available in the Open Science Framework (OSF) repository at DOI 10.17605/OSF.IO/8A4RW.

Consent for publication

Not applicable.

Use of AI and AI-assisted technologies

Not applicable.

ORCID iDs

Michał Zawistowski https://orcid.org/0000-0002-5173-6283
Piotr Niecikowski https://orcid.org/0009-0006-1997-1968
Magdalena Durlik https://orcid.org/0000-0002-4798-1497
Joanna Nowaczyk https://orcid.org/0000-0001-7438-3559
Jan Broda https://orcid.org/0009-0000-2102-7649
Bartosz Foroncewicz https://orcid.org/0000-0002-0757-4547
Krzysztof Mucha https://orcid.org/0000-0002-6613-7638
Monika Widera https://orcid.org/0009-0003-9213-5710
Robert Król https://orcid.org/0000-0002-3079-0168
Honorata Stadnik https://orcid.org/0000-0001-7910-2998
Marek Karczewski https://orcid.org/0000-0002-9642-0709
Tomasz Kruszyna https://orcid.org/0000-0002-7031-983X
Bogdan Niekowal https://orcid.org/0009-0006-5496-5117
Justyna Korus https://orcid.org/0000-0002-6260-8818
Dorota Kamińska https://orcid.org/0000-0003-2400-9328
Magdalena Krajewska https://orcid.org/0000-0002-2632-2409
Maciej Kosieradzki https://orcid.org/0000-0003-2889-1311
Piotr Domagała https://orcid.org/0000-0003-4801-1967

References

1. Palamuthusingam D, Nadarajah A, Johnson DW, Pascoe EM, Hawley CM, Fahim M. Morbidity after elective surgery in patients on chronic dialysis: A systematic review and meta-analysis. *BMC Nephrol*. 2021;22(1):97. doi:10.1186/s12882-021-02279-0
2. Harrison TG, Hemmelgarn BR, Farragher JF, et al. Perioperative management for people with kidney failure receiving dialysis: A scoping review. *Semin Dial*. 2023;36(1):57–66. doi:10.1111/sdi.13081
3. McGregor T. The PD catheter dilemma. *Can Urol Assoc J*. 2012;6(5):379. PMID:23093632.
4. Parks R, Saedon M. Outcomes of removal of peritoneal dialysis catheter at the time of renal transplant. *Saudi J Kidney Dis Transpl*. 2021;32(2):415. doi:10.4103/1319-2442.335453
5. Warren J, Jones E, Sener A, et al. Should peritoneal dialysis catheters be removed at the time of kidney transplantation? *Can Urol Assoc J*. 2012;6(5):376–378. doi:10.5489/cuaj.12112
6. Peluso G, Incollingo P, Carlomagno N, et al. Our timing to remove peritoneal catheter dialysis after kidney transplant. *Transplant Proc*. 2019;51(1):160–163. doi:10.1016/j.transproceed.2018.04.075
7. Glass NR, Miller DT, Sollinger HW, Zimmerman SW, Simpson D, Belzer FO. Renal transplantation in patients on peritoneal dialysis. *Perit Dial Int*. 1985;5(3):157–160. doi:10.1177/089686088500500305
8. McDonald MW, Sterioff S, Engen DE, Zincke H, Kurtz SB. Renal transplantation in patients with indwelling continuous ambulatory peritoneal dialysis catheters. *J Urol*. 1987;137(5):849–851. doi:10.1016/s0022-5347(17)44271-6
9. Kitada H, Doi A, Nishiki T, et al. Short-term outcome of renal transplantation treated with pre-transplant peritoneal dialysis. *Dial Transplant*. 2010;39(4):148–150. doi:10.1002/dat.20419
10. Steinmuller D, Novick A, Braun W, Vidt D, Nakamoto S. Renal transplantation of patients on chronic peritoneal dialysis. *Am J Kidney Dis*. 1984;3(6):436–439. doi:10.1016/s0272-6386(84)80007-4
11. Dombros N, Dratwa M, Feriani M, et al. European best practice guidelines for peritoneal dialysis: 9 PD and transplantation. *Nephrol Dial Transplant*. 2005;20(Suppl 9):ix34–ix35. doi:10.1093/ndt/gfi1123
12. Abboud O, Barsoum R, Berthoux F, et al. European Best Practice Guidelines for Peritoneal Dialysis acknowledged by ISN. *Nat Rev Nephrol*. 2007;3(1):6–7. doi:10.1038/ncpneph0381
13. Zawistowski M, Nowaczyk J, Domagała P. Peritoneal dialysis catheter removal at the time or after kidney transplantation: A systematic review and meta-analysis. *Langenbecks Arch Surg*. 2022;407(7):2651–2662. doi:10.1007/s00423-022-02637-y
14. Gardezi AI, Aziz F, Parajuli S. The role of peritoneal dialysis in different phases of kidney transplantation. *Kidney360*. 2022;3(4):779–787. doi:10.34067/kid.0000482022
15. Dębska-Ślizień A, Rutkowski B, Jagodziński P, et al. Current status of renal replacement therapy in Poland in 2022 [in Polish]. *Nephrol Dial Pol*. 2022;24(3–4):21–38. https://nefroldialpol.pl/wp-content/uploads/2023/05/Akualny-stan-leczenia-nerkozastepczego-w-Polsce-2022-Debska-Slizien-et-al..pdf. Accessed August 15, 2024.
16. Von Elm E, Altman DG, Egger M, Pocock SJ, Gøtzsche PC, Vandenbroucke JP. The Strengthening the Reporting of Observational Studies in Epidemiology (STROBE) statement: Guidelines for reporting observational studies. *Lancet*. 2007;370(9596):1453–1457. doi:10.1016/s0140-6736(07)61602-x
17. Mathew G, Agha R, Albrecht J, et al. STROCSS 2021: Strengthening the reporting of cohort, cross-sectional and case-control studies in surgery. *Int J Surg*. 2021;96:106165. doi:10.1016/j.ijsu.2021.106165
18. Zubizarreta JR, Paredes RD, Rosenbaum PR. Matching for balance, pairing for heterogeneity in an observational study of the effectiveness of for-profit and not-for-profit high schools in Chile. *Ann Appl Stat*. 2014;8(1):204–231. doi:10.1214/13-aoas713
19. Niknam BA, Zubizarreta JR. Using cardinality matching to design balanced and representative samples for observational studies. *JAMA*. 2022;327(2):173. doi:10.1001/jama.2021.20555
20. Visconti G, Zubizarreta JR. Handling limited overlap in observational studies with cardinality matching. *Observ Stud*. 2018;4(1):217–249. doi:10.1353/obs.2018.0012
21. Fortin SP, Schuemie M. Indirect covariate balance and residual confounding: An applied comparison of propensity score matching and cardinality matching. *Pharmacoepidemiol Drug Saf*. 2022;31(12):1242–1252. doi:10.1002/pds.5510
22. Ho D, Imai K, King G, Stuart E, Whitworth A, Greifer N. MatchIt: Nonparametric Preprocessing for Parametric Causal Inference. The Comprehensive R Archive Network; 2023. https://cran.r-project.org/web/packages/MatchIt/index.html. Accessed December 3, 2023.
23. Schwedinger F, Schumacher D, Hall J, Galabova I, Gottwald L, Feldmeier M. highs: "HiGHS" Optimization Solver. The Comprehensive R Archive Network; 2023. https://cran.r-project.org/web/packages/highs/index.html. Accessed December 3, 2023.
24. Kwong JCC, Kroczak T, Honey JRD, et al. Peritoneal dialysis catheter removal at the time of renal transplantation: Choosing the optimal candidate. *Can Urol Assoc J*. 2019;14(1):E13–E19. doi:10.5489/cuaj.5825
25. Faul F, Erdfelder E, Buchner A, Lang AG. Statistical power analyses using G*Power 3.1: Tests for correlation and regression analyses. *Behav Res Methods*. 2009;41(4):1149–1160. doi:10.3758/brm.41.4.1149
26. Snowden JM, Rose S, Mortimer KM. Implementation of G-computation on a simulated data set: Demonstration of a causal inference technique. *Am J Epidemiol*. 2011;173(7):731–738. doi:10.1093/aje/kwq472
27. Greifer N. cobalt: Covariate Balance Tables and Plots. The Comprehensive R Archive Network; 2023. https://cran.r-project.org/web/packages/cobalt/index.html. Accessed December 3, 2023.
28. Wickham H, Chang W, Henry L, et al. ggplot2: Create Elegant Data Visualisations Using the Grammar of Graphics. The Comprehensive R Archive Network; 2023. https://cran.r-project.org/web/packages/ggplot2/index.html. Accessed December 3, 2023.
29. Koneswarakantha B. easyalluvial: Generate Alluvial Plots with a Single Line of Code. The Comprehensive R Archive Network; 2023. https://cran.r-project.org/web/packages/easyalluvial/index.html. Accessed May 19, 2024.
30. Yoshida K, Bartel A, Chipman JJ, et al. tableone: Create "Table 1" to Describe Baseline Characteristics with or without Propensity Score Weights. The Comprehensive R Archive Network; 2023. https://cran.r-project.org/web/packages/tableone/index.html. Accessed December 10, 2023.
31. Arel-Bundock V, Diniz MA, Greifer N, Bacher E. marginaleffects: Predictions, Comparisons, Slopes, Marginal Means, and Hypothesis Tests. The Comprehensive R Archive Network; 2023. https://cran.r-project.org/web/packages/marginaleffects/index.html. Accessed December 12, 2023.
32. Benomar M, Vachey C, Lobbedez T, et al. Peritoneal dialysis after kidney transplant failure: A nationwide matched cohort study from the French Language Peritoneal Dialysis Registry (RDPLF). *Nephrol Dial Transplant*. 2019;34(5):858–863. doi:10.1093/ndt/gfy290

33. Gill JS, Abichandani R, Khan S, Kausz AT, Pereira BJG. Opportunities to improve the care of patients with kidney transplant failure. *Kidney Int*. 2002;61(6):2193–2200. doi:10.1046/j.1523-1755.2002.00373.x
34. Castledine C, Caskey FJ. Dialysis modality after renal transplant failure. *Perit Dial Int*. 2013;33(6):600–603. doi:10.3747/pdi.2013.00087
35. Tanriover C, Copur S, Basile C, Ucku D, Kanbay M. Dialysis after kidney transplant failure: How to deal with this daunting task? *J Nephrol*. 2023;36(7):1777–1787. doi:10.1007/s40620-023-01758-x
36. Irish WD, Ilsley JN, Schnitzler MA, Feng S, Brennan DC. A risk prediction model for delayed graft function in the current era of deceased donor renal transplantation. *Am J Transplant*. 2010;10(10):2279–2286. doi:10.1111/j.1600-6143.2010.03179.x
37. Issa N, Lakhani L. Peritoneal dialysis for delayed graft function after kidney transplantation: To do or not to do? *Kidney Int Rep*. 2021;6(6):1494–1496. doi:10.1016/j.ekir.2021.04.008
38. Najafi I, Hosseini M, Atabac S, et al. Patient outcome in primary peritoneal dialysis patients versus those transferred from hemodialysis and transplantation. *Int Urol Nephrol*. 2012;44(4):1237–1242. doi:10.1007/s11255-011-0068-x
39. Reyes Marin FA, Gómez-Villanueva D, Ballesteros-Santiago A, Amato D. Urgent peritoneal dialysis initiation: Is it better to wait a few days than to use the catheter immediately after its implantation? A randomized controlled trial. *Intern Med*. 2014;4(4):1000159. doi:10.4172/2165-8048.1000159
40. Kutcher SA, Brophy JM, Banack HR, Kaufman JS, Samuel M. Emulating a randomised controlled trial with observational data: An introduction to the Target Trial Framework. *Can J Cardiol*. 2021;37(9):1365–1377. doi:10.1016/j.cjca.2021.05.012
41. Fortin SP, Johnston SS, Schuemie MJ. Applied comparison of large-scale propensity score matching and cardinality matching for causal inference in observational research. *BMC Med Res Methodol*. 2021;21(1):109. doi:10.1186/s12874-021-01282-1

Correlations between OCT, OCT angiography and fundus autofluorescence in adults with superficial optic disc drusen: The importance of multimodal imaging

Paulina Szabelska[1,A–F], Joanna Brydak-Godowska[2,B,D,F], Przemysław Krajewski[2,B,F], Radosław Różycki[1,D,F], Joanna Gołębiewska[1,A,B,D–F]

[1] Department of Ophthalmology, Military Institute of Aviation Medicine, Warsaw, Poland
[2] Department of Ophthalmology, Infant Jesus Clinical Hospital, University Clinical Center, Medical University of Warsaw, Poland

A – research concept and design; B – collection and/or assembly of data; C – data analysis and interpretation;
D – writing the article; E – critical revision of the article; F – final approval of the article

Advances in Clinical and Experimental Medicine, ISSN 1899–5276 (print), ISSN 2451–2680 (online) *Adv Clin Exp Med*. 2025;34(11):1959–1968

Address for correspondence
Joanna Gołębiewska
E-mail: joanna.golebiewska@wp.pl

Funding sources
None declared

Conflict of interest
None declared

Received on December 5, 2024
Reviewed on January 15, 2025
Accepted on February 25, 2025

Published online on June 6, 2025

Abstract

Background. Optic nerve head drusen (ONHD) are benign calcified deposits that can compress local capillaries, disrupt blood flow and potentially lead to visual loss.

Objectives. The aim of the study was to present the correlations between optical coherence tomography (OCT), OCT angiography (OCTA) results and fundus autofluorescence (FAF) findings in patients with ONHD, and to highlight the importance of multimodal imaging in the diagnosis and management of this pathology.

Materials and methods. This retrospective study included 21 patients (36 eyes) with ONHD, with a mean age of 45.75 years (range: 19–71 years), who had no other ocular pathologies. All participants underwent a full ophthalmic examination and multimodal imaging using the DRI Triton OCT (Topcon). Drusen presence was divided into quadrants based on FAF and correlated with OCT and OCTA results.

Results. Optic nerve head drusen were unilateral in 6 patients (28.57%) and bilateral in 15 (71.43%). Drusen were most common in the nasal and superior quadrants (NQ and SQ) but were significantly more frequent in the inferior (IQ) and temporal (TQ) quadrants in patients with bilateral ONHD. Eyes with drusen located in the IQ and TQ showed a significantly decreased radial peripapillary capillary (RPCP) vessel density (VD). Retinal nerve fibre layer (RNFL) measurements showed the strongest positive correlations with RPCP, especially in the IQ ($r = 0.78$, $p < 0.001$). Ganglion cell layer and nerve fiber layer (GCL++) thickness showed significant correlations with RPCP VD, particularly in the IQ and TQ ($p < 0.001$ for both).

Conclusions. Fundus autofluorescence is a valuable tool for identifying superficial drusen. Optical coherence tomography and OCTA are effective in assessing optic nerve fiber integrity and microvascular changes. Microcirculation assessment using OCTA should focus not only on the radial peripapillary capillaries (RPCP), but also on the macular region. Multimodal imaging plays a crucial role in the accurate diagnosis and comprehensive evaluation of patients with ONHD. Further longitudinal studies are needed to investigate how these correlations evolve over time, particularly in the context of ONHD progression.

Key words: optical coherence tomography, multimodal imaging, fundus autofluorescence, optic nerve head drusen, OCT angiography

Cite as
Szabelska P, Brydak-Godowska J, Krajewski P, Różycki R, Gołębiewska J. Correlations between OCT, OCT angiography and fundus autofluorescence in adults with superficial optic disc drusen: The importance of multimodal imaging. *Adv Clin Exp Med*. 2025;34(11):1959–1968. doi:10.17219/acem/202319

DOI
10.17219/acem/202319

Highlights

- The study confirms fundus autofluorescence (FAF) as a sensitive method for detecting superficial optic nerve head drusen (ONHD).
- Optical coherence tomography (OCT) and OCT angiography (OCTA) reveal significant optic nerve fiber and microvascular changes in ONHD.
- Reduced RPCP vessel density (VD) correlates with thinner retinal nerve fibre layer (RNFL), particularly in inferior quadrants, indicating microvascular compromise.
- Macular ganglion cell layer (GCL++) thinning suggest strong associations with superficial capillary plexus (SCP) VD in susceptible superior and inferior quadrants, what should be confirmed in future studies.
- Multimodal imaging is crucial in monitoring ONHD progression.

Background

Optic nerve drusen (OND), also known as optic nerve head drusen (ONHD) or optic disc drusen (ODD), are calcified, acellular deposits that accumulate within the optic nerve head (ONH).[1,2] These deposits are composed of calcium, amino acids, nucleic acids, and mucopolysaccharides.[2]

They can be located superficially, where they are visible during an ophthalmologic examination and give the optic disc a lumpy appearance, or buried deeper in the ONH, where they may cause the disc to appear swollen and congested.[3,4] Recent studies have confirmed that ONHD generally occupy a prelaminar location in the ONH.[3] Buried ONHD creates an elevated optic nerve appearance with an irregular, scalloped border, while superficial ONHD appear as hardened yellow deposits on the surface of the optic nerve.[4]

Histological studies, like those by Tso, suggest that ONHD formation may result from disrupted axoplasmic transport, which causes mitochondria to extrude into the extracellular space.[5] Over time, calcium deposits in the mitochondria lead to the formation of drusen, typically in front of the lamina cribrosa.[4] Although the exact mechanism of ONHD formation remains unclear, it is thought that a small optic disc and a narrow scleral canal may contribute to their development. These anatomical features can restrict axoplasmic flow, leading to impaired transport within the optic nerve fibers and eventually causing ganglion cell axon degeneration.[6,7]

The ONHD affect approx. 0.3–2.4% of the general population.[3,8] They are often bilateral (in about 75% of cases), with a higher preponderance in the nasal, rather than temporal, optic disc quadrants.[2,4] They are more common in Caucasians and may have a genetic predilection.[9–11]

Patients with ONHD usually are asymptomatic and unaware of the condition. If occur, visual field defects are the most common symptom, observed in about 51% of children and 75% of all affected individuals, with reported rates ranging from 11.2% to 87%.[12] However, in cases where symptoms do arise, patients reported peripheral vision loss, reduced night vision, flickering lights, flashes, or brief visual distortions, and increased blind spot size.[13,14] In rare cases, significant loss of visual acuity can occur due to vascular complications associated with ONHD. Such complications may include secondary conditions like central retinal artery (CRAO) or vein (CRVO) occlusion, anterior ischemic optic neuropathy (AION), or the formation of choroidal neovascular membranes (CNV). These issues are often a result of mechanical pressure exerted by the drusen on nearby blood vessels.[15,16]

Diagnosing ONHD requires a comprehensive ophthalmic examination and specialized imaging techniques. Multimodal imaging allows proper diagnosis and those used in ONHD diagnostics include, i.a., color fundus photography, fundus autofluorescence (FAF), ultrasound B-scans, optical coherence tomography (OCT), OCT Angiography (OCTA), and visual field testing.[17]

Fundus autofluorescence exploits the natural fluorescence emitted by certain components of the drusen, allowing them to be visualized clearly. Autofluorescence imaging is valuable for identifying superficial ONHD.[17,18]

Optical coherence tomography is a noninvasive imaging technique that uses light waves to create cross-sectional images of the retina. This test can provide detailed images of the ONH and is particularly useful in assessing the location and extent of the drusen.[17]

Optical coherence tomography angiography provides detailed images of blood flow in the retina and optic nerve.[19] As drusen accumulate within the ONH, they can crowd this area, compressing the small capillaries that supply blood to the optic nerve. This crowding effect, particularly when drusen are superficial or located near major vessels, can cause disturbances in local blood flow. Such compression can lead to minor ischemia in certain areas, potentially affecting nerve fibers and leading to gradual visual field loss.[20] OCTA can show decreased capillary density and areas of peripapillary dropout in patients with ONHD, helping to assess the extent of vascular compromise.[19]

Objectives

The aim of the study was to present correlations between OCT and OCTA results and fundus autofluorescence (FAF) findings in patients with superficial ONHD and highlight the importance of multimodal imaging in this pathology.

Materials and methods

This retrospective study enrolled 21 patients (36 eyes) diagnosed with ONHD who attended the Outpatient Clinic of the Military Institute of Aviation Medicine in Warsaw (Poland) between January 2019 and November 2024. The study protocol was approved by the Bioethics Committee at the Military Medical Chamber (approval No. KB 77/2024).

The inclusion criterion was a diagnosis of superficial drusen, determined by their presence observed in FAF. Exclusion criteria included a history of any retinal or choroidal pathology that could have influenced the results, such as glaucoma, diabetic retinopathy, uveitis, or a refractive error greater than ±3.0 diopters (D).

All patients underwent a complete ophthalmic examination and multimodal imaging using swept-source DRI OCT Triton (SS-OCT; Topcon, Tokyo, Japan), which included color fundus photography, FAF, OCT, en face OCT, and OCTA. The Triton SS-OCT uses a wavelength of 1,050 nm with a scan speed of 100.000 A-scans per second. A 7.0 × 7.0 mm 3D macula scan centered on the fovea and a 6.0 × 6.0 mm 3D disc scan centered on the optic nerve head (ONH) were obtained. The RNFL and GCL++ parameters were measured automatically using the built-in OCT software. GCL++ refers to the combination of the ganglion cell layer (GCL) and the nerve fiber layer (NFL) in the macular region. The OCTA was performed using 4.5 × 4.5 mm images centered on the macula and ONH. Vessel density was automatically calculated by the software as a percentage, based on the area occupied by blood vessels in the superficial capillary plexus (SCP) and radial peripapillary capillaries (RPCP). Macular outcomes were measured in the fovea (0–1 mm) and parafoveally. The parafoveal area, as defined by the 3-mm partial early treatment diabetic retinopathy study (ETDRS) chart provided by the software, corresponds to the region between the 1-mm and 3-mm concentric rings centered on the fovea. This area was further divided into 4 sectors for quadrant analysis: temporal (TQ), superior (SQ), nasal (NQ), and inferior (IQ).

Eyes with low-quality scans (image quality <60), with motion artifacts or blurred images were excluded from the final analysis.

Statistical analyses

Numerical variables were presented as their mean and standard deviation (SD) values. Categorical variables were described through integer numbers and percentages. The Shapiro–Wilk W test was performed to verify the normality of distribution. Levene's test was fitted to assess the homogeneity of variances. A multifactor analysis of variance (ANOVA) without replications was carried out for normally distributed numerical traits with homogenic variances when estimating the significance of differences in the investigated traits by prevalence of drusen. Generalized linear models were applied otherwise, when dealing with non-normally distributed variables or heterogenic variances (normal distribution and identity link function were chosen). The parametric models were controlled for age. Their goodness-of-fit was assessed by calculating the Akaike information criterion (AIC) and Bayesian information criterion (BIC), instead of R^2, which cannot be computed for the Generalized Linear Models used. A special correction method for p-values was used when encompassing family hypotheses if applicable. Model testing was based on one main independent (grouping) variable, i.e., the presence of drusen in the examined eyes, along with participants' age as a control variable. No explicit "family of hypotheses" was established, as the analyses consistently focused on the presence of drusen, controlled for age, and investigated separate and independent retinal areas, which did not naturally infer one another. To estimate linear relationships between pairs of numerical traits, the Pearson's product-moment correlation coefficients were computed. For discrete variables, the significance of references in frequencies were tested by using Fisher's exact test. A level of $p < 0.05$ was considered statistically significant. All the statistical procedures were performed using Statistica v. 13.3 (TIBCO Software Inc., Palo Alto, USA)

Results

The study involved 14 female and 7 male participants. The mean age of the subjects was 45.75 years (range: 19–71 years; SD = 14.81). All participants were Caucasian, in good general health, and had a best-corrected visual acuity (BCVA) ranging from 0.8 to 1.0. Intraocular pressure (IOP) was within normal limits (ranging from 12 mm Hg to 20 mm Hg) in all patients.

Patients' demographic and clinical characteristics were summarized in Table 1. The ONHD occurred unilaterally

Table 1. Demographic and clinical characteristics of patients with ONHD

Characteristics	Patients (n = 21)
Age, range [years]	19–71 (M = 45.75; SD = 14.81)
Sex, n (%)	14 female (66.67), 7 male (33.33)
Race, n (%)	21 Caucasian (100%)
BCVA, range	0.8–1.0

n – integer number, M – mean, SD – standard deviation; BVCA – best-corrected visual acuity; ONHD – optic nerve head drusen.

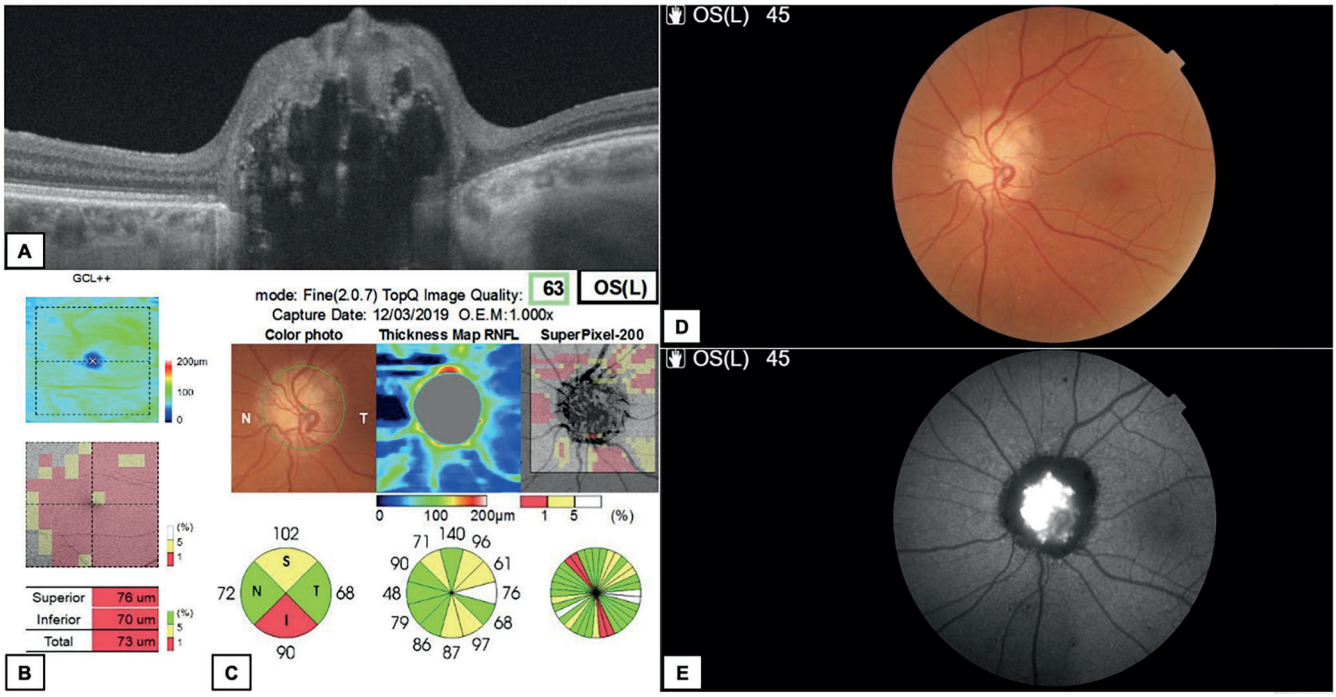

Fig. 1. Multimodal imaging of the left eye (LE) in patient with ONHD. A. SS-OCT B–scan showed hyporeflective core and hyperreflective halo around deposits visible in the ONH; B,C. Decreased RNFL in SQ and IQ and GCL++ values; D. Color fundus photography – indistinct margins and mild swelling of the ONH; E. FAF – irregular hyperautofluorescent round structures with irregular edges were observed in ONH

SQ – superior quadrant; IQ – inferior quadrant; NQ – nasal quadrant; TQ – temporal quadrant; ONHD – optic nerve head drusen.

Table 2. Baseline characteristics of the study cohort by number of eyes with ONHD

Analyzed trait	Overall	Unilateral drusen	Bilateral drusen	p-value*
Number of participants, n (%)	21 (100.00)	6 (28.57)	15 (71.43)	–
Number of eyes, n (%)	36 (100.00)	6 (16.67)	30 (83.33)	–
Drusen in quadrants, n (%)				
SQ	30 (83.33)	6 (100.00)	24 (80.00)	0.561
IQ	27 (75.00)	2 (33.33)	25 (83.33)	**0.024**
NQ	32 (88.89)	6 (100.00)	26 (86.67)	>0.999
TQ	15 (41.67)	0 (0.00)	15 (50.00)	**0.030**
Age [years], M (SD)	45.75 (14.81)	43.83 (19.97)	46.13 (13.97)	$F(1,34) = 0.12$ $\Delta = 2.30$ partial $\eta^2 < 0.00$ $p = 0.734$ (Levene's test $F(1,34) = 3.78$ $p = 0.060$)

n – integer number, M – mean; SD – standard deviation; SQ – superior quadrant; IQ – inferior quadrant; NQ – nasal quadrant; TQ – temporal quadrant; ONHD – optic nerve head drusen. * Fisher's two-sided test was performed, only p-values are presenteded. Values in bold are statistically significant.

in 6 (28.57%) and bilaterally in 15 patients (71.43%). Multimodal imaging findings of ONHD were presented in Fig. 1 and Fig. 2.

The FAF imaging technique was used to detect the presence of superficial drusen and to categorize them by their location into specific quadrants. Based on FAF findings, ONHD most frequently occurred in the NQ and SQ. However, we observed that ONHD in the TQ and IQ were more common in patients with bilateral drusen than in those with unilateral drusen, and the differences were statistically significant:

– for TQ ($p = 0.030$), as no eyes in the unilateral group exhibited temporal drusen, while 50% of eyes in the bilateral group did;

– for IQ ($p = 0.025$), with a higher percentage of affected eyes in the bilateral group (83.33%) compared to the unilateral group (33.33%) (Table 2).

The RNFL thickness decreased significantly with age in all quadrants except the TQ ($p = 0.362$). The GCL++ thickness also showed a decreasing trend, but without statistical significance (Table 3).

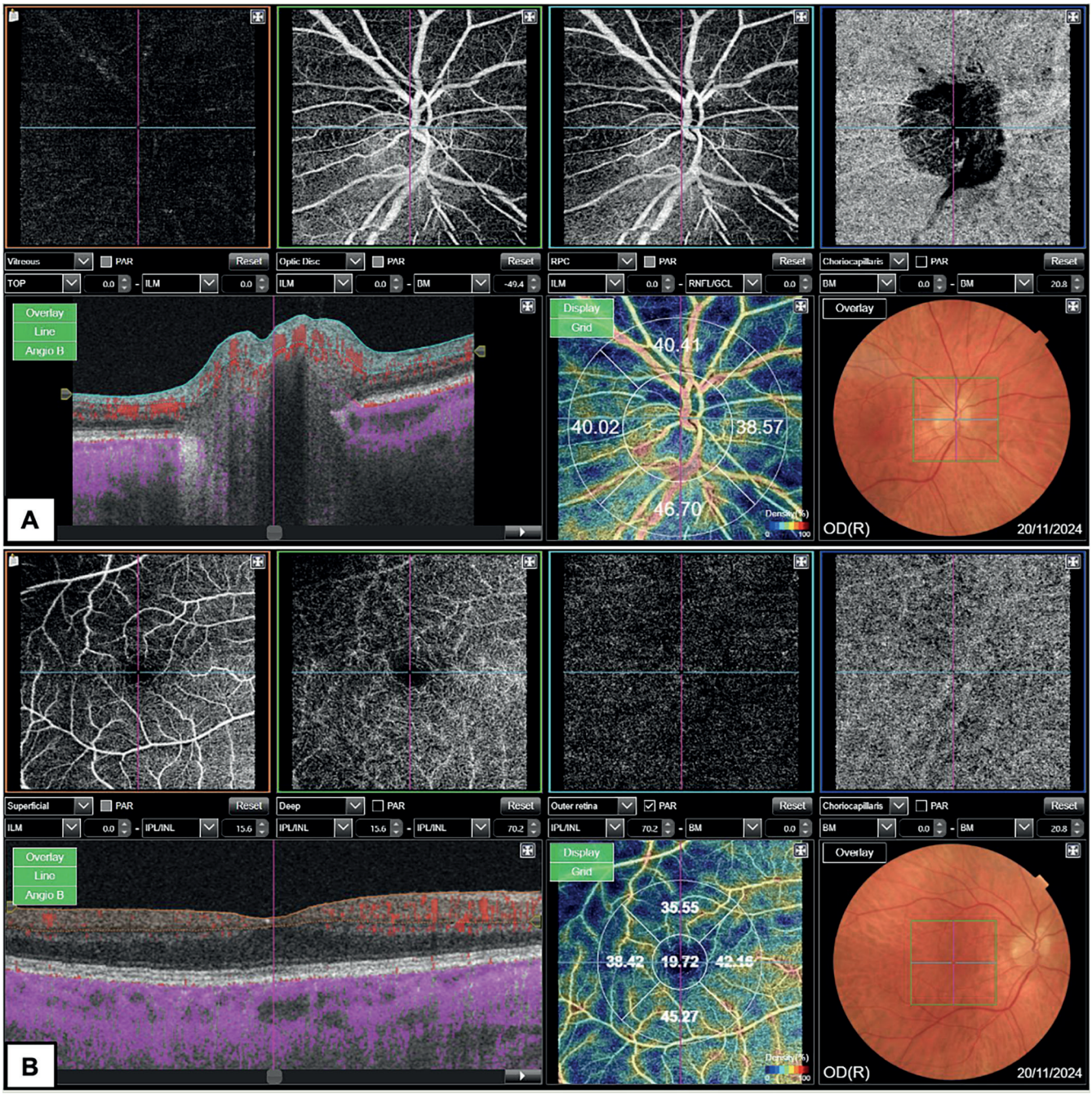

Fig. 2. OCTA of the ONH and macula in patient with ONHD (right eye (RE)). A. VD map of ONH region showed decreased RPCP density (dark blue color) in SQ and NQ; B. VD map of SCP showed decreased VD (dark blue color) in SQ, NQ and TQ of the macula

OCTA – optical coherence tomography angiography; ONH – optic nerve head; VD – vessel density; ONH – optic nerve head; RPCP – radial peripapillary capillaries; SQ – superior quadrant; NQ – nasal quadrant; TQ – temporal quadrant; SCP – superficial capillary plexus.

Age was significantly negatively correlated with RPCP VD in the SQ, IQ, and NQ, indicating reduced capillary density in these areas. The TQ RPCP VD showed a moderate negative trend; however, it did not reach statistical significance ($p = 0.053$). Significant negative correlations were found in the IQ and TQ of SCP VD, suggesting reduced VD with age. However, foveal VD (FVD) increased significantly with age ($r = 0.38$, $p = 0.044$) (Table 4).

A comparison was made between OCTA measurements and other structural parameters, including RNFL and GCL++.

RPCP VD was analyzed by comparing eyes with and without drusen detected by FAF. Eyes with ONHD in the IQ and TQ showed significantly lower RPCP VD compared to eyes without drusen. No significant difference was found in the SQ. While there was a trend for lower RPCP VD in the NQ, the difference was not statistically significant (Table 5).

Optical coherence tomography measurements and RPCP VD were compared. RNFL thickness showed positive correlations with RPCP VD, with the strongest correlation

Table 3. Pearson's product-moment correlation coefficients and corresponding p-values for the investigated OCT measurements vs age in the study participants' eyes

OCT	Age [years]		
	r	n	p-value
RNFL [µm]			
SQ	**–0.50**	36	**0.002**
IQ	**–0.51**	36	**0.002**
NQ	**–0.50**	36	**0.002**
TQ	–0.16	36	0.362
Total	**–0.51**	36	**0.001**
GCL++ [µm]			
Superior	–0.25	36	0.146
Inferior	–0.21	36	0.223
Total	–0.25	36	0.147

n – integer number, r – Pearson correlation coefficient; OCT – optical coherence tomography; RNFL – retinal nerve fibre layer; SQ – superior quadrant; IQ – inferior quadrant; NQ – nasal quadrant; TQ – temporal quadrant; GCL++ – ganglion cell layer and the nerve fiber layer. Values in bold are statistically significant.

Table 4. Pearson's product-moment correlation coefficients and corresponding p-values for the investigated OCTA measurements vs age in the study participants' eyes

OCTA	Age [years]		
	r	n	p-value
RPCP VD [%]			
SQ	**–0.52**	36	**0.001**
IQ	**–0.37**	36	**0.024**
NQ	**–0.57**	36	**<0.001**
TQ	–0.33	36	0.053
SCP VD [%]			
SQ	–0.34	36	0.074
IQ	**–0.37**	36	**0.049**
NQ	–0.29	36	0.126
TQ	**–0.42**	36	**0.024**
FVD	**0.38**	36	**0.044**

n – integer number, r – Pearson correlation coefficient; OCTA – optical coherence tomography angiography; SQ – superior quadrant; IQ – inferior quadrant; NQ – nasal quadrant; TQ – temporal quadrant; RPCP – radial peripapillary capillaries; SCP – superficial capillary plexus; FVD – foveal vessel density. Values in bold are statistically significant.

Table 5. RPCP VD values [%] in individual quadrants of the ONH by drusen occurrence in FAF

Quadrant	Drusen occurrence in FAF	Statistical parameter*			
		M	SD	normality	GLZ**
SQ	present	43.76	6.20	W = 0.95 p = 0.156	Wald stat. 0.90 estimate 1.01 ((–1.09)–3.12) Δ = 1.48 AIC = 222.85 BIC = 229.19 p = 0.344 **(Levene's test F(1,34) = 4.92** **p = 0.033)**
	absent	45.24	2.28	W = 0.96 p = 0.838	
IQ	present	44.76	5.74	W = 0.96 p = 0.457	**Wald stat. 7.71** **estimate 2.42 (0.71–4.13)** **Δ = 4.47** **AIC = 218.82** **BIC = 225.16** **p = 0.005** **(Levene's test F(1,34) = 6.96** **p = 0.008)**
	absent	49.23	2.46	W = 0.92 p = 0.436	
NQ	present	39.90	6.29	W = 0.93 p = 0.053	Wald stat. 0.93 estimate 1.31 ((–1.36)–3.98) Δ = 3.90 AIC = 227.54 BIC = 233.88 p = 0.335 (Levene's test F(1,34) = 0.14 p = 0.707)
	absent	43.80	6.97	W = 0.91 p = 0.459	
TQ	present	43.46	3.12	W = 0.98 p = 0.960	**Wald stat. 7.18** **estimate 1.55 (0.42–2.68)** **Δ = 3.38** **AIC = 197.96** **BIC = 204.30** **p = 0.007** (Levene's test F(1,34) = 0.07 p = 0.789)
	absent	46.84	3.98	W = 0.95 p = 0.285	

*M – mean; SD – standard deviation. **Generalized Linear Models were carried out, controlled for age. AIC – Akaike information criterion; BIC – Bayesian information criterion; SQ – superior quadrant; IQ – inferior quadrant; NQ – nasal quadrant; TQ – temporal quadrant; FAF – fundus autofluorescence; RPCP – radial peripapillary capillaries; VD – vessel density; ONH – optic nerve head; FAF – fundus autofluorescence. Values in bold are statistically significant.

Table 6. Pearson's product-moment correlation coefficients and corresponding p-values for the investigated OCT measurements vs RPCP VD in the study participants' eyes

OCT	RPCP VD, SQ [%]		RPCP VD, IQ [%]		RPCP VD, NQ [%]		RPCP VD, TQ [%]	
	r	p-value	r	p-value	r	p-value	r	p-value
RNFL [µm]								
SQ	**0.60**	**<0.001**	**0.57**	**<0.001**	**0.53**	**<0.001**	**0.43**	**0.009**
IQ	**0.59**	**<0.001**	**0.78**	**<0.001**	**0.53**	**<0.001**	**0.57**	**<0.001**
NQ	**0.42**	**0.010**	**0.39**	**0.017**	**0.64**	**<0.001**	0.09	0.606
TQ	**0.38**	**0.021**	**0.51**	**0.001**	**0.34**	**0.043**	**0.61**	**<0.001**
Total	**0.63**	**<0.001**	**0.70**	**<0.001**	**0.60**	**<0.001**	**0.53**	**<0.001**
GCL++ [µm]								
Superior	**0.35**	**0.036**	**0.50**	**0.002**	**0.38**	**0.023**	**0.54**	**<0.001**
Inferior	**0.44**	**0.007**	**0.57**	**<0.001**	**0.36**	**0.033**	**0.57**	**<0.001**
Total	**0.43**	**0.010**	**0.57**	**<0.001**	**0.39**	**0.018**	**0.59**	**<0.001**

Number of correlated pairs of variables was always n = 36. n – integer number, r – Pearson's correlation coefficient; OCT – optical coherence tomography; RNFL – retinal nerve fibre layer; SQ – superior quadrant; IQ – inferior quadrant; NQ – nasal quadrant; TQ – temporal quadrant; GCL++ – ganglion cell layer and the nerve fiber layer; RPCP – radial peripapillary capillaries; VD – vessel density. Values in bold are statistically significant.

Table 7. Pearson's product-moment correlation coefficients and corresponding p-values for the VD SCP vs RPCP in the study participants' eyes

SCP VD	RPCP VD, SQ (%)		RPCP VD, IQ (%)		RPCP VD, NQ (%)		RPCP VD, TQ (%)	
	r	p-value	r	p-value	r	p-value	r	p-value
SQ	**0.43**	**0.018**	**0.37**	**0.048**	0.34	0.068	**0.49**	**0.006**
IQ	**0.39**	**0.037**	**0.44**	**0.017**	0.29	0.132	**0.57**	**0.001**
NQ	0.27	0.149	0.31	0.099	**0.38**	**0.041**	**0.44**	**0.018**
TQ	**0.42**	**0.021**	0.28	0.143	0.35	0.060	**0.38**	**0.043**
Fovea	–0.31	0.096	–0.33	0.078	–0.37	0.049	–0.21	0.285

Number of correlated pairs of variables was always n = 36. n – integer number, r – Pearson's correlation coefficient; SQ – superior quadrant; IQ – inferior quadrant; NQ – nasal quadrant; TQ – temporal quadrant; RPCP – radial peripapillary capillaries; SCP – superficial capillary plexus; VD – vessel density. Values in bold are statistically significant.

observed between the IQ RNFL and RPCP VD (r = 0.78, p < 0.001). GCL++ measurements also showed moderate positive correlations with RPCP VD, particularly in the IQ and TQ (Table 6). The dependencies of VD in the SCP and RPCP across various quadrants were analyzed. Significant correlations were primarily observed in the SQ and IQ, particularly within their corresponding RPCP regions. The fovea showed weak or negative correlations with RPCP, with 1 significant negative correlation in the NQ (Table 7).

The OCT parameters and VD in SCP in different quadrants and the fovea were examined. The strongest positive correlations were found between total GCL++ and SCP VD in the SQ and IQ (r = 0.60–0.62, p < 0.001). The weakest and mostly nonsignificant correlations were found between RNFL, GCL++ and SCP VD in NQ (Table 8).

Discussion

The prevalence of ONHD is estimated at 0.2–2% in adults and 0.37–1% in children.[3,8,21] The patients in our study were between 19 and 71 years old, and age did not appear to have a significant impact on the distinction between unilateral and bilateral drusen cases. The exact pathogenesis of drusen is still uncertain, but they are believed to harm retinal nerve fibers directly through axonal compression and indirectly by inducing ischemia in the RNFL due to vascular compression.[22] Therefore, diagnostic tests are crucial for enhancing the management of patients with ONHD. Previous attempts to investigate the relationship between ONHD severity and optic nerve damage relied on subjective grading systems based on ONH photography, parameters such as ONHD diameter, or imaging techniques like Spectral-Domain OCT (SD-OCT) to assess disease severity.[14,23]

The FAF is a noninvasive diagnostic technique that detects drusen by utilizing the natural fluorescence emitted by their components, making them easily identifiable. In very young children, ONHD are typically located deeper within the tissue.[24] A major limitation of FAF is its reduced ability to detect deeper, buried drusen.[25] Nonetheless, drusen often becomes superficial by late childhood.[24] Given its capability to detect and map the distribution of drusen, FAF proves to be a valuable tool for diagnosing and managing superficial ONHD,[17,18] and therefore we chose this method to identify superficial drusen in our group.

Table 8. Pearson's product-moment correlation coefficients and corresponding p-values for the investigated OCT measurements vs SCP VD in the study participants' eyes

OCT	SCP VD, SQ [%]		SCP VD, IQ [%]		SCP VD, NQ [%]		SCP VD, TQ [%]		SCP VD, Fovea [%]	
	r	p-value	r	p-value	r	p-value	r	p-value	r	p-value
RNFL [µm]										
SQ	**0.43**	**0.021**	0.33	0.082	0.26	0.171	0.36	0.054	–0.10	0.609
IQ	**0.38**	**0.041**	**0.44**	**0.016**	0.18	0.351	0.34	0.067	–0.18	0.350
NQ	0.13	0.498	0.11	0.559	0.08	0.676	0.11	0.558	–0.17	0.363
TQ	**0.38**	**0.040**	**0.45**	**0.015**	0.32	0.093	0.34	0.074	0.13	0.487
Total	**0.42**	**0.022**	**0.42**	**0.024**	0.26	0.176	**0.37**	**0.048**	–0.11	0.577
GCL++ [µm]										
Superior	**0.54**	**0.002**	**0.50**	**0.006**	0.36	0.054	0.28	0.144	0.25	0.190
Inferior	**0.56**	**0.001**	**0.65**	**<0.001**	**0.46**	**0.012**	**0.48**	**0.009**	0.14	0.473
Total	**0.60**	**<0.001**	**0.62**	**<0.001**	**0.45**	**0.014**	**0.41**	**0.029**	0.22	0.255

Number of correlated pairs of variables was always n = 36. n – integer number, r – Pearson's correlation coefficient; OCT – optical coherence tomography; RNFL – retinal nerve fibre layer; SQ – superior quadrant; IQ – inferior quadrant; NQ – nasal quadrant; TQ – temporal quadrant; GCL++ – ganglion cell layer and the nerve fiber layer; SCP – superficial capillary plexus; VD – vessel density. Values in bold are statistically significant.

Consistent with the available literature, which states that ONHD is often bilateral (in approx. 75% of cases),[2,4] we found bilateral drusen in 71.43% of our patients. The authors reported that ONHD has a higher prevalence in the NQ compared to the TQ of the optic disc,[2,4] which was confirmed by our findings. Interestingly, in our study, drusen were significantly more common in TQ and IQ in bilateral than unilateral cases. This suggests that fluorescence in the TQ and IQ, as confirmed by FAF, may serve as an important biomarker for the presence of bilateral drusen and warrants further investigation.

Our research focused on the correlations between FAF, OCT and OCTA. To the best of our knowledge, this is the first study to examine the relationship between those diagnostic methods based on presence of superficial drusen in FAF.

The OCT allows for detailed analysis of both the RNFL and GCC by providing high-resolution images. It allows for the assessment of structural changes in these layers, which are crucial for the diagnosis and monitoring of diseases.[17] Optical coherence tomography-based studies report that both the RNFL and GCC undergo thinning with age.[26] These age-related changes were also confirmed in our study group (Table 3).

The OCTA provides detailed images of retinal and optic nerve blood flow, highlighting reduced capillary density and peripapillary dropout in ONHD patients.[19] Additionally, retinal VD declines with age. Previous studies suggest that age-related narrowing of retinal arteries leads to decreased perfusion pressure and lower blood flow, particularly in the peripapillary and parafoveal regions, contributing to reduced vascular function.[27] This trend was also observed in our study group (Table 4).

The introduction of OCTA has improved the assessment of the RPCP, overcoming limitations of previous dye-based methods. The RPCP is thought to supply blood to the RNFL in the peripapillary region. Mase et al. found that RPCP perfusion density is highest in the peripapillary area and decreases toward the macula, with a significant positive correlation to RNFL thickness in healthy eyes.[28] Cennamo et al. found that patients with ONHD exhibited a lower flow index and reduced VD in ONH in OCTA compared to the control group.[29] In our study, we observed a significant reduction in RPCP VD in all quadrants where drusen were present. We focused on RPCP perfusion within a 700 µm elliptical ring around the optic disc,[20] revealing significant VD differences in the TQ and IQ, which can be explained by the fact that the majority of cases were bilateral. Our results were consistent with the available literature, in which RPCP VD in the TQ in ONHD group was found to be lower.[30]

In the current literature, there are only a few publications addressing vascular changes in the macula in patients with ONHD.[16,30,31] Turker et al. found no statistically significant differences in the superficial capillary plexus (SCP) and deep capillary plexus (DCP) VD values of the parafoveal and foveal regions between patients with superficial drusen and healthy controls. Therefore, we focused on the SCP VD of the macula to simplify our analysis.[30] Yan et al. identified a negative correlation between the presence of drusen and macular flow measurements, suggesting that reduced macular perfusion may serve as a potential early biomarker, based on the analysis of 29 eyes compared to eyes without abnormalities.[16]

Based on current studies,[31] our research revealed a reduction in VD in both SCP and RPCP. Notable correlations were identified in the SQ and IQ of SCP VD, particularly in quadrants overlapping with RPCP regions. This suggests that regions of diminished VD detected via OCTA may be considered predictors for the development of future central scotoma,[31] confirming the findings of Yan et al. that reduced macular VD serves as an early and valuable biomarker of ischemia.[16] These findings are consistent

with the theory that enlarged ONHD could lead to acute or chronic ischemia by exerting pressure on adjacent nerve fibers or blood vessels. For now, our study represents the largest group of eyes in which vascular abnormalities in the macula have been confirmed among patients with ONHD. Furthermore, it is the first research comparing SCP VD of the macula with RNFL, suggesting strong correlations of these parameters, particularly in the SQ and IQ.

The origin of RNFL damage in ONHD – whether due to direct axonal compression by drusen or indirectly through vascular compromise – remains uncertain. Noval et al. reported that eyes with superficial ONHD exhibited thinner RNFL compared to controls, whereas those with buried ONHD did not show this correlation.[32] Similarly, Sato et al. found a significant negative correlation between ONHD diameter and RNFL thickness.[4] In our study, RNFL thickness demonstrated strong positive correlations with RPCP VD across all quadrants, particularly in the IQ, where the correlation was the highest ($r = 0.78$, $p < 0.001$). In our ONHD cohort, a reduction in RPCP VD was associated with thinner RNFL. These findings align with previous research, suggesting the association between thinner RNFL and decreased peripapillary microvascular circulation, as indicated by lower RPCP VD.[30]

Notably, total RNFL thickness showed a stronger correlation with RPCP VD than GCC, suggesting that RNFL measurements may serve as a more reliable indicator of microvascular integrity in the ONH. This is particularly relevant in conditions like ONHD, where microvascular changes might precede overt nerve fiber damage.

Advanced OCT technology enables precise macular GCC assessment through automated segmentation. The ganglion cell complex (GCC) encompasses 3 retinal layers: the macular retinal nerve fiber layer (mRNFL), the GCL and the inner plexiform layer (IPL). It is primarily used in assessing the health of the macular region, particularly for early optic nerve damage detection as in glaucoma, monitoring disease progression and advanced-stage evaluation of abnormalities.[33] Notably, asymmetry between macular hemifields in the ganglion cell–inner plexiform layer (GCIPL) can indicate early stages of optic nerve damage, such as in preperimetric glaucoma.[34] GCL++ refers to the combination of the GCL and the NFL, focusing on fewer layers than the GCC, and is often used to simplify assessments, particularly for the early detection of neural damage.[33] Based on this, we selected the GCL++ parameter to simplify our analysis and to evaluate early abnormalities in patients with ONHD. To the best of our knowledge, this is the first study to analyze the GCL++ parameter in patients with ONHD.

Our results demonstrated moderate positive correlations between GCL++ measurements and RPCP VD, particularly in the IQ and TQ (Table 6). The relationship between GCL++ and RPCP in these regions aligns with previous research indicating that ganglion cell loss can influence the vascular supply to the retina, particularly in areas prone to damage like the IQ and TQ. Studies, including those on the "macular vulnerability zone" (MVZ), have shown that GCC thinning in the IQ and TQ regions of the macula corresponds to structural fragility in these areas, particularly involving the lamina cribrosa.[34] The initial IQ loss of GCC and RNFL, compared to the SQ, is due to the increased fragility of the inferior lamina cribrosa and the higher fiber density in the inferior segment. This fragility is linked to the weak connective tissue and large pores, which are secondary to the high fiber density in the inferotemporal sector of the ONH.[35–37] The thinning of the GCC affects vascular supply, suggesting that its loss significantly impacts RPCP VD in susceptible zones. Additionally, as visual field deficits and GCC thinning progress, a more pronounced decline in RPCP VD values may serve as a late-stage biomarker in ONHD cases.[16]

This study is the first to compare SCP VD with GCL++. We found a positive correlation between total GCL++ and SCP VD in both the SQ and IQ ($r = 0.60–0.62$, $p < 0.001$), with the SQ being more affected, possibly due to the higher frequency of ONH drusen in this area. Furthermore, GCL++ suggested a stronger association with SCP VD than RNFL. Additional longitudinal research is required to investigate how these correlations develop over the time.

Limitations

The limitations of this study include the small patient cohort and its retrospective design.

Conclusions

This study confirmed that FAF is a useful, sensitive tool for identifying superficial drusen. The OCT and OCTA are valuable methods for assessing the impact of ONHD on optic nerve fibers and microvascular alterations. The assessment of microcirculation using OCTA should include not only the RPCP but also the macula, as we observed attenuation of macular flow, which should be confirmed in a larger study group.

Multimodal imaging plays a crucial role in accurately diagnosing and thoroughly evaluating patients with ONHD. Further longitudinal studies are needed to explore how these correlations evolve over time, particularly in the context of ONHD progression.

Data availability statement

The datasets supporting the findings of the current study are openly available in Zenodo at: https://doi.org/10.5281/zenodo.14790582.

Consent for publication

Not applicable.

Use of AI and AI-assisted technologies

Not applicable.

ORCID iDs

Paulina Szabelska https://orcid.org/0000-0002-6216-0646
Joanna Brydak-Godowska https://orcid.org/0000-0002-7567-4777
Przemysław Krajewski https://orcid.org/0000-0001-5136-1621
Radosław Różycki https://orcid.org/0000-0001-7040-026X
Joanna Gołębiewska https://orcid.org/0000-0002-3013-4363

References

1. Sadun AA, Wang MY. Abnormalities of the optic disc. *Handb Clin Neurol*. 2011;102:117–157. doi:10.1016/B978-0-444-52903-9.00011-X
2. Friedman AH, Beckerman B, Gold DH, Walsh JB, Gartner S. Drusen of the optic disc. *Surv Ophthalmol*. 1977;21(5):373–390. doi:10.1016/0039-6257(77)90041-8
3. Friedman AH, Gartner S, Modi SS. Drusen of the optic disc: A retrospective study in cadaver eyes. *Br J Ophthalmol*. 1975;59(8):413–421. doi:10.1136/bjo.59.8.413
4. Sato T, Mrejen S, Spaide RF. Multimodal imaging of optic disc drusen. *Am J Ophthalmol*. 2013;156(2):275–282.e1. doi:10.1016/j.ajo.2013.03.039
5. Tso MO. Pathology and pathogenesis of drusen of the optic nerve-head. *Ophthalmology*. 1981;88(10):1066–1080. doi:10.1016/s0161-6420(81)80038-3
6. Arbabi EM, Fearnley TE, Carrim ZI. Drusen and the misleading optic disc. *Pract Neurol*. 2010;10(1):27–30. doi:10.1136/jnnp.2009.200089
7. Davis PL, Jay WM. Optic nerve head drusen. *Semin Ophthalmol*. 2003;18(4):222–242. doi:10.1080/08820530390895244
8. Asli Dinc U, Tatlipinar S, Gorgun E, Yenerel M. Fundus autofluorescence in optic disc drusen: Comparison of confocal scanning laser ophthalmoscope and standard fundus camera. *Neuroophthalmology*. 2009;33(6):318–321. doi:10.3109/01658100903360338
9. Rosenberg MA, Savino PJ, Glaser JS. A clinical analysis of pseudopapilledema. I. Population, laterality, acuity, refractive error, ophthalmoscopic characteristics, and coincident disease. *Arch Ophthalmol*. 1979;97(1):65–70. doi:10.1001/archopht.1979.01020010005001
10. Kiegler HR. Comparison of functional findings with results of standardized echography of the optic nerve in optic disk drusen [in German]. *Wien Klin Wochenschr*. 1995;107(21):651–653. PMID:8578752.
11. Boldt HC, Byrne SF, DiBernardo C. Echographic evaluation of optic disc drusen. *J Clin Neuroophthalmol*. 1991;11(2):85–91. PMID:1832690.
12. Savino PJ, Glaser JS, Rosenberg MA. A clinical analysis of pseudopapilledema. II. Visual field defects. *Arch Ophthalmol*. 1979;97(1):71–75. doi:10.1001/archopht.1979.01020010011002
13. Lorentzen SE. Drusen of the optic disk: A clinical and genetic study. *Acta Ophthalmol (Copenh)*. 1966;Suppl 90:1–180. PMID:6012937.
14. Malmqvist L, Wegener M, Sander BA, Hamann S. Peripapillary retinal nerve fiber layer thickness corresponds to drusen location and extent of visual field defects in superficial and buried optic disc drusen. *J Neuroophthalmol*. 2016;36(1):41–45. doi:10.1097/WNO.0000000000000325
15. Abegão Pinto L, Vandewalle E, Marques-Neves C, Stalmans I. Visual field loss in optic disc drusen patients correlates with central retinal artery blood velocity patterns. *Acta Ophthalmol*. 2014;92(4):e286–291. doi:10.1111/aos.12314
16. Yan Y, Zhou X, Chu Z, et al. Vision loss in optic disc drusen correlates with increased macular vessel diameter and flux and reduced peripapillary vascular density. *Am J Ophthalmol*. 2020;218:214–224. doi:10.1016/j.ajo.2020.04.019
17. Allegrini D, Pagano L, Ferrara M, et al. Optic disc drusen: A systematic review: Up-to-date and future perspective. *Int Ophthalmol*. 2020;40(8):2119–2127. doi:10.1007/s10792-020-01365-w
18. Bonnin P, Passot N, Triolaire-Cotten T. Autofluorescence of papillary drusen in the diagnosis of false papillary edema [in French]. *Bull Soc Ophtalmol Fr*. 1976;76(4):331–335. PMID:1028524.
19. Gaier ED, Rizzo JF, Miller JB, Cestari DM. Focal capillary dropout associated with optic disc drusen using optical coherence tomographic angiography. *J Neuroophthalmol*. 2017;37(4):405–410. doi:10.1097/WNO.0000000000000502
20. Engelke H, Shajari M, Riedel J, Mohr N, Priglinger SG, Mackert MJ. OCT angiography in optic disc drusen: Comparison with structural and functional parameters. *Br J Ophthalmol*. 2020;104(8):1109–1113. doi:10.1136/bjophthalmol-2019-314096
21. Rotruck J. A review of optic disc drusen in children. *Int Ophthalmol Clin*. 2018;58(4):67–82. doi:10.1097/IIO.0000000000000236
22. Beck RW, Corbett JJ, Thompson HS, Sergott RC. Decreased visual acuity from optic disc drusen. *Arch Ophthalmol*. 1985;103(8):1155–1159. doi:10.1001/archopht.1985.01050080067022
23. Casado A, Rebolleda G, Guerrero L, et al. Measurement of retinal nerve fiber layer and macular ganglion cell-inner plexiform layer with spectral-domain optical coherence tomography in patients with optic nerve head drusen. *Graefes Arch Clin Exp Ophthalmol*. 2014;252(10):1653–1660. doi:10.1007/s00417-014-2773-5
24. Chang MY, Pineles SL. Optic disk drusen in children. *Surv Ophthalmol*. 2016;61(6):745–758. doi:10.1016/j.survophthal.2016.03.007
25. Auw-Haedrich C, Staubach F, Witschel H. Optic disk drusen. *Surv Ophthalmol*. 2002;47(6):515–532. doi:10.1016/s0039-6257(02)00357-0
26. Li C, Cheng Y, Zhang Y, et al. Variation in retinal nerve fiber layer and ganglion cell complex associated with optic nerve head size in healthy eyes. *Transl Vis Sci Technol*. 2023;12(3):26. doi:10.1167/tvst.12.3.26
27. Ding X, Lu L, Yang J, Chen Y, Ma J. The peripapillary retinal capillary density is highly correlated with its nerve fibre layer in normal population. *Clin Hemorheol Microcirc*. 2020;74(3):231–239. doi:10.3233/CH-180453
28. Mase T, Ishibazawa A, Nagaoka T, Yokota H, Yoshida A. Radial peripapillary capillary network visualized using wide-field montage optical coherence tomography angiography. *Invest Ophthalmol Vis Sci*. 2016;57(9):OCT504–510. doi:10.1167/iovs.15-18877
29. Cennamo G, Tebaldi S, Amoroso F, Arvanitis D, Breve M, Cennamo G. Optical coherence tomography angiography in optic nerve drusen. *Ophthalmic Res*. 2018;59(2):76–80. doi:10.1159/000481889
30. Turker IC, Uzun SU, Dogan CU, et al. Evaluation of peripapillary and macular vascular flow changes with OCT-A in patients with superficial optic disk drusen. *Sisli Etfal Hastan Tip Bul*. 2022;56(2):196–201. doi:10.14744/SEMB.2021.07348
31. Biçer Ö, Atilla H. Microvascular changes associated with optic disc drusen: Case report. *Turk J Ophthalmol*. 2019;49(5):300–304. doi:10.4274/tjo.galenos.2019.14194
32. Noval S, Visa J, Contreras I. Visual field defects due to optic disk drusen in children. *Graefes Arch Clin Exp Ophthalmol*. 2013;251(10):2445–2450. doi:10.1007/s00417-013-2384-6
33. Tan O, Chopra V, Lu ATH, et al. Detection of macular ganglion cell loss in glaucoma by Fourier-domain optical coherence tomography. *Ophthalmology*. 2009;116(12):2305–2314.e1–2. doi:10.1016/j.ophtha.2009.05.025
34. Ghita AM, Iliescu DA, Ghita AC, Ilie LA, Otobic A. Ganglion cell complex analysis: Correlations with retinal nerve fiber layer on optical coherence tomography. *Diagnostics (Basel)*. 2023;13(2):266. doi:10.3390/diagnostics13020266
35. Jonas JB, Fernández MC, Stürmer J. Pattern of glaucomatous neuroretinal rim loss. *Ophthalmology*. 1993;100(1):63–68. doi:10.1016/s0161-6420(13)31694-7
36. Jonas JB, Mardin CY, Schlötzer-Schrehardt U, Naumann GO. Morphometry of the human lamina cribrosa surface. *Invest Ophthalmol Vis Sci*. 1991;32(2):401–405. PMID:1993592.
37. Choi JA, Park HYL, Jung KI, Hong KH, Park CK. Difference in the properties of retinal nerve fiber layer defect between superior and inferior visual field loss in glaucoma. *Invest Ophthalmol Vis Sci*. 2013;54(10):6982–6990. doi:10.1167/iovs.13-12344

Analysis of changes in mental health, cognitive function and self-care behaviors in patients with heart failure: A prospective cohort study

Maria Jędrzejczyk[1,A–F], Christopher S. Lee[2,D–F], Ercole Vellone[3,1,D–F], Anna Gozdzik[4,5,D–F], Remigiusz Szczepanowski[6,7,D–F], Michał Czapla[8,9,D–F], Izabella Uchmanowicz[1,10,A,C–F]

[1] Department of Nursing, Faculty of Nursing and Midwifery, Wroclaw Medical University, Poland
[2] Boston College William F. Connell School of Nursing, Chestnut Hill, USA
[3] Department of Biomedicine and Prevention, University of Rome Tor Vergata, Italy
[4] Division of Cardiovascular Imaging, Institute of Heart Diseases, Faculty of Medicine, Wroclaw Medical University, Poland
[5] Institute of Heart Diseases, University Hospital, Wrocław, Poland
[6] Department of Computer Science and Systems Engineering, Wroclaw University of Science and Technology, Poland
[7] The J. Gromkowski Provincial Specialist Hospital, Wrocław, Poland
[8] Department Division of Scientific Research and Innovation in Emergency Medical Service, Department of Emergency Medical Service, Faculty of Nursing and Midwifery, Wroclaw Medical University, Poland
[9] Group of Research in Care (GRUPAC), Faculty of Health Science, University of La Rioja, Logroño, Spain
[10] Centre for Cardiovascular Health, Edinburgh Napier University, Sighthill Campus, UK

A – research concept and design; B – collection and/or assembly of data; C – data analysis and interpretation; D – writing the article; E – critical revision of the article; F – final approval of the article

Received on December 20, 2024
Reviewed on January 22, 2025
Accepted on March 9, 2025

Published online on April 8, 2025

Advances in Clinical and Experimental Medicine, ISSN 1899–5276 (print), ISSN 2451–2680 (online) *Adv Clin Exp Med*. 2025;34(11):1969–1979

Address for correspondence
Michał Czapla
E-mail: michal.czapla@umw.edu.pl

Funding sources
This study was funded by the National Science Centre, Poland (grant No. 2021/41/B/NZ7/01698).

Conflict of interest
None declared

Acknowledgements
Grateful acknowledgment is extended to Ms. Bernadetta Żółkowska and Mr. Karol Mirkowski for their invaluable contributions to data collection. Their dedication played a crucial role in gathering the essential information for this study.

Cite as
Jędrzejczyk M, Lee CS, Vellone E, et al. Analysis of changes in mental health, cognitive function and self-care behaviors in patients with heart failure: A prospective cohort study. *Adv Clin Exp Med*. 2025;34(11):1969–1979. doi:10.17219/acem/202773

DOI
10.17219/acem/202773

Abstract

Background. Heart failure (HF) is a chronic condition affecting tens of millions of people worldwide. Despite advances in treatment, its impact on mental health, cognitive function and self-care behaviors remains underexplored, particularly across ejection fraction phenotypes, underscoring the need for comprehensive investigations into these interconnected domains.

Objectives. This prospective cohort study investigated changes in affective symptoms, cognitive functioning and self-care behaviors in patients with HF stratified with ejection fraction (EF) phenotypes over 6 months.

Materials and methods. The study included 162 patients aged over 60 years with a diagnosis of HF. Participants were examined at enrollment and after 6 months. The Mini-Mental State Examination (MMSE), the Hospital Anxiety and Depression Scale (HADS) and Patient Health Questionnaire-9 (PHQ-9) and the European Heart Failure Self-care Behaviour Scale (EHFScB-9) were used to assess cognitive function, affective symptoms and self-care behaviors.

Results. Cognitive impairment indicated with the MMSE was less severe in patients with mildly-reduced HF (HFmrEF) compared to preserved EF (HFpEF) (MMSE median scores: 28 [interquartile range (IQR): 27–29] vs 27 [IQR: 25–28]; $p = 0.008$). The HADS showed that severity of depression worsened over 6 months, particularly in the HFpEF group (median scores increased from 1 [IQR: 0–4] to 3 [IQR: 0–6]; $p = 0.006$). Self-care ability declined in all groups as indicated in the increased EHFSc-9 (poorer self-care) median scores, which changed from 28 [IQR: 21–33] at baseline to 29 [IQR: 23–34] at 6 months ($p = 0.035$). Additionally, NT-proBNP parameters were higher in the HFrEF group (3437.7 pg/mL [IQR: 1336.33–6226.43) compared to both HFmrEF and HFpEF (2171.2 pg/mL [IQR: 806.65–4033.15] and 977.1 pg/mL [IQR: 576.9–3708.95, respectively, $p = 0.001$).

Conclusions. Patients with HF showed significant cognitive decline, increased depressive symptoms and reduced self-care over 6 months, with HFpEF patients exhibiting the most pronounced impairments. Differences in outcomes across HF phenotypes highlight the need for tailored diagnostic and therapeutic strategies to address cognitive and emotional challenges in this population.

Key words: anxiety, depression, self-care, heart failure, cognitive dysfunction

Highlights

- This study investigates changes in cognitive function, depressive symptoms and self-care behaviors among patients with heart failure (HF) over 6 months.
- Cognitive impairment was more pronounced in HF with preserved ejection fraction (HFpEF) compared to other phenotypes.
- Depressive symptoms increased significantly over 6 months, with the most severe progression observed in HFpEF patients.
- Self-care abilities declined across all HF phenotypes, highlighting the need for tailored interventions.
- The findings underscore the importance of integrating cognitive and psychological assessments into routine HF care to optimize patient outcomes.

Background

Heart failure (HF) is a chronic condition that represents a growing global health burden, affecting millions of patients worldwide. With an aging population and advances in medical interventions that improve survival after acute cardiovascular events, the prevalence of HF is rising, especially among older adults.[1] Heart failure, defined by the heart's inability to pump blood efficiently, causes significant physical, cognitive and emotional impairments reducing patients' quality of life (QoL) and increasing the burden on healthcare systems.[2]

Older adults with HF face an elevated risk for physical deconditioning, poor self-care and cognitive impairment (CI), irrespective of the ejection fraction (EF) subtype. Heart failure is categorized into 3 phenotypes of the EF: HF with reduced EF (HFrEF), mildly reduced EF (HFmrEF) and preserved EF (HFpEF).[3] Cognitive impairment in HF has emerged as a major concern, as HF patients commonly exhibit deficits in memory, executive function, attention, and processing speed compared to those without HF symptoms.[4] The underlying causes of CI in HF are multifactorial, involving reduced cerebral perfusion, vascular damage and the neurohormonal changes typical of chronic HF.[5]

Cognitive dysfunction appears to vary across HF phenotypes. For instance, HFpEF phenotype, which is more prevalent in older women, may be associated with milder CI compared to HFrEF.[6] In contrast, HFmrEF patients experience distinct cognitive challenges, with some studies indicating a higher risk for hospitalization due to cognitive deficits and difficulty in self-care.[7] These findings emphasize the need for clinicians to routinely assess cognitive function in HF patients, as unaddressed CI contributes to poorer self-care, increased hospital readmissions and higher mortality rates.[8]

Mental disorders, particularly depression and anxiety, are prevalent among patients with HF, and often exacerbate cognitive decline, contributing to poorer clinical outcomes. Depression in HF impairs cognition in terms of attention and executive function, which are critical for managing complex treatment regimens and self-care.[9] Symptoms of anxiety can further complicate the clinical picture. Some studies suggest that mild anxiety may have a protective effect on cognitive function, whereas severe anxiety is associated with worsening cognitive outcomes.[10]

Effective self-care behaviors such as medication adherence, symptom monitoring and lifestyle adjustments are essential for managing HF and improving patients' QoL.[11] However, cognitive and emotional challenges often hinder self-care in HF patients. However, cognitive deficits in memory and executive functioning make it difficult for patients to follow complex medical regimens, while depression and anxiety reduce motivation and confidence in self-care abilities.[12] This vicious cycle leads to worse health outcomes, including higher rates of hospitalization and mortality.[13]

Objectives

The aim of this study was to assess changes in affective symptoms, cognitive impairment and self-care behaviors in older adults with HF, categorized by HF phenotype, over a 6-month period.

Methods

Participants

This study was conducted 6 months after the 1st stage, participants were again re-examined. A total of 250 patients were enrolled in the 1st stage of the study. Of these, 77 did not participate in the 2nd stage due to inability to be contacted or other unspecified reasons. The 2nd stage included 162 participants, while 11 individuals died before the follow-up. To be eligible for inclusion in the 1st stage, participants had to meet the following criteria: age ≥60 years, a diagnosis of HF in accordance with the European Society of Cardiology (ESC) guidelines,[14] a duration of HF of at least 6 months, hospitalization for acute HF, New York Heart Association (NYHA) functional class II–IV, and intact cognitive function, as assessed by the Mini-Mental State Examination (MMSE) with a score ≥24 points. The exclusion criteria in the 1st stage

included NYHA class I, MMSE score <24 points, diagnosed and treated depressive disorder, and lack of consent to participate in the study.

Data collection

Patients were recruited from the Institute of Heart Diseases (Department of Cardiology) at University Hospital in Wrocław, Poland, between September 2022 and June 2023 for the 1st stage of the study. The 2nd stage of the study began 6 months after the 1st stage – starting in March 2023 and ending in December 2023. Patients were classified into 3 groups based on EF values: HFrEF: EF ≤40%, HFmrEF: EF 41–49% and HFpEF: EF ≥50%. The data were gathered during the hospitalization period after the successful treatment of acute decompensated HF, with clinical stability attained before discharge. Strengthening the Reporting of Observational Studies in Epidemiology (STROBE) guidelines were followed.

Research instruments

Cognitive function was assessed using the MMSE, a tool developed by Folstein et al. in 1975.[15] This test aimed to create a simple and rapid cognitive assessment tool that clinicians could easily use to identify disorders such as dementia or Alzheimer's disease. The MMSE has become one of the most widely used screening tests worldwide for diagnosing cognitive problems. The test consists of simple questions and tasks assessing various aspects of cognitive functioning, including orientation in time and space, short-term memory, language abilities, attention, and mathematical skills. The maximum score on the MMSE is 30, and scores below 24 may indicate potential dementia.[16] In this study, the Polish adaptation of MMSE developed by Stańczak was utilized.[17]

Depression and anxiety were measured using 2 instruments: The Hospital Anxiety and Depression Scale (HADS) and the Patient Health Questionnaire-9 (PHQ-9). The HADS was originally developed in 1983 by Zigmond and Snaith.[18] It allows to quickly and easily assess levels of anxiety and depression in hospitalized patients, especially those with somatic illnesses, in whom physical symptoms could mask emotional disturbances. Many researchers have studied HADS data to determine cut-off points for anxiety and depression. Bjelland et al. identified a cut-off point of 8/21 for anxiety and depression through a review of numerous studies.[19] This tool is extensively utilized in clinical and research settings to identify emotional disturbances. The HADS comprises 14 items, with 7 assessing anxiety and 7 assessing depression, each rated on a 4-point scale ranging from 0 to 3. The total score for each subscale ranges from 0 to 21, with higher scores indicating higher levels of anxiety or depression.[20] The present study used the Polish adaptation of the HADS, validated by Mihalca and Pilecka.[21]

The PHQ-9 is a highly regarded self-report tool for assessing depressive symptoms. Developed by Kroenke and Spitzer, it has consistently demonstrated reliability and accuracy in measuring depression severity in a wide range of settings, from primary care to specialist medical practices.[22] It includes 9 core questions and a supplementary question, providing a comprehensive assessment of depression. The respondent specifies the annoyance of the listed problems from "not annoyed at all" to "annoyed almost daily" in the past 2 weeks. Each question can be scored from 0 to 3 points, with a max of 27 points. Severe depression is indicated by a score greater than or equal to 20 points, moderate depression 15–19 points, moderate depression 10–14 points, and mild depression 5–9 points.[23] The study used the Polish adaptation of the PHQ-9, which was validated by Kokoszka et al.[24]

The European Heart Failure Self-Care Behaviour Scale (EHFScB) was developed by Jaarsma et al. in 2003.[11] The scale was created as part of research on self-care among patients with HF and is widely used in Europe and other regions. Its purpose is to support patients in better managing their health by assessing and monitoring their self-care behaviors. Subsequently, in 2009, the team led by Jaarsma revised the scale from a 12-item version to a 9-item scale, EHFScB-9, which can be used as an internally consistent and valid tool for measuring self-care behaviors related to HF.[25] The 9-point scale consists of statements focusing on self-care skills in HF management. Five of these refer to specific self-care aspects, such as monitoring body weight, restricting fluids, adhering to a low-salt diet, taking prescribed medications, and engaging in physical activity. The remaining 4 assess symptoms (such as shortness of breath, extreme fatigue, lower limb edema, and significant weight gain over a week) that may indicate disease progression and warrant medical assistance. Responses are rated on a 5-point scale from 1 ("strongly agree") to 5 ("strongly disagree"). The total score is calculated by summing the responses to all 9 statements, ranging from 9 to 45, where higher scores indicate lower self-care ability. A Polish adaptation of EHFSc-9 validated by Uchmanowicz et al. was used in the study.[26]

Ethical consideration

This study adhered to the principles of the Declaration of Helsinki and received approval from the Bioethics Committee of Wroclaw Medical University (approval No. KB-651/2022). Written informed consent was obtained from all participants before their inclusion in the study, and all patient data were anonymized to maintain confidentiality.

Statistical analyses

First, descriptive statistics were calculated for the quantitative variables, including mean, standard deviation (SD), median, quartiles, and minimum and maximum values. The analysis of qualitative variables was carried out by calculating the absolute frequencies and percentages of all values that these variables could assume. The comparison

of qualitative variables between groups was conducted using the χ^2 test of independence. If the assumptions of the χ^2 test were not met, Yates's correction was applied for 2 × 2 tables, while Fisher's exact test was used for larger contingency tables. Quantitative variables across the 3 groups were compared using the Kruskal–Wallis test, followed by Dunn's post hoc test if significant differences were identified. Correlations between quantitative variables were analyzed using Spearman's correlation coefficient. Scatter plots were examined to verify the assumption of a monotonic relationship, and representative examples are provided in the shared data. The Wilcoxon signed-rank test was employed to assess differences between 2 repeated measurements. A significance level of 0.05 was adopted for the analysis. Each examined relationship was assessed independently rather than as part of a broader statistical inference encompassing all tests. Therefore, multiple comparison corrections were not applied, as each analysis was treated as an independent result. In this analysis, HF phenotype was considered a key confounding factor influencing the relationships between affective symptoms, cognitive impairment and self-care behaviors. While we recognize the presence of other potential confounding factors, they were not included in the scope of this study. This approach aligns with the primary aim of our research, which focuses on the role of HF phenotype in these associations. The analysis was performed with R software v. 4.4.1 (R Foundation for Statistical Computing, Vienna, Austria).

Results

The demographic characteristics of the sample (n = 162) are summarized in Table 1. There were 76 patients with HFrEF, 55 patients with HFpEF and 31 patients with

Table 1. Demographic and clinical characteristics of patients by heart failure phenotype

Parameter		HFrEF (n = 76) – A	HFmrEF (n = 31) – B	HFpEF (n = 55) – C	Total (n = 162)	p-value
Age [years]	mean (SD)	70.63 (6.09)	71.87 (7.56)	72.85 (6.07)	71.62 (6.42)	0.133
	median (quartiles)	70.5 (65.75–74.25)	73 (65.5–77.5)	73 (69–75.5)	72 (67–75)	
Education period [years]	mean (SD)	12.32 (3.32)	12.71 (4.44)	62–91	60–91	0.996
	median (quartiles)	11.5 (10–14)	11 (10–14)	55	162	
Sex	woman	12 (15.79%)	8 (25.81%)	12.49 (3.99)	12.45 (3.77)	<0.001*
	man	64 (84.21%)	23 (74.19%)	12 (10–14)	12 (10–14)	
Marital status	single	25 (32.89%)	9 (29.03%)	7–27	7–27	0.667
	in a relationship	51 (67.11%)	22 (70.97%)	55	162	
Current place of residence	city	52 (68.42%)	27 (87.10%)	29 (52.73%)	49 (30.25%)	0.026*
	village	24 (31.58%)	4 (12.90%)	26 (47.27%)	113 (69.75%)	
Professional status	professionally active	13 (17.11%)	6 (19.35%)	21 (38.18%)	55 (33.95%)	0.065
	pensioner	63 (82.89%)	25 (80.65%)	34 (61.82%)	107 (66.05%)	
BMI [kg/m^2] (stage I)	mean (SD)	28.35 (4.76)	29.24 (7.34)	47 (85.45%)	126 (77.78%)	0.062
	median (quartiles)	27.92 (25.15–31.27)	27.73 (23.94–35.87)	8 (14.55%)	36 (22.22%)	
Initial BMI (stage I)	weight normal	18 (23.68%)	12 (38.71%)	3 (5.45%)	22 (13.58%)	0.018*
	overweight	34 (44.74%)	7 (22.58%)	52 (94.55%)	140 (86.42%)	
	obesity	24 (31.58%)	12 (38.71%)	30.96 (5.76)	29.41 (5.75)	
BMI after 6 months [kg/m^2] (stage II)	mean (SD)	28.1 (4.84)	28.78 (6.87)	29.73 (26.63–35.01)	28.52 (25.35–33.41)	0.075
	median (quartiles)	27.77 (24.75–30.77)	27.4 (23.66–36.17)	19.16–44.96	17.91–44.96	
BMI after 6 months (stage II)	weight normal	21 (27.63%)	13 (41.94%)	55	162	0.046*
	overweight	30 (39.47%)	6 (19.35%)	6 (10.91%)	36 (22.22%)	
	obesity	25 (32.89%)	12 (38.71%)	23 (41.82%)	64 (39.51%)	
Central obesity	no (waist circumference <94 cm for men or <80 cm for women)	13 (17.11%)	9 (29.03%)	26 (47.27%)	62 (38.27%)	0.03*
	yes (waist circumference >94 cm for men or >80 cm for women)	63 (82.89%)	22 (70.97%)	30.44 (5.54)	29.02 (5.58)	
NYHA class	II	32 (42.11%)	16 (51.61%)	21 (38.18%)	69 (42.59%)	0.239
	III	27 (35.53%)	13 (41.94%)	26 (47.27%)	66 (40.74%)	
	IV	17 (22.37%)	2 (6.45%)	8 (14.55%)	27 (16.67%)	

Table 1. Demographic and clinical characteristics of patients by heart failure phenotype – cont.

Parameter		HFrEF (n = 76) – A	HFmrEF (n = 31) – B	HFpEF (n = 55) – C	Total (n = 162)	p-value
NT-proBNP [pg/mL]	mean (SD)	4752.78 (4901.47)	2578.83 (2190.51)	3254.15 (5946.57)	3827.98 (4976.21)	0.001* A>B,C
	median (quartiles)	3437.7 (1336.33–6226.43)	2171.2 (806.65–4033.15)	977.1 (576.9–3708.95)	2178.45 (793.1–4988.75)	
Hospitalizations in the last year (stage I)	no hospitalizations	2 (2.63%)	1 (3.23%)	2 (3.64%)	5 (3.09%)	0.822
	1 hospitalization	18 (23.68%)	7 (22.58%)	19 (34.55%)	44 (27.16%)	
	2 hospitalizations	20 (26.32%)	11 (35.48%)	13 (23.64%)	44 (27.16%)	
	3 hospitalizations	13 (17.11%)	5 (16.13%)	9 (16.36%)	27 (16.67%)	
	more than 3 hospitalizations	23 (30.26%)	7 (22.58%)	11 (20.00%)	41 (25.31%)	
Hospitalizations in the last year (stage II)	no hospitalizations	9 (11.84%)	5 (16.13%)	5 (9.09%)	19 (11.73%)	0.472
	1 hospitalization	13 (17.11%)	2 (6.45%)	12 (21.82%)	27 (16.67%)	
	2 hospitalizations	21 (27.63%)	11 (35.48%)	17 (30.91%)	49 (30.25%)	
	3 hospitalizations	12 (15.79%)	6 (19.35%)	13 (23.64%)	31 (19.14%)	
	more than 3 hospitalizations	21 (27.63%)	7 (22.58%)	8 (14.55%)	36 (22.22%)	
Medications taken**	ACEI/ARB	76 (100.00%)	30 (96.77%)	53 (96.36%)	159 (98.15%)	0.198
	calcium antagonists	17 (22.37%)	8 (25.81%)	20 (36.36%)	45 (27.78%)	0.203
	alpha blockers	7 (9.21%)	4 (12.90%)	5 (9.09%)	16 (9.88%)	0.833
	beta-blockers	75 (98.68%)	31 (100.00%)	55 (100.00%)	161 (99.38%)	1
	MKS	66 (86.84%)	22 (70.97%)	34 (61.82%)	122 (75.31%)	0.004*
	diuretics	74 (97.37%)	23 (74.19%)	50 (90.91%)	147 (90.74%)	0.001*
	statins	65 (85.53%)	30 (96.77%)	45 (81.82%)	140 (86.42%)	0.146
	anticoagulants	51 (67.11%)	19 (61.29%)	37 (67.27%)	107 (66.05%)	0.824
	antiplatelet drugs	34 (44.74%)	17 (54.84%)	23 (41.82%)	74 (45.68%)	0.495
	flosins	52 (68.42%)	19 (61.29%)	31 (56.36%)	102 (62.96%)	0.361

ACEI – angiotensin converting enzyme inhibitors; ARB – angiotensin receptor antagonists; BMI – body mass index; HFrEF – heart failure with reduced ejection fraction; HFmrEF – heart failure with mildly reduced ejection fraction; HFpEF – heart failure with preserved ejection fraction; MKS – mineralocorticosteroids; NT-proBNP – N-terminal prohormone of brain natriuretic peptide; NYHA – New York Heart Association; SD – standard deviation; p-value – qualitative variables: χ^2 test of independence or Fisher's exact test; quantitative variables: Kruskal–Wallis test + post hoc analysis (Dunn's test); *statistically significant difference ($p < 0.05$); ** multiple choice question – percentages do not add up to 100.

Table 2. Results of questionnaires of people who died after stage I

Parameter	N	Mean	SD	Median	Min	Max	Q1	Q3
EHFSc-9	11	27.73	8.52	28	13	40	22.5	34
HADS: Anxiety	11	7.64	6.2	7	0	20	3	11
HADS: Depression	11	6.64	5.97	7	0	16	1.5	10.5
PHQ-9	11	12.91	8.42	12	0	27	7	19.5
MMSE	11	27.45	2.38	28	24	30	25.5	29.5

EHFSc-9 – European Heart Failure Self-Care Behviour Scale; HADS – Hospital Anxiety and Depression Scale; PHQ-9 – Patient Health Questionnaire-9; MMSE – Mini-Mental State Examination; SD – standard deviation; Q1 – lower quartile; Q3 – upper quartile.

HFmrEF. The percentage of women was highest in the HFpEF group and lowest in the HFrEF group. The percentage of individuals from cities was highest in the HFmrEF group and lowest in the HFrEF group. At the beginning of the study, the percentage of individuals with normal weight was highest in the HFmrEF group and lowest in the HFpEF group, while the percentage of overweight individuals was highest in the HFrEF group and lowest in the HFmrEF group. The percentage of individuals with obesity was highest in the HFpEF group and lowest in the HFrEF group. Additionally, the percentage of individuals with central obesity was highest in the HFpEF group and lowest in the HFmrEF group. NT-proBNP levels were higher in the HFrEF group than in both the HFmrEF and HFpEF groups.

Table 2 shows the results of the questionnaires that were completed by people who died after the 1st stage of the study.

Table 3. Differences in European Heart Failure Self-Care Behaviour Scale, Hospital Anxiety and Depression Scale, Patient Health Questionnaire, and Mini-Mental State Examination results in patients with heart failure after 6 months

Parameter	HF phenotype	N	Mean	SD	Median	Min	Max	Q1	Q3	p-value
HADS:A after 6 months	HFrEF	76	3.43	4.17	2	0	18	0	5	0.602
	HFmrEF	31	3.16	2.98	3	0	9	0	5.5	
	HFpEF	55	3.55	3.35	3	0	15	1	5	
HADS: Depression after 6 months	HFrEF	76	3.62	4.64	2	0	20	0	6	0.54
	HFmrEF	31	2.29	2.47	2	0	8	0	4	
	HFpEF	55	3.27	3.29	3	0	13	0	6	
PHQ-9 after 6 months	HFrEF	76	6.05	5.76	5	0	23	2	7	0.536
	HFmrEF	31	5.13	3.83	4	0	14	2	7.5	
	HFpEF	55	6.24	4.47	6	0	18	3	8	
MMSE after 6 months	HFrEF	76	26.97	1.71	27	23	29	26	28.25	0.008* B >C
	HFmrEF	31	27.55	1.59	28	23	29	27	29	
	HFpEF	55	26.42	1.75	27	23	29	25	28	
EHFSc-9 after 6 months	HFrEF – A	76	27.39	7.97	28	11	42	23	33.25	0.742
	HFmrEF – B	31	28.23	8.24	29	9	40	23	35	
	HFpEF – C	55	28.05	7.37	30	11	39	23.5	34	

EHFSc-9 – European Heart Failure Self-Care Behaviour Scale; HADS – Hospital Anxiety and Depression Scale; PHQ-9 – Patient Health Questionnaire-9; MMSE – Mini-Mental State Examination; HF – heart failure; HFrEF – heart failure with reduced ejection fraction; HFmrEF – heart failure with mildly reduced ejection fraction; HFpEF – heart failure with preserved ejection fraction; SD – standard deviation; Q1 – lower quartile; Q3 – upper quartile; p-value – Kruskal–Wallis test + post hoc analysis (Dunn's test); *statistically significant relationship ($p < 0.05$); A, B and C – 3 phenotypes of heart failure.

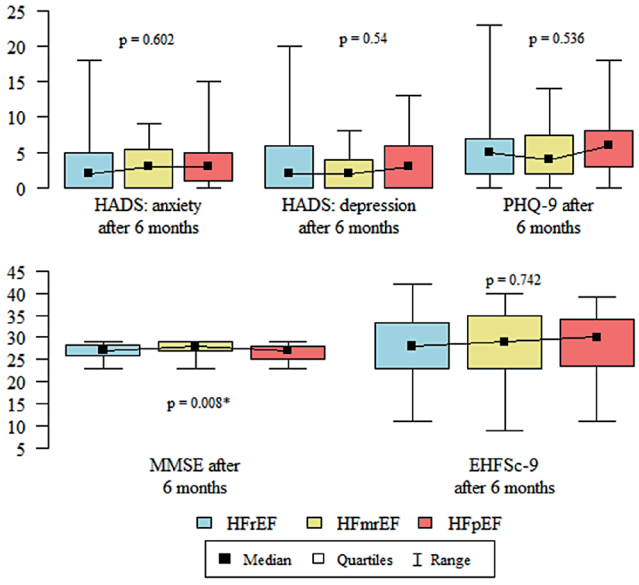

Fig. 1. Differences in European Heart Failure Self-Care Behaviour Scale, Hospital Anxiety and Depression Scale, Patient Health Questionnaire, and Mini-Mental State Examination in patients with heart failure after 6 months

EHFSc-9 – European Heart Failure Self-Care Behaviour Scale; HADS – Hospital Anxiety and Depression Scale; PHQ-9 – Patient Health Questionnaire-9; MMSE – Mini-Mental State Examination; HFrEF – heart failure with reduced ejection fraction; HFmrEF – heart failure with mildly reduced ejection fraction; HFpEF – heart failure with preserved ejection fraction; p – Kruskal–Wallis test + post hoc analysis (Dunn's test); *statistically significant relationship ($p < 0.05$).

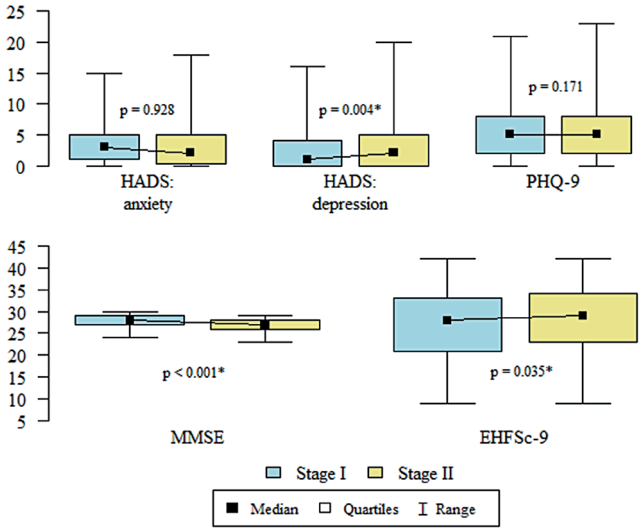

Fig. 2. Comparison of questionnaires results in stages I and II

EHFSc-9 – European Heart Failure Self-Care Behaviour Scale; HADS – Hospital Anxiety and Depression Scale; PHQ-9 – Patient Health Questionnaire-9; MMSE – Mini-Mental State Examination; p – Wilcoxon test for related pairs; *statistically significant relationship ($p < 0.05$).

Statistical analysis showed that CI according to the MMSE after 6 months was significantly less severe in the HFmrEF group than in the HFpEF group (Table 3, Fig. 1). The correlation between self-care behaviors and cognitive function and affective symptoms was examined within each HF phenotype group (Table 4).

Statistical analysis was performed, which compared the results of the questionnaires between the 1st and 2nd stages. The study showed that the level of self-care according to EHFSc-9 was significantly lower in stage II than in stage I. Depression, as measured with HADS, was

Table 4. Influence of cognitive function and affective symptoms on the level of self-care in patients by heart failure phenotype

HF phenotype	Parameter	EHFSc-9 after 6 months
		Spearman's correlation coefficient
HFrEF	HADS: Anxiety after 6 months	r = 0.075; p = 0.519
	HADS: Depression after 6 months	r = 0.078; p = 0.503
	PHQ-9 after 6 months	r = –0.045; p = 0.702
	MMSE after 6 months	r = 0.099; p = 0.396
HFmrEF	HADS: Anxiety after 6 months	r = 0.15; p = 0.421
	HADS: Depression after 6 months	r = 0.126; p = 0.498
	PHQ-9 after 6 months	r = 0.115; p = 0.537
	MMSE after 6 months	r = 0.146; p = 0.432
HFpEF	HADS: Anxiety after 6 months	r = –0.154; p = 0.261
	HADS: Depression after 6 months	r = –0.004; p = 0.98
	PHQ-9 after 6 months	r = –0.204; p = 0.136
	MMSE after 6 months	r = –0.012; p = 0.933

EHFSc-9 – European Heart Failure Self-Care Behaviour Scale; HADS – Hospital Anxiety and Depression Scale; PHQ-9 – Patient Health Questionnaire-9; MMSE – Mini-Mental State Examination; HF – heart failure; HFrEF – heart failure with reduced ejection fraction; HFmrEF – heart failure with mildly reduced ejection fraction; HFpEF – heart failure with preserved ejection fraction.

Table 5. Comparison of questionnaires results in stages I and II

Parameter	Measurement	N	Mean	SD	Median	Min	Max	Q1	Q3	p-value
HADS: Anxiety	stage I	162	3.44	3.33	3	0	15	1	5	0.928
	stage II	162	3.42	3.68	2	0	18	0.25	5	
HADS: Depression	stage I	162	2.70	3.50	1	0	16	0	4	0.004*
	stage II	162	3.25	3.88	2	0	20	0	5	
PHQ-9	stage I	162	5.73	4.94	5	0	21	2	8	0.171
	stage II	162	5.94	5.01	5	0	23	2	8	
MMSE	stage I	162	27.90	1.74	28	24	30	27	29	<0.001*
	stage II	162	26.90	1.74	27	23	29	26	28	
EHFSc-9	stage I	162	26.96	7.82	28	9	42	21	33	0.035*
	stage II	162	27.78	7.79	29	9	42	23	34	

EHFSc-9 – European Heart Failure Self-Care Behaviour Scale; HADS – Hospital Anxiety and Depression Scale; PHQ-9 – Patient Health Questionnaire-9; MMSE – Mini-Mental State Examination; SD – standard deviation; Q1 – lower quartile; Q3 – upper quartile; p-value – Wilcoxon signed-rank test; *statistically significant relationship ($p < 0.05$).

significantly higher in stage II compared to stage I. Cognitive impairment according to the MMSE was significantly less severe in stage I than in stage II (Table 5, Fig. 2).

Statistical analysis for patients with HFrEF and HFpEF showed that the level of depression according to HADS was significantly higher in stage II than in stage I. Statistical analysis for patients with HfmrEF, HfrEF and HFpEF CI according to the MMSE was significantly less severe in stage I than in stage II (Table 6, Fig. 3).

Discussion

The study presents a detailed analysis of HF subtypes (HFrEF, HFmrEF, HFpEF) in a diverse patient population, revealing significant differences in demographic, clinical and biomarker profiles. The predominance of women in the HFpEF group and the higher urban residency in HFmrEF suggest potential sociodemographic influences on disease presentation. Body mass index and central obesity differences across groups underscore the metabolic effects of HF phenotypes. Notably, the higher NT-proBNP in patients with HFrEF phenotype as compared to HFmrEF and HFpEF suggest the need of more aggressive management strategies in these patients.

These findings are in line with other major studies, such as the Framingham Heart Study (FHS) and the Multi-Ethnic Study of Atherosclerosis (MESA).[28] Both studies reported that the lifetime risk of HFpEF was higher than that of HFrEF, particularly among women. The FHS cohort reported a rise in lifetime risk across both sexes, with notable variations by race and ethnicity in MESA and the Cardiovascular Health Study (CHS). The higher prevalence of HFpEF and its associated risk factors in the above study

Table 6. Comparison of questionnaire results at stages I and II in patients by heart failure phenotype

Parameter	Measurement	N	Mean	SD	Median	Min	Max	Q1	Q3	p-value
HFrEF										
HADS: Anxiety	stage I	76	3.74	3.70	3	0	15	1	6	0.316
	stage II	76	3.43	4.17	2	0	18	0	5	
HADS: Depression	stage I	76	3.01	4.08	1	0	16	0	5	0.022*
	stage II	76	3.62	4.64	2	0	20	0	6	
PHQ-9	stage I	76	5.72	5.31	5	0	21	1	8.25	0.29
	stage II	76	6.05	5.76	5	0	23	2	7	
MMSE	stage I	76	27.97	1.71	28	24	30	27	29.25	<0.001*
	stage II	76	26.97	1.71	27	23	29	26	28.25	
EHFSc-9	stage I	76	26.95	8.35	27	9	42	21	33.25	0.351
	stage II	76	27.39	7.97	28	11	42	23	33.25	
HFmrEF										
HADS: Anxiety	stage I	31	3.29	3.49	2	0	13	1	5	0.975
	stage II	31	3.16	2.98	3	0	9	0	5.5	
HADS: Depression	stage I	31	2.84	3.00	3	0	12	0	4.5	0.38
	stage II	31	2.29	2.47	2	0	8	0	4	
PHQ-9	stage I	31	5.97	5.22	5	0	21	1.5	8.5	0.459
	stage II	31	5.13	3.83	4	0	14	2	7.5	
MMSE	stage I	31	28.55	1.59	29	24	30	28	30	<0.001*
	stage II	31	27.55	1.59	28	23	29	27	29	
EHFSc-9	stage I	31	27.10	7.44	28	11	41	23	32	0.248
	stage II	31	28.23	8.24	29	9	40	23	35	
HFpEF										
HADS: Anxiety	stage I	55	3.13	2.65	3	0	11	1	4	0.225
	stage II	55	3.55	3.35	3	0	15	1	5	
HADS: Depression	stage I	55	2.20	2.83	1	0	10	0	4	0.006*
	stage II	55	3.27	3.29	3	0	13	0	6	
PHQ-9	stage I	55	5.60	4.31	5	0	18	3	7.5	0.063
	stage II	55	6.24	4.47	6	0	18	3	8	
MMSE	stage I	55	27.42	1.75	28	24	30	26	29	<0.001*
	stage II	55	26.42	1.75	27	23	29	25	28	
EHFSc-9	stage I	55	26.91	7.38	29	11	39	21	32.5	0.123
	stage II	55	28.05	7.37	30	11	39	23.5	34	

EHFSc-9 – European Heart Failure Self-Care Behaviour Scale; HADS – Hospital Anxiety and Depression Scale; PHQ-9 – Patient Health Questionnaire-9; MMSE – Mini-Mental State Examination; HFrEF – heart failure with reduced ejection fraction; HFmrEF – heart failure with mildly reduced ejection fraction; HFpEF – heart failure with preserved ejection fraction; p-value – Wilcoxon signed-rank test; *statistically significant relationship ($p < 0.05$).

emphasizes the need for targeted interventions across different demographic groups.[6,27]

This study's findings align with existing research, confirming that CI is a significant issue in patients with HF. The observed cognitive decline mirrors findings from broader studies that indicate a high prevalence of CI among HF patients, with rates ranging from 10% to 79%. This cognitive decline is linked to poorer self-care, increased hospitalization and higher mortality rates. Studies such as the one by Kuipers et al. further highlight the importance of proactive CI screening and management in HF patients to enhance overall outcomes.[8] The implications of these findings are substantial. Given the demonstrated association between HF and CI, especially in HFpEF, it is crucial to incorporate regular cognitive assessments into standard care for HF patients. This approach would enable more personalized treatment strategies addressing both cardiovascular and cognitive needs. Additionally, as highlighted in the broader literature, the varied risks associated with different HF subtypes underscore the need for tailored interventions to mitigate risks and improve long-term outcomes.

Medication patterns, particularly the higher use of diuretics and mineralocorticoid receptor antagonists (MRA)

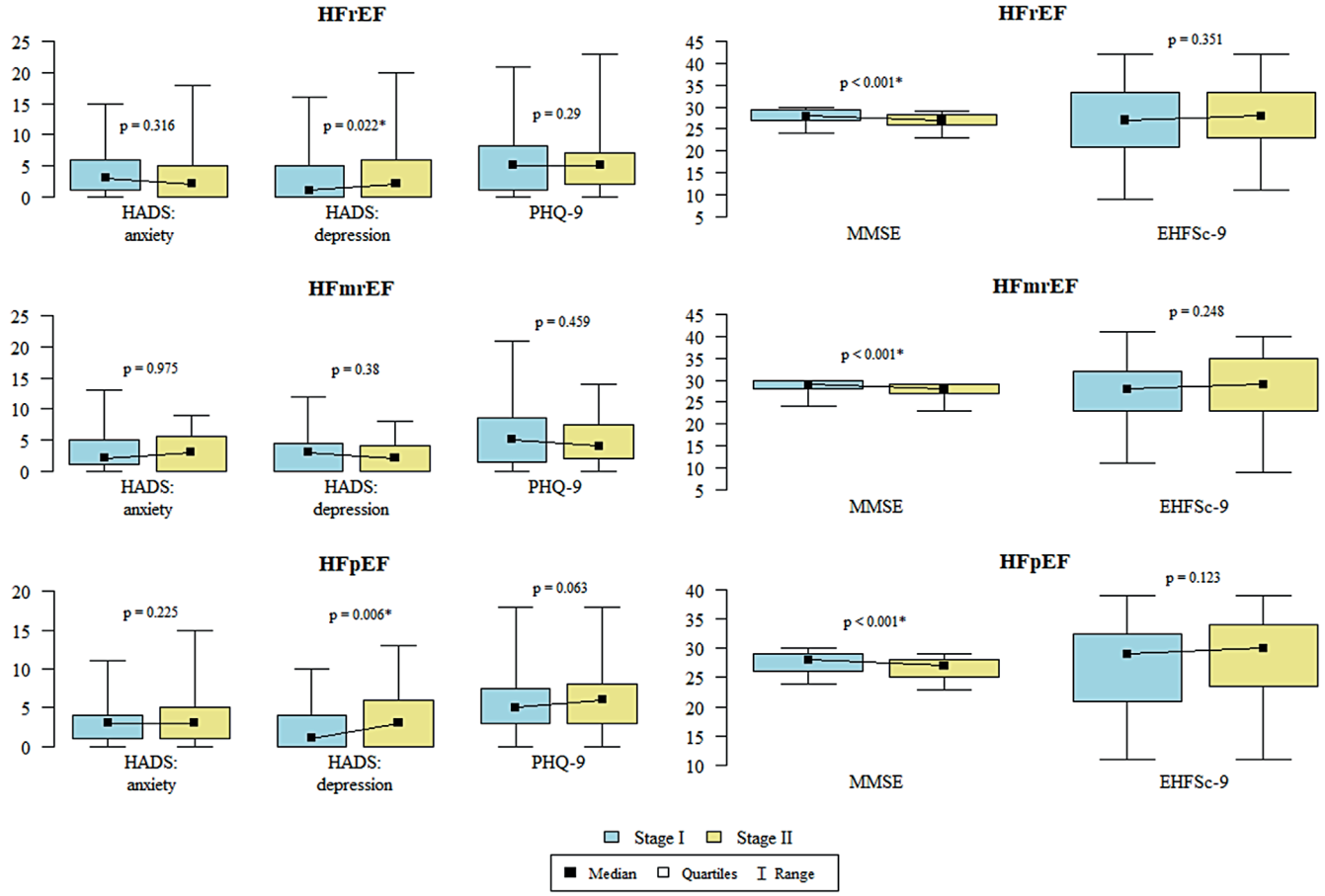

Fig. 3. Comparison of questionnaire results at stages I and II in patients by heart failure phenotype

EHFSc-9 – European Heart Failure Self-Care Behaviour Scale, HADS – Hospital Anxiety and Depression Scale, PHQ-9 – Patient Health Questionnaire-9, MMSE – Mini-Mental State Examination, HFrEF – heart failure with reduced ejection fraction, HFmrEF – heart failure with mildly reduced ejection fraction, HFpEF – heart failure with preserved ejection fraction, p – Wilcoxon test for related pairs; *statistically significant relationship ($p < 0.05$)

in HFrEF, reflect the necessity for tailored treatment approaches for each HF subtype. These findings are consistent with established guidelines that emphasize the critical role of these medications in managing HFrEF. While diuretics are essential for alleviating congestion and reducing hospitalizations, their use must be carefully balanced with other guideline-directed medical therapies (GDMT) to avoid complications such as hypotension and renal dysfunction. This tailored approach highlights that, while diuretics are not disease-modifying, they play a crucial role in symptom management and achieving euvolemia.[28–30] It emphasizes the importance of personalized care in HFrEF, where severity of symptoms and comorbidities demand a careful pharmacotherapy balance. Our findings highlight the need for vigilance in managing these complex cases, ensuring that life-saving treatments are maximized while minimizing adverse effects, in line with current clinical guidelines and evidence-based practices.

Cognitive impairment was more pronounced in HFpEF, which can affect how these patient manage their condition and present self-care behaviors. This finding emphasizes the importance of cognitive assessments as part of regular care for HF patients. Research by Uchmanowicz et al. supports this highlighting connection between frailty syndrome and cognitive decline in patients with HF condition. The combined presence of frailty and cognitive impairment significantly increases the risk of adverse outcomes, such as higher mortality, increased hospital readmissions and poorer QoL. These insights point to the need for comprehensive care strategies that address both the cognitive and physical challenges faced by older and frail HF patients.[12]

Finally, the mortality analysis revealed that patients who passed away after the initial stage had poorer scores in cognitive and depression assessments. This finding highlight potential for using risk stratification and management strategies, focusing on improving mental health and cognitive function as part of comprehensive HF care. Our study's findings that diminished cognitive functioning and more severe depression scores are associated with increased mortality in HF patients align closely with the broader literature. For example, Gathright et al. conducted a meta-analysis demonstrating that depression is a significant predictor of all-cause mortality in HF patients, particularly among older adults and during shorter

follow-up periods.[9] Similarly, Rutledge et al. found a strong link between depression and increased mortality in HF.[13] Moreover, studies emphasize the growing burden of HF, where mental health plays a crucial role in managing this chronic condition.[2,31,32]

Given the evidence from these studies, it is essential to integrate comprehensive mental health care into the routine HF management to earlier identify and treat at-risk individuals, improving survival rates and QoL. Consistent evidence from various studies and meta-analyses further highlights the need for a multidisciplinary approach that addresses both the physical and psychological dimensions of HF.

Overall, this study underscores the heterogeneity within HF populations and the importance of personalized treatment approaches to account for demographic, clinical and psychosocial factors to achieve the best outcomes for patients.

Limitations

Despite its strengths, this study has several limitations. First, its observational design makes it difficult to establish causal relationships between the identified factors and HF outcomes. Additionally, the sample size may have been insufficient to capture the full spectrum of variability within each HF subtype, particularly when examining less common comorbidities or demographic subgroups. Furthermore, the reliance on self-reported data for certain variables, such as cognitive function and depression, could introduce bias or inaccuracies, particularly if patients underreported or overreported their symptoms. Additionally, while the study considered a range of demographic and clinical variables, other potentially relevant factors, such as socioeconomic status, access to care and lifestyle factors, were not comprehensively analyzed. Finally, the follow-up period, although adequate for short-term outcomes, may not capture long-term trends and outcomes, particularly regarding the progression of cognitive impairment and its impact on mortality. Future studies with extended follow-up periods and larger, more diverse populations would help mitigate these limitations and offer a more comprehensive understanding of HF subtypes.

Practical implications

The findings of this study carry several practical implications for the management of patients with HF. The diversity in clinical profiles across HF subtypes suggests that a personalized approach to treatment is essential. Clinicians should consider demographic factors, such as gender and residence, alongside clinical indicators like BMI and NT-proBNP levels, to tailor treatment strategies effectively. Moreover, the significant cognitive impairment observed, particularly in HFpEF patients, underscores the necessity of incorporating cognitive and psychological assessments into routine care. This approach could enhance patient adherence to treatment and improve overall health outcomes. Finally, the higher mortality rates associated with worse cognitive and depression scores underline the importance of addressing mental health in HF management. Overall, these implications underscore the necessity of a holistic and individualized approach to treating HF, which may enhance patient outcomes and optimize the utilization of healthcare resources.

Conclusions

This study highlights significant differences among HF phenotypes in cognitive function, depression and self-care behaviors. Patients with HFpEF exhibited the most severe cognitive impairment and progressive depressive symptoms, while NT-proBNP levels were highest in HFrEF, highlighting the need for more intensive management. The findings underscore the importance of integrating routine cognitive and psychological assessments into HF care and developing phenotype-specific therapeutic strategies to optimize patient outcomes. Tailored interventions that address the specific challenges of each HF subtype, particularly cognitive deficits and depression, are essential for enhancing long-term health outcomes and QoL.

Data availability statement

The dataset used in this study is publicly available at Zenodo: https://doi.org/10.5281/zenodo.14996762.

Consent for publication

Not applicable.

Use of AI and AI-assisted technologies

Not applicable.

ORCID iDs

Maria Jędrzejczyk https://orcid.org/0000-0002-7208-3509
Christopher S. Lee https://orcid.org/0000-0002-2510-4071
Ercole Vellone https://orcid.org/0000-0003-4673-7473
Anna Gozdzik https://orcid.org/0000-0002-8182-5586
Remigiusz Szczepanowski https://orcid.org/0000-0003-2989-2172
Michał Czapla https://orcid.org/0000-0002-4245-5420
Izabella Uchmanowicz https://orcid.org/0000-0001-5452-0210

References

1. Ponikowski P, Anker SD, AlHabib KF, et al. Heart failure: Preventing disease and death worldwide. *ESC Heart Fail*. 2014;1(1):4–25. doi:10.1002/ehf2.12005
2. McMurray J, Stewart S. The burden of heart failure. *Eur Heart J Suppl*. 2002;4:D50–D58. doi:10.1016/S1520-765X(02)90160-4
3. Conrad N, Judge A, Tran J, et al. Temporal trends and patterns in heart failure incidence: A population-based study of 4 million individuals. *Lancet*. 2018;391(10120):572–580. doi:10.1016/S0140-6736(17)32520-5

4. Harkness K, Heckman GA, McKelvie RS. The older patient with heart failure: High risk for frailty and cognitive impairment. *Exp Rev Cardiovasc Ther*. 2012;10(6):779–795. doi:10.1586/erc.12.49
5. Almeida OP, Garrido GJ, Beer C, Lautenschlager NT, Arnolda L, Flicker L. Cognitive and brain changes associated with ischaemic heart disease and heart failure. *Eur Heart J*. 2012;33(14):1769–1776. doi:10.1093/eurheartj/ehr467
6. Pandey A, Omar W, Ayers C, et al. Sex and race differences in lifetime risk of heart failure with preserved ejection fraction and heart failure with reduced ejection fraction. *Circulation*. 2018;137(17):1814–1823. doi:10.1161/CIRCULATIONAHA.117.031622
7. Desai N, Olewinska E, Famulska A, Remuzat C, Francois C, Folkerts K. Heart failure with mildly reduced and preserved ejection fraction: A review of disease burden and remaining unmet medical needs within a new treatment landscape. *Heart Fail Rev*. 2024;29(3):631–662. doi:10.1007/s10741-024-10385-y
8. Kuipers S, Greving JP, Brunner-La Rocca HP, et al. Risk evaluation of cognitive impairment in patients with heart failure: A call for action. *IJC Heart Vasc*. 2022;43:101133. doi:10.1016/j.ijcha.2022.101133
9. Gathright EC, Goldstein CM, Josephson RA, Hughes JW. Depression increases the risk of mortality in patients with heart failure: A meta-analysis. *J Psychosom Res*. 2017;94:82–89. doi:10.1016/j.jpsychores.2017.01.010
10. Bierman EJM, Comijs HC, Rijmen F, Jonker C, Beekman ATF. Anxiety symptoms and cognitive performance in later life: Results from the longitudinal aging study Amsterdam. *Aging Mental Health*. 2008;12(4):517–523. doi:10.1080/13607860802224276
11. Jaarsma T, Strömberg A, Mårtensson J, Dracup K. Development and testing of the European Heart Failure Self-Care Behaviour Scale. *Eur J Heart Fail*. 2003;5(3):363–370. doi:10.1016/S1388-9842(02)00253-2
12. Uchmanowicz I, Rosano G, Piepoli M, et al. The concurrent impact of mild cognitive impairment and frailty syndrome in heart failure. *Arch Med Sci*. 2023;19(4):912–920. doi:10.5114/aoms/162369
13. Rutledge T, Reis VA, Linke SE, Greenberg BH, Mills PJ. Depression in heart failure. *J Am Coll Cardiol*. 2006;48(8):1527–1537. doi:10.1016/j.jacc.2006.06.055
14. McDonagh TA, Metra M, Adamo M, et al. 2021 ESC Guidelines for the diagnosis and treatment of acute and chronic heart failure. *Eur Heart J*. 2021;42(36):3599–3726. doi:10.1093/eurheartj/ehab368
15. Folstein MF, Folstein SE, McHugh PR. "Mini-mental state." *J Psychiatr Res*. 1975;12(3):189–198. doi:10.1016/0022-3956(75)90026-6
16. Creavin ST, Wisniewski S, Noel-Storr AH, et al. Mini-Mental State Examination (MMSE) for the detection of dementia in clinically unevaluated people aged 65 and over in community and primary care populations. *Cochrane Database Syst Rev*. 2016;2016(4):CD011145. doi:10.1002/14651858.CD011145.pub2
17. Stańczak J. *MMSE: polska normalizacja*. Warsaw, Poland: Pracownia Testów Psychologicznych Polskiego Towarzystwa Psychologicznego; 2010. ISBN:978-83-60733-70-7.
18. Snaith RP, Zigmond AS. The hospital anxiety and depression scale. *BMJ*. 1986;292(6516):344. doi:10.1136/bmj.292.6516.344
19. Bjelland I, Dahl AA, Haug TT, Neckelmann D. The validity of the Hospital Anxiety and Depression Scale. *J Psychosom Res*. 2002;52(2):69–77. doi:10.1016/S0022-3999(01)00296-3
20. Wichowicz HM, Wieczorek D. Screening post-stroke depression using the Hospital Anxiety and Depression Scale [in Polish]. *Psychiatr Pol*. 2011;45(4):505–514. https://www.psychiatriapolska.pl/Screening-post-stroke-depression-using-the-Hospital-Anxiety-and-Depression-Scale,154400,0,2.html.
21. Mihalca A, Pilecka W. The factorial structure and validity of the Hospital Anxiety and Depression Scale (HADS) in Polish adolescents. *Psychiatr Pol*. 2015;49(5):1071–1088. doi:10.12740/PP/38139
22. Kroenke K, Spitzer RL, Williams JBW. The PHQ-9: Validity of a brief depression severity measure. *J Gen Intern Med*. 2001;16(9):606–613. doi:10.1046/j.1525-1497.2001.016009606.x
23. Suchowiak S, Wszołek K, Suwalska J, Łojko D, Suwalska A. Screening for perinatal depression: A review of tools and barriers. *Neuropsychiatr Neuropsychol*. 2020;15(1-2):60–69. doi:10.5114/nan.2020.97402
24. Kokoszka A, Jastrzębski A, Obrębski M. Ocena psychometrycznych właściwości polskiej wersji Kwestionariusza Zdrowia Pacjenta-9 dla osób dorosłych. *Psychiatria*. 2016;13(4):187–193. https://journals.viamedica.pl/psychiatria/article/view/49966.
25. Jaarsma T, Årestedt KF, Mårtensson J, Dracup K, Strömberg A. The European Heart Failure Self-care Behaviour scale revised into a nine-item scale (EHFScB-9): A reliable and valid international instrument. *Eur J Heart Fail*. 2009;11(1):99–105. doi:10.1093/eurjhf/hfn007
26. Uchmanowicz I, Wleklik M. Polish adaptation and reliability testing of the nine-item European Heart Failure Self-care Behaviour Scale (9-EHFScBS). *Kardiol Pol*. 2016;74(7):691–696. doi:10.5603/KP.a2015.0239
27. Vasan RS, Enserro DM, Beiser AS, Xanthakis V. Lifetime risk of heart failure among participants in the Framingham Study. *J Am Coll Cardiol*. 2022;79(3):250–263. doi:10.1016/j.jacc.2021.10.043
28. Kapłon-Cieślicka A, Vardas P, Grabowski M, Lelonek M. Tailoring guideline-directed medical therapy in heart failure with reduced ejection fraction: A practical guide. *Kardiol Pol*. 2023;81(9):850–858. doi:10.33963/v.kp.97062
29. Straw S, McGinlay M, Witte KK. Four pillars of heart failure: Contemporary pharmacological therapy for heart failure with reduced ejection fraction. *Open Heart*. 2021;8(1):e001585. doi:10.1136/openhrt-2021-001585
30. McMurray JJV, Packer M. How should we sequence the treatments for heart failure and a reduced ejection fraction? A redefinition of evidence-based medicine. *Circulation*. 2021;143(9):875–877. doi:10.1161/CIRCULATIONAHA.120.052926
31. Grupper A, Chernomordik F, Herscovici R, et al. The burden of heart failure in cardiac intensive care unit: A prospective 7 years analysis. *ESC Heart Fail*. 2023;10(3):1615–1622. doi:10.1002/ehf2.14320
32. Liu Z, Li Z, Li X, et al. Global trends in heart failure from 1990 to 2019: An age-period-cohort analysis from the Global Burden of Disease study. *ESC Heart Fail*. 2024;11(5):3264–3278. doi:10.1002/ehf2.14915

The role of urinary biomarkers in the diagnosis, prognosis and pathophysiology of heart failure with preserved ejection fraction

Aleksandra A. Nasiadka[A–D], Alicja Rydzewska-Rosołowska[A–C,E,F], Katarzyna Kakareko[B,C,E], Irena Głowińska[B,C,E], Tomasz Hryszko[E,F]

2nd Department of Nephrology, Hypertension, and Internal Medicine with Dialysis Unit, Medical University of Bialystok, Poland

A – research concept and design; B – collection and/or assembly of data; C – data analysis and interpretation;
D – writing the article; E – critical revision of the article; F – final approval of the article

Advances in Clinical and Experimental Medicine, ISSN 1899–5276 (print), ISSN 2451–2680 (online) *Adv Clin Exp Med*. 2025;34(11):1981–1989

Address for correspondence
Aleksandra A. Nasiadka
E-mail: aleksandra.anna.nasiadka@gmail.com

Funding sources
None declared

Conflict of interest
None declared

Received on September 9, 2024
Reviewed on December 31, 2024
Accepted on January 18, 2025

Published online on August 1, 2025

Abstract

Heart failure with preserved ejection fraction (HFpEF) poses a significant clinical challenge due to its increasing incidence, diagnostic complexities and pathophysiological heterogeneity. This study offers valuable insights into the role of urinary biomarkers in patients with HFpEF. Our research focused on profiling alterations in urinary biomarkers, encompassing albumin, indicators of tubular injury, oxidative stress markers, and proteomic changes in individuals with this condition. These findings may provide a potential tool for addressing the diagnostic challenges associated with HFpEF, particularly given the absence of specific cutoff points in the diagnosis of this disease. Furthermore, we explored the potential pathophysiological relationships of these biomarkers, which, in a broader context, facilitate a deeper understanding of this complex disease and may identify potential pharmacotherapeutic targets. We also examined the prognostic value of the identified biomarkers, which could serve as useful instruments for predicting disease risk and forecasting clinical outcomes. Additionally, we emphasized the existing knowledge surrounding potential biomarkers, suggesting that a better understanding of these markers may contribute to the development of clinically relevant tools and enhance our comprehension of HFpEF. The findings from this study align with the current literature, which underscores the complexity of HFpEF and the need for innovative diagnostic, prognostic and therapeutic strategies.

Key words: diastolic dysfunction, albuminuria, HFpEF, heart failure with preserved ejection fraction, urinary biomarker

Cite as
Nasiadka AA, Rydzewska-Rosołowska A, Kakareko K, Głowińska I, Hryszko T. The role of urinary biomarkers in the diagnosis, prognosis and pathophysiology of heart failure with preserved ejection fraction. *Adv Clin Exp Med*. 2025;34(11):1981–1989. doi:10.17219/acem/200268

DOI
10.17219/acem/200268

Highlights

- Heart failure with preserved ejection fraction (HFpEF) is often misdiagnosed or inadequately diagnosed, as many diagnostic parameters lack clear cutoffs. Additionally, its pathophysiology remains incompletely understood.
- Studies have demonstrated a strong correlation between albuminuria and HFpEF, identifying it as a prognostic factor for HFpEF development. Albuminuria is associated with poor outcomes and echocardiographic parameters related to diastolic dysfunction.
- Urinary biomarkers N-acetyl-d-glucosaminidase (NAG), neutrophil gelatinase-associated lipocalin (NGAL) and kidney injury molecule-1 (KIM-1) are correlated with HFpEF. Patients with HFpEF exhibit higher levels of tubular kidney injury biomarkers in their urinary profile compared to those with HFrEF.
- Urinary oxidative stress markers, such as F2-isoprostanes, 8-hydroxy-2'-deoxyguanosine (8-OHdG) and biopyrrins, are potential biomarkers for HFpEF; however, further research is needed.
- In HFpEF, urinary proteome analysis has shown correlations with collagen metabolism proteins and pathways involved in immune system regulation.

Introduction

Heart failure with preserved ejection fraction (HFpEF) is a heterogeneous condition posing significant medical and societal challenges. Its prevalence is estimated to be approx. 1–2% in adults, rising to about 5% in those over 60 years.[1,2] These figures may be underestimated due to insufficient recognition of the condition.[3] The incidence of HFpEF is projected to rise with aging populations and the growing prevalence of lifestyle-related diseases, such as hypertension, diabetes and hyperlipidemia, which contribute to the pathogenesis of HFpEF. Research in HFpEF is becoming crucial for improving patients' quality of life and treatment outcomes.

Diagnosing HFpEF is challenging in clinical practice due to the absence of a definitive biochemical or echocardiographic marker. The mere presence of diastolic dysfunction is insufficient for establishing a diagnosis of HFpEF. Many diagnostic parameters lack clear cutoffs, and symptoms appear only during physical exertion, requiring exercise testing for accurate diagnosis. Although invasive hemodynamic testing is regarded as the reference standard, its use is limited by its benefit–risk ratio and the substantial number of suspected cases.[4] The lack of a universally accepted diagnostic guideline leads to many HFpEF patients being misdiagnosed or inadequately diagnosed in the early stages, often until the disease has progressed significantly.

The classification of HFpEF highlights its distinct pathophysiology compared to heart failure with reduced ejection fraction (HFrEF). Key components of HFpEF pathophysiology include systemic inflammation, increased oxidative stress and endothelial dysfunction, leading to structural cardiac remodeling and its subsequent effects.[5] Despite extensive research, these processes remain incompletely understood. This review summarizes current knowledge on urinary biomarkers in patients with HFpEF, evaluating their diagnostic and prognostic value while contributing to a better understanding of the pathophysiology of this complex clinical entity (see Fig. 1 and Table 1).

Objectives

This review consolidates current knowledge on urinary biomarkers in HFpEF patients, focusing on those specific to HFpEF rather than general heart failure (HF). Our study identifies both well-known biomarkers and highlights potential biomarkers that require further investigation. Understanding these biomarkers may shed light on the pathophysiological processes in patients diagnosed with HFpEF. Since these biomarkers are accessible through noninvasive urine collection, they provide valuable insights into the underlying pathology. This knowledge could facilitate the identification of new therapeutic targets and optimize the patient care. Urinary biomarkers may also serve as diagnostic tools, identifying individuals at risk of developing HFpEF or aiding its diagnosis. Additionally, this review examines the evidence for their predictive value in patients with HFpEF.

We conducted a comprehensive PubMed search from July 2023 to June 2024, using specific key words and relevant subheadings. The key words included: "heart failure with preserved ejection fraction urinary biomarker", "heart failure with preserved ejection fraction albuminuria", "HFpEF urinary biomarker", "diastolic dysfunction urinary biomarker", "diastolic dysfunction albuminuria", "heart failure with preserved ejection fraction NGAL", and "heart failure with preserved ejection fraction KIM-1". Results were combined, duplicates removed, and articles assessed for relevance based on titles, abstracts or full texts. Only English-language articles directly related to the topic were included, regardless of publication date. Studies involving animals were excluded.

Albuminuria

In physiological states, the glomerular barrier prevents filtration of large proteins, such as albumin, through size- and charge-selective membrane. The negatively charged

Table 1. Observed correlation between changes in echocardiographic parameters and increasing albuminuria, NGAL, KIM-1, and 8-OHdG

Biomarker	Albuminuria	NGAL	KIM-1	8-OHdG
Left ventricular parameters				
Left ventricular (LV) dimensions	↑, eccentric hypertrophy	↑	↑	ND
Left ventricular mass (LVM)	↑	ND	ND	ND
Left ventricular systolic function parameters				
Ejection fraction %	↓	ND	ND	↓
Tissue Doppler s' velocity	↓	ND	ND	ND
Preload recruitable stroke work (PRSW)	↓	ND	ND	ND
Global longitudinal strain (GLS)	↓	ND	ND	ND
Left ventricular diastolic function parameters				
e' tissue velocity	↓	↓	ND	↓
E/e' ratio	↑	↑	ND	↑
Right ventricular parameters				
RV dimensions	↑	ND	ND	ND
The right ventricular end-systolic area index (RVESRI)	↑	ND	ND	ND
Right ventricular fractional area change (RVFAC)	↓	ND	ND	ND
Pressures in the right heart (PASP and RAP)	↑	ND	ND	ND

ND – no data; e' tissue velocity – early diastolic mitral annular tissue velocity; E/e' ratio – ratio of early diastolic transmitral flow velocity (E) to early diastolic mitral annular tissue velocity (e'); RV – right ventricle; PASP – pulmonary artery systolic pressure; RAP – right atrial pressure; NGAL – neutrophil gelatinase-associated lipocalin; KIM-1 – kidney injury molecule-1; 8-OHdG – 8-hydroxy-2'-deoxyguanosine.

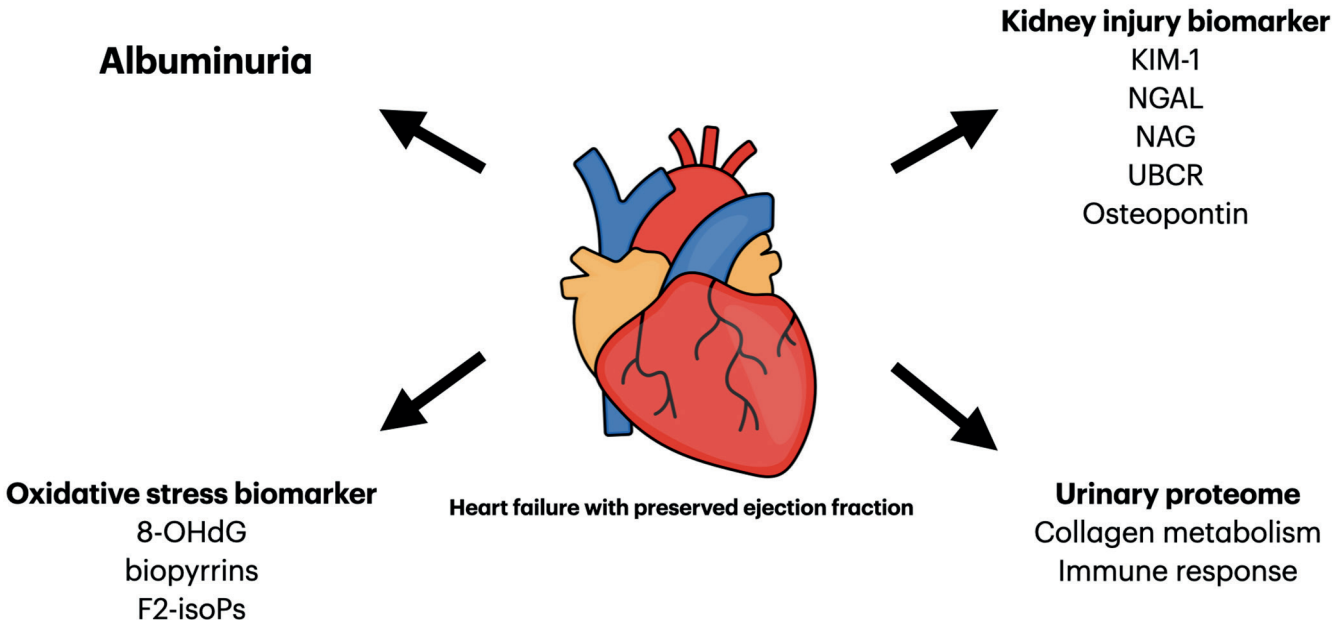

Fig. 1. Urinary biomarkers identified in the literature in patients with heart failure with preserved ejection fraction (HFpEF)

endothelial membrane with its fenestrations restricts the filtration of negatively charged albumin in the renal glomerulus.[6] This results in albumin concentrations in the ultrafiltrate within Bowman's space being 1000–10,000 times lower than in plasma. Most albumin molecules that pass through are absorbed by proximal tubule cells, where proteases break them down into fragments that can re-enter the urine. Elevated levels of albumin in urine are a recognized symptom of glomerular endothelial damage. Moreover, the population-based Maastricht Study demonstrated a direct relationship between albuminuria and microvascular endothelial dysfunction.[7] A significant correlation was observed between 24-h albuminuria and 2 established measures of microvascular endothelial function: retinal arteriolar dilation in response to flicker light stimulation and skin hyperemia induced by local heating. The presence of albuminuria also carries broader implications for systemic health. Transient albuminuria can occur in response to high-altitude hypoxia, myocardial hypoxia and physical exertion, whereas its persistent presence

is commonly associated with metabolic syndrome, type 2 diabetes and cardiovascular diseases.[8]

Albuminuria is a major risk factor for cardiovascular and overall mortality, independent of other cardiovascular risk factors, even in individuals with normal renal function.[9] An elevated urinary albumin-to-creatinine ratio (UACR) is common among patients with HF, and this association remains significant even in individuals without diabetes.[10] Moreover, it has been shown that low-grade albuminuria precedes the occurrence of both HFpEF and HFrEF.[11] According to these findings, elevated albuminuria indicates systemic vascular endothelial dysfunction and is pathophysiologically linked to HF, including HFpEF.[12] The association between albuminuria and HFpEF was demonstrated in the prospective multicenter PROMIS-HFpEF study.[13] It identified a link between albuminuria and coronary microvascular dysfunction, as well as systemic endothelial dysfunction, evidenced by elevated UACR and reduced coronary flow reserve. These dysfunctions correlated with markers of systemic endothelial dysfunction, including UACR. Therefore, albuminuria serves as an indicator of widespread microvascular and endothelial damage and may act as a surrogate marker for such pathological changes in multiple organs, including the heart. However, the precise pathomechanisms and causal link between albuminuria and HF remain unclear, although inflammation-induced endothelial dysfunction is considered a potential contributing factor.[13] In the RELAX study, 75% of patients with HFpEF exhibited elevated levels of C-reactive protein (CRP).[14] Correlations were observed between inflammatory markers, such as von Willebrand factor, in patients with both albuminuria and HF, with this factor further associated with increased levels of interleukin 6 (IL-6) and CRP.[15] Another marker supporting the link between inflammation and the pathophysiology of HFpEF is pentraxin 3 (PTX-3), a novel inflammatory biomarker. Its levels have been shown to correlate with the presence of left ventricular diastolic dysfunction in patients with preserved ejection fraction.[16] Moreover, elevated levels of PTX-3) have also been associated with diastolic remodeling in patients experiencing ST-elevation myocardial infarction (STEMI).[17]

Furthermore, hypervolemia is another potential mechanism linking albuminuria to HFpEF. Studies have confirmed associations between albuminuria and reduced renal artery blood flow, as well as physical signs of volume overload and elevated levels of NT-proBNP.[18] Additionally, according to this hypothesis, a reduction in albuminuria has been associated with an improvement in congestion-related symptoms, as well as a decrease in NT-proBNP levels.[19]

Albuminuria is also associated with echocardiographic parameters reflecting biventricular dysfunction and myocardial remodeling.[20] This relationship persisted even after excluding comorbid conditions such as diabetes and chronic kidney disease (CKD), and correlations with changes in echocardiographic parameters have been observed even at low levels of albuminuria in asymptomatic patients. Studies have shown that albuminuria is associated with increased left ventricular (LV) mass (LVM) and wall thickness in both hypertensive and non-hypertensive individuals.[21–23] In hypertensive patients, it correlates negatively with ejection fraction and left LV chamber size.[21] Renal impairment also affects left heart geometry; however, the specific alterations in cardiac structure and function vary depending on whether albuminuria or a reduced estimated glomerular filtration rate (eGFR) is present.[24] In patients with albuminuria but normal creatinine levels, eccentric hypertrophy is more common, while isolated reductions in eGFR are linked to concentric hypertrophy, increased LV mass and abnormal LV geometry alongside lower mid-wall fractional shortening (MWFS). Patients with both albuminuria and reduced eGFR exhibit mixed structural changes, including eccentric and concentric hypertrophy, as well as concentric remodeling.[24] The above observations suggest that albuminuria and eGFR are associated with different pathomechanisms leading to HFpEF. This also indicates the potential to identify subgroups of patients with diastolic dysfunction in future studies.

Higher UACR levels are linked to worse LV systolic function parameters, such as longitudinal systolic function (measured by tissue Doppler's velocity) and preload recruitable stroke work (PRSW, a load-independent indicator of contractility), despite the presence of preserved ejection fraction.[20,25] Global longitudinal strain (GLS), a sensitive echocardiographic parameter, is crucial for assessing subtle changes in LV systolic function in patients with HFpEF.[26] Studies indicate that HFpEF patients often exhibit abnormalities in GLS, suggesting underlying systolic dysfunction, which may be an inherent part of the HFpEF syndrome.[26–28] Notably, UACR exhibits an inverse relationship with GLS, and this association remains significant even after adjustment for multiple confounding variables. Another parameter indicative of LV diastolic relaxation is the e′ tissue velocity, which reflects the diastolic motion of the myocardium during the rapid filling phase of the ventricle.[29] While some studies have reported an association between albuminuria and reduced e′ velocity, the strength and significance of this relationship have varied across different analyses.[25,30] Nonetheless, albuminuria, even at low concentrations, consistently correlates with an elevated E/e′ ratio.[25] The E/e′ ratio is regarded as one of the most reliable noninvasive measures for assessing LV filling pressure in individuals with preserved diastolic function. Importantly, this relationship persists after accounting for diabetes and LV hypertrophy, indicating a subclinical connection between albuminuria and deteriorating function. Additionally, an analysis of B-type natriuretic peptide (BNP) levels and UACR in patients with preserved ejection fraction and normal LV volume revealed a strong positive correlation.[25] This suggests that elevated albuminuria may serve as a biomarker for heightened myocardial wall stress, a key contributor to HFpEF pathophysiology.

In patients with HFpEF, right ventricular dysfunction is common and associated with worse clinical outcomes in this population. Furthermore, research findings indicate that longitudinal subendocardial dysfunction, both diastolic and systolic, of the right ventricle is related to the symptomatology of patients.[20] Albuminuria is significantly associated with right ventricular (RV) remodeling. Structural changes such as increased RV wall thickness and chamber enlargement are frequently observed in patients with HFpEF.[20] The urinary albumin-to-creatinine ratio is significantly elevated in individuals with RV hypertrophy, and higher levels are correlated with increased RV wall thickness and a larger RV end-systolic area index. Furthermore, albuminuria is associated with RV systolic dysfunction, as indicated by reduced right ventricular fractional area change (RVFAC). These associations persist even after excluding patients with macroalbuminuria, and they remain significant after adjusting for increased pressures in the right heart, such as pulmonary artery systolic pressure (PASP) and right atrial pressure (RAP), as well as left ventricular diastolic pressure measured via catheterization. This suggests that albuminuria-related RV remodeling may result from mechanisms beyond preload or afterload increases, possibly involving inflammation and endothelial dysfunction.

In clinical terms, albuminuria emerges as a promising biomarker for HFpEF onset, as traditional cardiovascular biomarkers exhibit a stronger correlation with HFrEF. Low-grade albuminuria preceding HFpEF suggests its potential as an early indicator of cardiovascular pathology.[11] Studies have shown that elevated UACR is associated with a higher risk of hospitalization in HFpEF patients, an effect that is notably stronger in males.[31] In individuals with HFpEF, urinary albumin excretion has also been identified as an independent predictor of both cardiovascular and non-cardiovascular mortality across all eGFR levels.[32] Moreover, positive findings of albuminuria on urine dipstick tests in HFpEF patients have also been associated with poorer outcomes.[33,34] This evidence suggests that dipstick albuminuria could serve as a simple yet effective prognostic marker in HFpEF patients, enabling early risk stratification and guiding clinical management.

Tubular kidney injury biomarkers

Tubular kidney injury biomarkers are emerging as valuable tools for the early detection and evaluation of kidney damage. Unlike traditional markers such as serum creatinine, which often reflect kidney injury only after significant delays, tubular injury biomarkers can detect damage at earlier stages, allowing for differentiation of the site and degree of kidney injury.[35]

Kidney injury molecule-1 (KIM-1) is a type I cell membrane glycoprotein that is undetectable in healthy kidneys. However, in response to inflammation or injury of the proximal tubules, it is expressed in regenerating epithelial cells.[36] This upregulated expression is particularly prominent in the S3 segment of the proximal tubule, where KIM-1 functions as a scavenger receptor, facilitating the phagocytosis of necrotic epithelial cells.[37] In patients with chronic HF, elevated levels of KIM-1 in the urine correlate with worse clinical outcomes and increased risk of hospitalization.[38] Additionally, elevated KIM-1 levels are observed in symptomatic HF patients.[38] These elevations persist even in patients with normal kidney function and normal glomerular filtration rate (GFR). Furthermore, elevated levels of KIM-1 in urine are correlated with an increased risk of developing HF within the population.[39] Comparing the urinary marker profile in patients with HFrEF versus HFpEF, patients with diastolic dysfunction show greater evidence of tubular damage and/or dysfunction.[40] Among HFpEF patients, higher urinary KIM-1 levels are noted, while urinary creatinine levels are significantly lower compared to those with HFrEF.[40] Additionally, pediatric studies have linked elevated urinary KIM-1 concentrations to left ventricular hypertrophy (LVH), the most common myocardial structural abnormality in diastolic dysfunction.[41]

Another biomarker, neutrophil gelatinase-associated lipocalin (NGAL), is typically present at low levels in healthy individuals but rises markedly in response to kidney injury. It serves roles in innate immunity and acts as an acute-phase protein in inflammatory states and endothelial damage.[42] Its heightened concentration in urine stems from increased protein expression and impaired reabsorption in damaged proximal tubule epithelium.[42] Research has shown that NGAL levels in both serum and urine are significantly increased in outpatients with HF, suggesting its potential utility as a diagnostic and prognostic indicator in this condition.[43,44] This correlation remained significant in patients with reduced GFR. Interestingly, while serum NGAL levels are correlated with serum creatinine in acute HF,[45] urinary NGAL concentrations do not show this association. The data on the predictive value of urinary NGAL levels in predicting mortality in patients with chronic HF are inconclusive, with only 1 study demonstrating a weak correlation with elevated mortality in this patient cohort.[43,44,46] However, similarly to KIM-1, the study shows that patients with HFpEF exhibit higher urinary NGAL-1 levels compared to patients with reduced ejection fraction, particularly when there is no kidney dysfunction.[40] Furthermore, in patients with CKD, plasma NGAL concentration correlated with LVH and left ventricular diastolic dysfunction, as assessed by the E' parameter and the ratio of E to E' (E/E').[47]

Going further, N-acetyl-β-D-glucosaminidase (NAG), a lysosomal enzyme released from proximal tubules due to epithelial cell injury, is significantly elevated in patients with chronic HF.[48] Its levels correlate with poorer prognosis and increased risk of hospitalization.[37,46,48] However, no clear relationship has been established

between NAG levels and HF-related events in HFpEF, defined as hospitalization or death due to HF. In contrast, a study showed that the urinary β2-microglobulin to creatinine ratio (UBCR) indicated a significantly higher risk of cardiac events in patients with HFpEF, and this association persisted even after adjusting for other risk factors.[49] Levels of UBCR also correlate with HF severity, as classified by the New York Heart Association (NYHA) functional classification, in patients with HFpEF.[49] Another biomarker found in urine that shows significantly elevated levels in patients with HFpEF is osteopontin,[40] a protein secreted by cells in the distal tubule and loop of Henle in response to nephron injury. While its role in diastolic dysfunction remains unclear, further investigation is warranted.

The observed relationships between HFpEF and tubular kidney injury biomarkers highlight the need for deeper investigation into the underlying mechanisms. These biomarkers likely reflect the functional status of the renal tubules, which are responsible for electrolyte and water balance. A study conducted by Jungbauer et al. revealed that alterations in volume status induced by diuretics are linked to changes in markers of tubular dysfunction, such as KIM-1 and NGAL.[38] Disruption in salt and water excretion can result in fluid overload, and therefore elevated cardiac output, high blood pressure, LVH, and indirectly contribute to HFpEF development. Tubular injury, reduced nephron mass and ongoing inflammation may activate both the renin–angiotensin–aldosterone system and the sympathetic nervous system, causing endothelial dysfunction.[50] Moreover, the referenced studies observed higher concentrations of tubular injury biomarkers in patients with HFpEF compared to those with HFrEF, particularly in cases with normal eGFR.[40] This suggests that renal dysfunction may be present in HFpEF patients without diagnosed kidney disease, as eGFR primarily assesses kidney filtration capacity and may not accurately reflect existing damage in the distal nephron segments. Proximal tubules, which are highly susceptible to injury due to their substantial oxygen demand, play a central role in the progression of CKD. In turn, CKD is associated with the accumulation of uremic toxins, increased oxidative stress and microvascular dysfunction, i.e., key contributors to the development and progression of diastolic heart dysfunction.[51,52] While current data strongly suggest a connection between HFpEF and tubular injury biomarkers, causality remains unproven. Reverse causation, where HFpEF contributes to tubular injury, must also be considered.

Oxidative stress markers

In the literature on the HFpEF pathophysiology, oxidative stress, along with endothelial dysfunction and inflammation, plays a significant role in the development of diastolic dysfunction of the heart.[52] Oxidative stress arises from an imbalance between excessive production of reactive oxygen species (ROS) and insufficient antioxidant defenses, leading to cellular damage that affects proteins, lipids and DNA. Patients with HFpEF frequently present with comorbidities such as obesity, diabetes, dyslipidemia, hypertension, and renal impairment, all of which contribute to endothelial dysfunction and systemic inflammation, thereby enhancing ROS production in cardiac endothelial cells.[53] Moreover, studies have shown that the presence of HFpEF correlates with elevated levels of oxidative stress markers, such as nitrotyrosine, indicating nitrosative/oxidative stress.[54] Reactive oxygen species can alter titin phosphorylation, leading to increased passive stiffness of cardiomyocytes, which may adversely affect cardiac diastolic function.[55] Additionally, ROS-induced secretion of pro-fibrotic substances promotes myofibroblast differentiation and collagen deposition, contributing to cardiac fibrosis.[56] Mitochondrial structural and functional disruption in cardiomyocytes, another consequence of oxidative stress, is strongly implicated in the pathophysiology of HFpEF.[57]

One of the well-established biomarkers of oxidative stress is 8-hydroxy-2′-deoxyguanosine (8-OHdG), also known as 8-oxo-2′-deoxyguanosine (8-oxo-dG). It is generated as one of the main products of DNA oxidation by ROS. Formed from the oxidation of deoxyguanosine within DNA, 8-OHdG is repaired and removed by 8-oxoguanine DNA glycosylase-1, then transported into the bloodstream, filtered by the kidneys and excreted in urine.[58] Elevated 8-OHdG levels in serum and urine reflect systemic oxidative stress. In the conducted meta-analysis of studies focusing on 8-OHdG in patients with HF, a strong positive correlation has been demonstrated.[59] Furthermore, in studies of patients with HF, it has also not been shown that diabetes affects the concentration of the biomarker. Urinary 8-OHdG levels have been shown to correlate with HF symptom severity, as assessed using the NYHA functional classification, as well as with echocardiographic parameters including left ventricular ejection fraction (LVEF), pulmonary capillary wedge pressure, and left ventricular end-diastolic volume index (LVEDVI).[60] Laboratory markers like BNP60 also show significant associations. Urinary 8-OHdG has emerged as an independent prognostic marker for cardiac events in patients with chronic HF.[61] Furthermore, in asymptomatic individuals with hypertension, increased urinary 8-OHdG levels correlate with subclinical diastolic dysfunction. In the cohort of individuals without diagnosed HF but with arterial hypertension, the association between 8-OHdG levels and cardiac function has been evaluated. The investigation revealed that parameters of diastolic dysfunction, such as mitral annular early diastolic velocity (e') and the ratio of early transmitral flow velocity (E) to e' (E/e'), correlated with increased urinary 8-OHdG excretion.[62]

Biopyrrins, formed through the oxidative metabolism of bilirubin, serve as additional biomarkers of oxidative stress and can be detected in the blood and urine. Bilirubin, an antioxidant, captures circulating ROS to prevent lipid and low-density lipoprotein (LDL) oxidation. However, this process is self-limiting, and biopyrrins are subsequently excreted in urine, making them a noninvasive biomarker.[63] In a study conducted by Hokomaki et al., urinary biopyrrins concentrations are significantly elevated in patients with HF, with the highest levels observed in patients classified as NYHA III/IV.[64] Even in patients with milder symptoms (NYHA I) and preserved ejection fraction (average 54.8 ±2.7%), biopyrrin levels are significantly higher than in controls. A positive correlation has been observed between biopyrrin and BNP levels.[64] Further research has focused on bilirubin levels, which are associated with poorer prognosis, increased severity in patients with HF and elevated all-cause mortality.[65,66] However, in patients with HFpEF, lower blood bilirubin levels have been observed compared to control subjects, and this decrease correlates with the severity of diastolic dysfunction, with the lowest levels detected in those with grade 4 HFpEF.[67] This discrepancy in study results depending on the type of HF may be explained by the role of bilirubin as an antioxidant,[68] which may decrease in HFpEF due to increased oxidative stress. Regarding biopyrrins, it has been shown that their concentration in urine correlates with bilirubin levels.[69] Therefore, it seems reasonable to hypothesize about the potential value of biopyrrins as a biomarker in HFpEF. However, further studies are required to establish their clinical utility in specific HF subtypes.

Another potential biomarkers of oxidative stress in HFpEF measurable in urine are F2-isoprostanes (F2-isoPs). These compounds are advantageous due to the noninvasive nature of their assessment and their stability, as their concentrations are not significantly influenced by renal or hepatic dysfunction. Furthermore, F2-isoPs are considered one of the most reliable and stable markers for monitoring oxidative stress intensity in patients.[70] Research indicates that the concentration of F2-isoPs in urine is significantly elevated in patients with severe HF and correlates with the severity of symptoms as indicated by the NYHA scale.[70] Although promising, additional studies are needed to determine the predictive value of F2-isoPs and their specific relationship to HFpEF.

Urinary proteome

Urinary proteome analysis is an evolving field in biomarker discovery, offering insights into naturally occurring peptides in urine. This approach has become a valuable tool for understanding disease mechanisms and identifying novel biomarkers across various conditions. Heart failure, including HFpEF, presents a multifactorial etiology, making it challenging to unravel the precise molecular mechanisms involved. In all HF subtypes, including HFpEF, the strongest correlations have been observed with peptides representing collagen fragments, whose concentrations in urine have decreased.[71] The most pronounced reductions are observed in fragments derived from collagens with specialized structures that support network formation, particularly collagen types IV and VIII. While the exact cause of these changes is unclear, these findings suggest enhanced collagen network stability in HF and underscore the role of disrupted collagen turnover in patients with HFpEF.[72] Further alterations observed in the urinary proteome of patients with HF includes dysregulation in pathways responsible for immune response. The most prominent alterations are associated with innate immune responses, notably those involving toll-like receptors (TLRs), neutrophil degranulation and activation of the complement cascade.[71] Notably, these changes are characteristic of HF and remain distinct from those caused by CKD. Despite significant differences between patients with HF and the control group, no significant differences in peptide changes have been observed between patients with reduced and preserved ejection fraction. These findings may indicate that, irrespective of clinical distinctions, HFpEF and other HF subtypes involve overlapping molecular mechanisms. An analysis of data from the TOPCAT study was conducted to assess the prognostic value of urinary proteins in patients with HFpEF. The findings revealed that more than 40 urinary peptides were significantly associated with adverse outcomes, defined as an increased risk of mortality or hospital readmission. The proteins associated with the highest risk included angiopoietin-like protein 2 (ANGPTL2), deoxyribonuclease-1 (DNASE1) and α-amylase 2A (AMY2A). A weaker correlation was observed for proteins related to fibrosis, metabolism and inflammation. In this context, the findings align with other research indicating that urinary biomarkers can provide valuable insights into the prognosis of HFpEF patients.[73]

Conclusions

Urinary biomarkers show considerable potential as valuable instruments for the diagnosis, prognosis and elucidation of the pathophysiological mechanisms underlying HFpEF. This review consolidates current knowledge on urinary biomarkers, highlighting their utility in advancing the understanding of HFpEF and guiding future research. Given the substantial heterogeneity of HFpEF, it continues to pose a major clinical challenge. Further investigations are crucial to refine the understanding of biomarkers in HFpEF patients, paving the way for improved management and therapeutic strategies for these patients.

Consent for publication

Not applicable.

Use of AI and AI-assisted technologies

Not applicable.

ORCID iDs

Alicja Rydzewska-Rosołowska https://orcid.org/0000-0002-8126-3085
Katarzyna Kakareko https://orcid.org/0000-0001-8046-4179
Irena Głowińska https://orcid.org/0000-0002-4701-8422
Tomasz Hryszko https://orcid.org/0000-0002-0145-3103

References

1. Kapelios CJ, Shahim B, Lund LH, Savarese G. Epidemiology, clinical characteristics and cause-specific outcomes in heart failure with preserved ejection fraction. *Card Fail Rev*. 2023;9:e14. doi:10.15420/cfr.2023.03
2. Van Riet EES, Hoes AW, Wagenaar KP, Limburg A, Landman MAJ, Rutten FH. Epidemiology of heart failure: The prevalence of heart failure and ventricular dysfunction in older adults over time. A systematic review. *Eur J Heart Fail*. 2016;18(3):242–252. doi:10.1002/ejhf.483
3. Loai S, Cheng HLM. Heart failure with preserved ejection fraction: The missing pieces in diagnostic imaging. *Heart Fail Rev*. 2020;25(2):305–319. doi:10.1007/s10741-019-09836-8
4. Pieske B, Tschöpe C, De Boer RA, et al. How to diagnose heart failure with preserved ejection fraction: The HFA–PEFF diagnostic algorithm. A consensus recommendation from the Heart Failure Association (HFA) of the European Society of Cardiology (ESC). *Eur J Heart Fail*. 2020;22(3):391–412. doi:10.1002/ejhf.1741
5. Nair N. Epidemiology and pathogenesis of heart failure with preserved ejection fraction. *Rev Cardiovasc Med*. 2020;21(4):531. doi:10.31083/j.rcm.2020.04.154
6. Butt L, Unnersjö-Jess D, Höhne M, et al. A molecular mechanism explaining albuminuria in kidney disease. *Nat Metab*. 2020;2(5):461–474. doi:10.1038/s42255-020-0204-y
7. Martens RJH, Houben AJHM, Kooman JP, et al. Microvascular endothelial dysfunction is associated with albuminuria: The Maastricht Study. *J Hypertens*. 2018;36(5):1178–1187. doi:10.1097/HJH.0000000000001674
8. Prasad RM, Bali A, Tikaria R. Microalbuminuria. In: *StatPearls*. Treasure Island, USA: StatPearls Publishing; 2025:Bookshelf ID: NBK563255. http://www.ncbi.nlm.nih.gov/books/NBK563255/. Accessed January 18, 2025.
9. Claudel SE, Waikar SS, Schmidt IM, Vasan RS, Verma A. The relationship between low levels of albuminuria and mortality among adults without major cardiovascular risk factors. *Eur J Prev Cardiol*. 2024;31(17):2046–2055. doi:10.1093/eurjpc/zwae189
10. Agewall S, Wikstrand J, Ljungman S, Fagerberg B. Usefulness of microalbuminuria in predicting cardiovascular mortality in treated hypertensive men with and without diabetes mellitus. *Am J Cardiol*. 1997;80(2):164–169. doi:10.1016/S0002-9149(97)00312-3
11. De Boer RA, Nayor M, deFilippi CR, et al. Association of cardiovascular biomarkers with incident heart failure with preserved and reduced ejection fraction. *JAMA Cardiol*. 2018;3(3):215. doi:10.1001/jamacardio.2017.4987
12. Khan MS, Shahid I, Anker SD, et al. Albuminuria and heart failure. *J Am Coll Cardiol*. 2023;81(3):270–282. doi:10.1016/j.jacc.2022.10.028
13. Shah SJ, Lam CSP, Svedlund S, et al. Prevalence and correlates of coronary microvascular dysfunction in heart failure with preserved ejection fraction: PROMIS-HFpEF [published correction appears in *Eur Heart J*. 2019;40(6):541. doi:10.1093/eurheartj/ehy804]. *Eur Heart J*. 2018;39(37):3439–3450. doi:10.1093/eurheartj/ehy531
14. DuBrock HM, AbouEzzeddine OF, Redfield MM. High-sensitivity C-reactive protein in heart failure with preserved ejection fraction. *PLoS One*. 2018;13(8):e0201836. doi:10.1371/journal.pone.0201836
15. Abudoukelimu M, Ba B, Kai Guo Y, Xu J. Von Willebrand factor (vWF) in patients with heart failure with preserved ejection fraction (HFpEF): A retrospective observational study. *Medicine (Baltimore)*. 2022;101(31):e29854. doi:10.1097/MD.0000000000029854
16. Matsubara J, Sugiyama S, Nozaki T, et al. Pentraxin 3 is a new inflammatory marker correlated with left ventricular diastolic dysfunction and heart failure with normal ejection fraction. *J Am Coll Cardiol*. 2011;57(7):861–869. doi:10.1016/j.jacc.2010.10.018
17. Somuncu MU, Tatar FP, Serbest NG, Uygur B, Demir AR. Pentraxin-3 is associated with adverse diastolic remodeling in patients with ST-elevation myocardial infarction after successful reperfusion by primary percutaneous intervention. *J Cardiovasc Echography*. 2021;31(2):77–84. doi:10.4103/jcecho.jcecho_116_20
18. Brisco MA, Testani JM. Novel renal biomarkers to assess cardiorenal syndrome. *Curr Heart Fail Rep*. 2014;11(4):485–499. doi:10.1007/s11897-014-0226-4
19. Koyama S, Sato Y, Tanada Y, Fujiwara H, Takatsu Y. Early evolution and correlates of urine albumin excretion in patients presenting with acutely decompensated heart failure. *Circ Heart Fail*. 2013;6(2):227–232. doi:10.1161/CIRCHEARTFAILURE.112.000152
20. Katz DH, Burns JA, Aguilar FG, Beussink L, Shah SJ. Albuminuria is independently associated with cardiac remodeling, abnormal right and left ventricular function, and worse outcomes in heart failure with preserved ejection fraction. *JACC Heart Fail*. 2014;2(6):586–596. doi:10.1016/j.jchf.2014.05.016
21. Djoussé L, Kochar J, Hunt SC, et al. Relation of albuminuria to left ventricular mass (from the HyperGEN Study). *Am J Cardiol*. 2008;101(2):212–216. doi:10.1016/j.amjcard.2007.07.065
22. Dekkers IA, De Mutsert R, Rabelink TJ, et al. Associations between normal range albuminuria, renal function and cardiovascular function in a population-based imaging study. *Atherosclerosis*. 2018;272:94–100. doi:10.1016/j.atherosclerosis.2018.03.029
23. Wang T, Zhong H, Lian G, et al. Low-grade albuminuria is associated with left ventricular hypertrophy and diastolic dysfunction in patients with hypertension. *Kidney Blood Press Res*. 2019;44(4):590–603. doi:10.1159/000500782
24. Gori M, Senni M, Gupta DK, et al. Association between renal function and cardiovascular structure and function in heart failure with preserved ejection fraction. *Eur Heart J*. 2014;35(48):3442–3451. doi:10.1093/eurheartj/ehu254
25. Katz DH, Selvaraj S, Aguilar FG, et al. Association of low-grade albuminuria with adverse cardiac mechanics: Findings from the hypertension genetic epidemiology network (HyperGEN) study. *Circulation*. 2014;129(1):42–50. doi:10.1161/CIRCULATIONAHA.113.003429
26. DeVore AD, McNulty S, Alenezi F, et al. Impaired left ventricular global longitudinal strain in patients with heart failure with preserved ejection fraction: Insights from the RELAX trial. *Eur J Heart Fail*. 2017;19(7):893–900. doi:10.1002/ejhf.754
27. Buggey J, Alenezi F, Yoon HJ, et al. Left ventricular global longitudinal strain in patients with heart failure with preserved ejection fraction: Outcomes following an acute heart failure hospitalization. *ESC Heart Fail*. 2017;4(4):432–439. doi:10.1002/ehf2.12159
28. Diễm TN, Nguyễn VA, Đỗ LD, et al. Early detecting myocardial entity damage using 2D speckle tracking echocardiography through strain parameters in hypertensive patients. *Arter Hypertens*. 2022;26(1):15–25. doi:10.5603/AH.a2022.0001
29. Choi YJ, Park CS, Rhee TM, et al. Mitral annular tissue velocity predicts survival in patients with primary mitral regurgitation. *Korean Circ J*. 2024;54(6):311. doi:10.4070/kcj.2023.0292
30. Liu M, He A, Wang Y, et al. Association of urine albumin-to-creatinine ratio with subclinical systolic dysfunction in hypertensive patients but not normotensive subjects: Danyang study. *J Clin Hypertens (Greenwich)*. 2020;22(12):2230–2238. doi:10.1111/jch.14081
31. Wei FF, Xue R, Wu Y, et al. Sex-specific associations of risks and cardiac structure and function with microalbumin/creatinine ratio in diastolic heart failure. *Front Cardiovasc Med*. 2020;7:579400. doi:10.3389/fcvm.2020.579400
32. Bayes-Genis A, Cediel G, Domingo M, Codina P, Santiago E, Lupón J. Biomarkers in heart failure with preserved ejection fraction. *Card Fail Rev*. 2022;8:e20. doi:10.15420/cfr.2021.37
33. Oeun B, Hikoso S, Nakatani D, et al. Prognostic significance of dipstick proteinuria in heart failure with preserved ejection fraction: Insight from the PURSUIT-HFpEF registry. *BMJ Open*. 2021;11(9):e049371. doi:10.1136/bmjopen-2021-049371
34. Miura M, Shiba N, Nochioka K, et al. Urinary albumin excretion in heart failure with preserved ejection fraction: an interim analysis of the CHART 2 study. *Eur J Heart Fail*. 2012;14(4):367–376. doi:10.1093/eurjhf/hfs001

35. Jana S, Mitra P, Roy S. Proficient novel biomarkers guide early detection of acute kidney injury: A review. *Diseases*. 2022;11(1):8. doi:10.3390/diseases11010008
36. Huo W, Zhang K, Nie Z, Li Q, Jin F. Kidney injury molecule-1 (KIM-1): A novel kidney-specific injury molecule playing potential double-edged functions in kidney injury. *Transplant Rev (Orlando)*. 2010;24(3):143–146. doi:10.1016/j.trre.2010.02.002
37. Al-bataineh MM, Kinlough CL, Mi Z, et al. KIM-1-mediated anti-inflammatory activity is preserved by MUC1 induction in the proximal tubule during ischemia-reperfusion injury. *Am J Physiol Renal Physiol*. 2021;321(2):F135–F148. doi:10.1152/ajprenal.00127.2021
38. Jungbauer CG, Birner C, Jung B, et al. Kidney injury molecule-1 and *N*-acetyl-ß-D-glucosaminidase in chronic heart failure: Possible biomarkers of cardiorenal syndrome. *Eur J Heart Fail*. 2011;13(10):1104–1110. doi:10.1093/eurjhf/hfr102
39. Driver TH, Katz R, Ix JH, et al. Urinary kidney injury molecule 1 (KIM-1) and interleukin 18 (IL-18) as risk markers for heart failure in older adults: The Health, Aging, and Body Composition (Health ABC) Study. *Am J Kidney Dis*. 2014;64(1):49–56. doi:10.1053/j.ajkd.2014.01.432
40. Streng KW, Hillege HL, Ter Maaten JM, et al. Urinary marker profiles in heart failure with reduced versus preserved ejection fraction. *J Cardiovasc Transl Res*. 2024;17(1):3–12. doi:10.1007/s12265-023-10356-y
41. Jiang K, Greenberg JH, Abraham A, et al. Associations of biomarkers of kidney tubule health, injury, and inflammation with left ventricular hypertrophy in children with CKD. *Kidney360*. 2023;4(8):1039–1047. doi:10.34067/KID.0000000000000183
42. Romejko K, Markowska M, Niemczyk S. The review of current knowledge on neutrophil gelatinase-associated lipocalin (NGAL). *Int J Mol Sci*. 2023;24(13):10470. doi:10.3390/ijms241310470
43. Damman K, Van Veldhuisen DJ, Navis G, Voors AA, Hillege HL. Urinary neutrophil gelatinase associated lipocalin (NGAL), a marker of tubular damage, is increased in patients with chronic heart failure. *Eur J Heart Fail*. 2008;10(10):997–1000. doi:10.1016/j.ejheart.2008.07.001
44. Van Deursen VM, Damman K, Voors AA, et al. Prognostic value of plasma neutrophil gelatinase-associated lipocalin for mortality in patients with heart failure. *Circ Heart Fail*. 2014;7(1):35–42. doi:10.1161/CIRCHEARTFAILURE.113.000242
45. Akiyama E, Cinotti R, Čerlinskaitė K, et al. Improved cardiac and venous pressures during hospital stay in patients with acute heart failure: An echocardiography and biomarkers study. *ESC Heart Fail*. 2020;7(3):996–1006. doi:10.1002/ehf2.12645
46. Damman K, Masson S, Hillege HL, et al. Clinical outcome of renal tubular damage in chronic heart failure. *Eur Heart J*. 2011;32(21):2705–2712. doi:10.1093/eurheartj/ehr190
47. Kim IY, Kim JH, Kim MJ, et al. Plasma neutrophil gelatinase-associated lipocalin is independently associated with left ventricular hypertrophy and diastolic dysfunction in patients with chronic kidney disease. *PLoS One*. 2018;13(10):e0205848. doi:10.1371/journal.pone.0205848
48. Damman K, Van Veldhuisen DJ, Navis G, et al. Tubular damage in chronic systolic heart failure is associated with reduced survival independent of glomerular filtration rate. *Heart*. 2010;96(16):1297–1302. doi:10.1136/hrt.2010.194878
49. Otaki Y, Watanabe T, Shimizu M, et al. Renal tubular damage and clinical outcome in heart failure with preserved ejection fraction and chronic kidney disease. *ESC Heart Fail*. 2023;10(4):2458–2468. doi:10.1002/ehf2.14378
50. Schupp N, Kolkhof P, Queisser N, et al. Mineralocorticoid receptor-mediated DNA damage in kidneys of DOCA-salt hypertensive rats. *FASEB J*. 2011;25(3):968–978. doi:10.1096/fj.10-173286
51. Zwaenepoel B, De Backer T, Glorieux G, Verbeke F. Predictive value of protein-bound uremic toxins for heart failure in patients with chronic kidney disease. *ESC Heart Fail*. 2024;11(1):466–474. doi:10.1002/ehf2.14566
52. Budde H, Hassoun R, Mügge A, Kovács Á, Hamdani N. Current understanding of molecular pathophysiology of heart failure with preserved ejection fraction. *Front Physiol*. 2022;13:928232. doi:10.3389/fphys.2022.928232
53. Harper AR, Patel HC, Lyon AR. Heart failure with preserved ejection fraction. *Clin Med (Lond)*. 2018;18(Suppl 2):s24–s29. doi:10.7861/clinmedicine.18-2-s24
54. Momot K, Krauz K, Czarzasta K, Zarębiński M, Puchalska L, Wojciechowska M. Evaluation of nitrosative/oxidative stress and inflammation in heart failure with preserved and reduced ejection fraction. *Int J Mol Sci*. 2023;24(21):15944. doi:10.3390/ijms242115944
55. Mongirdienė A, Skrodenis L, Varoneckaitė L, Mierkytė G, Gerulis J. Reactive oxygen species-induced pathways in heart failure pathogenesis and potential therapeutic strategies. *Biomedicines*. 2022;10(3):602. doi:10.3390/biomedicines10030602
56. Sweeney M, Corden B, Cook SA. Targeting cardiac fibrosis in heart failure with preserved ejection fraction: Mirage or miracle? *EMBO Mol Med*. 2020;12(10):e10865. doi:10.15252/emmm.201910865
57. Martinez CS, Zheng A, Xiao Q. Mitochondrial reactive oxygen species dysregulation in heart failure with preserved ejection fraction: A fraction of the whole. *Antioxidants (Basel)*. 2024;13(11):1330. doi:10.3390/antiox13111330
58. Di Minno A, Turnu L, Porro B, et al. 8-hydroxy-2-deoxyguanosine levels and cardiovascular disease: A systematic review and meta-analysis of the literature. *Antioxid Redox Signal*. 2016;24(10):548–555. doi:10.1089/ars.2015.6508
59. Di Minno A, Turnu L, Porro B, et al. 8-hydroxy-2-deoxyguanosine levels and heart failure: A systematic review and meta-analysis of the literature. *Nutr Metab Cardiovasc Dis*. 2017;27(3):201–208. doi:10.1016/j.numecd.2016.10.009
60. Kobayashi S, Susa T, Tanaka T, et al. Urinary 8-hydroxy-2'-deoxyguanosine reflects symptomatic status and severity of systolic dysfunction in patients with chronic heart failure. *Eur J Heart Fail*. 2011;13(1):29–36. doi:10.1093/eurjhf/hfq178
61. Suzuki S, Shishido T, Ishino M, et al. 8-hydroxy-2'-deoxyguanosine is a prognostic mediator for cardiac event. *Eur J Clin Invest*. 2011;41(7):759–766. doi:10.1111/j.1365-2362.2010.02465.x
62. Masugata H, Senda S, Inukai M, et al. Association between oxidative stress assessed by urinary 8-hydroxydeoxyguanosine and the cardiac function in hypertensive patients without overt heart disease. *Clin Exp Hypertens*. 2013;35(5):308–312. doi:10.3109/10641963.2012.721842
63. Tada S, Shiota A, Hayashi H, Nakamura T. Reference urinary biopyrrin level and physiological variation in healthy young adults: Relation of stress by learning. *Heliyon*. 2020;6(1):e03138. doi:10.1016/j.heliyon.2019.e03138
64. Hokamaki J, Kawano H, Yoshimura M, et al. Urinary biopyrrins levels are elevated in relation to severity of heart failure. *J Am Coll Cardiol*. 2004;43(10):1880–1885. doi:10.1016/j.jacc.2004.01.028
65. Wu AH, Levy WC, Welch KB, et al. Association between bilirubin and mode of death in severe systolic heart failure. *Am J Cardiol*. 2013;111(8):1192–1197. doi:10.1016/j.amjcard.2012.12.048
66. Okada A, Sugano Y, Nagai T, et al. Usefulness of the direct and/or total bilirubin to predict adverse outcomes in patients with acute decompensated heart failure. *Am J Cardiol*. 2017;119(12):2035–2041. doi:10.1016/j.amjcard.2017.03.033
67. Zheng H, Li Y, Xie N. Association of serum total bilirubin levels with diastolic dysfunction in heart failure with preserved ejection fraction. *Biol Res*. 2014;47(1):7. doi:10.1186/0717-6287-47-7
68. DiNicolantonio JJ, McCarty MF, O'Keefe JH. Antioxidant bilirubin works in multiple ways to reduce risk for obesity and its health complications. *Open Heart*. 2018;5(2):e000914. doi:10.1136/openhrt-2018-000914
69. Kudo K, Inoue T, Sonoda N, Ogawa Y, Inoguchi T. Relationship between serum bilirubin levels, urinary biopyrrin levels, and retinopathy in patients with diabetes. *PLoS One*. 2021;16(2):e0243407. doi:10.1371/journal.pone.0243407
70. Ng ML, Ang X, Yap KY, et al. Novel oxidative stress biomarkers with risk prognosis values in heart failure. *Biomedicines*. 2023;11(3):917. doi:10.3390/biomedicines11030917
71. He T, Mischak M, Clark AL, et al. Urinary peptides in heart failure: A link to molecular pathophysiology. *Eur J Heart Fail*. 2021;23(11):1875–1887. doi:10.1002/ejhf.2195
72. Bonanni A, Vinci R, d'Aiello A, et al. Targeting collagen pathways as an HFpEF therapeutic strategy. *J Clin Med*. 2023;12(18):5862. doi:10.3390/jcm12185862
73. Carland C, Zhao L, Salman O, et al. Urinary proteomics and outcomes in heart failure with preserved ejection fraction. *J Am Heart Assoc*. 2024;13(9):e033410. doi:10.1161/JAHA.123.033410